Etude anatomique et fonctionnelle du noyau parasousthalamique chez le rongeur

Marie Barbier

THESE DE DOCTORAT

DE L'ETABLISSEMENT UNIVERSITE BOURGOGNE FRANCHE-COMTE

Préparée à la faculté des Sciences et Techniques de Besançon

Ecole doctorale n°554

Environnements-Santé

Spécialité : Sciences de la Vie et de la Sant , Neurosciences

Présentée et soutenue publiquement à Besançon

Le 11 septembre 2019

Par

Marie Barbier

Etude anatomique et fonctionnelle du noyau parasousthalamique chez le rongeur

Directeur de thèse : **Dr Pierre-Yves RISOLD**

EA481 : Laboratoire de Neurosciences Intégratives et Cliniques de Besançon

Composition du Jury :

Philippe VERNIER	DR, CNRS-Université Paris Sud	Rapporteur
Yves TILLET	DR, INRA-CNRS-Université de Tours	Rapporteur
Christelle PEYRON	CR, CNRS-Université Claude Bernard Lyon	Examinatrice
Dominique FELLMANN	Pr, Université Bourgogne Franche-Comté	Président du jury
Pierre-Yves RISOLD	CR, Université Bourgogne Franche-Comté	Directeur de thèse

“ Dans la vie on ne fait pas ce que l’on veut
mais on est responsable de ce que l’on est “

Jean-Paul Sartre

“ Il faut toujours viser la lune,
car même en cas d’échec on atterrit dans les étoiles “

Oscar Wilde

Remerciements

Je tiens tout d'abord à remercier le Dr Philippe Vernier et le Dr Yves Tillet de m'avoir fait l'honneur de juger ce travail de thèse.

Merci également au Dr Christelle Peyron d'avoir accepté de faire partie de ce jury de thèse. Je la remercie aussi pour sa participation active lors de mes comités de suivi de thèse, d'avoir écouté les avancées de mes travaux et d'avoir été de bon conseil lors de nos rencontres aux congrès à Copenhague, à Bordeaux et au laboratoire à Besançon.

J'exprime toute ma gratitude au Pr Dominique Fellmann pour ses conseils avisés et son écoute, et je le remercie de m'avoir fait l'honneur de présider mon jury de thèse.

Je remercie également le Dr Frédérique Datiche et le Dr Jean Gascuel pour leur accueil dans leur équipe à Dijon et avec qui j'ai eu la chance de travailler, notamment lors de réalisations d'injections de virus PRV chez la souris.

Pierre-Yves, je t'adresse mes plus profonds et chaleureux remerciements, pour la confiance que tu m'as accordée en acceptant de m'encadrer au cours de mon master 2 et de ma thèse, ainsi que pour tes multiples conseils et les connaissances que tu as su me transmettre. J'aimerais également te dire à quel point j'ai apprécié ta grande disponibilité et tes qualités humaines d'écoute et de compréhension tout au long de ce travail qui m'ont permis de progresser dans cette phase d'"apprenti-chercheur". J'ai beaucoup appris à tes côtés et pris énormément de plaisir à travailler avec toi. Je t'adresse ma gratitude pour tout cela. Je suis consciente d'avoir eu beaucoup de chance de t'avoir comme "chef" (oui, je l'ai dit et sans rire cette fois !) ou directeur de thèse. Tu m'as transmis ta passion de la neuroanatomie et je t'en suis très reconnaissante. Et puis, soyons un peu prétentieux, une fois n'est pas coutume et ce n'est pas bien grave…, mais travailler et apprendre aux côtés d'un des meilleurs neuroanatomistes de France et même du monde (même si je ne connais qu'une infime partie de la littérature, je n'en connais pas d'autre aussi "calé" que toi !) n'est pas donné à tout le monde. Ce sera un avantage certain pour ma carrière future, j'en suis persuadée. Et puis bien sûr, je te remercie de m'avoir guidée, encouragée et fait beaucoup voyager pendant presque quatre ans ! J'ai beaucoup apprécié nos visites "touristiques" lors des congrès dans les différentes villes, parcourues parfois au pas de course… (oui, je sais, c'est ma faute ! Je n'aime pas les transports en commun, y'a trop de microbes…). Mais bon, tu me connais maintenant, le sport c'est la vie alors considère que je prenais soin de toi ! J'espère que notre "binôme" ne s'arrêtera pas avec la fin de cette thèse et que je pourrai continuer à te "fatiguer" un peu comme tu dis ! C'est vrai que je n'ai pas toujours été facile, parfois "dure" émotionnellement, intransigeante avec les autres et avec moi-même, mais bon, on va dire que c'est toi qui as un peu déteint sur moi…. Et de toute façon, j'ai encore plein

de questions à te poser et on a encore pleins de papiers à écrire je crois… (et un livre, non ?? au pire, je te "pique" l'idée … et je le continue, vu que tu m'as tout dit et que j'ai un superbe stylo pour l'inspiration !!). Bref, tu ne souhaites pas encadrer de nouveau(elle) étudiant(e), mais tu as raison (pour une fois !) car tu ne vas pas te débarrasser de moi comme ça, et puis tu le sais, tu ne trouveras pas mieux que moi (dis-moi que j'ai raison … ou je sors la photo "dossier", tu sais, celle prise à Hollywood avec Bigfoot et Superwoman !!!). Pour terminer plus sérieusement, tu es quelqu'un que j'admire beaucoup, j'aimerais avoir ne serait-ce qu'un tier de tes connaissances, mais un jour tu verras… l'élève dépassera le maître !

Je remercie aussi tous les membres de mon équipe EA481 et ex-équipe EA3922 pour le climat sympathique dans lequel ils m'ont permis de travailler. Les nombreuses discussions que j'ai pu avoir avec chacun m'ont beaucoup apporté. Laurence, Vincent, Pierre-Edouard, Coralie mais aussi Jean-Louis, disparu brutalement, j'ai passé d'agréables moments en votre compagnie lors des TP de "Psycho". Je remercie également tous les stagiaires que j'ai eu l'occasion d'encadrer ou de croiser. Je remercie aussi mes étudiants de la licence au master, sans qui je n'aurais jamais pu être aussi à l'aise à l'oral que je ne le suis aujourd'hui et qui m'ont appris la pédagogie !

J'ai plus particulièrement une pensée pour Sandrine, doctorante m'ayant précédé et avec qui j'ai pu apprendre les bases de la coupe au cryostat et l'immunohistochimie ! Je te souhaite de réussir dans tes projets futurs. Martine, "du bureau de l'école doc", je te remercie également pour ta disponibilité, pour ton aide lors des réinscriptions sur ADUM et pour ta patience avec Pierre-Yves et moi au moment de l'attente des rapports, nécessaires à l'autorisation de soutenance !! Merci Gaby, "ma maman du labo" et Amandine (nos discussions sur Pedro, Iris et nos autres compagnons de tous poils me manquent) parties du labo toutes les deux un peu trop tôt (retraite pour l'une et jeune maman pour l'autre). On discutait bien tous ensemble à midi avec Christophe, à raconter des blagues et à faire des mots croisés…ce n'était plus aussi vivant et joyeux le midi après votre départ. Que de bons moments passés avec vous à l'animalerie, en salle histo et à la cafet' le midi. Christophe, mon technicien préféré et maintenant ami (enfin si tu veux bien !), tu vas énormément me manquer, je t'emmènerais bien avec moi en post-doc (je te fais signe s'ils ont besoin d'un technicien !). Mais je passerai te saluer à Port-Lesney si l'occasion se présente. Je te souhaite le meilleur pour la suite avec ta femme et tes enfants. Merci également à Hervé, Anna et maintenant Emmanuel d'avoir pris soin de mes rats et de mes souris. Merci aussi à toutes ces petites bêtes, sans qui cette thèse n'existerait pas, compagnons de travail facétieux et avec qui j'ai développé une relation particulière, parfois non conventionnelle ("Marie, on ne fait pas de bisous aux rats, ce n'est pas autorisé !"). Bahrie, Lidia, Angélique et Stéphanie, nous avons eu l'occasion de discuter un petit peu (parfois au labo, mais travail oblige, "Marie, on ne papote pas, aller hop, au boulot !" et quelques fois en dehors…), j'ai été ravie de vous connaitre. Je suis certaine que vous prendrez soin de Christophe (il est bien entouré, bon…

je ne sais pas si les filles c'est de tout repos, mais il ne va pas s'ennuyer, j'en suis sûre !). Je vous souhaite de réussir vos projets respectifs et de vous épanouir autant professionnellement que personnellement.

Sophie, je ne t'ai pas connue étudiante au laboratoire mais ta présence à ma soutenance m'a beaucoup touchée, je t'en remercie. J'espère pouvoir te recroiser en trail, et si l'occasion se présentait, je serais ravie de collaborer avec toi ! Merci aussi aux membres du bureau de l'A'Doc, anciens et nouveaux, Jé, Alex, Marie, François, Romain … pour m'avoir fait découvrir la vie associative. Un grand merci également à Sandra et Alice, que j'ai appris à connaitre lors de nos soirées "jeux" notamment. Merci pour votre bonne humeur et pour votre participation à la préparation de mon pot de thèse et de mes cadeaux je crois...

Bien sûr, mes bichons et mes bichettes, je ne vous remercierai jamais assez pour tous ces bons moments passés depuis nos débuts à la fac et tous nos fous rires. Mention spéciale à ma bichette n°1 et ancienne binôme de TP, Coralie, merci pour ton écoute, ta gentillesse et ta positivité même lors des périodes parfois difficiles que nous avons surmontées ensemble. Merci à vous tous de m'avoir encouragée pendant ces années de thèse même si je n'ai pas été beaucoup présente lors des différentes soirées organisées ici et là ! Mais chacune de nos retrouvailles me redonnaient un moral d'acier, et ce n'est bien évidemment pas terminé !

Mes remerciements vont aussi à ma famille et mes amis, qui, avec cette question récurrente, "quand est-ce que tu la soutiens cette thèse ?", bien qu'angoissante en période de doutes, m'ont permis de ne jamais dévier de mon objectif final. Je tiens aussi à adresser mes plus vifs remerciements à nos infirmières préférées, Estelle, Christine, Delphine et Lydie, merci pour vos encouragements et votre présence à ma soutenance. Et bien sûr, une petite pensée pour tous mes "compagnons sportifs" rencontrés lors de randonnées, trails et sorties VTT, dans notre belle région, la Franche-Comté, avec comme terrain de jeu, les falaises et sentiers escarpés du Doubs.

Jérôme, merci pour tout le soutien que tu m'as apporté pendant cette thèse même si ça n'a pas toujours été facile. Merci de m'avoir accompagnée lors de mes sorties plus ou moins rocambolesques avec mes compagnons à quatre pattes (Okapi puis Dorlane alias Nanou), à sabots (Flicka, Caline, Symphonie et Becky) et à grandes oreilles (Pitchoune et Ratoune) !!! Merci d'être là tout simplement.

Enfin, j'adresse toute mon affection à mes parents ; leur confiance, leur tendresse et leur amour me portent et me guident tous les jours. Merci d'avoir fait de moi ce que je suis aujourd'hui. Je vous aime.

Table des matières

Table des illustrations

Abréviations

ACB : noyau accumbens

AId : aire insulaire agranulaire, partie dorsale

AIp : aire insulaire agranulaire, partie postérieure

ARNm : acide ribonucléique messager

BMAa : partie antérieure du noyau basomédian de l'amygdale

BST : noyau du lit de la strie terminale

CbN : noyau calbindine

CEA : noyau central de l'amygdale

CEAc : partie capsulaire du noyau central

CEAi : partie intermédiaire du noyau central

CEAl : partie latérale du noyau central

CEAm : partie médiane du noyau central

CGRP: calcitonin gene-related peptide

CNO : clozapine-N-oxide

COAa : partie antérieure du noyau cortical amygdalien

CP : caudoputamen

CRH : corticolibérine

Ctb : cholera toxine B

DREADD : *Designer Receptor Exclusively Activated by Designer Drugs*

EGL : éminence ganglionnaire latérale

EGM : éminence ganglionnaire médiane

Enk : enképhaline

FG : fluorogold

FS : fundus striatum

GABA : acide gamma-aminobutyrique

GAD : acide glutamique décarboxylase

GP : globus pallidus

GPe : segment externe du GP

GPi : segment interne du GP

GU : aire gustative

Hcrt : hypocrétine

HRP : *horseradish peroxidase*

INS : région insulaire

LHA : aire hypothalamique latérale

LHAd : région dorsale du LHA

LHApfx : région périfornicale du LHA

LHApm : région prémamillaire du LHA

LHAppstn : région pré-PSTN du LHA

LHAs : région suprafornicale du LHA

LPS : lipopolysaccharide bactérien

MCH : hormone de mélanoconcentration

mfb : faisceau médian du télencéphale

NG : noyau gémini

NT : neurotensine

NTS : noyau du tractus solitaire

PB : noyau parabrachial

pTac1 : préprotachykinine 1

PHAL : *Phaseolus vulgaris* leucoagglutinine

PKC-δ : protéine kinase C delta

PMd : noyau prémamillaire dorsal

PMv : noyau prémamillaire ventral

PSTN : noyau parasousthalamique

SI : substance innominée

SN : substance noire

SNc : partie compacte de la substance noire

SNr : partie réticulée de la substance noire

SNC : système nerveux central

STN : noyau sousthalamique

TAC1 : tachykinine 1

TH : tyrosine hydroxylase

VISC : aire viscérale

vlt : tractus hypothalamique ventro-latéral

vlah : tractus amygdalo-hypothalamique ventro-latéral

VMPGN : *viscero motor pattern generator network*

VTA : aire tegmentale ventrale

PREAMBULE

L'hypothalamus a été identifié en tant que structure dans le système nerveux central (SNC) à la fin du XIX^{ème} siècle, mais les premières hypothèses quant à son organisation anatomique n'ont été formulées qu'au milieu du XX^{ème} siècle. Le terme même "hypothalamus" vient de sa position "sous-thalamique", définit selon un axe longitudinal dont le télencéphale est le pôle antérieur, l'hypothalamus en arrière de celui-ci occupant la partie ventrale du diencéphale et le thalamus la partie dorsale. Il pouvait alors être confondu avec d'autres structures "sous-thalamiques", telles que le corps de Luys (noyau sousthalamique (STN)) ou le champ de Forel ; le terme de région "sous-thalamique" étant dû à Auguste Forel (1877). C'est W.E. Le Gros Clark qui révisa l'organisation des structures "sous-thalamiques" qu'il associa soit au thalamus ventral (noyau du lit de la strie terminale (BST), zona incerta, STN), soit aux régions hypothalamiques dont les frontières furent alors fixées jusqu'à la fin du XX^{ème} siècle. Ainsi, l'hypothalamus est limité rostralement par la lame terminale, caudalement par le tegmentum mésencéphalique et latéralement par le pédoncule cérébral. Au début du XXI^{ème} siècle, l'hypothalamus est par convention divisé en quatre aires rostrocaudales (préoptique, antérieure, tubérale et postérieure) et trois zones longitudinales (périventriculaire, médiane et latérale) qui circonscrivent douze secteurs (Le Gros Clark *et al*, 1939; Crosby & Woodburne, 1940; Swanson, 1987). Cependant, sur des coupes histologiques, les limites entre ces différentes régions de l'hypothalamus n'apparaissent pas clairement.

Des années1980 jusqu'aux années 2000, l'organisation de circuits intra-hypothalamiques, de même que leur intégration dans des réseaux plus larges avec le télencéphale, a fait l'objet de nombreux travaux chez le rongeur. Il y a vingt-cinq ans, plusieurs de ces circuits ont été décrits (Risold *et al*, 1994; Risold & Swanson, 1995, 1996; Risold *et al*, 1997) impliquant les noyaux de la zone médiane de l'hypothalamus. Ces circuits interviennent dans l'expression de comportements sociaux, la mémorisation spatiale ou encore dans la genèse des rythmes circadiens. Ils agissent en interaction avec les neurones neuroendocriniens et non neuroendocriniens de la zone périventriculaire afin de contrôler les réponses périphériques en lien avec l'expression de ces comportements, le bilan énergétique et le maintien du poids corporel (Swanson, 1999, 2000; Saper *et al*, 2005; Berthoud & Münzberg, 2011; Swanson, 2012). Ces travaux anatomiques menés pour beaucoup d'entre eux dans le laboratoire du Professeur Larry W. Swanson à Los Angeles entre 1989 et 1998 furent concomitants à des progrès importants dans l'étude du développement embryonnaire de l'hypothalamus et du télencéphale (Puelles & Rubenstein, 1993; Rubenstein & Puelles, 1994; Rubenstein *et al*, 1994; Puelles, 1995; Eisenstat *et al*, 1999). Les deux approches, anatomique et développementale, s'accordent sur la conclusion que les frontières "classiques" de l'hypothalamus ne sont pas satisfaisantes mais aboutissent à des modèles d'organisation de l'hypothalamus différents. Un bref résumé des hypothèses et conclusions développementales sera fourni dans l'introduction puisque des données du développement sont indispensables afin de comprendre l'organisation anatomique de l'hypothalamus. Néanmoins, nos travaux s'inscrivent dans la ligne des hypothèses émanant de ceux du groupe de L.W.

Swanson, et donc essentiellement sur la base de données anatomiques du cerveau adulte. Ces travaux amènent à des modèles encore hypothétiques mais qui ont le mérite de prendre en compte l'organisation des réseaux du cerveau antérieur (prosencéphale) dans leur globalité. D'après le modèle de L.W. Swanson, les réseaux impliquant notamment les noyaux de la zone médiane de l'hypothalamus sont organisés suivant un plan qui se rapproche de celui des "ganglions de la base" (terme introduit en 1876 par Ferrier, que nous appelons plutôt "noyaux de la base") (Ferrier, 1876; Swanson, 2000, 2012). Cependant, à ce jour, ce modèle s'accommode mal des aires hypothalamiques latérales qui sont encore très peu comprises. Identifier et caractériser les réseaux impliquant l'aire hypothalamique latérale (LHA) doit permettre de placer les dernières pièces d'un puzzle, afin de compléter le schéma d'une certaine organisation anatomique de l'hypothalamus.

Dans ce travail, nous avons cherché à comprendre comment l'hypothalamus latéral postérieur s'insère dans des réseaux cérébraux, via l'étude d'un complexe nucléaire formé du noyau parasousthalamique (PSTN) et du noyau calbindine (CbN) (Chometton *et al*, 2016; Barbier *et al*, 2017). Ces deux noyaux sont localisés entre le STN et les noyaux prémamillaires, le premier étant associé aux "noyaux de la base" et les seconds, aux réseaux de l'hypothalamus médian décrits par le groupe de L.W. Swanson.

INTRODUCTION

I. Résumé des différentes hypothèses concernant le développement du prosencéphale et incluant l'hypothalamus

Le cerveau primitif est composé de trois vésicules cérébrales primaires liées par des faisceaux de fibres en développement (commissures) orientés transversalement. On distingue alors le cerveau antérieur (ou prosencéphalon ou prosencéphale) issu de l'archencéphale, le cerveau médian (ou mésencéphalon ou mésencéphale) et le cerveau postérieur (ou rhombencéphalon ou rhombencéphale) issus du deutérencéphale (Figure 1A). Le prosencéphalon et le rhombencéphalon se différencient ensuite en deux parties. Le prosencéphalon donne naissance au télencéphalon (ou télencéphale) et au diencéphalon (ou diencéphale), le mésencéphalon reste comme une seule vésicule et le rhombencéphalon se subdivise en métencéphalon (ou métencéphale) (rostral) et en myélencéphalon (ou myélencéphale) (caudal) (Huxley, 1871). Le cerveau dit « à cinq vésicules » est formé (Figure 1B).

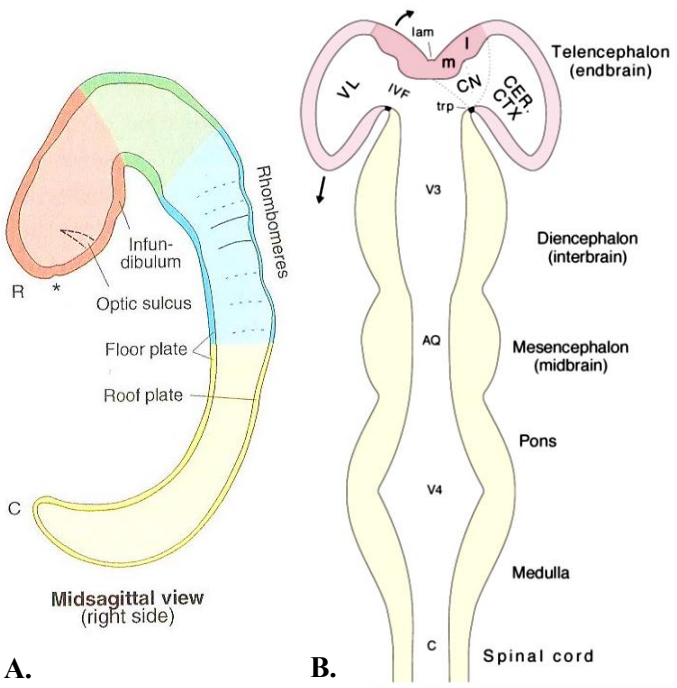

Figure 1. Représentations schématiques d'une coupe sagittale et horizontale d'un tube neural embryonnaire humain (Swanson, 2000, 2012).

(A) Représentation des principales vésicules cérébrales en vue sagittale (prosencéphalon en rouge, mésencéphalon en vert, rhombencéphalon en bleu et moelle épinière en jaune). "*" : localisation de la fermeture du neuropore rostral.
(B) Coupe horizontale, dont l'axe longitudinal a été "redressé". Evagination (flèches) des hémisphères cérébraux (en rose) formés de leurs deux divisions, cortex et noyaux cérébraux.

AQ : aqueduc ; C : caudal (en A), canal central (en B) ; CER. CTX : cortex cérébral ; CN (l, m) : "noyaux de la base" (crêtes ventriculaires latérale et médiane) ; IVF : foramen interventriculaire de Monro ; lam : lame terminale ; trp : plaque du toit (*"roof plate"*) ; R : rostral ; VL : ventricule latéral ; V3 : 3ème ventricule ; V4 : 4ème ventricule.

Selon les hypothèses classiques, le diencéphalon peut ensuite lui-même être divisé en épithalamus (dorsalement), thalamus dorsal et ventral, et hypothalamus (ventralement), grâce à l'étude de plusieurs sulci sur la face ventriculaire du cerveau en développement. Le télencéphalon est formé de deux vésicules latérales, les futurs hémisphères cérébraux, ainsi que d'une partie médiane, la lame terminale qui correspond à la fusion du neuropore rostral. C'est dans le toit des vésicules télencéphaliques (pallium) que se développe le futur cortex cérébral, alors que leurs parois rostrales ventromédianes formeront le septum, en particulier les noyaux médian et latéral (Figure 2). Enfin, la partie ventrale/sous-palliale de ces vésicules donnera naissance aux éminences ganglionnaires

médianes (EGM) et latérales (EGL) qui formeront le pallidum et le striatum (Marin *et al*, 2000; Bayer & Altman, 2004).

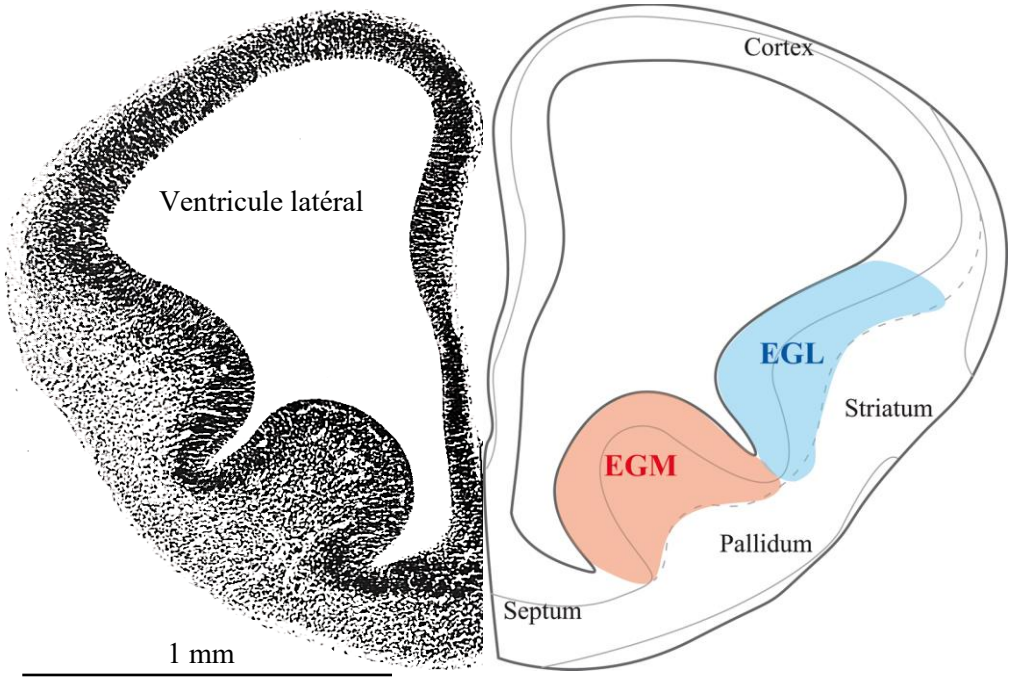

Figure 2. Représentation des éminences ganglionnaires latérale et médiane sur une coupe coronale de prosencéphale de rat au 15ème jour embryonnaire.

Photographie (à gauche) d'une coupe coronale de prosencéphale de rat au 15ème jour embryonnaire, traitée en paraffine et colorée avec la méthode de Nissl (Bayer and Altman, 2004). Représentation schématique (à gauche) de la coupe adjacente avec localisation des EGL et EGM.

EGL : éminence ganglionnaire latérale ; EGM : éminence ganglionnaire médiane.

L'organisation anatomique du télencéphale repose donc sur des différences très nettes entre cortex et "noyaux de la base". Le cortex est majoritairement organisé en couches chez les mammifères, et les neurones pyramidaux qui le composent utilisent majoritairement le glutamate, alors que les noyaux cérébraux sont organisés en formations nucléaires et utilisent l'acide gamma-aminobutyrique (GABA) (Figure 3). De plus, les neurones pyramidaux des couches corticales génèrent l'immense réseau de connexions intra-corticales, projetant ensuite sur les autres régions du SNC de manière topographiquement organisée. Le cortex partage ainsi des connections bidirectionnelles avec le thalamus, et envoie aussi des efférences topographiquement organisées aux "noyaux de la base", qui eux-mêmes projettent topographiquement sur le tronc cérébral. Le cortex et les "noyaux de la base" sont donc des structures bien distinctes. Les "noyaux de la base" se développent vers l'intérieur des vésicules formant les éminences ganglionnaires.

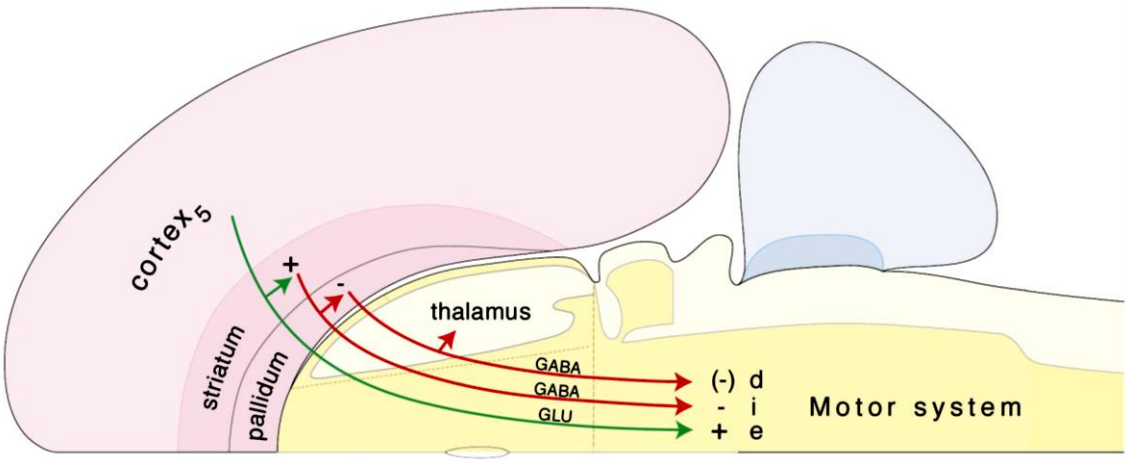

Figure 3. Organisation générale des projections caudales descendantes directes depuis les régions corticales, striatales et pallidales au système moteur du tronc cérébral (Swanson, 2012).

Ce circuit "prototype" met en jeu des projections glutamatergiques excitatrices (e) (qui utilisent le glutamate GLU, flèches vertes) depuis les neurones pyramidaux de la couche 5 isocorticale avec des collatérales dans le striatum. Le striatum génère ensuite des projections GABAergiques inhibitrices (i) (qui utilisent le GABA, flèches rouges) au système moteur et dans le pallidum. Enfin, le pallidum envoie des projections GABAergiques au système moteur avec des collatérales dans le thalamus dorsal. Ces projections pallidales peuvent être désinhibitrices (d) lorsqu'elles sont inhibées par les afférences striatales.

Cependant, *"il règne encore aujourd'hui une grande confusion et beaucoup de discordances quant à ce qui constitue les "noyaux de la base" et à la façon de regrouper les différentes structures des hémisphères cérébraux pour lesquelles il existe une multitude de termes, allant de système limbique, amygdale étendue, corps striés, néocortex et plus encore"* (d'après L.W. Swanson, 2012). En principe, pour comprendre l'organisation d'une région du SNC, il faut comprendre les processus conduisant à son histogenèse neurale ; mais il est aussi nécessaire de confronter les données développementales aux particularités de la région considérée dans le cerveau adulte. Plusieurs modèles vertébrés et invertébrés sont couramment utilisés pour l'étude du développement du cerveau et ont permis l'accumulation de nombreuses données (morphologiques, histologiques, neurochimiques, hodologiques et génétiques). Toutefois, dans la littérature, certains auteurs se concentrent sur les principes fonctionnels alors que d'autres considèrent les données morphologiques et/ou ontogéniques comme plus pertinentes (Puelles *et al*, 2013). Ceci abouti à l'émergence de nombreuses théories et modèles d'organisation du SNC. Cependant, un "bon" modèle et une "bonne" théorie amènent à une compréhension des phénomènes de manière durable et largement acceptée par l'ensemble de la communauté scientifique. Ils doivent permettre d'assembler logiquement et de mettre en avant une vraie cohérence entre les données se référant au développement, à l'anatomie, à l'anatomie comparée mais encore à la fonction de la structure étudiée, et, à fortiori, du cerveau lui-même. De nombreux modèles, basés sur des approches génétiques, remettent en question les limites même du télencéphale, notamment avec l'hypothalamus. En fait, dès l'origine, les frontières entre hypothalamus et télencéphale ont été difficiles à établir. Si un certain consensus semblait avoir émergé pendant la seconde moitié du XX^{ème} siècle, avec une frontière entre région préoptique et septale, les

données développementales récentes changent encore une fois la donne. Ainsi, pour certains auteurs, le télencéphale pourrait inclure tout ou en partie l'hypothalamus. Quoi qu'il en soit, il est maintenant devenu évident que pour comprendre l'organisation du cerveau antérieur, il est indispensable de s'intéresser à celle de l'hypothalamus. Les efforts pour comprendre l'organisation de l'hypothalamus ont été beaucoup influencés par l'étude de son développement en relation avec les modèles en colonnes et les modèles segmentaires déjà appliqués au SNC dans son ensemble, et qui vont être présentés succinctement ci-après.

1. Modèles segmentaires

A la fin du XIX^{ème} siècle, Orr invente le terme "neuromère" (Orr, 1887) et propose le modèle segmentaire, également à l'origine du modèle proposé par His, qui comprend le cerveau comme un tube divisé en un ensemble de segments transversaux successifs (neuromères). Bien qu'il ne soit pas explicitement neuromérique, le modèle de His a introduit des concepts importants telles que les parties alar (sensorielle) et basale (motrice), séparées par le *sulcus limitans* (His, 1893), ou encore le concept d'isthme et de déformation du tube neural due à la flexion axiale. His est également le premier à avoir utilisé le terme "hypothalamus" en 1893 (Figure 4).

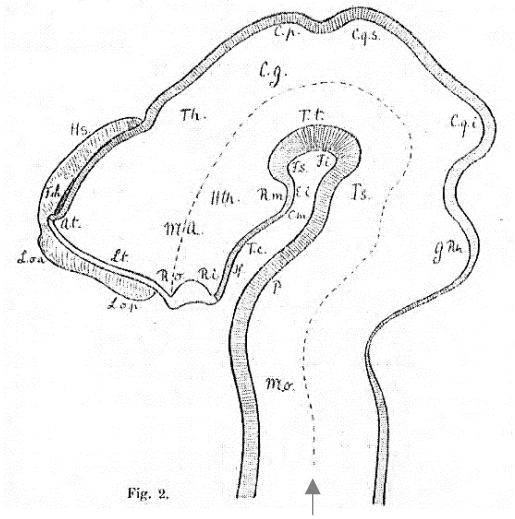

Sulcus limitans

A. t.	=	Angulus terminalis	If.	=	Ort der Infundibulumbildung
C. g.	=	Ort des Corpora geniculata	Is.	=	Isthmus mit seiner charakteristischen Einbiegung
C. m.	=	Corpus mamillare			
C. q. i.	=	Corp. quadrigem. inferius	L. o. a.	=	Lobus olfactorius anterior
C. q. s.	=	Corp. quadrigem. superius	L. o. p.	=	Lobus olfactorius posterior
C. p.	=	Corpus pineale	L. t.	=	Lamina terminalis
E. i.	=	Eminentia interpeduncularis	M. o.	=	Medulla oblongata
F. ch.	=	Fissura chorioidea	R. i.	=	Recessus infundibuli, s. basilaris
F. i.	=	Fossa interpeduncularis	R. o.	=	Recessus opticus
F. s.	=	Fossa supramamillaris	P.	=	Ponsgebiet
G. Rh.	=	Genu Rhombencephali	T. c.	=	Tuber cinerum
Hs.	=	Hemisphäre	Th.	=	Thalamus
Hth.	=	Hypothalamus	Tt.	=	Tuber tegmentale, Haubenwulst

Figure 4. Dessin du tube neural et liste des abréviations, réalisés par His en 1893.

Le terme "hypothalamus", écrit dans la liste des abréviations ci-dessus, est noté "Hth." sur le dessin.

Le relief ventriculaire du cerveau en développement étant en changement perpétuel, il est difficile de donner une description exacte des neuromères et des sulci aboutissant notamment à une divergence d'opinions concernant la place du *sulcus limitans* (sillon permettant de délimiter la plaque basale et alar (dorsale) du tube neural) (Rubenstein *et al*, 1994; Alvarez-Bolado *et al*, 1995; Alvarez-Bolado & Swanson, 1996; Moreno & González, 2011; Diez-Roux *et al*, 2011). Certains auteurs doutent de son existence dans le diencéphale alors que d'autres ont des avis divergents quant aux régions où il se termine (Keyser, 1979; Alvarez-Bolado & Swanson, 1996; Nieuwenhuys *et al*, 1998).

En fait, la limite rostrale du *sulcus limitans* semble dépendre du stade embryonnaire auquel sont faites les observations. L'axe longitudinal du corps et donc du SNC n'étant pas rectiligne, celui de l'embryon de vertébrés subit alors un changement de forme complexe durant le développement (Figure 5).

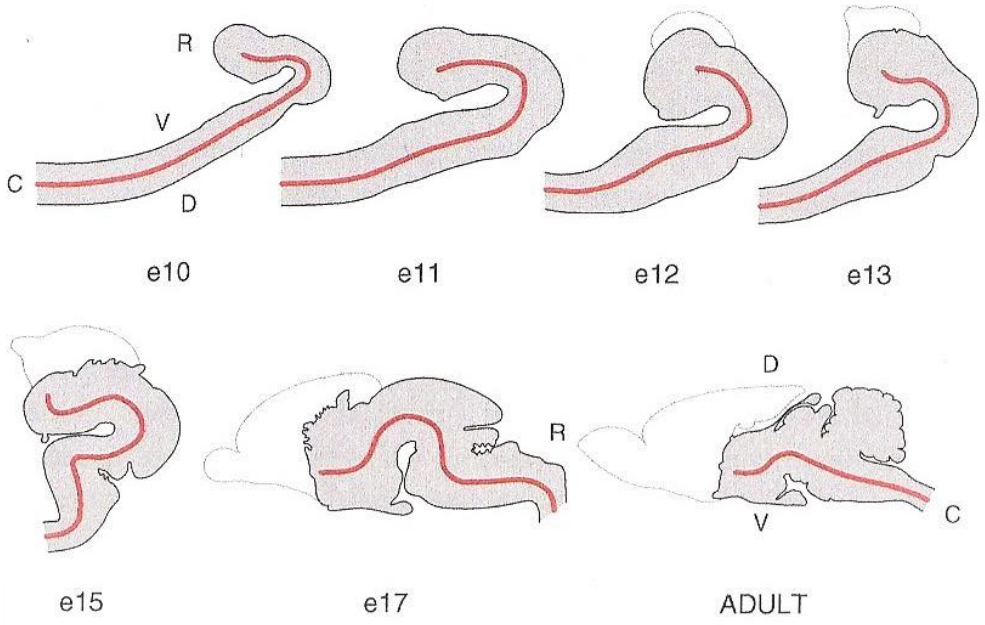

Figure 5. Illustrations des changements de forme de l'axe longitudinal du tube neural au cours du développement embryonnaire chez le rongeur (Alvarez-Bolado & Swanson, 1996).

La ligne rouge représente l'axe longitudinal.

C : caudal ; D : dorsal ; e10-e17 : jours embryonnaires 10-17 ; R : rostral ; V : ventral.

Des données de notre équipe semblent assez en faveur de l'hypothèse d'un changement dans l'organisation de l'axe longitudinal du prosencéphale, induit par l'accroissement du télencéphale et le développement du faisceau médian du télencéphale (mfb) (Croizier *et al*, 2011). Si l'on ne se base que sur des liens physiques, il est évident qu'il n'y a pas de moyen logique d'appliquer le système de coordonnées Cartésien au cerveau des vertébrés en général si l'actuel axe rostro-caudal se réfère à l'axe longitudinal. Il faut d'avantage se référer aux liens topographiques qu'entretiennent les structures entre elles plutôt qu'à leurs relations physico-géométriques ; ce qui revient à déformer l'axe de la même manière chez les différentes espèces durant l'embryogenèse.

Un exemple de modèle segmentaire est le modèle prosomérique (Figure 6), basé sur les patrons d'expression de facteurs de transcription et de molécules de signalisation impliquées dans le développement cérébral des mammifères (Puelles & Rubenstein, 1993; Puelles *et al*, 2013, 2019). Ce modèle suggère une organisation hypothalamique alternative à celle indiquée dans les modèles en colonnes. Tout d'abord, il prend en charge l'aire préoptique dans le cadre du télencéphale, appelé télencéphale non évaginé (Medina *et al*, 2011; Moreno & González, 2011) et fait valoir que l'hypothalamus est situé sous le télencéphale plutôt que sous le thalamus. Cependant, des incertitudes

persistent, comme l'existence de certains neuromères et particulièrement les prosomères (Puelles *et al*, 2013; Nieuwenhuys & Puelles, 2016; Puelles *et al*, 2019).

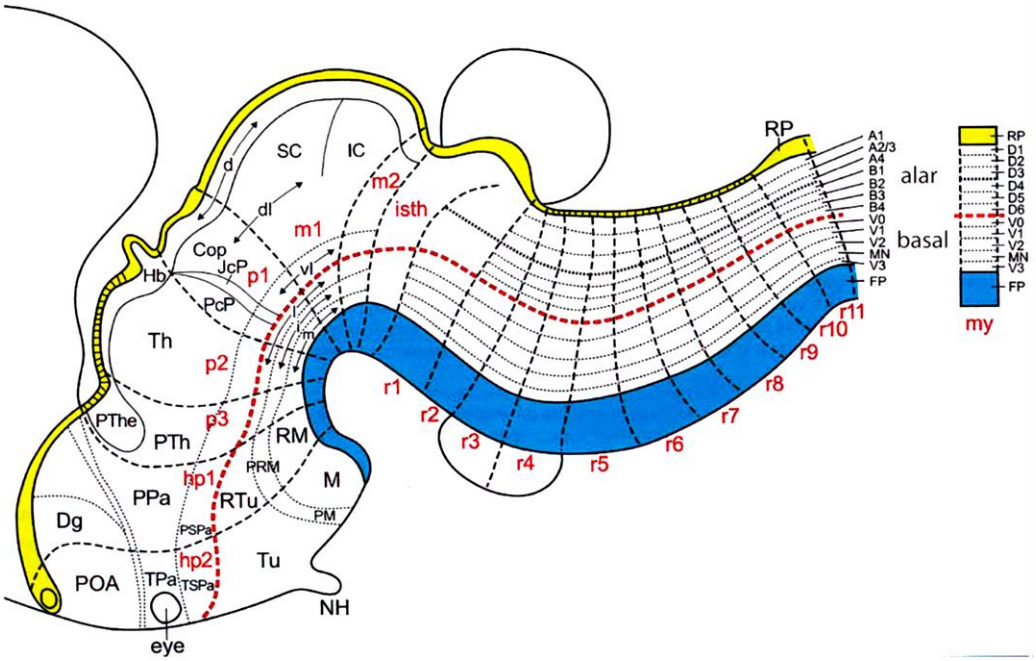

Figure 6. Schéma du prosencéphale d'après le modèle prosomérique (Puelles *et al*, 2019).

Subdivisions de zones neuromériques mises à jour d'après le modèle prosomérique (Nieuwenhuys & Puelles, 2016), et extrapolées aux régions mésencéphaliques, diencéphaliques et hypothalamiques.

Ligne pointillée rouge : limite entre la plaque alar et la plaque basale ; partie bleue : plaque du plancher ; partie jaune : plaque du toit.

D'après l'ouvrage de R. Nieuwenhuys, H.J. Donkelaar et C. Nicholson, chez la plupart des vertébrés, le diencéphale comporte trois neuromères appelés synencéphale, parencéphale postérieur et parencéphale antérieur (Nieuwenhuys *et al*, 1998). Ces derniers étant respectivement limités par le *fasciculus rétroflexus* et par la *zona limitans intrathalamica* (zli). De plus, les auteurs signalent aussi que l'organisation de la partie la plus rostrale du tube neural (hypothalamus, aire préoptique, hémisphères télencéphaliques) n'est pas claire et n'offre aucune limite fiable pour une sous-division "naturelle" de cette région. Selon lui, le télencéphale et l'hypothalamus dérivent probablement du même groupe de neuromères et la plaque basale ne serait pas impliquée dans la formation du télencéphale. Le télencéphale moyen (régions préoptiques) serait ainsi la continuité du diencéphale. Toutes ces données amènent l'idée que l'hypothalamus ne constituerait plus une entité ventrale mais rostrale au thalamus (Bergquist & Kallen, 1953, 1954).

2. Modèles à colonnes et modèles intermédiaires

Le premier modèle en colonnes a été proposé par C.J. Herrick au début du XX^{ème} siècle (Herrick, 1910), influençant la compréhension de l'organisation cérébrale depuis 1910 à nos jours. Ce modèle, basé sur l'organisation des nerfs crâniens et rachidiens en colonnes fonctionnelles, propose que cette organisation colonnaire se propage dans tout le cerveau, y compris le prosencéphale. D'après ce point de vue, l'hypothalamus fait partie du diencéphale et est littéralement "situé sous le thalamus". Pour W.E. Le Gros Clark (1938), le continuum préopto-hypothalamique était divisé en quatre régions rostrocaudales : préoptique, antérieure, tubérale et mamillaire. D'autres modèles proposent un changement de certains traits du modèle prosomérique, telle que la position du *sulcus limitans*, donnant une configuration s'adaptant à celle du modèle en colonnes (Diez-Roux *et al*, 2011).

Des modèles alternatifs d'organisation hypothalamique ont aussi été proposés à partir de certains gènes du développement. T. Shimogori a ainsi identifié une "diagonale intra-hypothalamique", qui n'est ni le modèle en colonne ni le modèle prosomérique, mais un peu entre les deux (Shimogori *et al*, 2010), donnant une interprétation assez différente de celle proposée par L. Puelles et ses collaborateurs (Puelles *et al*, 2012; Puelles & Rubenstein, 2015). D'autres modèles sont basés sur la gliogenèse et la neurogenèse (Alvarez-Bolado *et al*, 2012; Xie & Dorsky, 2017) impliquant des progéniteurs en division, localisés dans la zone ventriculaire, qui produisent des précurseurs neuronaux (Aujla *et al*, 2013; Duncan *et al*, 2016) et gliaux (Timsit *et al*, 1995; Grupp *et al*, 2010; Robins *et al*, 2013) migrant latéralement dans le parenchyme.

Récemment, en 2015, travaillant sur le poisson, le groupe de P. Vernier a proposé un nouveau modèle de régionalisation du prosencéphale basé sur l'organisation ventriculaire (Affaticati *et al*, 2015; Yamamoto *et al*, 2017). Il existe, entre le télencéphale et l'hypothalamus, une région nommée récessus optique (ORR) qui est le continuum de la rétine dans l'embryon téléostéen (Figure 7). Elle correspond en fait à la zone identifiée comme étant la tige optique, chez la souris et le poisson zèbre, entre les commissures antérieure et post-optique. Ce modèle accentue l'hypothèse selon laquelle l'hypothalamus n'est pas une structure homogène et démontre aussi que la région préoptique est différente, dans sa nature, des régions postérieures. Un autre point très intéressant avec cette dernière théorie, concerne le rapprochement qu'elle permet avec l'observation par le groupe de D. Arendt que la même région nommée "ORR" correspond à un territoire qui exprime des gènes conservés, suggérant une origine phylogénétique très ancienne de certains types cellulaires qui le composent (Arendt *et al*, 2016).

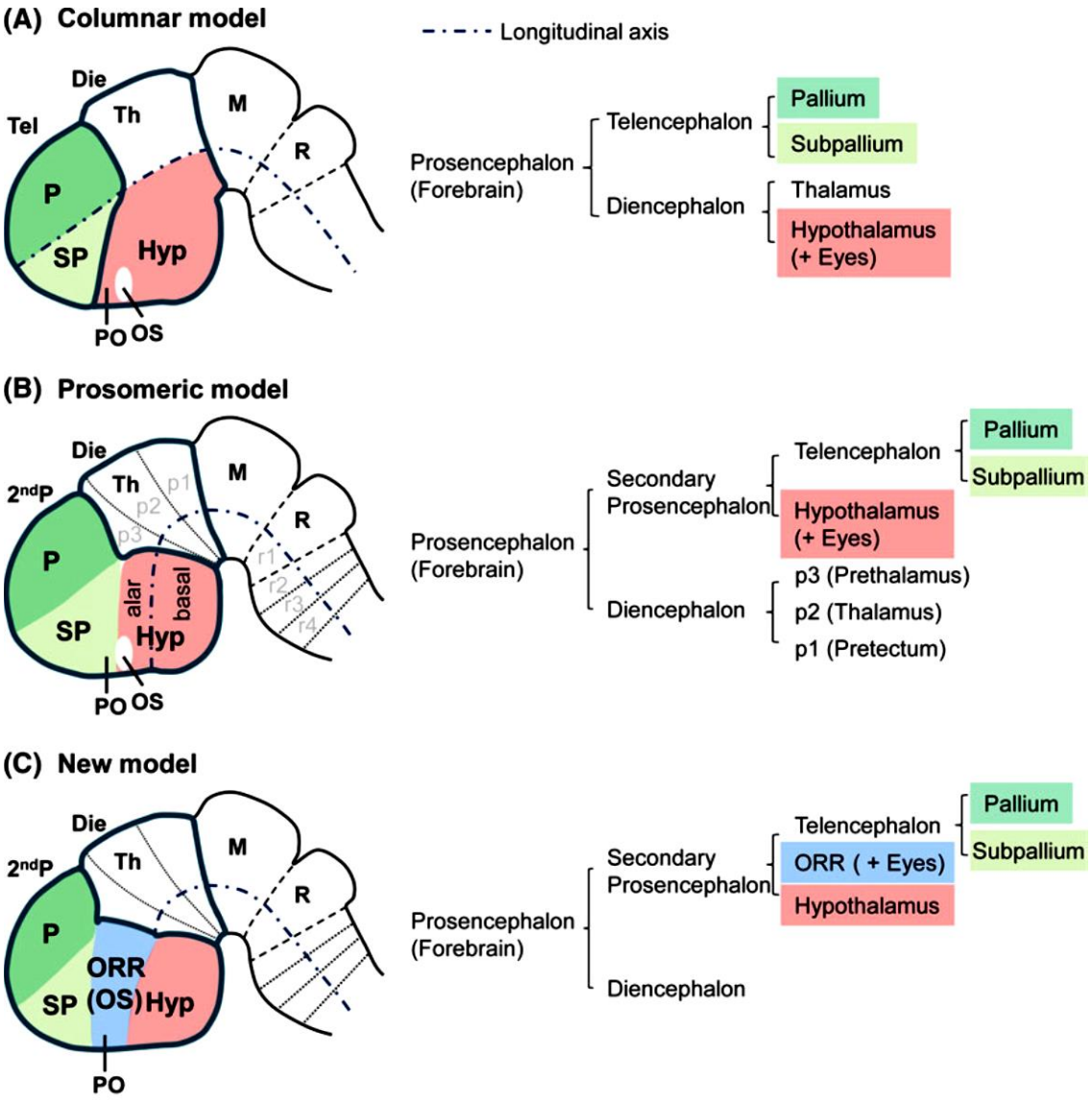

Figure 7. Trois modèles de subdivision du prosencéphale de vertébrés en vue latérale (Yamamoto *et al*, 2017).

(A) Le modèle en colonnes dans lequel l'hypothalamus occupe la moitié ventrale du diencéphale. (B) Le modèle prosomérique proposé à l'origine par Puelles et Rubenstein au début des années 1990 et modifié au cours du temps. Dans ce modèle, l'hypothalamus représente la moitié ventrale de la partie la plus antérieure du prosencéphale ; le télencéphale et l'hypothalamus forment alors le prosencéphale secondaire. (C) Le nouveau modèle, proposé par Affaticati *et al* (2015), dans lequel le prosencéphale secondaire est divisé en trois parties : le télencéphale, l'hypothalamus et la région du récessus optique (ORR).

2ndP : prosencéphale secondaire ; Die : diencéphale ; Hyp : hypothalamus ; M : mésencéphale ; ORR : région du récessus optique ; OS : tige optique ; P : pallium ; p : sous-division prosomérique : PO : aire préotique ; R : rhombencéphale ; r : sous-division rhombomérique ; SP : sous-pallium ; Tel : télencéphale ; Th : thalamus.

3. Conclusions

Tous ces modèles, basés sur le développement, comprennent l'hypothalamus de différentes manières en se fondant sur des principes différents. Ils en fournissent des frontières également souvent divergentes. Ils associent très souvent tout ou partie de l'hypothalamus (comme par exemple l'aire préoptique) au télencéphale plutôt qu'au diencéphale. En ce sens, il devient évident que, si, comme il a été dit précédemment, comprendre l'hypothalamus va permettre de comprendre l'organisation du

cerveau antérieur, comprendre l'organisation du télencéphale devient de même indispensable à l'interprétation des données concernant l'hypothalamus. Suivant ce point de vue, ces modèles ont souvent tendance, parce qu'ils s'intéressent au cerveau à des stades précoces, à ignorer les connaissances acquises dans le domaine de l'organisation des liens anatomiques entre les structures du télencéphale et les diverses structures et noyaux de l'hypothalamus. Ces réseaux ont été très étudiés dans le cerveau adulte et ils seront évoqués dans les chapitres suivants.

II. Organisation anatomique du télencéphale : hypothèse de L.W. Swanson

L'organisation du télencéphale est décrite dans tous les ouvrages de neuroanatomie. On y trouve le reflet de sa complexité avec tous les "systèmes" qui le composent et qui ont été décrits depuis l'origine des neurosciences modernes : systèmes moteur et sensoriels qui impliquent l'isocortex et le striatum/pallidum dorsal, ou système limbique connecté au système olfactif mais qui est aussi étroitement associé à l'hypothalamus. Ce système limbique peut être divisé en système septohippocampal d'une part (Risold, 2004) et amygdale/amygdale étendue d'autre part (de Olmos & Heimer, 1999; Elias *et al*, 2008b). Il empiète aussi sur le réseau cortico-striatal classique, tout comme le système magnocellulaire cholinergique du télencéphale basal qui s'étend du septum médian au noyau de Meynert et implique le pallidum (Pombero *et al*, 2011). Ces neurones cholinergiques participent à l'innervation du manteau cortical dans son ensemble (Figure 8).

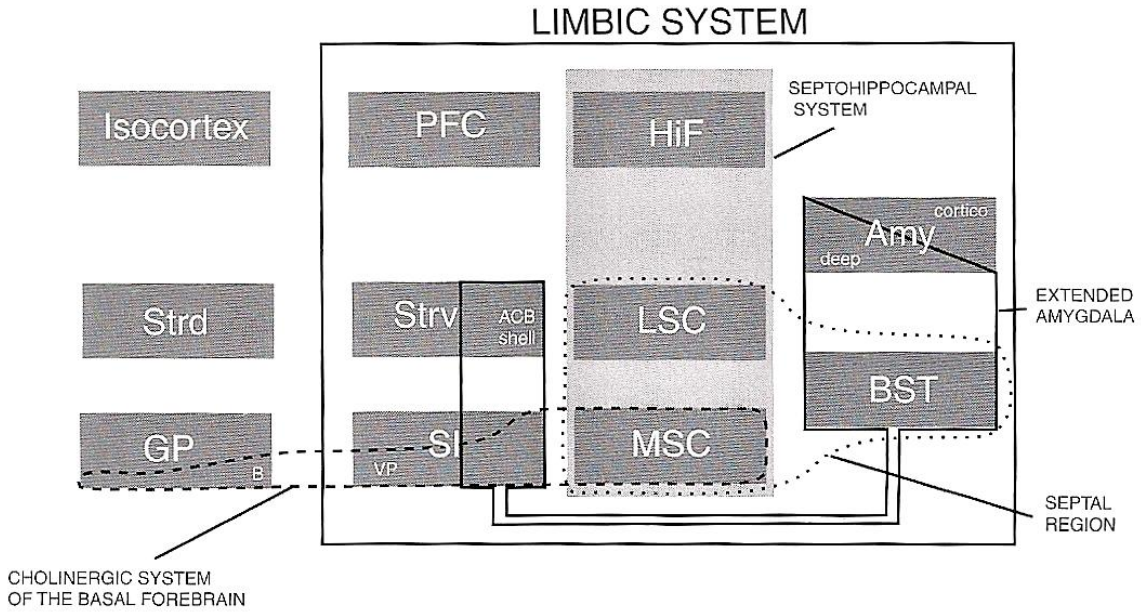

Figure 8. Représentation schématique de quelques "systèmes" du télencéphale (Risold, 2004).

ACB : noyau accumbens ; Amy : amygdale ; B : noyau basal de Meynert ; BST : noyau du lit de la strie terminale ; GP : globus pallidus ; HiF : formation hippocampale ; LSC : complexe septal latéral ; MSC : complexe septal médian ; PFC : cortex préfrontal ; Strd/v : striatum dorsal/ventral ; VP : pallidum ventral.

Dans le chapitre précédent, il a été montré que les données récentes, notamment dans le domaine du développement, incitent à penser l'organisation de l'hypothalamus avec celle du télencéphale. La question se pose alors : de quelle organisation télencéphalique parle-t-on ? Système limbique ? Amygdale étendue ? Système septohippocampal ? Et ceux-là sont-ils sans rapport avec l'organisation cortico-striatale, alors que du point de vue développement l'amygdale se distribue entre pallium, striatum, voir pallidum ?

Comme l'a proposé L.W. Swanson, une façon de s'en sortir avec la multitude des modèles et systèmes décrits dans le télencéphale est de considérer simplement les hémisphères cérébraux comme étant constitués du pallium et sous-pallium : le premier donnant le cortex et le second comprenant les noyaux cérébraux, divisés en striatum et pallidum (Swanson, 2012). Cette vue simplifiée de la régionalisation des hémisphères cérébraux est supportée par l'embryologie, par l'action des neurotransmetteurs, impliqués dans les connexions depuis le cortex aux noyaux sous-corticaux et par l'organisation des connexions depuis le cortex au système moteur (Swanson, 2000). C'est cette vision de l'organisation du télencéphale qui va être brièvement décrite dans les parties suivantes. On retrouve ces principales divisions dans les atlas de L.W. Swanson (Swanson, 1998, 2004) mais c'est aussi celles utilisées dans l'atlas de l'Allen Brain Institute (Allen Institute, 2004). Les principales divisions télencéphaliques sont alors le pallium et les régions striatum/pallidum dorsal, ventral, postérieur et médian.

1. Le manteau cortical est issu du pallium

Chez l'embryon, le sillon cortico-striatal divise les vésicules télencéphaliques en une partie dorsale, le cortex cérébral et une partie ventrale, les noyaux cérébraux. Ce sillon est suivi, peu de temps après, par l'apparition du sillon striato-pallidal qui divise la région nucléaire de la vésicule en une crête dorsale (striatale) et une crête ventrale (pallidale). L'expansion corticale est sous la dépendance de deux centres organisateurs appelés "hem" et "anti-hem" (Medina & Abellán, 2009; Subramanian *et al*, 2009; Montiel & Aboitiz, 2015; Puelles, 2017; García-Cabezas *et al*, 2019). Le premier occupe une position adjacente à la plaque du toit (*"roof plate"*) alors que le second est à la jonction striato-corticale. L'action des gradients inverses de facteurs morphogènes, secrétés par ces centres organisateurs, conduit à la différenciation des différentes structures corticales (Figure 9).

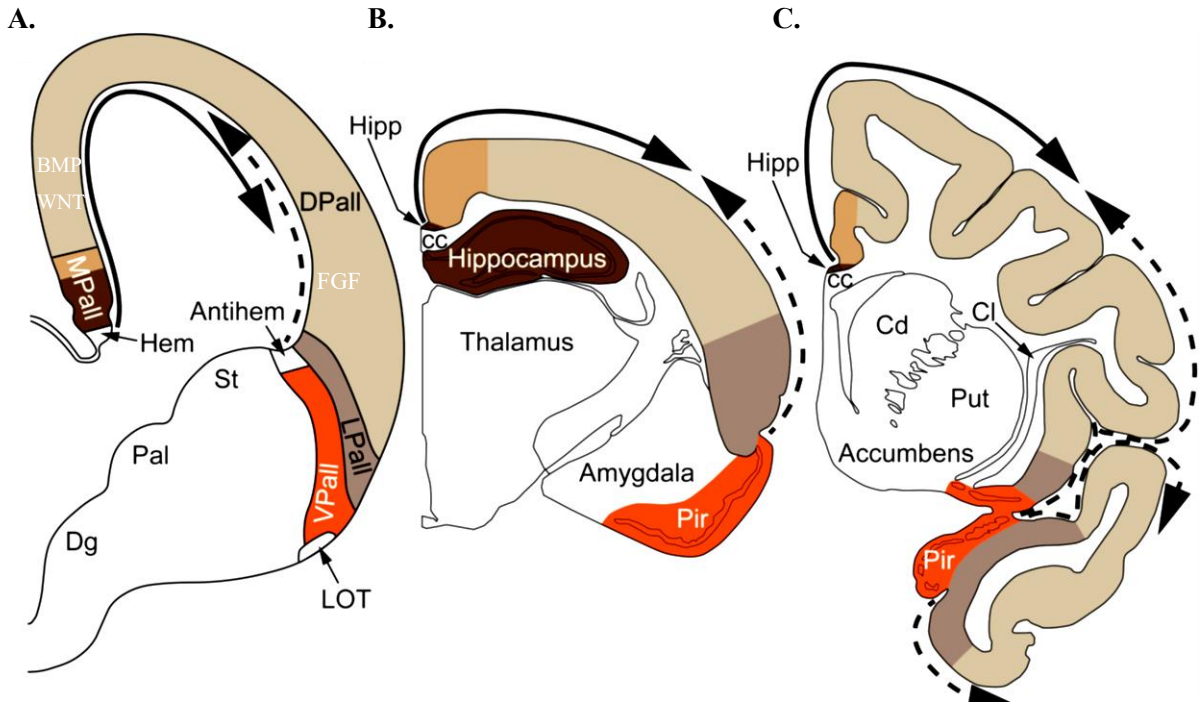

Figure 9. Représentations des centres organisateurs, "hem" et "anti-hem", sur des schémas de coupes sagittales du télencéphale de mammifères (García-Cabezas *et al*, 2019).

(A) Télencéphale en développement qui montre les secteurs du pallium (corticaux) [pallium médian (MPall), pallium dorsal (DPall), pallium latéral (LPall) et pallium ventral (VPall)], l'"hem", et l'"anti-hem". Les deux parties ajoutées sur le secteur de MPall correspondent à l'allocortex (hippocampe) et au périallocortex (aires cingulaires agranulaires/dysgranulaires) chez le rat (B) et le primate (C) d'après l'analyse architectonique chez l'adulte. L'"hem" et l'"anti-hem" sécrètent des protéines morphogènes (BMP, WNT et FGF respectivement) qui forment deux gradients qui se chevauchent (flèches en trait plein et en pointillés).

(B) et (C) Télencéphales de rat (B) et de singe rhésus adultes (C) ; les dérivés adultes des secteurs du pallium en développement sont colorés comme en A. Les flèches en traits pleins indiquent la tendance à la différenciation laminaire attribuée au cortex hippocampique ; les flèches en pointillés montrent la tendance à la différenciation laminaire attribuée au cortex olfactif (cortex piriforme (Pir)).

Cc : corps calleux ; Cd : noyau caudé ; Cl : claustrum ; Dg : domaine diagonal sous-pallial ; Hipp : extension antérieure de la formation hippocampale ; LOT : tractus olfactif latéral ; Pal : pallidum ; Put : putamen ; St : striatum.

Ces progrès récents dans la compréhension de l'origine du pallium et par extension du cortex cérébral sont largement en accord avec l'un des premiers postulats de l'hypothèse de L.W. Swanson. L'organisation du télencéphale, énoncée il y a près de 20 ans, reste cohérente avec des nuances et des précisions que l'expression des marqueurs moléculaires sont seuls à même d'atteindre.

De façon générale, il semble que la neurogenèse progresse du pallidum au striatum jusqu'au cortex. La plus grande partie des précurseurs des neurones du cortex cérébral migrent selon un axe radial à travers la zone sous-ventriculaire adjacente pour coloniser l'ébauche corticale en formation (de Carlos *et al*, 1996; Rakic, 2009). Cependant, d'autres cellules migrent tangentiellement à la surface du cortex cérébral et proviennent des EGL et EGM du télencéphale basal (Cobos *et al*, 2001). Les premières donnent les cellules pyramidales adultes qui utilisent le glutamate. Les secondes sont des interneurones GABAergiques (Welagen & Anderson, 2011). Le glutamate, très majoritairement

utilisé par les efférences caudales, est un des critères qui aide à classer une région de substance grise comme appartenant au cortex ou aux noyaux cérébraux (striatum et pallidum) (Swanson, 2012). Sur la base de ce principe, le cortex cérébral se divise en différentes parties : l'isocortex, qui concerne les régions précédemment assimilées au "néocortex", organisé en six couches de cellules ; l'allocortex, dont l'organisation diffère, il s'agit alors de l'hippocampe et des noyaux corticaux de l'amygdale. Entre ces deux territoires est aussi décrit un cortex périallocortical qui est dépourvu de la couche granulaire (couche IV) ; il s'agit notamment des régions préfrontales médianes et insulaires (INS). L'organisation de ce pallium a été analysée par plusieurs auteurs et d'autres schémas d'organisation ont également été décrits (Vogt & Vogt, 1919; Kappers *et al*, 1936; Filimonoff, 1947; Yakovlev, 1959; Sanides, 1970; Braak, 1980; Swanson, 2012; Puelles, 2017; García-Cabezas *et al*, 2019) (Figure 10) et ne seront pas plus approfondis ici.

<table>
<tr><th>Brodmann (1909/1999)</th><th>Vogt and Vogt (1919)</th><th>Ariëns Kapers et al. (1936)</th><th>Filimonoff (1947)</th><th>Yakovlev (1959)</th><th>Sanides (1970)</th><th>Braak (1980)</th><th>Puelles (2017)</th><th>García-Cabezas et al. (2019)</th></tr>
<tr><td rowspan="2">Hétérogénétique</td><td rowspan="2">Allocortex</td><td>Archicortex (hippocampe)</td><td rowspan="2">Cortex incompletus (hippocampe et cortex olfactif)</td><td rowspan="2">Entopallium (hippocampe et cortex olfactif)</td><td rowspan="2">Allocortex (hippocampe et cortex olfactif)</td><td rowspan="2">Allocortex sensu stricto (hippocampe et cortex olfactif)</td><td>Pallium médian</td><td rowspan="2">Allocortex (hippocampe et cortex olfactif)</td></tr>
<tr><td>Paléocortex (cortex olfactif)</td><td>Pallium ventral</td></tr>
<tr><td rowspan="3">Homogénétique</td><td rowspan="3">Isocortex</td><td rowspan="3">Néocortex</td><td rowspan="2">Cortex intermedius</td><td rowspan="2">Mésopallium</td><td>Périallocortex (agranulaire)</td><td>Mésocortex (Périallocortex)</td><td>Pallium latéral</td><td>Cortex limbique agranulaire</td></tr>
<tr><td>Proisocortex (dysgranulaire)</td><td>Mésocortex (Proisocortex)</td><td>Pallium médian</td><td>Cortex limbique dysgranulaire</td></tr>
<tr><td>Cortex completus</td><td>Ectopallium</td><td>Isocortex</td><td>Isocortex sensu stricto</td><td>Pallium dorsal</td><td>Euliminate</td></tr>
</table>

Figure 10. Nomenclature des types corticaux selon différents auteurs (García-Cabezas *et al*, 2019).

2. Striatum et pallidum dorsal

Les données développementales, neurochimiques et anatomiques montrent que chez tous les vertébrés à mâchoires et même chez les agnathes, les "noyaux de la base" contiennent une division striatale et une division pallidale (Moreno *et al*, 2009; Ocaña *et al*, 2015; Grillner & Robertson, 2016). Chez les mammifères, le striatum et le pallidum proviennent respectivement de l'EGL qui exprime abondamment le facteur de transcription *Pax6* et de l'EGM (Holmgren, 1925) qui exprime *Nkx2.1*, un facteur de transcription également abondant dans l'hypothalamus. Cependant, il existe plusieurs subdivisions de progéniteurs au sein de l'EGL et de l'EGM, chacune donnant lieu à des sous-populations de neurones différentes (Stenman *et al*, 2003; Flames *et al*, 2007; Bupesh *et al*, 2011a, 2011b). De plus, il a été observé une migration tangentielle de neurones de l'EGM et de l'EGL, respectivement vers le striatum et le pallidum en développement, contribuant aussi à la diversité neuronale trouvée dans les "noyaux de la base" (Marin *et al*, 2000, 2001; Marin & Rubenstein, 2001; Zhao *et al*, 2003; Cocas *et al*, 2009; Bupesh *et al*, 2011a, 2011b, 2014). Les premières cellules à être

décrites sont celles de l'EGM et de la zone entopédonculaire, d'où il a été démontré qu'elles produisaient la plupart des interneurones striataux (Marin *et al*, 2000).

Des études ont aussi montré que la majorité des interneurones cholinergiques du caudoputamen (CP) sont originaires de la région préoptique et dépendent de l'expression de *Lhx7/8* et de *Islet1* (Elshatory & Gan, 2008; García-López *et al*, 2008). La plupart des interneurones dopaminergiques du striatum migrent de manière tangentielle à partir de la région préoptique (Bupesh *et al*, 2014). Contrairement à la plupart des interneurones, les neurones de projection du CP (contenant la substance P ou enképhaline) et également appelés neurones épineux (*medium "spiny" neurons*), représentant 90 à 95% de tous les neurones striataux (Kemp & Powell, 1971; Medina & Reiner, 1995), sont originaires de l'EGL et migrent de manière radiale dans le manteau (Marin & Rubenstein, 2001). Ces découvertes, associées aux résultats sur le développement du cortex cérébral, suggèrent que dans le télencéphale, les neurones principaux arrivent par migration radiale à partir de leur zone progénitrice (située topologiquement plus profondément), tandis que la migration tangentielle est réservée aux interneurones (Marin & Rubenstein, 2001). Cependant, ces observations ne peuvent pas être considérées comme une règle générale (Nóbrega-Pereira *et al*, 2010; Bupesh *et al*, 2011a).

En ce qui concerne le pallidum dorsal, le globus pallidus (GP) des rongeurs contient deux sous-populations majeures de neurones à projections GABAergiques issues de l'EGL et de l'EGM (Medina *et al*, 2014). Les neurones du GP contenant la parvalbumine et la neurotensine (NT) liée à un hexapeptide (LANT6), et qui envoient des projections descendantes au STN et à la substance noire (SN), proviennent de progéniteurs exprimant *Nkx2.1* (et *Lhx6*), principalement localisés dans l'EGM. Quant aux neurones contenant la pré-proenképhaline qui ont des projections ascendantes sur le striatum, ils proviennent de progéniteurs exprimant *lslet1* dans l'EGL (Sussel *et al*, 1999; Flandin *et al*, 2010; Nóbrega-Pereira *et al*, 2010; Bupesh *et al*, 2011a) (Figure 11).

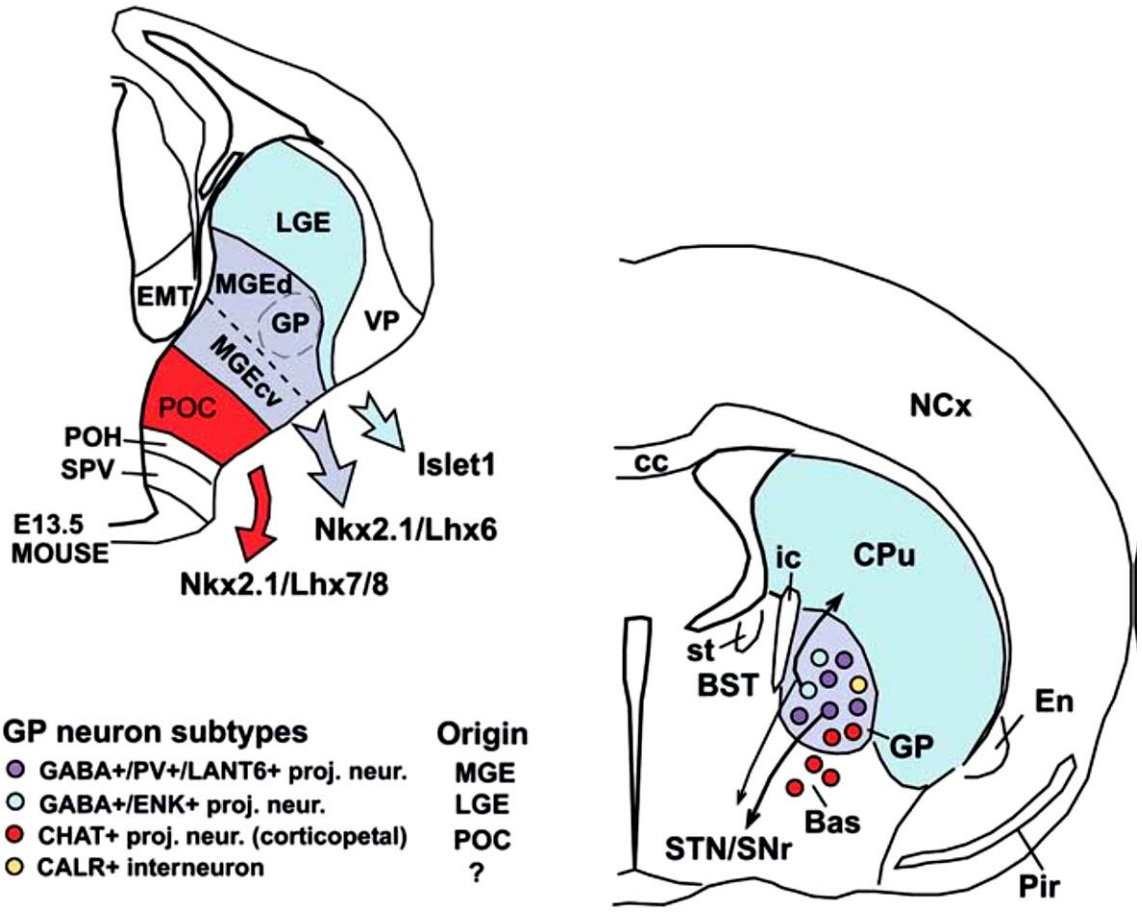

Figure 11. Schémas de coupes frontales du télencéphale embryonnaire et postnatal de souris représentant les sous-types de neurones du GP chez les rongeurs et indiquant leur origine embryonnaire (Medina *et al*, 2014).

Le manteau pallidal contient aussi des neurones exprimant *Lhx7/8*, mais ceux-ci représentent des neurones cholinergiques appartenant au système corticopetal qui proviennent principalement du domaine préoptique commissural (POC).

Bas : noyau de Meynert ; BST : noyau du lit de la strie terminale ; CALR : calrétinine ; cc : corps calleux ; CHAT : choline acétyltransférase ; CPu: caudoputamen ; E13,5: 13,5ème jour embryonnaire ; EMT: éminence thalamique ou préthalamique ; En : noyau endopiriforme ; ENK : enképhaline ; GP : globus pallidus ; ic : capsule interne ; LGE : EGL ; MGEcv/d : partie caudoventrale/dorsale de l'EGM ; NCx : néocortex ; Pir : cortex piriforme ; POH : sous-division préopto-hypothalamique ; SNr : substance noire réticulée ; SPV : domaine supraopto-paraventriculaire de l'hypothalamus alar ; st : strie terminale ; STN : noyau sousthalamique ; VP : pallium ventral.

Comme rappelé par Gerfen et Wilson, les "noyaux de la base" sont un excellent modèle permettant l'étude de l'organisation fonctionnelle d'autres systèmes cérébraux (Gerfen & Wilson, 1996). Ces "noyaux de la base", composés d'un certain nombre de noyaux sous-corticaux, mettent en jeu des circuits en boucles directs et indirects topographiquement organisés depuis le cortex (Webster, 1961; Künzle, 1975; McGeorge & Faull, 1989; Gerfen & Wilson, 1996), susceptibles de fournir un "circuit modèle" pour les autres systèmes (Alexander *et al*, 1986). D'après L.W. Swanson, l'étude du système moteur (Figure 3) et, par conséquent, de l'organisation anatomique et fonctionnelle des "noyaux de la base" permet d'étendre, par comparaison, ce schéma d'organisation au télencéphale dans son entier (Swanson, 2012).

Les cibles des afférences corticales sont les neurones épineux GABAergiques. Ces neurones sont à l'origine des deux principaux composants du circuit des "noyaux de la base" : les projections striatales "directes" et "indirectes" (Figure 12) (Gerfen & Bolam, 2016).

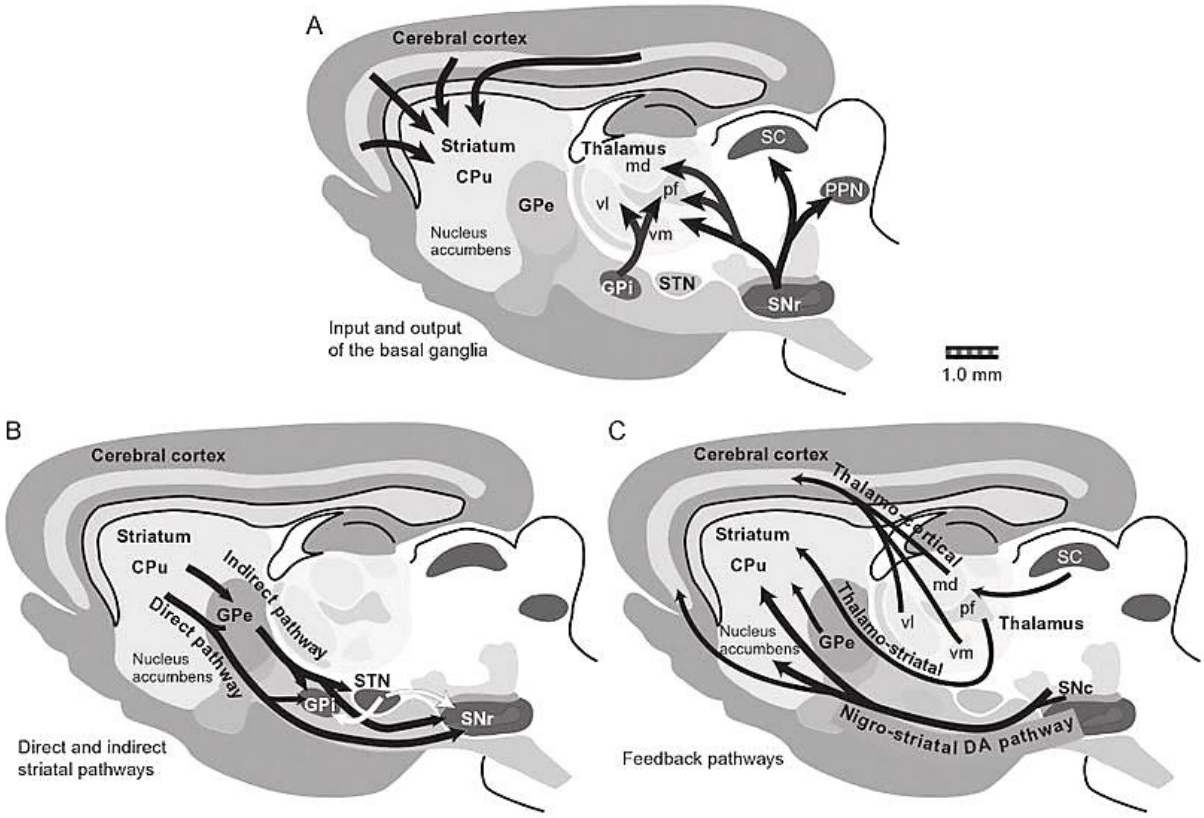

Figure 12. Schémas des connexions des "noyaux de la base" avec le cortex dans l'encéphale de rat en vues sagittales (Gerfen & Bolam, 2016).

(A) Principales afférences et efférences des "noyaux de la base". Les neurones pyramidaux de la couche corticale 5 fournissent la majorité des afférences au striatum (CPu, noyau accumbens). Les efférences des "noyaux de la base" dans les noyaux thalamiques, le SC et le PPN proviennent des neurones GABA du GPi et de la SNr.

(B) Projections striatales formant les voies directes et indirectes depuis des *mediums "spiny" neurons*.

(C) Voies de retour des informations des "noyaux de la base" impliquant les projections nigrostriées dopaminergiques, thalamo-striatales et thalamo-corticales.

CPu : caudoputamen ; DA : dopamine ; GPe/i : segments externe/interne du globus pallidus ; md : noyau thalamique médiodorsal ; pf : complexe thalamique intralaminaire parafasciculaire ; PPN : noyau pédonculopontine ; SC : colliculus supérieur ; STN : noyau sousthalamique ; vl/vm : noyaux thalamiques ventrolatéral/ventromédian.

La voie directe met en jeu le CP qui projette dans le segment interne du GP (GPi) projetant ensuite dans la partie réticulée de la SN (SNr), tandis que les projections du CP de la voie indirecte innervent le segment externe du GP (GPe) qui projette dans le STN (Gerfen & Wilson, 1996; Tecuapetla *et al*, 2016). Ce dernier envoie ensuite des projections dans la SNr et dans le GPi. Il existe également une voie hyperdirecte dans laquelle le STN reçoit des projections topographiquement organisées depuis l'isocortex et impliquées dans des réponses motivationnelles (Albin *et al*, 1989; Nambu *et al*, 2002; Gerfen & Bolam, 2016; Chu *et al*, 2017). Les neurones GABAergiques du GPe projettent dans le striatum, le GPi, la SNr et dans le STN, qui lui-même fournit des projections excitatrices aux neurones du GPi et de la SNr. En fait, les efférences GABA des "noyaux de la base"

entrainent une inhibition de leur cibles qui peuvent être désinhibées par les afférences striatales du circuit indirect (Chevalier *et al*, 1985; Deniau & Chevalier, 1985) qui inhibent les projections pallidales inhibitrices. En complément de ces circuits hyperdirect, direct et indirect, il existe des boucles de retour formées par les systèmes nigrostrié (depuis les neurones dopaminergiques de la partie compacte de la SN (SNc) dans le striatum), thalamo-striatal et thalamo-cortical, ainsi que des projections depuis le GP et le STN au striatum (Gerfen & Wilson, 1996). Les interneurones cholinergiques du striatum peuvent également interagir avec les terminaisons dopaminergiques de la SN (Bolam *et al*, 1984, 1986).

3. Striatum et pallidum ventral

En 1975, L. Heimer et R.D. Wilson ont suggéré, avec une brillante perspicacité, qu'il existait un striatum ventral et un pallidum ventral qui complètent le "classique" striatum dorsal (caudé et putamen) et pallidum dorsal (GP) (Heimer & Wilson, 1975). Le striatum ventral est composé du noyau accumbens (ACB) et du tubercule olfactif. Le fundus striatum (FS) qui est une structure ventralement adjacente au CP est aussi associé au striatum ventral. Toutes ces structures qui appartiennent au striatum ventral projettent sur des secteurs antérieurs mais distincts d'une région dont les contours sont mal définis et nommée substance innominée (SI). Ces territoires qui sont la cible du striatum ventral ont été renommés "pallidum ventral" dans l'optique de leur comparaison au GP devenu alors le pallidum dorsal. Bien qu'en accord sur le concept de pallidum ventral, L.W. Swanson conserve aux régions correspondantes le nom de substance innominée.

Les bases de la comparaison entre ce réseau avec celui du striatum dorsal sont solides et très largement acceptées. Elles sont fondées sur des données de divers ordres dont :

1- Le type cellulaire principal du striatum ventral : comme dans le striatum dorsal, le neurone épineux est le type cellulaire dominant dans l'ACB et le tubercule olfactif.

2- Ces cellules projettent dans le pallidum ventral et reçoivent des afférences glutamatergiques des régions corticales et dopaminergiques de l'aire tegmentale ventrale (VTA) et de la SN (Millhouse, 1987; Walaas & Ouimet, 1989; Zahm & Heimer, 1990). Les projections descendantes de l'ACB et du CP adjacent sont topographiquement organisées le long d'axes médio-latéral et dorso-ventral (Mogenson *et al*, 1983). L'ACB (striatum ventral) projette dans la SI (pallidum ventral) tout comme le CP (striatum dorsal) projette dans le GP (pallidum dorsal) projetant ensuite dans la VTA et la SN. Les projections de l'ACB, connecté à la VTA, sont donc comparables à celles de la voie directe décrite pour le striatum dorsal puisque la VTA et la SN forment un complexe mésencéphalique (Yamamoto & Vernier, 2011; Yetnikoff *et al*, 2014). En revanche, une voie indirecte issue du striatum ventral n'a jamais été définie de façon très claire (Fujiyama *et al*, 2015), même si des projections du pallidum

ventral sont observées dans la partie dorso-médiane du STN et dans le noyau pédonculopontique (Mogenson *et al*, 1985).

3- Enfin, les données du développement sont cohérentes avec la théorie d'un striatum ventral et pallidum ventral. Les cellules épineuses du tubercule olfactif et de la majorité de l'ACB ont la même origine et la même signature moléculaire que celles du striatum dorsal (Stenman *et al*, 2003). Enfin le pallidum ventral est issu de l'EGM d'où sont issus de nombreux neurones du pallidum dorsal.

Cependant, s'il y a des similitudes évidentes entre les réseaux des corps striés dorsal et ventral, il y a aussi des différences notables. Les plus évidentes d'entre elles concernent le *"shell"* de l'ACB. Le terme de noyau accumbens septal, parce qu'adjacent au septum, persiste encore dans la littérature (*accumbens septi*) et est une résurgence d'un passé lointain où ce noyau était comparé au septum adjacent. Il faut dire que les afférences intenses du subiculum ventral dans cette région rappellent celles de l'hippocampe dans les noyaux du septum. Ainsi, le *"shell"* de l'ACB est connecté à l'allocortex, alors que le striatum dorsal est associé à l'isocortex. Le *"shell"* de l'ACB est aussi connecté à l'hypothalamus, notamment à l'hypothalamus latéral. Par extension, ces projections ont longtemps été interprétées comme des connexions avec le système nerveux autonome, alors que les réseaux striato-pallidaux sont plutôt considérés comme jouant un rôle dans des processus cognitifs et en lien avec la motricité volontaire. Le *"shell"* de l'ACB est encore directement et indirectement connecté à plusieurs noyaux profonds de l'amygdale, ce qui avait incité L. Heimer, J.S. de Olmos et d'autres à intégrer cette région à l'amygdale étendue (de Olmos & Heimer, 1999; de Olmos *et al*, 2004; Elias *et al*, 2008b). Ce concept sera très rapidement évoqué dans le chapitre suivant. Malgré tout, son innervation dopaminergique abondante, issue de la VTA, souligne son appartenance au bloc formé avec le striatum dorsal et, d'une manière générale, son appartenance au striatum ventral est assez peu discutée.

4. Striatum et pallidum caudal

Dans l'Allen Brain Atlas (Allen Institute, 2004), le striatum caudal est appelé *"striatum like amygdalar nuclei"* car il correspond à certains noyaux profonds de l'amygdale. Le pallidum caudal est composé du BST. Ce concept est très controversé et il est dominé dans la littérature courante par celui de l'amygdale étendue. Il n'entre pas dans nos objectifs de comparer ici ces deux théories. Dans un article publié en 2003, G.F. Alheid admettait cependant qu'il existe des points de convergence entre les deux concepts (Alheid, 2003), notamment en ce qui concerne l'organisation des réseaux et leur ressemblance avec celui du striatum (Figure 13) et également avec celui du septum qui sera évoqué très brièvement plus bas.

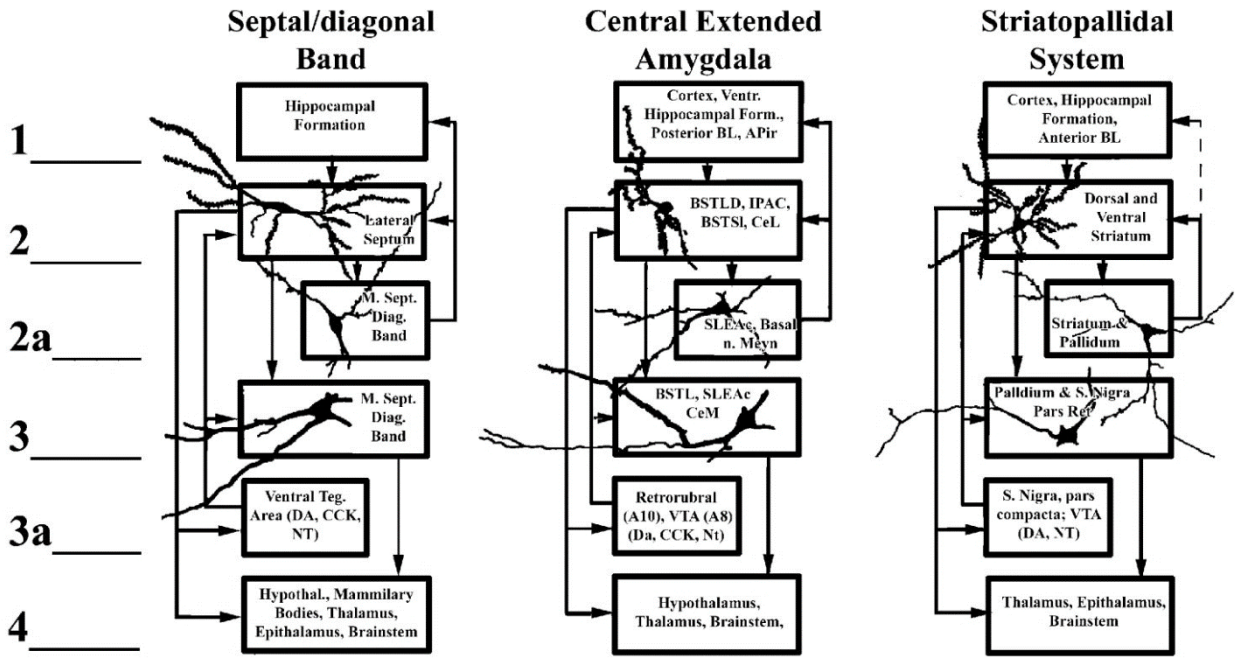

Figure 13. Schéma du plan d'organisation du télencéphale selon G.F. Alheid (2003).

Les circuits des trois principaux systèmes sont représentés : système septohippocampal et bandelette diagonale, amygdale étendue centrale, système cortico-striato-pallidal. Le niveau 1 représente les neurones corticaux glutaminergiques et les neurones amygdaliens projetant sur des *medium "spiny"* neurones GABAergiques (niveau 2). Ces derniers projettent sur les neurones du noyau de la bandelette diagonale dans l'amygdale étendue centrale (niveau 3) et dans l'aire tegmentale ventrale (VTA). Les neurones du niveau 2 projettent également dans l'hypothalamus, le thalamus et le tronc cérébral (niveau 4).

BSTLD : division latérale du noyau du lit de la strie terminale, partie dorsolatérale ; CeL, M : partie latérale et médiane du CEA ; CCK : cholécystokinine ; Da ou DA : dopamine ; IPAC : noyau interstitiel de la région postérieure de la commissure antérieure ; Nt ou NT : neurotensine ; SLEAc : division centrale de la partie sous-lenticulaire de l'amygdale étendue.

Ainsi, l'amygdale est une région très hétérogène. Elle est composée de cortex olfactif (noyau du tractus olfactif latéral, noyau cortical, post-piriforme et piriforme amygdalien) et de noyaux latéraux, basaux et postérieurs qui semblent correspondre à l'extension ventromédiane du claustrum. Ces deux régions de l'amygdale sont d'origine palliale et contiennent des neurones GABAergiques dispersés (Hirata *et al*, 2009). La partie ventromédiane (noyaux central et médian, et zone antérieure) a une organisation striatale que confirme l'étude de la distribution de l'acide glutamique décarboxylase (GAD). Cette enzyme, qui convertit le glutamate en GABA, révèle une bande très dense de neurones marqués qui s'étend ventralement à travers le CP et les noyaux central (CEA) et médian (MEA) de l'amygdale (Swanson & Petrovich, 1998) (Figure 14).

Figure 14. Photographie d'une coupe sagittale de télencéphale de rat montrant la distribution des neurones exprimant l'acide glutamique décarboxylase (*GAD65*) après hybridation *in situ* (Swanson & Petrovich, 1998).

BLA : noyau amygdalien basolatéral ; cc : corps calleux ; CEA : noyau central de l'amygdale ; CLA : claustrum ; COAa : partie rostrale du noyau amygdalien cortical ; CP : caudoputamen ; ec : capsule externe ; EP : noyau endopiriforme ; GPl/m : segments latéral/médian du globus pallidus ; HIP : hippocampe ; INS : région insulaire ; LA : noyau amygdalien latéral ; MEA : noyau médian de l'amygdale ; MO : aires motrices ; PERI : aire périrhinale ; PIR : aire piriforme ; RSP : aire rétrospléniale ; SI : substance innominée ; SS : aires somatosensorielles ; V3 : 3ème ventricule ; VL : ventricule latéral.

D'un point de vue développemental, les neurones du CEA et du BST dérivent de l'EGL (partie dorsale et ventrale) et de l'EGM (Figure 15). Comme dans le striatum, les neurones du CEA sont GABAergiques et contiennent un ou plusieurs neuropeptides.

La partie dorsale de l'EGL (EGLd) produit des neurones qui expriment *Pax6* et qui envahissent préférentiellement les parties capsulaire (excepté la partie ventromédiane du CEAc) et latérale (région latérale du CEAl) du CEA ainsi que la partie latérale du BST. La partie ventrale de l'EGL (EGLv) génère des cellules qui expriment *Islet1* et qui vont former la partie médiane (CEAm) et la zone centromédiane du CEAl ainsi que la partie latérale du BST. Le BST latéral, en plus des neurones exprimant *Nkx2.1* dérivés de l'EGM, est formé de cellules exprimant *Pax6* et *Islet1*. Quant aux parties médianes de l'amygdale et du BST, caractérisées par l'expression de *Lhx6*, elles partagent une origine embryologique commune dans la partie ventrocaudale de l'EGM et correspondraient donc davantage à du pallidum. Cela confirme les affirmations précédentes concernant le BST, suggérant qu'il représente la partie pallidale de l'amygdale étendue (Swanson, 2000). Ainsi, les neurones proviennent de différents domaines embryonnaires, mais les mêmes domaines contribuent aussi à la formation des neurones de plusieurs subdivisions de "l'amygdale étendue".

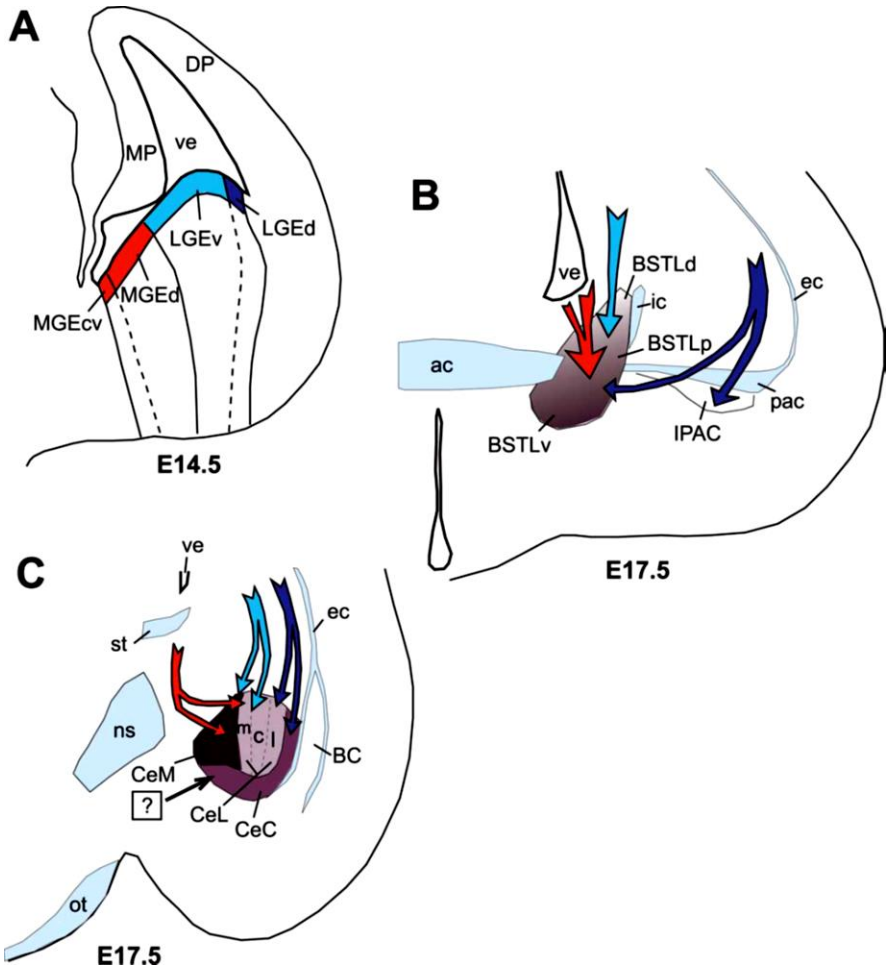

Figure 15. Schémas de coupes frontales du télencéphale embryonnaire, aux stades précoce et prénatal, montrant les principales sous-divisions des EGL et EGM aboutissant à la formation des différentes parties du CEA et du BST (Bupesh *et al*, 2011a).

Le point d'interrogation en C montre la partie ventromédiane du CEAc (riche en cellules exprimant la tyrosine hydroxylase mais qui ne contient que peu de cellules exprimant *Pax6*, *ppENK*, *Islet1* ou *SS*).

ac : commissure antérieure ; BC : complexe amygdalien basal ; BSTLd/p/v : division latérale du noyau du lit de la strie terminale, partie dorsale/postérieure/ventrale ; CeC, CeL (c, l, m), CeM : partie capsulaire, latérale (centrale, latérale et médiane) et médiane du CEA ; DP : pallium dorsal ; ec : capsule externe ; ic : capsule interne ; IPAC : noyau interstitiel de la région postérieure de la commissure antérieure ; LGEd/v : EGL, partie dorsale/ventrale ; MGEcv/d : EGM, partie ventrocaudale/dorsale ; MP : pallium médian ; ot : tractus optique ; pac : région postérieure de la commissure antérieure ; ns : nigro-striatum ; st : strie terminale ; ve : ventricule.

Pour conclure, il ne fait quasi plus aucun doute que les régions latérales du CEA ont une origine striatale. Il est également admis par tous que les réseaux qui impliquent ces structures présentent des ressemblances aussi compatibles avec cette notion de striatum caudal. Il est en revanche probablement caricatural de voir le CEA uniquement comme du striatum et le BST uniquement comme du pallidum ; les deux structures pouvant chacune renfermer des composantes striatales et pallidales. Par ailleurs, la place de certaines régions de la SI dont l'existence n'a pas été évoquée ici, mais qui font partie intégrale de l'"amygdale étendue", seront mentionnées plus loin dans ce travail. Enfin et pour terminer, toute région du striatum est innervée par du pallium. L'organisation de ces projections sur le striatum caudal n'a pas été systématiquement investiguée et l'identification de voies directes, indirectes et hyperdirectes n'est pas encore claire. Cependant, le CEA projette sur la SN permettant une

comparaison avec la voie nigro-striée (Gonzales & Chesselet, 1990; Wallace *et al*, 1992; Petrovich & Swanson, 1997; Lee *et al*, 2005, 2010; Shirasu *et al*, 2011).

5. Striatum et pallidum médian

Aux alentours du XX^{ème} siècle, Cajal a identifié plusieurs noyaux composant le septum (Cajal, 1909). Ce septum comprend les complexes du septum latéral et médian, connectés à l'hippocampe (Daitz & Powell, 1954; Swanson & Cowan, 1979) et le septum ventral – BST, connecté à l'amygdale et au subiculum ventral et déjà décrits car associés à l'amygdale étendue ou division caudale du pallidum. La région hippocampale et en particulier le septum médian est riche en neurones cholinergiques mais qui se distribuent aussi dans la SI et le GP (Risold, 2004; Engelhardt, 2013). Cependant, les connexions topographiquement organisées entre l'hippocampe et l'amygdale, avec respectivement le noyau latéral du septum et le BST, mais aussi entre ces structures et le tronc cérébral (hypothalamus et mésencéphale), suggèrent des circuits spécifiques mais d'organisation similaire impliqués dans l'expression de comportements en lien avec la reproduction ou le comportement de défense (Risold *et al*, 1997; Swanson & Risold, 2000). La nature sous-corticale de la région septale et sa richesse en neurones GABAergiques sont des indices soulignant sa ressemblance avec les noyaux cérébraux susmentionnés (Köhler & Chan-Palay, 1983; Panula *et al*, 1984; Onteniente *et al*, 1986; Feldblum *et al*, 1993; Risold & Swanson, 1997a).

Plus spécifiquement, la formation hippocampale, la région septale et l'hypothalamus forment des circuits parallèles complexes qui peuvent constituer des boucles largement interconnectées (Swanson, 2000) (Figure 16). Dans le réseau neuronal moteur qui contrôle les comportements motivés, le complexe septal latéral est décrit par P.Y. Risold et L.W. Swanson comme un composé médian du striatum pour le cortex hippocampal dont la corne d'Ammon (Risold & Swanson, 1996, 1997b; Risold, 2004). Il reçoit des afférences glutamatergiques abondantes depuis cette région corticale qui innerve des neurones épineux GABAergiques. A leur tour, les neurones épineux du noyau latéral du septum innervent topographiquement le noyau septal médian associé au pallidum médian.

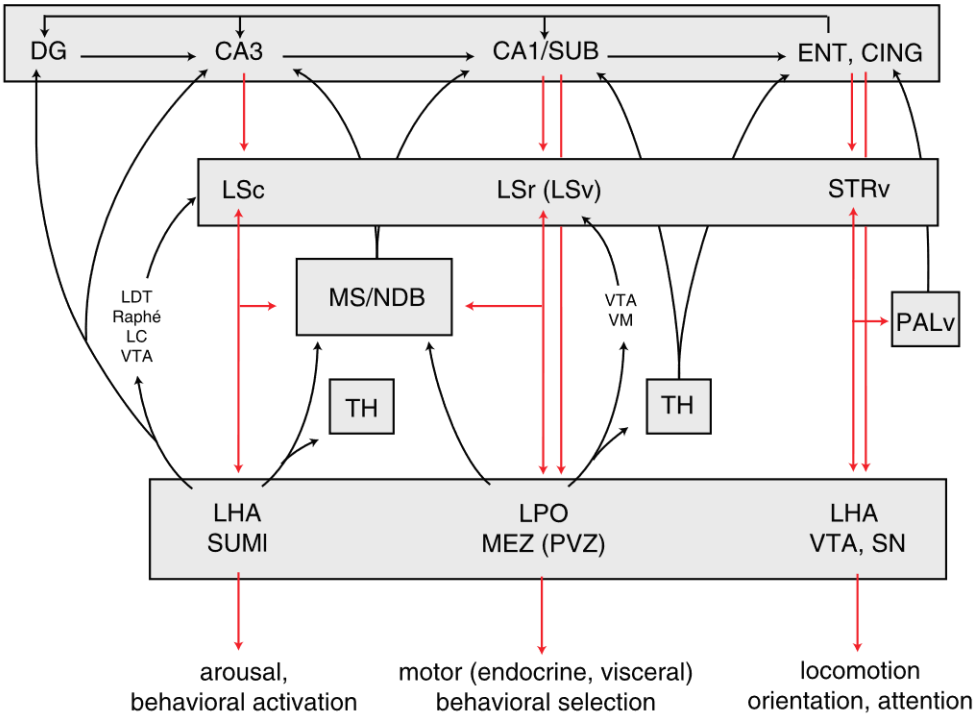

Figure 16. Modèle de circuiterie impliquant la formation hippocampale, le septum latéral et l'hypothalamus (Risold & Swanson, 1997b).

Schéma illustrant l'organisation des réseaux impliquant l'hippocampe et les aires périallocorticales associées, les noyaux latéral et médian du septum, le striatum et pallidum ventral ainsi que l'hypothalamus. Ce réseau intervient dans l'élaboration de réponses comportementales complexes. D'après ces auteurs, ce réseau présente dans son organisation de nombreuses similitudes avec celui classique des "noyaux de la base".

CA1-3 : cornes d'Ammon, champs 1 à 3 ; CING : cortex cingulaire ; DG : gyrus denté ; ENT : cortex entorhinal ; LC : locus ceruleus ; LDT : noyau tegmental latérodorsal ; LHA : aire hypothalamique latérale ; LPO : aire préoptique latérale ; LSc/r/v : noyau latéral du septum, parties caudale/rostrale/ventrale ; MEZ : zone hypothalamique médiane ; MS : noyau septal médian ; NDB : noyau de la bandelette diagonale ; Palv : pallidum ventral ; PVz : zone hypothalamique périventriculaire ; SN : substance noire ; Strv : striatum ventral ; SUB : subiculum ; SUMl : partie latérale du noyau supramamillaire ; TH : thalamus ; VM : médulla ventrale ; VTA : aire tegmentale ventrale.

D'un point de vue développemental, les cellules du septum latéral et médian se développent à partir de la crête septale qui forme la paroi rostro-ventro-médiane des vésicules télencéphaliques (Bayer, 1979a, 1979b; Alvarez-Bolado *et al*, 1995; Swanson & Risold, 2000). Le développement des tractus de fibres qui caractérisent la région septale comme la strie terminale et la strie médullaire apparaissent assez tôt sur les atlas de cerveau de rat en développement (Alvarez-Bolado & Swanson, 1996). Le septum exprime un marqueur moléculaire spécifique nommé *Steel* qui encode un ligand pour le récepteur à activité tyrosine kinase c-Kit (Bulchand *et al*, 2001). Ce marqueur est fortement exprimé dans le septum embryonnaire et faiblement dans les éminences ganglionnaires.

Ainsi, l'assimilation des noyaux latéral et médian du septum à une composante médiane des "noyaux de la base" est basée sur l'analyse de l'organisation structurelle du réseau qui les concerne, bien que l'origine développementale soit différente.

6. Conclusions

La division du télencéphale en pallium et sous-pallium et l'assimilation de ce dernier au striatum et pallidum permet de concevoir l'organisation du télencéphale selon un "plan de base" relativement simple dans son principe (Tableau 1). L'isocortex, le striatum et le pallidum dorsal forment avec le STN et la SN, le circuit composant le système extrapyramidal appelé des "noyaux de la base". L'allocortex par le striatum et le pallidum caudal et médian est connecté à l'hypothalamus. Il reste maintenant à comprendre l'organisation de l'hypothalamus.

	Dorsal	***Ventral***	***Médian***	***Caudal***
STRIATUM	CP	ACB FS OT	LSC	MEA CEA AAA IA
PALLIDUM	GPe GPi	SI MA	MS/DBB	BST

Tableau 1. Organisation topographique des "noyaux de la base", d'après L.W. Swanson (2000).

AAA : aire amygdalienne antérieure ; ACB : noyau accumbens ; BST : noyau du lit de la strie terminale ; CEA : noyau amygdalien central ; CP : caudoputamen ; FS : fundus striatum ; GPe/i : segments externe/interne du globus pallidus ; IA : noyaux amygdaliens intercalés ; LSC : complexe du septum latéral ; MA : noyau (préoptique) magnocellulaire ; MEA : noyau amygdalien médian ; MS/DBB : septum médian/noyau du complexe de la bandelette diagonale ; OT : tubercule olfactif ; SI : substance innominée.

III. L'hypothalamus

Une des principales difficultés à retracer avec précision le cheminement historique des idées se rapportant à l'organisation de l'hypothalamus est due, en grande partie, à la multiplicité des noms utilisés par les différents investigateurs pour définir les mêmes structures (Morgane & Panksepp, 1979). Les premières avancées majeures concernant l'étude de la région entourant le troisième ventricule ont été portées par G.T. Ziehen et par S.R. Cajal dans lesquelles ils ont identifiés clairement plusieurs formations nucléaires appartenant entre autres à l'hypothalamus ((Ziehen, 1901; Cajal, 1909) cités dans (Morgane & Panksepp, 1979)).

Avant les années 1900, des observations cliniques associées à des pathologies fournissaient de vagues indices quant aux fonctions des aires entourant le troisième ventricule. C'est par coopération entre neuropathologistes et cliniciens qu'émergèrent les premières tentatives de compréhension du fonctionnement de l'hypothalamus. Par exemple, en 1840, H. Mohr fut le premier à décrire des symptômes d'obésité causés par une tumeur hypophysaire comprimant la base du cerveau. De la même manière, C. Rokitansky (1842) avait associé certaines infections de la base du troisième ventricule à des déséquilibres du tractus gastrointestinal. Plus tard, en 1890, le pathologiste L. Mauthner relia également les phénomènes de somnolence à cette région hypothalamique (cités dans (Morgane &

Panksepp, 1979)). S'en suivi une période de 30 ans de confusion, notamment entre des symptômes attribuables à des désordres du diencéphale ventral et d'autres à l'hypophyse. Puis, en 1910, J.P. Karplus et A. Kreidl (cités dans (Morgane & Panksepp, 1979)) démontrèrent par stimulation électrique l'implication de la région hypothalamique dans le contrôle du système nerveux autonome (fréquence cardiaque, salivation, transpiration, miction…). D'autres scientifiques tentèrent alors, à l'aide de techniques de stimulations combinées à des lésions, de fractionner l'hypothalamus en aires ayant chacune un rôle physiologique.

En 1940, J.F. Fulton rappela que l'hypothalamus fait partie d'un réseau fonctionnel dans le cerveau. Il insiste sur le fait que cette aire influence, certes, le tronc cérébral mais est elle-même sous l'influence de structures plus antérieures comme le cortex cérébral (Fulton *et al*, 1940). Curieusement, malgré cette mise au point, pendant les 40 années qui ont suivi, les chercheurs se sont concentrés sur l'hypothalamus lui-même, prenant très peu en considération ses relations avec les autres structures. Ainsi, la plupart des études comportementales des années 1950 à 1970 ont placé l'hypothalamus comme "chef suprême" de lui-même et comme une sorte de "centre des centres". On y démontra par exemple le "centre de la douleur" dans la région hypothalamique médiane ou encore dans le contrôle du comportement de faim à la suite de travaux d'A.E. Hetherington et S. Ranson dès 1939, puis de ceux de B.K. Anand et J.R. Brobeck, en 1951 (Hetherington & Ranson, 1939; Anand & Brobeck, 1951). Les premiers démontraient que la destruction du noyau ventromédian chez le rat produisait une hyperphagie et une obésité, tandis que les seconds découvraient qu'une lésion importante du LHA entraînait à l'inverse une aphagie (et une adipsie). Ces résultats amenèrent E. Stellar, en 1954 (cité dans (Morgane & Panksepp, 1979)), à proposer une "théorie hypothalamique" de l'appétit et de la faim qui n'a été remise en question que depuis peu d'années. Plusieurs psychophysiologistes mirent aussi en évidence son rôle dans le comportement de soif (Fitzsimons, 1979; Swanson & Mogenson, 1981; Rolls & Rolls, 1982), ou encore dans le cycle veille-sommeil (Hendrickson *et al*, 1972; Moore & Lenn, 1972; Vertes, 1984), la thermorégulation (Boulant & Bignall, 1973; Schulze *et al*, 1981), les comportements d'agressivité (Fernandez De Molina & Hunsperger, 1962), de reproduction et d'affection (Szechtman *et al*, 1978; Morgane & Panksepp, 1979). En 1979, P.J. Morgane et J. Panksepp, rappellent encore les relations de l'hypothalamus avec les autres structures et comme un membre d'un circuit complexe plutôt qu'une entité à lui seul. Aujourd'hui, sur le plan fonctionnel, l'hypothalamus est considéré comme un centre intégrateur conservé qui coordonne les réponses autonomes, endocriniennes mais aussi émotionnelles et cognitives (Swanson, 2000; Watts, 2011).

Pour mieux appréhender le fonctionnement de l'hypothalamus, il est nécessaire de comprendre son organisation anatomique. Tout d'abord, chez tous les vertébrés, l'hypothalamus est divisé en deux grandes régions : une région antérieure/préoptique (au-dessus et en avant du chiasma optique) et une région postérieure (postoptique). Certes, l'hypothalamus semble bien conservé mais les données modernes interrogent sur cette organisation et une question se pose : est-il vraiment plus "conservé"

que le système moteur impliquant pallium, striatum, pallidum et tegmentum ventral (Ocaña *et al*, 2015) ? Ensuite, l'hypothalamus est une région traversée par des systèmes de fibres diffuses parmi les plus complexes du cerveau (Simerly, 2004) et dont les groupes cellulaires ne définissent pas toujours clairement des noyaux ; notamment avec l'apparition de régions latérales riches en cellules parmi les fibres reliant le tronc cérébral au télencéphale. Même si sa compréhension s'est améliorée via l'identification de gènes impliqués dans son développement (sonic hedgehog (*Shh)*, *BMP*, *Wnt* par exemple) et la fonction de certaines de ses cellules (Swanson, 1999; Puelles & Rubenstein, 2003; Griffond & Risold, 2009), il n'en reste pas moins que le débat autour de sa structure et de son organisation est toujours ouvert.

Les travaux fondamentaux du début du XX^{ème} siècle avaient permis à W.E. Le Gros Clark, E.C. Crosby et R.T. Woodburne de définir l'hypothalamus comme étant divisé en quatre aires antéropostérieures et trois zones longitudinales (Figure 17).

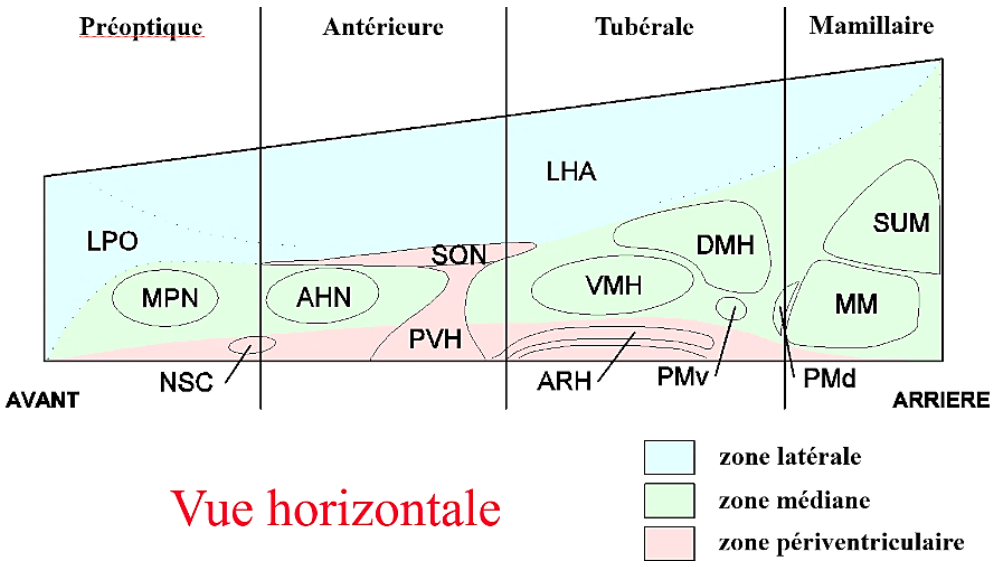

Figure 17. Représentation schématique des quatre aires antéropostérieures et trois zones longitudinales de l'hypothalamus, adapté de Risold et Swanson (1996).

AHN : noyau hypothalamique antérieur ; ARH : noyau arqué ; DMH : noyau dorsomédian ; LHA : aire hypothalamique latérale ; PMd/v : noyau prémamillaire dorsal/ventral ; LPO : aire préoptique latérale ; PVH : noyau paraventriculaire ; MM : noyau mamillaire médian ; MPN : noyau préoptique médian ; NSC : noyau suprachiasmatique ; SON : noyau supraoptique ; SUM : noyau supramamillaire ; VMH : noyau ventromédian.

Ce schéma d'organisation a été relativement bien accepté, même si des discussions persistaient quant à l'existence d'une région antérieure (souvent confondue avec la région préoptique - on parlait alors de région préoptico-antérieure), voire même si cette région préoptique appartenait à l'hypothalamus ou au télencéphale (Moreno & González, 2011; Puelles *et al*, 2012). Les années 1970-1980 voient la généralisation de l'utilisation des techniques immunohistochimiques et le développement de nouvelles techniques de traçage plus performantes chez l'animal (peroxydase de raifort dite HRP, de l'anglais *"horseradish peroxidase"*, et HRP conjuguée à un transport antérograde

d'agglutinine de germe de blé avec immunocytochimie à l'or nommée WGA-HRP). Les progrès dans l'étude des petits noyaux qui composent l'hypothalamus sont alors rapides et permettent la caractérisation des aires, zones et noyaux de l'hypothalamus. Il a notamment été décrit la zone périventriculaire de l'hypothalamus formée de noyaux bien différenciés et contenant la majorité des motoneurones neuroendocriniens ; zone qui se révèle très riche en neuropeptides. Pour exemple, c'est dans les années 1983 que L.W. Swanson et P.E. Sawchenko ont décrit les connexions de deux noyaux majeurs de cette zone que sont les noyaux paraventriculaire et noyau supraoptique (Swanson & Sawchenko, 1983) qui avaient déjà retenu l'attention dans le passé car ils contiennent les neurones magnocellulaires neurosécréteurs d'ocytocine et de vasopressine (Scharrer & Scharrer, 1940; Bargmann, 1949). Cependant, les méthodes de transport axonal (thymidine tritiée et HRP) antérogrades et rétrogrades, couplées parfois à des marquages immunohistochimiques, ont permis de définir de multiples afférences et efférences de ces différents noyaux des zones périventriculaire et médiane de l'hypothalamus, aboutissant à la description de circuits cérébraux complexes. De manière générale, les afférences et efférences de la zone périventriculaire impliquent le télencéphale, le diencéphale et le tronc cérébral ; cette zone recevant des afférences importantes du système moteur autonome. Par contraste, la zone adjacente, médiane, contient de larges groupes cellulaires bien délimités, influencés par le système de contrôle émotionnel et cognitif du télencéphale et qui apparaissent donc jouer un rôle dans l'initiation de comportements motivés spécifiques. Cette série de noyaux reçoit des afférences de différentes régions télencéphaliques du système dit "limbique" qui ont servi à définir les niveaux rostrocaudaux par W.E. Le Gros Clark, mais aussi de noyaux du tronc cérébral sur lesquels ils projettent en retour. La schématisation qu'en a fait L.W. Swanson, dans son chapitre intitulé *"The hypothalamus"* en 1987 (Swanson, 1987), se présente sous la forme d'un "circuit imprimé" (Figure 18). Cette représentation, qui résulte des données répertoriées au cours des années 1975 à 1983, reflète extrêmement bien toute la complexité quant à la compréhension et à l'organisation des connexions entre cette région et le reste du cerveau.

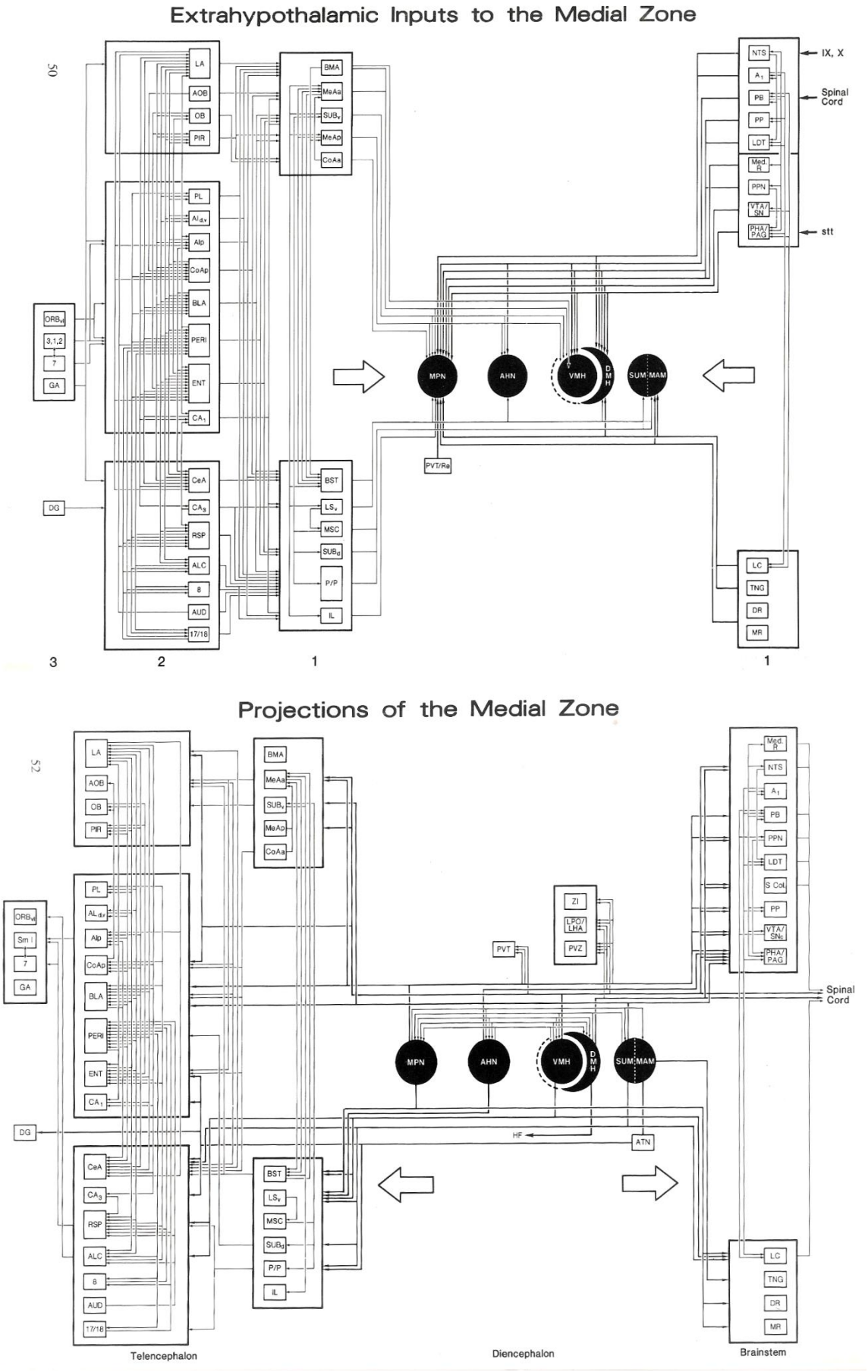

Figure 18. Représentations schématiques des principales afférences et efférences des noyaux de l'hypothalamus médian chez le rat (Swanson, 1987).

Les noyaux hypothalamiques de la zone médiane sont représentés par les cercles noirs.

De ce fait, les données anatomiques accumulées pendant les deux décennies 70-80 semblent corroborer l'organisation de l'hypothalamus suivant les concepts imaginés par W.E. Le Gros Clark, E.C. Crosby et R.T. Woodburne. Cependant, il faut reconnaître que cette organisation ne permet pas l'émergence de concepts clairs quant à l'organisation fonctionnelle de l'hypothalamus. Pendant les années 1990, des traceurs plus fins, tels que le *Phaseolus vulgaris* leucoagglutinine (PHAL), permettent d'affiner l'analyse de l'organisation des noyaux de l'hypothalamus médian et de leurs sous-divisions. Le groupe de L.W. Swanson est à la pointe sur le sujet avec une étude systématique de ces noyaux chez le rat (Swanson & Sawchenko, 1983; Risold *et al*, 1994). Les résultats obtenus permettent alors les premières modifications majeures du modèle précédent d'organisation de l'hypothalamus. Il serait trop long de détailler ici toutes ces données, mais leur conséquence sur la compréhension de l'organisation de l'hypothalamus adulte va rapidement être énoncée.

Tout d'abord, il devient évident que les noyaux de l'hypothalamus médian forment des réseaux intra-hypothalamiques distincts (Figure 19) (Risold & Swanson, 1995). Le premier implique le noyau préoptique médian, les régions ventrolatérales du noyau ventromédian et le noyau prémamillaire ventral (PMv). Ce réseau, aussi appelé sexuellement dimorphique, exprime abondamment les récepteurs alpha et beta aux estrogènes, mais aussi les récepteurs à la progestérone et testotérone. Impliqué dans les comportements liés à la reproduction, il est sous la dépendance d'informations phéromonales issues du bulbe olfactif accessoire par le noyau médian de l'amygdale, dont les axones suivent la strie terminale. Le second circuit implique le noyau hypothalamique antérieur, les parties centrale et dorsomédiane du noyau ventromédian et le noyau prémamillaire dorsal (PMd). Ce circuit reçoit aussi des afférences du noyau médian de l'amygdale, mais il semble surtout gouverné par des projections issues de l'hippocampe ventral, incluant le subiculum ventral et le champ CA1 ventral de la corne d'Ammon, par l'intermédiaire du noyau latéral du septum.

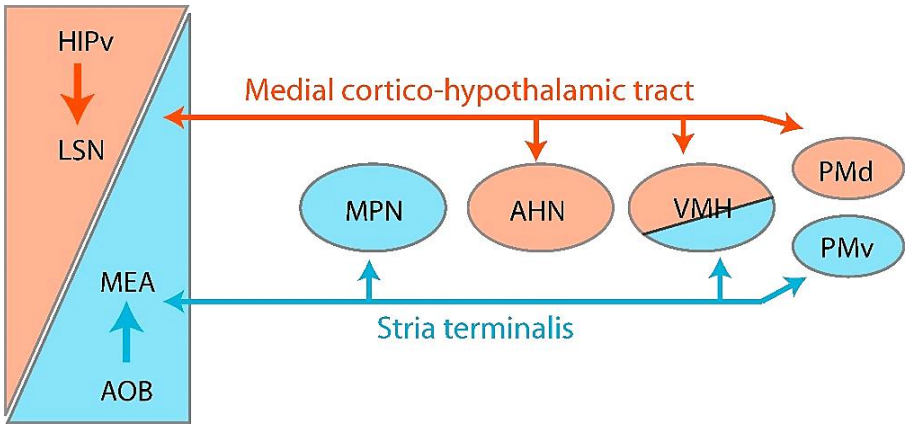

Figure 19. Représentation schématique des réseaux intra-hypothalamiques des noyaux de l'hypothalamus médian sous contrôle du septum et du noyau amygdalien médian.

AHN : noyau hypothalamique antérieur ; AOB : bulbe olfactif accessoire ; HIPv : hippocampe ventral ; LSN : noyau latéral du septum ; MEA : noyau médian de l'amygdale ; MPN : noyau préoptique médian ; PMd/v : noyau prémamillaire dorsal/ventral.

Il a été souligné, dans les parties précédentes, que les projections de l'hippocampe sur le noyau latéral du septum partagent de nombreuses ressemblances avec les connexions du cortex sur le striatum. Il se trouve qu'une des particularités de ce réseau est qu'il projette sur le noyau réuniens du thalamus (Risold *et al*, 1994) (Figure 20). Ce dernier noyau étant la source des afférences thalamiques à l'hippocampe ventral, il était ainsi décrit un circuit en boucle dont les projections par le thalamus sur le cortex évoquaient le circuit de Papez (Papez, 1995). Ce circuit en boucle implique les projections des noyaux mamillaires sur le cortex et le subiculum dorsal par les noyaux antérieurs du thalamus. Ces réseaux partagent des ressemblances avec le réseau des "noyaux de la base" par l'organisation des projections de l'hippocampe sur le noyau latéral du septum, étant lui-même bidirectionnellement connecté notamment au noyau hypothalamique antérieur.

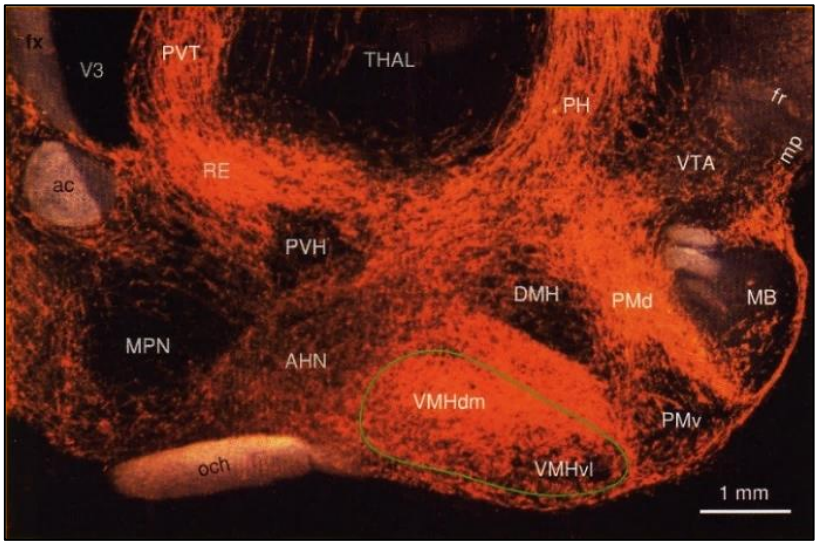

Figure 20. Photographie d'une coupe sagittale de cerveau de rat illustrant les projections du noyau hypothalamique antérieur (Risold *et al*, 1994).

L'injection de traceur PHAL réalisée dans le AHN met en évidence une innervation intense du VMH et du PMd avec une innervation collatérale abondante dans le RE.

ac : commissure antérieure ; AHN : noyau hypothalamique antérieur ; DMH : noyau hypothalamique dorsomédian ; fr : fasciculus retroflexus ; fx : fornix ; MB : mésencéphale ; mp : pédoncule mamillaire ; MPN : noyau préoptique médian ; ch : chiasma optique ; PH : noyau hypothalamique postérieur ; PMd/v : noyau prémamillaire dorsal/ventral ; PVH : noyau hypothalamique paraventriculaire ; PVT : noyau thalamique paraventriculaire ; RE : noyau réuniens ; THAL : thalamus ; VMHdm/vl : noyau ventromédian, partie dorsomédiane/ventrolatérale ; VTA : aire tegmentale ventrale ; V3 : 3ème ventricule.

Ainsi, ces noyaux de l'hypothalamus médian forment, d'après L.W. Swanson, un ensemble de structures interconnectées impliquées dans le contrôle de l'expression de comportements. Ils gouvernent certains centres moteurs postérieurs (substance grise périaqueducale) et renseignent en retour les centres supérieurs par des projections thalamiques et des connexions bidirectionnelles avec des structures appartenant aux formations des "noyaux de la base". Ces travaux et conclusions, qui ont été largement obtenus pendant la période 1990 à 1997 (Risold *et al*, 1994; Risold & Swanson, 1995, 1996; Risold *et al*, 1997), furent ensuite complétés par l'analyse des régions périnucléaires et du noyau dorsomédian. Ces derniers travaux aboutirent au concept de réseau générateur des schémas

viscéromoteurs (*"viscero motor pattern generator network"* ou VMPGN) qui coordonne l'activité neuroendocrinienne et celle du système nerveux autonome à l'expression des comportements (Figure 21). Il serait hors de propos de les décrire tous ici et sont détaillés dans la référence suivante (Thompson & Swanson, 2003). Il est important cependant de les mentionner puisqu'ils permettent de comprendre que le schéma d'organisation de l'hypothalamus évolue, au moins dans son organisation médio-latérale puisque le concept de zone périventriculaire et zone médiane au sens stricte s'effiloche quelque peu. Au moins trois secteurs peuvent être identifiés : des noyaux périventriculaires différenciés à fonctions neuroendocriniennes et contenant les prémotoneurones des systèmes nerveux autonomes ; des aires extranucléaires mais qui rassemblent aussi le noyau suprachiasmatique et le noyau dorsomédian, et formant le VMPGN ; et enfin, des noyaux de l'hypothalamus médian formant une "colonne de contrôle des comportements", de l'anglais "*behavioral control column*", qui inclue en arrière les noyaux mamillaires et même, selon L.W. Swanson, la SNr (Swanson, 2000; Thompson & Swanson, 2003; Swanson, 2012).

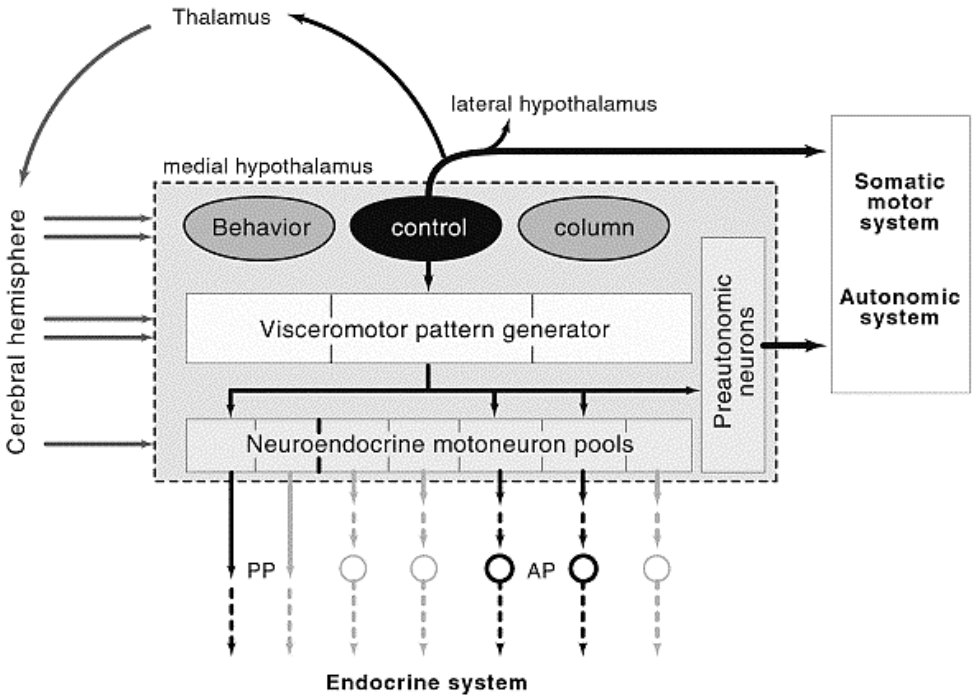

Figure 21. Schéma du modèle du "plan de base" de l'hypothalamus (Thompson & Swanson, 2003).

Les flèches indiquent les projections descendantes au tronc cérébral, les boucles ascendantes thalamo-corticales et les projections dans le LHA et le VMPGN depuis la "colonne de contrôle des comportements".

AP : hypophyse ou glande pituitaire antérieure ; PP : hypophyse ou glande pituitaire postérieure.

Par conséquence, l'image même de l'hypothalamus se modifie. Selon ce schéma, le noyau préoptique médian a toute sa place dans l'organisation hypothalamique, mais il y a un acteur essentiel qui semble totalement négligé : l'hypothalamus latéral.

IV. Le LHA

Le terme "aire hypothalamique latérale" a été utilisé pour la première fois en 1913 par Nissl et E.S. Gurdjian le nomme "*nucleus hypothalamicus lateralis"* dans son célèbre papier sur le cerveau du rat (Gurdjian, 1927; Morgane & Panksepp, 1979). Il est communément admis que le LHA est limité en avant par le télencéphale (SI et septum), en arrière par le mésencéphale (VTA), dorsalement par le thalamus ventral, médialement par les noyaux de l'hypothalamus médian et latéralement par la capsule interne. C'est une région traversée par le fornix qui est un tractus prenant son origine dans l'hippocampe et se terminant dans les noyaux mamillaires, mais aussi par le mfb qui est le système de fibres le plus complexe du cerveau des mammifères. Déjà en 1882, Ganser avait été le premier à dire que cette aire était le noyau du mfb (Ganser, 1882). Le mfb connecte les régions mésencéphaliques, bulbaires et médullaires aux aires télencéphaliques. Il contient des fibres ascendantes et descendantes provenant de régions du cortex préfrontal, de l'hypothalamus et des parties ventrales de la formation réticulée du tronc cérébral, laissant percevoir le LHA comme une extension rostrale de cette dernière (Swanson, 1987). Le LHA est situé comme un centre majeur d'intégration d'informations entre la formation réticulée, le tronc cérébral et l'hypothalamus médian. Cette région complexe, qui semble participer à de nombreuses fonctions (après des études d'ablation ou de stimulation de ses neurones), suscite depuis longtemps beaucoup d'intérêt (Olds, 1962; Epstein, 1971).

1. Organisation anatomique du LHA

Le LHA est une des dernières structures du SNC dont l'organisation anatomique reste très obscure. D'un point de vue strictement cytoarchitectural, les travaux anciens par les méthodes de Golgi ou de Nissl ont surtout mis l'accent sur la nature "réticulée" de cette région : le LHA est une extension rostrale des aires réticulées plus postérieures. L'absence de noyau différencié a orienté certains auteurs à tenter d'identifier des divisons basées sur l'organisation topographique du mfb. Notamment, dans le début des années 1980, J.G. Veening et ses collègues ont montré que les fibres ascendantes et descendantes du mfb, qui occupent une position précise et constante, peuvent selon leur origine diviser le LHA en plusieurs parties : ventrale/dorsale et latérale/médiane (Nieuwenhuys *et al*, 1982; Veening *et al*, 1982; Geeraedts *et al*, 1990). Cependant, ces travaux avaient une portée limitée afin de comprendre l'hypothalamus latéral puisque, d'une part, les neurones du LHA émettent des dendrites (Millhouse, 1969, 1979) capables de ramifier dans plusieurs secteurs déterminés par R. Nieuwenhuys et J.G. Veening. D'autre part, ils ne permettent pas d'identifier des divisions suivant l'axe antéro-postérieur. Enfin, les projections du mfb peuvent souvent ne faire que traverser le LHA sans l'innerver. Conscients de la complexité de cette région hypothalamique, R. Nieuwenhuys et ses collaborateurs (Nieuwenhuys *et al*, 1998) annonçaient déjà que la compréhension de son organisation structurelle et fonctionnelle allait prendre plusieurs années !

La découverte des neurones producteurs de l'hormone de mélanoconcentration (MCH) en 1989 (Bresson *et al*, 1989; Vaughan *et al*, 1989), puis celle des neurones producteurs d'orexine (ou hypocrétine (Hcrt)) en 1998 (Peyron *et al*, 1998), ont permis de faire un bond très important dans l'identification d'une certaine organisation structurelle du LHA. Notre équipe a beaucoup travaillé sur les neurones à MCH chez le rat, mais aussi chez d'autres espèces de vertébrés (Brischoux *et al*, 2001; Cvetkovic *et al*, 2003; Risold *et al*, 2009; Croizier *et al*, 2013). Elle a émis l'hypothèse du concept de "zone à MCH" dans l'hypothalamus. Ce concept était en partie basé sur l'analyse de la distribution de ces neurones comparée à celle d'autres systèmes peptidergiques mais spécifiques du LHA. Il était alors illustré que ces neurones occupaient un territoire particulier qui correspond, plus ou moins, à la partie tubérale du LHA. Avec la distribution de ces neurones, il a été confirmé que le LHA n'est pas homogène mais peut être divisé de manière objective en différentes parties caractérisées par leur chémoarchitecture. La codistribution des neurones à Hcrt dans la même région que ceux à MCH confirmait ces observations. Peu après, J.D. Hahn et L.W. Swanson divisaient le LHA tubéral en différentes parties essentiellement sur la base de la distribution comparée de MCH et d'Hcrt (Swanson *et al*, 2005; Hahn, 2010; Hahn & Swanson, 2010). L'utilisation de cette nouvelle division chémoarchitecturale du LHA n'a pas été reprise dans la littérature dans son ensemble. En effet, les études d'anatomie comparée de la distribution de MCH indiquent que des différences interspécifiques importantes existent (Figure 22) (Croizier *et al*, 2013). La position médio-latérale des neurones à MCH, notamment par rapport aux neurones à Hcrt, est différente chez les mammifères (herbivores, carnivores, primates). Par exemple, les péricaryons à MCH sont principalement situés dans la région latérale dorsale de l'hypothalamus postérieur chez le rat et la souris (Bittencourt *et al*, 1992; Croizier *et al*, 2010) alors qu'ils sont majoritairement situés ventro-latéralement au fornix chez le cochon (Chometton *et al*, 2014). Chez le mouton, ils sont situés dans le LHA ventral (Tillet *et al*, 1996), dans la région périfornicale (LHApfx) chez le chat (Torterolo *et al*, 2006) et ils sont plus médians chez l'homme (Bresson *et al*, 1989; Krolewski *et al*, 2010).

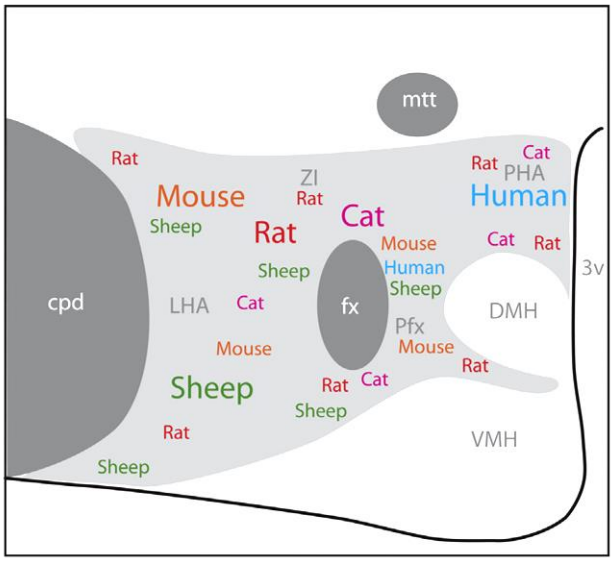

Figure 22. Schéma de la distribution des neurones à MCH dans l'hypothalamus chez le rat, la souris, le mouton, le chat et l'homme (Croizier *et al*, 2013).

La zone de distribution globale des neurones à MCH est représentée en gris clair.

cpd : pédoncule cérébral ; DMH : noyau dorsomédian ; fx : fornix ; mtt : tractus mammillothalamique ; LHA : aire hypothalamique latérale ; PH : noyau hypothalamique postérieur ; Pfx : région périfornicale du LHA ; VMH : noyau ventromédian ; ZI : zona incerta ; 3v : 3ème ventricule.

Ainsi, les divisions de L.W. Swanson et J.D. Hahn ne sont peut-être valables que chez certains rongeurs, mais peuvent ne pas exister de la même manière et s'appliquer à toutes les espèces.

Il existe d'autres structures du LHA qui, dans la même période, furent caractérisées sur la base de données neurochimiques. Notamment le noyau Parvafox, structure ventrale du LHA, a été montré dans l'hypothalamus de souris adulte. La localisation de neurones exprimant le facteur de transcription *Foxb1* coïncide avec le noyau PV1 (Bilella *et al*, 2014, 2016). Ce noyau, qui apparait dans les atlas de cerveaux de souris (Hof *et al*, 2000) et de rat sous l'acronyme PV1, avait été caractérisé chez le rat et la souris adulte comme étant parvalbumine positif (Celio, 1990; Mészár *et al*, 2012). Dans son atlas de 2005, G. Paxinos l'avait également observé et le nommait noyau *parateretе* (Paxinos & Watson, 2005).

Par ailleurs, des neurones enképhalinergiques dans le LHA antérieur occupent une région ventro-latérale au fornix. Ces neurones sont bien connus car à l'origine de l'innervation très intense du noyau latéral du septum (Poulain, 1983; Poulain *et al*, 1984; Risold & Swanson, 1997a; Risold, 2004). Chez le rat, ils ne constituent pas, d'après les atlas, une division spécifique du LHA, mais ils forment un noyau appelé noyau magnocellulaire dorsal, dorsal au fornix chez le cochon d'inde. Cet exemple illustre encore les différences interspécifiques importantes qui peuvent affecter des populations de neurones du LHA et la prudence qu'il convient d'appliquer à la caractérisation de structures par la neurochimie seule. Il peut être signalé ici que ces différences entre espèces observées, concernant la structure et l'organisation neurochimique du LHA, ne sont pas identifiées de la même manière pour l'hypothalamus médian, pour lequel il semble exister une plus grande stabilité phylogénétique chez les mammifères.

Enfin, il faut évoquer le cas du PSTN, caractérisé sur la base de l'expression de substance P, qui fait l'objet du présent travail et qui sera plus largement décrit plus loin.

Ainsi, si les données des 30 dernières années ont permis de comprendre certains éléments de la complexité du LHA, son organisation anatomique et fonctionnelle est encore loin d'être claire. A ce sujet, des données du développement peuvent apporter un éclairage important.

2. Organisation développementale du LHA

a. Développement de la zone à MCH

Le concept de zone à MCH n'était pas seulement né de l'étude de la distribution des neurones à MCH dans l'hypothalamus adulte, mais aussi de sa mise en place ontogénétique (Brischoux *et al*, 2001, 2002; Croizier *et al*, 2013, 2015). Notamment, les neurones à MCH s'expriment précocement chez l'embryon. Ils naissent dans une zone faisant partie d'une bande longitudinale (appelée *"cell cord"* par Keyser en 1972 et qui inclut la *"diagonale intrahypothalamica"* de T. Shimogori *et al*, (2010)) caractérisée par l'expression des gènes de développement *Shh*, *Nkx2.1*, *Nkx2.2*, *Dlx1-2*, *Lhx6*, *Lhx9* et à la limite postérieure du territoire d'expression de *Pax6*. Cette zone est dans la continuité des territoires *Nkx2.2* et *Shh* positifs du mésencéphale ventral (Alvarez-Bolado *et al*, 2012) d'où sont générés les neurones dopaminergiques mésencéphaliques et sérotoninergiques du Raphé. L'expression de *Dlx1-2* dans la région où se développent les neurones à MCH est corrélée avec le phénotype GABAergique (Stühmer *et al*, 2002; Potter *et al*, 2009) exprimé chez l'adulte par les neurones à MCH (Elias *et al*, 2001, 2008a).

Associée à l'observation du gradient de neurogenèse latéro-médian décrit dans l'hypothalamus (Altman & Bayer, 1986; Risold *et al*, 2009; Croizier *et al*, 2011), l'analyse des aires de distribution des neurones à MCH et à Hcrt dans l'hypothalamus adulte montre qu'elles sont cohérentes. En effet, les neurones à Hcrt, générés en un pic étroit, ont une aire de distribution plus réduite (aire périfornicale) que celle des neurones à MCH, générés en un pic évasé. Cette observation indique que les différences observées dans la distribution comparée de MCH et Hcrt dans l'hypothalamus tubéral sont à rapprocher des différences dans la chronologie de la genèse de ces neurones. Cependant, un parallèle avec des différences dans les facteurs de transcription potentiellement impliqués dans leur neurogenèse respective n'est pas encore faite.

Le concept de "zone à MCH" suggère implicitement que d'autres régions du LHA peuvent être caractérisées. S'il manque actuellement des marqueurs neurochimiques dans l'hypothalamus adulte pour les identifier, les travaux chez l'embryon sur la base de l'expression des facteurs de transcription peuvent aider à combler ce déficit. Notamment, *Dlx1-2* est clairement un outil particulièrement pertinent connu pour son implication dans la différenciation des cellules prosencéphaliques et précisément des neurones GABAergiques.

L'expression de *Dlx1-2* est alternée dans le manteau au 13ème jour de vie embryonnaire (E13), stade correspondant à la différenciation du LHA (Figure 23 A-C). Cette alternance est corrélée à celle de l'ARNm du marqueur *GAD*, enzyme de synthèse du GABA chez l'adulte (Chometton, 2015) (Figure 23 D). On ne connait pas l'expression de GABA chez tous les vertébrés, mais des travaux chez le cerveau larvaire de *Xenopus laevis* (amphibien) montrent que la distribution des neurones GABAergiques est similaire à l'expression de *Dlx1-2* à E13 dans l'hypothalamus de rongeur (Roberts *et al*, 1987; González *et al*, 2002) (Figure 23 E et F). L'alternance de l'expression de *GAD* dans le LHA chez les mammifères est imprimée dans la zone périventriculaire de l'hypothalamus de Xénope et est donc un caractère conservé (Puelles *et al*, 2012). L'alternance de l'expression de *GAD*, soulignée dans des divisions dans le LHA, peut être résumée ainsi : les neurones exprimant *GAD* sont très présents dans la région préoptique, en particulier dans l'aire préoptique latérale (LPO). La région antérieure est quant à elle coupée en deux domaines. En effet, la partie rostrale de l'hypothalamus antérieur et donc le LHA antérieur expriment *Dlx1-2* et sa partie caudale est dépourvue de neurone exprimant *GAD*. Le LHA tubéral est également *GAD*-positif comprenant la région MCH. Pour terminer, la région postérieure aux neurones à MCH, nommée plus loin dans ce mémoire LHA prémamillaire (LHApm), est *GAD*-négative.

Ces divisions forment donc une succession de régions *GAD*-positives et *GAD*-négatives susceptibles de correspondre à des entités fonctionnelles. Ces observations ont été affinées via l'analyse, chez le rat, de la distribution comparée de plusieurs neuropeptides dans ces territoires *GAD*-positifs ou *GAD*-négatifs, permettant la caractérisation de divisions supplémentaires dans certains domaines du LHA (Chometton, 2015). Comparé au LHA tubéral et aux neurones à MCH qui envoient des projections diffuses dans tout le cerveau, le LHApm est bien différencié. Même si peu de données existent concernant ces régions très postérieures du LHA, plusieurs noyaux y ont été identifiés.

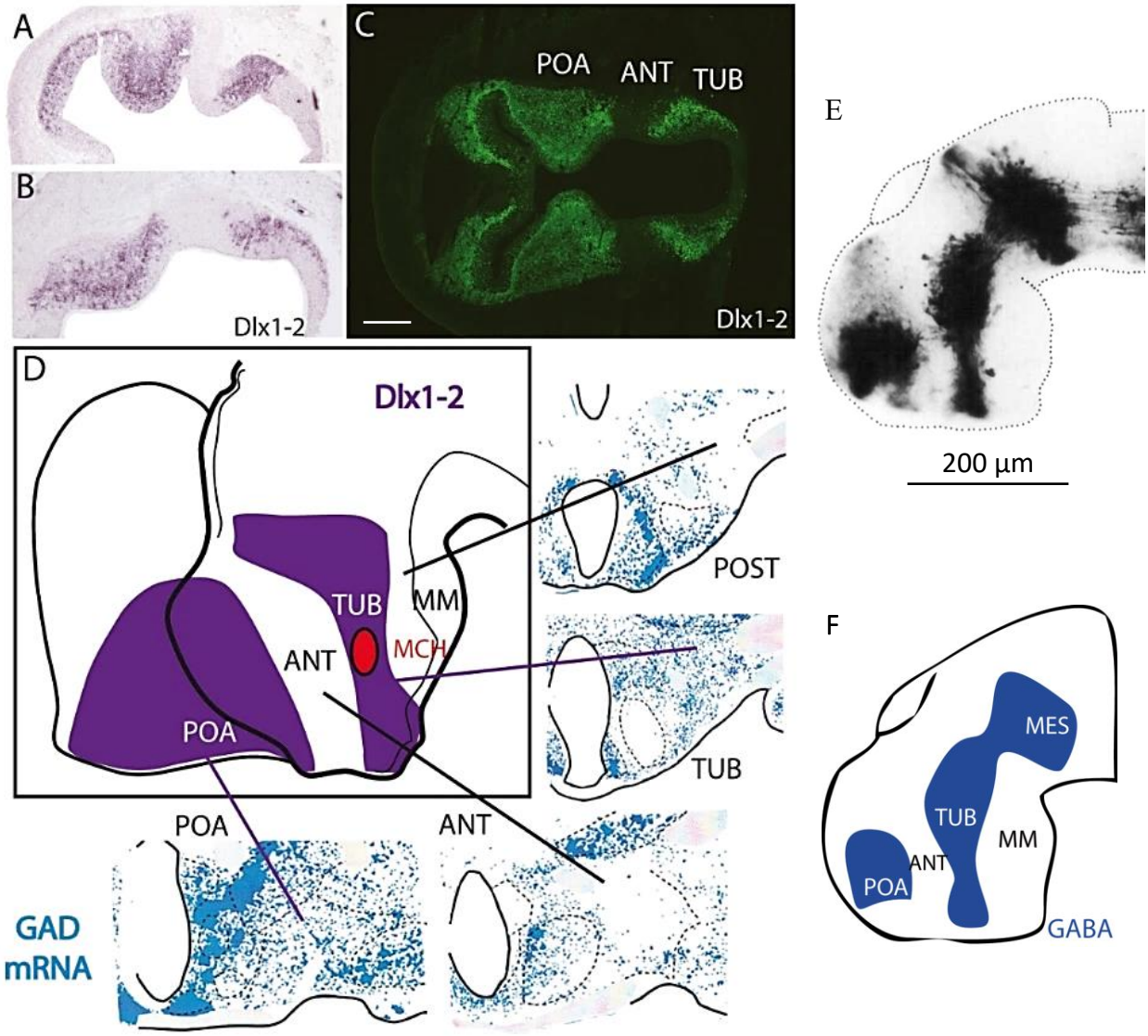

Figure 23. Photographies et s as illustrant l'expression de *Dlx1-2* dans le pros phale chez l'embryon et de *GAD* dans le LHA chez l'adulte, d'après Chometton (2015).

L'expression de *Dlx1-2* chez l'embryon à E13 révélée par hybridation *in situ* (A, B) et immunohistochimie (C). La comparaison avec l'expression de *GAD* dans l'hypothalamus latéral du rat adulte (D) montre que la succession de régions *GAD*-positives et *GAD*-négatives dans le LHA concorde avec l'alternance dans le patron d'expression du gène *Dlx1-2* chez l'embryon. De plus, la distribution des neurones GABAergiques dans le cerveau d'un Xénope au stade 37/38 [E et F, (Roberts et al., 1987)] correspond à l'expression de *Dlx1-2* dans l'hypothalamus d'un embryon de rat à E13 (D). Barre d'échelle = 200 µm.

ANT : région antérieure ; E13 : 13ème jour de vie embryonnaire ; GABA : acide gamma-aminobutyrique ; GAD : acide glutamique décarboxylase ; MCH : hormone de mélanoconcentration ; MES : mésencéphale ; MM : noyau mamillaire médian ; mRNA (ARNm) : acide ribonucléique messager ; opt : tractus optique ; POA : région préoptique ; POST : région postérieure ; TUB : région tubérale.

b. Le LHApm et le PSTN

Dans l'hypothalamus postérieur, deux grandes régions sont reconnues : le corps mamillaire qui a été identifié dès l'origine du concept d'hypothalamus et la région prémamillaire. La première description de la région prémamillaire est due à Krieg (1932) bien que le terme soit retrouvé dans des textes de E.S. Gurdjian (Gurdjian, 1927). D'après les atlas actuels, un certain nombre de noyaux constituent cette région prémamillaire, parmi lesquels les noyaux prémamillaires ventral et dorsal ont déjà été mentionnés dans le cadre des réseaux impliquant les noyaux de l'hypothalamus médian. Il faut y ajouter les noyaux tubéro-mamillaires riches en neurones histaminergiques, ou encore le noyau postérieur de l'hypothalamus et le noyau supramamillaire d'après certains auteurs.

Ces dernières années, notre équipe s'est beaucoup intéressée aux aires latérales de cette division de l'hypothalamus. Peu étudiée et mal caractérisée jusqu'alors, il a été constaté qu'elle occupait le secteur *GAD*-négatif postérieur du LHA, juste en avant de la VTA (Chometton, 2015). Il a été reconnu qu'à la différence des aires tubérales du LHA, cette région prémamillaire est caractéristique car elle contient un certain nombre de noyaux bien différenciés dont le principal dans notre étude est le PSTN (Chometton *et al*, 2016; Barbier *et al*, 2017). Une description plus complète de cette région est fournie dans les figures 24 et 25 ainsi que dans les informations supplémentaires de l'article 4 (pages 160-161).

Dans les années 1985, il avait été remarqué l'existence dans le LHA postérieur d'une population cellulaire adjacente au STN qui ne contient pas de neurones à Hcrt ni à MCH, mais associée à l'INS et au noyau parabrachial (PB) (Köhler *et al*, 1984; Saper *et al*, 1986; Saper, 2004). Chez le rat, P.Y. Wang et F.C. Zhang (1995) ont identifié et nommé ce groupe cellulaire PSTN sur la base de l'expression de l'ARNm de la préprotachykinine 1 (*pTac1*), précurseur de la tachykinine 1 (TAC1) et du peptide substance P (Wang & Zhang, 1995). Cette observation a ensuite été confirmée par M. Goto et L.W. Swanson qui en ont étudié les projections (Goto & Swanson, 2004). Le PSTN est illustré depuis dans les atlas (Swanson, 2004; Paxinos & Watson, 2005, 2013). Plus récemment, sur du matériel issu des hybridations *in situ pTac1*, notre équipe a observé que cette condensation cellulaire, proche du pédoncule cérébral, correspondant au PSTN est dans une zone *GAD*-négative dans les régions postérieures au LHA tubéral. Cette région du LHA postérieur, bordée dorsalement par la zona incerta *GAD*-positive et latéralement par le STN *GAD*-négatif, a été nommée LHApm car l'absence de *GAD* et l'expression de *pTac1* sont également observées dans les noyaux prémamillaires ventral et dorsal voisins (Chometton, 2015) (Figure 24). L'analyse de la distribution de parvalbumine et de calbindine a aussi permis d'identifier d'autres condensations cellulaires au voisinage du PSTN. On y retrouve ainsi le noyau Parvafox, parvalbumine positif, associé au tractus hypothalamique ventro-latéral (vlt) et au noyau gémini (NG) (Figure 25). De la même manière, en 2016, dans le travail de S. Chometton *et al*, notre équipe a identifié le noyau CbN, calbindine positif et ventral au PSTN, mais qui présente de nombreuses ressemblances hodologiques avec celui-ci.

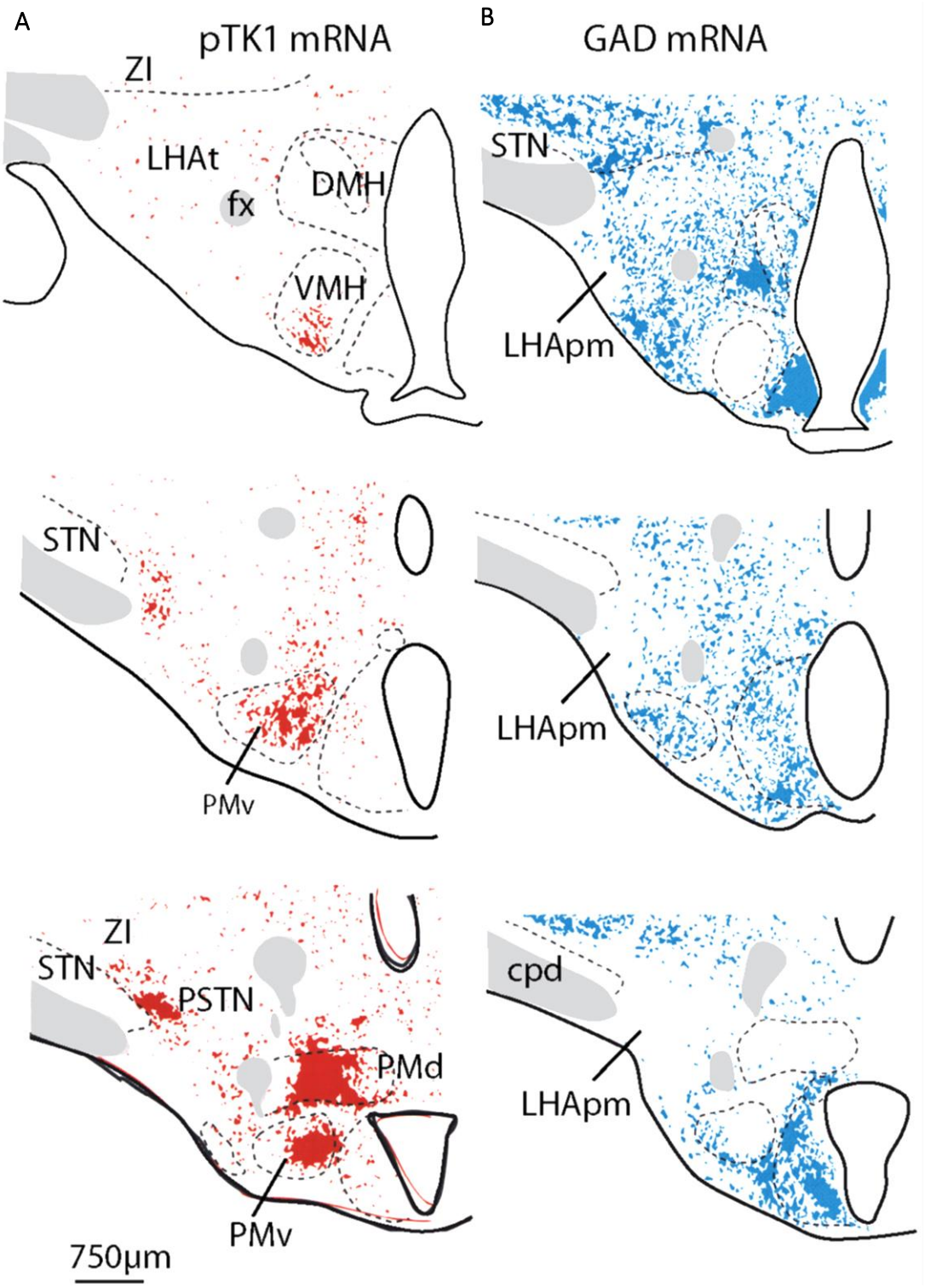

Figure 24. Distribution de l'ARNm de la *pTac1* (pTK1) et de la *GAD* dans le LHA postérieur (Chometton *et al*, 2016).

Les marquages des ARNm obtenus par hybridation *in situ* sur des coupes frontales de l'hypothalamus postérieur de rat montrent que les cellules exprimant la glutamate décarboxylase (*GAD*) (B) sont abondantes dans le LHAt mais absentes dans le LHApm. A l'inverse, l'ARNm préprotachykinine 1 (*pTac1*) (A) est abondamment exprimé dans le PSTN et les noyaux prémamillaires ventral et dorsal.

cpd : pédoncule cérébral ; DMH : noyau dorsomédian ; fx : fornix ; LHApm : aire hypothalamique latérale prémamillaire ; LHAt : aire hypothalamique latérale tubérale ; PMd/v : noyau prémamillaire dorsal/ventral ; PSTN : noyau parasousthalamique ; STN : noyau sousthalamique ; VMH : noyau ventromédian ; ZI : zona incerta.

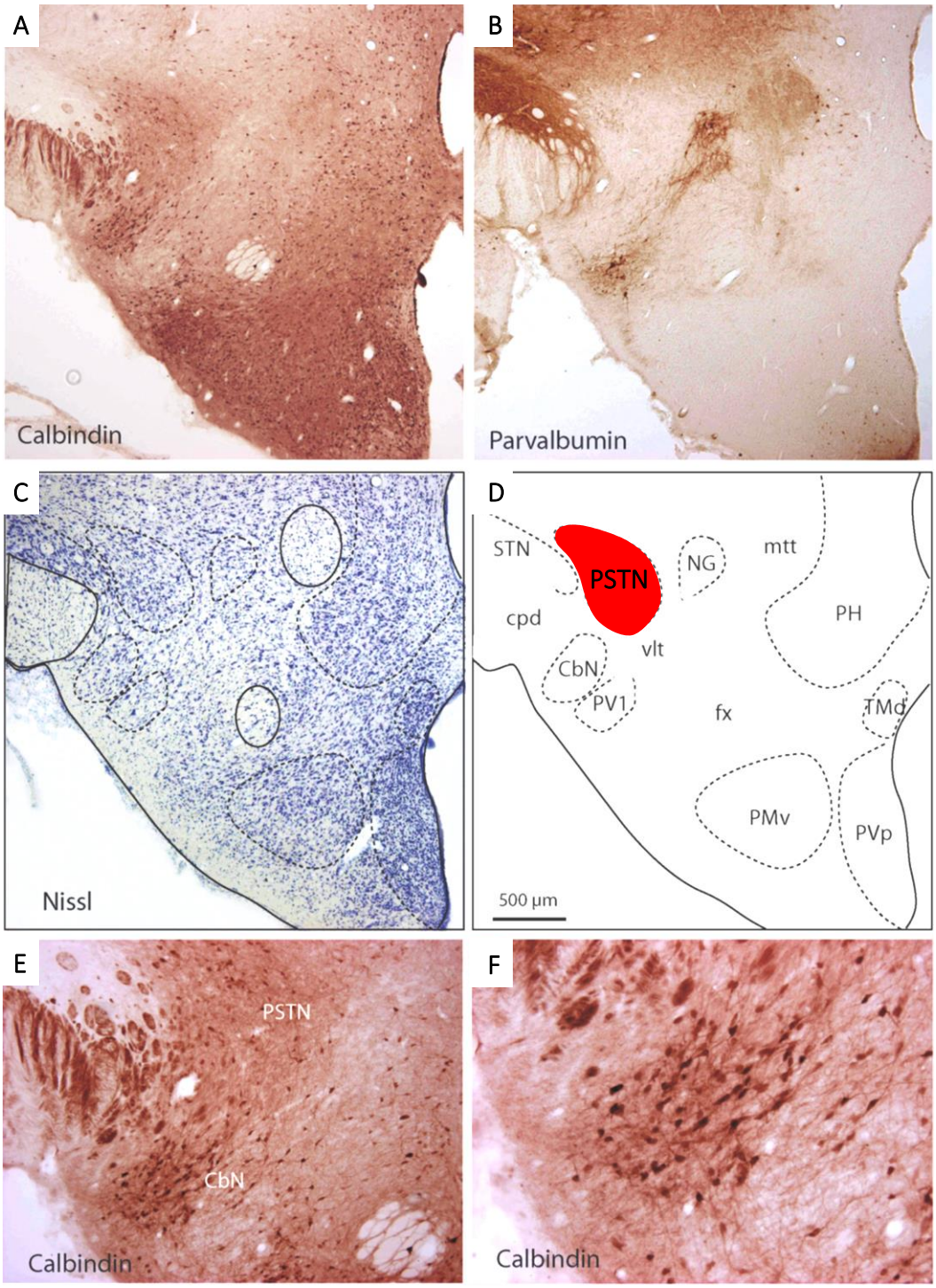

Figure 25. Photographies et schéma illustrant la distribution des neurones à parvalbumine et à calbindine dans le LHApm rostral (Chometton *et al*, 2016).

La distribution des marquages calbindine (A, E, F) et parvalbumine (B), détectés par immunohistochimie dans le LHApm rostral sur des coupes frontales adjacentes d'hypothalamus de rat, permet de voir que le signal parvalbumine est présent dans le PV1 (Parvafox) et le NG, deux structures connectées par le vlt (B). Entre les noyaux PV1/NG et le STN (marqués par la parvalbumine), le PSTN et le CbN sont marqués par la calbindine (A, E, F). La coupe C est marquée par un bleu de toluidine pour déterminer la cytoarchitecture (D).

CbN : noyau calbindine ; cpd : pédoncule cérébral ; fx : fornix ; LHApm : aire hypothalamique latérale prémamillaire ; mtt : tractus mamillothalamique ; NG : noyau gémini ; PH : noyau postérieur ; PMv : noyau prémamillaire ventral ; PSTN : noyau parasousthalamique ; PV1 : noyau parvalbumine ; PVp : partie postérieure du noyau périventriculaire ; STN : noyau sousthalamique ; TMd : partie dorsale du noyau tubéromamillaire ; vlt : tractus ventrolatéral.

En 2004, M. Goto et L.W. Swanson ont identifié, chez le rat, par injection de traceur antérograde PHAL dans le PSTN, les efférences de ce noyau (Goto & Swanson, 2004). Ils ont mis en évidence des projections massives dans le noyau salivaire et dans le noyau moteur dorsal du nerf vague, aussi identifiées par G.V. Allen et D.V. Cechetto en 1992 (Allen & Cechetto, 1992), ainsi que dans le noyau du tractus solitaire (NTS). Ce groupe cellulaire envoie également des projections descendantes dans le PB et ascendantes dans le cortex cérébral, directes ou indirectes via le thalamus, ainsi que dans le CEA, le FS, le BST et la SI (Saper, 1985; Saper *et al*, 1986; Moga *et al*, 1990; Allen & Cechetto, 1993; Goto & Swanson, 2004) (Figure 26).

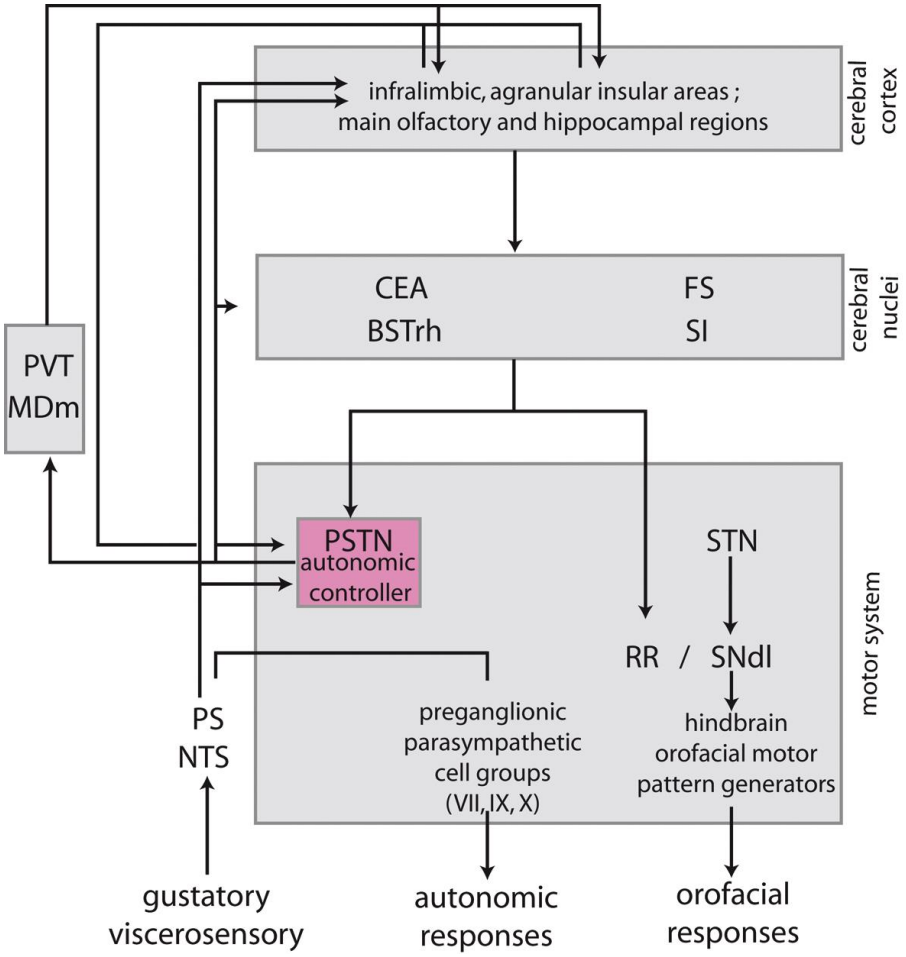

Figure 26. Schéma des connexions axonales du PSTN, d'après Goto & Swanson (2004).

BSTrh : noyau rhomboïde du noyau du lit de la strie terminale ; CEA : noyau amygdalien central ; MDm : partie médiane du noyau thalamique médiodorsal ; FS : fundus striatum ; NTS : noyau du tractus solitaire ; PB : noyau parabrachial ; PSTN : noyau parasousthalamique ; PVT : noyau thalamique paraventriculaire ; RR : aire rétrorubrale du noyau réticulaire mésencéphalique ; SI : substance innominée ; SN : substance noire ; STN : noyau sousthalamique.

Les afférences descendantes et ascendantes au PSTN ont ensuite été étudiées après injection du traceur rétrograde fluorogold (FG) et confirmées par des traçages antérogrades dans le CEA et l'INS (Chometton *et al*, 2016). Comme l'avait montré G.V. Allen et D.V. Cechetto (1992, 1993), cette région du LHA postérieur reçoit des afférences du PB et des aires corticales insulaires et

infralimbiques. L'étude des connexions du PSTN montre que ce dernier est associé à différentes structures liées au circuit de la gustation, de l'hédonisme et du contrôle de l'appétit (Goto & Swanson, 2004; Shin *et al*, 2011; Chometton *et al*, 2016). Il reçoit notamment les projections des neurones à CGRP (*Calcitonin Gene-Related Peptide*) (Dobolyi *et al*, 2005) du PB. Ces projections sont impliquées dans le contrôle de l'appétit via un circuit incluant la partie parvicellulaire du noyau ventro-postéromédian du thalamus et le CEA (Carter *et al*, 2013).

Les résultats fonctionnels observés dans le PSTN et le CbN montrent que cette région est fortement impliquée dans les réponses liées à la prise alimentaire et réagit au goût des aliments ingérés (Chometton *et al*, 2016). En effet, le complexe PSTN/CbN répond par l'expression du marqueur c-Fos à la nature hédonique palatable de l'aliment ingéré ainsi qu'à son aspect nouveauté. D'autres études corroborent ces résultats et avaient montré que le PSTN est la seule région hypothalamique qui reçoit des projections à la fois du système lié au besoin en sodium et du système lié au goût (Shin *et al*, 2011). Cette région est aussi impliquée dans l'organisation du comportement de prédation, lors de l'ingestion d'une proie après une phase de traque, via l'activation du PSTN et du CEA augmentant la motivation de l'animal pour la chasse (Comoli *et al*, 2005; Han *et al*, 2017).

Les premières données antomiques de L.W. Swanson (Goto & Swanson, 2004), illustrées dans la figure 26, suggèrent un lien entre le PSTN et le STN associé au réseau des "noyaux de la base". L'absence d'expression de *GAD* dans le LHA postérieur et le STN renforce ce lien entre ce noyau et l'hypothalamus postérieur. Par ailleurs, le STN, classiquement associé au thalamus ventral, est maintenant reconnu comme faisant partie de l'hypothalamus.

c. Le STN, un nouveau noyau hypothalamique

Le STN, identifié au milieu du XIX^{ème} siècle et alors appelé corps de Luys, était dès son origine associé au "sub-thalamus", puis a été incorporé au thalamus ventral au milieu du XX^{ème} siècle. Il faut attendre le début des années 1980 et l'observation par Altman et Bayer que ce noyau est issu des mêmes zones du neuroépithélium germinatif donnant naissance aux noyaux prémamillaires (Altman & Bayer, 1986) pour amorcer son assimilation définitive à l'hypothalamus. L'observation plus tardive de l'expression par ce noyau de marqueurs du développement spécifiques de l'hypothalamus, tels que le facteur de transcription *Nkx2.1*, confirmeront les observations d'Altman et Bayer.

Parmi les marqueurs exprimés par le STN pendant le développement, il faut s'intéresser au gène *Pitx2* (Figure 27). L'absence d'expression de ce gène entraine des déficits de la formation du STN, mais affecte aussi d'autres structures de l'hypothalamus postérieur et notamment les noyaux mamillaires (Martin *et al*, 2004; Skidmore *et al*, 2008; Waite *et al*, 2013). Il est encore à noter que l'expression de *Pitx2* est conservée chez l'animal adulte (Figure 28) (Smidt *et al*, 2000). Le territoire d'expression de ce gène englobe alors l'hypothalamus postérieur et cette expression est

particulièrement intense dans chacun des noyaux *GAD* négatifs de cette région incluant STN, PSTN, PMd, PMv et noyaux mamillaires. Ainsi, dans l'embryon, l'expression de *Pitx2* associée à celle de *Nkx2.1* en l'absence de *Dlx1-2* pourrait constituer la signature moléculaire de cette région de l'hypothalamus. La signification de la position anatomique du STN dans l'hypothalamus, maintenant validée dans les atlas (Allen Institute, 2004; Swanson, 2004; Paxinos & Franklin, 2007; Paxinos & Watson, 2013), n'est pas encore claire. Il faut cependant signaler la place de ce noyau dans le réseau des "noyaux de la base", notamment par les projections qu'il reçoit de l'isocortex et qui forment la voie hyperdirecte (Albin *et al*, 1989; Gerfen & Bolam, 2016), ou depuis le pallidum (voie indirecte) que nous avons déjà décrite.

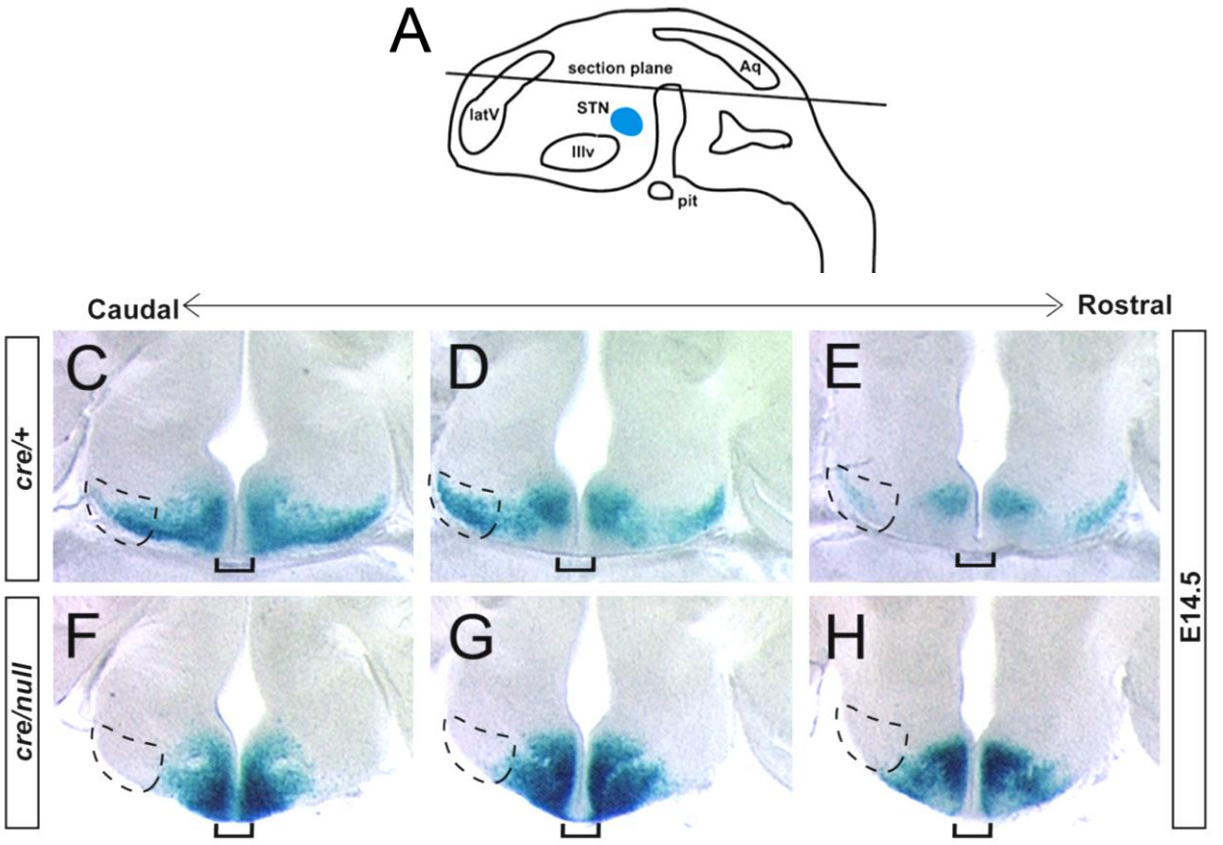

Figure 27. Schéma et photographies de coupes d'embryons exprimant ou non le gène *Pitx2*, d'après Skidmore *et al* (2008).

L'emplacement du STN chez l'embryon est symbolisé en bleu sur le schéma A (le schéma B a été volontairement supprimé, n'étant pas nécessaire ici). Cette expérience de traçage a été réalisée chez des embryons de souris qui expriment ou non le gène *Pitx2* sous la dépendance du rapporteur nucléaire lacZ (génotypées *Pitx2*-cre/+ ; N-lacZ ou *Pitx2*-cre/null ; N-lacZ, respectivement) afin de suivre les neurones embryonnaires qui expriment *Pitx2*. Les embryons ont été fixés, colorés pour l'activité β-galactosidase, et coupés selon le plan de coupe indiqué en A. Les zones en pointillés représentent l'hypothalamus latéral où se trouvent les neurones du STN. Des coupes d'hypothalamus adjacentes d'embryons (E14,5) de souris *Pitx2*-cre/null ont été comparées à celles de souris *Pitx2*-cre/+ (C – H). Ces coupes révèlent l'absence de cellules positives pour la β-galactosidase dans l'hypothalamus latéral des souris *Pitx2*-cre/null ; NlacZ et une abondance médiane de cellules positives à la β-galactosidase. Les mutants *Pitx2*-cre/null présentent également une expression accrue de la β-galactosidase au niveau de la ligne médiane ventrale (crochet sur les photographies), ce qui suggère que ces cellules ne respectent pas la limite de la ligne médiane. La migration du STN et des neurones hypothalamiques est perturbée dans les embryons *Pitx2*-cre/null. Ces mutants présentent donc des défauts de localisation des neurones hypothalamiques.

Aq : aqueduc cérébral ; latV : ventricule latéral ; pit : glande pituitaire (hypophyse) ; STN : noyau sousthalamique ; IIIv : 3ème ventricule.

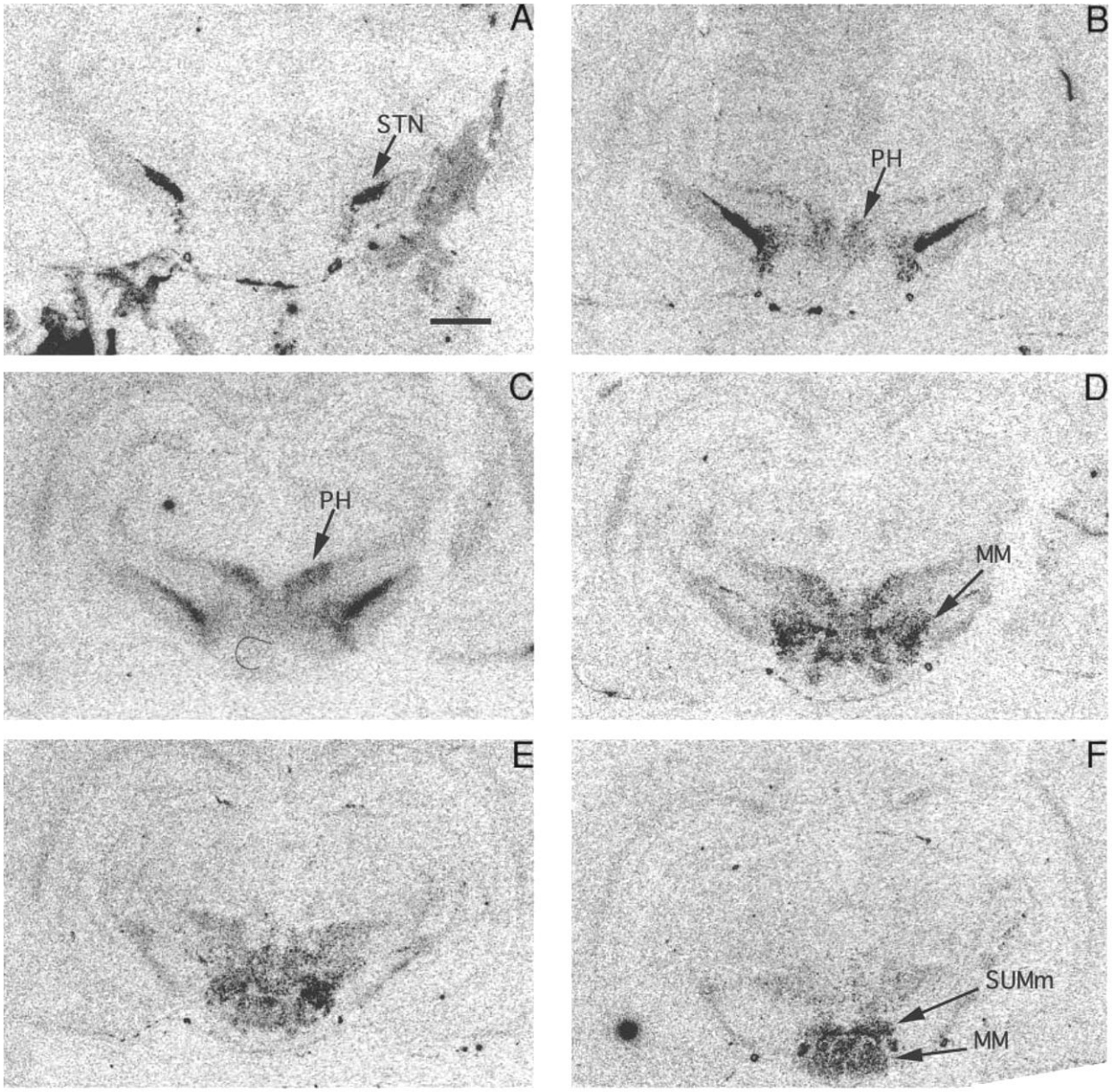

Figure 28. Photographies de coupes coronales d'encéphale de rat adulte marquées *Pitx2* par hybridation *in situ*, d'après Smidt *et al* (2000).

Les coupes sont présentées de rostral (A) à caudal (D). Le MM signalé sur la photographie D correspond au PSTN. MM : noyau mamillaire médian ; PH : noyau hypothalamique postérieur ; STN : noyau sousthalamique ; SUM : noyau supramamillaire. Barre d'échelle = 1 mm.

V. Hypothèses de travail et objectifs de notre étude

D'après L.W. Swanson, il existe un schéma d'organisation anatomique du prosencéphale dans lequel s'insère l'hypothalamus. C'est notamment le cas de l'hypothalamus médian qui est intégré dans des réseaux d'organisation similaire à ceux décrits pour les "noyaux de la base". Mais en ce qui concerne le LHA, très peu d'études intègrent cette région dans de tels réseaux. Il a été montré dans l'introduction que des données ontogénétiques, phylogénétiques et chémoarchitectoniques du LHA sont de bonnes bases permettant de mieux appréhender certains aspects de son organisation anatomique et fonctionnelle.

Les travaux de notre équipe avec le modèle des neurones à MCH ont apporté de nombreuses informations (Brischoux *et al*, 2001, 2002; Cvetkovic *et al*, 2003; Risold *et al*, 2009; Croizier *et al*, 2013; Chometton *et al*, 2014). Cependant, il a fallu se rendre à l'évidence que les caractéristiques de ce système n'en font pas un modèle adapté à l'objectif d'intégrer les aires du LHA aux réseaux prosencéphaliques. La raison essentielle à ce constat est que les projections des neurones à MCH sont diffuses dans tout le cerveau. Elles ressemblent en ce sens beaucoup plus à celles d'autres systèmes du tronc cérébral postérieur comme le noyau tubéro-mamillaire (TMN) histaminergique, sérotoninergique du Raphé ou noradrénergique du locus ceruleus.

En revanche, le complexe PSTN présente des caractéristiques idéales pour notre approche. C'est un noyau différencié qui forme un petit complexe nucléaire très net avec son voisin immédiat le CbN. Sa position anatomique est aussi particulière ; il est adjacent au STN qui est un acteur clé du réseau des "noyaux de la base", mais il partage des caractéristiques neurochimiques avec les noyaux prémamillaires (substance P) qui sont une partie intégrante des réseaux des noyaux de l'hypothalamus médian. Contrairement aux neurones à MCH, le complexe PSTN/CbN présente des connexions différenciées non diffuses qui peuvent donc être comparées à celles des structures voisines. Ce complexe nucléaire peut par conséquent être un bon modèle pour l'étude du LHA et notamment, pour analyser l'organisation du réseau qui l'implique et vérifier à quel schéma il est possible de le comparer. Enfin, cette structure a fait l'objet de peu d'études et en déterminer certaines fonctions est également un objectif original utile à la compréhension de l'organisation fonctionnelle de l'hypothalamus.

Plus spécifiquement, les objectifs de ce travail sont les suivants :

1. Analyser en détail le réseau impliquant des noyaux de l'hypothalamus postérieur et plus particulièrement du complexe PSTN/CbN en lien avec des aires corticales (INS) et striato-pallidales, notamment le CEA, puisque des liens anatomiques entre ces structures sont mentionnés dans la littérature, mais leur organisation n'est pas encore clairement établie.

2. Etudier les fonctions de ce complexe PSTN/CbN dans différentes conditions expérimentales.

Pour réaliser ces objectifs, nos premières expériences ont été menées, chez le rat, dans la continuité des précédents travaux effectués au laboratoire concernant l'étude des connexions du complexe PSTN/CbN et parce que c'est chez cette espèce que les réseaux sont les plus décrits. En parallèle de ce travail, la collecte de données sur d'autres régions du LHA ou proches, telles que les régions périfornicale et mamillaire (données en annexe) a également été poursuivie. Tous ces travaux font appel à des techniques classiques de neuroanatomie via l'utilisation de traceurs neuronaux antérograde et rétrograde (PHAL, FG et cholera toxine B (Ctb)).

Les travaux d'anatomie ont ensuite été complétés par des expériences comportementales chez le rat mais aussi chez la souris via des approches de pharmacogénétique. Des données sur l'anatomie du PSTN chez cette espèce ont alors aussi été obtenues.

RESULTATS

I. Etude neurochimique et hodologique du CEA et du LHA (Publications n°1, 2 et 3)

La première partie de notre travail a concerné l'analyse des liens anatomiques entre le complexe PSTN/CbN et l'amygdale. Pour cette étude exclusivement anatomique, des méthodes de traçage des voies nerveuses ont été utilisées chez des rats adultes. Des injections iontophorétiques ou par pression de traceurs classiques antérograde (PHAL) et rétrograde (FG) ont donc été réalisées. Le FG, un traceur intra-axonal fluorescent (permettant sa détection directe au microscope à fluorescence) capté par les terminaisons axonales des neurones, permet de repérer les corps cellulaires des neurones projetant dans la région où l'injection a été réalisée. A contrario, le PHAL, capté par les corps cellulaires des neurones au niveau du site d'injection, permet de repérer leurs axones dans toute leur longueur et leurs détails. Sa détection se fait par immunohistochimie enzymatique ou fluorescente indirecte. Pour préciser nos observations anatomiques, des analyses chémoarchitectoniques de la distribution de plusieurs neuropeptides ont également été réalisées. Des méthodes immunohistochimiques enzymatiques (par méthode "avidine-biotine-peroxydase") et fluorescentes multiples ont été utilisées, dont les procédures sont décrites dans chacun des articles de ce mémoire. Les anticorps primaires utilisés pour nos études ainsi que leurs principales caractéristiques sont listés dans les publications 1 à 6.

1. Etude des connexions entre l'amygdale et le complexe PSTN/CbN (Publication n°1)

Les travaux effectués au laboratoire avant mon arrivée concernaient l'étude d'une petite région du LHApm. Cette zone, neurochimiquement et cytoarchitectoniquement distincte du LHA tubéral chez le rat, contient le complexe PSTN/CbN. En 2014-2015, notre équipe avait montré que le LHA caudal, en particulier la région du PSTN et du CbN est la cible spécifique de projections CGRP intenses provenant du PB. Ces projections avaient été décrites chez le rat mais leurs cibles n'avaient pas été identifiées avec précision. Dans le travail publié par Chometton *et al*, en 2016, le complexe PSTN/CbN avait été identifié comme la cible exclusive de l'innervation CGRP dans le LHA depuis le PB. Notre équipe a ensuite confirmé les observations de M. Goto et L.W. Swanson concernant les efférences descendantes et ascendantes depuis le complexe PSTN/CbN (Goto & Swanson, 2004) grâce à des injections de PHAL chez le rat. Par ailleurs, S. Chometton *et al* (2016) ont aussi identifié le complexe PSTN/CbN comme une source spécifique des efférences depuis le LHA postérieur dans le CEA. Les neurones marqués par le FG dans le LHA après injection de FG dans le CEA formaient deux condensations différenciées, correspondant aux frontières du complexe PSTN/CbN, délimitées par les projections CGRP depuis le PB. Ainsi, les premiers travaux de l'équipe

pointaient vers des connexions bidirectionnelles intenses entre le CEA et le complexe PSTN/CbN, ce qui était en accord avec de nombreuses données de la littérature concernant le LHA postérieur (Krettek & Price, 1978; Ottersen, 1980; Veening *et al*, 1982, 1984; Ono *et al*, 1985; Gray *et al*, 1989; Gonzales & Chesselet, 1990; Petrovich & Swanson, 1997; Bourgeais *et al*, 2001; Tsumori *et al*, 2006; Oka *et al*, 2008; Shirasu *et al*, 2011; Niu *et al*, 2012; Chometton *et al*, 2016). Cependant, des informations importantes concernant la place du complexe PSTN/CbN dans les circuits depuis le CEA manquaient encore, notamment avec les différentes divisions du CEA et les trajets suivis par leur projections respectives vers ce complexe.

Les travaux associés à la publication n°1 de cette première partie des résultats concernent d'autres injections de traceurs rétrograde FG dans le PSTN ainsi que des injections de traceur antérograde PHAL dans l'amygdale. Cette étude anatomique a permis, non seulement, d'analyser en détail les projections spécifiques depuis les noyaux de l'amygdale dans le LHA postérieur, mais aussi de mettre en évidence deux trajets différenciés de fibres. Ainsi, il a été montré que le PSTN et le CbN reçoivent respectivement des projections du CEAm et de la partie antérieure du noyau basomédian de l'amygdale (BMAa) à travers deux voies, l'une dorsale et l'autre ventrale dans le mfb. Le trajet dorsal est formé d'axones, originaires du CEA, qui innervent modérément le noyau paraventriculaire et le LHApfx avant d'innerver abondamment le PSTN. Quant au trajet ventral, il forme un tractus différencié, nommé le tractus amygdalo-hypothalamique ventro-latéral (vlah) qui est adjacent mais distinct du vlt. Ce tractus achemine les informations originaires à la fois du BMAa, du CEA et de structures télencéphaliques telles que le FS et se termine dans le CbN, adjacent au noyau Parvafox cible du vlt. Ces deux tractus vlt et vlah forment une voie dite olfactive dans le LHA. En conclusion, l'analyse détaillée des projections depuis l'amygdale sur le PSTN et le CbN, couplée à la distribution convergente des projections CGRP et de l'expression des neurones à calbindine, met en évidence le CEAm et le BMAa comme sources d'afférences majeures dans le LHA postérieur. Par ailleurs, elle identifie le complexe PSTN/CbN comme la cible majeure des projections du CEA sur l'hypothalamus. Ces travaux soulèvent cependant des questions concernant l'organisation du CEA qui sont abordées dans les articles suivants.

Brain Struct Funct
DOI 10.1007/s00429-017-1379-1

ORIGINAL ARTICLE

Parasubthalamic and calbindin nuclei in the posterior lateral hypothalamus are the major hypothalamic targets for projections from the central and anterior basomedial nuclei of the amygdala

Marie Barbier[1] · Sandrine Chometton[1] · Yvan Peterschmitt[1] · Dominique Fellmann[1] · Pierre-Yves Risold[1]

Received: 16 September 2016 / Accepted: 26 January 2017

Abstract The parasubthalamic nucleus (PSTN) and the ventrally adjacent calbindin nucleus (CbN) form a nuclear complex in the posterior lateral hypothalamic area (LHA), recently characterized as connected with the central nucleus of the amygdala (CEA). The aim of the present work is to analyze in detail the projections from the amygdala into the PSTN/CbN, also focusing on pathways into the LHA. After fluorogold injections into the PSTN/CbN, the medial part of the CEA (CEAm) appears to be the main supplier of projections from the CEA. Other amygdalar nuclei contribute to the innervation of the PSTN/CbN complex, including the anterior part of the basomedial nucleus (BMAa). Injections of the anterograde tracer, *Phaseolus vulgaris* leucoagglutinin (PHAL), into the CEAm and BMAa revealed that projections from the CEAm follow two pathways into the LHA: a dorsal pathway formed by axons that also innervate the paraventricular hypothalamic nucleus, the anterior perifornical LHA and the PSTN, and a ventral pathway that runs laterally adjacent to the ventrolateral hypothalamic tract (vlt) and ends in the CbN. By contrast, the BMAa and other telencephalic structures, such as the fundus striatum project to the CbN via the ventral pathway. Confirming the microscopic observation, a semi-quantitative analysis of the density of these projections showed that the PSTN and the CbN are the major hypothalamic targets for the projections from the CEAm and the BMAa, respectively. PSTN and CbN receive these projections through distinct dorsal and ventral routes in the LHA. The ventral pathway forms a differentiated tract, named here the ventrolateral amygdalo-hypothalamic tract (vlah), that is distinct from, but runs adjacent to, the vlt. Both the vlt and the vlah had been previously described as forming an olfactory path into the LHA. These results help to better characterize the CbN within the PSTN/CbN complex and are discussed in terms of the functional organization of the network involving the PSTN and the CbN as well as the CEA and the BMAa.

Keywords Calbindin · Parvalbumin · CGRP · Olfaction · Parabrachial nucleus

Abbreviations

AAA	Anterior amygdalar area
Act	Anterior commissure, temporal limb
AHN	Anterior hypothalamic nucleus
AMB	Nucleus ambiguus
ARH	Arcuate hypothalamic nucleus
B	Barrington's nucleus
BA	Bed nucleus accessory olfactory tract
BLA	Basolateral amygdalar nucleus
BLAa	Basolateral amygdalar nucleus, anterior part
BLAp	Basolateral amygdalar nucleus, posterior part
BMAa	Basomedial amygdalar nucleus, anterior part
BMAp	Basomedial amygdalar nucleus, posterior part
BST	Bed nuclei stria terminalis
BSTad	Bed nuclei stria terminalis, anterior division, anterodorsal area
CA	Ammon's horn
Cb	Calbindin
CbN	Calbindin nucleus

✉ Pierre-Yves Risold
pierre-yves.risold@univ-fcomte.fr

[1] Laboratoire de Neurosciences Intégratives et Cliniques, EA481, University of Bourgogne-Franche-Comté, UFR Sciences Médicales et Pharmaceutiques, 25000 Besançon, France

Published online: 03 March 2017

CEA	Central amygdalar nucleus
CEAc	Central amygdalar nucleus, capsular part
CEAl	Central amygdalar nucleus, lateral part
CEAm	Central amygdalar nucleus, medial part
CGRP	Calcitonin gene-related peptide
CM	Central medial thalamic nucleus
COAa	Cortical amygdalar nucleus, anterior part
COApl	Cortical amygdalar nucleus, posterior part, lateral zone
COApm	Cortical amygdalar nucleus, posterior part, medial zone
CP	Caudoputamen
cpd	Cerebral peduncle
ddp	Dorsal descending pathway
DMH	Dorsomedial hypothalamic nucleus
ENTl	Entorhinal area, lateral part
ENTm	Entorhinal area, medial part, dorsal zone
EPd	Endopiriform nucleus, dorsal part
EPv	Endopiriform nucleus, ventral part
FG	Fluorogold
FS	Fundus striatum
fx	Columns of the fornix
GABA	Gamma-aminobutyric acid
GAD	Glutamic acid decarboxylase
GP	Globus pallidus
GRN	Gigantocellular reticular nucleus
IA	Intercaleted amygdalar nuclei
ic	Internal capsule
IC	Insular cortex
LA	Lateral amygdalar nucleus
LDT	Laterodorsal tegmental nucleus
LHA	Lateral hypothalamic area
LHApfx	Lateral hypothalamic area, perifonical region
LHAvl	Lateral hypothalamic area, ventral region, lateral zone
LRN	Lateral reticular nucleus
LS	Lateral septal nucleus
MA	Magnocellular preoptic nucleus
MCH	Melanin-concentrating hormone
MD	Mediodorsal thalamic nucleus
MDRN	Medullary reticular nucleus
MEA	Medial amygdalar nucleus
MEApv	Medial amygdalar nucleus, posteroventral part
mfb	Medial forebrain bundle
MG	Medial geniculate complex
MRN	Mesencephalic reticular nucleus
MS	Medial septal nucleus
mtt	Mammillothalamic tract
NDB	Diagonal band nucleus
NG	Nucleus gemini
NLOT	Nucleus of the lateral olfactory tract
NTS	Nucleus of the solitary tract
opt	Optic tract
OT	Olfactory tubercle
PA	Posterior amygdalar nucleus
PAG	Periaqueductal gray
PARN	Parvicellular reticular nucleus
PB	Parabrachial nucleus
PH	Posterior hypothalamic nucleus
PHAL	*Phaseolus vulgaris* leucoagglutinin
PIR	Piriform area
PMv	Ventral premammillary nucleus
POR	Periolivary region
PRN	Pontine reticular nucleus
PV	Parvalbumin
PV1/parvafox	Parvalbumin-positive (PV1) nucleus/ parvafox nucleus
PVH	Paraventricular hypothalamic nucleus
PVHlp-f	Paraventricular hypothalamic nucleus, lateral parvicellular part–forniceal part
PVT	Paraventricular thalamic nucleus
PSTN	Parasubthalamic nucleus
PSV	Principal sensory nucleus of the trigeminal
RE	Nucleus reuniens
RH	Rhomboid nucleus
RM	Nucleus raphe magnus
SC	Superior colliculus
SI	Substantia innominate
sm	Stria medullaris
SN	Substantia nigra
SO	Supraoptic nucleus
SPVI	Spinal nucleus of the trigeminal, interpolar part
st	Stria terminalis
STN	Subthalamic nucleus
SUM	Supramammillary nucleus
Sup	Supraoptic commissures
TU	Tuberal nucleus
V	Motor nucleus of the trigeminal nerve
VII	Facial nucleus
vlah	Ventrolateral amygdalo-hypothalamic pathway
vlt	Ventrolateral hypothalamic tract
VMH	Ventromedial hypothalamic nucleus
VP	Ventral pallidum
VTA	Ventral tegmental area
ZI	Zona incerta

Introduction

Although the anatomy of the mammalian hypothalamus is thought to be quite settled, anatomists know that mysterious and still unsuspected cell groups in this complex region

await discovery and characterization. Cytoarchitecture was the essential criterion during most of the 20th century. However, histological advances tied to neurochemistry and tract tracing have provided new ways to identify and characterize specific cell groups. These cell groups may be scattered through large volumes of hypothalamic tissue, such as neurons producing melanin-concentrating hormone (MCH) or hypocretin in the lateral hypothalamic area (LHA) (Croizier et al. 2013). They may also form discrete but subtly differentiated nuclei. Two such examples are the PV1/parvafox nucleus described by Celio's and Alvarez-Bolado's groups (Celio 1990; Mészár et al. 2012; Celio et al. 2013; Bilella et al. 2014, 2016a) and the parasubthalamic nucleus (PSTN) identified in the rodent primarily on the basis of substance P expression (Wang and Zhang 1995; Goto and Swanson 2004). This last nucleus has attracted our attention, in part, because it is intensely connected with the amygdala and receives very distinct calcitonin gene-related peptide (CGRP) projections from the parabrachial nucleus (PB) (Chometton et al. 2016). Adjacent to the PV1 and PSTN, we observed a small cell group labeled by antibodies against calbindin (Cb). We named this cell group the calbindin nucleus (CbN), with reference to the PV1/parvafox nucleus, although it partially corresponds to the ventrolateral part of the LHA (LHAvl) of Swanson's Brain Maps (Swanson 2004). The CbN appears to be associated with the PSTN, because both nuclei receive a dense CGRP input from the PB and project to the central nucleus of the amygdala (CEA) (Chometton et al. 2016). These connections between the amygdala and the region of the LHA that contains the PSTN/CbN have been reported several times in the literature (Krettek and Price 1978; Ottersen 1980; Veening et al. 1982; Ono et al. 1985; Gonzales and Chesselet 1990; Canteras et al. 1995; Petrovich et al. 1996; Petrovich and Swanson 1997; Bourgeais et al. 2001; Tsumori et al. 2006; Niu et al. 2012; Chometton et al. 2016), although they have not yet been carefully analyzed. Functionally, they might be part of a circuit involved in controlling appetite (Carter et al. 2013, 2015; Campos et al. 2016; Zséli et al. 2016).

The aim of the present article is, therefore, to analyze specific projections from amygdalar nuclei in the PSTN/CbN complex, with an emphasis on the CbN and on Cb expression but also with attention to the distribution of CGRP projections in the caudal LHA. This work will lead to a better characterization of both the PSTN and the CbN and of the posterior lateral hypothalamus in the rat brain, which we refer to as the premammillary LHA region and that corresponds to a glutamic acid decarboxylase (GAD) free region sitting caudal to MCH/GAD rich LHA regions (Chometton et al. 2016). This work also shows that projections from amygdalar nuclei in the LHA take two distinct routes: a dorsal pathway and a ventral "olfactory" pathway that is adjacent to, but distinct from the ventrolateral hypothalamic tract (vlt).

Materials and methods

Animals

All animal use and care protocols were in accordance with institutional guidelines, and the investigators were authorized. All animal protocols were carried out in accordance with the Directive 2010/63/EU of the European Parliament and of the Council of 22 September 2010 on the protection of animals used for scientific purposes and were approved by Franche-Comté University's Animal Care Committee (protocol number: 2015-002). Twenty Sprague–Dawley male rats, each weighing 300–350 g, were obtained from Janvier (Le Genest-Saint-Isle, France). Rats were housed with a standard 12 h light/dark cycle at a constant room temperature and had free access to the standard laboratory diet and water.

Tracer injections

Rats were anesthetized with an intraperitoneal (i.p.) injection of a mixture of xylazine and ketamine (1 mg/100 g and 10 mg/100 g of body weight, respectively; Vetoquinol®, France) and placed in a stereotaxic device.

Retrograde tracer into the PSTN

Rats received a unilateral iontophoretic injection of 10% solution of fluorogold (FG) (Interchim®) diluted in 0.9% sodium chloride (NaCl) into the PSTN. Coordinates were taken from Bregma using the Paxinos' atlas (Paxinos and Watson 2005). For the PSTN, the coordinates are AP: −4.2 mm, ML: 1.5 mm, DV: −8.4 mm. A glass micropipette (tip diameter: 30–50 µm) was used to inject the FG iontophoretically into this region (intermittent current of 5 mA and 7 s on/off time for 5 min). To avoid FG diffusion along the micropipette track, the micropipette was left in place for another 5 min before being removed.

Anterograde tracer into the amygdala and neighboring telencephalon

Rats received a unilateral iontophoretic injection of 2.5% *Phaseolus vulgaris* leucoagglutinin (PHAL) (Vector®) diluted in sodium phosphate buffer saline (NaPBS) pH 7.2. Glass micropipettes were used to inject the PHAL iontophoretically into the anterior part of the basomedial nucleus of the amygdala (BMAa), into the medial part of the central nucleus of the amygdala (CEAm) and into the fundus

striatum (FS) using an intermittent current (5 mA; 7 s on/off time for 20 min). For the CEA, the coordinates were AP: −1.4 mm, ML: 4 mm, DV: −7.5 mm; AP: −1.4 mm, ML: 4 mm, DV: −8 mm; for the basomedial nucleus of the amygdala (BMA), the coordinates were AP: −1.5 mm, ML: 4 mm, DV: −9 mm and for the FS, the coordinates were AP: −0.8 mm, ML: 4 mm, DV: −7.5 mm. The micropipette was left in place for another 5 min before being removed.

At 10–15 days after the injection, the rat brain was removed, frozen, cut, and processed for immunohistochemistry, as described in the following.

Tissue preparation

Rats were deeply anesthetized with an i.p. injection of Pentobarbital (CEVA®, 50 mg/kg). Animals were perfused transcardially with 0.9% NaCl, followed by ice-cold 4% paraformaldehyde (PFA, Roth®) fixative in 0.1 M phosphate buffer (PB) at pH 7.4. Brains were extracted, post-fixed for 20 h in the same fixative at 4 °C, and cryoprotected by saturation in a 15% sucrose solution (Sigma®) in 0.1 M PB for 24 h at 4 °C. Tissues were cut in four series of coronal sections at 30 µm thick, collected in a cryoprotective solution [1:1:2 glycerol/ethylene glycol/ phosphate buffer saline (PBS)], and stored at −40 °C.

Enzymatic immunohistochemistry

Free-floating sections were incubated with primary anti-FG or anti-PHAL antibodies (Table 1) dissolved in PBS at pH 7.4 containing 0.3% Triton X-100 (PBS-T), 1% bovine serum albumin, 10% lactoproteins, and 0.01% sodium azide for 48 h at 4 °C. Then, tissues were incubated for 4 h at room temperature in a solution of biotinylated goat anti-rabbit IgG (Vector Laboratories®) at a dilution of 1:1000 in PBS-T. Sections were placed in the mixed avidin–biotin horseradish peroxidase (HRP) complex solution with PBS (ABC Elite Kit, Vector Laboratories®) for 1 h at room temperature. The peroxidase complex was visualized by an exposure to a chromogen solution containing 0.04% 3,3′-diaminobenzidine tetrahydrochloride (DAB, Sigma®) with 0.006% hydrogen peroxide (Sigma®) in PBS. The reaction was stopped by extensive washing in PBS when the labeling was satisfactory. Sections were mounted on gelatin-coated slides, and then dehydrated and coverslipped with Canada balsam (Roth®). An adjacent series was always stained in a solution of 1% toluidine blue (Roth®) in water to serve as a reference series for cytoarchitectonic purposes.

Triple immunofluorescent staining

After rinsing in PBS-T, free-floating sections were incubated with primary antibodies (Table 1) dissolved in PBS-T, 1% bovine serum albumin, 10% lactoproteins, and 0.01% sodium azide or only in PBS-T for 24 h at 4 °C. Tissues were washed three times with PBS-T (5 min each) and incubated for 2 h with secondary antibodies diluted in PBS-T (Table 2) at room temperature. For triple labeling, this procedure was repeated twice with primaries raised in different species (Table 1). Finally, sections were washed with PBS-T, mounted on gelatin-coated slides, and coverslipped with 60/40 glycerol: PBS-T.

Image acquisition and processing

Sections were analyzed on an ApoTome.2 microscope (Axio Imager Zeiss), and images were obtained through a numeric camera (Digital Camera Hamamatsu C11440) using the Imager.Z2 software (Zen 2).

Table 2 Fluorescent secondary antibodies used in this study

Antibody	Type	Source	Dilution
Alexa Fluor 488	Anti-rabbit IgG	Invitrogen®, goat, A11034, Lot 1141875	1:1000
Cyanine 5	Anti-mouse IgG	Donkey, A31570	1:500
Cyanine 3	Anti-goat IgG	Donkey	1:1000

Table 1 Primary antibodies used in this study

Antibody	Type	Source	Dilution
Calbindin (Cb) (mouse)	Monoclonal	Swant	1:1000
α-Calretinin (rabbit)	Polyclonal	Swant	1:5000
CGRP (rabbit)	Polyclonal	Our laboratory, (Risold et al. 1992)	1:1000
Fluorogold (FG) (rabbit)	Polyclonal	Millipore	1:3000
PHAL (rabbit and goat)	Polyclonal	Vector Laboratories	1:1000
Parvalbumin (PV) (mouse)	Monoclonal	Swant	1:1000

Pictures were taken using regular epifluorescence and the advanced features "Z-Stack" and "Deconvolution" of the Zen software. No additional processing was performed, except to correct the fluorescence intensity.

Semi-quantitative analysis of the ABC peroxidase signal was performed by the experimenter using the free software ImageJ. The following procedure was followed: black and white pictures of the brain region were taken using the 10× objective. The regions were the CEAm [level 27 of the Swanson's Brain maps (Swanson 2004)], the bed nuclei of the stria terminalis (BST) (level 19), the perifonical region of the lateral hypothalamic area (LHApfx) (level 29), PSTN (level 33), CbN (level 31), and the nucleus of the solitary tract (NTS) (level 63). Images were then binarised by ImageJ, using the same threshold for each picture. A rectangle of 0.015 mm^2 was defined as a region of interest (ROI) and was placed over the structure of interest, where the signal was the most intense to the experimenter judgment. Then, the software determined the area occupied by the signal within the ROI. The results were then reported as a percentage of the total surface of the ROI.

Nomenclature and nuclear parcellation are from Swanson (2004), except for the premammillary LHA region that contains the PSTN/CbN, for which we used the parcellation of Chometton et al. (2016) (see Fig. 1).

Results

Distribution of retrogradely labeled neurons in the amygdala after fluorogold injection into the PSTN/CbN

In a previous report (Chometton et al. 2016), an illustration of the distribution of retrogradely labeled neurons in the central nervous system was provided after retrograde tracer injections in the PSTN. That report was quite succinct for the amygdala, and a more detailed account of the distribution of retrogradely labeled neurons in this region of the telencephalon after PSTN fluorogold injection is provided here.

Fluorogold injection sites in the PSTN/CbN complex

A total of seven FG injections were obtained in the region of the PSTN/CbN complex (Fig. 1). Because of the small size of these nuclei, none were completely restricted to one or the other or both, but the halo of diffusion extended into adjacent structures, such as the subthalamic nucleus (STN) or the surrounding LHA and nucleus gemini (NG). The caudal-most injection (3FG) extended into the ventral tegmental area (VTA). Of all these injections, only the 7FG experiment involved the CbN significantly more than the PSTN, but it also contaminated the adjacent cerebral peduncle (cpd), and retrograde signal could be seen in locations, such as the dorsal caudoputamen, clearly indicating that the injection site was not restricted to the CbN.

The illustration of the distribution of retrogradely labeled cells in Fig. 2 is based on the 6FG experiment. This selection was made, because the injection site is centered in the PSTN and does not extend into the STN, while the halo in the adjacent LHA, NG, and zona incerta suggested minimal transport from these regions. However, our description in the text is based on observations made in all seven experiments, as the patterns of retrogradely labeled cells in the amygdala were very similar, with some differences for the more ventral 7FG experiment.

Distribution of fluorogold labeled cells in the amygdala

For all the experiments with an injection site centered in the PSTN, the CEAm contained the greatest concentration of retrogradely labeled cells (Fig. 2). In contrast, the lateral part of the CEA (CEAl) contained very few retrogradely labeled cells (Fig. 2d–f). Labeled cells were slightly more abundant in the capsular part than in the lateral part, but there were still very few compared to the CEAm (Fig. 2b–f). Medially to the CEAm, the substantia innominata (SI) contained very large numbers of FG-containing neurons. In fact, retrogradely labeled cells seemed to be distributed through the CEAm and adjacent SI with a gradient in favor of the CEAm. The morphology of labeled cells was very similar between the CEAm and the SI. Consequently, borders between these two structures were not clear when based only on the distribution and aspect of FG-labeled cells.

In an attempt to identify the phenotypes of retrogradely labeled neurons, indirect immunofluorescence was performed on sections passing through the CEAm. Some neurons containing FG were found to be labeled by the calretinin antibody (Fig. 3). Other attempts were made using corticotropin-releasing hormone (CRH) and somatostatin antibodies, but cells expressing these peptides are mostly in the CEAl and no-double labeled neurons were observed (data not shown).

In addition to the CEAm, several other nuclei of the amygdala, including the anterior amygdala area, the BMAa, and the anterior part of the cortical nucleus of the amygdala (COAa), contained significant numbers of FG-labeled cells. These cells were particularly abundant in the BMAa and COAa in the 7FG experiment. However, this experiment showed a large contamination of the adjacent cpd, and many cells could be seen in the caudoputamen and the globus pallidus. The medial amygdalar nucleus (MEA), mostly its anterior parts, also contained some retrogradely labeled cells, and scattered neurons were found in the posterior

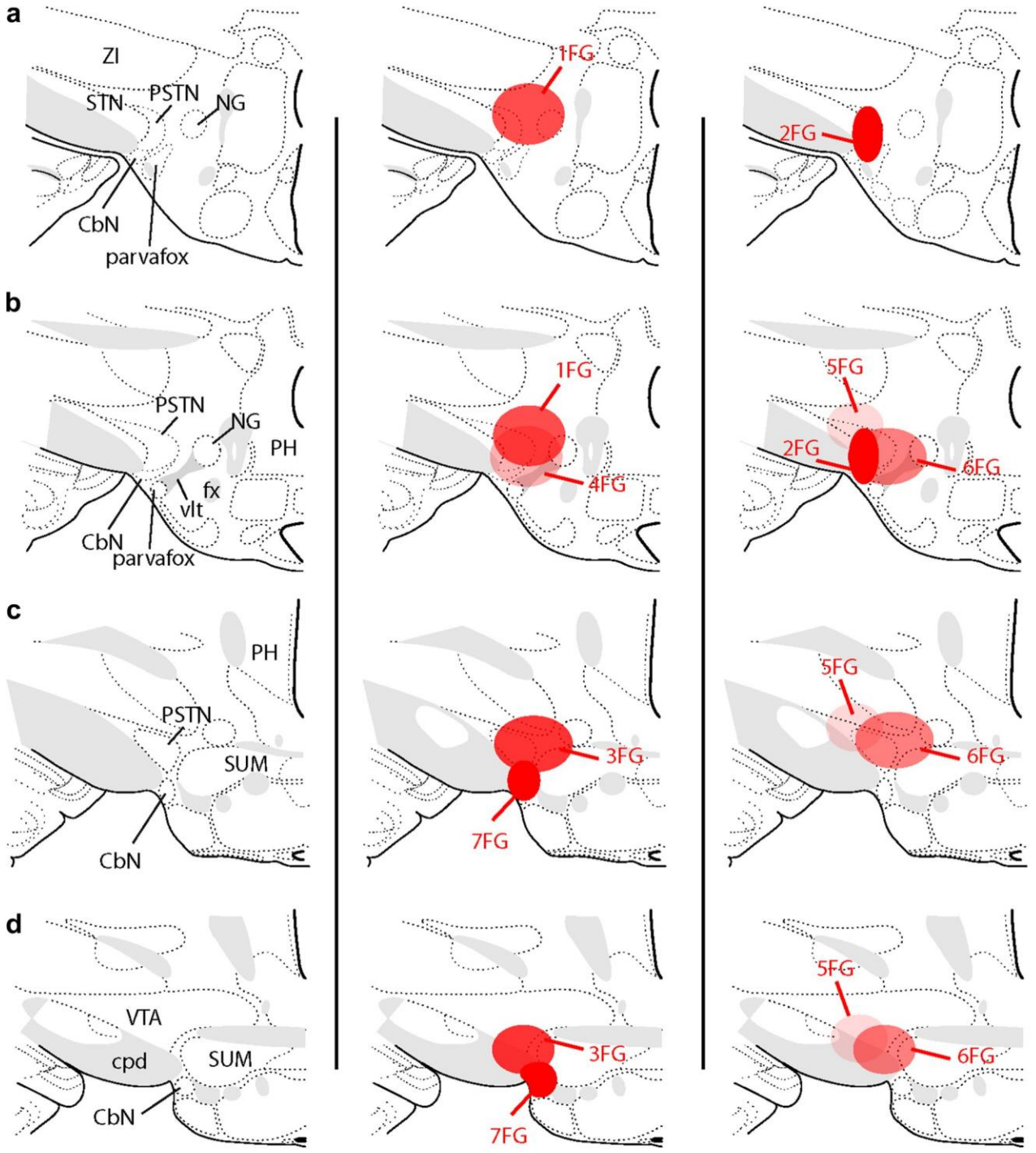

Fig. 1 Line drawings of coronal sections passing through the PSTN/CbN region, arranged from rostral (**a**) to caudal (**d**) and illustrating the FG injection sites in the region of the PSTN/CbN. The parcellation of the PSTN/CbN is from Chometton et al. (2016)

part of the basomedial amygdalar nucleus (BMAp) and in the basolateral amygdalar complex (BLA). In these last nuclei, retrogradely labeled cells were more abundant after injection at a ventral site (7FG). Finally, some cells were also observed in the FS rostral to the CEAm, especially when the injection site was close to the STN (1FG, 5FG).

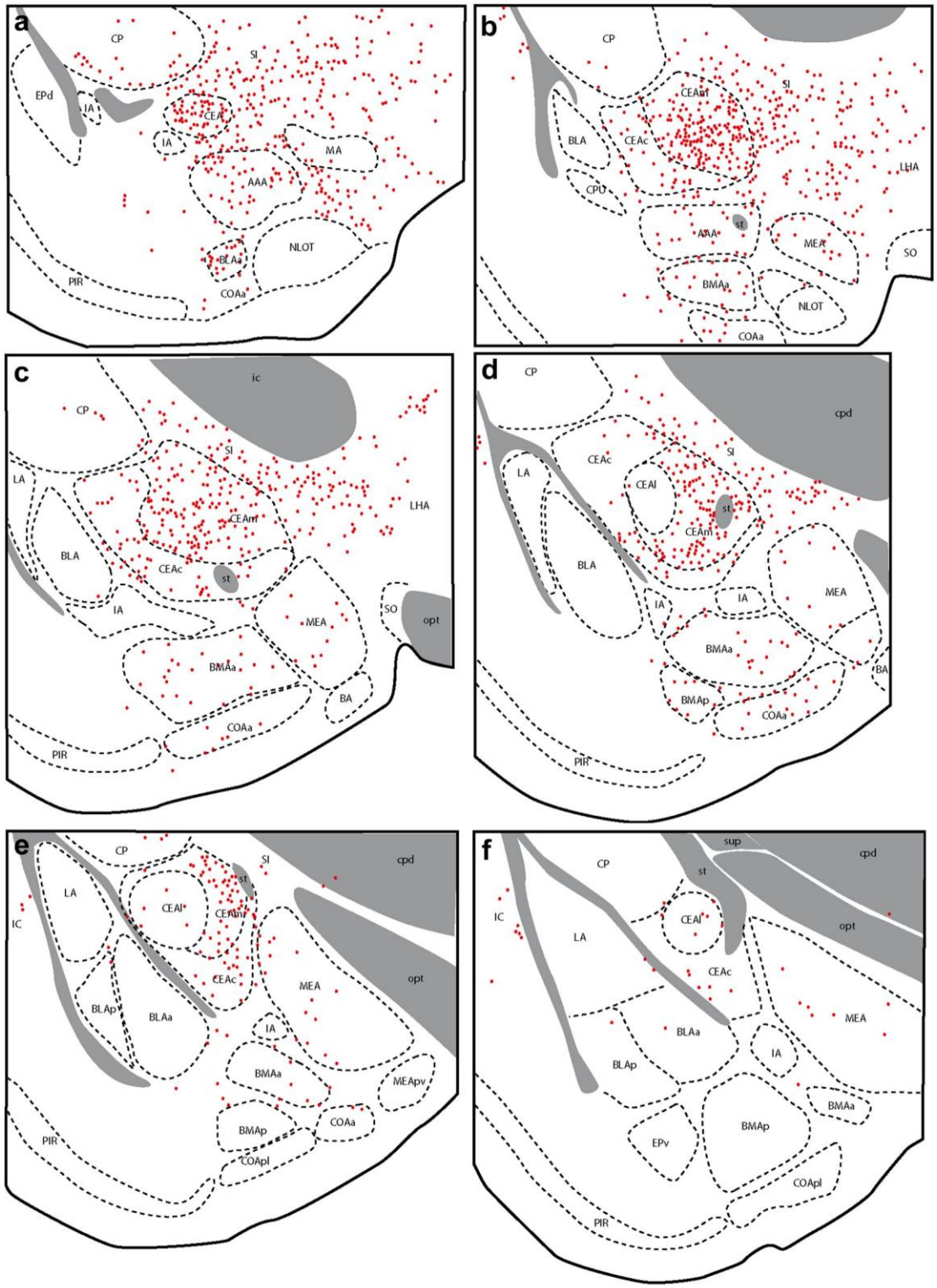

Fig. 2 Line drawings of coronal sections passing through the amygdala, arranged from rostral (**a**) to caudal (**f**) and illustrating the distribution of retrogradely labeled cells (containing the FG) in the amygdala in experiment 6FG

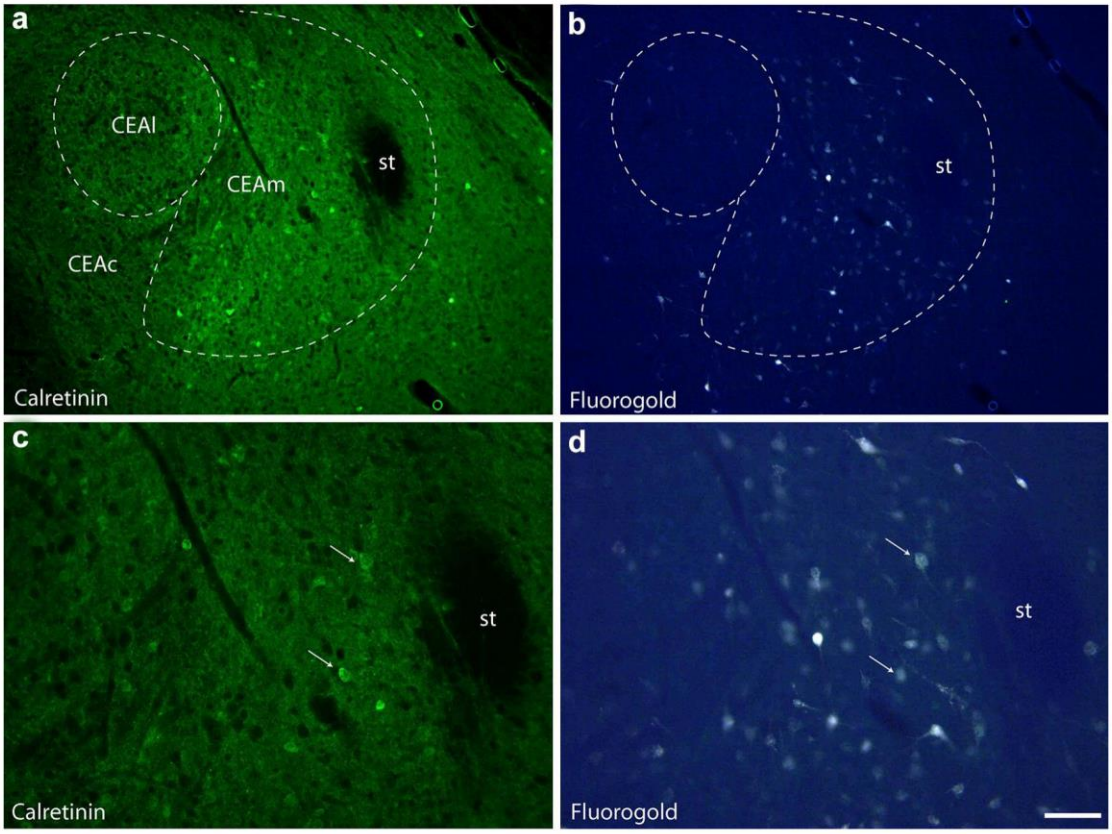

Fig. 3 Photomicrographs of calretinin-labeled perikarya using indirect immunofluorescence (**a**) and the same section with FG-retrogradely labeled neurons (**b**) after an FG injection in the PSTN (experiment 6FG). Note that numerous FG cell bodies are observed in the CEAm. **c, d** At higher magnification, some calretinin-expressing cells also contain FG (*arrows*). However, double labeled neurons are only a fraction of all retrogradely labeled neurons. *Scale bar* in **d** 100 µm (**a, b**) or 50 µm (**c, d**)

Distribution in the lateral hypothalamic area of PHAL-labeled projections from the medial part of the central amygdalar nucleus or the anterior part of the basomedial amygdalar nucleus

To confirm the projections from the amygdala into the PSTN/CbN complex and to identify pathways taken by the axons, PHAL was injected into the amygdala, particularly aiming at the CEA and BMAa.

PHAL injection sites

Twelve PHAL injections were obtained (Fig. 4), among which eight were in the amygdala, three in the FS, and one in the caudal dorsal piriform cortex. In the amygdala, injection sites involved several nuclei that contained retrograde labeling after the FG PSTN injections.

In one experiment (AMY1, Fig. 4b, d), the injection site was centered in the CEAm, with a few cells in the capsular part of the central amygdalar nucleus (CEAc) and the CEAl. In the experiment AMY3 (Fig. 4c, e), the site was centered in the BMAa, with negligible involvement of the dorsally adjacent intercalated nucleus of the amygdala.

Among the other injections, two (AMY2 and 7) were in the CEAc, one in the BMAa/BMAp (AMY5), and one in the posterior part of the basolateral nuclear amygdala (BLAp) (AMY8).

Of all these experiments, AMY1 and 3 were at the origin of the most abundant projections in the PSTN/CbN complex and are described in the following.

Aspects of PHAL-labeled axons

PHAL is an anterograde tracer used for more than 30 years, because it has the great advantage to entirely fill the axons of the labeled cells, showing their finest details. Figure 5 illustrates aspects of such PHAL-labeled axons and will serve to explain the nomenclature used in the following descriptions, as well as to provide a scale for terms as 'weak', 'moderate', or 'intense' innervations or again to explain some technical terms, such as passing fibers or axons, boutons-of-passage, and pericellular nets.

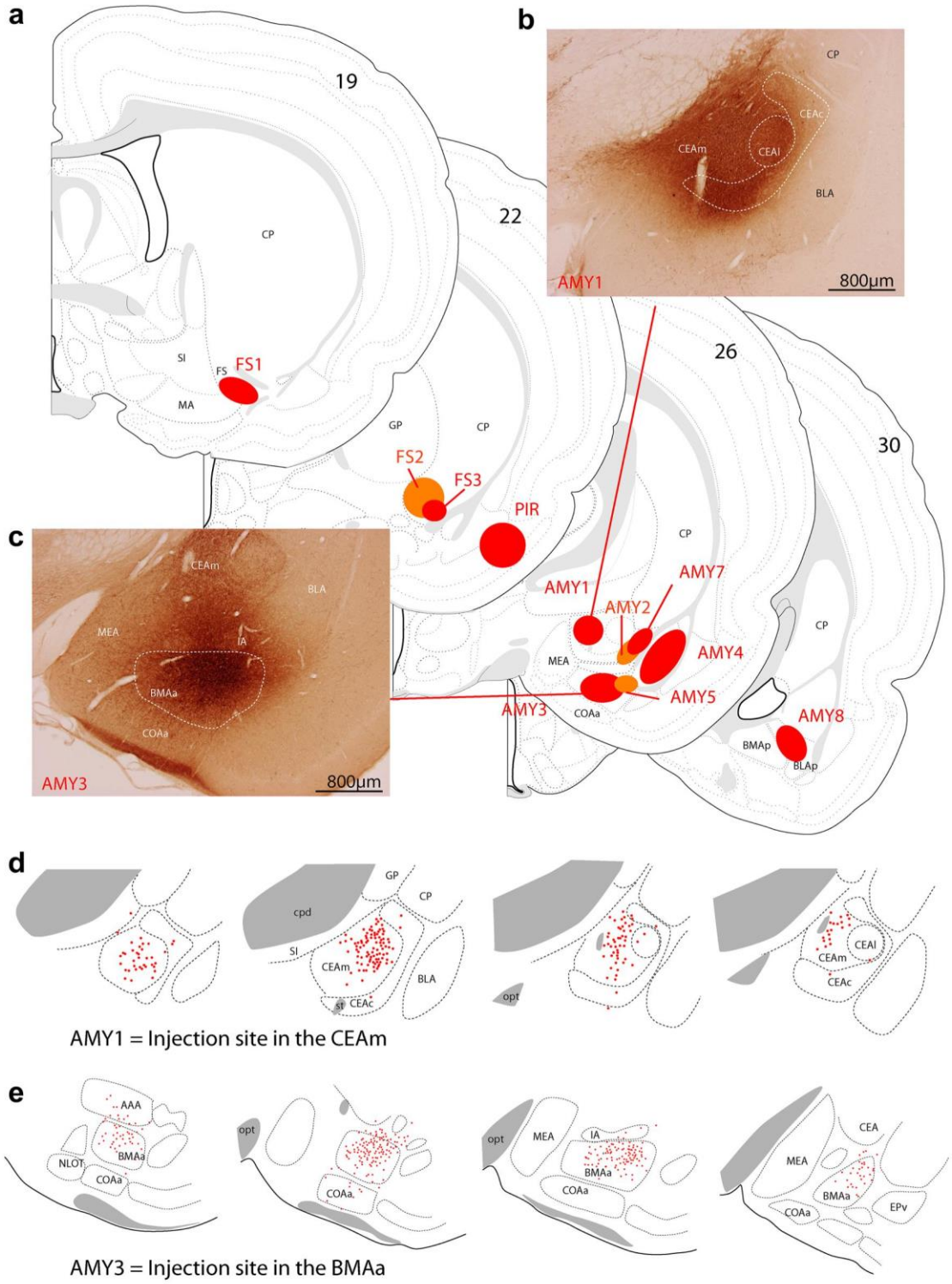

Fig. 4 **a** Line drawings illustrating the PHAL injection sites in the ventral telencephalon. **b, c** Photomicrographs of the injection sites in experiments AMY1 and AMY3 and centered respectively in the CEAm and BMAa. **d** Line drawings illustrating the distribution of PHAL-labeled cells in experiment AMY1. **e** Line drawings illustrating the distribution of PHAL-labeled cells in experiment AMY3

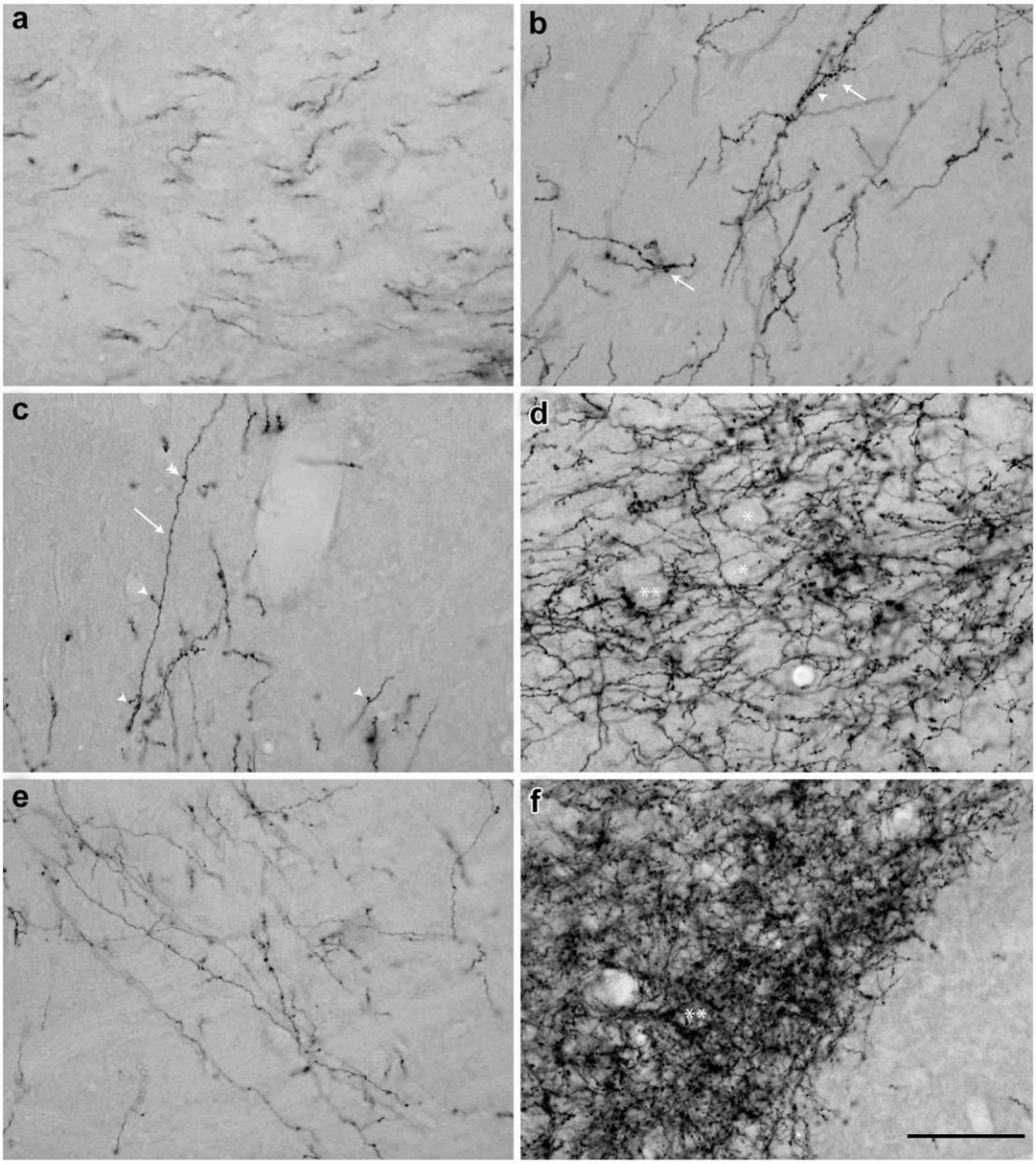

Fig. 5 Photomicrographs to illustrate aspects of PHAL axons. Aspects of axons passing without providing any input (**a**) or a weak "en passant" innervation (**c, e**). In **a**, axons run parallel to each other in the cpd. They are followed on a short distance, because they are cut in the coronal plan. In **b**, a typical axon-of-passage (*arrow*) can be seen displaying few boutons terminating a short collateral (*arrowheads*), and few varicosities (*double arrowhead*). Other similar axons are illustrated on **e. b, d, f** Example of axons providing an innervation. In **f**, we have an illustration of axons providing a weak innervation. Typically, those axons (*arrows*) show a very complex morphology upon arriving at the contact of the target. These axons suddenly ramify and exhibit chaplets of varicosities (*arrowhead*) as well as many collaterals with boutons. These axons are also thicker than surrounding passing axons. In **d**, the input provided by axons is more intense and can be qualified of moderate to intense. Labeled axons show complex morphologies, and they are difficult to individually follow. However, not all cells in the area are innervated. For example, the stars show empty shapes that may signal the location of cell bodies surrounded by axons but without any clear boutons at their immediate vicinity. Figures suggest that other cells (*double star*) are surrounded by complex axons with many varicosities and boutons. This picture was taken in the dorsal perifornical region in the LHA of experiment AMY1. In **f**, we illustrated a very dense or intense innervation of a structure. This is the PSTN in AMY1. It is impossible to follow individual axons as they have very complex morphologies. Furthermore, the picture appears fuzzy as most labeled elements cannot be on focus. Playing with the *z* on the microscope, we can see empty shapes resembling cell bodies (*double star*) completely surrounded by labeled boutons. *Scale bar* 50 µm

Pathways and innervation of the PSTN/CbN

Of all the PHAL experiments obtained in the amygdala, only injections centered in the CEAm and BMAa (AMY1 and AMY3) provided very intense anterograde labeling in the PSTN/CbN complex. The objective of the present work also includes analysis of the pathways in the lateral hypothalamus, but a full description of the anterograde labeling in the brain is beyond the scope of this paper. Nevertheless, the general patterns of distribution are illustrated in Fig. 6 and can then be compared to other reports after anterograde tracer injections in the CEA (Veening et al. 1982, 1984; Gray et al. 1989; Petrovich and Swanson 1997; Bourgeais et al. 2001; Oka et al. 2008; Shirasu et al. 2011) or BMAa (Petrovich et al. 1996; Niu et al. 2012).

From the anterior part of the basomedial amygdalar nucleus The distribution of PHAL axons from the BMAa in our experiment AMY3 was virtually identical to that described by Petrovich et al. (1996), with innervation of the cerebral cortex, including insular, perirhinal, transitional areas. Intense projection in the CEAm was also noted (Figs. 4c, 6d, e).

The LHA is innervated mostly by projections that pass through the ansa peduncularis. PHAL axons that followed this pathway formed a compact bundle in the SI (Fig. 6c, d). At level 27 of the Swanson's Brain maps (Swanson 2004), they joined axons that directly exited the CEAm to enter the LHA just dorsal to the optic tract and the supraoptic commissures (Figs. 6e, 7d). This bundle runs laterally to the vlt. Few boutons were observed. Axons run parallel to each other and resemble 'axons of passage' (Fig. 7f).

More caudally, roughly corresponding to levels 28–29 from the Brain Maps (Corresponding to the rostral tuberal area; Swanson 2004) (Figs. 6f, 8d–f), the bundle is still very clear and follows a route parallel and immediately lateral to the vlt. Very few axons coursed within the vlt. An India ink drawing of axons illustrates that they display more boutons and short collaterals (Fig. 8f) indicating that they may provide a weak innervation. A few of these axons also either arched dorsomedially to reach the perifornical region or took a more ventromedial direction to innervate the tuberal nucleus.

With more caudal sections (level 30—caudal tuberal area; Fig. 9d, e), the appearance of the axons clearly suggested an innervation of cell bodies along the path. Adjacent Nissl-stained sections revealed that this region corresponds to the CbN, as it contained a cluster of small neurons characteristic of this nucleus. This point will be better illustrated in the following (part 3 of the results).

In the posterior hypothalamus [premammillary level—close to level 33 from Swanson's Brain Maps (Swanson 2004)], more axons were observed with a dorsal orientation. They participated in a moderate innervation of the PSTN, while the CbN was intensely innervated (Fig. 10c, d). Caudal to the hypothalamus, few axons entered the VTA. This structure received sparse inputs (Fig. 6), and the caudal brainstem was largely empty. Therefore, we must deduce that most of the axons terminated in the CbN and to a lesser extent in the PSTN.

From the medial part of the central amygdalar nucleus The injection site in the experiment AMY1 was centered in the CEAm and showed a very negligible contamination of the CEAl/CEAc (Fig. 4d). Projections to other nuclei of the amygdala and to the temporal lobe of the cerebral cortex were sparse (Fig. 6). Basal forebrain structures, such as the FS and large parts of the SI, were innervated in a pattern similar to that described for the BMAa (Fig. 6a–c). In the BST, several nuclei were very heavily innervated, including the oval, juxtacapsular and fusiform nuclei.

In the LHA, projections from the CEAm followed two distinct routes. At level 27 of Swanson's Brain Maps (Swanson 2004), the ventral pathway that was described above for the BMAa was also taken by axons from the CEAm (Figs. 6e, 7a–c). However, a larger bundle of axons followed a more dorsal route in the LHA, dorsally adjacent to the cpd. These axons also diverged from the ansa peduncularis or the stria terminalis (st) (Fig. 6c, d), but they followed the internal capsule and cpd at anterior hypothalamic levels. Therefore, at this level, a dorsal and a ventral pathway reaching the hypothalamus appeared very clear, as they were segregated. At the same level, a bundle of axons entered the paraventricular hypothalamic nucleus (PVH) through its lateral parvicellular and forniceal parts. This input to the PVH was provided by axons from the dorsal pathway. Only caudal parts of the PVH were innervated, as rostral parts contained only scattered axons.

At levels 28–29 (Figs. 6f, 8a–c), the two dorsal and ventral pathways were well labeled. However, many axons of the ventral pathway changed direction to join the more dorsal route (Fig. 8c). Many other axons followed a more medial direction and innervated the dorsal perifornical region. A close examination of the sections revealed that most of these axons innervating the perifornical LHA were issued from the dorsal pathway, with the ventral route being a minor contributor.

At the caudal tuberal level (level 30; Fig. 9a–c), the dorsal perifornical region was not innervated, but some axons entered the posterior hypothalamic nucleus to reach the periaqueductal gray (PAG) (Fig. 6). However, the dorsolateral LHA, adjacent to the cpd, received very intense innervation, especially neurons adjacent to the STN, which were completely surrounded by boutons. India ink drawings of axons of the ventral pathway again showed that many of the axons of the ventral route had adopted a dorsal orientation

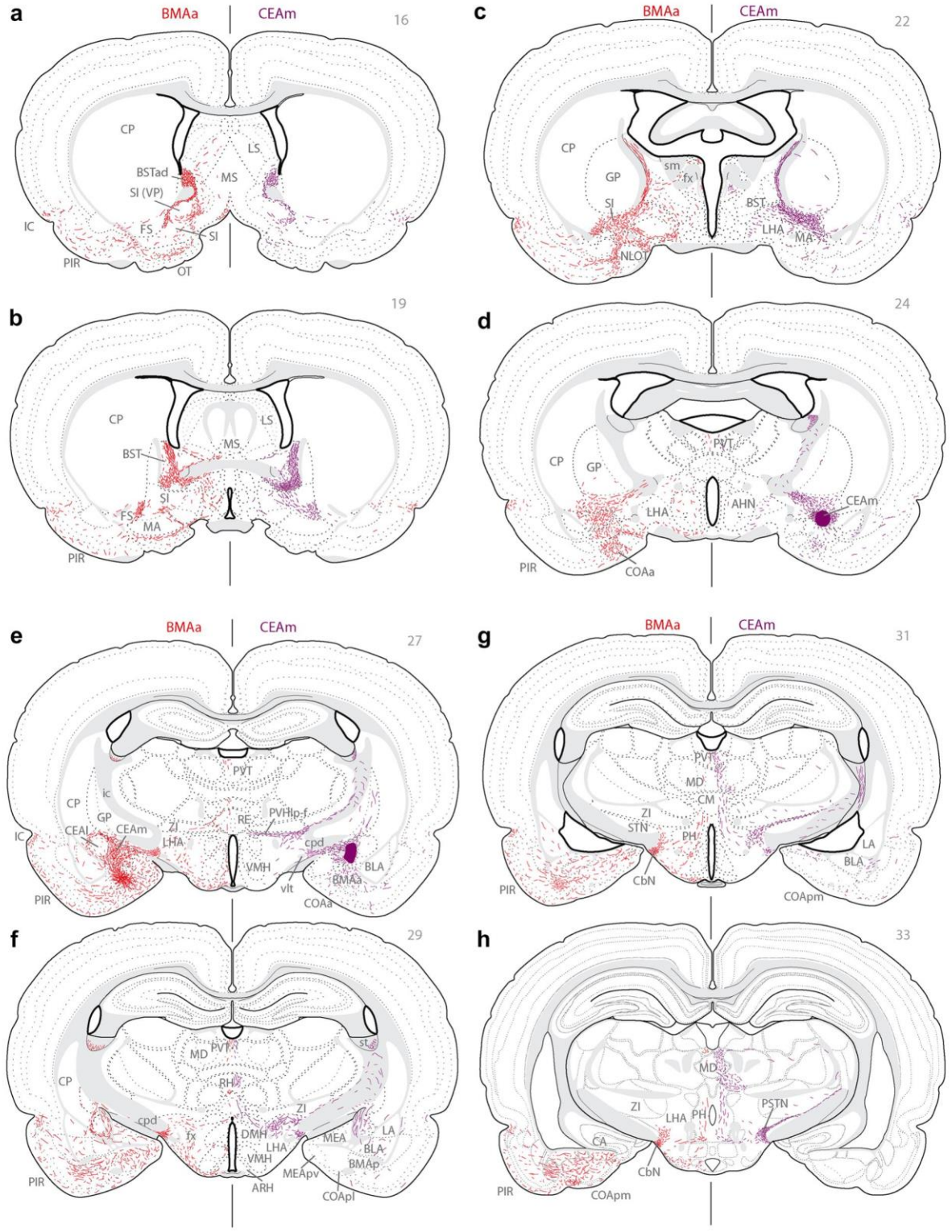

Fig. 6 Line drawings of coronal sections of the rat brain arranged from rostral (**a**) to caudal (**m**) and illustrating the distribution of PHAL-labeled axons in experiments AMY1 and AMY3. Projections labeled in experiment AMY3 (injection site centered in the BMAa) are illustrated on the *left side* of the line drawings, while projections labeled in experiment AMY1 (injection centered in the CEAm) are illustrated on the *right half* of each drawing. *Numbers in the right corner* of each drawing correspond to the atlas level in Brain Maps (Swanson 2004)

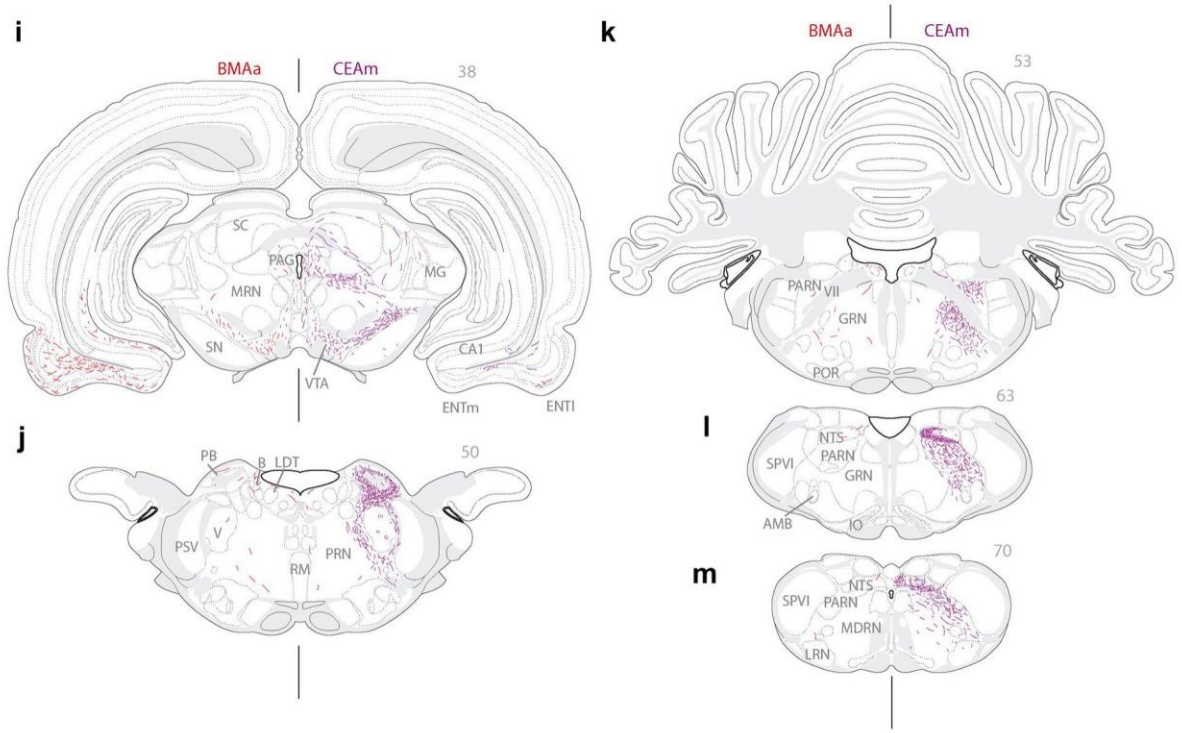

Fig. 6 (continued)

to reach the dorsal LHA region (Fig. 9c). This region could correspond to the very beginning of the PSTN, but Nissl staining on an adjacent section suggested that this level is still somewhat anterior to the cytoarchitectonic border of the nucleus. The presence of large and darkly Nissl-stained perikarya suggested the presence of MCH neurons which correspond to a level rostral to the PSTN per se (see Chometton et al. 2016). This would agree with the work of Nakamura et al. (2009), which showed that CEA projections to the caudal dorsal LHA innervate MCH neurons adjacent to the rostral tip of the STN [see Fig. 3d of Nakamura et al. (2009)]. In the ventral corner of the LHA, innervation of the CbN was obviously due to axons of the ventral pathway (see below).

At the premammillary level (Figs. 6h, 10a, b), the terminal field provided by PHAL axons in the dorsolateral LHA was very impressive, with clear pericellular nets. Cytoarchitecture in the adjacent Nissl-stained section showed that this innervation concerned the whole PSTN, but that areas closest to the STN were more densely targeted. The STN itself was completely spared by these projections. The innervation of the CbN by CEAm axons is less intense, although, at this level, many boutons were observed in this nucleus.

Finally, caudal to the premammillary level, axons of the dorsal pathway entered the ventral midbrain. Projections following this route provided an innervation of the pars compacta of the substantia nigra (Fig. 6i). Some continued and arched dorsomedially to reach the PAG (Fig. 6i). The PB and the anterior NTS received a very intense innervation (Fig. 6l). These last projections from the CEAm have frequently been described in the literature (Veening et al. 1982, 1984; Gray et al. 1989; Bourgeais et al. 2001; Oka et al. 2008; Shirasu et al. 2011).

Semi-quantitative analysis

The description of the PHAL projections from the injection sites in the BMAa and CEAm clearly suggested that the PSTN and the CbN contain densest projections in the hypothalamus and these projections might be as intense as those already well admitted and reported in innervated centers in the telencephalon and brainstem. An ROI in the form of a rectangle (150×100 µm; 0.015 mm^2) was chosen as to fit within the border of the smallest investigated region, the NTS. It was then applied over pictures of the section of the BST, perifornical LHA, PSTN, CbN, NTS, as well as CEAm only after BMAa injection. In each region, the ROI was placed, where the labeling was the densest and the surface taken by the labeling determined. The results are provided in Fig. 10e. They illustrate that the PSTN for the CEAm and the CbN for the BMAa contained dense projections, comparable to that

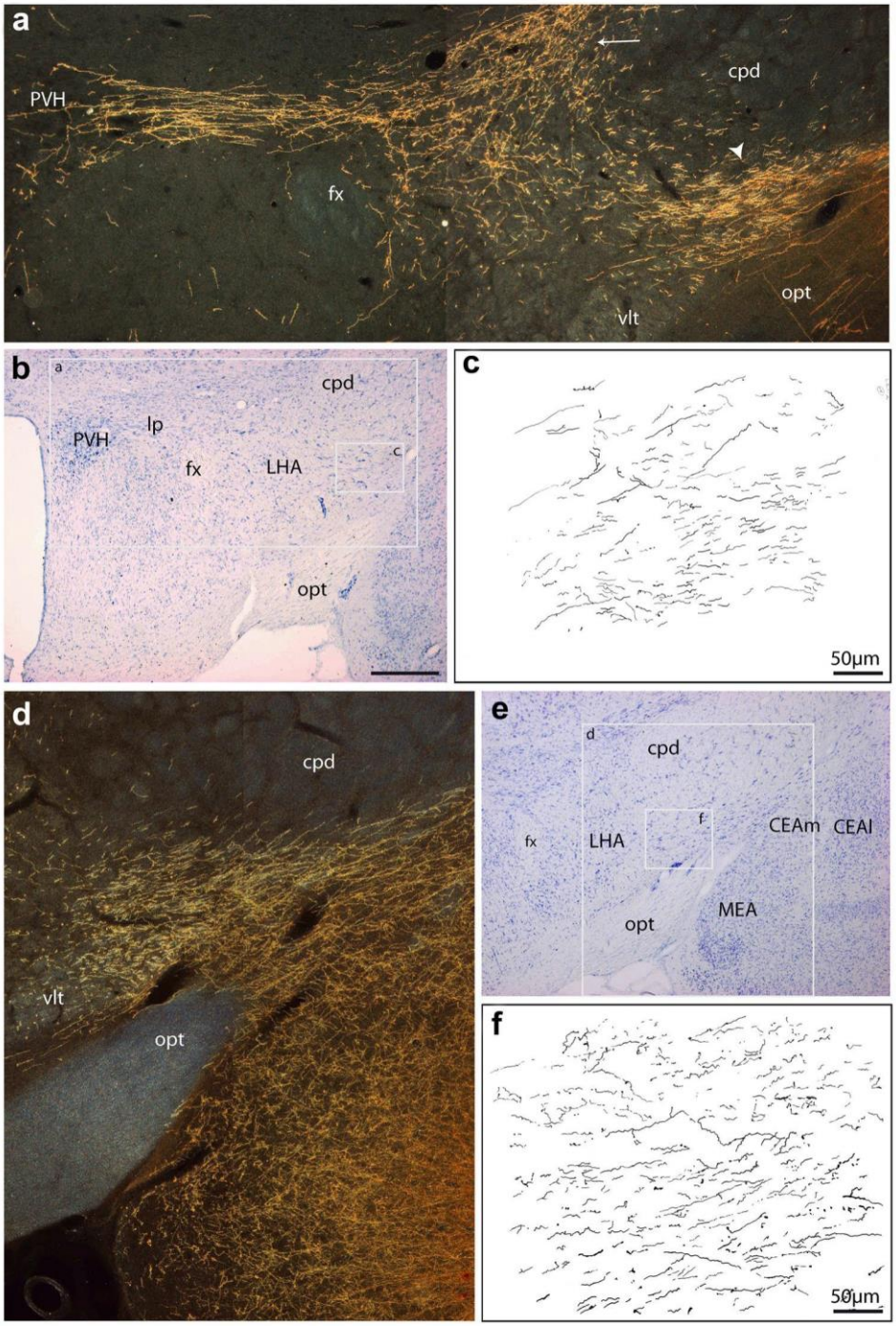

Fig. 7 Projections from the CEAm: darkfield photomicrograph (**a**) illustrating the distribution of PHAL axons in the LHA at the anterior hypothalamic level—level 27 in the Brain Maps (Swanson 2004). **b** Adjacent Nissl-stained section for cytoarchitectonic purposes. Axons enter this region following two pathways: a dorsal pathway (*arrow* in **a**) adjacent to the dorsomedial aspect of the cpd and formed of axons that followed ventral aspects of the internal capsule in the ansa peduncularis (see Fig. 6). Note that many axons enter the forniceal and lateral parvicellular parts of the PVH. A ventral pathway (*arrowhead*) formed of axons that enter the LHAvl between the optic tract and the cpd and coming directly from the injection site in the CEAm. The morphology of these axons is shown in an India ink drawing (**c**), and they mostly resemble axons of passage with few varicosities. Projections from the BMAa: darkfield photomicrograph (**d**) illustrating the distribution of PHAL axons in the LHA at the anterior hypothalamic level—level 27 in Brain Maps (Swanson 2004) and an adjacent Nissl-stained section (**e**) for cytoarchitectonic purposes. Axons enter this region following a ventral pathway in the LHA. They reach this region from the CEAm that is intensely innervated. India ink drawing of axons in the LHA at this level (**f**) shows that they also resemble axons of passage. *Scale bar* in **b** 500 μm for **b, e**; 250 μm for **a, d**

in the BST or NTS for the CEAm. Projections from the BMAa do not extend far beyond the CbN which then can be seen as containing terminals from this nucleus. This results associated with the aspect of the PHAL axons displaying many boutons and varicosities clearly signal the PSTN and CbN as major targets for the projections from the CEAm and the BMAa.

Control experiments

Other injections in the amygdala In all our experiments with an injection site in the amygdala, we observed at least a few fibers scattered through the medial forebrain bundle (mfb). After an injection in the CEAc (experiment AMY2), the ventral pathway was labeled, as well as the dorsal pathway, but far fewer axons were traced in the LHA compared

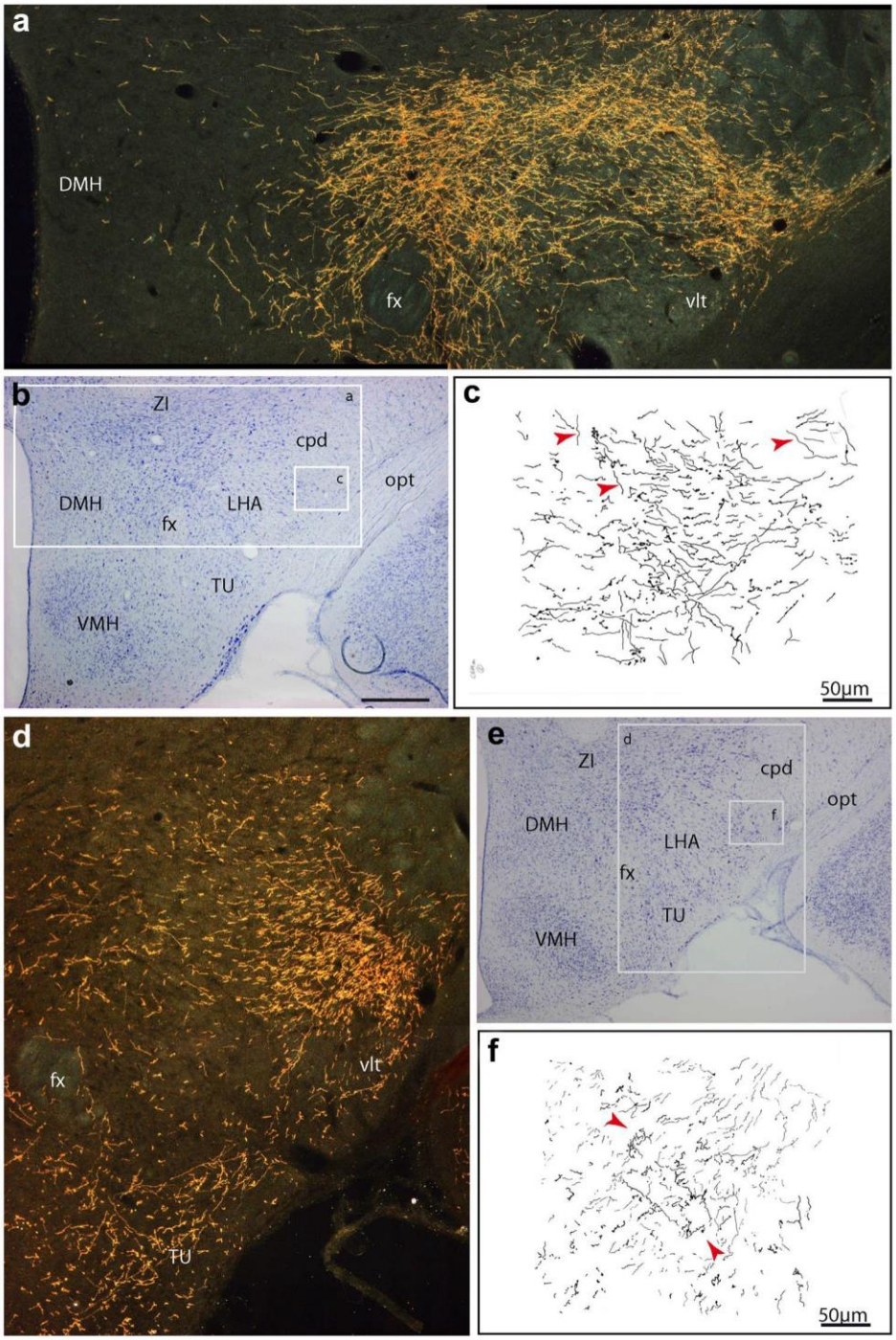

Fig. 8 Projections from the CEAm: darkfield photomicrograph (**a**) illustrating the distribution of PHAL axons in the LHA at the anterior tuberal hypothalamic level—level 28 in Brain Maps (Swanson 2004) and an adjacent Nissl-stained section (**b**) for cytoarchitectonic purposes. PHAL-labeled axons course through dorsal and ventral parts of the LHA. Some take a medial direction from these pathways and provide an innervation of dorsal perifornical regions. This innervation comes mostly from dorsal axons in the LHA. However, a close analysis (**c**) of the morphology and direction of axons in the ventral pathway show that some of them take a dorsomedial direction (*arrowheads*). Axons remaining in these ventral parts of the LHA display more varicosities than those at level 27, but they still mostly resemble fibers-of-passage. Projections from the BMAa: darkfield photomicrograph (**d**) illustrating the distribution of PHAL axons in the LHA at the anterior tuberal hypothalamic level—level 28 in Brain Maps (Swanson 2004) and an adjacent Nissl-stained section (**e**) for cytoarchitectonic purposes. Axons still mostly run through ventrolateral aspects of the LHA, forming a clear bundle immediately lateral to the vlt. Some leave this tract to innervate more medial parts of the ventral hypothalamus, including the tuberal nucleus. An India ink drawing of fibers in this ventral tract (**f**) shows that many still resemble fibers-of-passage, but some exhibit more complex morphologies with boutons (*arrowheads*), indicating that they innervate neurons along this path. *Scale bar* in **b** 500 µm for **b, e**; 250 µm for **a, d**

to the experiment AMY1 (CEAm). After the BLAp injection (AMY8), axons appeared scattered through the mfb and even in the vlt. Finally, we consistently observed axons taking a dorsomedial pathway to innervate the dorsal perifornical regions or the dorsal posterior hypothalamic area. In the experiment AMY8, more medial structures, such as the ventromedial hypothalamic nucleus, contained a moderate innervation (data not shown).

PSTN and CbN were very lightly innervated in all these experiments.

Injections into the fundus striatum Three injections were obtained in the FS. The experiment FS1 provided the strongest input to the LHA (Fig. 11). Axons from the injection site intensely innervated the CEAm (Fig. 11b), and some continued in the LHA. All along the path through

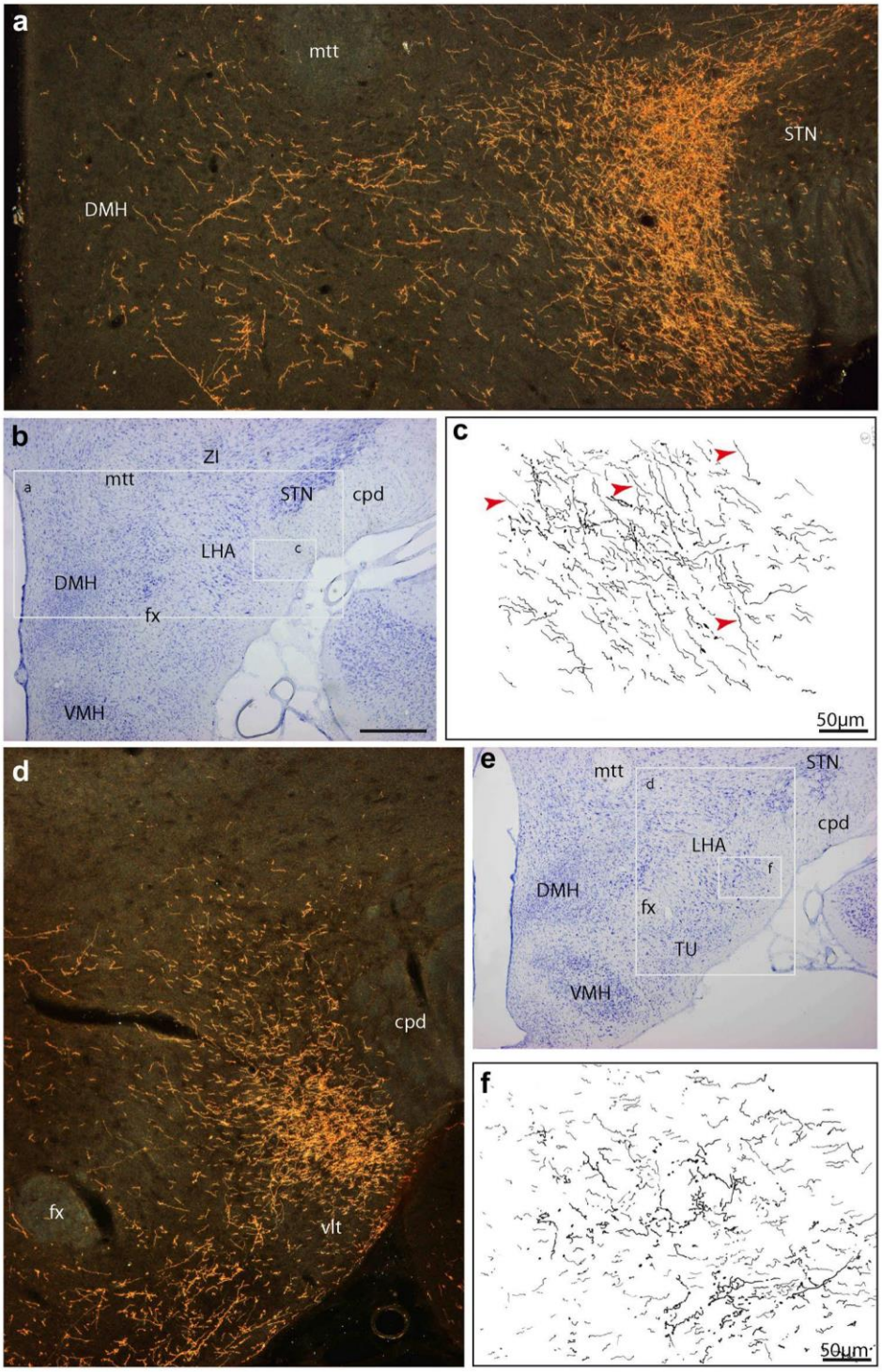

Fig. 9 Projections from the CEAm: darkfield photomicrograph (**a**) illustrating the distribution of PHAL axons in the LHA at posterior tuberal hypothalamic level—corresponding to level 30 in Brain Maps (Swanson 2004) and an adjacent Nissl-stained section (**b**) for cytoarchitectonic purposes. Most of the PHAL-labeled axons innervate a region in the far lateral LHA adjacent to rostral aspects of the STN. The perifornical region is no longer innervated, but axons run through more medial aspects of the mfb to reach the posterior hypothalamic nucleus in direction of the PAG. Axons running through the ventral pathway are still abundant, but a detailed drawing (**c**) shows that many of them take a dorsal direction (*arrowheads*) to merge with axons of the dorsal pathway. Innervation of neurons along the ventral pathway also becomes more noticeable. Projections from the BMAa: darkfield photomicrograph (**d**) illustrating the distribution of PHAL axons in the LHA at anterior hypothalamic level—level 30 in Brain Maps (Swanson 2004) and an adjacent Nissl-stained section (**e**) for cytoarchitectonic purposes. Projections are still mostly confined to the ventral pathway. An India ink drawing more clearly shows that fewer axons take a dorsal direction compared to the CEAm experiment (**d**). In contrast, innervation of neurons along the path is more prominent. *Scale bar* in **b** 500 µm for **b, e**; 250 µm for **a, d**

the ventrolateral LHA, axons or collaterals changed directions to take a dorsomedial direction (Fig. 11c, e). These axons terminated in the dorsal perifornical region, providing a light innervation of this region. At posterior hypothalamic levels, the CbN nucleus was innervated, but the axons arched dorsally and entered the PSTN (Fig. 11d). Innervation of the PSTN, however, concerned primarily dorsolateral, ventral, and posterior regions of this nucleus. Central and medial regions contained few or no axons. In the two other cases involving the FS, axons ran more laterally in ventral aspects of the cpd, and they did not contribute to the innervation of the CEAm. Nevertheless, in the

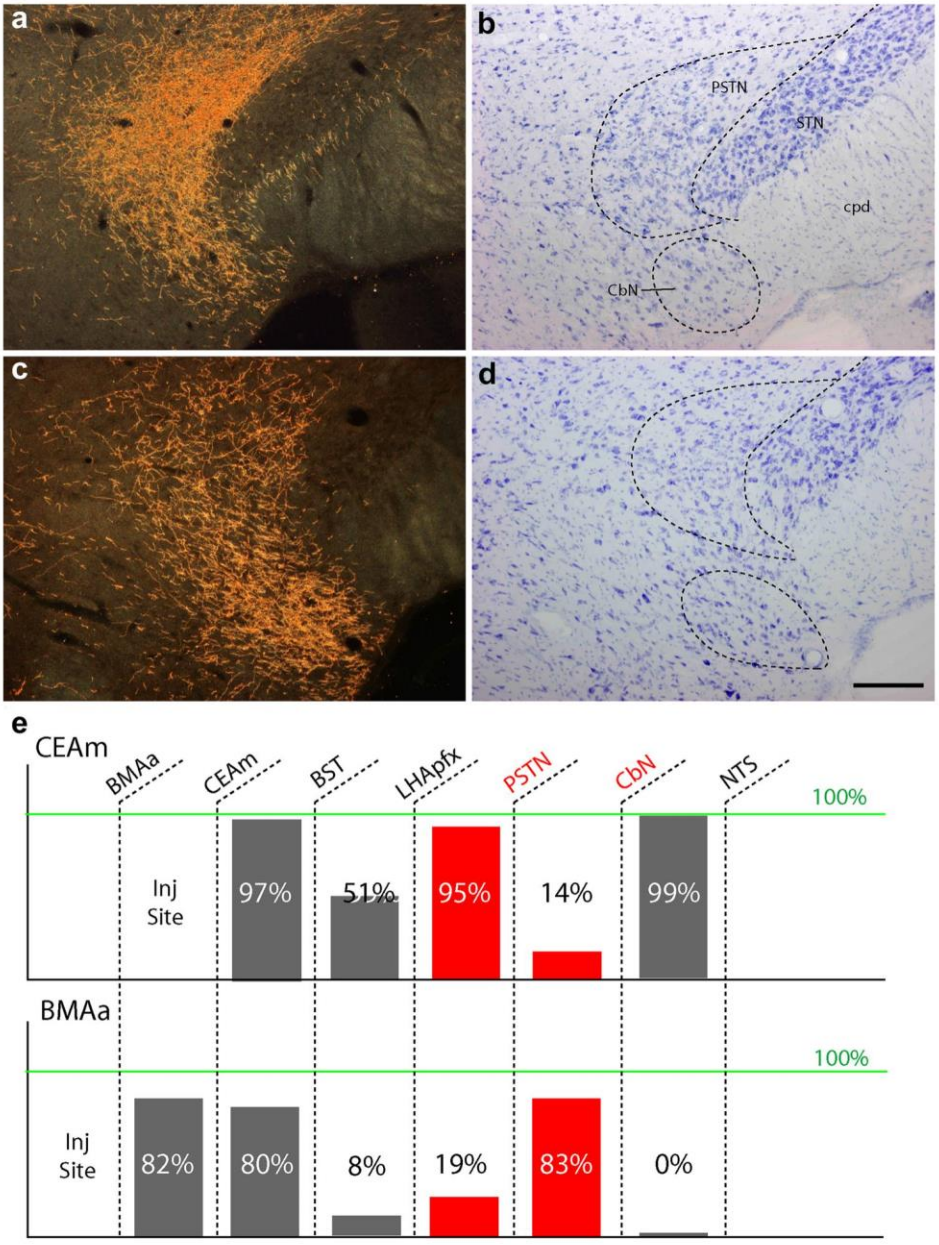

Fig. 10 **a, b** Photomicrographs illustrating the innervation of the PSTN/CbN in the experiment AMY1 (CEAm PHAL injection) in the premammillary LHA and an adjacent Nissl-stained section for cytoarchitectonic purposes. PHAL-labeled axons provide a very intense terminal field in the PSTN. This innervation is especially intense in tissue immediately adjacent to the STN and decreases slightly more laterally in the nucleus. The CbN is also innervated, but this innervation is only moderate. **c, d** Photomicrographs illustrating the innervation of the PSTN/CbN in the experiment AMY3 (BMAa PHAL injection) in the premammillary LHA and an adjacent Nissl-stained section for cytoarchitectonic purposes. PHAL-labeled axons provide a very intense terminal field in the CbN. However, this experiment shows only moderate innervation of the PSTN. *Scale bar* 100 µm. **e** Semi-quantitative analysis of the signal intensity in several structures innervated by PHAL axons in experiment AMY1 (CEAm) and AMY3 (BMAa). The surface taken by the staining were close to 100% in an ROI of structures containing very abundant PHAL axons. After CEAm injection, the surface occupied by the staining in the PSTN is comparable to that in BST or in NTS that are two structures innervated by this nucleus. After injection in the BMAa, the CbN contains a signal that is comparable in its intensity to that observed in the CEAm or BST. No structure caudal to the CbN contained such a signal. PSTN and CbN bars are highlighted (in *red*)

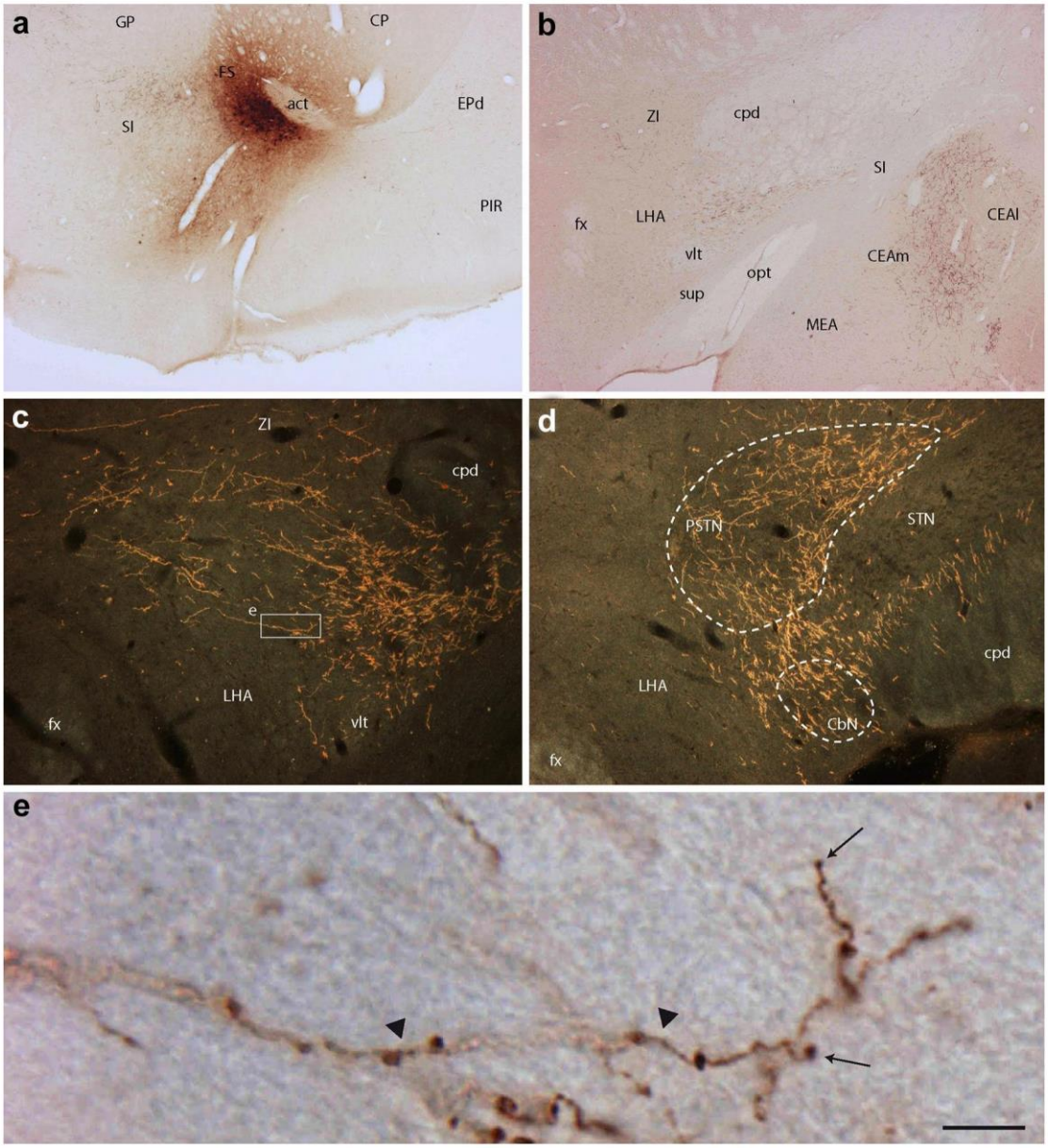

Fig. 11 Control PHAL injection in the FS: **a** injection site in the FS in experiment FS1. **b** Axons from the FS were traced in the CEAm which receives a dense innervation. They also enter the ventral LHA and follow a pathway similar to that of projections from the BMAa. **c, e** All along the course in the LHA, we observed axons taking a dorsomedial direction to innervate more medial parts of the LHA. In some instances, we noted that some of these axons were collaterals of axons continuing more caudally. We can see that this axons displays boutons-of-passage (*arrow*) but few varicosities (*arrowheads*). **d** PHAL-labeled axons from the FS provided moderate input to the PSTN and CbN. *Scale bar* in **e** 500 µm for **a, b**; 250 µm for **c, d**; 20 µm in **e**

posterior hypothalamus, they provided a small input to the CbN/PSTN complex in a pattern similar to that of FS1.

This pattern of projections within the PSTN may explain some discrepancies in observations after FG injections in the PSTN (Chometton et al. 2016). The distribution of FG-labeled neurons mapped in our previous report was centered in the PSTN, to avoid any STN contaminations. However, after more caudal and more voluminous injections, many retrogradely labeled cells can be observed in the FS.

Injections in the piriform cortex One PHAL injection was obtained in the dorsal and posterior piriform cortex (Fig. 12), and this injection site involved only a few contaminating cells in the adjacent dorsal endopiriform nucleus. Interestingly, a large bundle of axons left the injection site to extend

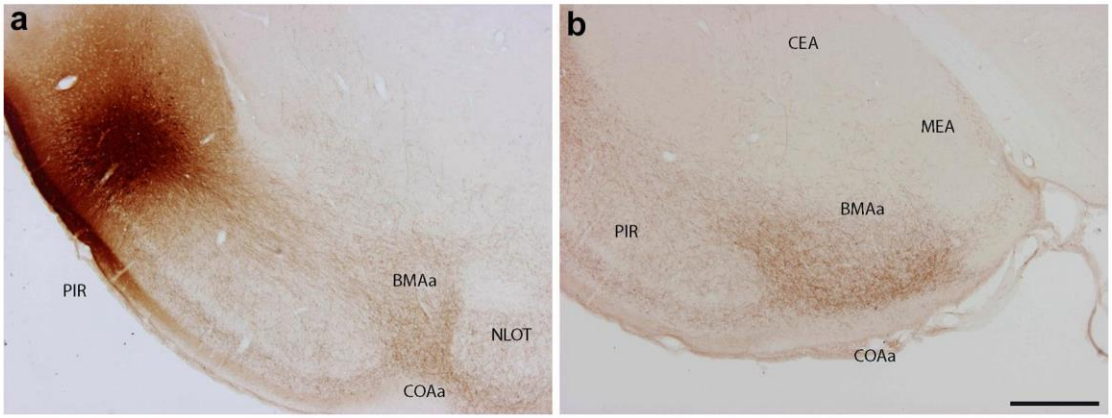

Fig. 12 After a control injection in the perirhinal cortex (**a**), we observed a large bundle of axons running straight into the BMAa and the COAa, providing intense innervation (**a, b**). *Scale bar* 500 µm

in a straight line into the BMAa and the COAa that received a very intense projection. Other outputs were observed in all aspects of the piriform cortex and olfactory tubercle. Innervation of the FS as well as of the CEAc was observed. From this injection, only a few axons were observed in the LHA and they traveled mostly via the vlt.

Co-distribution of PHAL with calbindin/parvalbumin and CGRP in the PSTN/CbN complex

Considering that the posterior lateral hypothalamus was obviously the main hypothalamic target for descending projections from the CEAm and BMAa, it is clearly important to compare the distribution of these projections with that of neurochemical markers of the PSTN/CbN complex.

Expression of the preprotachykinin 1 (precursor to substance P) gene has been reported several times in neurons of the PSTN based on in situ hybridization (Goto and Swanson 2004; Chometton et al. 2016). However, mention in the literature of a cluster of perikarya labeled for substance P using immunological methods in this region are inconsistent: after colchicine injection, Larsen (1992) failed to detect many, but Lantos et al. (1995) did reveal some. We also failed to detect many perikarya in this region using immunohistochemistry or immunofluorescence on un-colchicinized animals (data not shown), perhaps indicating that the peptide is very rapidly transported and released. Our group reported that Cb is abundantly expressed throughout the PSTN/CbN complex, with a ventral cell cluster, corresponding to the CbN. In the PSTN, the neuropil is labeled but this nucleus contains as well a few Cb-expressing cells. The CbN and PSTN are surrounded by several parvalbumin (PV)-expressing structures: laterally, the STN is very intensely labeled for PV and medially the parvafox nucleus and the NG are also characterized by PV expression. In addition to Cb, the PSTN/CbN contain a very dense CGRP innervation that originates in the PB (Shimada et al. 1985; Chometton et al. 2016). This input is restricted to the PSTN/CbN complex in the posterior lateral hypothalamus, even if a few cells outside these nuclei may be marginally affected.

Thus, the distribution of PHAL-labeled axons was subsequently analyzed with regard to the distribution of Cb, PV, and CGRP in the posterior LHA.

PHAL-calbindin-CGRP triple labeling

Using triple immunofluorescence procedures, PHAL axons from the BMAa very densely innervated the region containing the CbN cell cluster as revealed with the anti-Cb antibodies. The same region contained a dense network of CGRP projections (Fig. 13). At higher magnifications (Fig. 13e), Cb-containing neurons in the CbN seemed innervated by both PHAL and CGRP axons. The PSTN showed less innervation by PHAL axons from the BMAa, and the CGRP input was clearly predominant.

In contrast, the PSTN contained a very dense input after PHAL injection in the CEAm, and the distribution pattern of PHAL-labeled axons overlapped with that of CGRP (Fig. 14). Projections from the CEAm were less abundant in the CbN, but the pattern of PHAL axons is still close to the CGRP distribution. After 3D reconstructions using the "Z-stack" module of the Zen Software (Fig. 15), we observed CGRP and PHAL axons in close apposition of the same cell bodies. Moreover, we very frequently observed very close putative contacts between PHAL and CGRP boutons as they appear to contact Cb neurons, suggesting that the CGRP input from the PB and the projections from the CEAm interact as they innervate the same cells in the CbN. Similar putative contacts between PHAL and CGRP axons were observed in the PSTN, but the targeted cells in this nucleus were not identified (data not shown).

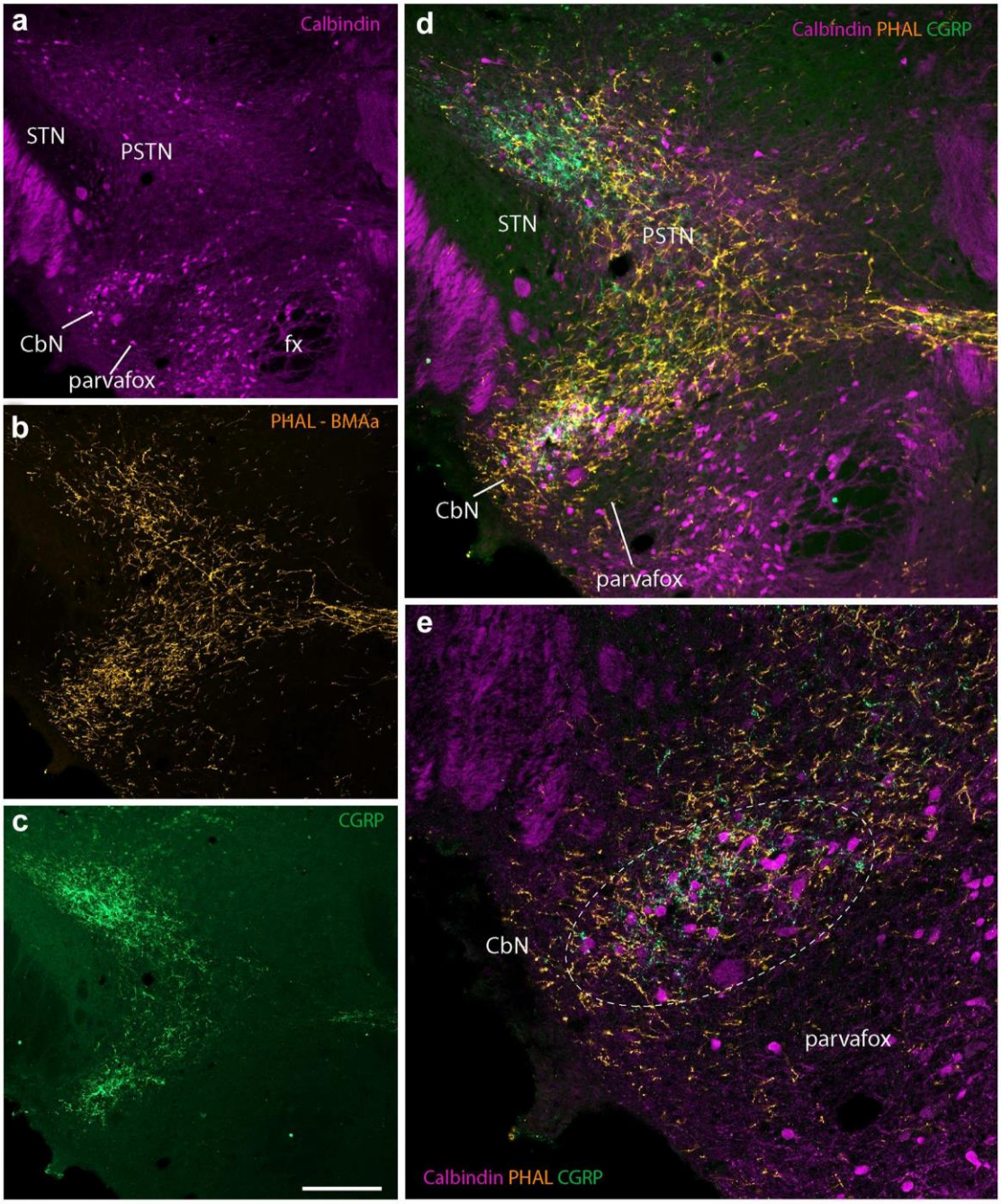

Fig. 13 Distribution of PHAL-labeled axons from the BMAa (AMY3) with CGRP and Cb in the PSTN/CbN complex using immunofluorescence. **a** Immunofluorescence photomicrograph showing that a Cb antibody labels a cell group ventral to the PSTN and termed the CbN. **b** Immunofluorescence photomicrograph showing that PHAL-labeled axons from the BMAa intensely innervate the region of the CbN. **c** Immunofluorescence photomicrograph showing that CGRP-labeled axons intensely innervate both the PSTN and the CbN. **d, e** Merged images showing the three immunofluorescent labels. The distributions of CGRP and PHAL axons are superimposed on the CbN; at higher magnification (**e**), many putative contacts can be seen on Cb-labeled cells by both CGRP- and PHAL-labeled axons. *Scale bar* 200 µm for **a**–**c**; 100 µm for **d**; 50 µm for **e**

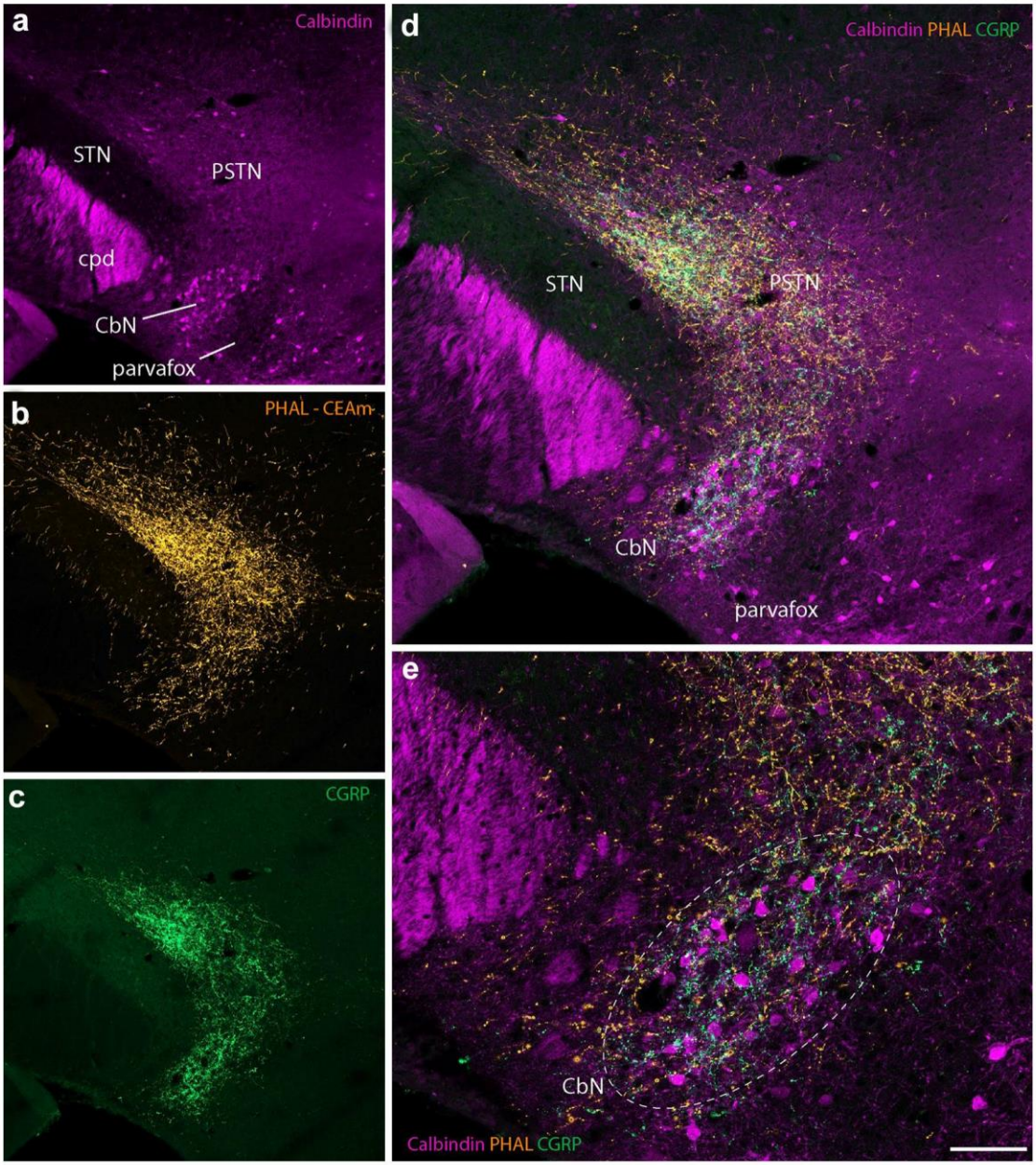

Fig. 14 Distributions of PHAL axons from the CEAm (AMY1) with CGRP and Cb in the PSTN/CbN complex using immunofluorescence. **a** Immunofluorescence photomicrograph showing that a Cb antibody labels a cell group ventral to the PSTN and termed the CbN. **b** Immunofluorescence photomicrograph showing that PHAL-labeled axons from the CEAm intensely innervate the region of the PSTN. **c** Immunofluorescence photomicrograph showing that CGRP-labeled axons intensely innervate both the PSTN and the CbN on the same section that **a, b. d, e** Merged images of the three immunofluorescent labels, showing that CGRP and PHAL axon distributions overlap in the PSTN. Furthermore, at higher magnification (**e**), many contacts can also be seen on Cb-labeled cells from both CGRP- and PHAL-labeled axons in the CbN. *Scale bar* 200 µm for **a**–**c**; 100 µm for **d**; 50 µm for **e**

PHAL-parvalbumin-CGRP triple labeling

PHAL/CGRP/PV triple labeling experiments clearly showed that the CbN, innervated by CGRP and PHAL from the BMAa or CEAm, lies immediately lateral to the parvafox nucleus, which is stained by the PV antibody (Fig. 16). A few PHAL axons could be observed within the borders of the parvafox nucleus, but they resembled fibers-of-passage and PV cell bodies were not innervated.

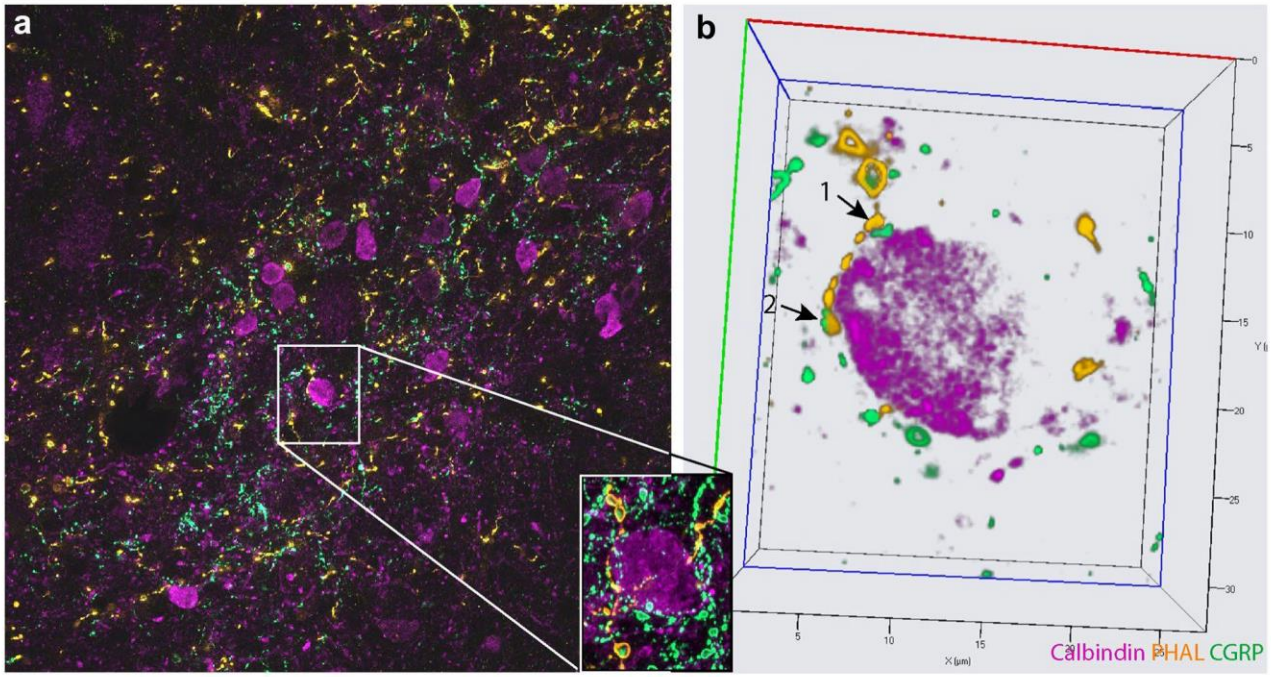

Fig. 15 Interactions between CGRP-labeled axons and PHAL-labeled axons from the CEAm (experiment AMY1) on neurons labeled by Cb in the CbN. **a** Triple immunofluorescence labeling on a section passing through the CbN and showing PHAL- and CGRP-labeled axons in the immediate vicinity of Cb neurons in the CbN. Many interactions between PHAL and CGRP axons are apparent. **b** Neuron in the frame was analyzed using the Z-Stack module of the Zen software. This allowed us to extract a thin section through this neuron to observe that PHAL axons (*orange*) appear to make contact on Cb cells (*purple*). However, some varicosities also contact CGRP boutons that innervate the same Cb neurons (*1*). CGRP boutons (*2*) also appear to be in close apposition to some of the PHAL boutons innervating the Cb neuron

Discussion

One of the main findings of this study is that the PSTN/CbN complex is a major target of descending connections from the amygdala. Projections from the amygdala to the LHA have been reported in the literature (Krettek and Price 1978; Veening et al. 1982; Ono et al. 1985; Gray et al. 1989; Gonzales and Chesselet 1990; Canteras et al. 1992, 1995; Petrovich et al. 1996; Petrovich and Swanson 1997; Bourgeais et al. 2001; Tsumori et al. 2006), but the specific targets, particularly the identification of the PSTN/CbN complex as a preferred target at least from the CEAm and BMAa, have not been clear to date. The present study also focused on the pathways taken by the fibers to reach the posterior LHA, as this information has rarely been clearly stated in the literature. We found that these axons form differentiated paths in the mfb.

Origin and pathways from the amygdala to the PSTN/CbN

Previous works reporting projections from the CEA to the caudal LHA are abundant, using both retrograde and anterograde approaches (Krettek and Price 1978; Ottersen 1980; Veening et al. 1982, 1984; Ono et al. 1985; Gray et al. 1989; Gonzales and Chesselet 1990; Petrovich and Swanson 1997; Bourgeais et al. 2001; Shirasu et al. 2011; Bienkowski and Rinaman 2013; Reppucci and Petrovich 2016). However, the characterization of the PSTN is quite recent, and our group identified the CbN even more recently (Chometton et al. 2016), making it necessary to evaluate the distribution of these projections with regard to the borders of these hypothalamic nuclei. The cell condensation labeled for Cb that characterizes the CbN has a clear oval and elongated appearance. This nucleus should not be confused with the LHAvl of the Swanson's brain maps (Swanson 2004): its borders do not fit within the LHAvl, and it extends more caudally (Hahn and Swanson 2012). Among all the papers reporting projections from the CEA into the posterior LHA, the work of Bourgeais et al. (2001) provided a precise description of projections into what they called the posterior region of the LHA as the most caudal and lateral part of the LHA. These authors showed that the CEAm is a main contributor to these projections. In their illustration (their Fig. 10), the distribution of PHAL axons clearly encompasses a ventral and a dorsal region adjacent

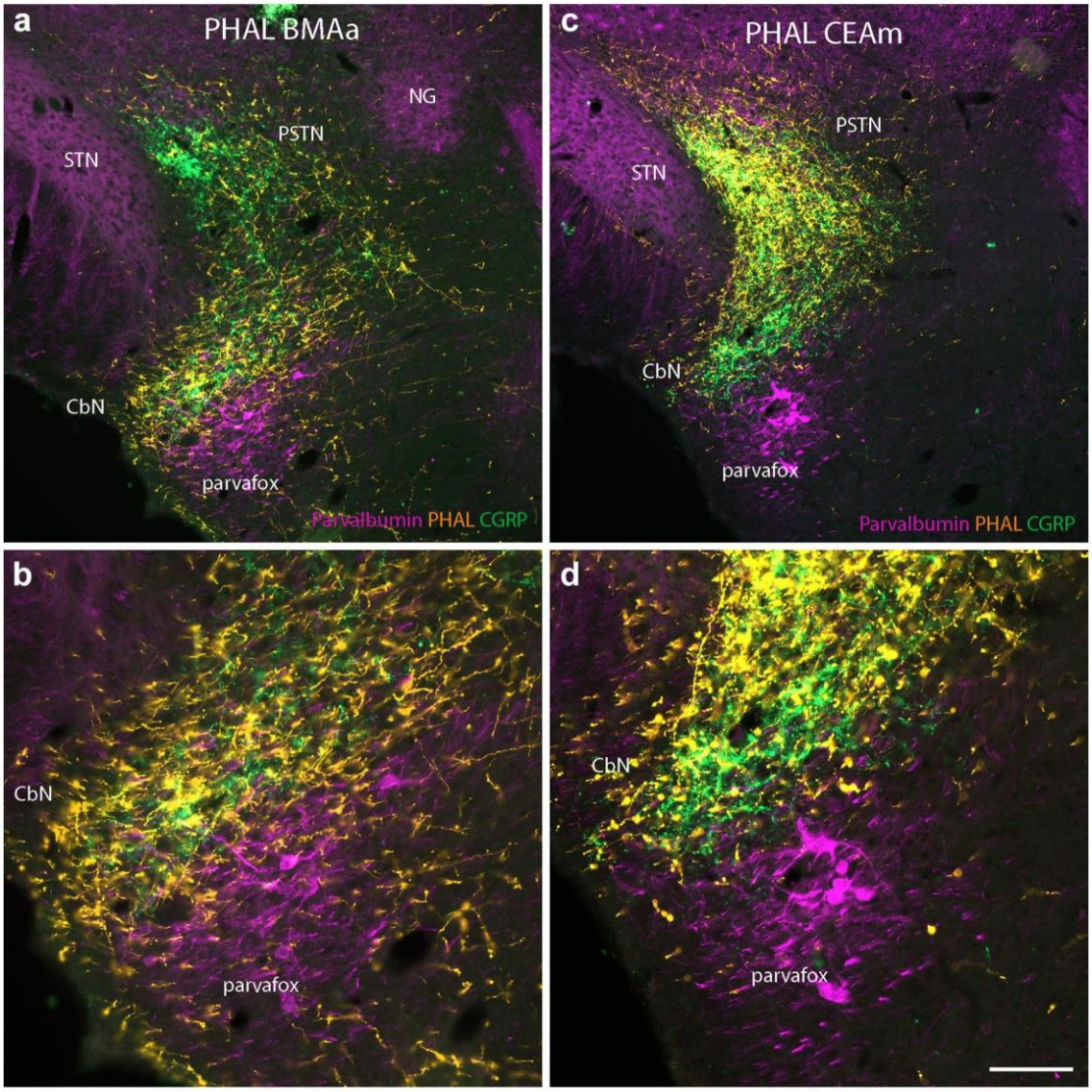

Fig. 16 Distributions of PHAL axons from the BMAa (**a, b**) or from the CEAm (**c, d**) with those labeled by CGRP and the PV labeling of axons and cell bodies in the PSTN/CbN region using immunofluorescence. **a, b** Using triple immunofluorescence labeling, PHAL axons from the BMAa (AMY3) innervate the PSTN and mostly the CbN, both of which also receive a dense CGRP input. The parvafox nucleus, which is medially adjacent to the CbN, is not innervated by either CGRP or PHAL axons. **c, d** Using triple immunofluorescence labeling, PHAL axons from the CEAm (AMY1) innervate mostly the PSTN and moderately the CbN. Both nuclei also receive a dense CGRP input. The parvafox nucleus, which is medially adjacent to the CbN, is not innervated by either CGRP or PHAL axons. *Scale bar* 100 μm for **a, c**; 50 μm for **b, d**

to the STN. This pattern is reminiscent of the innervation of the CbN and PSTN reported here. In our study, however, the PSTN receives more innervation from the CEAm than does the CbN, which is not clearly apparent in their figures. This point will be discussed further in the section addressing the pathways. The same authors also noted that the CEAc and CEAl send far fewer inputs into this region. After PHAL injections centered in the CEAl, Gray et al. (1989) and Petrovich and Swanson (1997) also described a light input into the LHA. Our present results are thus consistent with these reports: our retrograde experiment clearly illustrated that most of the retrogradely labeled cells were observed in the CEAm, but not in the CEAc or in the CEAl, and a PHAL injection in the CEAc labeled only few axons in the PSTN/CbN. Dorsal regions of the SI also contained many retrogradely labeled neurons, suggesting that this part of the SI, adjacent to the CEAm, also intensely innervates the PSTN/CbN. We did not perform control anterograde injections in the SI, but data published by Grove (1988a) and then confirmed by Spooren et al. (1991) and Groenewegen

et al. (1993), showed that a caudal LHA region corresponding to the PSTN is a major target for projections from several parts of the SI. The details of the connections from the ventral pallidum/SI (Zahm et al. 1996) into the PSTN/CbN will require a specific study and is not further addressed here. In addition to the CEA, the BMAa sends a dense projection into the caudal LHA, but this nucleus mostly targets the CbN. Only one of our FG injections primarily involved the CbN and that experiment was imperfect, as contamination of adjacent structures was obvious. However, using the HRP method, Ono et al. (1985) had reported the distribution of retrogradely labeled neurons in the amygdala after a similar experiment, but with a nearly perfect injection in the region of the CbN (their experiment C53), although the CbN was not identified at that time. In that experiment, they observed an intense labeling in the COAa and BMAa. Similar observations were made by Price et al. (1991) (see their Fig. 5). Anterograde studies also confirmed these data. Price et al. (1991) had identified this projection from the COAa and BMAa after a large injection of tritiated amino acid, as did Veening et al. (1982) using the same technique. Using PHAL, Petrovich et al. (1996) again observed axons from the BMAa and COAa coursing in the ventrolateral LHA, but it was not considered a major projection. Niu et al. (2012), on the contrary, had described some more abundant projections. In this last study, some of the projections innervated MCH cell bodies in the ventrolateral LHA, but obviously a large proportion of the axons continued caudally, with a pattern clearly reminiscent of the CbN. The pattern reported in our study is again similar to those previously described, and the CbN is clearly a target of these projections: PHAL axons formed many boutons on Cb cell bodies. Caudally to the CbN, only a few axons extended into the ventral tegmental area. The semi-quantitative analysis confirmed that projections in the CbN from BMAa are as intense as those from this nucleus in the BST. A very few were seen more caudally in the brainstem from this injection site. Therefore, projections from the BMAa mostly end in the CbN.

Thus, the comparison of the projection patterns from the CEA and BMAa into the LHA enabled us to characterize two distinct pathways: a dorsal pathway followed here by axons from the CEA, and a ventral pathway followed by projections from both the CEA and BMAa.

Characterization of two pathways within the medial forebrain bundle

Authors have often referred to the ansa peduncularis or the ventral amygdalofugal pathway as the main entrance pathway into the LHA (Leonard and Scott 1971). More caudally, the path within the mfb is rarely clearly characterized. The work of Veening et al. (1982) reported the course of axons from several telencephalic sites into the mfb. These authors had shown that projections from the amygdala coursed mostly very laterally and ventrally in the LHA, but our current observations indicate that these axons follow several more differentiated paths through the mfb. The two paths observed here were clearly different as they provided innervation to distinct structures within the hypothalamus (Fig. 17).

The dorsal pathway was observed only after CEA injections. PHAL in the CEAm very intensely labeled axons in the dorsolateral LHA. Axons from the CEAc also followed the same route. Petrovich and Swanson (1997) showed that projections from the CEAl exclusively run through a dorsal route similar to the dorsal pathway described here. However, many axons from the CEAm innervated more medial structures not innervated by the CEAl. A bundle of medially oriented axons entered the PVH through its forniceal and lateral parvicellular parts. Input from the CEA into the PVH has been reported previously (Gray et al. 1989; Wallace et al. 1992), and our observations indicate that this innervation originates from dorsal path fibers. At anterior tuberal levels, we observed a clear innervation of the dorsal perifornical region. This pattern was interesting as it concerns only rostral perifornical areas and not the caudal dorsal perifornical areas. This region has been mentioned in the literature as it contains a condensation of neurons projecting in the dorsal vagal complex along the CEAm and caudolateral LHA (PSTN) (Veening et al. 1984, 1987; Grove 1988b). More recently, non-MCH and non-hypocretin neurons in the same area, possibly containing neurotensin, were reported in feeding responses (Lantos et al. 1995; Allen and Cechetto 1995; Leinninger et al. 2009, 2011; Goforth et al. 2014).

A short review of the literature under the form of a table (Table 3) illustrates that the dorsal pathway was not consistently described by authors; some described a ventral route in the LHA from the CEAm or only a dorsal one, even if several studies reported or illustrated both dorsal and ventral paths for axons from the CEAm.

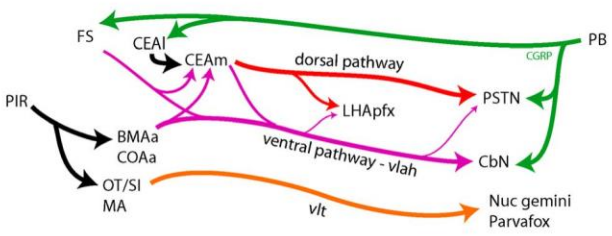

Fig. 17 Diagram illustrating the dorsal pathway, ventral pathway (also named the vlah) and vlt in the far lateral and ventral LHA. PSTN/CbN as well as CEAl and FS receive intense CGRP projections from the PB (see text for details)

Table 3 Dorsal and ventral pathways from the CEAm in the literature

References	Ventral path	Dorsal path
Gray et al. (1989)	+	+
Gonzales and Chesselet (1990)	+	−
Bourgeais et al. (2001)	+	−
Nakamura et al. (2009)	+	+
Shirasu et al. (2011)	−	+
Our study	+	+

Dorsal and ventral pathways from the CEA were not reported by all anterograde studies. Some studies illustrated only one or the other, even if a short majority reported both dorsal and ventral pathways from the CEAm

This is important, because studies that do not signal or illustrate a dorsal pathway do not signal perifornical and PVH projections by the CEAm. The discrepancies among anterograde studies, including our own results, regarding ventral and/or dorsal pathways in the LHA must come from the location of the respective injection sites. For example, the injection sites are very well described in Bourgeais et al. (2001) and appear ventral and caudal in the CEAm compared to our own. The difficulty in comparing all these studies also comes from the parcellation of the nucleus. We used the Swanson's nuclear delineation of the CEA (Swanson 2004), while Bourgeais et al. (2001) followed the nomenclature and parcellation of Bernard et al. (1993). Following the present delineation, their injection site was centered ventral to the CEAm, in the 'horizontal/ventral' CEAc, while our injection dodge the rostral edge of the CEAl. Authors such as Swanson 2004, McDonald (1982), Cassell et al. (1986) and Paxinos and Watson (2005), to cite only a few of the most recognized authors, differently outlined borders of the CEA. Depending on the precise localization of the injection site in the CEAm and on the parcellation used, distinct patterns of projections in the LHA can be reported. Retrograde studies such as that of Veening et al. (1984) are useful to analyze the origin of an innervation, but they do not illustrate the specific pathways taken by the axons. Nevertheless, most anterograde studies reported dense projections into the caudal portion of the LHA, corresponding to the projections in the PSTN/CbN described here.

The ventral pathway: in our experiments, both the BMAa and the CEAm send abundant axons into the ventral pathway. This ventrolateral amygdalo-hypothalamic pathway (vlah) runs immediately lateral to the well-recognized vlt (Figs. 17, 18) that can be labeled using PV antibodies (Chometton et al. 2016).

Both the vlah and the vlt form the olfactory pathway into the LHA, as described in the previous studies (Fig. 17). The presence of olfactory inputs in the hypothalamus was described first by Cajal and then labeled with greater precision in the 1970s (Scott and Pfaffmann 1967; Scott and Leonard 1971; Scott and Chafin 1975). These inputs were later confirmed by Price (1985) and Price et al. (1991). Especially in the 1985 paper, Price illustrated two pathways: one corresponding to the vlt, originating in the deep layers of the olfactory tubercle (SI, see also Heimer et al. (1990) albeit using different terminology), and another one just lateral to the vlt and originating in the COAa. The two pathways are visible in Fig. 8 of Price (1985). Panel A of this Fig. 8 illustrates the projections from the deep olfactory tubercle in what we now call the vlt. These projections arch at the level of the premammillary hypothalamus to innervate the NG (Fig. 18) (Scott and Chafin 1975). Today, this pathway can be very well visualized using antibodies against PV. The vlt is associated with an elongated nucleus initially named PV1 by Celio (1990), Mészár et al. (2012) and Celio et al. (2013) and renamed parvafox as neurons expressing the transcription factor Fox-b1 are associated with the PV neurons (Bilella et al. 2014, 2016a, b; Alvarez-Bolado and Celio 2016). Little is known about the functions of this nucleus, except that it projects very heavily in the PAG, and Price had observed that neurons in this region respond to olfactory stimuli (Price 1985; Price et al. 1991). Other origins for descending projections coursing in the vlt are found in the diagonal band nucleus and magnocellular preoptic nucleus (at the origin of the PV pathway), as well as some axons from ventral orbital prefrontal cortical fields (Groenewegen et al. 1993; Alvarez-Bolado and Celio 2016).

The vlah originates mainly from the BMAa and the COAa. Projections from these nuclei in the ventrolateral LHA were illustrated by Price (1985), Price et al. (1991) and Petrovich et al. (1996). The olfactory nature of this path is, therefore, confirmed, as these nuclei of the amygdala are influenced by the lateral olfactory tract (Millhouse and Uemura-Sumi 1985; Santiago and Shammah-Lagnado 2004), and we also observed that at least parts of the piriform cortex send very dense projections into both the BMAa and the COAa; Price also recorded responses from neurons after sensory stimuli along this path. However, the vlah conveys information from other sources: Canteras et al. (1995), had shown that projections from the anterodorsal part of the MEA form a small bundle ventrally adjacent to the cpd. These axons course through the exact same ventral pathway that we identified here as the vlah. Our FG injections in the PSTN/CbN retrogradely labeled neurons in the anterodorsal part of the MEA as well. The FS also projects through this path (Heimer et al. 1990).

The vlt is associated with the paravafox nucleus along its course in the LHA, but the vlah is associated with the CbN. Like the parvafox, the CbN is a cylindrical

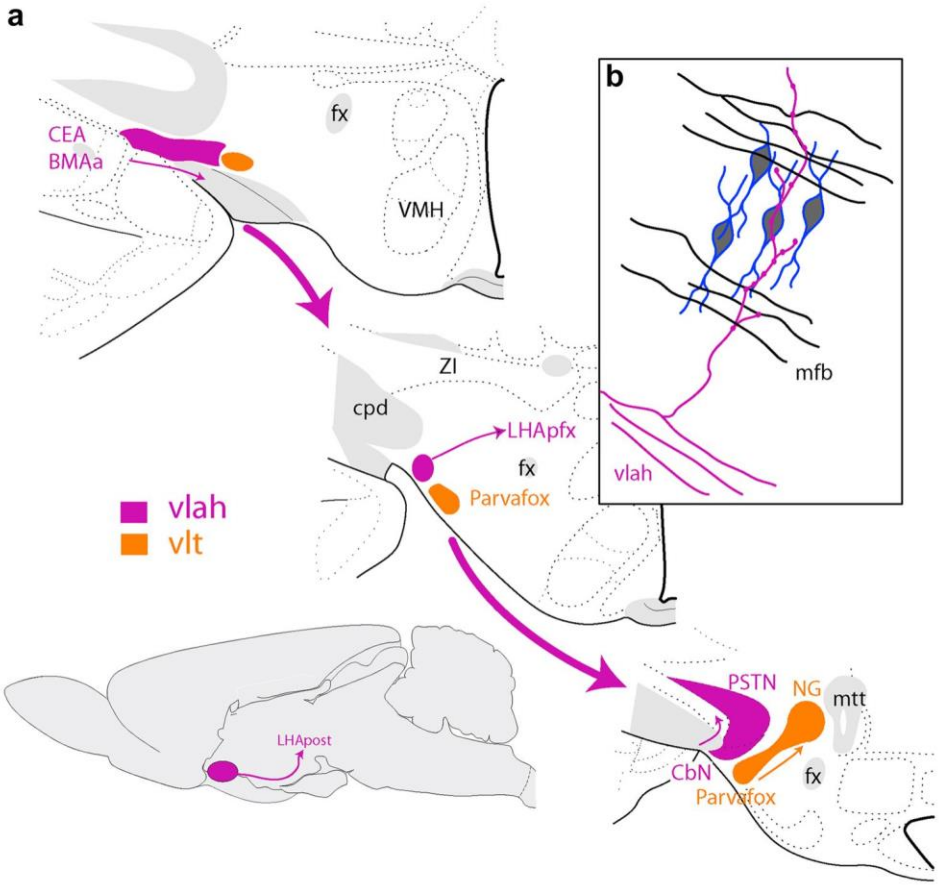

Fig. 18 **a** Diagram summarizing the parallel courses of the vlah (ventral pathway) and vlt in the ventral LHA. Both paths terminate at the premammillary level; the vlt terminates in the NG, while axons from the vlah terminate in the CbN or in the PSTN. **b** We noted that some axons leave the vlah to innervate more medial and dorsal regions of the LHA. Millhouse (1969) had reported that while the mfb runs orthogonal to the dendrites in the LHA, some collaterals of ventrally running axons left this longitudinal path and were able to innervate dendrites and neurons along their path (see text for details)

nucleus. It is shorter than the parvafox, as we were not able to distinguish it in levels rostral to the posterior tuberal region [approximately level 30 of the Swanson's Brain maps (Swanson 2004)] (Figs. 17, 18). Another difference between the vlah and the vlt is that the vlah distributes collaterals to the hypothalamus throughout its path: we observed branches, some of which, though not necessarily all, are collaterals that take a medial route to innervate LHA neurons dorsally or the tuberal nuclei ventrally. By contrast, the vlt appears more differentiated. A review of the classical literature that used the Golgi method revealed that such collaterals were described by Millhouse (1969), who had noted that, although axons of the mfb run perpendicular to the dendritic organization of LHA neurons, collaterals from ventral axons take a dorsal route parallel to the dendrites of LHA neurons and provide inputs to these neurons. At the premammillary level, as the vlt axons arch dorsally to innervate the NG, we observed axons of the vlah entering the PSTN. However, in most cases, the innervation of the PSTN by axons through this pathway was more moderate than the innervation of the CbN. Therefore, the CbN appears to be a main target of this tract, as few axons could be followed in the VTA caudal to this level.

In addition to projections from the amygdala, the PSTN/CbN receives inputs from multiple other brain areas, including a strong projection from the PB (Bernard et al. 1993; Shin et al. 2011; Zséli et al. 2016). At least a fraction of these PB projections into the PSTN/CbN contain CGRP (Shimada et al. 1985; Chometton et al. 2016). This input is interesting, because it is very functionally significant, but this point will be addressed in the 'functional considerations'. This input also helps to define the PSTN/CbN complex as it respects the borders of both nuclei (Chometton et al. 2016).

Functional considerations

The functions of the PSTN/CbN complex remain mysterious. Our recently published data confirmed previous studies indicating that this complex responds to gustatory cues, but the hedonic nature of this information is essential (Chometton et al. 2016). Projections from the PB are also crucial for determining the functions of these intriguing cell groups. Bester et al. (1997) had carefully analyzed the projections from the PB to the hypothalamus. The gustatory parts of the PB (waist and medial subnuclei) are those that send the densest inputs to the posterior LHA, following

a pattern that fully corresponds to the PSTN/CbN (Norgren 1976; Shin et al. 2011). These inputs are consistent with our previous observations regarding responses induced by hedonic taste in the PSTN/CbN (Chometton et al. 2016). Interestingly, the same injection sites also provided extremely dense innervation of dorsomedial or central parts of the ventromedial hypothalamic nucleus. These divisions of the ventromedial hypothalamic nucleus are parts of the hypothalamic defensive circuit, and these connections suggest an indirect link between the PSTN/CbN network and the defensive circuit of the hypothalamus. However, the CGRP projections also clearly define the borders of the PSTN/CbN. Dobolyi et al. (2005) as well as Shimada et al. (1985) indicated that the CGRP projections innervating the posterior LHA derived exclusively from the PB, and at least in the rat, these projections are very intense. These CGRP projections connect the PSTN/CbN to pain pathways that include the PB and the amygdala (Bernard et al. 1993; Bourgeais et al. 2001; Shin et al. 2011; Carter et al. 2015; Han et al. 2015; Liang et al. 2016). The group of JF Bernard had shown that a lateral component of the PB is involved in pain processing through connections with the CEAc (Bourgeais et al. 2001). This was again recently elegantly demonstrated by the group of Palmiter (Han et al. 2015). Using pharmacogenetics and optogenetics, this last group demonstrated that the CGRP input to the CEA is the determining factor for inducing anorexic responses and conditioned taste aversion (Carter et al. 2013, 2015). These authors mentioned a CGRP input to the caudal LHA using genetic tract tracing, suggesting that at least some collaterals of that pathway innervated the PSTN/CbN.

The main telencephalic target of the PB CGRP projections is the CEA, especially the CEAc and CEAl (Schwaber et al. 1988; D'Hanis et al. 2007). This input carries pain information, and it may be correlated to other sensory information in this nucleus. The results of this processing are then sent to the CEAm. Based on the current literature, the CEAm is responsible for the behavioral responses via its projections into the PAG (Oka et al. 2008; Carvalho et al. 2015). The PSTN/CbN complex is clearly also a main target for projections from the CEAm, and based on previous studies (Ono et al. 1985; Goto and Swanson 2004; Chometton et al. 2016), we know that the PSTN/CbN reciprocates these projections to the CEAm. The nature of the responses mediated by these projections remains unknown. However, the PSTN/CbN complex is thought to be glutamatergic, and the two nuclei do not express the glutamic acid decarboxylase but do contain VGlut2 (Chometton et al. 2016). They may, therefore, have an excitatory influence on the CEAm. The body of work showing the importance of the CEAl and its projections onto the CEAm in pain and defensive responses is growing rapidly (Yasoshima et al. 2006; Pape and Pare 2010; Han et al. 2015; Yu et al. 2016). In

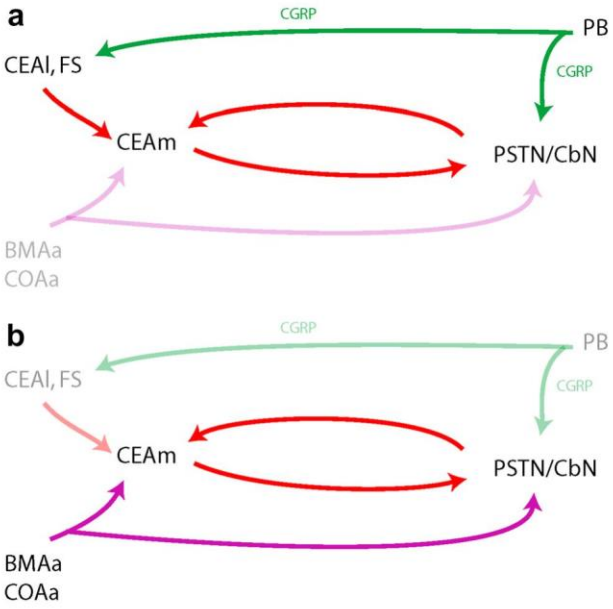

Fig. 19 Diagram illustrating the hypothesis of the functional organization of the circuitry linking the PSTN/CbN complex, the amygdala and the PB (see text for details)

brief, nociceptive inputs carried by CGRP/glutamatergic axons activate GABAergic neurons in the CEAl that in turn inhibit GABAergic neurons of the CEAm. We can then hypothesize (Fig. 19a) that inhibition of the CEAm relieves inhibition of PSTN/CbN neurons that are also activated by CGRP/glutamate from the PB. The reciprocal connections between the PSTN/CbN and the CEAm resemble a regulatory loop that could control the activity in the CEAl. Very interestingly, triple-immunofluorescent images obtained of the CbN show probable interactions between CGRP terminals from the PB and PHAL-labeled axons from the CEAm in contact with Cb neurons in the CbN. Furthermore, the distribution patterns of PHAL and CGRP in the PSTN overlap. These data argue in favor of a strong functional network involving the CEA, PSTN/CbN, and PB. The CEAm also receives projections from the FS (Shammah-Lagnado et al. 2001). This input is again very probably GABAergic. As the FS receives inputs from insular cortical fields, similar mechanisms may be involved in relation to interoceptive and possibly gustatory information. Finally, we observed that the BMAa also projects into the CEAm and CbN. A similar circuit with the BMAa and COAa could be responsible for the control of CEAm activity under olfactory stimuli (Fig. 19b). The overall circuit involving the PSTN/CbN and the CEA clearly suggests that the functions of the caudal hypothalamic complex are related to satiety/anorectic responses under the influence of nociceptive and/or cognitive information, as well as olfactory, gustatory and probably other sensory and cognitive

afferences (Petrovich et al. 2009; Cai et al. 2014). The PSTN/CbN react to the hedonic nature of food (Chometton et al. 2016). It is, therefore, tempting to see this information related to pleasure, susceptible to modulate pain related stimuli within this circuitry.

Structural organization of the amygdalo-hypothalamic connections

Concepts of the morphofunctional organization of the amygdala deem information flow funneled through two main components in this structure before information is sent toward the brainstem: basically, it is recognized that there is an olfactory/medial component with the MEA as the main output structure, whereas the output nucleus of the frontotemporal/autonomic component is the CEA (Heimer et al. 1997; Swanson and Petrovich 1998).

The function and organization of the medial component have long been associated with the st and the medial zone nuclei of the hypothalamus. Olfactory, but mostly vomeronasal (pheromonal) information would reach the MEA that then projects in a topographically arranged way into medial hypothalamic sub-circuits involved in reproduction (sexual dimorphic circuit) and/or defense reaction. These sub-circuits involve the medial premammillary region of the hypothalamus, and the st ends in the ventral premammillary nucleus. These structures act then through projections into the PAG. The reader may refer to several review articles or books that describes these pathways (Risold et al. 1997; Swanson 2000, 2012).

The results reported here can be summarized as follows:

- The pathway composed of the vlt and vlah may relay main olfactory information to the parvafox nucleus/NG, the CbN and to a lesser extent the PSTN in the premammillary hypothalamus.
- Furthermore, the PSTN may be an output target of projections from frontotemporal/autonomic component of the amygdala. We also observed that an anterior perifornical part of the LHA is included in this circuit, as well as the lateral parvicellular/forniceal parts of the PVH. Therefore, as it has already been described for the medial zone of the hypothalamus, our results suggest a pathway in the LHA in relation with the frontotemporal/autonomic component of the amygdala and maybe involved in the control of appetite and in relation with fear and pain. This pathway in the LHA would be the counterpart for the frontotemporal/autonomic component of the amygdala of the sub-circuits formed by hypothalamic medial zone nuclei with the medial component of the amygdala and involving the postcommissural part of the st.

In Chometton et al. (2016), we suggested the existence of a premammillary component in the LHA characterized as the caudal-most part of the LHA, an absence of GAD expression, but the expression of the tachykinin1 gene as in medial premammillary nuclei. The present work completes this picture by suggesting that the premammillary part of the hypothalamus contains a collection of discrete nuclei that receive topographically organized inputs from specific structures of the basal telencephalon, some of which are listed here (Fig. 20).

Conclusions

In conclusion, the PSTN and CbN form a caudal LHA nuclear group that is involved in complex and strong connections with several amygdalar nuclei. The CbN receives projections from the BMAa, while both the PSTN and the CbN are innervated by intense inputs from the CEA. Therefore, these nuclei are a major target in the hypothalamus for projections from the amygdala. One of the pathways travelling along the vlt may convey olfactory information to this nuclear complex in the premammillary LHA in a way similar to the relay of vomeronasal information to the hypothalamic ventral premammillary nucleus by the st. Although, the functions of these LHA nuclei remain under investigation, they seem to be related to the feeding behavior through the control of appetite.

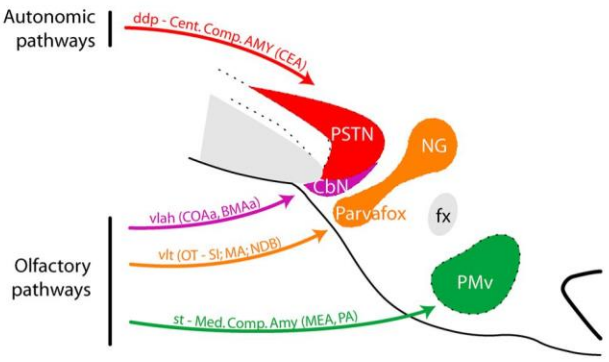

Fig. 20 Summary diagram to illustrate that the premammillary level of the hypothalamus contains several cell groups associated with specific basal telencephalic structures: the ventral premammillary nucleus receives the terminal input from the st that originates in the MEA and posterior (PA) nuclei of the amygdala (Canteras et al. 1992, 1995), the parvafox nucleus and NG receive the terminal projections from the vlt originating in the deep olfactory tubercle and magnocellular preoptic nucleus (Price 1985; Price et al. 1991), and the CbN receives the terminal projections from the COAa and BMAa (this study and Price 1985; Price et al. 1991). Finally, the PSTN is less involved by these olfactory inputs, but is innervated by projections transiting through a dorsal descending pathway (ddp) originating in the CEA (this study)

Acknowledgements This work was supported by the Region Franche-Comté, France. Authors wish to thank C. Houdayer and G. Franchi for technical assistances.

Compliance with ethical standards

Conflict of interest The authors declare that they have no conflict of interest.

References

Allen GV, Cechetto DF (1995) Neurotensin in the lateral hypothalamic area: origin and function. Neuroscience 69:533–544

Alvarez-Bolado G, Celio MR (2016) The ventrolateral hypothalamic area and the parvafox nucleus: role in the expression of (positive) emotions? J Comp Neurol 524:1616–1623. doi:10.1002/cne.23853

Bernard J-F, Alden M, Besson J-M (1993) The organization of the efferent projections from the pontine parabrachial area to the amygdaloid complex: a *Phaseolus vulgaris* leucoagglutinin (PHA-L) study in the rat. J Comp Neurol 329:201–229. doi:10.1002/cne.903290205

Bester H, Besson JM, Bernard JF (1997) Organization of efferent projections from the parabrachial area to the hypothalamus: a *Phaseolus vulgaris*-leucoagglutinin study in the rat. J Comp Neurol 383:245–281

Bienkowski MS, Rinaman L (2013) Common and distinct neural inputs to the medial central nucleus of the amygdala and anterior ventrolateral bed nucleus of stria terminalis in rats. Brain Struct Funct 218:187–208. doi:10.1007/s00429-012-0393-6

Bilella A, Alvarez-Bolado G, Celio MR (2014) Coaxiality of Foxb1- and parvalbumin-expressing neurons in the lateral hypothalamic PV1-nucleus. Neurosci Lett 566:111–114. doi:10.1016/j.neulet.2014.02.028

Bilella A, Alvarez-Bolado G, Celio MR (2016a) Birthdate of parvalbumin-neurons in the Parvafox-nucleus of the lateral hypothalamus. Brain Res 1633:111–114. doi:10.1016/j.brainres.2015.12.054

Bilella A, Alvarez-Bolado G, Celio MR (2016b) The Foxb1-expressing neurons of the ventrolateral hypothalamic parvafox nucleus project to defensive circuits: *Foxb1*-expressing neurons of the VL hypothalamic Parvafox nucleus. J Comp Neurol 524:2955–2981. doi:10.1002/cne.24057

Bourgeais L, Gauriau C, Bernard JF (2001) Projections from the nociceptive area of the central nucleus of the amygdala to the forebrain: a PHA-L study in the rat. Eur J Neurosci 14:229–255

Cai H, Haubensak W, Anthony TE, Anderson DJ (2014) Central amygdala PKC-δ^{+} neurons mediate the influence of multiple anorexigenic signals. Nat Neurosci 17:1240–1248. doi:10.1038/nn.3767

Campos CA, Bowen AJ, Schwartz MW, Palmiter RD (2016) Parabrachial CGRP neurons control meal termination. Cell Metab 23:811–820. doi:10.1016/j.cmet.2016.04.006

Canteras NS, Simerly RB, Swanson LW (1992) Connections of the posterior nucleus of the amygdala. J Comp Neurol 324:143–179. doi:10.1002/cne.903240203

Canteras NS, Simerly RB, Swanson LW (1995) Organization of projections from the medial nucleus of the amygdala: a PHAL study in the rat. J Comp Neurol 360:213–245. doi:10.1002/cne.903600203

Carter ME, Soden ME, Zweifel LS, Palmiter RD (2013) Genetic identification of a neural circuit that suppresses appetite. Nature 503:111–114. doi:10.1038/nature12596

Carter ME, Han S, Palmiter RD (2015) Parabrachial calcitonin gene-related peptide neurons mediate conditioned taste aversion. J Neurosci 35:4582–4586. doi:10.1523/JNEUROSCI.3729-14.2015

Carvalho MC, Santos JM, Brandão ML (2015) Dorsal periaqueductal gray post-stimulation freezing is counteracted by neurokinin-1 receptor antagonism in the central nucleus of the amygdala in rats. Neurobiol Learn Mem 121:52–58. doi:10.1016/j.nlm.2015.04.001

Cassell MD, Gray TS, Kiss JZ (1986) Neuronal architecture in the rat central nucleus of the amygdala: a cytological, hodological, and immunocytochemical study. J Comp Neurol 246:478–499. doi:10.1002/cne.902460406

Celio MR (1990) Calbindin D-28k and parvalbumin in the rat nervous system. Neuroscience 35:375–475

Celio MR, Babalian A, Ha QH et al (2013) Efferent connections of the parvalbumin-positive (PV1) nucleus in the lateral hypothalamus of rodents. J Comp Neurol 521:3133–3153. doi:10.1002/cne.23344

Chometton S, Pedron S, Peterschmitt Y, et al (2016) A premammillary lateral hypothalamic nuclear complex responds to hedonic but not aversive tastes in the male rat. Brain Struct Funct 221:2183–2208. doi:10.1007/s00429-015-1038-3

Croizier S, Cardot J, Brischoux F et al (2013) The vertebrate diencephalic MCH system: a versatile neuronal population in an evolving brain. Front Neuroendocrinol 34:65–87. doi:10.1016/j.yfrne.2012.10.001

D'Hanis W, Linke R, Yilmazer-Hanke DM (2007) Topography of thalamic and parabrachial calcitonin gene-related peptide (CGRP) immunoreactive neurons projecting to subnuclei of the amygdala and extended amygdala. J Comp Neurol 505:268–291. doi:10.1002/cne.21495

Dobolyi A, Irwin S, Makara G et al (2005) Calcitonin gene-related peptide-containing pathways in the rat forebrain. J Comp Neurol 489:92–119. doi:10.1002/cne.20618

Goforth PB, Leinninger GM, Patterson CM et al (2014) leptin acts via lateral hypothalamic area neurotensin neurons to inhibit orexin neurons by multiple GABA-independent mechanisms. J Neurosci 34:11405–11415. doi:10.1523/JNEUROSCI.5167-13.2014

Gonzales C, Chesselet MF (1990) Amygdalonigral pathway: an anterograde study in the rat with *Phaseolus vulgaris* leucoagglutinin (PHA-L). J Comp Neurol 297:182–200. doi:10.1002/cne.902970203

Goto M, Swanson LW (2004) Axonal projections from the parasubthalamic nucleus. J Comp Neurol 469:581–607. doi:10.1002/cne.11036

Gray TS, Carney ME, Magnuson DJ (1989) Direct projections from the central amygdaloid nucleus to the hypothalamic paraventricular nucleus: possible role in stress-induced adrenocorticotropin release. Neuroendocrinology 50:433–446

Groenewegen HJ, Berendse HW, Haber SN (1993) Organization of the output of the ventral striatopallidal system in the rat: ventral pallidal efferents. Neuroscience 57:113–142

Grove EA (1988a) Efferent connections of the substantia innominata in the rat. J Comp Neurol 277:347–364. doi:10.1002/cne.902770303

Grove EA (1988b) Neural associations of the substantia innominata in the rat: afferent connections. J Comp Neurol 277:315–346. doi:10.1002/cne.902770302

Hahn JD, Swanson LW (2012) Connections of the lateral hypothalamic area juxtadorsomedial region in the male rat. J Comp Neurol 520:1831–1890. doi:10.1002/cne.23064

Han S, Soleiman MT, Soden ME et al (2015) Elucidating an affective pain circuit that creates a threat memory. Cell 162:363–374. doi:10.1016/j.cell.2015.05.057

Heimer L, Zahm DS, Schmued LC (1990) The basal forebrain projection to the region of the nuclei gemini in the rat; a combined light and electron microscopic study employing horseradish peroxidase, fluorescent tracers and *Phaseolus vulgaris*-leucoagglutinin. Neuroscience 34:707–731

Heimer L, Harlan RE, Alheid GF et al (1997) Substantia innominata: a notion which impedes clinical-anatomical correlations in neuropsychiatric disorders. Neuroscience 76:957–1006

Krettek JE, Price JL (1978) Amygdaloid projections to subcortical structures within the basal forebrain and brainstem in the rat and cat. J Comp Neurol 178:225–253. doi:10.1002/cne.901780204

Lantos TA, Görcs TJ, Palkovits M (1995) Immunohistochemical mapping of neuropeptides in the premamillary region of the hypothalamus in rats. Brain Res Brain Res Rev 20:209–249

Larsen PJ (1992) Distribution of substance P-immunoreactive elements in the preoptic area and the hypothalamus of the rat. J Comp Neurol 316:287–313. doi:10.1002/cne.903160304

Leinninger GM, Jo Y-H, Leshan RL et al (2009) Leptin acts via leptin receptor-expressing lateral hypothalamic neurons to modulate the mesolimbic dopamine system and suppress feeding. Cell Metab 10:89–98. doi:10.1016/j.cmet.2009.06.011

Leinninger GM, Opland DM, Jo Y-H et al (2011) Leptin action via neurotensin neurons controls orexin, the mesolimbic dopamine system and energy balance. Cell Metab 14:313–323. doi:10.1016/j.cmet.2011.06.016

Leonard CM, Scott JW (1971) Origin and distribution of the amygdalofugal pathways in the rat: an experimental neuronatomical study. J Comp Neurol 141:313–329. doi:10.1002/cne.901410304

Liang S-H, Yin J-B, Sun Y et al (2016) Collateral projections from the lateral parabrachial nucleus to the paraventricular thalamic nucleus and the central amygdaloid nucleus in the rat. Neurosci Lett 629:245–250. doi:10.1016/j.neulet.2016.07.017

McDonald AJ (1982) Cytoarchitecture of the central amygdaloid nucleus of the rat. J Comp Neurol 208:401–418. doi:10.1002/cne.902080409

Mészár Z, Girard F, Saper CB, Celio MR (2012) The lateral hypothalamic parvalbumin-immunoreactive (PV1) nucleus in rodents. J Comp Neurol 520:798–815. doi:10.1002/cne.22789

Millhouse OE (1969) A Golgi study of the desending medial forebrain bundle. Brain Res 15:341–363

Millhouse OE, Uemura-Sumi M (1985) The structure of the nucleus of the lateral olfactory tract. J Comp Neurol 233:517–552. doi:10.1002/cne.902330411

Nakamura S, Tsumori T, Yokota S et al (2009) Amygdaloid axons innervate melanin-concentrating hormone- and orexin-containing neurons in the mouse lateral hypothalamus. Brain Res 1278:66–74. doi:10.1016/j.brainres.2009.04.049

Niu J-G, Yokota S, Tsumori T et al (2012) Projections from the anterior basomedial and anterior cortical amygdaloid nuclei to melanin-concentrating hormone-containing neurons in the lateral hypothalamus of the rat. Brain Res 1479:31–43. doi:10.1016/j.brainres.2012.08.011

Norgren R (1976) Taste pathways to hypothalamus and amygdala. J Comp Neurol 166:17–30. doi:10.1002/cne.901660103

Oka T, Tsumori T, Yokota S, Yasui Y (2008) Neuroanatomical and neurochemical organization of projections from the central amygdaloid nucleus to the nucleus retroambiguus via the periaqueductal gray in the rat. Neurosci Res 62:286–298. doi:10.1016/j.neures.2008.10.004

Ono T, Luiten PG, Nishijo H et al (1985) Topographic organization of projections from the amygdala to the hypothalamus of the rat. Neurosci Res 2:221–238

Ottersen OP (1980) Afferent connections to the amygdaloid complex of the rat and cat: II. Afferents from the hypothalamus and the basal telencephalon. J Comp Neurol 194:267–289. doi:10.1002/cne.901940113

Pape HC, Pare D (2010) Plastic synaptic networks of the amygdala for the acquisition, expression, and extinction of conditioned fear. Physiol Rev 90:419–463. doi:10.1152/physrev.00037.2009

Paxinos G, Watson C (2005) The rat brain in stereotaxic coordinates†, 5th ed. Elsevier Academic Press, Amsterdam

Petrovich GD, Swanson LW (1997) Projections from the lateral part of the central amygdalar nucleus to the postulated fear conditioning circuit. Brain Res 763:247–254

Petrovich GD, Risold PY, Swanson LW (1996) Organization of projections from the basomedial nucleus of the amygdala: a PHAL study in the rat. J Comp Neurol 374:387–420. doi:10.1002/(SICI)1096-9861(19961021)374:3<387::AID-CNE6>3.0.CO;2-Y

Petrovich GD, Ross CA, Mody P et al (2009) Central, but not basolateral, amygdala is critical for control of feeding by aversive learned cues. J Neurosci 29:15205–15212. doi:10.1523/JNEUROSCI.3656-09.2009

Price JL (1985) Beyond the primary olfactory cortex: olfactory-related areas in the neocortex, thalamus and hypothalamus. Chem Senses 10:239–258. doi:10.1093/chemse/10.2.239

Price JL, Slotnick BM, Revial M-F (1991) Olfactory projections to the hypothalamus. J Comp Neurol 306:447–461. doi:10.1002/cne.903060309

Reppucci CJ, Petrovich GD (2016) Organization of connections between the amygdala, medial prefrontal cortex, and lateral hypothalamus: a single and double retrograde tracing study in rats. Brain Struct Funct 221:2937–2962. doi:10.1007/s00429-015-1081-0

Risold PY, Fellmann D, Rivier J et al (1992) Immunoreactivities for antisera to three putative neuropeptides of the rat melanin-concentrating hormone precursor are coexpressed in neurons of the rat lateral dorsal hypothalamus. Neurosci Lett 136:145–149

Risold PY, Thompson RH, Swanson LW (1997) The structural organization of connections between hypothalamus and cerebral cortex. Brain Res Rev 24:197–254. doi:10.1016/S0165-0173(97)00007-6

Santiago AC, Shammah-Lagnado SJ (2004) Efferent connections of the nucleus of the lateral olfactory tract in the rat. J Comp Neurol 471:314–332. doi:10.1002/cne.20028

Schwaber JS, Sternini C, Brecha NC et al (1988) Neurons containing calcitonin gene-related peptide in the parabrachial nucleus project to the central nucleus of the amygdala. J Comp Neurol 270(416–426):398–399

Scott JW, Chafin BR (1975) Origin of olfactory projections to lateral hypothalamus and nuclei gemini of the rat. Brain Res 88:64–68

Scott JW, Leonard CM (1971) The olfactory connections of the lateral hypothalamus in the rat, mouse and hamster. J Comp Neurol 141:331–344. doi:10.1002/cne.901410305

Scott JW, Pfaffmann C (1967) Olfactory input to the hypothalamus: electrophysiological evidence. Science 158:1592–1594

Shammah-Lagnado SJ, Alheid GF, Heimer L (2001) Striatal and central extended amygdala parts of the interstitial nucleus of the posterior limb of the anterior commissure: evidence from tract-tracing techniques in the rat. J Comp Neurol 439:104–126. doi:10.1002/cne.1999

Shimada S, Shiosaka S, Emson PC et al (1985) Calcitonin gene-related peptidergic projection from the parabrachial area to the forebrain and diencephalon in the rat: an immunohistochemical analysis. Neuroscience 16:607–616. doi:10.1016/0306-4522(85)90195-2

Shin J-W, Geerling JC, Stein MK et al (2011) FoxP2 brainstem neurons project to sodium appetite regulatory sites. J Chem Neuroanat 42:1–23. doi:10.1016/j.jchemneu.2011.05.003

Shirasu M, Takahashi T, Yamamoto T et al (2011) Direct projections from the central amygdaloid nucleus to the mesencephalic trigeminal nucleus in rats. Brain Res 1400:19–30. doi:10.1016/j.brainres.2011.05.026

Spooren WP, Veening JG, Groenewegen HJ, Cools AR (1991) Efferent connections of the striatopallidal and amygdaloid components of the substantia innominata in the cat: projections to the nucleus accumbens and caudate nucleus. Neuroscience 44:431–447

Swanson LW (2000) Cerebral hemisphere regulation of motivated behavior. Brain Res 886:113–164

Swanson LW (2004) Brain maps: structure of the rat brain, 3 edn. Elsevier, San Diego

Swanson LW (2012) Brain architecture: understanding the basic plan. Oxford University Press

Swanson LW, Petrovich GD (1998) What is the amygdala? Trends Neurosci 21:323–331

Tsumori T, Yokota S, Qin Y et al (2006) A light and electron microscopic analysis of the convergent insular cortical and amygdaloid projections to the posterior lateral hypothalamus in the rat, with special reference to cardiovascular function. Neurosci Res 56:261–269. doi:10.1016/j.neures.2006.07.005

Veening JG, Swanson LW, Cowan WM et al (1982) The medial forebrain bundle of the rat. II. An autoradiographic study of the topography of the major descending and ascending components. J Comp Neurol 206:82–108. doi:10.1002/cne.902060107

Veening JG, Swanson LW, Sawchenko PE (1984) The organization of projections from the central nucleus of the amygdala to brainstem sites involved in central autonomic regulation: a combined retrograde transport-immunohistochemical study. Brain Res 303:337–357

Veening JG, Te Lie S, Posthuma P et al (1987) A topographical analysis of the origin of some efferent projections from the lateral hypothalamic area in the rat. Neuroscience 22:537–551

Wallace DM, Magnuson DJ, Gray TS (1992) Organization of amygdaloid projections to brainstem dopaminergic, noradrenergic, and adrenergic cell groups in the rat. Brain Res Bull 28:447–454

Wang PY, Zhang FC (1995) Outline and atlas of learning rat brain slices. Westnorth University Press, China

Yasoshima Y, Scott TR, Yamamoto T (2006) Memory-dependent c-Fos expression in the nucleus accumbens and extended amygdala following the expression of a conditioned taste aversive in the rat. Neuroscience 141:35–45. doi:10.1016/j.neuroscience.2006.03.019

Yu K, Garcia da Silva P, Albeanu DF, Li B (2016) Central amygdala somatostatin neurons gate passive and active defensive behaviors. J Neurosci 36:6488–6496. doi:10.1523/JNEUROSCI.4419-15.2016

Zahm DS, Williams E, Wohltmann C (1996) Ventral striatopallidothalamic projection: IV. Relative involvements of neurochemically distinct subterritories in the ventral pallidum and adjacent parts of the rostroventral forebrain. J Comp Neurol 364:340–362. doi:10.1002/(SICI)1096-9861(19960108)364:2<340::AID-CNE11>3.0.CO;2-T

Zséli G, Vida B, Martinez A et al (2016) Elucidation of the anatomy of a satiety network: focus on connectivity of the parabrachial nucleus in the adult rat: refeeding-activated contacts of the PB. J Comp Neurol 524:2803–2827. doi:10.1002/cne.23992

2. Analyse chémoarchitecturale du CEA (Publication n°2)

Le CEA, impliqué dans de nombreuses fonctions en relation avec les émotions, l'alimentation et les addictions, est une importante source de projections sur le LHA postérieur et le tronc cérébral. Dans notre précédent travail, les projections de l'amygdale dans le complexe PSTN/CbN ont été analysées avec attention (Barbier *et al*, 2017). Cependant, certaines zones d'ombres persistaient concernant les limites des différentes parties du CEA et, par conséquent, concernant l'origine de certaines projections dans l'hypothalamus. En effet, quelques difficultés émergent lorsqu'il s'agit de corréler nos observations anatomiques avec les frontières du CEA comme définit dans les atlas (Swanson, 2004; Paxinos & Watson, 2005, 2013). Classiquement divisé en une partie capsulaire, une partie médiane et une partie latérale, ses frontières ne sont cependant pas toujours clairement définies. Cette complexité cytoarchitecturale est accentuée par les études neurochimiques, divisant par exemple la partie latérale en trois zones (Cassell *et al*, 1999; Marchant *et al*, 2007; Kim *et al*, 2017).

Dans l'étude faisant l'objet de l'article 2, il a été observé qu'après injection de FG dans la région tubérale antérieure du LHA (le LHApfx), des neurones marqués formaient une condensation compacte dans le CEA chez le rat. Ce groupe de neurones étant comparable à ce qu'avait initialement décrit A.J. McDonald en 1982 sur la base d'observations histologiques (McDonald, 1982, 1997) identifiant ainsi une partie intermédiaire du CEA (CEAi). Dans ce travail, des marqueurs neurochimiques susceptibles de caractériser ce groupe cellulaire ont été recherchés. La partie intermédiaire a été généralement englobée dans le CEAl, mais elle est clairement une division à part entière de ce noyau. A.J. McDonald avait montré un marquage calbindine spécifique chez le rat qui la distingue des autres divisions du CEA (McDonald, 1997). Ce groupe cellulaire calbindine positif est également intensément innervé par des projections tyrosine hydroxylase (TH) et méthionine-Enk, modérément par la corticolibérine (CRH) et faiblement par CGRP. Au niveau de ses connexions, le patron de projections du CEAi présente des similarités avec celui du CEAm. Cependant, concernant ses afférences, le CEAi, contrairement au CEAm, est dépourvu de toute innervation du FS mais est la cible de projections de la partie postérieure de l'aire agranulaire insulaire dorsale (AId). Chez la souris, après injection de Ctb dans la région périfornicale antérieure du LHA, les neurones rétrogradement marqués dans la partie antérieure et médiane du CEAl forment un groupe cellulaire moins distinct et moins bien organisé que chez le rat. Ces cellules n'expriment pas la calbindine et sont localisées dans la partie médiane de la zone exprimant la protéine kinase C delta (PKC-δ) positive du CEAl. Le marquage Ctb rétrograde s'étend sur une bande dorso-ventrale par rapport à la "zone PKC-δ" débordant dans le CEAm, soulignant une différence d'organisation chez la souris comparée au rat.

En conclusion, les données des études passées concernant notamment les frontières du CEAl ont donc été complétées par l'analyse de la distribution de calbindine, CRH, NT, Enk et PKC-δ avec d'autres marqueurs, tels que CGRP et TH qui ne sont exprimés que par des axones afférents. Les

parties capsulaire et latérale du CEA ne sont pas homogènes comme en témoigne la division spécifique du CEAl, nommée CEAi. Particulièrement bien différenciée chez le rat par ses projections sur le LHApfx et son marquage calbindine, elle n'avait jamais été décrite chez la souris. Soulignant des différences entre ces deux espèces, tant dans l'organisation que la neurochimie du CEA, le CEAi forme néanmoins une condensation cellulaire plus discrète chez la souris. Ce travail a montré que le CEA, bien que très étudié, est une structure hétérogène et très complexe dont certaines frontières des différentes parties sont encore assez floues et mal comprises. Ce noyau amygdalien central nécessite encore des investigations. Par exemple, la délimitation actuelle de sa partie capsulaire ne correspond pas entièrement à son innervation CGRP. De la même manière, le CEAm ne semble pas projeter uniformément dans l'hypothalamus selon la localisation plus antérieure ou postérieure du site d'injection d'un traceur antérograde comme le PHAL.

Received: 8 February 2018 | Revised: 14 May 2018 | Accepted: 17 May 2018

DOI: 10.1002/cne.24470

WILEY JCN RESEARCH IN SYSTEMS NEUROSCIENCE THE JOURNAL OF COMPARATIVE NEUROLOGY

RESEARCH ARTICLE

Characterization of McDonald's intermediate part of the Central nucleus of the amygdala in the rat

Marie Barbier | Dominique Fellmann | Pierre-Yves Risold

EA481, UFR Sciences Médicales et Pharmaceutiques, 19 rue Ambroise Paré, Université Bourgogne Franche-Comté, Besançon cedex, 25030, France

Correspondence
Pierre-Yves Risold, EA481, UFR Sciences Médicales et Pharmaceutiques, 19 rue Ambroise Paré, Université Bourgogne Franche-Comté, Besançon cedex 25030, France.
Email: pierre-yves.risold@univ-fcomte.fr

Funding information
Région Franche-Comté

Abstract

The actual organization of the central nucleus of the amygdala (CEA) in the rat is mostly based on cytoarchitecture and the distribution of several cell types, as described by McDonald in 1982. Four divisions were identified by this author. However, since this original work, one of these divisions, the intermediate part, has not been consistently recognized based on Nissl-stained material. In the present study, we observed that a compact condensation of retrogradely labeled cells is found in the CEA after fluorogold injection in the anterior region of the tuberal lateral hypothalamic area (LHA) in the rat. We then searched for neurochemical markers of this cell condensation and found that it is quite specifically labeled for calbindin (Cb), but also contains calretinin (Cr), tyrosine hydroxylase (TH) and methionine-enkephalin (Met-Enk) immunohistochemical signals. These neurochemical features are specific to this cell group which, therefore, is distinct from the other parts of the CEA. We then performed cholera toxin injections in the mouse LHA to identify this cell group in this species. We found that neurons exist in the medial and rostral CEAl that project into the LHA but they have a less tight organization than in the rat.

KEYWORDS

calbindin, calretinin, intermediate part of the central amygdalar nucleus, tyrosine hydroxylase, RRID:AB_10000347, RRID:AB_725807, RRID:AB_10000321, RRID:AB_518251, RRID:AB_726859, RRID:AB_2314412, RRID:AB_572250, RRID:AB_572254, RRID:AB_10000343, RRID:AB_2315142, RRID:AB_10000080, RRID:AB_397781, RRID:AB_2201528, RRID:AB_10562715; RRID:AB_2536180; RRID:AB_2313606; RRID:AB_2340819; RRID:AB_2340411; RRID:SCR_013672

Abbreviations: ac, Anterior commissure; AHN, Anterior hypothalamic nucleus; AId, Agranular insular area, dorsal part; ARH, Arcuate hypothalamic nucleus; AS, Antiserum; BLA, Basolateral amygdalar nucleus; BST, Bed nuclei stria terminalis; Cb, Calbindin; CbN, Calbindin nucleus; CEA, Central amygdalar nucleus; CEAc, Central amygdalar nucleus, capsular part; CEAc, d, Central amygdalar nucleus, capsular part, dorsal zone; CEAc, v, Central amygdalar nucleus, capsular part, ventral zone; CEAi, Central amygdalar nucleus, intermediate part; CEAl, Central amygdalar nucleus, lateral part; CEAl, c, Central amygdalar nucleus, lateral part, central zone; CEAl, l, Central amygdalar nucleus, lateral part, lateral zone; CEAm, Central amygdalar nucleus, medial part; CGRP, Calcitonin gene-related peptide; cpd, Cerebral peduncle; Cr, Calretinin; CRH, Corticotropin-releasing factor; Ctb, Cholera toxin subunit B; DMH, Dorsomedial hypothalamic nucleus; FG, Fluorogold; fx, Columns of the fornix; IA, Intercaleted amygdalar nuclei; IPAC, Interstitial nucleus of the posterior limb of the anterior commissure; LHA, Lateral hypothalamic area; LHAd, Lateral hypothalamic area, dorsal region; LHAjd, Lateral hypothalamic area, juxtadorsomedial region; LHAjvd, Lateral hypothalamic area, juxtaventromedial region, dorsal zone; LHAjvv, Lateral hypothalamic area, juxtaventromedial region, ventral zone; LHAm, Lateral hypothalamic area, magnocellular nucleus; LHApc, Lateral hypothalamic area, parvicellular region; LHAs, Lateral hypothalamic area, suprafornical region; LHAsfp, Lateral hypothalamic area, subfornical region, posterior zone; LHAvm, Lateral hypothalamic area, ventral region, medial zone; Met-Enk, Methionine Enkephalin; mtt, Mammillothalamic tract; NG, Nucleus gemini; NT, Neurotensin; PH, Posterior hypothalamic nucleus; PHAL, *Phaseolus vulgaris* leucoagglutinin; PKC-δ, Protein Kinase C delta; PS, Parastrial nucleus; PV, Parvalbumin; PVH, Paraventricular hypothalamic nucleus; PVHf, Paraventricular hypothalamic nucleus, forniceal part; PSTN, Parasubthalamic nucleus; RRID, Research Resource Identifiers; st, Stria terminalis; STN, Subthalamic nucleus; TH, Tyrosine Hydroxylase; TU, Tuberal nucleus; TUi, Tuberal nucleus, intermediate part; TUsv, Tuberal nucleus, subventricular part; V3h, Third ventricle, hypothalamic part; vlt, Ventrolateral hypothalamic tract; VMH, Ventromedial hypothalamic nucleus; ZI, Zona incerta; ZIda, Zona incerta, dopaminergic group

1 | INTRODUCTION

The CEA has a strategic position within the amygdala network (Swanson & Petrovich, 1998). This nucleus is a major output station for amygdalo-fugal projections toward the lateral hypothalamus and brainstem, and is involved in a large range of functions in relation to emotion, feeding, and addiction (Holland, Petrovich, & Gallagher, 2002; Paré, Quirk, & Ledoux, 2004; Koob & Volkow, 2010; Cole, Powell, & Petrovich, 2013; Koob, 2013; Partin et al., 2013; George, Koob, & Vendruscolo, 2014; Holland & Hsu, 2014). This nucleus has a quite complex organization, only imperfectly rendered by the current parceling in atlases of the rodent brain. In these reference books, the CEA is divided onto a capsular, a lateral and a medial part. However, the borders of the nucleus and of each part diverge (Allen Institute, 2004; Swanson, 2004; Paxinos & Keith, 2012; Paxinos & Watson, 2013). The cheer complexity of the nucleus is also keenly illustrated by neurochemical studies. For example, the lateral part can be subdivided into three divisions (Cassell, Freedman, & Shi, 1999; Marchant, Densmore, & Osborne, 2007; Kim, Zhang, Muralidhar, LeBlanc, & Tonegawa, 2017). It encloses a particular cell group that reacts to calbindin antibodies and that was initially identified by McDonald as a fourth part in the CEA and named the intermediate part (McDonald, 1988, 1997). It is notable that in the mouse, such an intermediate part was not described yet and it is a matter of fact that a cell group labeled for calbindin is not reported in this species. The Allen Brain Atlas does not signal intense expression of the caldindin1 gene in the mouse CEA (Allen Institute, 2004). Besides, these neurochemical considerations, connectional evidence also suggest that the CEAl is not homogeneous. Many works in the mouse report specific intra-nuclear connections with important functional implications (Haubensak et al., 2010; Kim et al., 2017) and in the rat, several studies signaled projections into the hypothalamus from a rostral portion, but not from caudal regions of the CEAl (Petrovich & Swanson, 1997; Swanson & Petrovich, 1998; Petrovich, Setlow, Holland, & Gallagher, 2002; Reppucci & Petrovich, 2016). In a recent work in which we analyzed connections from the CEA into the parasubthalamic nucleus (PSTN) of the posterior LHA (Barbier et al., 2017), we signaled that it was difficult to correlate anatomical observations with actual borders of and within the CEA as defined in atlases. We also signaled discrepancies in the literature concerning projections into the hypothalamus, especially from the medial part of the nucleus. Therefore, we believe that important aspects of the connections with the hypothalamus of this otherwise very well studied nucleus still need investigations.

In the present work, we combined retrograde tract tracing from the LHA with a neurochemical analysis of the CEA in the rat. We also added observation in the mouse using a similar approach. It seems that slight differences in the organization of the nucleus exist between the two species. However, both have cells in the medial CEAl region, also referred here as the CEAi, that project into the perifornical hypothalamus.

2 | MATERIAL AND METHODS

2.1 | Animals

All animal use and care protocols were in accordance with institutional guidelines and with the Directive 2010/63/EU of the European Parliament and of the Council of 22 September 2010 on the protection of animals used for scientific purposes. The protocols were approved by the Franche-Comté University's Animal Care Committee (protocol number: 2015-002) and the investigators were authorized. Eleven Sprague–Dawley rats, weighing 300–350 g, were obtained from Janvier (Le Genest-Saint-Isle, France). Rats were housed with a standard 12 hr light/dark cycle at a constant room temperature and had free access to the standard laboratory diet and water.

2.2 | Characterization of primary antisera

Table 1 lists the antigen, immunogen, manufacturer, catalog/lot number, species in which the antibodies were raised, and working dilution for each of the primary antibodies. Information about the specificity of the antibodies in the following paragraphs are from the manufacturers and/or the cited references.

2.2.1 | Anti-Cb and anti-Cr

The monoclonal Cb antibody reacts specifically with Cb D-28k on immunoblots of extracts of tissue originating from human, monkey, guinea pig, rabbit, rat, mouse, and chicken (but probably not fish). It specifically stains the 45Ca-binding protein spot of Cb D-28k in a two-dimensional gel.

The polyclonal Cr antibody reacts specifically with Cr in tissue originating from human, monkey, rat, mouse, guinea pig, chicken and fish. This antiserum does not cross-react with Cb D-28k or other known calcium binding-proteins, as determined by immunoblots and by its distribution in the brain. Antibodies against the calcium-binding protein Cr and Cb D28K have been shown to label photoreceptors and horizontal cells in the studies of the amphibian retina (Pasteels, Rogers, Blachier, & Pochet, 1990; Deng et al., 2001; Zhang, Zhang, & Wu, 2006).

2.2.2 | Anti-calcitonin gene-related peptide (CGRP)

This CGRP antibody is thought to react with the whole molecule (1-37) and the 23-37 fragment (C term). It is specifically used to visualize CGRP in brain cells. This antibody produced the same staining pattern in the rat brain as previously reported for other CGRP antibodies (Shimada et al., 1985; Yasui, Saper, & Cechetto, 1991; Holtz, Fu, Loflin, Corson, & Erisir, 2015).

2.2.3 | Anti-corticotropin-releasing hormone (CRH)

According to the manufacturer's data, this CRH antibody has been shown via enzyme and radioimmunoassay to cross-react at 100% with the rat CRH peptide and to show no cross-reactivity with other neuropeptides. Piekut and Phipps (1998) have shown that pre-absorption of the antiserum with the CRH peptide abolished the immunolabeling. In this study, the antibody produced the same staining pattern in the rat brain as previously reported for other CRH antibodies (Olschowka, O'Donohue, Mueller, & Jacobowitz, 1982; Swanson, Sawchenko, Rivier, & Vale, 1983; Asan et al., 2005; Li & Kirouac, 2008).

TABLE 1 Primary antibodies used in this study

Antibody	Immunogen	Source	Dilution
Anti-Cb	IgG1 produced by hybridization of mouse myeloma cells with spleen cells from mice immunized with calbindin D-28k purified from chicken gut	Mouse, monoclonal, Swant, Cat# 300, RRID:AB_10000347	1:1,000
Anti-CGRP	Synthetic peptide corresponding to rat CGRP (C terminal)	Goat, polyclonal, Abcam Cat# ab36001, RRID:AB_725807	1:3,000
Anti-Cr	Produced by immunization with recombinant human calretinin containing a 6-his tag at the N-terminal	Rabbit, polyclonal, Swant, Cat# 7699/3H, RRID:AB_10000321	1:5,000
Anti-CRH	Collected from rabbits immunized with a synthetic peptide as the immunogen	Rabbit, polyclonal, Peninsula Laboratories Cat# T-4036.0400, RRID:AB_518251	1:10,000
Anti-Ctb	Purified Choleragenoid. Reacts with the beta subunit of Cholera toxin	Rabbit, polyclonal, Abcam Cat# ab34992, RRID:AB_726859	1:1,000
Anti-FG	Fluorogold	Rabbit, polyclonal, Millipore® Cat# 153, Lot LV1644476, RRID:AB_2314412	1:3,000
Anti-Met-Enk	Synthetic methionine enkephalin coupled to bovine thyroglobulin (BTg) with glutaraldehyde	Rabbit, polyclonal, ImmunoStar Cat# 20065, RRID:AB_572250	1:5,000
Anti-NT	Synthetic peptide (human) neurotensin coupled to bovine thyroglobulin (BTg) with glutaraldehyde	Rabbit, polyclonal, ImmunoStar Cat# 20072, RRID:AB_572254	1:8,000
Anti-PV	IgG1 produced by hybridization of mouse myeloma cells with spleen cells from mice immunized with parvalbumin purified from carp muscles	Mouse, monoclonal, Swant Cat# 235, RRID:AB_10000343	1:2,000
Anti-PHAL	PHA-E et PHA-L	Rabbit, polyclonal, Vector Laboratories® Cat# AS-2300, lot No. ZC0303, RRID:AB_2315142	1:1,000
Anti- PHAL	PHA-E et PHA-L	Goat, polyclonal, Vector Laboratories® Cat# AS-2224 W0131, RRID:AB_10000080	1:1,000
Anti- PKC-δ	Human PKCδ aa. 114-289	Mouse, monoclonal, BD Biosciences Cat# 610398, RRID:AB_397781	1:5,000
Anti-TH	Purified from PC12 cells	Mouse, monoclonal, Millipore Cat# MAB318, RRID:AB_2201528	1:10,000

2.2.4 | Anti- cholera toxin subunit B (Ctb), anti-fluorogold (FG) and anti- *Phaseolus vulgaris* leucoagglutinin (PHAL)

Antibody to Ctb showed no signal in the absence of injected Ctb (Quina et al., 2015).

The Fluorescent Gold (hydroxystilbamidine or FG) antibody used in the present study was a rabbit polyclonal antibody raised against a peptide mapping to hydroxystilbamidine (Schmued & Fallon, 1986; García Del Caño, Gerrikagoitia, & Martínez-Millán, 2000). This antibody reacts with any species sample treated with FG; we did not observe any FG-like immunostaining when using the anti-FG antibody in animals not injected with FG. The cells labeled by the FG antibody also displayed their endogenous fluorescence when viewed with UV illumination (White et al., 2016).

To detect PHAL, we used polyclonal antibodies directed against PHAL and raised in rabbit or goat immunized with the purified lectin. They recognize both PHAL and the related *Phaseolous vulgaris* erythroagglutinin, neither of which is found in the mammalian brain. Hence, specificity is established by the absence of immunoreactivity for PHAL in brain sections from naïve animals, from cases in which the uptake and transport of PHAL failed, and from regions that do not receive innervation from the area of tracer injection (Balcita-Pedicino, Omelchenko, Bell, & Sesack, 2011).

2.2.5 | Anti-Met-Enk and anti-neurotensin (NT)

These antibodies were collected from rabbits immunized with a synthetic Met-Enk or NT coupled to bovine thyroglobulin (BTg) with glutaraldehyde. As a control for antibody specificity, pre-absorption of the Met-Enk and NT antibody with an excess of the native peptide resulted in the complete absence of immunolabeling for NT. Method specificity controls for Met-Enk or NT immunocytochemistry, performed by omitting the primary antibody at either of the two successive incubation steps, also failed to reveal immunolabeling for the respective antigens (Emson, Goedert, Williams, Ninkovic, & Hunt, 1982; Woulfe & Beaudet, 1992; François et al., 2017).

2.2.6 | Anti-parvalbumin (PV)

Anti-PV mouse monoclonal antibody was raised against purified carp muscle PV (Celio, Baier, Schärer, de Viragh, & Gerday, 1988; Clarke, Emson, & Irvine, 2009). The antibody reacts specifically with PV in human, monkey, rabbit, rat, mouse, chicken and fish tissue. The antibody specifically identifies 12-kDa, IEF-4.9 PV by 2D immunoblot and shows an absence of staining in the brain of a PV knockout mouse (manufacturer's technical information).

2.2.7 | Anti-protein kinase C Delta (PKC-δ)

We used the monoclonal anti-PKC-δ antibody (Han, Soleiman, Soden, Zweifel, & Palmiter, 2015; Campos, Bowen, Schwartz, & Palmiter, 2016). This antibody is routinely tested by western blot analysis by the manufacturer.

2.2.8 | Anti-TH

We used the monoclonal anti-TH antibody raised in mouse monoclonal IgG1k ascites fluid containing 0.01 M PBS, pH 7.1. According to the manufacturer's description, the specificity of this antibody was examined using Western blot. It recognizes an epitope on the outside

of the regulatory N-terminus corresponding to a protein of approximately 59–61 kDa. It does not cross-react with dopamine-beta hydroxylase, phenylalanine hydroxylase, tryptophan hydroxylase, dehydropteridine reductase, sepiapterin reductase, or phenyl ethanolamine-N-methyl transferase (as reported by the manufacturer). This antibody provides strong labeling of all regions known to contain dopaminergic and noradrenergic neuronal elements such as the ventral midbrain and the striatum. Milman and Woulfe (2013) have detected intense TH-immunoreactive cell bodies in the substantia nigra pars compacta and in locus coeruleus, areas which are known to contain catecholaminergic neurons.

2.3 | Tracer injections

Rats were anesthetized with an intraperitoneal (i.p.) injection of a mixture of xylazine and ketamine (1 mg/100 g and 10 mg/100 g of body weight, respectively; Vetoquinol®, France) and placed in a stereotaxic device. Mice were anesthetized with isoflurane (0.5 l/min) before the stereotaxic surgery.

2.3.1 | Anterograde tracer into the central amygdala nucleus, the fundus striatum (FS) and the dorsal part of the agranular insular cortex (AId) in the rat

Six rats received a unilateral iontophoretic injection of 2.5% PHAL diluted in sodium phosphate buffer saline (NaPBS) pH 7.2. Glass micropipettes (tip diameter: 10–20 μm) were used to inject the PHAL iontophoretically (intermittent current of 5 μA and 7 s on/off time for 20 min). Coordinates were taken from Bregma using the Paxinos' atlas (Paxinos & Watson, 2005). For the CEA, the coordinates were AP: −1.53 mm, ML: 3.2 mm, and DV: −8.2 mm; AP: −1.78 mm, ML: 3.5 mm, and DV: −8.5 mm; AP: −1.78 mm, ML: 3.8 mm, and DV: −8.2 mm; and AP: −2.45 mm, ML: 4.0 mm, and DV: −8.6 mm. For the FS, the coordinates were AP: −0.26 mm, ML: 3.2 mm, and DV: −7.4 mm, and for the AId, the coordinates were AP: 1.45 mm, ML: 2.0 mm, and DV: −7.2 mm, with an angle of 30 °. To avoid PHAL diffusion along the micropipette track, the micropipette was left in place for another 5 min before being removed. Two experiments (FS and AId) were from our collection of PHAL-injected brains and were not performed specifically for this study. The fundus experiment was already described in Barbier et al. (2017).

2.3.2 | Retrograde tracer into the perifornical region of the LHA in the rat

Five rats received a unilateral iontophoretic injection of a 10% solution of FG diluted in 0.9% sodium chloride (NaCl) into the LHA. The coordinates were AP: −2.45 mm, ML: 1.6 mm, and DV: −8.4 mm; and AP: −3.25 mm, ML: 1.7 mm, DV: −8.3 mm. Glass micropipettes (tip diameter: 30–50 μm) were used to inject the FG iontophoretically into these regions (intermittent current of 5 μA and 7 s on/off time for 5 min). After the injection, the micropipettes were left in place for another 5 min before being removed. At 10–15 days after the injection, the brains were processed for immunohistochemistry, as described below.

2.3.3 | Retrograde tracer into the perifornical region of the LHA in the mouse

Four mice received a unilateral iontophoretic injection of a 10% solution of FG diluted in 0.9% NaCl into the LHA. Three mice received a unilateral iontophoretic injection of a solution of Ctb (10 mg/ml) diluted in distilled water into the LHA. The coordinates, based on standard atlas coordinates (Paxinos & Keith, 2012), were AP: −1.0 mm, ML: 0.8 mm, and DV: −5.0 mm; and AP: −1.2 mm, ML: 1.0 mm, DV: −5.2 mm. Glass micropipettes (tip diameter: 30–50 μm for the FG and 10–20 μm for the Ctb) were used to inject the tracers iontophoretically into these regions (intermittent current of 4 μA and 7 s on/off time for 5 min for the FG and 30 min for the Ctb). After the injection, the micropipettes were left in place for another 5 min before being removed. At 15 days (for the FG) or 5 days (for the Ctb) after the injection, the brains were processed for immunohistochemistry, as described below.

2.4 | Tissue preparation

Rats and mice were deeply anesthetized with an i.p. injection of Pentobarbital (CEVA®, 50 mg/kg). Animals were perfused transcardially with 0.9% NaCl, followed by ice-cold 4% paraformaldehyde (PFA, Roth®) fixative in 0.1 M phosphate buffer (PB) at pH 7.4. Brains were extracted, post-fixed for 20 hr in the same fixative at 4 °C, and cryoprotected by saturation in a 15% sucrose solution (Sigma®) in 0.1 M PB for 24 hr at 4 °C. Tissues were cut in four series of coronal 30 μm thick sections, collected in a cryoprotective solution [1:1:2 glycerol/ethylene glycol/phosphate buffer saline (PBS)], and stored at −40 °C.

2.5 | Enzymatic immunohistochemistry

After rinsing in PBS with 0.3% Triton X100 (PBS-T), free-floating sections were incubated with the anti-Cb, anti-Cr, anti-FG, anti-PHAL, or anti-PV antibodies (Table 1) in a milk solution for 48 hr at 4 °C. Sections were incubated for 4 hr at room temperature in a solution of biotinylated goat anti-rabbit IgG at a dilution of 1:1,000 in PBS-T. Then, sections were placed in the mixed avidin-biotin horseradish peroxidase (HRP) complex solution (ABC Elite Kit, Vector Laboratories®) for 1 hr at room temperature. The peroxidase complex was visualized by 6 min exposure to a chromogen solution containing 0.04% 3,3′diaminobenzidine tetrahydrochloride (DAB, Sigma®) with 0.006% hydrogen peroxide (Sigma®) in PBS. The reaction was stopped by extensive washing in PBS. Sections were mounted on gelatin-coated slides. Sections of another series of the same brain were mounted and then stained in a solution of 1% toluidine blue (Roth®) in water to serve as a reference for cytoarchitectonic purposes. Finally, sections were dehydrated and cover-slipped with Canada balsam (Roth®).

2.6 | Immunofluorescent staining

After rinsing in PBS-T, free-floating sections were incubated with primary antibodies (Table 1) dissolved in PBS-T, 1% bovine serum albumin, 10% lactoproteins, and 0.01% sodium azide or only in PBS-T for 24 hr at 4 °C. Tissues were washed three times with PBS-T (5 min each) and incubated for 2 hr with appropriate secondary antibodies

TABLE 2 Secondary antibodies used in this study

Antibody	Type	Source	Dilution
Alexa Fluor 488	Anti-rabbit IgG	Invitrogen®, goat, Thermo Fisher Scientific Cat#A11034, Lot 1141875, RRID:AB_10562715	1:1,000
Alexa Fluor 555	Anti-mouse IgG	Invitrogen®, donkey, Thermo Fisher Scientific Cat#A31570, Lot 1117032, RRID:AB_2536180	1:1,000
Biotinylated	Anti-rabbit IgG	Vector Laboratories®, goat, Cat#BA-1000, Lot ZA0520, RRID:AB_2313606	1:1,000
Cyanine 5	Anti-mouse IgG	Jackson Immunoresearch, donkey, Cat#715-175-150, Lot A31570, RRID:AB_2340819	1:1,000
Cyanine 3	Anti-goat IgG	Jackson Immunoresearch, donkey, Cat# 705-165-003, RRID:AB_2340411	1:1,000

(Table 2) diluted in PBS-T at room temperature. For triple-labeling, this procedure was repeated twice with primaries raised in different species (Table 1). In some cases, FG was detected by auto-fluorescence. Finally, sections were washed with PBS-T, mounted on gelatin-coated slides and cover-slipped with 60/40 glycerol: PBS-T.

2.7 | Image acquisition and processing

Sections were analyzed on an ApoTome.2 microscope (Axio Imager Zeiss) and images were obtained through a numeric camera (Digital Camera Hamamatsu C11440) using the Imager.Z2 software (Zen 2) (ZEN Digital Imaging for Light Microscopy, RRID:SCR_013672). The labeling was observed with appropriate filters: 38 HE Green Fluorescent Protein (BP excitation 450-490, emission 500-550), 43 HE DsRed (BP excitation 538-562, emission 570-540) and 50 Cy5 (BP excitation 625-655, emission 665-715). Some pictures were taken using the advanced features "Z-Stack" and "Deconvolution" of the Zen software. Neither additional treatment was made, except to enhance fluorescent intensities. Nomenclature and nuclear parcellation are from Swanson (2004), except for the PSTN-calbindin nucleus (CbN)-nucleus gemini (NG) region, whose nomenclature and parceling is from Chometton et al. (2016).

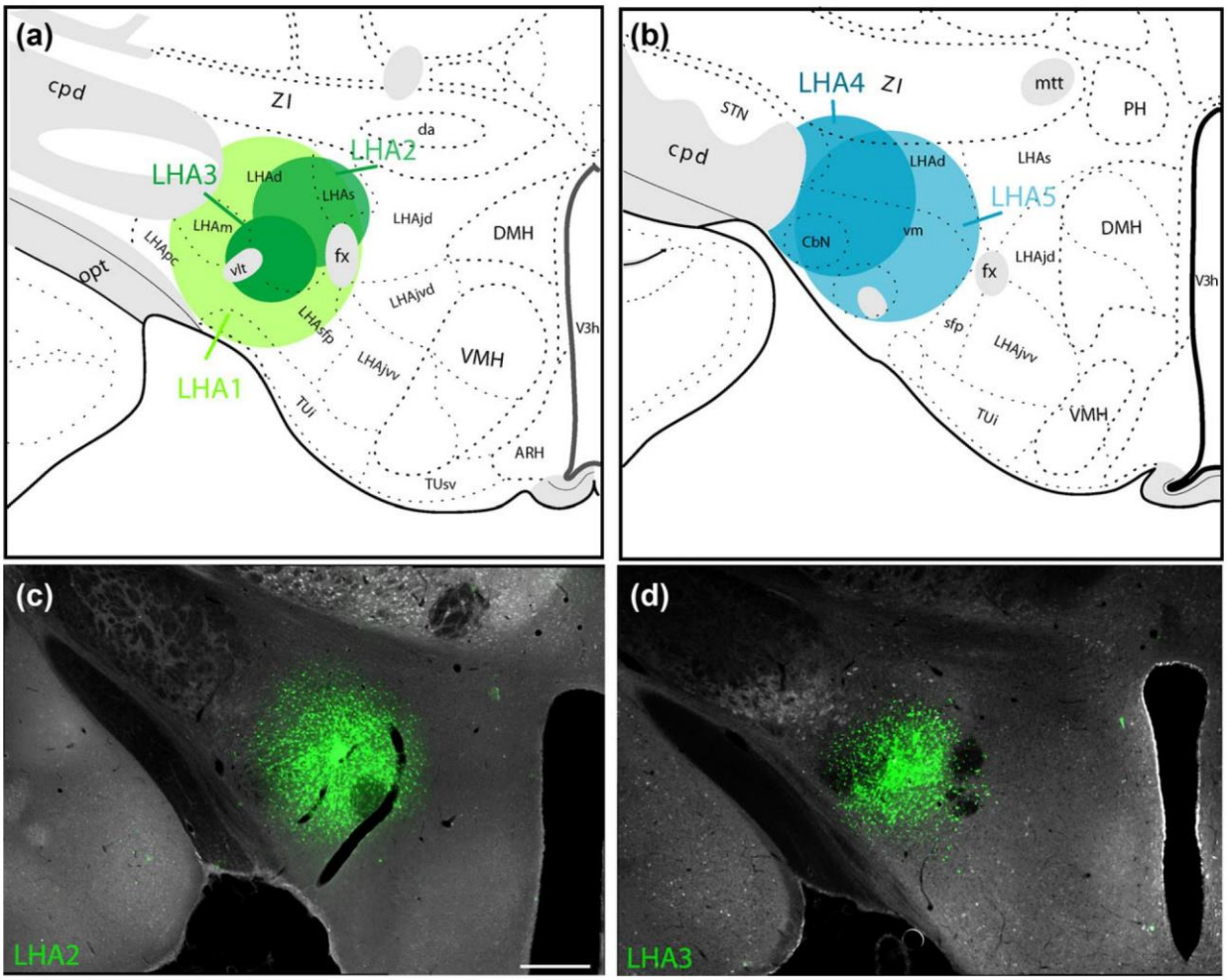

FIGURE 1 (a, b) Line drawings to illustrate the localization of the five FG injection sites into the LHA. In (a) three experiments are represented (LHA1-3) that intensely labeled the CEAi. All three involved the anterior tuberal perifornical region. In (b) are the two sites (LHA4-5) that provided less retrograde labeling in the CEAi but more in the CEAm. (c, d) Photomicrographs illustrating the injection sites in experiment LHA2 and LHA3. (The injection site of experiment LHA1 is illustrated in the Figure 2) [Color figure can be viewed at wileyonlinelibrary.com]

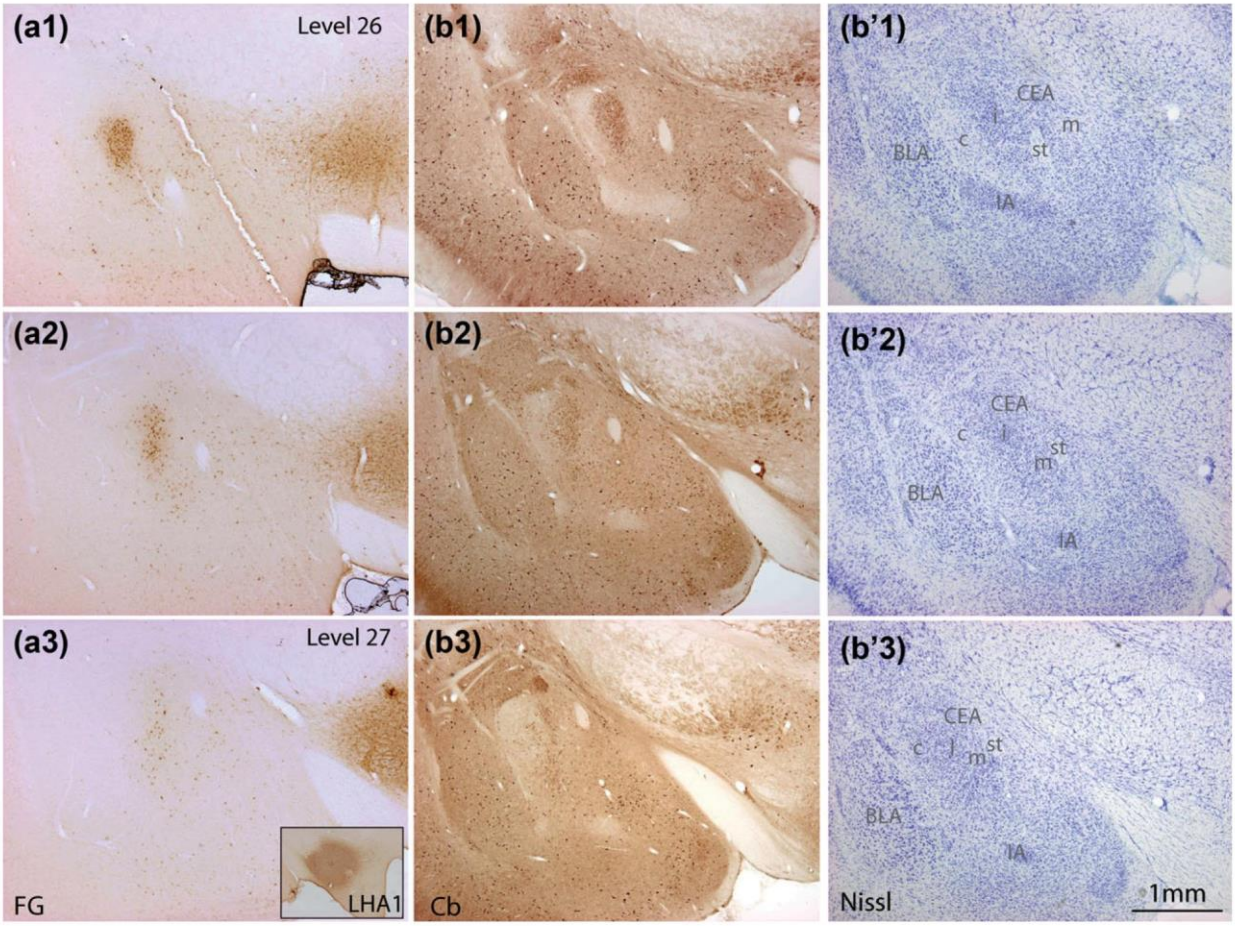

FIGURE 2 (a1–a3) Photomicrographs of FG retrogradely labeled cells in the CEA (experiment LHA1) on coronal sections corresponding to the levels 26 to 27 of the Swanson's Brain Maps (Swanson, 2004). The injection site is illustrated in the frame of a3. Note the dense condensation of labeled cells at the level 26 that has almost disappeared at level 27. The FG labeling is revealed using immunohistochemistry. (b1–b3) Photomicrographs illustrating the distribution of Cb immunolabeling on sections through the amygdala and corresponding to the levels 26 to 27 of the Swanson's Brain Maps (Swanson, 2004). This experiment was done on a different brain than in (a) but the plans of sections are close. Note the dense condensation of Cb cells at the level 26 and how it disappears at level 27. The distribution of these cells is very similar to that of the FG neurons in (a1–a3). (b'1–b'3) Sections adjacent to those in (b1–b3) that were stained with toluidine blue for cytoarchitectonic purposes. Note that the Cb condensation correspond to a group of darkly stained cells that are tightly packed and corresponds to the McDonald's CEAi (McDonald, 1982). See text for details [Color figure can be viewed at wileyonlinelibrary.com]

3 | RESULTS

3.1 | Identification of the CEAi after FG injection into the perifornical region of the LHA in the rat

Five FG injections were obtained into or involving the perifornical region of the LHA (Figure 1). Of those, three were centered laterally close to the fornix in the rostral tuberal LHA and labeled the greatest number of cells in a tight cell condensation in the CEA at level 26 of Swanson's Brain Maps (Swanson, 2004) and level 50 of Paxinos and Watson's atlas (Paxinos & Watson, 2005; Paxinos & Watson, 2013) (Figure 2). This cell condensation corresponded to the rostral CEAl in both atlases. However, this retrogradely-labeled cell condensation was already disappearing on sections corresponding to level 27 of the Brain Maps (Swanson, 2004) or level 53 of Paxinos and Watson's atlas (Paxinos & Watson, 2005, Paxinos & Watson, 2013). In the following parts of the paper, and for practical reasons, this cell group shall be referred to as the CEAi for the intermediate part of the CEA, even if the correspondence with the CEAi characterized by McDonald (1982) is only advocated in the discussion. Unless the FG injection site involved the far lateral hypothalamus and cerebral peduncle, the caudal CEAl contained only a few labeled cells. This caudal CEAl will only be named CEAl in the rest of the text. The CEAm contained retrogradely-labeled cells, but they did not form a compact group and were scattered through this part of the nucleus.

We then searched for neurochemical markers to differentiate the CEAi from other CEA parts. Antibodies against Cb labeled a cell group with a distribution in the CEA that closely resembled that of FG cells after FG injections in the anterior perifornical region. Additional but less abundant Cb cells were observed in the CEAm and medial aspects of the CEAl (Figure 2). This cell group does not extend far caudally: it fades on sections corresponding to level 27 of Swanson's Brain Maps (Swanson, 2004) and is absent more caudally. An anti-Cr antibody also labeled the CEAi, but the intensity of this labeling was weaker than

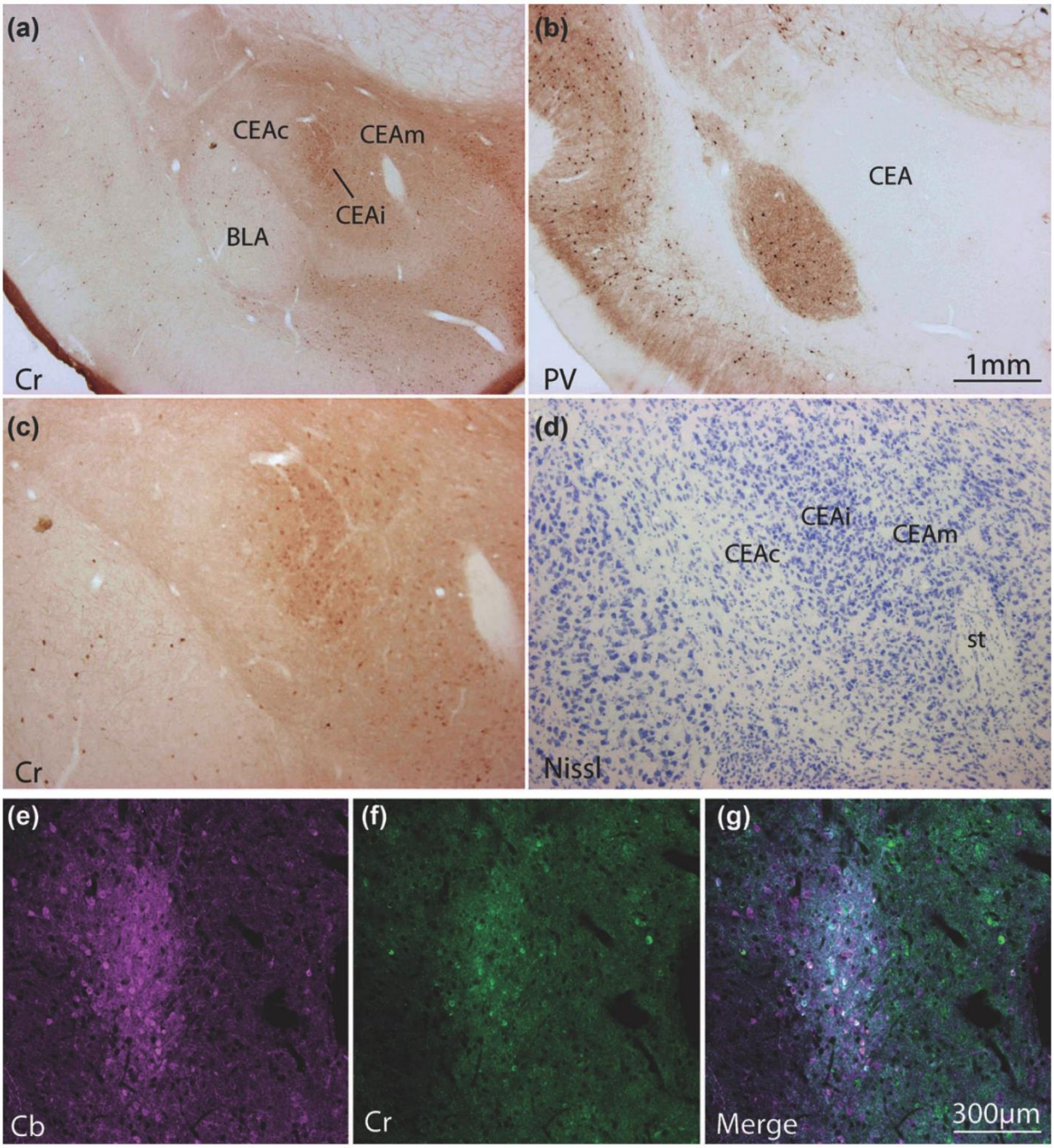

FIGURE 3 (a, b) Photomicrographs illustrating the distribution of Cr and PV in the amygdala at low magnification. Note the condensation in the CEAi labeled by the Cr-AS. No labeling of the CEA is obtained with the anti-PV antibody. (c, d) Higher magnification of the labeling in the CEAi obtained for Cr and the adjacent section stained with toluidine blue for cytoarchitectonic purpose. The labeling of the CEAi cells is not very intense with this AS. (e–g) Dual immunofluorescence with anti-Cb (e) and anti-Cr (f) antibodies. Most cells are double labeled and appear orange in the merged picture (g) [Color figure can be viewed at wileyonlinelibrary.com]

that with the Cb-antiserum (AS) (Figure 3). The CEAl contained scattered Cr-labeled cells. Such cells were more abundant in the CEAm. No labeling was observed for PV (Figure 3b).

Double immunofluorescent experiments were then implemented to verify that FG cells in the CEAi expressed Cb and/or Cr. Double Cr/Cb experiments showed that a very large majority of the cells in the CEAi co-expressed the immunofluorescent signal for both Cb and Cr (Figure 3e–g). We estimated that over 80% of Cb neurons contained the Cr signal (Figure 3g, a precise estimation was difficult as the Cr labeling was weak in some cells). Double FG-Cb immunofluorescent staining on sections of two experiments (LHA2 and LHA3), with abundant retrograde-labeling in the CEAi, indicated that about half (47%; 46 intensely brilliant but otherwise randomly chosen FG neurons were counted on three sections of which 20 were calbindin positive) of the retrogradely-labeled cells were also labeled with the Cb antibody (Figure 4). One triple-labeling experiment indicated that all FG/Cb cells were also Cr (not shown). The nature of the FG+/Cb- cells remains unknown, but we cannot exclude that we failed to

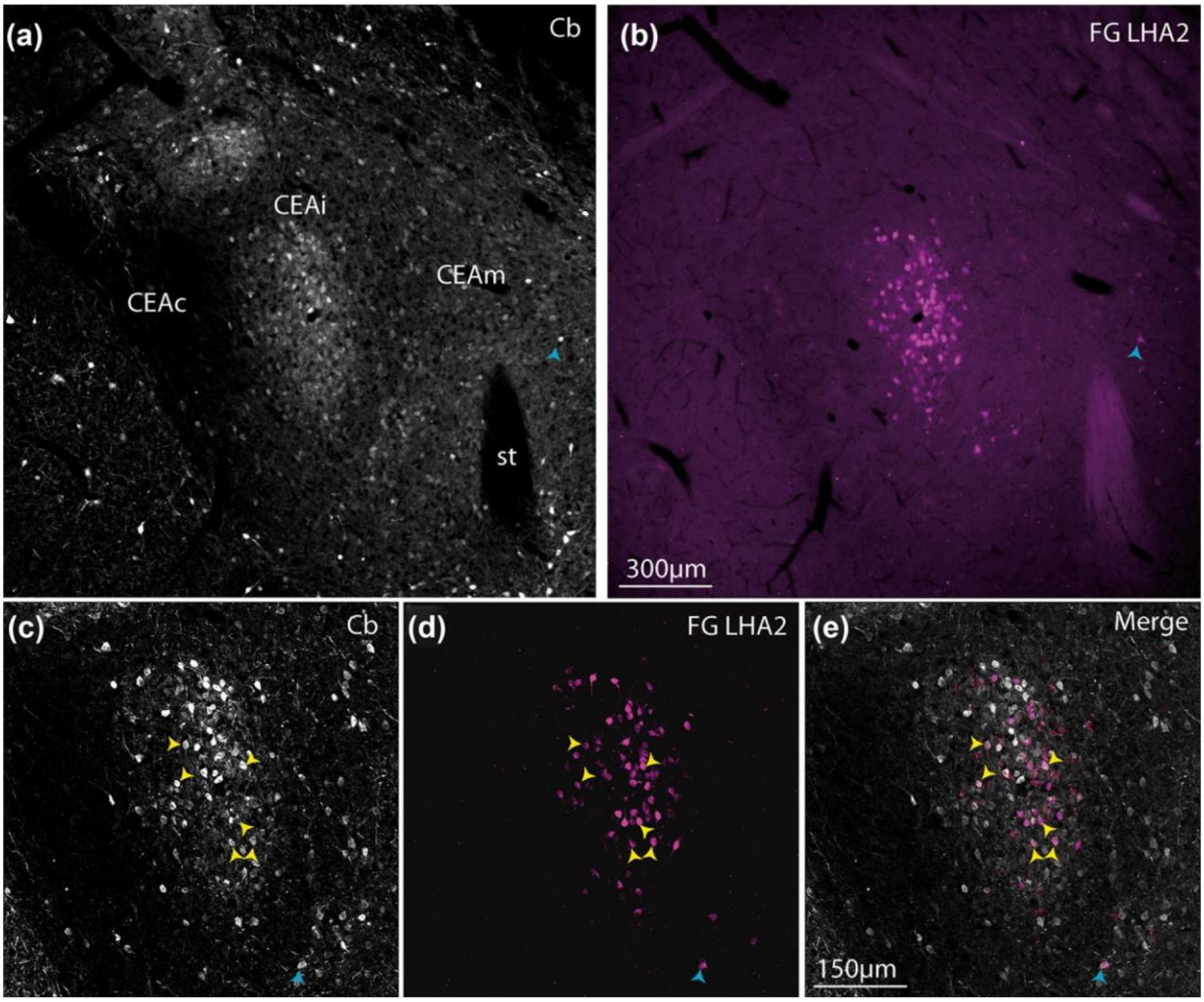

FIGURE 4 (a, b) Photomicrographs of a section from the experiment LHA2 and labeled using double immunofluorescences for Cb (a) and FG (b). (c–e) Photomicrographs using the Apotome device of the microscope at a slightly higher magnification of the same section and illustrating double labeled cells. The yellow arrowheads show some of the numerous double labeled cells in the CEAi. Some cells in the CEAm are also double labeled (blue arrowheads in a, b and in c–e) [Color figure can be viewed at wileyonlinelibrary.com]

detect very low levels of Cb expression. Some Cb cells in the CEAm were also retrogradely-labeled by FG after anterior perifornical injection.

3.2 | Comparison with the distribution of PKC-δ, CRH, CGRP, TH, Met-Enk, and NT in the rat

The CEA, and especially the CEAl, is rich in cell bodies and axons expressing a large panel of neuropeptides and enzymes (Veening, Swanson, & Sawchenko, 1984; Cassell, Gray, & Kiss, 1986; Chieng, Christie, & Osborne, 2006). We have just emphasized the expression of Cb and Cr in the CEAi. However, PKC-δ, CRH, NT, and Met-Enk have also been reported in many cell bodies and axons of the CEA (Cassell et al., 1986; Poulin, Chevalier, Laforest, & Drolet, 2006; Marchant et al., 2007; Campos et al., 2016). Furthermore, intense innervation by CGRP and TH axons have proven to correspond to some functional organization of the nucleus (Marchant et al., 2007; Carter, Han, & Palmiter, 2015). We then compared the distribution of the labeling provided by FG or the Cb-AS with that of PKC-δ-, CRH-, NT-, Met-Enk-, CGRP-, and TH-AS. This analysis was performed on un-colchicinized rats and, therefore, not all CRH, NT or Met-Enk perikarya could be revealed as they were in such previous studies, as Veening et al. (1984) and Cassell et al. (1986). Nevertheless, this analysis was useful to better characterize the CEAi from the CEAm and CEAl.

Overall, the CEAi shows specific neurochemical features: in addition to Cb, this part of the CEA contains moderate to intense TH and Met-Enk innervations, a moderate CRH and weak CGRP innervation and an absence of PKC-δ and NT expression. A concise description of these patterns with regard to the CEA parceling is provided in the following paragraphs as well as in the legend of Figures 5 to 10.

PKC-δ: Antibodies against this enzyme labeled a large population of cells (Figure 5a, a1). These cells formed a dense ovoid (level 27) or round (from level 28) condensation that corresponded to the lateral part of the CEA in the LWS Brain Maps (Swanson, 2004). We therefore used this marker to delimit the CEAl. At the level of section 26, only a few PKC-δ cells can be detected. Compared to the FG labeling in experiment LHA2, they are lateral to the condensation that forms the CEAi (Figure 5e–g).

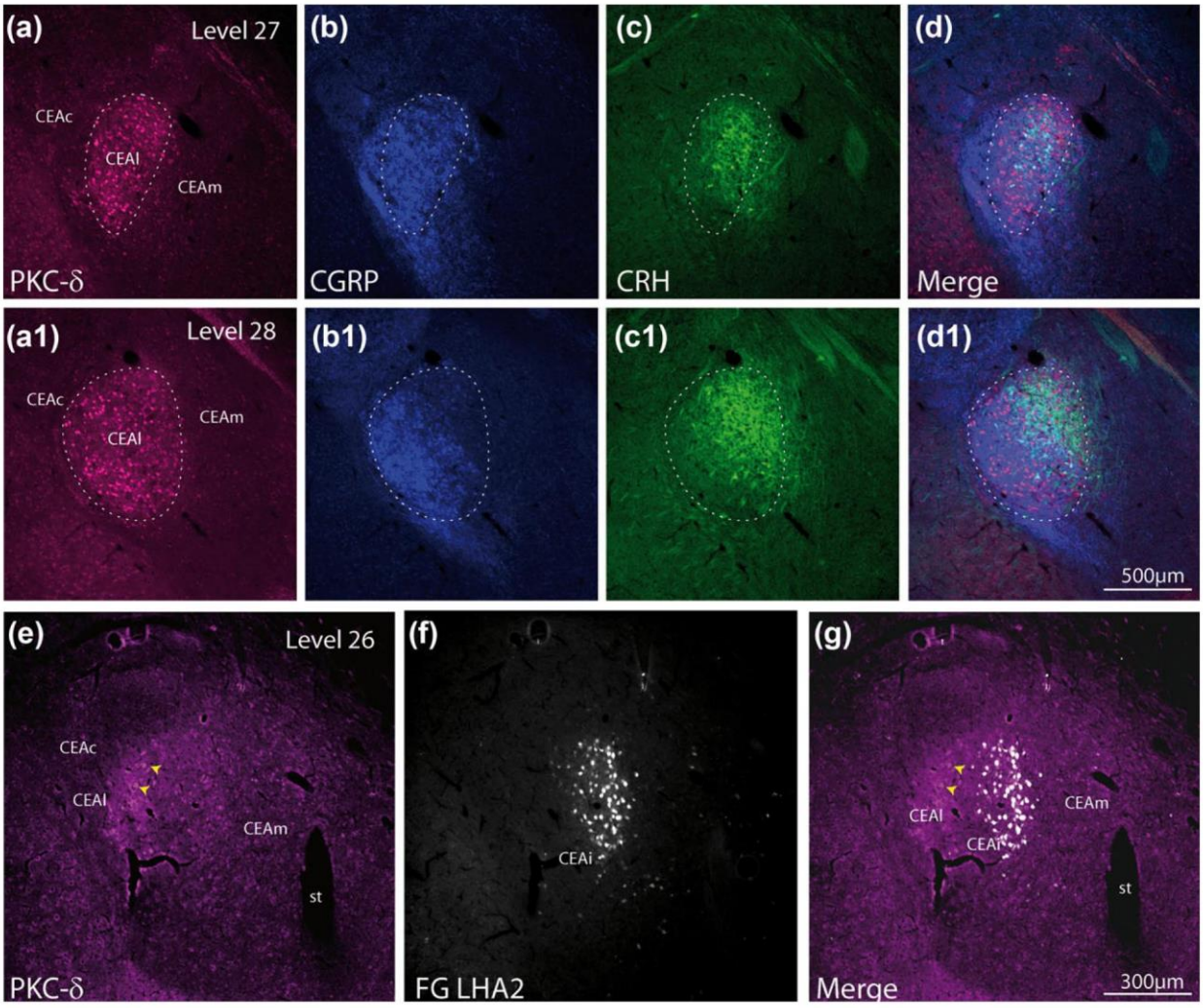

FIGURE 5 (a–d) Photomicrographs to illustrate the distribution of PKC-δ, CGRP, and CRH on a section passing through the CEA at the level 27 of Swanson's Brain Maps (Swanson, 2004). The PKC-δ-AS (a) labels an intense cell group forming an ovoid condensation that corresponds to the CEAl. CGRP labeled axons (b) provide a very intense innervation of the CEAl and laterally of the CEAc. CRH labeled cells and axons (c) are also abundant in the CEAl. The merged image (d) shows that CRH is mostly in the dorsomedial aspect of the CEAl. (a1–d1) Triple immunofluorescence to illustrate the distribution of PKC-δ, CGRP, and CRH on a section passing through the CEA at the level 28 of Swanson's Brain Maps (Swanson, 2004). The PKC-δ-AS (a1) labels an intense cell group forming a round condensation that corresponds to the CEAl. CGRP labeled axons (b1) provided a very intense innervation of the CEAl and laterally of the CEAc. CRH labeled cells and axons (c1) are also abundant in the CEAl. The merged image (d1) shows that CGRP is in the ventrolateral region of the CEAl and CRH is in the dorsomedial aspect of the CEAl. (e–g) Dual immunofluorescence labelings to illustrate PKC-δ and FG on a section at the level 26. Only few PKC-δ cell are observed that are located lateral to the CEAi. Furthermore, these cells (red arrowheads) are faintly labeled [Color figure can be viewed at wileyonlinelibrary.com]

CRH: Cell bodies and axons were labeled by the CRH antibody (Figures 5c, c1, 6b–b2, and 7c, c1). Cell bodies were essentially found within the borders of the CEAl, concentrated in the dorsomedial aspect of this part. Comparing the distribution of CRH with that of Cb (Figure 6) or FG (Figure 7b–d1), CRH perikarya surrounded the dorsal and caudal aspect of the CEAi. However, the border between the CEAi and the CEAl appeared somewhat fuzzy and some Cb cells were seen in the CEAl mixed with CRH cell bodies; also, an occasional CRH cell body was labeled in the caudal CEAi (Figure 6a, a1, b, b1). CRH axons were abundant in the CEAl, but we observed that the CEAi contained a moderate innervation that poorly extended into the neighboring CEAm. The CRH labeling was absent from the CEAc.

CGRP: The CEA does not contain any CGRP perikaryon, but is innervated by a very intense input that originates in the lateral parabrachial nucleus and is known to convey pain information (Carter, Soden, Zweifel, & Palmiter, 2013, Carter et al., 2015; Han et al., 2015). CGRP projections distribute mostly in lateral aspects of the nucleus, spreading over capsular and lateral parts. The CEAi and CEAm contained only a weak input by CGRP axons (Figures 5–6, 8–9, and 10).

TH: The TH expression pattern in the CEA is complex. The very intense innervation of the caudoputamen nucleus extended into the dorsal aspect of the CEAc (Figures 7a, a1 and 8a-a3). In this region, the TH labeling co-localizes with the CGRP innervation, but no TH/CGRP co-expression within the same neuronal elements was found. As well as this input, we observed an innervation of the CEAi that continues with an increased intensity in the dorso-medial region of the CEAl (Figures 7 and 8). The rostral and CGRP-rich ventrolateral

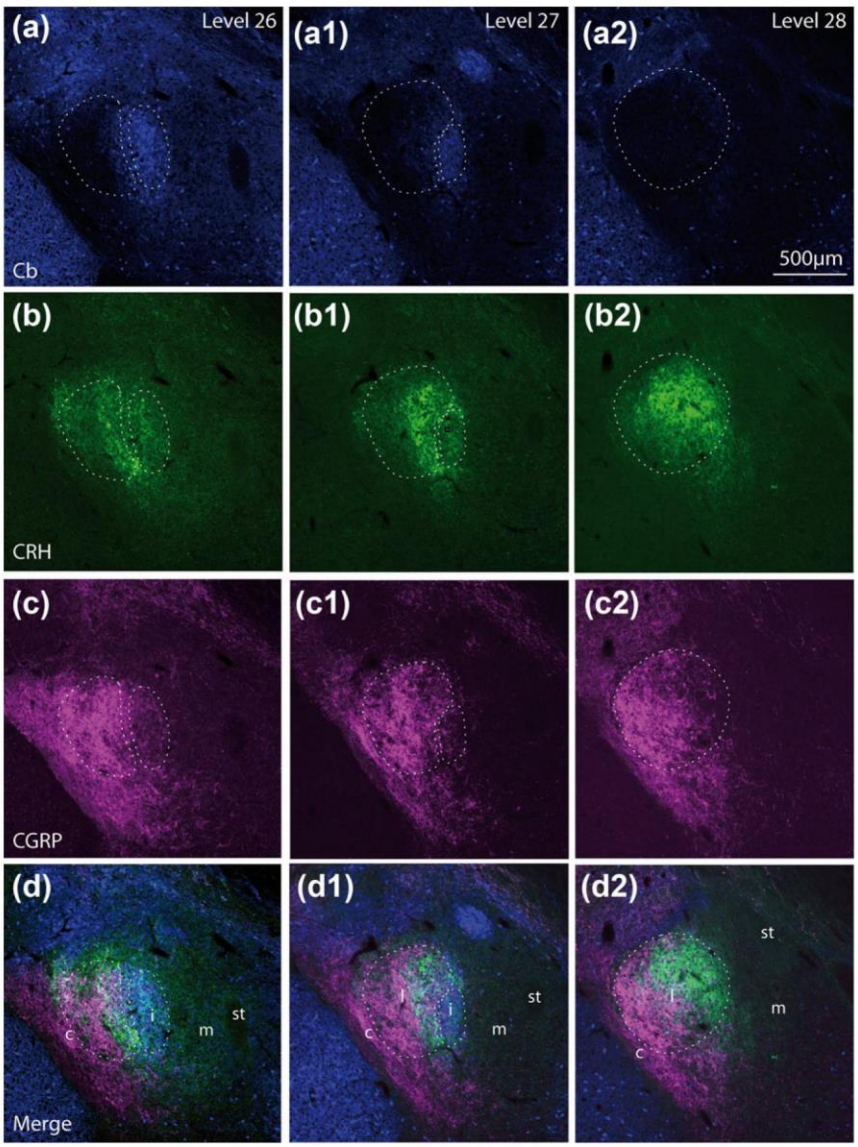

FIGURE 6 (a–d) Photomicrographs to illustrate the distribution of Cb, CRH, and CGRP on a section passing through the CEA at the level 26 of Swanson's Brain Maps (Swanson, 2004). The Cb-AS (a) labels an intense cell condensation that corresponds to the CEAi. A few CRH labeled cells are observed just lateral to the CEAi, but one or two can be seen within this division (b). The CEAi also receives an innervation by CRH axons. The CGRP-labeled axons (c) provide a very intense innervation of the CEAl and of the CEAc The CEAi contains a weak CGRP innervation. (a1–d1) Photomicrographs to illustrate the distribution of Cb, CRH, and CGRP on a section passing through the CEA close to the level 27 of the Swanson's Brain Maps (Swanson, 2004). The cell condensation that corresponds to the CEAi and labeled by the Cb-AS is disappearing (a1). CRH labeled cells are more abundant and aggregate in a medial aspect of the CEAl (b1). The CGRP labeled axons (c1) provide a very intense innervation of the CEAc and lateral region of the CEAl. (a2–d2) Photomicrographs to illustrate the distribution of Cb, CRH, and CGRP on a section passing through the CEA at the level 28 of the Swanson's Brain Maps (Swanson, 2004). Very few labeled elements can be seen in the CEAl and the CEAi is not found (a2). CRH labeled cells are abundant in a medial aspect of the CEAl (b2). The CGRP labeled axons (c2) provide a very intense innervation of the CEAc and lateral region of the CEAl [Color figure can be viewed at wileyonlinelibrary.com]

aspects of the CEAl are minimally innervated by TH axons, as also seen for the ventral CEAc and the CEAm.

Met-Enk: The Met-Enk signal was quite diffuse in the CEA. Nevertheless, we found a denser expression in a cell mass labeled by Cb and corresponding to the CEAi (Figure 9a1–d1). At higher magnification, using the Apotome device, we observed that Met-Enk fibers closely surrounded Cb cell bodies. We also noted that a few Cb neurons expressed the Met-Enk signal (Figure 9e–h), indicating that some of them are enkephalinergic.

NT: The NT-AS provided a very intense labeling of axons in the ventral aspect of the CEAc. Multiple immunofluorescent labeling showed that this signal co-localized with the CGRP signal in axons of this region (Figure 10). Therefore, the ventral CEAc is innervated by axons containing both CGRP and NT while the dorsal CEAc and CEAl are mostly innervated by CGRP+/NT- axons. At caudal levels of the nucleus, we could see that some cells labeled by the PKC-δ-AS and belonging to the ventral margin of the CEAl were innervated by CGRP/NT axons (Figure 10e–h).

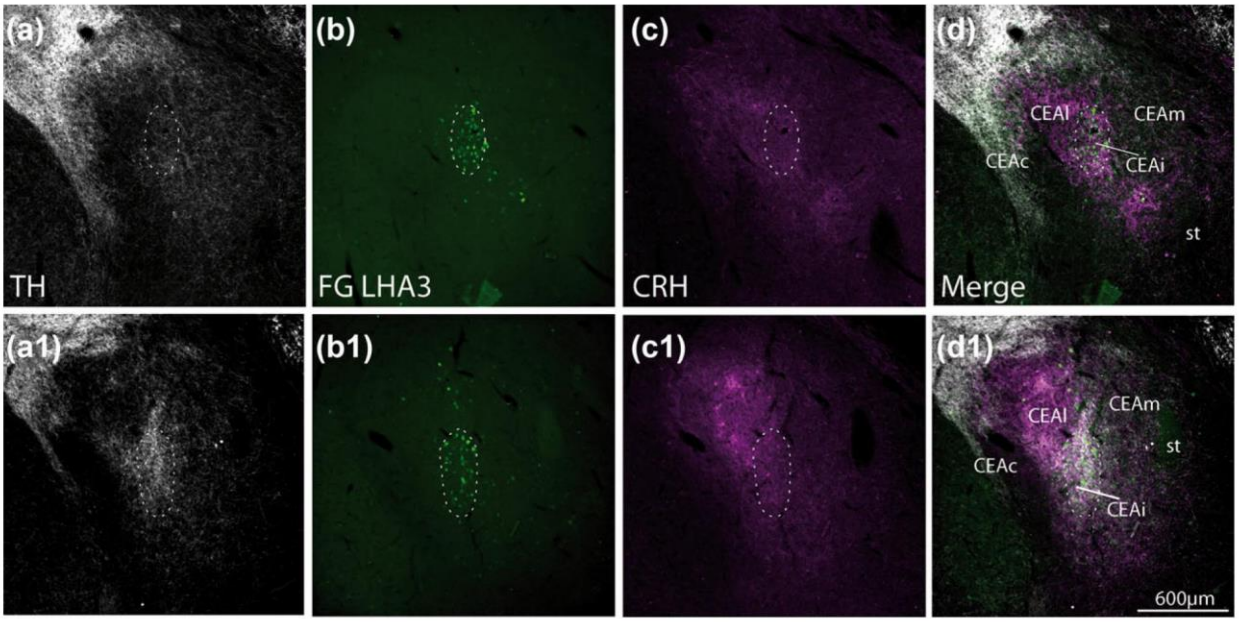

FIGURE 7 (a–d) and (a1–d1) Photomicrographs to illustrate the distribution of TH, FG, and CRH on two close sections passing through the CEAi around the level 26 of Swanson's Brain Maps (Swanson, 2004). The level of the a-d section is more rostral than that of the a1–d1 section. The TH-AS (a, a1) labels many axons that extend from the striatum into dorsal aspects of the CEAc. In addition, a moderate innervation of the CEAm and CEAi is also clearly visible. The innervation of the CEAi is more intense on the caudal section (a1). The CEAi is characterized by the distribution of FG-containing neurons in experiment LHA3 (b, b1). CRH neurons are few at the rostral-most level of the CEAl (c), but their number increases rapidly in a more caudal section (c1). They are co-distributed with TH axons in the CEAl (d1) [Color figure can be viewed at wileyonlinelibrary.com]

3.3 | Projections from the CEAi and CEAm into the perifornical LHA in the rat

The CEAi is characterized as containing a dense cluster of FG cells after rostral perifornical LHA injections. However, not all injection sites in the LHA provided such specific retrograde labeling of the CEAi as the one illustrated in Figure 2. More caudal and lateral injection sites in the LHA provided more abundant labeling in the CEAm and less abundant labeling in the CEAi (Figure 11). Such distinct distribution patterns of FG cells suggested that the CEAi and CEAm innervate different parts of the LHA.

In order to confirm and understand the organization of projections from the CEAi and CEAm into the LHA, PHAL injections were aimed at these subnuclei (Figure 12a–e). Four PHAL injections were obtained, one of which was centered in the caudal portion of the CEAi with a more ventral contamination in the CEAm. Of the three other injections, one was in the CEAm rostral to the CEAi and extended as far as the FS, the second was in the CEAm medially adjacent to CEAi, and the last one was mostly in the ventral aspect of the CEAc (Brain Maps; Swanson, 2004) caudal to the CEAi. This last one had significant contaminations in the neighboring medial and basomedial nuclei.

The striking results of these experiments was that the projection patterns from the CEAi were very similar to that from the CEAm. Differences were nevertheless observed. At the level of the bed nuclei of the stria terminalis (BST), projections from CEAi and CEAm experiments were very similar in the lateral and fusiform parts of the BST. However, an intense innervation of the parastrial nucleus (PS) was observed from the CEAi that was absent in the CEAm experiments (Figure 12f, g). Within the hypothalamus, the patterns were more similar than suggested by the FG experiments. Axons coursed through dorsal and ventral LHA pathways, as already described (Barbier et al., 2017). Axons innervated the paraventricular hypothalamic nucleus (PVH), essentially the perifornical part (PVHf) (Figure 12h–l). These projections were more intense from the CEAi and, in addition, innervation of the rostral most PVH was also noted. Within the LHA, each of our experiments provided a distinct pattern of innervation of the rostral tuberal region. The experiment PHAL #1 innervated the far lateral and dorsal anterior LHA regions (Figure 12h–l). The CEAi and PHAL #2, PHAL #3 experiments labeled axons closer to the fornix, but the innervations by the CEAi injection site were more intense and formed very clear pericellular nets. At caudal levels of the tuberal LHA (level 30 of the Brain Maps, Swanson, 2004), innervation of the perifornical region disappeared in all experiments; however, some axons penetrated the borders of the dorsomedial hypothalamic nucleus (DMH). Finally, at the caudal tuberal and premammillary levels of the LHA, a very intense innervation of the PSTN was obvious, as previously described (Barbier et al., 2017). These projections were however less intense from the CEAi (PHAL #2) than from the CEAm (PHAL #1 and PHAL #3). Caudal to this level, the pattern of projections toward the parabrachial nucleus and the nucleus of the solitary tract was very similar to that described for the CEAm in previous studies (Veening, Swanson, Cowan, Nieuwenhuys, & Geeraedts, 1982; Gray, Carney, & Magnuson, 1989; Bourgeais, Gauriau, & Bernard, 2001; Oka, Tsumori, Yokota, & Yasui, 2008; Shirasu et al., 2011).

3.4 | Afferent connections from the FS and the AId in the rat

From the preceding results, it appears that the CEAi shares many features of the CEAm, in particular concerning projections into the

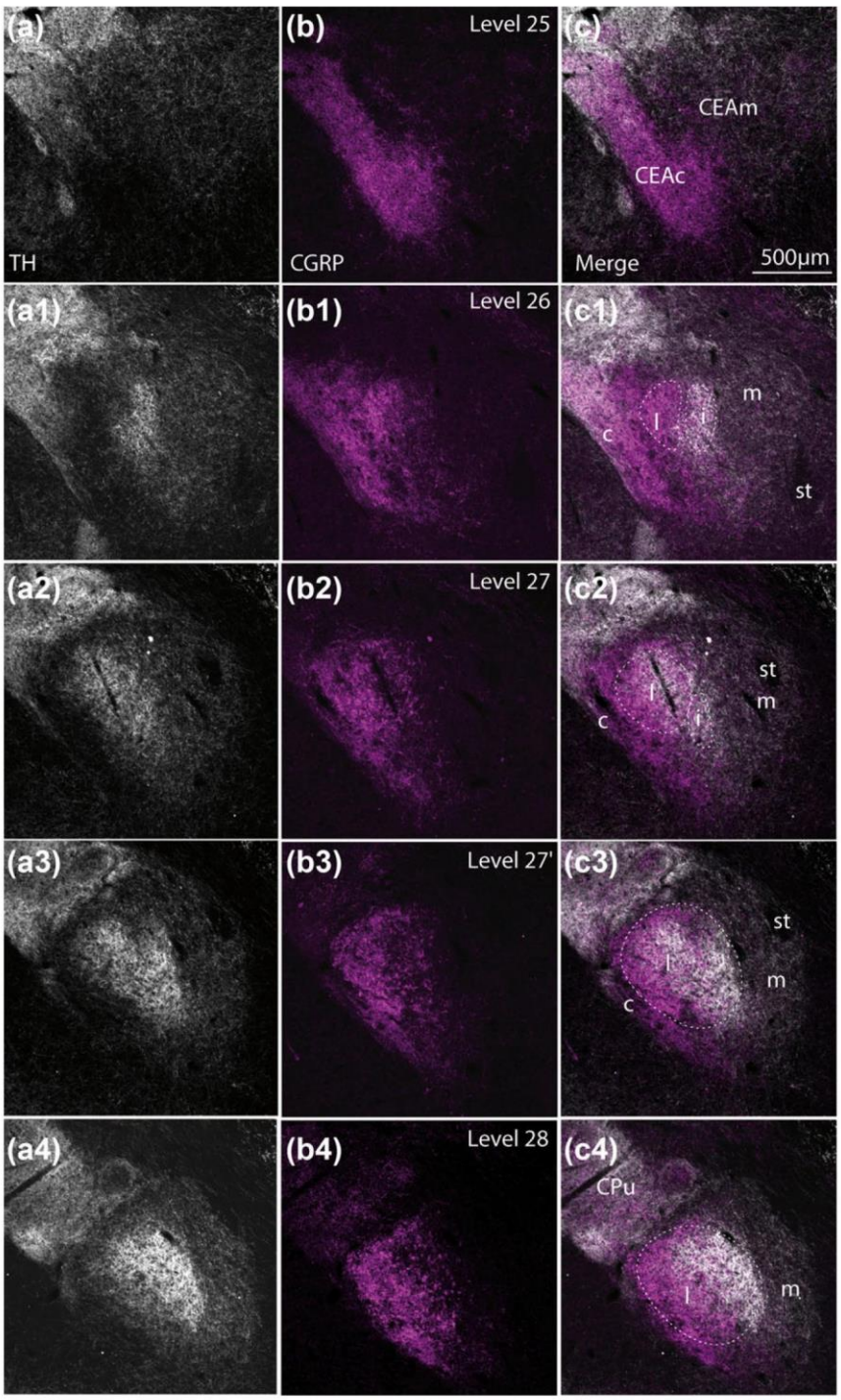

FIGURE 8 (a–a4) Photomicrographs illustrating the distribution of TH on sections passing through the CEA from level 25 to level 28. TH axons extend from the caudoputamen nucleus and innervate the dorsal aspects of the CEAc. This innervation is intense rostrally (levels 25–26) but is almost absent of the ventral and caudal CEAc (level 28). A moderate innervation of the CEAm and rostral CEAi is apparent. The innervation by TH axons becomes more intense with caudal levels in the CEAi (a1) and extends in the CEAl (a2). Caudal aspects of the CEAl is as intensely labeled than the dorsal CEAc (a4). (b–b4) Photomicrographs illustrating the distribution of CGRP on sections passing through the CEA from level 25 to level 28. The CEAc and then the CEAl are very intensely innervated by CGRP axons. (c–c4) Merged images of the TH and CGRP labelings to illustrate that the dorsal CEAc receives convergent TH and CGRP innervation. The ventral CEAc and caudal CEAc are innervated only by CGRP axons. In the CEAl, lateral regions of this division of the CEA are intensely innervated by CGRP axons, but little by TH axons. On the contrary, medial regions of this division are mostly innervated by TH axons but CGRP projections are less intense [Color figure can be viewed at wileyonlinelibrary.com]

LHA and more caudally into the brainstem. Analyzing afferent projections to the CEAi is a difficult task, as this part is not surrounded by a capsule that would restraint the diffusion of the tracer. Furthermore, because of its small size, it is unfortunately almost impossible to perform an FG injection without contaminating adjacent parts. Therefore, we went through our collection of PHAL

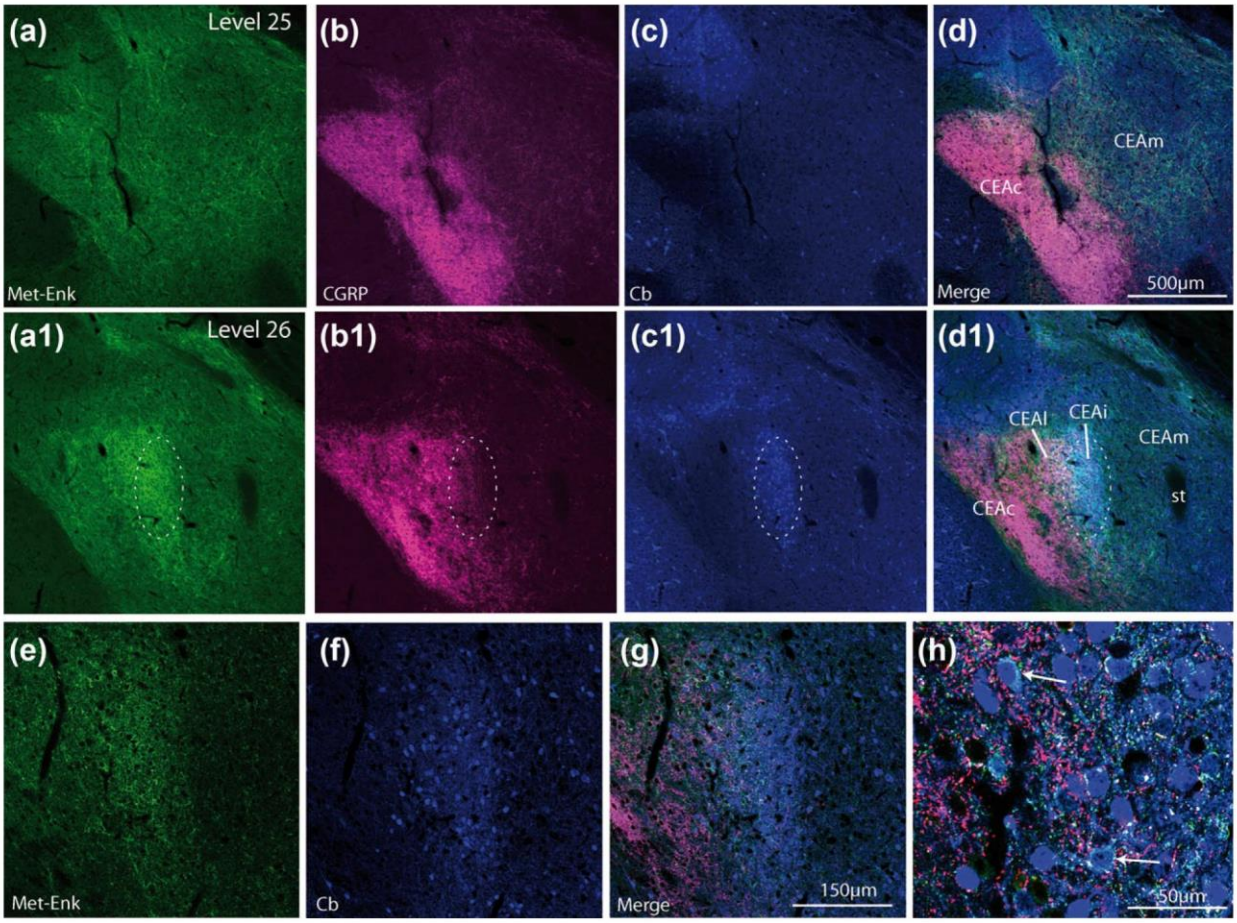

FIGURE 9 (a–d) Photomicrographs to illustrate the distribution of Met-Enk, CGRP, and Cb on a section passing through the CEA at the level 25 of the Swanson's Brain Maps (Swanson, 2004). The labeling provided by the Met-Enk- and Cb-AS are quite diffuse through this rostral level of the CEA. The CGRP projection is very intense in the CEAc. (a1–d1) Photomicrographs to illustrate the distribution of Met-Enk, CGRP and Cb on a section passing through the CEA at the level 26 of the Swanson's Brain Maps (Swanson, 2004). The Met-Enk-AS provides a more intense staining of the CEAi characterized by the Cb distribution. This Met-Enk labeling extends in the CEAl. (e–h) Using the Apotome device, Met-Enk axons surround Cb cells in the CEAi. The cytoplasm of some Cb cells also displayed a punctiform labeling with the Met-Enk-AS suggesting that they contain this peptide (arrows in d) [Color figure can be viewed at wileyonlinelibrary.com]

experiments to identify particular inputs that would differentiate the CEAi from the CEAm.

The current literature often refers to the concept of "extended amygdala" when considering the functional organization of the CEA and its network. Following this concept, the CEAm is closely related to parts of the FS, which is also named the interstitial nucleus of the posterior limb of the anterior commissure (IPAC), and more specifically to the medial part of the IPAC (Heimer, Harlan, Alheid, Garcia, & de Olmos, 1997; Shammah-Lagnado, Alheid, & Heimer, 1999; De Olmos, Beltramino, & Alheid, 2004). In a previous study, we obtained a PHAL injection in this region and confirmed a very intense projection through the CEAm (Barbier et al., 2017). A re-examination of this previous experiment in light of the present findings showed that innervation from the FS tends to completely avoid the CEAi (Figure 13a). A double-staining PHAL/Cb on the remaining sections of this experiment confirmed that this injection site in the FS labeled axons innervating the whole CEAm but avoided the CEAi (Figure 13b).

On the other hand, the CEAl is known to receive intense projections from insular cortical areas. We re-examined PHAL projections from injection sites in the posterior AId (Figure 13c–g). This area of the insular cortex very intensely innervates the CEAl. Dual-labeling PHAL/Cb showed that the CEAi is also a target for these projections. Many buttons were seen in the immediate vicinity of Cb-containing cell bodies, suggesting that they are synaptically connected. The CEAm was not innervated in this experiment.

3.5 | Data in the mouse

Several FG or Ctb injections were obtained in the perifornical region of the LHA in the mouse. Both tracers provided the same pattern of retrograde labeling in the CEA. However, the intensity of the FG signal was clearly weaker in this species compared to results in the rat and we choose to show only data obtained with Ctb (experiment mLHA1).

Similarly, to our findings in the rat, Ctb injections in the rostral perifornical region labeled many perikarya in the rostral and medial CEAl (Figures 14 and 15). However, we noted a weaker Cb and Cr expression in the mouse CEA compared to that in the rat. We were unable to clearly identify an intense expression of Cb or Cr in the retrogradely labeled cells. The Allen Brain Atlas reports expression of

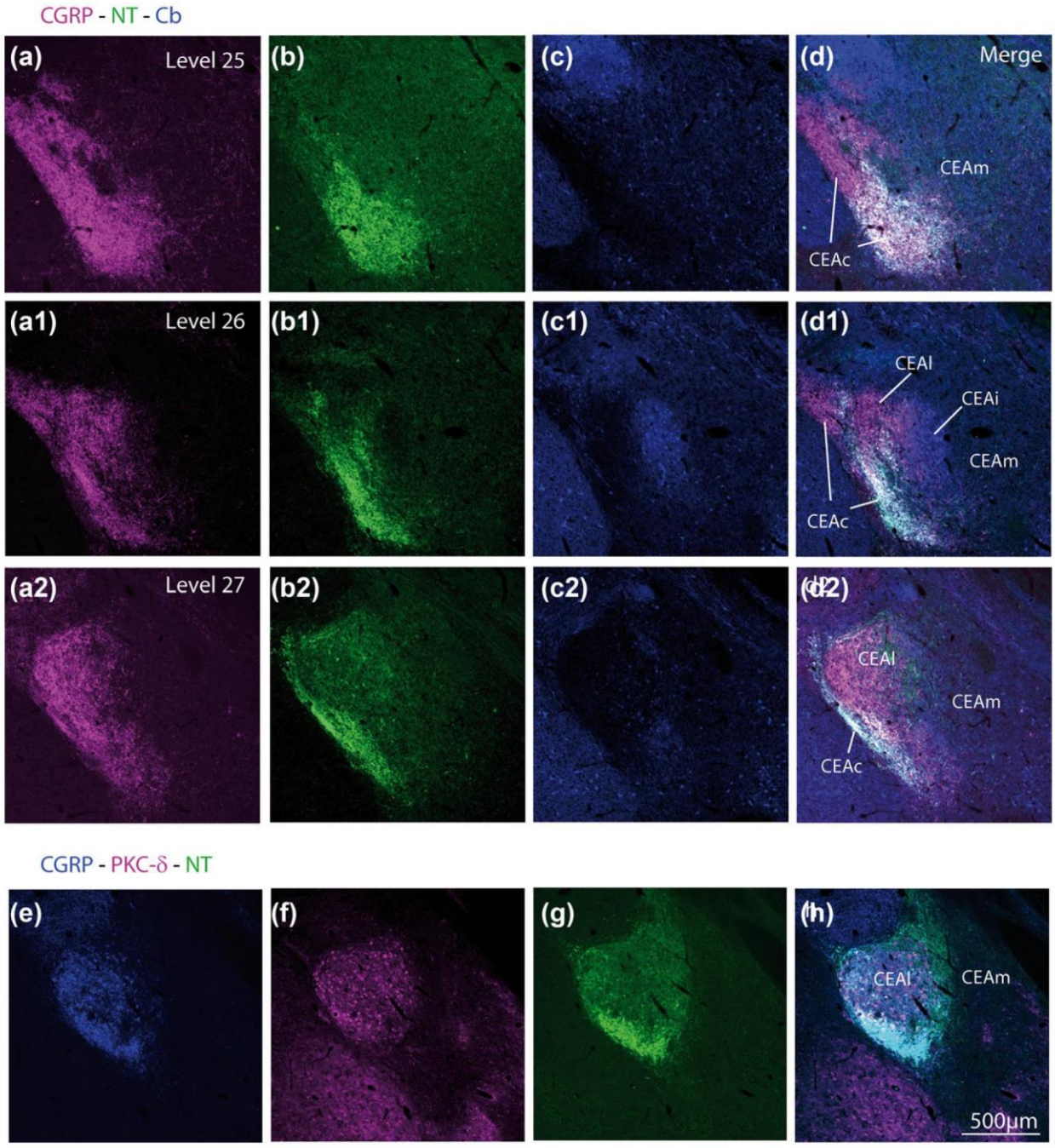

FIGURE 10 (a–d; a1–d1; a2–d2) Photomicrographs to illustrate the distribution of CGRP, NT and Cb on sections passing through the CEA at respectively the levels 25, 26, 27 of the Swanson's Brain Maps (Swanson, 2004). The CEAi is not innervated by NT axons (b1, c1, d1). However, a very intense labeling for NT is observed in axons innervating the ventral aspect of the CEAc. Superimposing NT and CGRP labelings showed that axons in the ventral CEAc co-express both CGRP and NT signals and they are double labeled. Dorsal CEAc and in the CEAl that are also intensely innervated by CGRP axons, double labeled axons were less frequent. (e–h) Photomicrographs to illustrate the distribution of CGRP, PKC-δ, and NT on a section passing through the CEA at the levels 28 of the Swanson's Brain Maps (Swanson, 2004). This experiment showed that some very ventral PKC-δ cells in the CEAl received a CGRP/NT innervation, but these double labeled axons were in general rarer in the CEAl [Color figure can be viewed at wileyonlinelibrary.com]

mostly calbindin 1 but few or no calbindin 2 in the mouse CEA. A dense Cb labeled cell groups that would remind the CEAi in the rat is not apparent in any of the illustrated series of the atlas, corroborating our immunohistochemical observation (data not shown). Furthermore, retrogradely labeled cells do not form a dense cluster as in the rat. They show a loose organization, extending in a dorsoventrally oriented band of tissue. The distribution of these retrogradely labeled cell bodies was then compared with that of PKC-δ, CGRP, and TH. PKC-δ intensely labeled the CEAl as in the rat. However, comparison with CGRP showed that its expression also involved a ventral component of the rostral CEAc (Figure 14a–d). Co-labeling with the NT-AS showed that, as in the rat, CGRP axons contained NT in this ventral region of the CEAc (data not shown). Attentive examination of the distribution of Ctb cells showed that they are within the medial

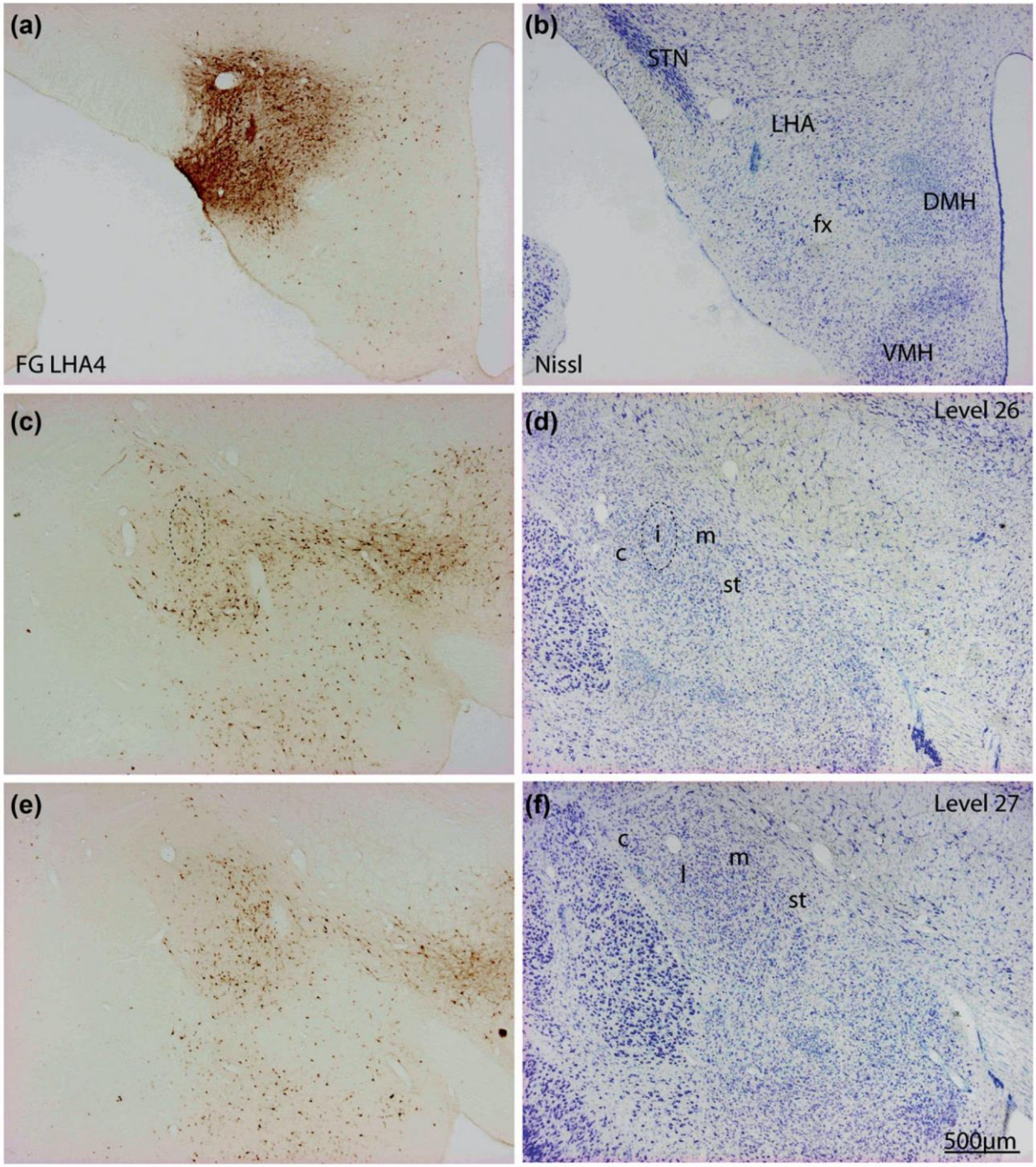

FIGURE 11 (a, b) Photomicrographs illustrating the FG injection site in experiment LHA4 (a) and the adjacent Nissl stained section (b). This injection involved the caudal tuberal LHA and extended in the PSTN caudally to this level. (c–f) Photomicrographs to illustrate the distribution of FG retrogradely labeled cells in the CEA at the levels 26 (c, d) and 27 (e, f) of the Swanson's Brain Maps (Swanson, 2004). Note that the pattern is very different to that illustrated in Figure 2. The CEAi is more faintly labeled, but the CEAm contains abundant and darkly stained cells [Color figure can be viewed at wileyonlinelibrary.com]

aspect of the PKC-δ labeled zone, that is, the CEAl but avoid the core of this zone where the PKC-δ labeling is more intense (Figure 14). Co-expression of PKC-δ and Ctb was observed in literally one single cell in the experiment mLHA1. The distribution of the retrogradely labeled cells extended rostrally (Figure 14a–d) and ventrally (Figure 14e–i) to the PKC-δ labeled zone and therefore in the CEAm (Figure 14). Very few Ctb cells were observed in the regions innervated by CGRP axons (Figures 14 and 15), but the co-labeling with TH showed that most of them were in the region innervated by TH axons (Figure 15), in that remembering the observations made in the rat.

4 | DISCUSSION

The CEA is a complex nucleus. All current atlases directly or indirectly reference the seminal work of McDonald (1982) for the

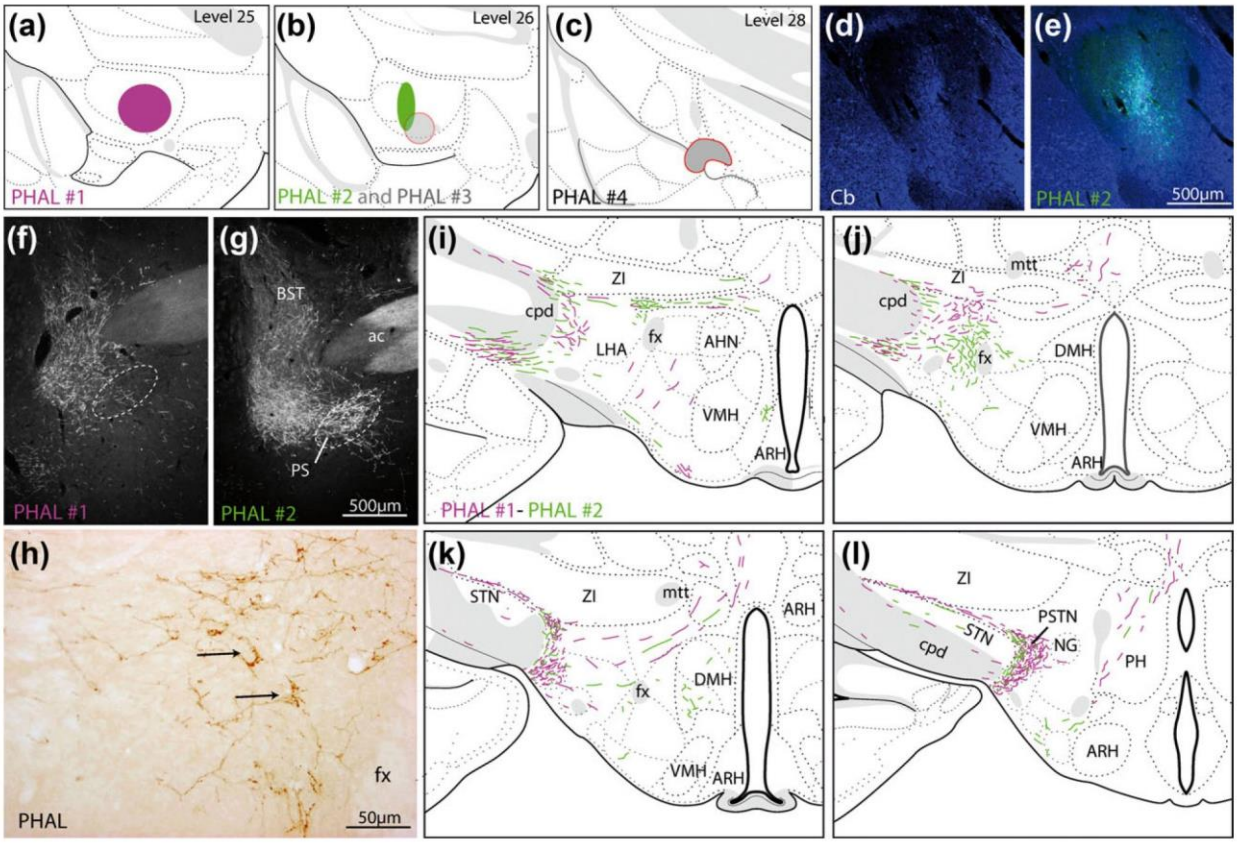

FIGURE 12 (a–e) PHAL injection sites in (PHAL #2) and around (PHAL #1, #3, #4) the CEAi. The injection site of experiment PHAL2 is also illustrated in the photomicrograph (e) and compared to the distribution of the Cb labeling (d). (f, g) CEAm (PHAL #1) and CEAi (PHAL #2) provide a similar innervation of the BST. However, a clear innervation of the PS is observed after CEAi injection and is not found after CEAm injection. (h) Photomicrograph illustrating the innervation of the lateral perifornical region in experiment PHAL #2. Note the pericellular nets provided by some axons (arrows). (i–l) Line drawings to compare the distribution of PHAL axons in experiments PHAL #1 and PHAL #2. PHAL #2 (CEAi) provide a more intense innervation of the caudal PVH (i), anterior perifornical area and DMH. It innervates the PSTN as well but in this nucleus the projection from the CEAm are more intense [Color figure can be viewed at wileyonlinelibrary.com]

cytoarchitectonic organization and nomenclature of the different parts of the nucleus. However, based on Nissl and Golgi stains and an analysis of the different cell types that assemble this nucleus, McDonald (1982) distinguished four parts. He described a lateral part, which he also named the core of the nucleus, and a capsular part, which is poorer in cell bodies and richer in axons. Both were characterized as containing striatal-like medium spiny neurons. He also identified an intermediate part and a medial part sharing similar larger cells with smoother dendrites. McDonald (1982) described the intermediate part as follows: "Near the rostral pole of the 'central nucleus' a small region of tightly packed intensely stained neurons is interposed between CL and CM." This author later showed a dense Cb expression in the CEAi (McDonald, 1997) and advocated that it display specific projection patterns (McDonald, 1988). Since then, several studies of the chemoarchitecture of the nucleus pleaded for an integration of the CEAi within the borders of the CEAl, in that agreeing with current atlases. In the present work, we completed these past studies by analyzing the distribution of PKC-δ with that of other markers previously used, such as CGRP and TH. We confirmed that the CEAl and CEAc are not homogeneous. Most importantly, we illustrated that a specific medial and rostral division of the CEAl corresponding to the CEAi of MacDonald in the rat, sends dense projections into the rostral perifornical LHA. These LHA projecting cells in the medial CEAl exist in both rat and mouse, but they form a less differentiated condensation in the mouse. The term CEAi was used in the present work to acknowledge the initial observations by McDonald, although arguments in favor of it being associated to the CEAl shall also be discussed.

Indices existed in the recent literature indicating that the rostral and caudal poles of the CEAl, as defined in atlases, show some differences, in particular concerning projections into the LHA (Swanson, Sanchez-Watts, & Watts, 2005; Reppucci & Petrovich, 2016). In the present work, the distribution of retrogradely labeled cells in the nucleus after rostral perifornical LHA injection, is clearly reminiscent of the CEAi in the rat, as described by McDonald (1982). McDonald (1982) noted that the CEAi and CEAm shared similar cell types, distinct from those in more lateral parts of the CEA. Indeed, both CEAi and CEAm show similar projection patterns and send axons into the LHA, while most of the CEAl and the CEAc do not send abundant axons in the LHA (Petrovich & Swanson, 1997; Cassell et al., 1999; Pomrenze et al., 2015). Our PHAL experiment agrees in that with the previous observations by McDonald using retrograde tracer (McDonald, 1988). It could therefore be tempting to associate CEAi and CEAm into the same medial part of the CEA. In the rat, Chieng et al. (2006) argued that the CEAi contains both Cb containing cell

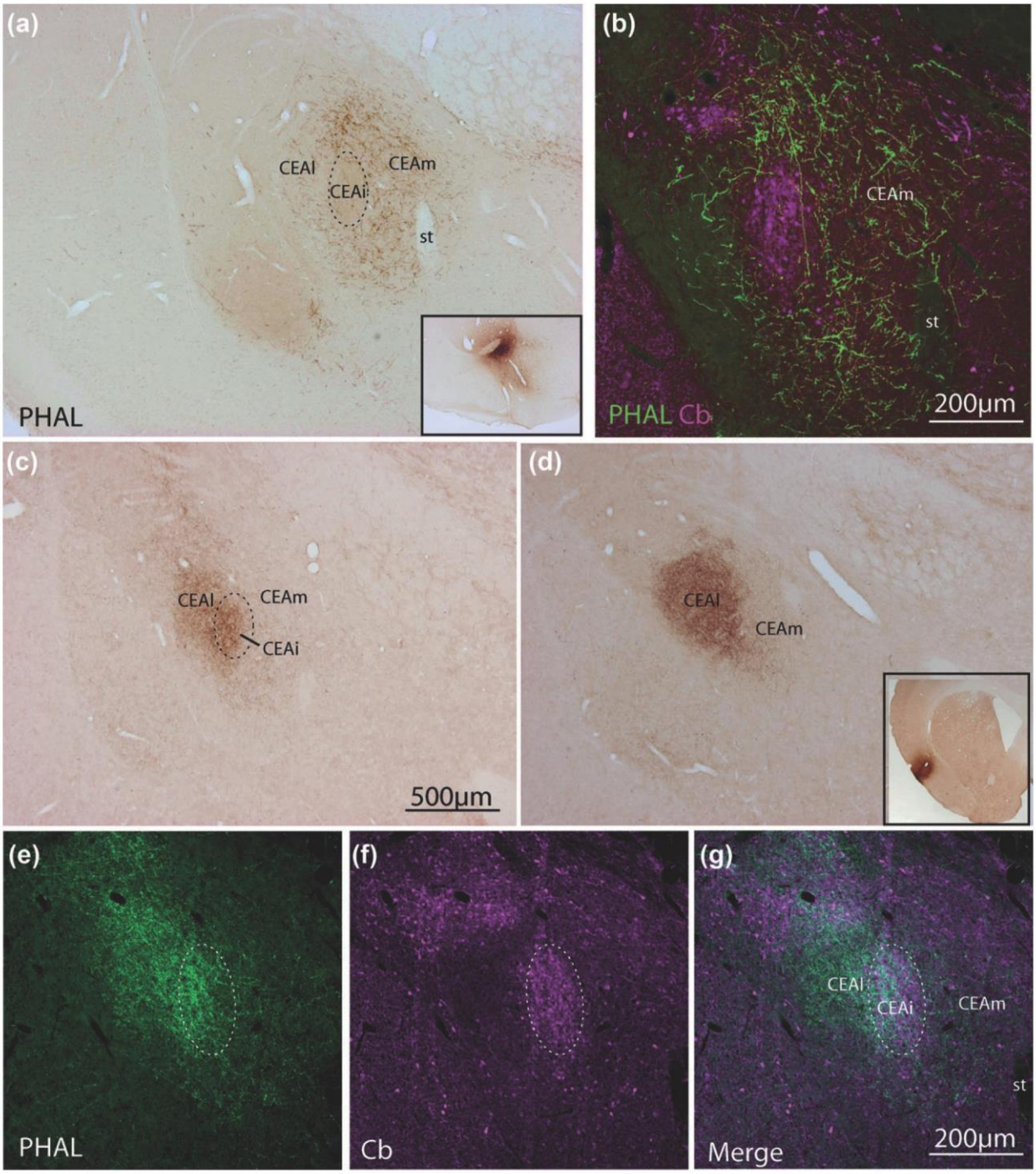

FIGURE 13 (a, b) Photomicrographs illustrating the distribution of PHAL axons in the CEAm after injection of the tracer in the ventral part of the FS. The injection site is illustrated in the frame of (a). Using double immunofluorescence for PHAL and Cb, we observe that PHAL axons (green) innervate the CEAm, few are in the CEAl, but they mostly avoid the CEAi. (c–g) After PHAL injection in the posterior AId, a very intense innervation of the CEAl is observed. At rostral level we can see that projections enter the CEAi, but not the CEAm. Using double immunofluorescence for PHAL and Cb, we can confirm that PHAL axons from the AId innervate the CEAi that contains the Cb labeling [Color figure can be viewed at wileyonlinelibrary.com]

along some CRH neurons. In our material, CRH cell bodies were not abundant within the borders of the CEAi. More in agreement with a view of the CEAi included within the CEAl is the observation in the mouse that Ctb cells lies within the region labeled for PKC-δ that can be seen as belonging to the CEAl. Therefore, retrogradely labeled cells from the perifornical LHA mostly distributed at the medial edge of the CEAl but their distribution area extended into the adjacent CEAm. Hence, the cell group at the origin of intense projections into the LHA perifornical region does not form in the mouse a tight cell condensation as in the rat, nevertheless intermediate cells also exist in this species.

In the rat, the CEAm receives intense inputs from parts of the FS which are also named IPAC in the Paxinos and Watson atlas (2013). These projections carefully avoided the CEAi. On the contrary, the

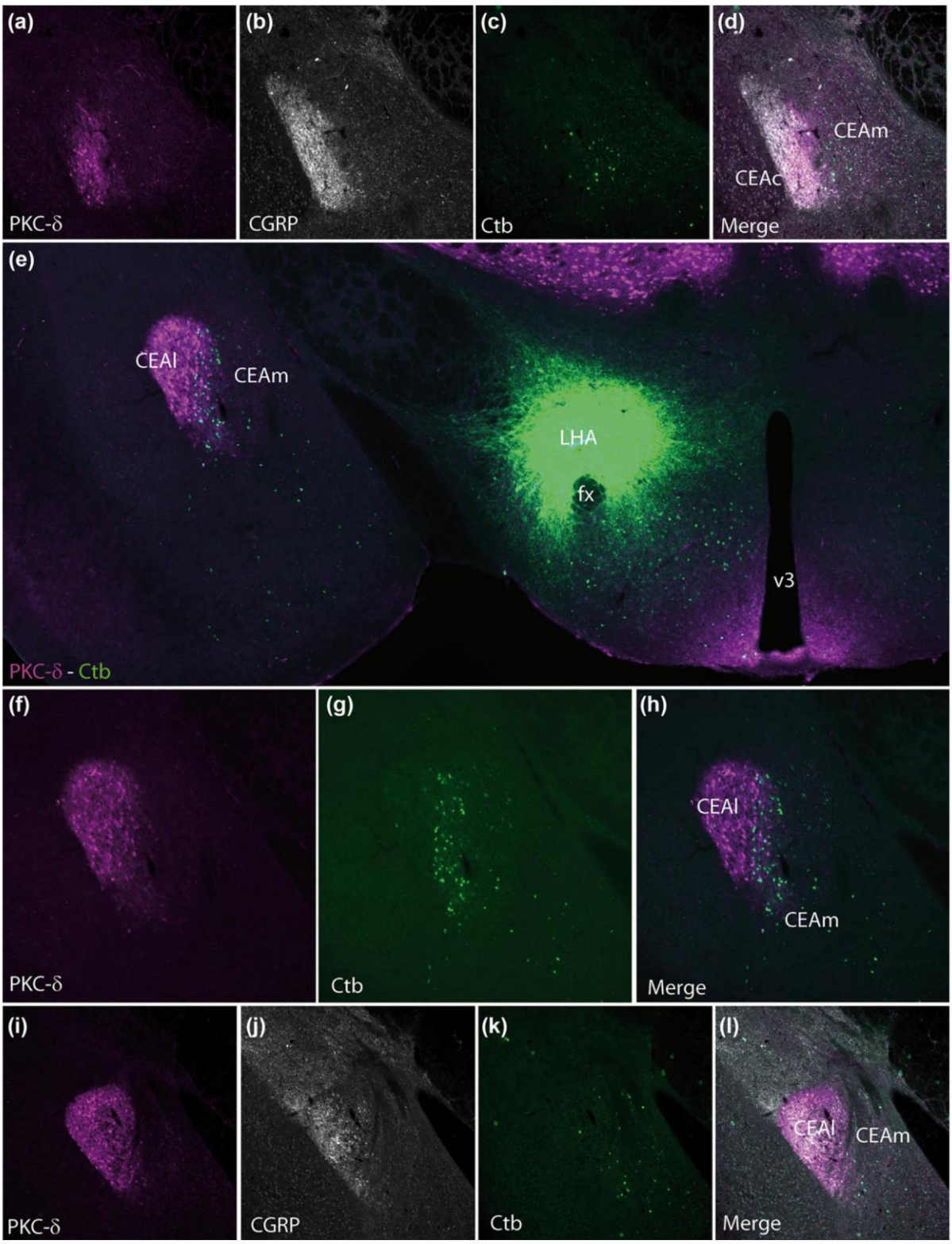

FIGURE 14 Photomicrographs to compare the distribution of Ctb in the CEA after injection in the LHA (e), with that of CGRP and PKC-δ. (a–d) At the rostral most level of the nucleus, CGRP axons innervate the CEAc as in the rat. However, PKC-δ antibodies intensely label a group of cells in the ventral aspect of the CEAc. Ctb containing neurons are immediately medial to the CEAc. (d–g) The Ctb injection site of the experiment mLHA1 is illustrated in (d). At this level in the CEA, Ctb retrogradely labeled neurons form a loosely arranged condensation. This condensation is mostly within the medial aspect of the CEAl that is labeled for PKC-δ. It avoid however the more lateral region of the CEAl in which the PKC-δ labeling is more intense. The Ctb condensation also extends ventrally into the CEAm. (h–l) At caudal levels of the CEA, the patterns of labeling for CGRP and PKC-δ provide a very similar to that in the rat, with intense CGRP in lateral regions of the CEAl [Color figure can be viewed at wileyonlinelibrary.com]

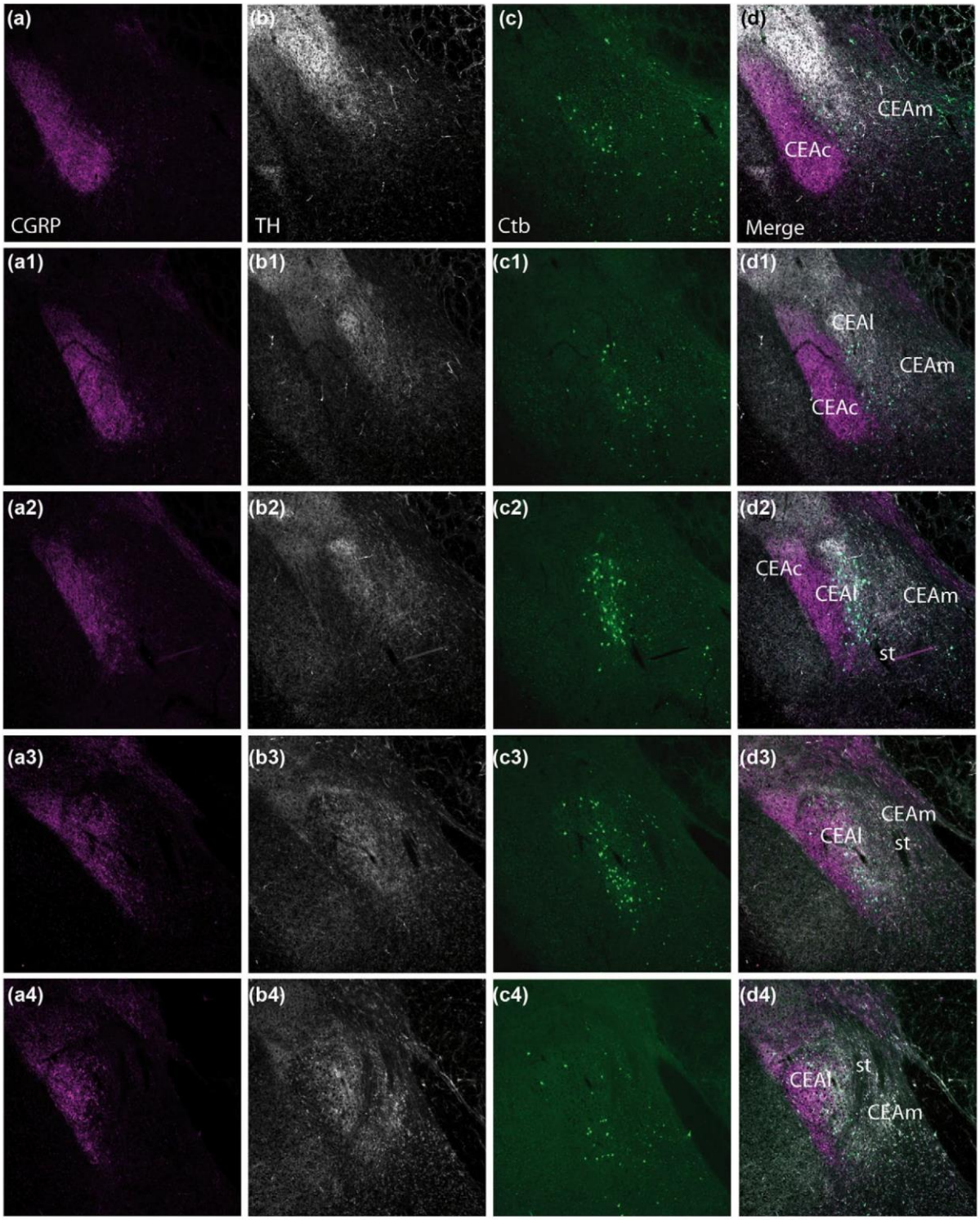

FIGURE 15 Photomicrographs illustrating the distribution of Ctb in the CEA after injection in the LHA (e), with that of CGRP and TH from sections arranged from rostral (a, b, c, d) to caudal (a4, b4, c4, d4). The relative distribution of CGRP and TH is very similar to that in the rat, with CGRP mostly in the CEAc and lateral CEAl and TH in the medial aspect of CEAl. Ctb retrogradely labeled cells are mostly observed forming a loosely organized condensation within TH innervated region, in that remembering what was observed in the rat [Color figure can be viewed at wileyonlinelibrary.com]

CEAi received intense inputs from the posterior AId that did not innervate the CEAm. The CEAi is innervated by CRH-, Met-Enk-, and TH-labeled axons while the CEAm does not contain such intense innervation by similar neurochemically defined axons. This evidence indicates that the CEAi and CEAm are parts of two distinct networks, implying that they may serve distinct functions. The CEAi appears to be more closely associated and receives similar sets of afferents than the CEAl. Cassell et al. (1999) and Chieng et al. (2006) suggested that it is part of an intra-CEAl network. It is interesting to note that several functional studies in the mouse indicated that the rostral pole of the

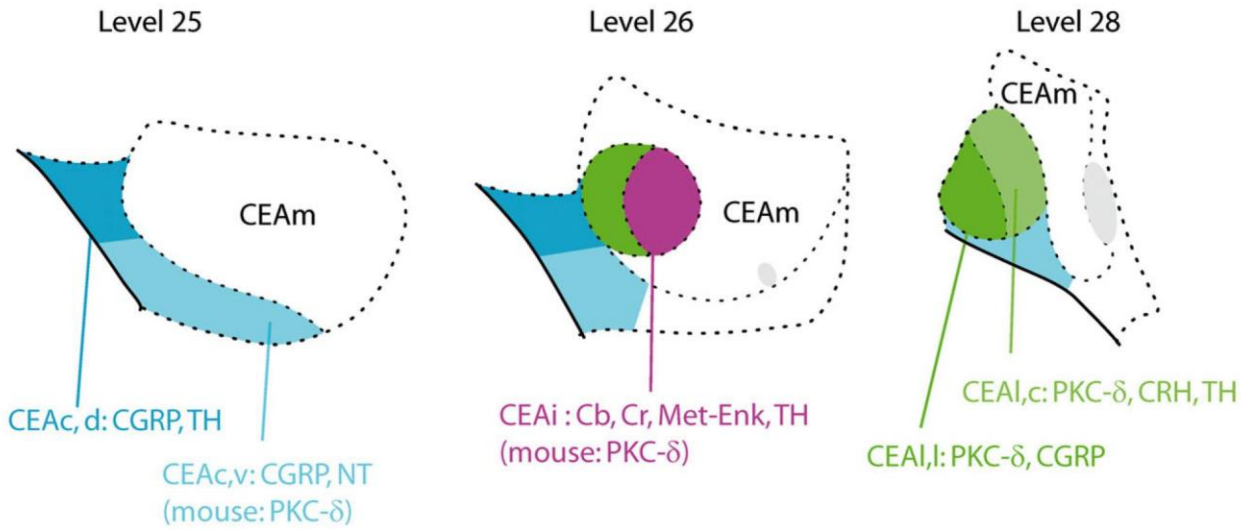

FIGURE 16 Line drawings to summarize the subdivisions of the CEA as suggested by chemoarchitecture in this study. See text for detail

CEAl could serve somewhat specific functions (Haubensak et al., 2010; Han et al., 2015; Kim et al., 2017). Another interesting point is that CEAm and CEAi may innervate different cell groups in the LHA, especially in the perifornical region. However, both send convergent projections into the PSTN. These inputs into the PSTN are more intense from the CEAm (Barbier et al., 2017). It was unfortunately impossible to specifically target the CEAi using conventional retrograde tracers and therefore more work is obviously needed to characterize precisely its output/input and functions.

Our study confirmed a great heterogeneity in the neurochemical organization of the CEAl and CEAc. Studies of the chemoarchitecture of the CEA in un-colchicinized animals are available in the literature to which we can compare our data. The expression of Cb within the CEAi was already described by McDonald (1997), Cassell et al. (1999), Kemppainen and Pitkänen (2000), and Pitkänen and Kemppainen (2002). In a study that was very similar to ours, Marchant et al. (2007) compared the distribution of Cb-containing neurons with that of several molecules including CRH, TH, CGRP, and dynorphin. The patterns described by these authors are virtually identical to those reported here for Cb, CRH, TH and CGRP. They concluded as Cassell et al. (1999), that the CEAl should be divided into three zones. The Cb cell condensation corresponded to the medial zone of the CEAl in their study. We also found that the CEAl is characterized as a whole by PKC-δ-expressing neurons, with the exception of the CEAi in the rat, but not in the mouse. The CEAl is also divided into a central zone containing dynorphin (Marchant et al., 2007), CRH, and TH (Marchant et al. (2007), and probably other peptides such as somatostatin (Chieng & Christie, 2010; Yu, Garcia da Silva, Albeanu, & Li, 2016). It is also divided into a lateral zone that is intensely innervated by CGRP axons that make very clear pericellular nets around cell bodies that correspond to PKC-δ cells. In the mouse, the CGRP innervation of PKC-δ cells was also observed in the ventral aspect of the CEAc. The CEAi contains an intense innervation by Met-Enk axons. A paper by Poulin et al. (2006) illustrated a similar pattern in the rostral CEAl that we found here corresponding to the CEAi. These authors showed that lateral parts of the CEA are rich in enkephalinergic neurons using in situ hybridization, which also confirms that neurons of the CEAi may contain Met-Enk. Poulin et al. (2006) further indicated that most of the Met-Enk innervations of the CEA mostly have intra-amygdala and BST origins.

Finally, the CEAc is also a heterogeneous division of the CEA. McDonald (1982) divided the rostral CEAc into dorsal and ventral zones. Cassel (1999) identified a dorsal and ventral wings while De Olmos et al. (2004) observed an antero-posterior difference that is not incoherent with a dorsal/ventral parceling, as the ventral part extends more caudally. The dorsal CEAc contains CGRP and TH projections, while the ventral zone is innervated by axons co-expressing CGRP and NT. The CGRP innervation of the CEAc originates in the lateral parabrachial nucleus (Schwaber, Sternini, Brecha, Rogers, & Card, 1988; Bernard, Alden, & Besson, 1993; Bourgeais et al., 2001; D'Hanis, Linke, & Yilmazer-Hanke, 2007; Carter et al., 2013, Carter et al., 2015; Han et al., 2015; Campos et al., 2016; Liang et al., 2016). Neurons in this nucleus have been reported to co-express CGRP and NT as well as substance P (Shinohara, Yamano, Matsuzaki, & Tohyama, 1988). Veening et al. (1984) showed similar NT and SP expression in the ventral CEAc. Our observation indicates that CGRP/NT and CGRP only cells may innervate distinct divisions of the CEA in the rat. Similar observations were made in the mouse (data not shown).

To conclude, and as stated by Swanson in the Brain Maps (Swanson, 2004), the CEA is a very heterogeneous and complex structure. The chemoarchitecture of the nucleus may reveal this complexity better than the sole cytoarchitecture (Figure 16). Using the Golgi method, McDonald (1982) had identified parts in the CEA that were not always recognized based solely on Nissl staining. Agreeing with McDonald, we found that the projections of the CEAi are closer to those of the CEAm, but it might receive afferences common with and be more functionally related to the CEAl.

ACKNOWLEDGMENTS

This work was financed by the Region Franche-Comté, France.

CONFLICT OF INTEREST

The authors declare that they have no conflict of interest.

AUTHOR CONTRIBUTIONS

Conceived and designed the experiments: Pierre-Yves Risold. Performed the experiments and illustration production: Marie Barbier and Pierre-Yves Risold. Animal handling: Marie Barbier. Analyzed the data and wrote the text: Marie Barbier, Dominique Fellmann and Pierre-Yves Risold.

REFERENCES

Allen Institute. (2004). Allen Mouse Brain Atlas. Available from: http://mouse.brain-map.org/

Asan, E., Yilmazer-Hanke, D. M., Eliava, M., Hantsch, M., Lesch, K.-P., & Schmitt, A. (2005). The corticotropin-releasing factor (CRF)-system and monoaminergic afferents in the central amygdala: Investigations in different mouse strains and comparison with the rat. Neuroscience, 131, 953–967.

Balcita-Pedicino, J. J., Omelchenko, N., Bell, R., & Sesack, S. R. (2011). The inhibitory influence of the lateral habenula on midbrain dopamine cells: Ultrastructural evidence for indirect mediation via the rostromedial mesopontine tegmental nucleus. The Journal of Comparative Neurology, 519, 1143–1164.

Barbier, M., Chometton, S., Peterschmitt, Y., Fellmann, D., & Risold, P.-Y. (2017). Parasubthalamic and calbindin nuclei in the posterior lateral hypothalamus are the major hypothalamic targets for projections from the central and anterior basomedial nuclei of the amygdala. Brain Structure and Function, 222(7), 2961–2991.

Bernard, J.-F., Alden, M., & Besson, J.-M. (1993). The organization of the efferent projections from the pontine parabrachial area to the amygdaloid complex: A phaseolus vulgaris leucoagglutinin (PHA-L) study in the rat. The Journal of Comparative Neurology, 329, 201–229.

Bourgeais, L., Gauriau, C., & Bernard, J. F. (2001). Projections from the nociceptive area of the central nucleus of the amygdala to the forebrain: A PHA-L study in the rat. The European Journal of Neuroscience, 14, 229–255.

Campos, C. A., Bowen, A. J., Schwartz, M. W., & Palmiter, R. D. (2016). Parabrachial CGRP neurons control meal termination. Cell Metabolism, 23, 811–820.

Carter, M. E., Han, S., & Palmiter, R. D. (2015). Parabrachial calcitonin gene-related peptide neurons mediate conditioned taste aversion. The Journal of Neuroscience, 35, 4582–4586.

Carter, M. E., Soden, M. E., Zweifel, L. S., & Palmiter, R. D. (2013). Genetic identification of a neural circuit that suppresses appetite. Nature, 503, 111–114.

Cassell, M. D., Freedman, L. J., & Shi, C. (1999). The intrinsic organization of the central extended amygdala. Annals of the New York Academy of Sciences, 877, 217–241.

Cassell, M. D., Gray, T. S., & Kiss, J. Z. (1986). Neuronal architecture in the rat central nucleus of the amygdala: A cytological, hodological, and immunocytochemical study. The Journal of Comparative Neurology, 246, 478–499.

Celio, M. R., Baier, W., Schärer, L., de Viragh, P. A., & Gerday, C. (1988). Monoclonal antibodies directed against the calcium binding protein parvalbumin. Cell Calcium, 9, 81–86.

Chieng, B., & Christie, M. J. (2010). Somatostatin and nociceptin inhibit neurons in the central nucleus of amygdala that project to the periaqueductal grey. Neuropharmacology, 59, 425–430.

Chieng, B. C. H., Christie, M. J., & Osborne, P. B. (2006). Characterization of neurons in the rat central nucleus of the amygdala: Cellular physiology, morphology, and opioid sensitivity. The Journal of Comparative Neurology, 497, 910–927.

Chometton, S., Pedron, S., Peterschmitt, Y., Van Waes, V., Fellmann, D., & Risold, P.-Y. (2016). A premammillary lateral hypothalamic nuclear complex responds to hedonic but not aversive tastes in the male rat. Brain Structure and Function, 221, 2183–2208.

Clarke, J. H., Emson, P. C., & Irvine, R. F. (2009). Distribution and neuronal expression of phosphatidylinositol phosphate kinase IIÎ³ in the mouse brain. The Journal of Comparative Neurology, 517, 296–312.

Cole, S., Powell, D. J., & Petrovich, G. D. (2013). Differential recruitment of distinct amygdalar nuclei across appetitive associative learning. Learning & Memory (Cold Spring Harbor, N.Y.), 20, 295–299.

De Olmos, J. S., Beltramino, C. A., & Alheid, G. (2004). CHAPTER 19 - Amygdala and Extended Amygdala of the Rat: A Cytoarchitectonical, Fibroarchitectonical, and Chemoarchitectonical Survey. In G. Paxinos (ed.), *The rat nervous system* (3rd edn, pp. 509–603). Burlington: Academic Press. Available from: https://www.sciencedirect.com/science/article/pii/B9780125476386500201

Deng, P., Cuenca, N., Doerr, T., Pow, D. V., Miller, R., & Kolb, H. (2001). Localization of neurotransmitters and calcium binding proteins to neurons of salamander and mudpuppy retinas. Vision Research, 41, 1771–1783.

D'Hanis, W., Linke, R., & Yilmazer-Hanke, D. M. (2007). Topography of thalamic and parabrachial calcitonin gene-related peptide (CGRP) immunoreactive neurons projecting to subnuclei of the amygdala and extended amygdala. The Journal of Comparative Neurology, 505, 268–291.

Emson, P. C., Goedert, M., Williams, B., Ninkovic, M., & Hunt, S. P. (1982). Neurotensin: Regional distribution, characterization, and inactivation. Annals of the New York Academy of Sciences, 400, 198–215.

François, A., Low, S. A., Sypek, E. I., Christensen, A. J., Sotoudeh, C., Beier, K. T., … Scherrer, G. (2017). A brainstem-spinal cord inhibitory circuit for mechanical pain modulation by GABA and enkephalins. Neuron, 93, 822–839.e6.

García Del Caño, G., Gerrikagoitia, I., & Martínez-Millán, L. (2000). Morphology and topographical organization of the retrospleniocollicular connection: A pathway to relay contextual information from the environment to the superior colliculus. The Journal of Comparative Neurology, 425, 393–408.

George, O., Koob, G. F., & Vendruscolo, L. F. (2014). Negative reinforcement via motivational withdrawal is the driving force behind the transition to addiction. Psychopharmacology, 231, 3911–3917.

Gray, T. S., Carney, M. E., & Magnuson, D. J. (1989). Direct projections from the central amygdaloid nucleus to the hypothalamic paraventricular nucleus: Possible role in stress-induced adrenocorticotropin release. Neuroendocrinology, 50, 433–446.

Han, S., Soleiman, M. T., Soden, M. E., Zweifel, L. S., & Palmiter, R. D. (2015). Elucidating an affective pain circuit that creates a threat memory. Cell, 162, 363–374.

Haubensak, W., Kunwar, P. S., Cai, H., Ciocchi, S., Wall, N. R., Ponnusamy, R., … Anderson, D. J. (2010). Genetic dissection of an amygdala microcircuit that gates conditioned fear. Nature, 468, 270–276.

Heimer, L., Harlan, R. E., Alheid, G. F., Garcia, M. M., & de Olmos, J. (1997). Substantia innominata: A notion which impedes clinical-anatomical correlations in neuropsychiatric disorders. Neuroscience, 76, 957–1006.

Holland, P. C., & Hsu, M. (2014). Role of amygdala central nucleus in the potentiation of consuming and instrumental lever-pressing for sucrose by cues for the presentation or interruption of sucrose delivery in rats. Behavioral Neuroscience, 128, 71–82.

Holland, P. C., Petrovich, G. D., & Gallagher, M. (2002). The effects of amygdala lesions on conditioned stimulus-potentiated eating in rats. Physiology & Behavior, 76, 117–129.

Holtz, S. L., Fu, A., Loflin, W., Corson, J. A., & Erisir, A. (2015). Morphology and connectivity of parabrachial and cortical inputs to gustatory thalamus in rats. The Journal of Comparative Neurology, 523, 139–161.

Kemppainen, S., & Pitkänen, A. (2000). Distribution of parvalbumin, calretinin, and calbindin-D(28k) immunoreactivity in the rat amygdaloid complex and colocalization with gamma-aminobutyric acid. The Journal of Comparative Neurology, 426, 441–467.

Kim, J., Zhang, X., Muralidhar, S., LeBlanc, S. A., & Tonegawa, S. (2017). Basolateral to central amygdala neural circuits for appetitive behaviors. Neuron, 93, 1464–1479.e5.

Koob, G. F. (2013). Negative reinforcement in drug addiction: The darkness within. Current Opinion in Neurobiology, 23, 559–563.

Koob, G. F., & Volkow, N. D. (2010). Neurocircuitry of Addiction. Neuropsychopharmacology, 35, 217–238.

Li, S., & Kirouac, G. J. (2008). Projections from the paraventricular nucleus of the thalamus to the forebrain, with special emphasis on the extended amygdala. The Journal of Comparative Neurology, 506, 263–287.

Liang, S.-H., Yin, J.-B., Sun, Y., Bai, Y., Zhou, K.-X., Zhao, W.-J., … Li, Y.-Q. (2016). Collateral projections from the lateral parabrachial nucleus to the paraventricular thalamic nucleus and the central amygdaloid nucleus in the rat. Neuroscience Letters, 629, 245–250.

Marchant, N. J., Densmore, V. S., & Osborne, P. B. (2007). Coexpression of prodynorphin and corticotrophin-releasing hormone in the rat central amygdala: Evidence of two distinct endogenous opioid systems in the lateral division. The Journal of Comparative Neurology, 504, 702–715.

McDonald, A. J. (1982). Cytoarchitecture of the central amygdaloid nucleus of the rat. The Journal of Comparative Neurology, 208, 401–418.

McDonald, A. J. (1988). Projections of the intermediate subdivision of the central amygdaloid nucleus to the bed nucleus of the stria terminalis and medial diencephalon. Neuroscience Letters, 85, 285–290.

McDonald, A. J. (1997). Calbindin-D28k immunoreactivity in the rat amygdala. The Journal of Comparative Neurology, 383, 231–244.

Milman, P., & Woulfe, J. (2013). Novel variant of neuronal intranuclear rodlet immunoreactive for 40 kDa huntingtin associated protein and ubiquitin in the mouse brain. Journal of Comparative Neurology, 521, 3832–3846.

Oka, T., Tsumori, T., Yokota, S., & Yasui, Y. (2008). Neuroanatomical and neurochemical organization of projections from the central amygdaloid nucleus to the nucleus retroambiguus via the periaqueductal gray in the rat. Neuroscience Research, 62, 286–298.

Olschowka, J. A., O'Donohue, T. L., Mueller, G. P., & Jacobowitz, D. M. (1982). The distribution of corticotropin releasing factor-like immunoreactive neurons in rat brain. Peptides, 3, 995–1015.

Paré, D., Quirk, G. J., & Ledoux, J. E. (2004). New vistas on amygdala networks in conditioned fear. Journal of Neurophysiology, 92, 1–9.

Partin, A. C., Hosek, M. P., Luong, J. A., Lella, S. K., Sharma, S. A. R., & Ploski, J. E. (2013). Amygdala nuclei critical for emotional learning exhibit unique gene expression patterns. Neurobiology of Learning and Memory, 104, 110–121.

Pasteels, B., Rogers, J., Blachier, F., & Pochet, R. (1990). Calbindin and calretinin localization in retina from different species. Visual Neuroscience, 5, 1–16.

Paxinos, G., & Keith, F. (2012). *Paxinos and Franklin's the mouse brain in stereotaxic coordinates*, fourth edition. Amsterdam: Academic Press.

Paxinos, G., & Watson, C. (2005). *The rat brain in stereotaxic coordinates* (5th ed.). Amsterdam: Elsevier Academic Press.

Paxinos, G., & Watson, C. (2013). *The rat brain in stereotaxic coordinates*. Amsterdam: Academic Press.

Petrovich, G. D., Setlow, B., Holland, P. C., & Gallagher, M. (2002). Amygdalo-hypothalamic circuit allows learned cues to override satiety and promote eating. The Journal of Neuroscience, 22, 8748–8753.

Petrovich, G. D., & Swanson, L. W. (1997). Projections from the lateral part of the central amygdalar nucleus to the postulated fear conditioning circuit. Brain Research, 763, 247–254.

Piekut, D. T., & Phipps, B. (1998). Increased corticotropin-releasing factor immunoreactivity in select brain sites following kainate elicited seizures. Brain Research, 781, 100–113.

Pitkänen, A., & Kemppainen, S. (2002). Comparison of the distribution of calcium-binding proteins and intrinsic connectivity in the lateral nucleus of the rat, monkey, and human amygdala. Pharmacology, Biochemistry, and Behavior, 71, 369–377.

Pomrenze, M. B., Millan, E. Z., Hopf, F. W., Keiflin, R., Maiya, R., Blasio, A., … Messing, R. O. (2015). A transgenic rat for investigating the anatomy and function of corticotrophin releasing factor circuits. Frontiers in Neuroscience, 9, 487.

Poulin, J.-F., Chevalier, B., Laforest, S., & Drolet, G. (2006). Enkephalinergic afferents of the centromedial amygdala in the rat. The Journal of Comparative Neurology, 496, 859–876.

Quina, L. A., Tempest, L., Ng, L., Harris, J. A., Ferguson, S., Jhou, T. C., & Turner, E. E. (2015). Efferent pathways of the mouse lateral habenula. The Journal of Comparative Neurology, 523, 32–60.

Reppucci, C. J., & Petrovich, G. D. (2016). Organization of connections between the amygdala, medial prefrontal cortex, and lateral hypothalamus: A single and double retrograde tracing study in rats. Brain Structure & Function, 221, 2937–2962.

Schmued, L. C., & Fallon, J. H. (1986). Fluoro-Gold: a new fluorescent retrograde axonal tracer with numerous unique properties. Brain Research, 377, 147–154.

Schwaber, J. S., Sternini, C., Brecha, N. C., Rogers, W. T., & Card, J. P. (1988). Neurons containing calcitonin gene-related peptide in the parabrachial nucleus project to the central nucleus of the amygdala. The Journal of Comparative Neurology, 270, 416–426. 398–399.

Shammah-Lagnado, S. J., Alheid, G. F., & Heimer, L. (1999). Afferent connections of the interstitial nucleus of the posterior limb of the anterior commissure and adjacent amygdalostriatal transition area in the rat. Neuroscience, 94, 1097–1123.

Shimada, S., Shiosaka, S., Emson, P. C., Hillyard, C. J., Girgis, S., Macintyre, I., & Tohyama, M. (1985). Calcitonin gene-related peptidergic projection from the parabrachial area to the forebrain and diencephalon in the rat: An immunohistochemical analysis. Neuroscience, 16, 607–616.

Shinohara, Y., Yamano, M., Matsuzaki, T., & Tohyama, M. (1988). Evidences for the coexistence of substance P, neurotensin and calcitonin gene-related peptide in single neurons of the external subdivision of the lateral parabrachial nucleus of the rat. Brain Research Bulletin, 20, 257–260.

Shirasu, M., Takahashi, T., Yamamoto, T., Itoh, K., Sato, S., & Nakamura, H. (2011). Direct projections from the central amygdaloid nucleus to the mesencephalic trigeminal nucleus in rats. Brain Research, 1400, 19–30.

Swanson, L. W. (2004). *Brain maps: Structure of the rat brain* (3rd edn). San Diego: Elsevier.

Swanson, L. W., & Petrovich, G. D. (1998). What is the amygdala?. Trends in Neurosciences, 21, 323–331.

Swanson, L. W., Sanchez-Watts, G., & Watts, A. G. (2005). Comparison of melanin-concentrating hormone and hypocretin/orexin mRNA expression patterns in a new parceling scheme of the lateral hypothalamic zone. Neuroscience Letters, 387, 80–84.

Swanson, L. W., Sawchenko, P. E., Rivier, J., & Vale, W. W. (1983). Organization of ovine corticotropin-releasing factor immunoreactive cells and fibers in the rat brain: An immunohistochemical study. Neuroendocrinology, 36, 165–186.

Veening, J. G., Swanson, L. W., Cowan, W. M., Nieuwenhuys, R., & Geeraedts, L. M. (1982). The medial forebrain bundle of the rat. II. An autoradiographic study of the topography of the major descending and ascending components. The Journal of Comparative Neurology, 206, 82–108.

Veening, J. G., Swanson, L. W., & Sawchenko, P. E. (1984). The organization of projections from the central nucleus of the amygdala to brainstem sites involved in central autonomic regulation: A combined retrograde transport-immunohistochemical study. Brain Research, 303, 337–357.

White, M. G., Cody, P. A., Bubser, M., Wang, H.-D., Deutch, A. Y., & Mathur, B. N. (2016). Cortical hierarchy governs rat claustrocortical circuit organization: Cortical hierarchy and claustrocortical circuitry. Journal of Comparative Neurology, 525(6), 1347–1362.

Woulfe, J., & Beaudet, A. (1992). Neurotensin terminals form synapses primarily with neurons lacking detectable tyrosine hydroxylase immunoreactivity in the rat substantia nigra and ventral tegmental area. The Journal of Comparative Neurology, 321, 163–176.

Yasui, Y., Saper, C. B., & Cechetto, D. F. (1991). Calcitonin gene-related peptide (CGRP) immunoreactive projections from the thalamus to the striatum and amygdala in the rat. The Journal of Comparative Neurology, 308, 293–310.

Yu, K., Garcia da Silva, P., Albeanu, D. F., & Li, B. (2016). Central amygdala somatostatin neurons gate passive and active defensive behaviors. The Journal of Neuroscience, 36, 6488–6496.

Zhang, J., Zhang, A.-J., & Wu, S. M. (2006). Immunocytochemical analysis of GABA-positive and calretinin-positive horizontal cells in the tiger salamander retina. The Journal of Comparative Neurology, 499, 432–441.

How to cite this article: Barbier M, Fellmann D, Risold P-Y. Characterization of McDonald's intermediate part of the Central nucleus of the amygdala in the rat. *J Comp Neurol*. 2018; 1–22. https://doi.org/10.1002/cne.24470

3. Analyse détaillée des projections du CEA dans le LHA (Publication n°3)

L'article suivant a été écrit à la suite d'une invitation du journal *Frontiers in neurology*, section *Neuropharmacology* dans le topic *"The LHA hub"*. Dans notre première publication, il a été montré que les axones du CEAm empruntent deux trajets différents dans le LHA : un dorsal et un ventral, avec une innervation de régions périfornicales (Barbier *et al*, 2017) qui n'était pas toujours mentionnée dans la littérature. Ce travail a ensuite mené à l'analyse de l'origine des projections dans le LHApfx, et à l'identification du CEAi comme principale source d'innervation de cette région (Barbier *et al*, 2018a), attestant d'une organisation complexe des projections du CEA dans le LHA. En effet, il semble que des aspects importants des connexions avec l'hypothalamus de ce noyau, par ailleurs très étudié, nécessitent encore des investigations. Dans cette troisième étude, une analyse de l'innervation du LHApfx par les fibres depuis le CEAm et le CEAi a été réalisée. Dans le LHA tubéral, la distribution des axones PHAL a été comparée à celle des neurones à MCH et à Hcrt. La distribution de ces neurones étant très stéréotypée dans ce territoire, elle s'avère pertinente pour l'identification de sous-divisions sur la base de ce qu'avait décrit J.D. Hahn et L.W. Swanson (Hahn, 2010; Hahn & Swanson, 2010; Swanson *et al*, 2005). Les axones qui convergent dans les régions postérieures latérales du LHA depuis le CEA présentent des patrons distincts dans les régions antérieures tubérales. Par exemple, la partie antérieure du CEAm projette dans le LHA tubéral antérieur puis dans les aires dorsales de la région dorsale du LHA (LHAd) et dans le LHA pré-PSTN (LHAppstn). De plus, des neurones rétrogradement marqués après injection de FG dans le PSTN sont innervés par les axones PHAL positifs issus de l'amygdale. Les projections issues du CEAm et du CEAi innervent donc différentes divisions du LHA : la région suprafornicale du LHA (LHAs) est innervée par la partie postérieure du CEAm et le LHAd est ciblé par le CEAm postérieur et le CEAi. Ce travail peut ainsi permettre de commencer l'analyse fine de microcircuits dans le LHA, sous le contrôle du CEA, associés peut-être à des fonctions qui restent à déterminer.

frontiers in Neurology

ORIGINAL RESEARCH
published: 24 August 2018
doi: 10.3389/fneur.2018.00688

Morphofunctional Organization of the Connections From the Medial and Intermediate Parts of the Central Nucleus of the Amygdala Into Distinct Divisions of the Lateral Hypothalamic Area in the Rat

*Marie Barbier, Dominique Fellmann and Pierre-Yves Risold**

Laboratoire de Neurosciences Intégratives et Cliniques, EA481, UFR Sciences Médicales et Pharmaceutiques, Université de Bourgogne Franche-Comté, Besançon, France

OPEN ACCESS

Edited by:
Remi Martin-Fardon, The Scripps Research Institute, United States

Reviewed by:
Ling-Ling Hwang, Taipei Medical University, Taiwan
Pascal Carrive, University of New South Wales, Australia

***Correspondence:**
Pierre-Yves Risold
pierre-yves.risold@univ-fcomte.fr

Specialty section:
This article was submitted to Neuropharmacology, a section of the journal Frontiers in Neurology

Received: *18 April 2018*
Accepted: *30 July 2018*
Published: *24 August 2018*

Citation:
Barbier M, Fellmann D and Risold P-Y (2018) Morphofunctional Organization of the Connections From the Medial and Intermediate Parts of the Central Nucleus of the Amygdala Into Distinct Divisions of the Lateral Hypothalamic Area in the Rat. Front. Neurol. 9:688. doi: 10.3389/fneur.2018.00688

Projections from the central nucleus of the amygdala (CEA) into the lateral hypothalamic area (LHA) show a very complex pattern. After injection of an anterograde tracer (*Phaseolus vulgaris* leucoagglutinin—PHAL) into the medial and intermediate parts of the CEA, we observed that labeled axons converged onto the caudal lateral LHA but provided distinct patterns in rostral tuberal regions. These projections were compared to that of neurons containing the peptides "melanin-concentrating hormone" (MCH) or hypocretin (Hcrt). Because the distribution of these neurons is stereotyped, it was possible to characterize distinct divisions into the LHA. Some of them in the rostral tuberal LHA [the dorsal (LHAd) and suprafornical regions (LHAs)] received a distinct innervation by projections that originated from neurons in respectively anterior or posterior regions of the medial part (CEAm) or from the intermediate part (CEAi) of the central nucleus. Therefore, this work illustrates that projections from the CEAm and CEAi converge into the caudal lateral LHA but diverge into the rostral tuberal LHA.

Keywords: lateral hypothalamus, amygdala, melanin-concentrating hormone, hypocretin, tract tracing

INTRODUCTION

The lateral hypothalamic area (LHA) receives inputs from a very large number of brain sites and is involved in a large range of functions from ingestive behaviors to the control of behavioral state and sleep/wake cycle (1–6). Many studies have focused on the role of specific neuron populations of the LHA, including the melanin-concentrating hormone (MCH) and hypocretin (Hcrt) containing cells that form conspicuous populations in the tuberal hypothalamus (7–10). However, despite these efforts, we must acknowledge that the internal organization of the LHA is still poorly understood.

One of the main function associated with the LHA is the initiation of feeding behavior (1, 10). Literature data indicates that neuropeptide Y (NPY) and proopiomelanocortin (POMC)

neurons from the arcuate nucleus provide metabolic information to second order LHA neurons (MCH, Hcrt) that may then initiate the feeding response (2, 9, 11–16). Other works point to projections from the bed nucleus of the stria terminalis or accumbens nucleus that are important for this response from the LHA, but involving non-MCH and non-Hcrt, glutamatergic, or GABAergic cells (17–19). The central nucleus of the amygdala (CEA) is another telencephalic structure innervating the LHA and is involved in the initiation of feeding (20–26). This nucleus is closely connected to the parasubthalamic nucleus (PSTN), a caudal LHA nucleus devoid of MCH and Hcrt neurons (7, 21). However, the CEA also projects into the perifornical LHA. In a recent study (27), we identified that these projections originate from the medial part of the CEA (CEAm), but also from the intermediate part (CEAi), while the capsular and lateral parts of the CEA send only very sparse projections into the hypothalamus. We noted that mostly the anterior perifornical region of the LHA was innervated by the CEAm/i, but this term is quite vague and this region can be sub-divided as in the Rat Brain Maps (28).

Different strategies can be implemented to increase our knowledge of the LHA organization. One of the most accessible mean to gather meaningful information, is to carefully analyze the distribution pattern of afferents from specific brain sites and compare these patterns with what is known of the cyto- and chemoarchitecture of the LHA.

In the present study, we aimed at carefully analyze the distribution of projections from the CEA into the LHA and compare these distributions with that of MCH and Hcrt neurons. We would then more easily characterize the distribution of the projections from the CEA, with regard to the parceling scheme of this region proposed by Swanson (28).

Abbreviations: AAA, Anterior amygdaloid area; ac, Anterior commissure; amc, Amygdalar capsule; AHN, Anterior hypothalamic nucleus; BLAa, Basolateral amygdalar nucleus, anterior part; BLAp, Basolateral amygdalar nucleus, posterior part; BMAa, Basomedial amygdalar nucleus, anterior part; BMAp, Basomedial amygdalar nucleus, posterior part; CbN, Calbindin nucleus; CEA, Central amygdalar nucleus; CEAc, Central amygdalar nucleus, capsular part; CEAl, Central amygdalar nucleus, lateral part; CEAi, Central amygdalar nucleus, intermediate part; CEAm, Central amygdalar nucleus, medial part; CLA, Claustrum; COAa, Cortical amygdalar nucleus, anterior part; cpd, Cerebral peduncle; DMH, Dorsomedial hypothalamic nucleus; ec, External capsule'; EPd, Endopiriform nucleus, dorsal part; EPv, Endopiriform nucleus, ventral part; FG, Fluorogold; fx, Columns of the fornix; GABA, Gamma-aminobutyric acid; GPe, Globus pallidus, external segment; Hcrt, Hypocretin/orexin; IA, Intercaleted amygdalar nuclei; LA, Lateral amygdalar nucleus; LHA, Lateral hypothalamic area; LHAav, Lateral hypothalamic area, anterior region, ventral zone; LHAd, Lateral hypothalamic area, dorsal region; LHAs, Lateral hypothalamic area, suprafornical region; lot, Lateral olfactory tract; MA, Magnocellular preoptic nucleus; MCH, Melanin-concentrating hormone; MEAad, Medial amygdalar nucleus, anterodorsal part; MEAav, Medial amygdalar nucleus, anteroventral part; MEApd-a,b,c, Medial amygdalar nucleus, posterodorsal part, sublayers a-c; MEApv, Medial amygdalar nucleus, posteroventral part; mtt, Mammillothalamic tract; NLOT, Nucleus of the lateral olfactory tract; NLOT2, Nucleus of the lateral olfactory tract, pyramidal layer; opt, Optic tract; PHAL, *Phaseolus vulgaris* leucoagglutinin; PVH, Paraventricular hypothalamic nucleus; PST, Preparasubthalamic nucleus; PSTN, Parasubthalamic nucleus; SI, Substantia innominate; sm, Stria medullaris; SO, Supraoptic nucleus, proper; st, Stria terminalis; STN, Subthalamic nucleus; sup, Supraoptic commissures; V3, Third ventricle; vlt, Ventrolateral hypothalamic tract; VMH, Ventromedial hypothalamic nucleus.ZI, Zona incerta.

MATERIALS AND METHODS

Animals

All animal use and care protocols were in accordance with institutional guidelines and with the Directive 2010/63/EU of the European Parliament and of the Council of 22 September 2010 on the protection of animals used for scientific purposes. The protocols were approved by Franche-Comté University's Animal Care Committee (protocol number: 2015-002) and the investigators authorized. Four Sprague–Dawley male rats, weighing 300–350 g, were obtained from Janvier (Le Genest-Saint-Isle, France). Rats were housed with a standard 12 h light/dark cycle at a constant room temperature and had free access to the standard laboratory diet and water.

Tracer Injections

PHAL experiments were already reported in previous works (AMY1 in 22, PHAL#1, PHAL#2, PAHL#3 in 27). In two experiments (PHAL#1, PHAL#2) a fluorogold (FG) injection was performed into the PSTN as well as a PHAL injection respectively in the CEAm or the CEAi. Experimental procedures are briefly described below.

Rats were anesthetized with an intraperitoneal (i.p.) injection of a mixture of xylazine and ketamine (1 mg/100 g and 10 mg/100 g of body weight, respectively; Vetoquinol®, France), and placed in a stereotaxic device.

Rats received a unilateral iontophoretic injection of 2.5% PHAL diluted in sodium phosphate buffer saline (NaPBS) pH 7.2. Glass micropipettes (tip diameter: 10–20 μm) were used to inject the PHAL iontophoretically (intermittent current of 5 μA and 7 s on/off time for 20 min). Coordinates were taken from Bregma using the Paxinos' atlas (29). For the CEA, the coordinates were: PHAL#1: AP: −1.53 mm, ML: 3.4 mm, and DV: −8.1 mm; PHAL#2: AP: −1.78 mm, ML: 3.72 mm, and DV: −8.5 mm; and PHAL#3: AP: −2.45 mm, ML: 4.0 mm, and DV: −8.6 mm. Coordinates of AMY 1 were close to those of PHAL#1 but ended more caudally. For the PSTN, the coordinates were AP: −4.2 mm, ML: 1.5 mm, DV: −8.4 mm. To avoid PHAL or FG diffusion along the micropipette track, the micropipette was left in place for another 5 min before being removed.

Tissue Preparation

Rats were deeply anesthetized with an i.p. injection of Pentobarbital (CEVA®, 50 mg/kg). Animals were perfused transcardially with 0.9% NaCl, followed by ice-cold 4% paraformaldehyde (PFA, Roth®) fixative in 0.1 M phosphate buffer (PB) at pH 7.4. Brains were extracted, postfixed for 20 h in the same fixative at 4°C, and cryoprotected by saturation in a 15% sucrose solution (Sigma®) in 0.1 M PB for 24 h at 4°C. Tissues were cut in four series of coronal sections at 30 μm thick, collected in a cryoprotective solution [1:1:2 glycerol / ethylene glycol / phosphate buffer saline (PBS)], and stored at −40°C.

Enzymatic Immunohistochemistry

After rinsing in PBS with 0.3% Triton X100 (PBS-T), free-floating sections were incubated with the anti-PHAL (Rabbit polyclonal, 1:1000, Vector Laboratories®, RRID:AB_2315142) in a solution containing 10% of lactoproteins (commercial

dry milk) during 48 h at 4°C. Sections were incubated for 4 h at room temperature in a solution of biotinylated goat anti-rabbit IgG (Vector Laboratories®, RRID:AB_2313606) at a dilution of 1:1000 in PBS-T. Then, sections were placed in the mixed avidin-biotin horseradish peroxidase (HRP) complex solution (ABC Elite Kit, Vector Laboratories®) for 1 h at room temperature. The peroxidase complex was visualized by a 6 min exposure to a chromogen solution containing 0.04% 3,3'diaminobenzidine tetrahydrochloride (DAB, Sigma®) with 0.006% hydrogen peroxide (Sigma®) in PBS. The reaction was stopped by extensive washing in PBS. Sections were mounted on gelatin-coated slides, and then stained in a solution of 1% toluidine blue (Roth®) in water to serve as a reference for cytoarchitectonic purposes. Finally, sections were dehydrated and coverslipped with Canada balsam (Roth®).

Immunofluorescent Staining

After rinsing in PBS-T, free-floating sections were incubated with primary antibodies [anti-Hcrt (Mouse monoclonal, 1:1,000, ANGIO-PROTEOMIE®); anti-MCH [Rabbit polyclonal, 1:1,000, our laboratory (21), RRID:AB_2616562]; anti-PHAL (Goat polyclonal, 1:1,000, Vector Laboratories®, RRID:AB_10000080)] dissolved in PBS-T, 1% bovine serum albumin, 10% lactoproteins, and 0.01% sodium azide or only in PBS-T for 24 h at 4°C. Tissues were washed three times with PBS-T (5 min each) and incubated for 2 h with appropriate secondary antibodies (Cyanine 5, donkey anti-mouse IgG, 1:1,000, Jackson Immunoresearch®, RRID:AB_2340819; Alexa Fluor 488, donkey anti-rabbit IgG 1:1,000, Invitrogen®, RRID:AB_2535792; Cyanine 3, donkey anti-goat IgG, 1:1,000, Jackson Immunoresearch®, RRID:AB_2340411) diluted in PBS-T at room temperature. For triple labeling, this procedure was repeated twice with primaries raised in different species. In some cases, only the FG labeling was detected by epifluorescence under UV illumination. Finally, sections were washed with PBS-T, mounted on gelatin-coated slides and coverslipped with 60/40 glycerol: PBS-T. An adjacent series was always stained in a solution of 1% toluidine blue (Roth) in water to serve as a reference series for cytoarchitectonic purposes.

Image Acquisition and Processing

Sections were analyzed on an ApoTome.2 microscope (Axio Imager Zeiss) and images were obtained through a digital camera (Digital Camera Hamamatsu C11440) using the Imager.Z2 software (Zen 2) (ZEN Digital Imaging for Light Microscopy, RRID:SCR_013672). The labeling was observed with appropriate filters: 38 HE Green Fluorescent Protein (BP excitation 450–490, emission 500–550), 43 HE DsRed (BP excitation 538–562, emission 570–540), and 50 Cy5 (BP excitation 625–655, emission 665–715), 49 DAPI (BP excitation 372–401, emission 421–456).

Some pictures were taken using the advanced features "Z-Stack" and "Deconvolution" of the Zen software. Finally, an orthogonal view was performed to obtain a 2D image. Neither additional treatment was made, except the fluorescence intensity. Nomenclature and nuclear parceling are from Swanson (28).

To perform the mapping of PHAL axons in the LHA, photomicrographs of the DAB stained sections and adjacent Nissl stained sections were taken. Drawings of the histological features and axons were made on tracing paper. Drawings were then scanned and transferred as jpeg files into Photoshop. This procedure was chosen as it allowed the most accurate representation of the labeled axon distributions.

RESULTS

Our initial objective was to compare the distribution of PHAL axons from injection sites in the CEAm and CEAi to the cytoarchitectonic divisions of the LHA as in Swanson (28). Unfortunately, we found very difficult to reliably identify the borders of these divisions on our Nissl stained material and, therefore, we choose to describe these distributions in two steps: (i) a detailed mapping on drawings made from the histological material on which main cytoarchitectonic borders (excluding intra-LHA borders) and fiber tracts are identified; (ii) in a second step, these distributions were compared with that of MCH and Hcrt neurons. The distributions of these neurons are truly stereotyped in the rat hypothalamus and they can be very useful to identify borders of LHA subdivisions as in Swanson et al. (7), or Swanson (28).

Injection Sites

All injection sites reported in this work are from experiments that were already used in previous articles. In the course of our study, we obtained many injections within the borders of the CEA. Only experiments with injection sites restricted to the CEAm/CEAi are reported here as only these parts of the CEA project into the LHA (22, 27). The CEAl and the CEAc do not send significant projections into the LHA (22, 27).

The experiment AMY1 was described in Barbier et al. (22). It consisted in a large injection involving most of the CEAm (**Figure 1**). This injection site extends through the rostrocaudal extend of the CEAm, but with a caudal predominance. It involves a few cell bodies in the CEAi.

The experiment PHAL#1 is a rostral injection extending from the level 24–26 of the Swanson's Brain Maps. It does not involve contamination of the CEAi.

The experiment PHAL#3 is a caudal injection, immediately adjacent to the CEAi, and extends caudally and ventrally into the CEAm with little contamination of the CEAi.

The experiment PHAL#2 is centered in the CEAi with contamination of the CEAm. This injection site overlaps slightly with the PHAL#3 experiment.

In experiments PHAL#1 and PHAL#2, the PHAL injections in the CEA were combined with FG injections in the PSTN. Injection sites in the PSTN are illustrated in the **Figure 4**. The reason for these co-injections is that the PSTN is the major target for CEA projections in the LHA. However, the LHA may as well innervate the PSTN and we wanted to start investigating on some putative intra-LHA microcircuits under CEA control.

Patterns of Innervation of the LHA

Experiment AMY1: As the experiment AMY1 involved most of the CEAm, it labeled the most complete pattern of projections

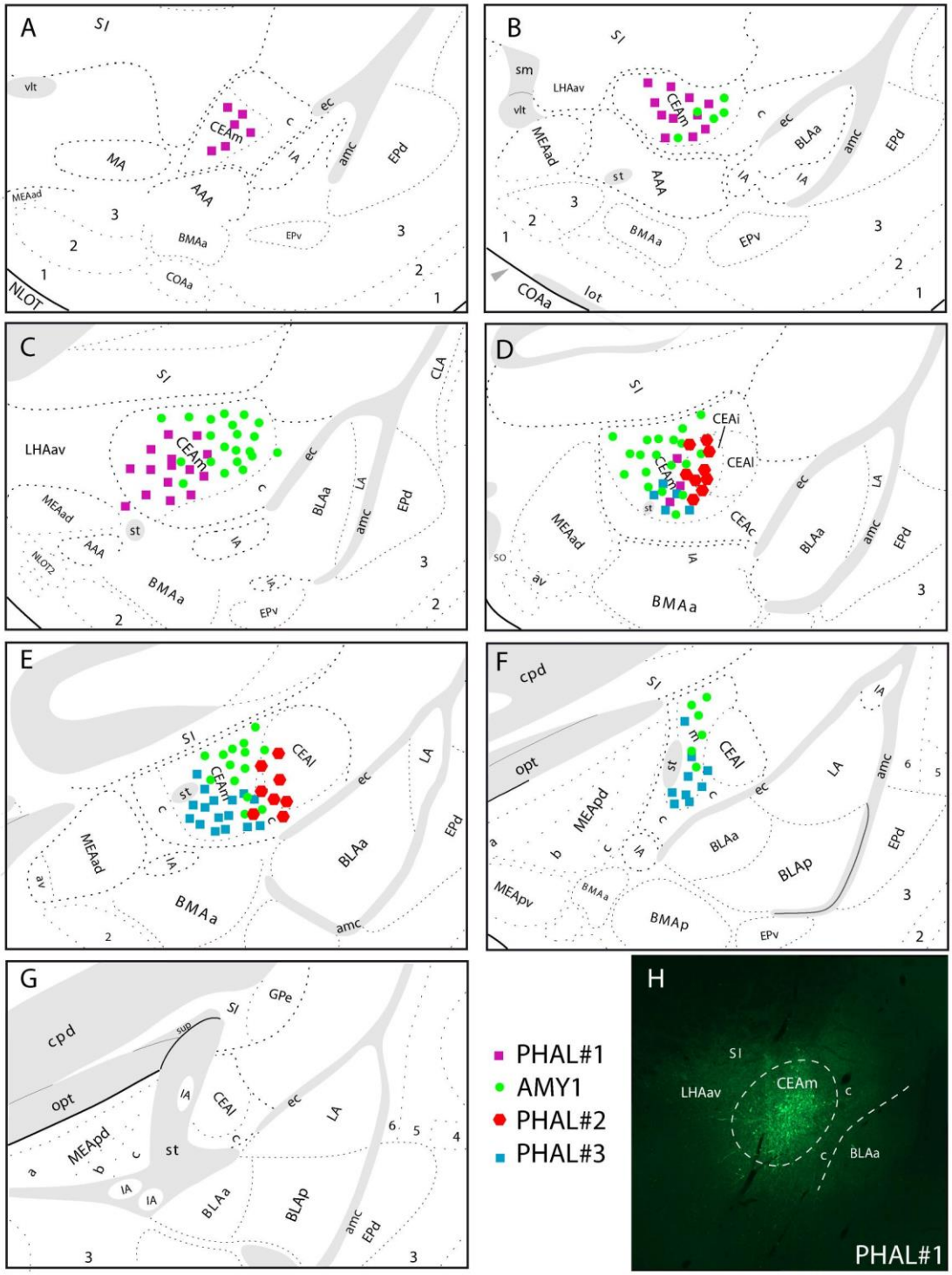

FIGURE 1 | (A–G) Line drawings to illustrate the relative extend of PHAL injection sites in the CEAm and CEAi that contributed to significant innervations of the LHA. PHAL#1 was centered in the rostral CEAm **(A–C)**. AMY1 mainly extended into central and caudal CEAm **(D–F)**. PHAL#2 was in the CEAi **(D,E)**. PHAL#3 is restricted to the caudal CEAm. **(H)** Photomicrograph to illustrate the PHAL injection site in the experiment PHAL#1.

FIGURE 2 | Line drawings describing the distribution patterns of PHAL axons in the LHA of sections corresponding to the levels 26–31 of the Swanson's Brain Maps (28) in experiments AMY1, PHAL#1, and PHAL#2.

in the LHA. The description of these patterns is illustrated in the **Figure 2**.

Anterior region of the LHA, e.g., corresponding to the level 26 of the Brain Maps (28), was little innervated (**Figure 2A1**). A few axons were observed in the paraventricular hypothalamic nucleus (PVH). These axons entered the nucleus by its perifornical part at level 27 (**Figure 2A2**). The perifornical part of the nucleus is well innervated as well as caudal parvicellular neurons. The LHA contains only a loose innervation at these rostral levels, and most axons resembled to passing axons in the two dorsal and ventral pathways that were described in the work of Barbier et al. (22).

Caudal to the PVH, corresponding to inter-level 27–28 (**Figures 2A3–A4, 3B**), cells dorsal to the fornix received an intense innervation. Immediately caudal to the PVH (**Figure 2A3**), this region was quite restricted in size. It concerned cells in the dorsal perifornical LHA. In the next caudal sections, the innervation encompassed the whole dorsal perifornical region as well as a band of tissue immediately lateral to the fornix (**Figure 2A5**). The innervated perifornical area was largest on sections corresponding to the level 28 of the Brain Maps. Within this region, axons displayed the typical complex aspect with many buttons suggesting that they make many synaptic contacts. We also noted clear pericellular nets around neuronal soma.

In contrary to the perifornical region in which the intensity of the innervation decrease with more caudal tuberal levels, far lateral hypothalamic regions received a more intense innervation by PHAL axons with more caudal hypothalamic levels. Far lateral regions of the LHA contain the ventral and dorsal pathways taken by axons from the CEAm that were described in a previous study (22). At rostral levels (levels 26–28), axons provide a sparse innervation of the ventrolateral and dorsolateral LHA. From levels 29/30, the dorsolateral LHA receives a clear innervation as the morphology of PHAL axons change, displaying a complex organization and many buttons. At the level 30, this innervation is intense in an area adjacent to the subthalamic nucleus (STN) (**Figures 2A6–A8**).

Experiment PHAL#1: Although restricted to the cytoarchitectonic borders of the CEAm, the injection site in this experiment was confined to the rostral part of the subnucleus, caudal most perikarya being observed in sections corresponding to the level 26 (**Figure 1**). Compared to the experiment AMY1, axons essentially run through the ventral pathway (**Figures 2, 3A**). The innervation of the anterior perifornical region was weaker than that in the preceding experiment and seemed slightly more dorsal (**Figures 2B3, B4, 3E**). In the caudal LHA, the far lateral area adjacent to the STN was intensely innervated as in experiment AMY1 (**Figures 2B6, B7**), but again the PSTN appeared as the main target of the projections from this experiment (**Figure 4A**).

Experiment PHAL#2: The pattern of projections from this injection site centered into the CEAi was very different to that from experiment PHAL#1. Projections coursed through the dorsal and ventral pathways and entered the posterior PVH through its periforniceal part (**Figure 2C2**). Immediately caudal to this level, an innervation of dorsal perifornical regions was apparent, similar to the experiment AMY1 (**Figures 2C3, C4**). At inter-level 27–28, the area innervated by these axons clearly involved lateral perifornical regions in addition to dorsal region. Axons formed clear pericellular nets on scattered neurons of this region (**Figures 3C,F**). At level 29, the perifornical region is less innervated, but axons took a medial direction and a light innervation of the dorsomedial hypothalamic nucleus (DMH) was evident (**Figure 2C6**). At the levels 30–31, far lateral regions that were intensely innervated in experiment AMY1 and in experiment PHAL#1, were only slightly innervated by axons in experiment PHAL#2 (**Figures 2C7, C8**). The PSTN was also slightly labeled compared to that in experiments PHAL#1 or AMY1 (**Figure 4D**).

Experiment PHAL#3: Projections from this experiment are little illustrated, but their distribution patterns were identical to that described for experiment AMY1, although they were less abundant and thinner as the injection site was smaller (**Figures 3D,G**).

Co-distribution of PHAL With MCH, Hcrt, and FG

To better characterize the LHA regions innervated in each experiment, series of sections were co-labeled for MCH and Hcrt. Furthermore, in experiments PHAL#1 and PHAL#2, PHAL injections in the CEA were combined with FG injections in the PSTN (**Figure 4**). Therefore, in these two experiments, PHAL, MCH, and Hcrt immunolabeling were also compared with the distribution of FG retrogradely labeled neurons.

Experiment AMY1: Axons followed in the dorsal perifornical region a distribution that by in large corresponded to the distribution of Hcrt cell bodies from levels 28 to 30 (**Figure 5**). At the level 30, Hcrt perikarya occupy a more medial position compared to the fornix, and PHAL axons in this experiment followed the same pattern, explaining the decrease of innervation of the dorsal perifornical area described in the preceding paragraph. This pattern of distribution of Hcrt cell bodies, corresponded at least partly to the suprafornical part of the LHA described by Hahn (30). The PHAL labeling may be interpreted as an innervation of this part in this experiment. More laterally, axons provided an intense innervation of a triangular shaped region dorsally adjacent to the cerebral peduncle from the levels 30–31. This region corresponded to a condensation of MCH cell bodies and is named PST in the Swanson's Brain Maps (28), see as well Swanson et al. (7) and Hahn (30). However, a dense MCH condensation around the fornix at the same levels was not innervated as well as the MCH rich region in the ZI and sub-incertal territories. At high magnifications, we could see that many MCH or Hcrt cell bodies in the LHAd, s, as well as in the PST, could receive an "en passant" innervation (**Figures 5D–E**). Pericellular nets provided by axons in the perifornical regions were never observed around MCH or Hcrt neurons.

Experiment PHAL#1: Projections in this experiment were dorsal in the rostral tuberal LHA and involved an MCH rich zone immediately ventral to the ZI (**Figures 6A,B**). This zone corresponds to parts of the dorsal region of the LHA in Swanson's Brain Maps. In this experiment, FG was injected in the PSTN. FG retrogradely labeled cells were mostly observed in a ventrolateral corner of the LHA and lateral to the fornix. We observed very few

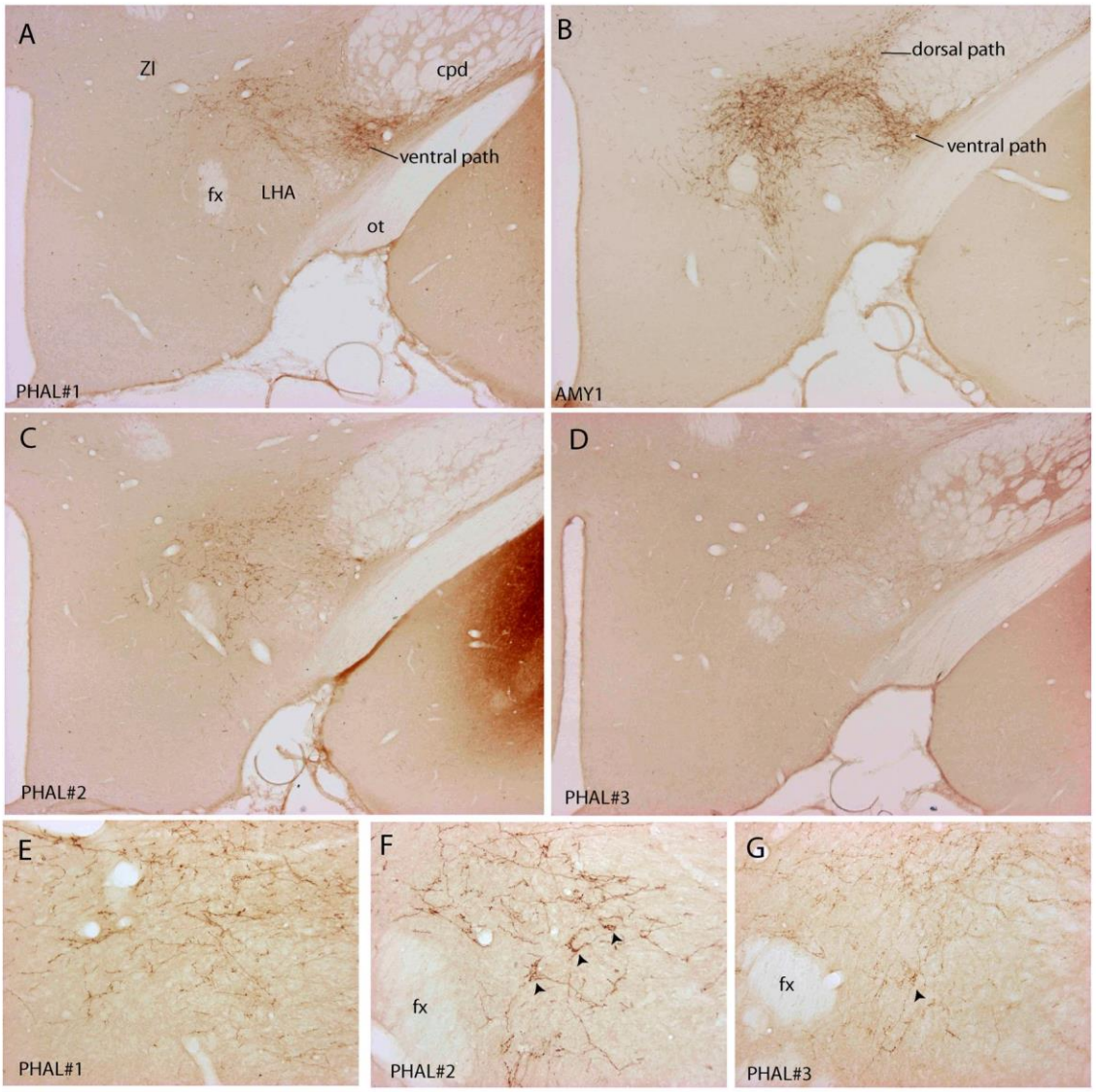

FIGURE 3 | Photomicrographs illustrating the distribution of PHAL axons in the rostral tuberal LHA of the four experiments PHAL#1, AMY1, PHAL#2, and PHAL#4. **(A–D)** Low magnification pictures. Note in A (PHAL#1) that only the ventral pathway is labeled, but axons innervate dorsal LHA regions. By comparison, the dorsal and ventral pathways are clear in the experiment AMY1. Injections in experiments PHAL#2 and #3 resulted in smaller sites and the number of axons is lower than in the two other cases. In the latter **(D)** axons are also thinner and more difficult to see at this magnification. **(E–G)** Higher magnification pictures to illustrate aspects of axons in the experiments PHAL#1, #2, and #3. Note the clear pericellular nets (arrowheads) in the lateral perifornical region of experiment PHAL#2, and even one in PHAL#3. Such figures could not be seen in the experiment PHAL#1. In this last experiment, axons displayed less collaterals and buttons. Therefore, even if the axons were very well labeled, this was interpreted as a weaker innervation of the LHA that than in the other experiments.

double labeled FG/MCH or FG/Hcrt perikarya. If axons of the ventral pathway could innervate "en passant" ventrolateral FG cells, little correspondence with FG containing neurons lateral to the fornix could be observed.

Experiment PHAL#2: The FG distribution was identical in this experiment to that in the case PHAL#1. PHAL innervation of the suprafornical part was observed, extending into the DMH. Obviously, PHAL axons were more abundant lateral to the fornix where FG retrogradely labeled neurons were observed (**Figures 6C, D**). Many FG cells appeared targeted by PHAL axons and, in a few instances, we also observed that pericellular nets by PHAL axons surrounded FG retrogradely labeled cell bodies (**Figure 6C**). Again, in this experiment, a total of <10 FG cells contained MCH or Hcrt.

DISCUSSION

The present work illustrates the complex patterns of innervation of the LHA by the CEA. PHAL injections in the rat CEAm

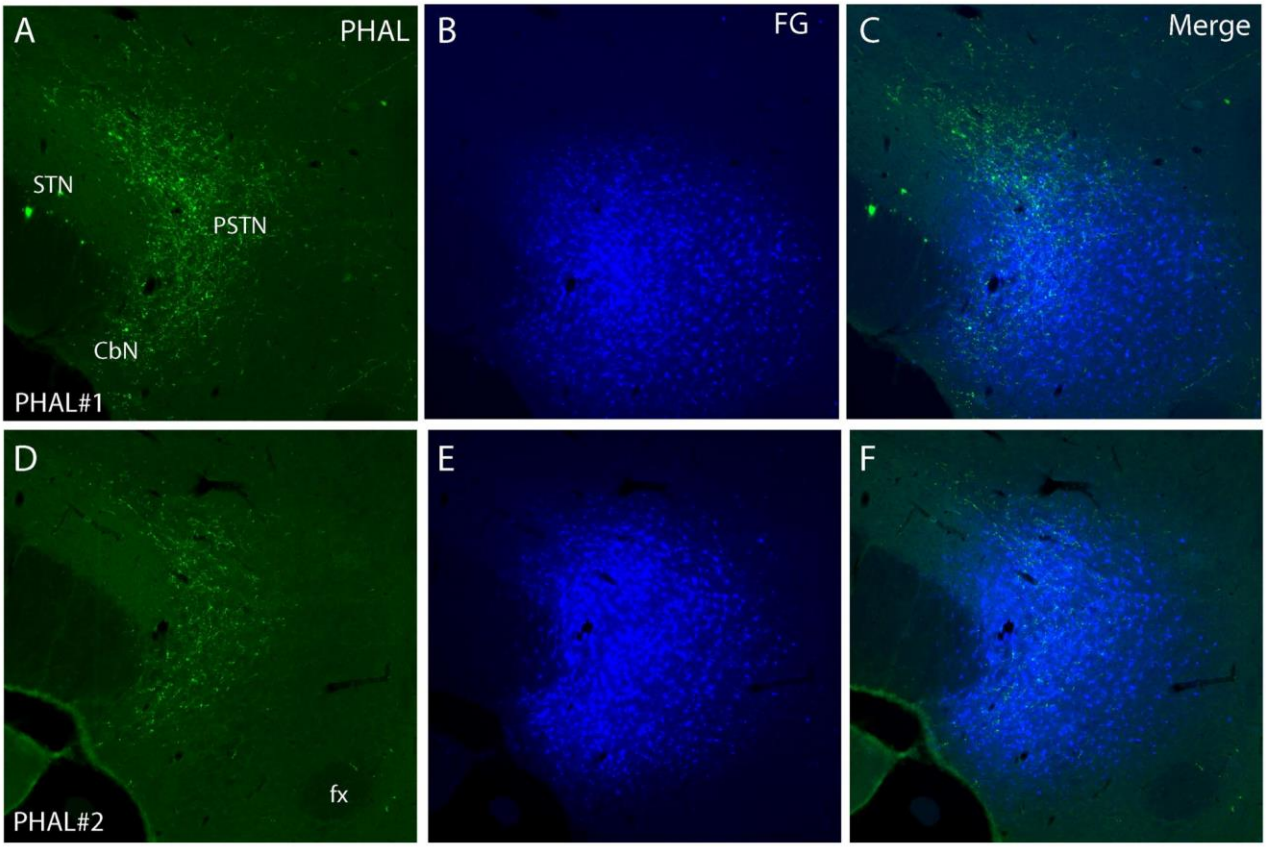

FIGURE 4 | Photomicrographs of PHAL **(A, D)** and FG **(B, E)** dual labeling in fluorescence in experiments PHAL#1 and PHAL#2. Note the innervation of the PSTN region, adjacent to the STN, by PHAL axons. The innervation in experiment PHAL#1 is however more intense than in experiment PHAL#2. A FG injection was aimed at the PSTN in both experiments that slightly involved adjacent STN and LHA areas (**C, F** Merge images from **A, B** and **D, E** respectively).

and CEAi provided a distinct pattern of innervation of the tuberal region of the LHA. Several comments can be drawn from this observation and will be discussed in the following paragraphs.

Convergence of Projections Into the Caudal Lateral LHA

The caudal lateral LHA, in which we include the PST and the PSTN, receives projections from every PHAL sites in the CEAm and CEAi. These projections are especially intense from the CEAm. This observation confirms results presented in a previous article in which we already mentioned that the PSTN is the main hypothalamic target for the CEAm projections (22). However, the PSTN is part of the premammillary hypothalamus and is devoid of MCH and Hcrt neurons (7, 21, 30). It is also very poor in GABAergic neurons (21). The region just rostral to this nucleus, named PST by Swanson, receives an intense CEAm input as well. This part is rich in MCH cell bodies and therefore GAD containing cells. It is associated to the tuberal LHA that is rich in such MCH and GAD neurons, even if MCH cells may not systematically use GABA as a neurotransmitter (31). Projections into the PST are however less intense than those observed in the PSTN. Finally, the CEAi appears to innervate only moderately both cell groups compared to the CEAm.

Divergence of Projections From the CEAm and CEAi Into the LHAd and LHAs

Rostral parts of the LHA received projections from the CEA, but these projections showed different patterns depending on their origin. They essentially concerned areas named LHAd and LHAs by Swanson (28). The LHAs is a bit easier to distinguish as it contains many Hcrt perikarya, few MCH cell bodies and lies dorsal to the fornix at levels 28/29 and then extends dorso-medially to this tract at the level 30. The LHAd corresponds to a larger and latero-dorsal LHA region. Our results suggest that this last region is not homogeneous. FG injections into the PSTN labeled cells in the lateral perifornical region in a rostral tuberal hypothalamus attached to the LHAd in Swanson (28). This region contains few MCH or Hcrt cell bodies and it is obviously innervated by the caudal CEAm and CEAi but not by the rostral CEAm. It is therefore very likely that future chemoarchitectonic and hodologic studies will further subdivide the LHAd.

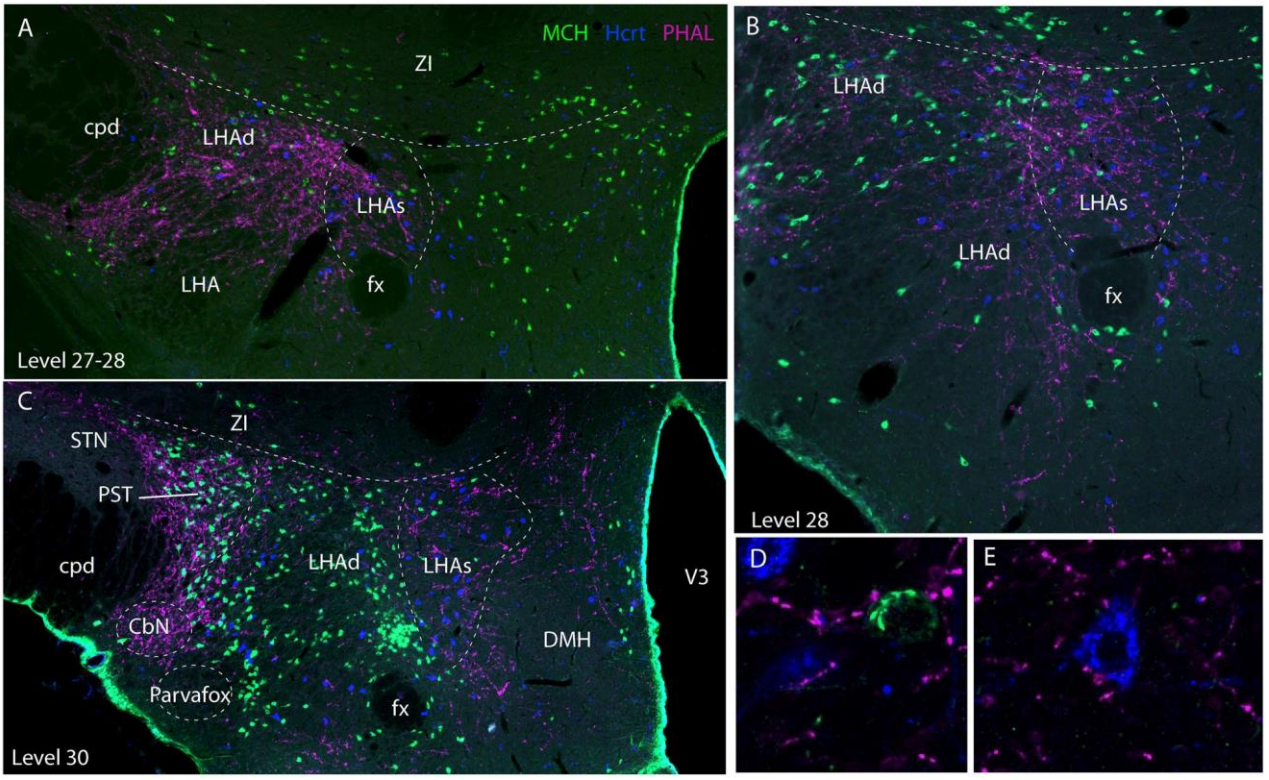

FIGURE 5 | Photomicrographs illustrating the co-distribution of PHAL axons, MCH and Hcrt cell bodies using a triple immunofluorescence procedure. **(A–C)** are low magnification pictures on sections at levels 27 (in fact better seen as inter-level 27/28), 28 and 30. Note the innervation of regions containing MCH and Hcrt cell bodies and corresponding to the dorsal and suprafornical regions of the LHA. However, the ZI, or the caudal perifornical regions (level 30) that are rich in MCH cell bodies but poor in Hcrt neurons are not innervated. By contrast at level 30, the PST that contains a dense group of MCH neurons is intensely innervated. **(D,E)** Higher magnification illustrations showing that buttons by PHAL axons could be seen close to MCH and Hcrt cell bodies. However, it seemed to be mostly *en passant* putative contacts.

Injection in the anterior CEAm (experiment PHAL#1) labeled fewer projections in the LHAd than other experiments and did not innervated the LHAs. Projections from this injection site labeled mainly axons passing through the ventral pathway described by Barbier et al. (22). This pattern is reminiscent of the projections from the CEAm in the study of Gonzales and Chesselet (32) and Bourgeais et al. (33) in which it was shown that such projections traveled in the ventrolateral LHA and provided light LHA innervation. We confirm here that a rostral PHAL injection site in the CEAm is at the origin of such a light pattern of inputs into the anterior tuberal LHA, and this input innervate mostly dorsal aspects of the LHAd. Therefore, as illustrated in the **Figure 7**, the rostral CEAm innervate lightly the LHAd, does not innervate the LHAs, but sends a heavy input into the PST and PSTN.

Injection sites in experiments AMY1 and PHAL#3 involved more caudal CEAm regions (AMY1 involve both rostral and caudal CEAm). In these two experiments, dorsal and ventral pathways were observed, as described in Barbier et al. (22). Projections, not seen in experiment PHAL#1, extended into the LHAs. Therefore, the caudal CEAm appears to send a heavier input into the rostral LHA than the rostral region of this subnucleus, and this input involved LHAd and LHAs.

The pattern of projections in the LHAd and s in experiment PHAL#2 was reminiscent to that in experiment AMY1 and PHAL#3. We also showed that axons in a region immediately lateral to the fornix and belonging to the LHAd, contained FG retrogradely labeled cells after FG PSTN injection. PHAL axons in experiment PHAL#2 clearly innervated some of these cells, while in a comparable FG injection in experiment PHAL#1, lateral perifornical cells were observed but PHAL axons were not observed close to them. The innervation of such cells in experiment PHAL#2 is interesting as it suggests that the CEAi may indirectly influence the PSTN through an intra-LHA circuit, which can be correlated to the observation of a lighter direct innervation of the PSTN by PHAL axons (**Figure 7**).

These patterns of projections are supported by literature data. In a recent study about the characterization of the perifornical projections from the CEA (27), we noted that retrograde tracer injections into the caudal lateral hypothalamus labeled many more neurons in the CEAm than in the CEAi, while rostral perifornical injections labeled a dense cluster in the CEAi. The study of Han and Swanson (34) is also interesting as these authors

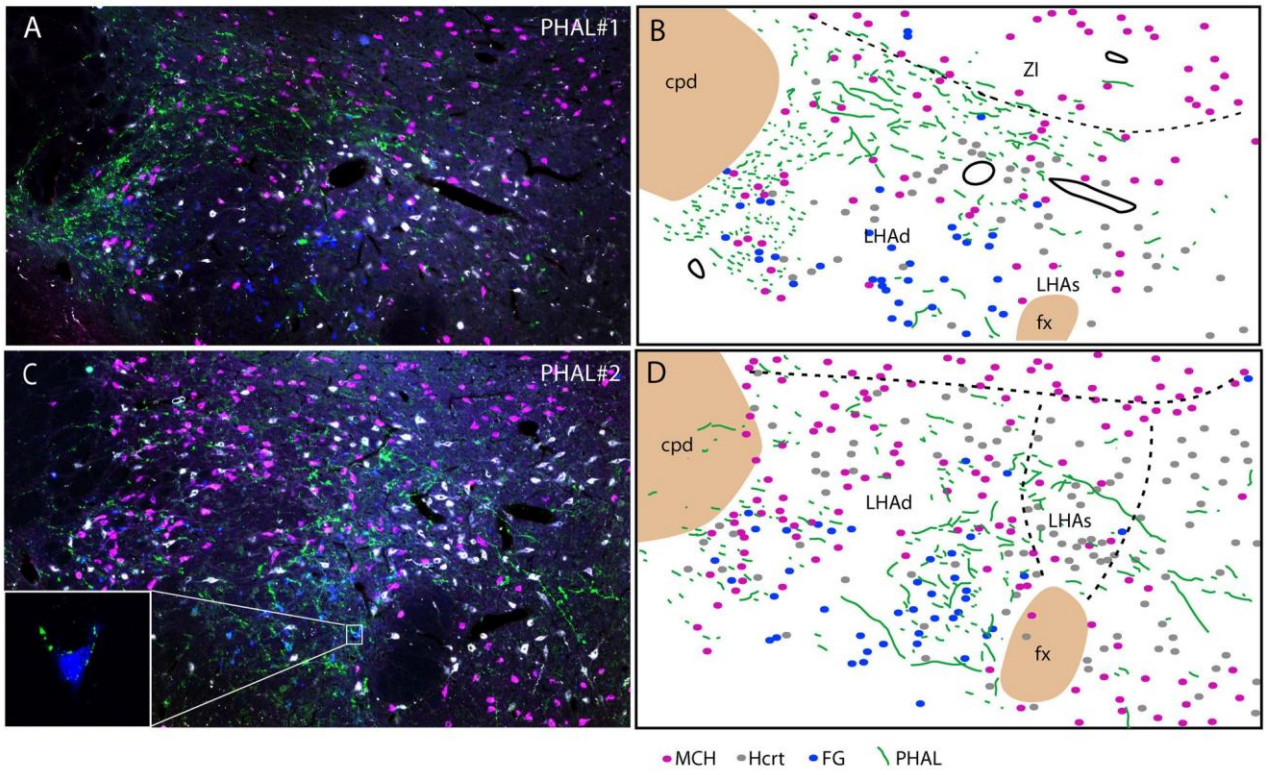

FIGURE 6 | Photomicrographs after quadruple labeling experiments with the detection using immunofluorescence of PHAL, MCH, and Hcrt, the fourth signal being the native fluorescence of the FG. Because it is difficult to separate signals from each other on the picture, we added line drawings that schematize the distribution of these signals. Sections are from experiments PHAL#1 **(A,B)** or PHAL#2 **(C,D)** respectively, and pass approximately through the level 28. Note that the PHAL distribution is distinct in these two cases, with an innervation restricted to the LHAd in experiment PHAL#1, while the LHAs is innervated in the experiment PHAL#2. Furthermore in this experiment, innervation of FG retrogradely labeled neurons from the PSTN are observed. In fact in a few occasion we could see PHAL axons forming pericellular nets around FG-containing cell bodies lateral to the fornix [framed picture in **(C)**, optical slice taken using the Apotome feature of the microscope]. FG labeled neurons were observed lateral to the fornix, in an area that belong to the LHAd, and in the far ventrolateral LHA. However, we cannot rule out the possibility that the labeling of these far latero-ventral neurons could not be the result of an uptake of the FG through dendrites extending into the injection site. In the two experiments, as in the experiment AMY1, only passing axons seemed to contact MCH or Hcrt cell bodies.

injected retrograde and anterograde tracers into the LHAs. They illustrated that the rostral CEAm contained no retrogradely labeled cells, while the rostral CEAl [corresponding to the CEAi, see (27)], and adjacent caudal CEAm contained such retogradely labeled cells. The paper of Reppucci and Petrovich (35) also noted intense labeling in the rostral CEAl after retrograde tracer injections into the perifornical region.

Functional Considerations

The experimental evidence exposed in this work point to a complex pattern of projection from the CEAm,i into the LHA, and the question of the functional meaning of this observation therefore arises, even if it is very difficult to provide a satisfactory answer at this stage.

The PSTN receives a convergent input from all parts of the CEAm and the CEAi. This nucleus is suspected to play a role in the feeding response. The expression of c-Fos increases in this nucleus when the animal ingests palatable food (21), and other studies suggest it might be part of a satiety circuit (36).

The LHAs has also been little investigated by itself, but its projections were well described in the work of Han and Swanson (34). Several features are reminiscent of those from the CEAm,i. In particular projections into the caudal PVH are similar. This region is also connected to the parastrial nucleus and to the DMH which are also targeted by the CEAm and/or CEAi [see (27)]. Interestingly, this region does not project into the PSTN, and our retrograde injections also failed to label perikarya in this part of the LHA. Han and Swanson extensively discussed the connections of this zone and pointed its association with ingestive behavior (30, 34). As a perifornical structure, there is also a considerable amount of work associating this general region to ingestive behaviors (37–43). In particular, the LHAs contains many Hcrt neurons that seemed targeted by PHAL axons. Hcrt is involved in reward-related food intake and flavor/taste learning through a network that involves the accumbens, the ventral pallidum, the VTA and the amygdala including the CEA (44–49). Our results are in range with these previous findings, but suggests that the caudal CEAm might more

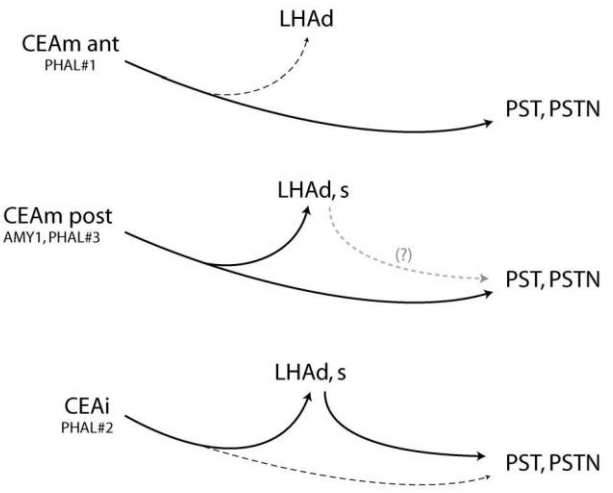

FIGURE 7 | Summary diagram and showing that the CEAm and CEAi send convergent projections into the posterior and lateral LHA but divergent projections into the LHAd, s. After CEAli injection, projections into the PSTN may require a relay into the perfornical LHA, suggesting an intra-LHA network under the control of the CEAi. It may also exist from the caudal CEAm but was not investigated in this study. (Dashed lines represent weak inputs).

directly intervene in the innervation of Hcrt cell bodies in the LHAs.

The LHAd contains a mix of loosely organized MCH and Hcrt cells, but the area lateral to the fornix contains fewer such cells. It is however quite intensely labeled by FG after injection in the PSTN. This area contains neurons expressing neurotensin (50, 51). Neurotensinergic cells are involved in the homeostatic control of food intake and express c-Fos after administration of leptin.

Therefore, the divergent innervation of the tuberal LHA by CEA axons reflects that they innervate cell populations controlling distinct aspects of the feeding response. This hypothesis is speculative, but coherent with the actual anatomical data.

Finally, the PST is filled with MCH cell bodies, and some of our previous works pointed that many spinally projecting MCH neurons are found in this region (8) and may influence autonomic output.

Nonetheless, the distribution of MCH and Hcrt cells being so stereotyped, they prove to be excellent tools to identify and characterize divisions in the LHA, as was stated by Swanson et al. (7) and Hahn (30). Further analysis of the co-distribution of specific afferences with that of these neurons appears to be a good way to better understand a certain parceling of the LHA which may help to understand its organization.

AUTHOR CONTRIBUTIONS

P-YR conceived and designed the experiments. MB and P-YR performed the experiments and illustration production. MB animal handling. MB, DF, and P-YR analyzed the data and wrote the text.

ACKNOWLEDGMENTS

This work was financed by the Region Franche-Comté, France.

REFERENCES

1. Saper CB, Chou TC, Elmquist JK. The need to feed: homeostatic and hedonic control of eating. *Neuron* (2002) 36:199–211. doi: 10.1016/S0896-6273(02)00969-8
2. Elmquist JK, Coppari R, Balthasar N, Ichinose M, Lowell BB. Identifying hypothalamic pathways controlling food intake, body weight, and glucose homeostasis. *J Comp Neurol.* (2005) 493:63–71. doi: 10.1002/cne.20786
3. Luppi P-H, Clément O, Fort P. Paradoxical (REM) sleep genesis by the brainstem is under hypothalamic control. *Curr Opin Neurobiol.* (2013) 23:786–92. doi: 10.1016/j.conb.2013.02.006
4. Verret L, Goutagny R, Fort P, Cagnon L, Salvert D, Léger L, et al. A role of melanin-concentrating hormone producing neurons in the central regulation of paradoxical sleep. *BMC Neurosci.* (2003) 4:19. doi: 10.1186/1471-2202-4-19
5. Carter ME, Adamantidis A, Ohtsu H, Deisseroth K, de Lecea L. Sleep homeostasis modulates hypocretin-mediated sleep-to-wake transitions. *J Neurosci.* (2009) 29:10939–49. doi: 10.1523/JNEUROSCI.1205-09.2009
6. González JA, Iordanidou P, Strom M, Adamantidis A, Burdakov D. Awake dynamics and brain-wide direct inputs of hypothalamic MCH and orexin networks. *Nat Commun.* (2016) 7:11395. doi: 10.1038/ncomms11395
7. Swanson LW, Sanchez-Watts G, Watts AG. Comparison of melanin-concentrating hormone and hypocretin/orexin mRNA expression patterns in a new parceling scheme of the lateral hypothalamic zone. *Neurosci Lett.* (2005) 387:80–4. doi: 10.1016/j.neulet.2005.06.066
8. Brischoux F, Fellmann D, Risold PY. Ontogenetic development of the diencephalic MCH neurons: a hypothalamic "MCH area" hypothesis. *Eur J Neurosci.* (2001) 13:1733–44. doi: 10.1046/j.0953-816x.2001.01552.x
9. Bouret SG. Development of hypothalamic circuits that control food intake and energy balance. In: Harris RBS, editor. *Appetite and Food Intake: Central Control*. Boca Raton, FL: CRC Press/Taylor & Francis (2017). p. 310.
10. Sohn JW. Network of hypothalamic neurons that control appetite. *BMB Rep.* (2015) 48:229–33. doi: 10.5483/BMBRep.2015.48.4.272
11. Krashes MJ, Koda S, Ye C, Rogan SC, Adams AC, Cusher DS, et al. Rapid, reversible activation of AgRP neurons drives feeding behavior in mice. *J Clin Invest.* (2011) 121:1424–8. doi: 10.1172/JCI46229
12. Hillebrand JJ, de Wied D, Adan RA. Neuropeptides, food intake and body weight regulation: a hypothalamic focus. *Peptides* (2002) 23:2283–306. doi: 10.1016/S0196-9781(02)00269-3
13. Lau J, Farzi A, Qi Y, Heilbronn R, Mietzsch M, Shi YC, et al. CART neurons in the arcuate nucleus and lateral hypothalamic area exert differential controls on energy homeostasis. *Mol Metab.* (2018) 7:102–18. doi: 10.1016/j.molmet.2017.10.015
14. Barsh GS, Schwartz MW. Genetic approaches to studying energy balance: perception and integration. *Nat Rev Genet.* (2002) 3:589–600. doi: 10.1038/nrg862
15. Broberger C, De Lecea L, Sutcliffe JG, Hökfelt T. Hypocretin/orexin- and melanin-concentrating hormone-expressing cells form distinct populations in the rodent lateral hypothalamus: relationship to the neuropeptide Y and agouti gene-related protein systems. *J Comp Neurol.* (1998) 402:460–74.
16. Qu D, Ludwig DS, Gammeltoft S, Piper M, Pelleymounter MA, Cullen MJ, et al. A role for melanin-concentrating hormone in the central regulation of feeding behaviour. *Nature* (1996) 380:243–7. doi: 10.1038/380243a0

17. Jennings JH, Rizzi G, Stamatakis AM, Ung RL, Stuber GD. The inhibitory circuit architecture of the lateral hypothalamus orchestrates feeding. *Science* (2013) 341:1517–21. doi: 10.1126/science.1241812
18. O'Connor EC, Kremer Y, Lefort S, Harada M, Pascoli V, Rohner C, et al. Accumbal D1R neurons projecting to lateral hypothalamus authorize feeding. *Neuron* (2015) 88:553–64. doi: 10.1016/j.neuron.2015.09.038
19. Stamatakis AM, Van Swieten M, Basiri ML, Blair GA, Kantak P, Stuber GD. Lateral hypothalamic area glutamatergic neurons and their projections to the lateral habenula regulate feeding and reward. *J Neurosci.* (2016) 36:302–11. doi: 10.1523/JNEUROSCI.1202-15.2016
20. Douglass AM, Kucukdereli H, Ponserre M, Markovic M, Gründemann J, Strobel C, et al. Central amygdala circuits modulate food consumption through a positive-valence mechanism. *Nat Neurosci.* (2017) 20:1384–94. doi: 10.1038/nn.4623
21. Chometton S, Pedron S, Peterschmitt Y, Van Waes V, Fellmann D, Risold PY. A premammillary lateral hypothalamic nuclear complex responds to hedonic but not aversive tastes in the male rat. *Brain Struct Funct.* (2016) 221:2183–208. doi: 10.1007/s00429-015-1038-3
22. Barbier M, Chometton S, Peterschmitt Y, Fellmann D, Risold P-Y. Parasubthalamic and calbindin nuclei in the posterior lateral hypothalamus are the major hypothalamic targets for projections from the central and anterior basomedial nuclei of the amygdala. *Brain Struct Funct.* (2017) 222:2961–91. doi: 10.1007/s00429-017-1379-1
23. Cai H, Haubensak W, Anthony TE, Anderson DJ. Central amygdala PKC-δ+ neurons mediate the influence of multiple anorexigenic signals. *Nat Neurosci.* (2014) 17:1240–8. doi: 10.1038/nn.3767
24. Carter ME, Soden ME, Zweifel LS, Palmiter RD. Genetic identification of a neural circuit that suppresses appetite. *Nature* (2013) 503:111–4. doi: 10.1038/nature12596
25. Carter ME, Han S, Palmiter RD. Parabrachial Calcitonin gene-related peptide neurons mediate conditioned taste aversion. *J Neurosci.* (2015) 35:4582–6. doi: 10.1523/JNEUROSCI.3729-14.2015
26. Petrovich GD, Setlow B, Holland PC, Gallagher M. Amygdalo-hypothalamic circuit allows learned cues to override satiety and promote eating. *J. Neurosci.* (2002) 22:8748–53. doi: 10.1523/JNEUROSCI.22-19-08748.2002
27. Barbier M, Fellmann D, Risold PY. Characterization of McDonald's intermediate part of the central nucleus of the amygdala in the rat. *J Comp Neurol.* (2018). doi: 10.1002/cne.24470. [Epub ahead of print].
28. Swanson LW. *Brain Maps: Structure of the Rat Brain*. 3rd ed. San Diego, CA: Elsevier (2004).
29. Paxinos G, Watson C. *The Rat Brain in Stereotaxic Coordinates*. 5th ed. Amsterdam ; Boston, MA: Elsevier Academic Press (2005).
30. Hahn JD. Comparison of melanin-concentrating hormone and hypocretin/orexin peptide expression patterns in a current parceling scheme of the lateral hypothalamic zone. *Neurosci Lett.* (2010) 468:12–7. doi: 10.1016/j.neulet.2009.10.047
31. Chee MJ, Arrigoni E, Maratos-Flier E. Melanin-concentrating hormone neurons release glutamate for feedforward inhibition of the lateral septum. *J Neurosci.* (2015) 35:3644–51. doi: 10.1523/JNEUROSCI.4187-14.2015
32. Gonzales C, Chesselet MF. Amygdalonigral pathway: an anterograde study in the rat with *Phaseolus vulgaris* leucoagglutinin (PHA-L). *J Comp Neurol.* (1990) 297:182–200. doi: 10.1002/cne.902970203
33. Bourgeais L, Gauriau C, Bernard JF. Projections from the nociceptive area of the central nucleus of the amygdala to the forebrain: a PHA-L study in the rat. *Eur J Neurosci.* (2001) 14:229–55. doi: 10.1046/j.0953-816x.2001.01640.x
34. Hahn JD, Swanson LW. Distinct patterns of neuronal inputs and outputs of the juxtaparaventricular and suprafornical regions of the lateral hypothalamic area in the male rat. *Brain Res Rev.* (2010) 64:14–103. doi: 10.1016/j.brainresrev.2010.02.002
35. Reppucci CJ, Petrovich GD. Organization of connections between the amygdala, medial prefrontal cortex, and lateral hypothalamus: a single and double retrograde tracing study in rats. *Brain Struct Funct.* (2016) 221:2937–62. doi: 10.1007/s00429-015-1081-0
36. Zséli G, Vida B, Martinez A, Lechan RM, Khan AM, Fekete C. Elucidation of the anatomy of a satiety network: focus on connectivity of the parabrachial nucleus in the adult rat: refeeding-activated contacts of the PB. *J Comp Neurol.* (2016) 524:2803–27. doi: 10.1002/cne.23992
37. Barbano MF, Wang HL, Morales M, Wise RA. Feeding and reward are differentially induced by activating GABAergic lateral hypothalamic projections to VTA. *J Neurosci.* (2016) 36:2975–85. doi: 10.1523/JNEUROSCI.3799-15.2016
38. Navarro M, Olney JJ, Burnham NW, Mazzone CM, Lowery-Gionta EG, Pleil KE, et al. Lateral hypothalamus GABAergic neurons modulate consummatory behaviors regardless of the caloric content or biological relevance of the consumed stimuli. *Neuropsychopharmacology* (2016) 41:1505–12. doi: 10.1038/npp.2015.304
39. Stanley BG, Magdalin W, Seirafi A, Thomas WJ, Leibowitz SF. The perifornical area: the major focus of (a) patchily distributed hypothalamic neuropeptide Y-sensitive feeding system(s). *Brain Res.* (1993) 604:304–17.
40. Stanley BG, Urstadt KR, Charles JR, Kee T. Glutamate and GABA in lateral hypothalamic mechanisms controlling food intake. *Physiol Behav.* (2011) 104:40–6. doi: 10.1016/j.physbeh.2011.04.046
41. Stuber GD, Wise RA. Lateral hypothalamic circuits for feeding and reward. *Nat Neurosci.* (2016) 19:198–205. doi: 10.1038/nn.4220
42. Wu Z, Kim ER, Sun H, Xu Y, Mangieri LR, Li DP, et al. GABAergic projections from lateral hypothalamus to paraventricular hypothalamic nucleus promote feeding. *J Neurosci.* (2015) 35:3312–8. doi: 10.1523/JNEUROSCI.3720-14.2015
43. Qualls-Creekmore E, Yu S, Francois M, Hoang J, Huesing C, Bruce-Keller A, et al. Galanin-expressing GABA neurons in the lateral hypothalamus modulate food reward and noncompulsive locomotion. *J Neurosci.* (2017) 37:6053–65. doi: 10.1523/JNEUROSCI.0155-17.2017
44. Risco S, Mediavilla C. Orexin A in the ventral tegmental area enhances saccharin-induced conditioned flavor preference: The role of D1 receptors in central nucleus of amygdala. *Behav Brain Res.* (2018) 348:192–200. doi: 10.1016/j.bbr.2018.04.010
45. Avolio E, Alò R, Mele M, Carelli A, Canonaco A, Bucarelli L, et al. Amygdalar excitatory/inhibitory circuits interacting with orexinergic neurons influence differentially feeding behaviors in hamsters. *Behav Brain Res.* (2012) 234:91–9. doi: 10.1016/j.bbr.2012.06.013
46. Castro DC, Terry RA, Berridge KC. Orexin in rostral hotspot of nucleus accumbens enhances sucrose "liking" and intake but scopolamine in caudal shell shifts "liking" toward "disgust" and "fear." *Neuropsychopharmacology* (2016) 41:2101–11. doi: 10.1038/npp.2016.10
47. Ho CY, Berridge KC. An orexin hotspot in ventral pallidum amplifies hedonic "liking" for sweetness. *Neuropsychopharmacology* (2013) 38:1655–64. doi: 10.1038/npp.2013.62
48. Haynes AC, Jackson B, Overend P, Buckingham RE, Wilson S, Tadayyon M, et al. Effects of single and chronic intracerebroventricular administration of the orexins on feeding in the rat. *Peptides* (1999) 20:1099–105.
49. Thorpe AJ, Kotz CM. Orexin A in the nucleus accumbens stimulates feeding and locomotor activity. *Brain Res.* (2005) 1050:156–62. doi: 10.1016/j.brainres.2005.05.045
50. Woodworth HL, Beekly BG, Batchelor HM, Bugescu R, Perez-Bonilla P, Schroeder LE, et al. Lateral hypothalamic neurotensin neurons orchestrate dual weight loss behaviors via distinct mechanisms. *Cell Rep.* (2017) 21:3116–28. doi: 10.1016/j.celrep.2017.11.068
51. Allen Institute. *Allen Mouse Brain Atlas*. Available online at: http://mouse.brain-map.org/ (Accessed May 2, 2018) (2004).

Conflict of Interest Statement: The authors declare that the research was conducted in the absence of any commercial or financial relationships that could be construed as a potential conflict of interest.

II. Etude anatomique et fonctionnelle du seau impliquant l'INS, le CEA et le complexe PSTN/CbN (Publication n°4)

Dans la ligne directrice du travail mené au laboratoire concernant l'étude des connexions du complexe PSTN/CbN et après analyse de l'injection de FG réalisée par Chometton *et al* en 2016 dans le PSTN chez le rat, des neurones ont été retrouvés dans la partie agranulaire dorsale (AId) et dans une partie du cortex gustatif (GU de L.W. Swanson). De plus, après injection de FG dans le CEA, les neurones FG rétrogradement marqués dans le complexe PSTN/CbN sont innervés par les axones CGRP provenant du PB. Ces projections CGRP dessinent les mêmes frontières que les projections descendantes depuis l'INS. Ce travail a donc pour objectif d'analyser l'organisation des connexions entre l'INS, le CEA et le PSTN. Le but est de comprendre si cette organisation peut s'interpréter dans le cadre plus global de l'organisation des liens anatomiques qui relient le télencéphale au tronc cérébral et qui ont été décrits dans l'introduction de ce mémoire. Des injections de traceur PHAL ont été réalisées dans l'INS afin d'analyser le trajet des fibres dans l'amygdale jusque dans le complexe PSTN/CbN. Nos données indiquent que les projections des différentes aires insulaires innervent de manière topographiquement organisée différentes parties du CEA, convergeant ensuite dans le complexe PSTN/CbN du LHApm. Un certain nombre d'observations amènent à proposer l'hypothèse d'une similitude dans l'organisation des circuiteries impliquant les "noyaux de la base" (striatum, pallidum et STN) et celles impliquant le CEA et le complexe PSTN/CbN.

En plus des aspects purement anatomiques, des investigations fonctionnelles ont été entamées afin d'identifier des rôles plus spécifiques associés au complexe PSTN/CbN. Les premières données concernant l'étude des connexions du complexe PSTN/CbN ont montré qu'il est associé à des structures liées au circuit de la gustation, de l'hédonisme et du contrôle de l'appétit (Chometton *et al*, 2016). En première exploration, afin de comprendre les fonctions de ce complexe, Chometton *et al* (2016) avaient réalisé des expériences susceptibles de modifier l'expression de la protéine c-Fos dans cette région à la suite d'expériences d'éveil, d'exploration, d'attention et d'ingestion de nourriture habituelle (nourriture standard de laboratoire) ou palatable (salami) (Chometton, 2015). Les résultats ont mis en évidence une forte expression de la protéine c-Fos dans le complexe PSTN/CbN chez le rat après ingestion d'un aliment à valence hédonique positive. L'ingestion d'une nourriture nouvelle conduit également à une activation de ce complexe supérieure à celle induite par la consommation répétée du même aliment (Chometton, 2015). Ce travail initial a donc été poursuivi par des expériences complémentaires afin de mieux comprendre la signification de l'expression de la protéine c-Fos dans ce complexe. Un protocole de consommation volontaire d'une solution d'alcool à 15% a été élaboré. En analysant nos premiers résultats "alcool", il a été observé une forte activation du complexe PSTN/CbN après une alcoolisation importante de nos animaux. Leur comportement laissant penser à un malaise, l'hypothèse selon laquelle le complexe PSTN/CbN pourrait être impliqué dans des

comportements de maladie a donc été testée. Des injections à des rats de lipopolysaccharide bactérien (LPS) mimant un malaise de type viscéral, ou de cisplatine entrainant un malaise de type nauséeux ont été réalisées. Le rôle du complexe PSTN/CbN a ensuite été testé dans le comportement d'ingestion d'une solution hédonique sucrée à 20% mais inconnue (néophobie). Un test de *"licking"* a été mis en place afin de mesurer le profil de consommation de la solution des animaux au cours du temps. A la fin de chaque expérimentation, les animaux ont été anesthésiés et perfusés. Pour les expériences "alcool" et "malaise" notamment, du sang a également été prélevé avant la perfusion de chaque rat en prévision de dosage de protéines ou substances diverses. Après dissection, congélation et coupe des cerveaux, des immunohistochimies ont été réalisées et la présence du marqueur d'activité neuronale c-Fos a été analysée.

Afin d'investiguer plus amplement le rôle de ce complexe, il était devenu nécessaire de travailler sur le modèle souris. Ce dernier permettant l'accès aux techniques plus contemporaines de traçage génétique et d'activation/inhibition de populations neuronales. A la fin de ma première année de thèse, des souris génétiquement modifiées tachyckininergiques exprimant l'enzyme recombinase Cre (souris TAC1-Cre) ont été importées (*The Jackson Laboratory*®). Le complexe PSTN/CbN exprimant majoritairement la substance P, il s'agissait du modèle le plus approprié à l'étude des fonctions de ce noyau. Ces souris ont été mises en reproduction au CSGA (Centre des Sciences du Goût et de l'Alimentation) à Dijon; notre animalerie n'étant, à cette époque, pas encore agréée à les détenir. De février à juin 2016, j'ai appris à injecter des virus traceurs PRV (PRV152 et PRV2001) à des souris TAC1-Cre avec l'aide du Dr Frédérique Datiche et du Dr Jean Gascuel à Dijon. Dans le même temps, des dossiers de demandes d'autorisations de détentions de modèles murins OGM Cre et d'adénovirus (AAV) dans nos locaux, ainsi que la soumission de notre projet au comité d'éthique ont été réalisés. Ce n'est qu'à la fin de ma deuxième année de thèse que l'autorisation de travailler avec ces AAV sur ces modèles souris a été délivrée. Après rapatriement de la lignée dans nos locaux, août 2017, la technique d'injection de virus AAV a commencé à être mise en place. Le but étant de permettre au laboratoire l'acquisition de la technique dite DREADD ("*Designer Receptor Exclusively Activated by Designer Drugs"*) qui est basée sur l'expression de récepteurs spécifiques à la surface des neurones Cre, activés par une drogue de synthèse, la clozapine-N-oxide (CNO). Dès le début de ma troisième année de thèse, des séries d'injections sur ces souris ont donc été réalisées, non sans difficultés. En effet, il était souhaitable d'obtenir de petites injections très localisées dans le complexe PSTN/CbN. Ce dernier étant de très petite taille, injecter un très faible volume (50 nL) semblait nécessaire afin d'éviter toute lésion et toute diffusion du virus aux structures voisines. Des injections de virus AAV activateurs et inhibiteurs ont donc été réalisées avec la méthode iontophorétique à l'aide de micropipettes en verre. Par cette méthode, peu de signal fluorescent traduisant la présence du virus n'avait été obtenu. Plusieurs tentatives ont été effectuées avec différents systèmes, notamment en pression à l'aide d'une micropompe et en augmentant le volume injecté (100 nL). Les résultats furent

très aléatoires et le pourcentage de réussite assez faible. Ce n'est qu'après observations et essais successifs que certaines défaillances de ce système d'injection en pression et de l'imprécision de la technique en général ont enfin pu être pointées. En effet, il a été remarqué que le virus n'était pas injecté à chaque fois et que même si le virus parvenait à atteindre sa cible, le volume injecté n'était absolument pas le volume théorique. La pression intracérébrale et le sang coagulant empêchaient bien souvent l'éjection du virus de la pipette en verre. En mai 2018, il a donc été fait l'acquisition d'un "nanofil" (à la place des micropipettes en verre), utilisé avec le système à micropompe pour l'injection des AAV (DREADD). Après injection du virus (AAV-hSyn-DIO-hM4D(Gi)-mCherry) dans une série de souris TAC1-Cre, suivie de l'injection intrapéritonéale de CNO qui se lie spécifiquement aux récepteurs inhibiteurs hM4D(Gi), différents tests comportementaux ont été effectués (décrits dans le manuscrit *"Supplemental data 1"* pages 158 et 159) afin de tester le rôle du complexe PSTN/CbN. Nos premiers résultats attestant de l'injection bilatérale de l'AAV dans le complexe PSTN/CbN ont été obtenus mai 2018. D'autres séries d'injections ont ensuite été réalisées afin de compléter nos données. Des injections iontophorétiques de virus AVV traçage couplées à des injections de traceurs classiques (Ctb, retrobeads, PHAL, FG) ont également été effectuées en parallèle chez des souris TAC1-Cre mais aussi NT-Cre et CRH-Cre, afin de poursuivre et compléter l'étude anatomique du réseau dans lequel est impliqué le complexe. Curieusement, la technique d'injection iontophorétique avec des pipettes en verre des AVV traçage donne de bons résultats. De la même façon qu'il avait été fait chez le rat, des co-marquages multiples et des analyses de la protéine c-Fos à la suite des différents tests comportementaux ont aussi été réalisés, mais tous ne sont pas rapportés ici.

The insular cortex-central amygdala-parasubthalamic nucleus network maps onto a basal ganglia like organization and mediates cognitive and interoceptive gating of feeding behavior

Marie Barbier, Sandrine Chometton, Arnaud Pautrat, Carole Miguet-Alfonsi, Yvan Peterschmitt, Frédérique Datiche, Jean Gascuel, Dominique Fellmann, Véronique Coizet, Pierre-Yves Risold

Abstract

Anterograde tract tracing from the insular cortex labels a pathway to the parasubthalamic nucleus in the caudal lateral hypothalamus that runs parallel to the canonical hyperdirect pathway from the isocortex to the subthalamic nucleus. Besides, an indirect pathway with a relay in the lateral central amygdala and then medial parts of the central amygdala or the caudal substantia innominata was also observed that is similar in its structure to the classical indirect pathway of the basal ganglia. Finally, physiological and behavioral experiments illustrated PSTN-dependent responses in gating feeding behavior homologous to the motor No Go response of the adjacent STN. The in-depth anatomical characterization of such modular networks connected by parallel pathways opens the way to formally identify a basic holistic plan in the hodological organization of the forebrain highly relevant for many homeostatic functions (motor, feeding behaviors...).

Developmental, neurochemical and cytoarchitectural evidence shows that the central nucleus of the amygdala (CEA) is mostly striatal in nature and therefore can be seen as a part of the basal ganglia *(1, 2)*. The classical basal ganglia network includes cortical afferents, direct/indirect pathways from the striatum and pallidum onto the substantia nigra (SN) and the subthalamic nucleus (STN) *(3, 4)*. This network is completed by an hyperdirect pathway from the cortex onto STN. The CEA projects into the SN but it has no ties with the STN *(5-10)* and classical basal ganglia pathways are not recognized for this nucleus. It is however bi-directionally connected with the parasubthalamic nucleus (PSTN) in the caudal lateral hypothalamic area *(11, 12)*, and both the CEA and PSTN are connected with the insular cortex (INS). In the present work, we took into consideration the anatomical vicinity of the PSTN with the STN to analyze the network connecting the INS, the CEA and the PSTN in the rodent. We observed that the structural organization of this network is strikingly reminiscent of the canonical hyperdirect and indirect pathways. We also illustrate functional PSTN-dependent electrophysiological and behavioral responses homologous to those of the adjacent STN.

In order to determine the anatomical organization of connections from the INS into the PSTN, anterograde (*Phaseolus vulgaris* Leucoagglutinin, PHAL) and retrograde (Fluorogold, FG) tract tracers were respectively injected in the former and latter structures of adult male rats (see fig. S1 for the methods and S2, S3 for the parceling of the PSTN and INS regions as well as injection sites in the INS). The retrograde labeling from the PSTN distributed throughout the antero-posterior INS with the agranular insular dorsal (AId) and posterior (AIp) areas being the most intensely labeled (Fig. 1A-C). PHAL injections targeted the whole INS and neighboring isocortical areas (Fig. 1E; fig. S3). The projections from the isocortex to the STN form the well described *basal ganglia* hyperdirect pathway (Fig. 1G). Likewise, INS, rather than targeting the STN, topographically innervated the adjacent PSTN/Calbindin Nucleus (CbN) and a region encompassing the CbN and the Parvafox nucleus (Fig. 1 E-L; fig. S4) featuring a non-canonical hyperdirect pathway.

To characterize the putative equivalent of an indirect pathway, description of the topographic organization of the projections from the cortex to the STN, PSTN/CbN has been completed with mapping of the corresponding cortico-striatal projections. Whereas the motor (MO) and somatosensory (SS) cortices innervated specific lateral and dorsal sectors of the STRd (CPU), INS targeted ventral components of the CPU, including the amygdalostriatal transition area (ASt). INS also innervated the ventral striatum (STRv) including the nucleus accumbens (ACB) and, from the AIv and AIp, the olfactory tubercle (Fig. 2A; fig. S5). From most INS injection sites, the innervation of the ASt extended into the CEA. This was evident for the gustatory (GU) and visceral (VISC) projections that innervated the capsular part of the CEA (Fig. 2B, C; fig. S5 and S6) and this input was exclusively provided by axons exiting the innervation field in the

ASt. From the anterior part of GU, axons also abundantly innervated the lateral domain of the CEAl. Finally, the CEAl as a whole was abundantly innervated by the caudal AId and the AIp.

The CEA is bidirectionally connected with the PSTN through its medial division while the CEAc and CEAl send sparse inputs to this nucleus *(12)* but innervate the substantia nigra *(5-10)*. To determine if CEAc and CEAl could indirectly target the PSTN, we combined PHAL injections into the lateral calcitonin-gene-related peptide (CGRP)-rich regions of the CEA with FG injections into the PSTN (Fig. 2D-F; fig. S7). The distribution of PHAL axons matched that of the FG cells in the CEAm. However, we observed that the caudal substantia innominata (SI) contained a denser innervation by PHAL axons as well as abundant FG labeled cells. Apotome-assisted optical slicing and 3D reconstructions identified many boutons in close contact with FG-containing cells, showing that lateral CEA divisions target cells in the CEAm and the caudal SI adjacent to the globus pallidus, that in turn innervate the PSTN (Fig. 2F, fig. S7).

Therefore, anatomy data point to topological homologies between the networks involving the STN or the PSTN. *In vivo* electrophysiological recordings in both nuclei were also performed demonstrating physiological similarities (fig. S8). In fact, PSTN neurons had a significant lower spontaneous firing, but both STN and PSTN exhibited the same pattern of activity and neurons in both structures also similarly responded to a peripheric noxious stimulus (footshock).

We further sought to functionally better characterize the PSTN. The only information to date is c-Fos responses related to palatable food ingestion and satiety *(11, 13-15)*. Owing to its intense CGRP inputs from the parabrachial neurons that also innervate the CEAc and CEAl, we hypothesized the PSTN could be involved in sickness induced anorexia, in line with its reactivity to peripheral aversive stimuli. As the CEA is involved in emotional processing and reinforcing/rewarding properties of palatable food and drugs, its deregulation is often associated with mood- and substance-use disorders *(16-22)*. Besides, INS and CEA are involved in neophobia-induced prevention of feeding *(23, 24)*. Therefore, we evaluated the influence of the PSTN/CbN in experiments (i) where feeding is prevented by neophobia, bacterial-endotoxin lipopolysaccharide (LPS)- or anti-cancer chemotherapy drug cisplatin, and (ii) after alcoholic intoxication.

Firstly, rats exposed to a novel sucrose (20% v/v) solution consumed less but displayed a greater number of c-Fos expressing neurons in the PSTN (but not in the CbN) than sucrose-habituated counterparts (Fig. 3A, B and fig. S9). Secondly, intraperitoneal injection of LPS (5mg/kg) or cisplatin (6mg/kg) also triggered increases of c-Fos responses in the PSTN and the CbN (Fig. 3C, D; fig. S10). Thirdly, rats were habituated to drink either an ethanol (15% v/v) solution or a bitter solution (0,3 mM quinine) instead of water (Fig. 3E-G; fig. S11). Ingestion of large quantities of the alcoholic solution, but not of large quantities of the quinine solution paralleled the increased c-Fos immunoreactivity in the PSTN and CbN. Additionally, the alcohol blood level directly correlated with c-Fos expression in the CbN (Fig. 3H). Whereas these data

support the involvement of the PSTN/CbN in response to alcoholic intoxication, the quinine experiment suggests that c-Fos expression is independent of ingested volumes (fig. S11).

Therefore, the PSTN/CbN is involved in the modulation of consummatory behavior depending on cognitive (novelty) and interoceptive (sickness or food intoxication) signals. To confirm and extend this observation we further manipulated the PSTN using pharmacogenetic tools in mice. The combination of results from a pilot study using viral tract tracing in mice with resources from the Allen Brain Institute data base *(25)* provided convincing evidence that the PSTN in mice shares many features of the rat PSTN, especially with respect to the connections with the INS and CEAm/SI (fig. S12). Ultimately, prominent substance P transcripts expression in the PSTN pointed toward the TAC1-Cre mouse line (expressing the Cre-recombinase under the control of the substance P gene promoter) as a relevant model to achieve this goal (fig. S12).

Designer receptors exclusively activated by designer drugs (DREADD) experiments were conducted with pAAV-4hSyn-DIO-hM4D(Gi)-mCherry recombinant viral vector bilaterally injected in the PSTN of TAC1-Cre mice (Fig. 3I-M). Remarkably, whereas clozapine-N-oxide (CNO)-induced inhibition of substance P-expressing PSTN neurons had no effect on spontaneous food intake, locomotion (open field test) or affective/coping behavior (forced swim test) (fig. S13), it did suppress the neophobic response reinstating consummatory behavior (Fig. 3Q).

In a last experiment, we tested whether feeding/drinking behavior could be reinstated in sick animals by manipulating the PSTN circuitry. To prevent neophobia confound, AAV-injected-Tac1-Cre mice were first habituated for one week to drink a sucrose (10% v/v) solution before being deprived for twenty-four hours. Mice then received ip injections of LPS (50 µg/kg) and CNO (1 mg/kg; 2 injections, 1h apart) solutions and placed 1h later in operant chambers equipped with lickometers (MedAssociates) to monitor sucrose (10% v/v) solution consumption. As expected, control mice refrained from drinking. In contrast, accurate chemogenetic inactivation of the PSTN relieved this inhibition and experimental mice performed a significantly higher number of licks than the control and mistargeted (AAV injections in the zona incerta, VTA or supramammillary nucleus) mice (fig. S13).

Overall, anatomical data point to a complex network connecting the INS, the CEA and the PSTN (Fig. 3N). We first described projections that are parallel to and topographically organized as the isocortex-to-STN hyperdirect pathway. We also identified INS-to-PSTN indirect pathways with relay through the CEA and the caudal SI. As a side note, the CEA has direct projections to the SN that may be associated to a direct pathway. Considering that the lateral CEA is made of medium spiny neurons that have a striatal molecular signature during development, and that the STN has a hypothalamic premammillary embryonic origin, it is again sound to state that the INS-CEA/SI-PSTN and the isocortex-CPU/GP-STN networks are related and similarly organized. Physiologically, PSTN and STN neurons behave alike and inhibition of the PSTN

suppresses the anorexic response associated to neophobia or sickness, indicating that the PSTN modulates ingestion of palatable food. Hence the PSTN gates a stop or warning "no-eat" signal for survival purposes in conflicting situations of potentially noxious (sickness-associated or previously unknown) source of food to refrain from or initiate feeding, by integrating interoceptive and cognitive signals. Somehow, the gating of CEA-triggered feeding exerted by the PSTN can be compared to the role of the adjacent STN in movement inhibition preventing information flow from the striatum (Fig. 3N) in a no-go pathway. Collectively, these results highlight the basal ganglia like hyperdirect and indirect organization of the projections from the insular cortex to the PSTN and emphasize the role of the PSTN which exerts cognitive and interoceptive gating of feeding behavior.

1. L. W. Swanson, G. D. Petrovich, What is the amygdala? *Trends Neurosci.* **21**, 323–331 (1998).

2. M. Bupesh, A. Abellán, L. Medina, Genetic and experimental evidence supports the continuum of the central extended amygdala and a mutiple embryonic origin of its principal neurons. *J. Comp. Neurol.* **519**, 3507–3531 (2011).

3. R. L. Albin, A. B. Young, J. B. Penney, The functional anatomy of basal ganglia disorders. *Trends Neurosci.* **12**, 366–375 (1989).

4. C. R. Gerfen, J. P. Bolam, in *Handbook of Behavioral Neuroscience*, H. Steiner, K. Y. Tseng, Eds. (Elsevier, 2016), vol. 24 of *Handbook of Basal Ganglia Structure and Function, Second Edition*, pp. 3–32.

5. C. Gonzales, M. F. Chesselet, Amygdalonigral pathway: an anterograde study in the rat with Phaseolus vulgaris leucoagglutinin (PHA-L). *J. Comp. Neurol.* **297**, 182–200 (1990).

6. D. M. Wallace, D. J. Magnuson, T. S. Gray, Organization of amygdaloid projections to brainstem dopaminergic, noradrenergic, and adrenergic cell groups in the rat. *Brain Res. Bull.* **28**, 447–454 (1992).

7. G. D. Petrovich, L. W. Swanson, Projections from the lateral part of the central amygdalar nucleus to the postulated fear conditioning circuit. *Brain Res.* **763**, 247–254 (1997).

8. H. J. Lee *et al.*, Role of Amygdalo-Nigral Circuitry in Conditioning of a Visual Stimulus Paired with Food. *J. Neurosci.* **25**, 3881–3888 (2005).

9. H. J. Lee, M. Gallagher, P. C. Holland, The central amygdala projection to the substantia nigra reflects prediction error information in appetitive conditioning. *Learn. Mem.* **17**, 531–538 (2010).

10. M. Shirasu *et al.*, Direct projections from the central amygdaloid nucleus to the mesencephalic trigeminal nucleus in rats. *Brain Res*. **1400**, 19–30 (2011).

11. S. Chometton *et al.*, A premammillary lateral hypothalamic nuclear complex responds to hedonic but not aversive tastes in the male rat. *Brain Struct Funct*. **221**, 2183–2208 (2016).

12. M. Barbier, S. Chometton, Y. Peterschmitt, D. Fellmann, P.-Y. Risold, Parasubthalamic and calbindin nuclei in the posterior lateral hypothalamus are the major hypothalamic targets for projections from the central and anterior basomedial nuclei of the amygdala. *Brain Struct Funct*. **222**, 2961–2991 (2017).

13. A. M. Douglass *et al.*, Central amygdala circuits modulate food consumption through a positive-valence mechanism. *Nat. Neurosci.* **20**, 1384–1394 (2017).

14. G. Zséli *et al.*, Elucidation of the anatomy of a satiety network: Focus on connectivity of the parabrachial nucleus in the adult rat. *J. Comp. Neurol.* **524**, 2803–2827 (2016).

15. G. Zséli *et al.*, Neuronal connections of the central amygdalar nucleus with refeeding-activated brain areas in rats. *Brain Struct Funct*. **223**, 391–414 (2018).

16. P. Namburi *et al.*, A circuit mechanism for differentiating positive and negative associations. *Nature*. **520**, 675–678 (2015).

17. G. de Guglielmo *et al.*, Recruitment of a Neuronal Ensemble in the Central Nucleus of the Amygdala Is Required for Alcohol Dependence. *J. Neurosci.* **36**, 9446–9453 (2016).

18. J. Kim, X. Zhang, S. Muralidhar, S. A. LeBlanc, S. Tonegawa, Basolateral to Central Amygdala Neural Circuits for Appetitive Behaviors. *Neuron*. **93**, 1464-1479.e5 (2017).

19. B. E. Schmeichel, M. A. Herman, M. Roberto, G. F. Koob, Hypocretin Neurotransmission Within the Central Amygdala Mediates Escalated Cocaine Self-administration and Stress-Induced Reinstatement in Rats. *Biol. Psychiatry*. **81**, 606–615 (2017).

20. S. M. Warlow, M. J. F. Robinson, K. C. Berridge, Optogenetic Central Amygdala Stimulation Intensifies and Narrows Motivation for Cocaine. *J. Neurosci.* **37**, 8330–8348 (2017).

21. J. A. Hardaway *et al.*, Central Amygdala Prepronociceptin-Expressing Neurons Mediate Palatable Food Consumption and Reward. *Neuron*. **102**, 1037-1052.e7 (2019).

22. B. Li, Central amygdala cells for learning and expressing aversive emotional memories. *Curr Opin Behav Sci*. **26**, 40–45 (2019).

23. J.-Y. Lin, J. Arthurs, S. Reilly, Gustatory insular cortex, aversive taste memory and taste neophobia. *Neurobiol Learn Mem*. **119**, 77–84 (2015).

24. A. Skórzewska *et al.*, GABAergic control of the activity of the central nucleus of the amygdala in low- and high-anxiety rats. *Neuropharmacology*. **99**, 566–576 (2015).

25. Allen Institute, Allen Mouse Brain Atlas (2004), (available at http://mouse.brain-map.org/).

26. V. Coizet, E. J. Dommett, P. Redgrave, P. G. Overton, Nociceptive responses of midbrain dopaminergic neurones are modulated by the superior colliculus in the rat. *Neuroscience*. **139**, 1479–1493 (2006).

27. V. Coizet, E. J. Dommett, E. M. Klop, P. Redgrave, P. G. Overton, The parabrachial nucleus is a critical link in the transmission of short latency nociceptive information to midbrain dopaminergic neurons. *Neuroscience*. **168**, 263–272 (2010).

28. E. Dommett *et al.*, How visual stimuli activate dopaminergic neurons at short latency. *Science*. **307**, 1476–1479 (2005).

29. V. Coizet *et al.*, Short-latency visual input to the subthalamic nucleus is provided by the midbrain superior colliculus. *J. Neurosci.* **29**, 5701–5709 (2009).

30. P. Y. Wang, F. C. Zhang, *Outline and atlas of learning rat brain slices* (1995).

31. L. W. Swanson, *Brain Maps: Structure of the Rat Brain* (Elsevier, San Diego, Third Edition., 2004).

32. G. Paxinos, C. Watson, *The Rat Brain in Stereotaxic Coordinates: Hard Cover Edition* (Academic Press, 2013).

33. L. Puelles, M. Martinez-de-la-Torre, S. Bardet, J. L. R. Rubenstein, in *The Mouse Nervous System* (Watson C., Paxinos G., Puelles L., London; San Diego, CA, :Academic Press/Elsevier., 2012), pp. 221–312.

34. A. Bilella, G. Alvarez-Bolado, M. R. Celio, The Foxb1-expressing neurons of the ventrolateral hypothalamic parvafox nucleus project to defensive circuits. *J. Comp. Neurol.* **524**, 2955–2981 (2016).

35. J. L. Price, B. M. Slotnick, M.-F. Revial, Olfactory projections to the hypothalamus. *J. Comp. Neurol.* **306**, 447–461 (1991).

36. M. Barbier, D. Fellmann, P.-Y. Risold, Characterization of McDonald's intermediate part of the Central nucleus of the amygdala in the rat. *J. Comp. Neurol.* **526**, 2165–2186 (2018).

37. A. Pautrat *et al.*, Revealing a novel nociceptive network that links the subthalamic nucleus to pain processing. *Elife*. **7** (2018), doi:10.7554/eLife.36607.

38. M. Goto, L. W. Swanson, Axonal projections from the parasubthalamic nucleus. *J. Comp. Neurol.* **469**, 581–607 (2004).

Legends of figures

Figure 1: The insular cortex to PSTN projections form a basal ganglia like hyperdirect pathway.

The PSTN/CbN is a nuclear complex characterized by dense CGRP projections lying adjacent to the STN labeled for parvalbumin as the Parvafox nucleus (A). The PSTN receives afferents from INS, mostly AId as evidenced by Fluorogold (FG) retrograde tracer labeling (B-D) and confirmed by PHAL anterograde tracer data with injection sites illustrated by line drawings in the cortex (E), and the topographic organization of the projections observed in the STN, PSTN/CbN and Parvafox regions (F). Whereas the isocortex innervates the STN as part of the basal ganglia hyperdirect pathway, most of the INS innervates the PSTN with the exception of the AIv that targets the CbN and Parvafox nucleus. Photomicrographs illustrating the innervation of the STN and PSTN/CbN after respectively PHAL injection in the motor cortex (G) or the AId (H). Darkfiled illumination after immunohistochemical detection of PHAL tracer (G, H). Photomicrograph after dual immunofluorescence for CGRP and PHAL (I). The tracer was injected in the AIv and the axons are observed in a region encompassing the CbN and Parvafox nucleus. PHAL results underline a similar topographic organization of projections from the isocortex into the STN and from the INS to PSTN/CbN, Parvafox regions. Scale bar = 1 mm in A, B and 500 µm in C to I.

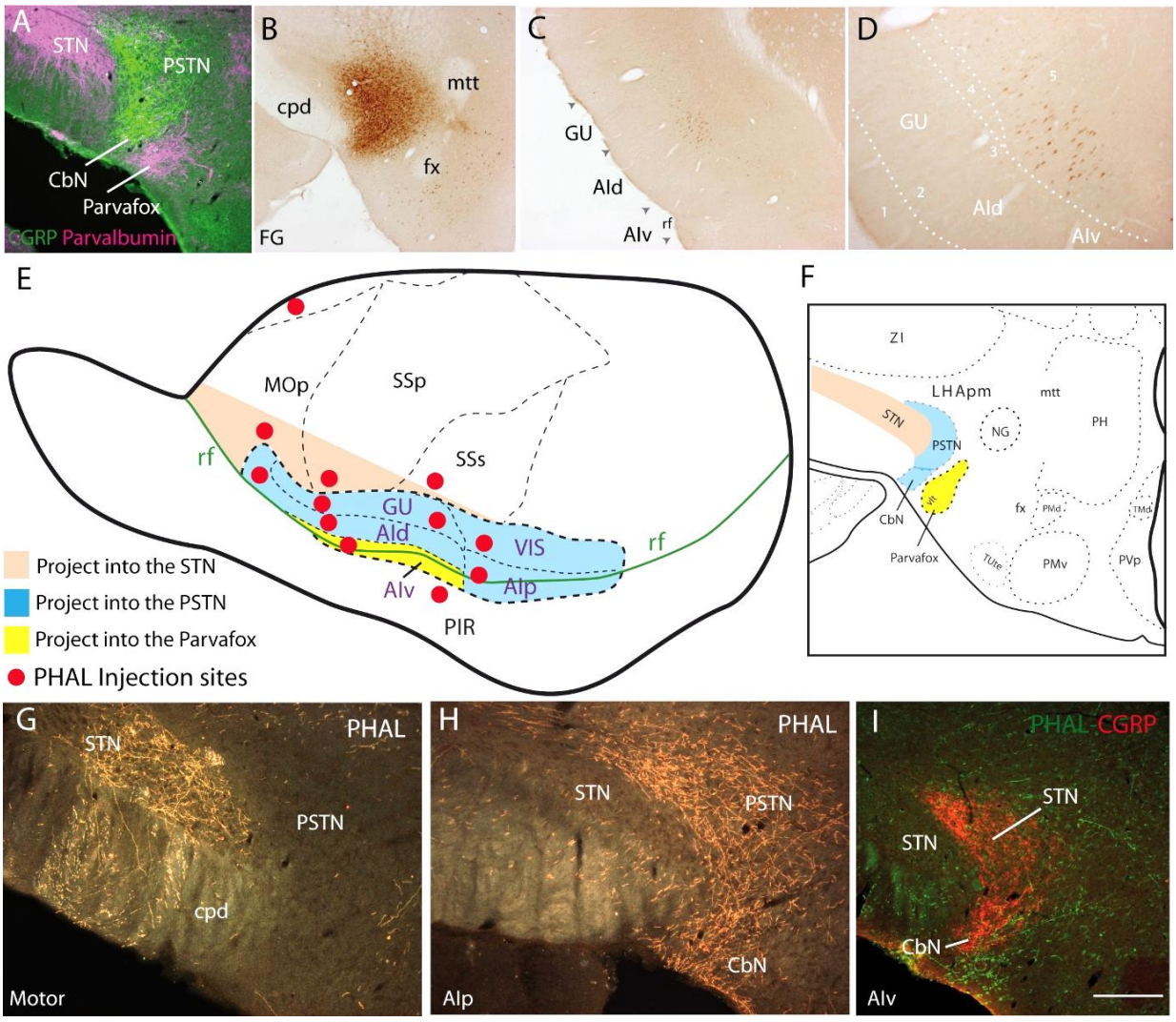

Figure 2: The insular cortex-ventral striatum/CeA-PSTN network maps onto a basal ganglia like indirect pathway organization.

(A) Line drawing illustrating the topographic organization of the projections from the cortex into the STR with the isorcortex innervating the STRd (CPU) while the INS as a whole, targets STRd and STRv including the ASt, ACB, FS, OT. From the ASt, the INS also innervates the CEAc and CEAl. (B, C) Dual immunofluorescence to detect PHAL and CGRP. After PHAL injection in the GU, intense labeling of the ASt is observed, but axons exit this region to further reach the CEAc that is characterized by dense CGRP positive PBN input. (D) Photomicrograph showing a PHAL injection site in the CGRP-rich CEAc. (E) Line drawing illustrating the pathway from the CEAc to the PSTN as evidenced after PHAL injection in the CEAc and FG injection in the PSTN. (E) Dual immunofluorescence photomicrograph of a section through the caudal SI. This region contains abundant FG labeled cells in close apposition with PHAL axons after injections of FG in the PSTN and PHAL in the CEAc. (F) Higher magnification (frame) clearly shows that most FG cells are contacted by PHAL axons. Scale bar = 250 µm in B to D and 500 µm in F.

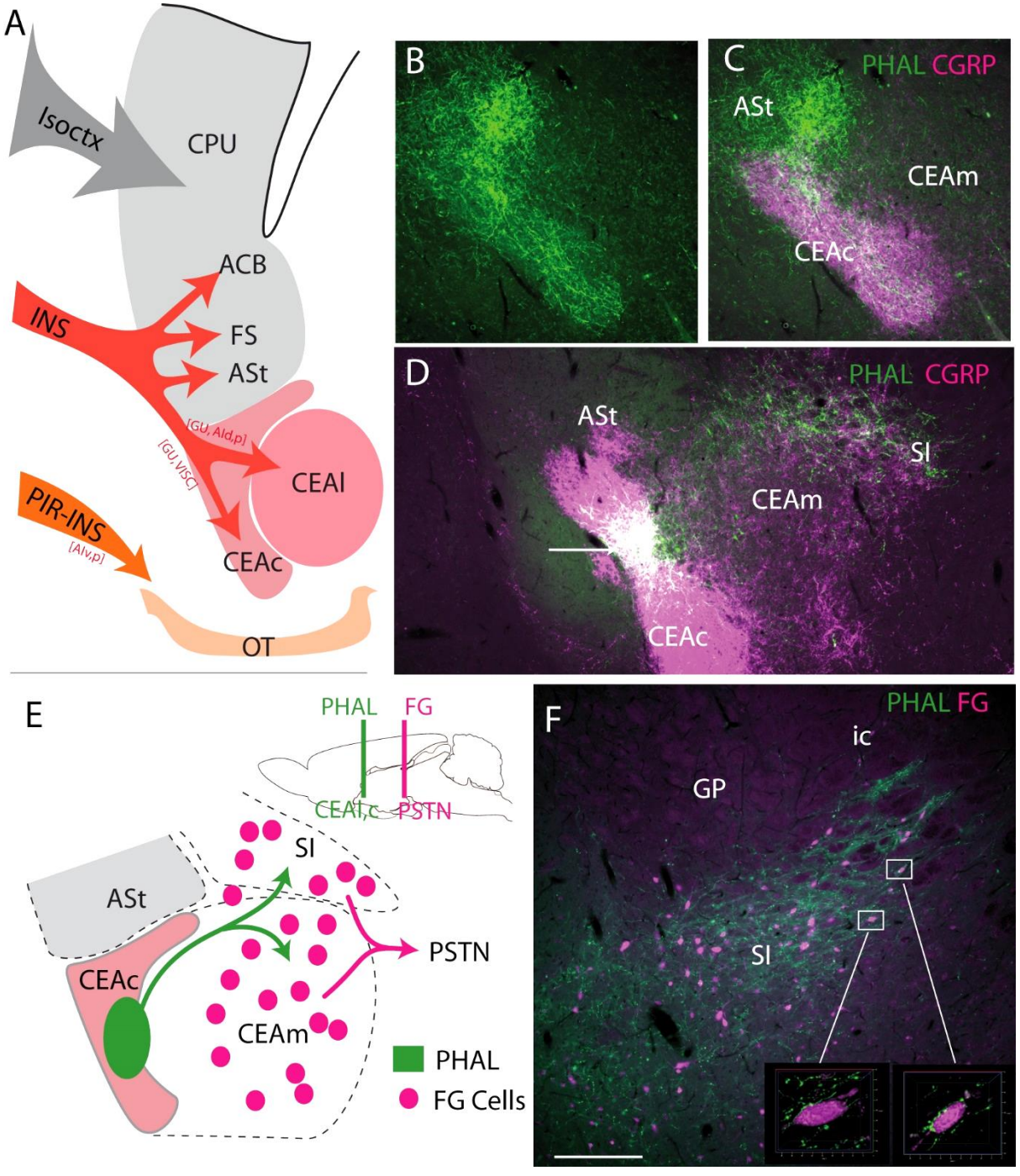

Figure 3: The activated PSTN refrains animals from consuming while sick or encountering novel drink whereas its inactivation relieves inhibitory control reinstating drinking behavior.

(A, B) Neophobic rats display higher number of c-Fos expressing nuclei in the PSTN as compared to habituated controls that already encountered the sucrose (20% v/v) solution (n = 5 rats; unpaired t-test p = 0.0181). The increase in number of c-Fos nuclei in the CbN was non-significant (n = 5 rats; unpaired t-test p = 0.3526). (C, D) LPS and cisplatin very significantly increase the number of c-Fos nuclei in the PSTN and CbN (n = 9 rats; One-way ANOVA and Bonferroni's post hoc multiple comparison test, for the PSTN, F = 13.91 and for the CbN, F = 29.67). (E-H) Additionally, from rats trained for weeks to develop alcohol binge drinking (procedure described in Sup data 1 and 11), those titrating the highest blood alcohol level (D20-group rats in E (n = 5 per group; One-way ANOVA and Bonferroni's multiple comparison test, F = 31.28) also show a very significant increase in the number of c-Fos labeled nuclei in the PSTN (F) and CbN (G) as compared to earlier timepoints (n = 5 rats per group; One-way ANOVA and Bonferroni's multiple comparison test, for the PSTN, F = 9.444; for the CbN, F = 8.939). Moreover, the c-Fos response in the CbN, correlates with the blood alcohol level (H, n = 20, correlation coefficient r = 0.568, p = 0.009). (I-M) Diagram showing pAAV-4hSyn-DIO-hM4D(Gi)-mCherry bilateral injection into the PSTN of TAC1-Cre mice. Scale bar = 250 µm. (N-P) Chemogenetic inhibition of PSTN (TAC1 neurons) suppresses neophobia (L) with mice initiating more consummatory behaviors (number of licks) toward the never encountered solution (10% sucrose) during the first period of the trial (minutes 1-5) compared to vehicle (VEH) mice (n = 5 mouse; Two-way ANOVA and Bonferroni's multiple comparison test, p = 0.026, F = 11.25). (M) Similarly, CNO inhibition of the PSTN reinstates consummatory behavior suppressed by LPS-induced sickness with CNO-accurate PSTN mice displaying more licks than VEH mice and CNO mice with misplaced (MP) AAV injections (ctrl n = 13; DREADD n = 10; DREADD MP n = 7; One-way ANOVA and Bonferroni's multiple comparison test, p = 0.0015, F = 8.377). (N) Diagram highlighting the homologies of hyperdirect and indirect pathways involving on the one hand the isocortex-CPU-STN network and on the other hand the INS-CEA-PSTN/CbN circuit with focus on cognitive and interoceptive inputs influencing the latter. *P < 0.05; **P < 0.001; ***P < 0.0001.

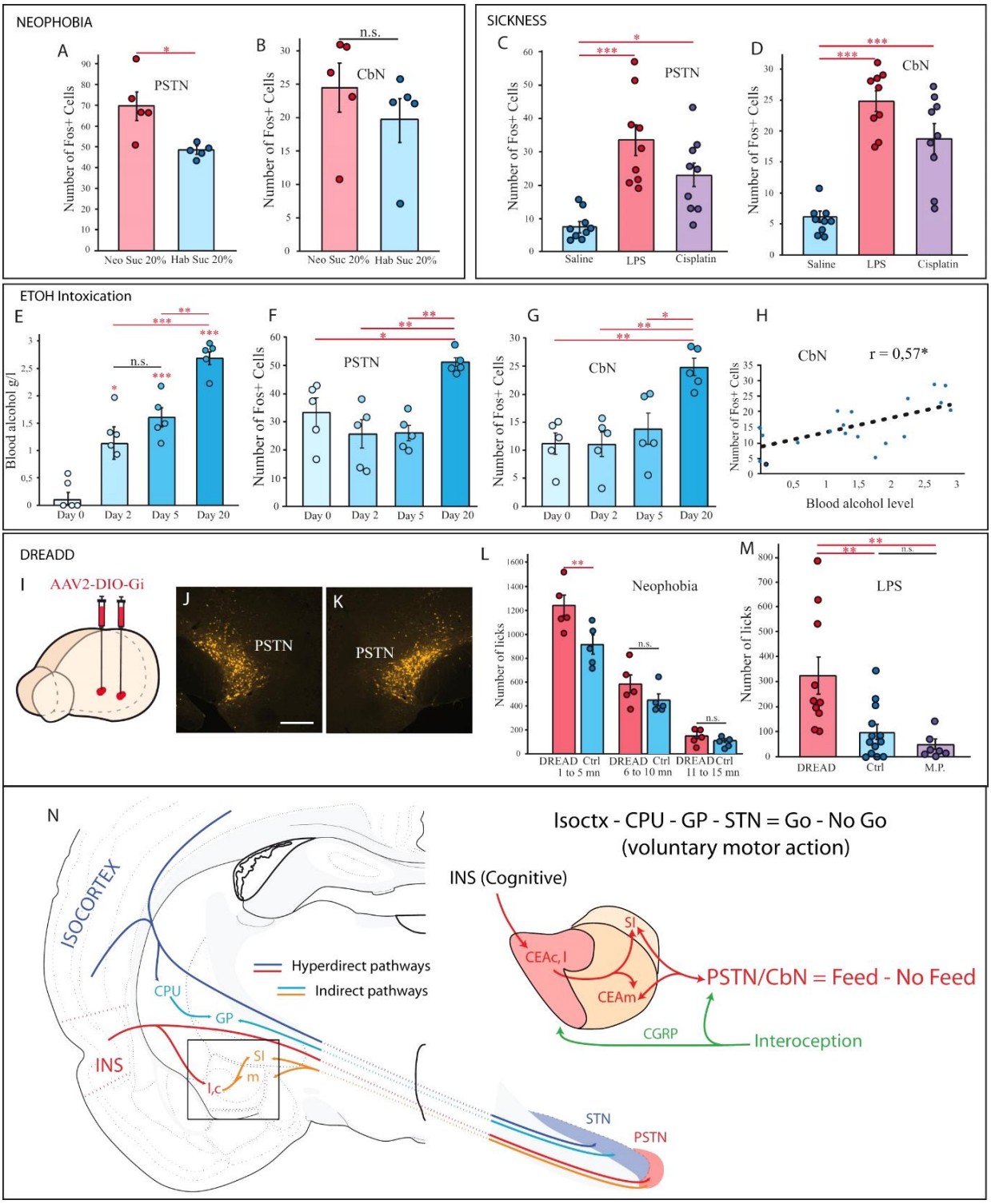
NEOPHOBIA
A
PSTN
Number of Fos+ Cells
Neo Suc 20%
Hab Suc 20%
B
CbN
n.s.
SICKNESS
C
PSTN
Saline
LPS
Cisplatin
D
CbN
ETOH Intoxication
E
Blood alcohol g/l
Day 0
Day 2
Day 5
Day 20
F
PSTN
G
CbN
H
CbN
r = 0,57*
Blood alcohol level
DREADD
I
AAV2-DIO-Gi
J
PSTN
K
PSTN
L
Neophobia
Number of licks
DREAD
Ctrl
1 to 5 mn
6 to 10 mn
11 to 15 mn
M
LPS
M.P.
N
ISOCORTEX
CPU
GP
INS
SI
m
l,c
Hyperdirect pathways
Indirect pathways
STN
PSTN
Isoctx - CPU - GP - STN = Go - No Go
(voluntary motor action)
INS (Cognitive)
CEAc, l
CEAm
PSTN/CbN = Feed - No Feed
CGRP
Interoception

Supplemental data 1: Material and methods.

EXPERIMENTAL MODEL

All experiments presented in this study were conducted according to the animal research guidelines from the Directive 2010/63/EU of the European Parliament, and of the Council of 22 September 2010, on the protection of animals used for scientific purposes. The protocols were approved by the Franche-Comté University's Animal Care Committee, and the investigators received authorization to conduct the study.

All rats and mice used in experiments were housed under a 12 hr light/dark cycle. The rats (Sprague Dawley unless otherwise specified) were obtained from Janvier (Le Genest-Saint-Isle, France) and Tac1-Cre (B6;129S-Tac1tm1.1(cre)Hze/J) mice were obtained from Jackson Laboratories. At the time of the experiments, mice were 15–20 weeks old and weighted approximately 25-28 g; Rats were 10–15 weeks old and weighted 300–320 g. All animals were used in scientific experiments for the first time. This includes no previous exposures to pharmacological substances or altered diets. Health status was normal for all animals.

METHOD DETAILS

Surgical procedures

Rats were anesthetized with an intraperitoneal (i.p.) injection of a mixture of xylazine and ketamine (1 mg/100 g and 10 mg/100 g of body weight, respectively; Vetoquinol®, France) and placed in a stereotaxic device. For mice, anesthesia was induced with 2% isoflurane and maintained under constant flow of ~1% isoflurane anesthesia (1.5 l min−1) and each mouse was placed on a stereotaxic apparatus. For each animal, a postoperative analgesia was maintained with 5 mg/Kg Carprofen (s.c.) twice per day for consecutive 3 days or paracetamol (1 g/l) in the drinking water for one week.

Tracer injections

Retrograde tracer
Rats received a unilateral iontophoretic injection of 10% solution of fluorogold (FG) (Interchim®) diluted in 0.9% sodium chloride (NaCl) into the PSTN. Coordinates were taken from Bregma using the Swanson atlas (2004). For the PSTN, the coordinates are AP: −4.0 mm, ML: 1.5 mm, DV: −8.4 mm. A glass micropipette (tip diameter: 30–50 µm) was used to inject the FG iontophoretically into this region (intermittent current of 5 mA and 7 s on/off time for 5 min). To avoid FG diffusion along the track, the micropipette was left in place for another 5 min before being removed.

Anterograde tracer
Rats received a unilateral iontophoretic injection of 2.5% *Phaseolus vulgaris* leucoagglutinin (PHAL) (Vector®) diluted in sodium phosphate buffer saline (NaPBS) pH 7.2. Glass micropipettes were used to inject the PHAL iontophoretically into the insular cortex and into the CEA (for coordinates see below) using an intermittent current (5 mA; 7 s on/off time for 20 min). All injections in the CEA were done with a retrograde FG injection in the PSTN. For the MO1, the coordinates were AP: 3.2 mm, ML: 2.0 mm, and DV: −4.0 mm, with an angle of 30°; for the AId, the coordinates were AP: 3.2 mm, ML: 1.5 mm, DV: -5.6 mm, with an angle of 25°; and AP: 2.8 mm, ML: 2.0 mm, DV: -5.6 mm, with an angle of 21°; for the ORB, the coordinates were AP: 3.2 mm, ML: 1.5 mm, DV: -5 mm, with an angle of 13°; for the AIv, the coordinates were AP: 2.8 mm, ML: 2.0 mm, DV: -5.7 mm, with an angle of 14°; for the SS1, the coordinates were AP: 0.95 mm, ML: 4.0 mm, DV: -4.8 mm, with an angle of 30°; for the GUant, the coordinates were AP: 0.95 mm, ML: 3.5 mm, DV: -6.2 mm, with an angle of 19°; for the AIdpost, the coordinates were AP: 0.95 mm, ML: 3.0 mm, DV: -7.2 mm, with an angle of 21°; for the GUpost, the coordinates were AP: 0.10 mm, ML: 3.5 mm, DV: -6.6 mm, with an angle of 23°; for the AIp, the coordinates were AP: 0.10 mm, ML: 3.5 mm, DV: -6.8 mm, with an angle of 16°; for the VISC, the coordinates were AP: -0.26 mm, ML: 4.0 mm, DV: -6.5 mm, with an angle of 21°**.** For the CEAc, the coordinates were AP: -1.78 mm, ML: 4.4 mm, and DV: -8.0 mm and for the CEAi, the coordinates were AP: -1.78 mm, ML: 3.8 mm, and DV: -8.2 mm. The

micropipette was left in place for another 5 min before being removed. At 10–15 days after the injection, the rat brain was removed, frozen, cut, and processed for immunohistochemistry, as described in the following.

Stereotaxic viral injections

For anatomical experiments

Retrograde virus: Viral injections of PRV152 and PRV2001 were done unilateral in the CEAm (with blue Fluorospheres carboxylates-modified (diameter 1 µm; F8814, Molecular Probes®) to see the injection site after sacrifice of mice) using a nanofil on modified microliter syringes (Hamilton) with a 33-needle gauge. The tip of the needle was placed at the target regions and the injections were performed at a rate of 0.1 µl min−1 (for coordinates and volumes see below). Once the injection was finished the needle was left in place for 5 min and then slowly removed. To allow time for viral migration, animals were housed for at least 1 day for the PRV152 (one synapse) and 7 days for the PRV2001 following injection before sacrifice. TAC1-cre mice were used for injections of cre-dependant PRV 2001 virus in the CEAm. The coordinates were taken from Bregma using the Paxinos and Watson atlas (2013). The coordinates used were AP = -1.2 mm, ML = 2.3 mm and DV = -4.7 mm and 300 nl of PRV virus was injected.

Anterograde virus: Iontophoretic viral injections of AAV1.CAG-FLEX-EGFP-WPRE and AAV1.CAG.LSL.tdTomato were done unilateral in the PSTN using glass micropipette and an intermittent current (4 mA; 7 s on/off time for 10 min). The micropipette was left in place for another 5 min before being removed. To allow the axonal labeling, animals were housed for at least 2 weeks following injection before sacrifice. TAC1-cre mice were used for injections in the PSTN, and the coordinates were AP = -2.0 mm, ML = 1.1 mm and DV = -5.2 mm (from skull surface).

For functional experiments

All viral injections were done bilateral in the PSTN, using a nanofil on modified microliter syringes (Hamilton) with a 33-needle gauge. The tip of the needle was placed at the target regions and the injections were performed at a rate of 0.1 µl min−1 (for coordinates and volumes see below). Once the injection was finished the needle was left in place for 5 min and then slowly removed. Animals were housed for at least 3 weeks following injection before any experiments were initiated. The coordinates used were AP = -2.0 mm, ML = 1.1 mm and DV = -5.2 mm (from skull surface) and 200 nl of AAV2-hSyn-DIO-hM4D(Gi)-mCherry virus was injected per hemisphere.

Chemogenetic inhibition

Clozapine-N-Oxide (1mg/kg, Sigma) was injected i.p., 1 h before the start of the behavioral sessions.

After sacrifice of TAC1-Cre mice, brains were dissected out frozen and serially sectioned. The injection sites were determined by microscopic observation, and animals with an injection site in adjacent regions to the PSTN/CbN complex were included in a group named "Miss Placed" (M.P.).

Histological procedures

Rats and mice were deeply anesthetized with a lethal dose of Dolethal (1ml/Kg – intraperitoneal (i.p.)). All animals were transcardially perfused with filtered saline (0.9% NaCl), followed by 4% paraformaldehyde (wt/vol). Following perfusion, brains were left in 4% paraformaldehyde for 24 h and then moved to a 20% sucrose solution (wt/vol) in phosphate-buffered saline (PBS) for 12 h. Brains were then frozen and cut into four series 30-µm coronal sections with a sliding microtome equipped with a freezing stage. To identify injection site locations, relevant sections were identified and mounted on slides.

Enzymatic immunohistochemistry

Free-floating sections were incubated with primary antibodies (Table 1) dissolved in PBS at pH 7.4 containing 0.3% Triton X-100 (PBS-T), 1% bovine serum albumin, 10% lactoproteins, and 0.01% sodium

azide for 48 h at 4 °C. Then, tissues were incubated for 4 h at room temperature in a solution of biotinylated goat anti-rabbit IgG (Vector Laboratories®) at a dilution of 1:1000 in PBS-T. Sections were placed in the mixed avidin–biotin horseradish peroxidase (HRP) complex solution with PBS (ABC Elite Kit, Vector Laboratories®) for 1 h at room temperature. The peroxidase complex was visualized by an exposure to a chromogen solution containing 0.04% 3,3'-diaminobenzidine tetrahydrochloride (DAB, Sigma®) with 0.006% hydrogen peroxide (Sigma®) in PBS. The reaction was stopped by extensive washing in PBS when the labeling was satisfactory. Sections were mounted on gelatin coated slides, and then dehydrated and coverslipped with Canada balsam (Roth®). An adjacent series was always stained in a solution of 1% toluidine blue (Roth®) in water to serve as a reference series for cytoarchitectonic purposes. Finally, sections were washed in PBS and mounted, air-dried, dehydrated in alcohol, cleared in xylene, and coverslipped.

Immunofluorescent staining
After rinsing in PBS-T, free-floating sections were incubated with primary antibodies (Table 1) dissolved in PBS-T, 1% bovine serum albumin, 10% lactoproteins, and 0.01% sodium azide or only in PBS-T for 24 h at 4 °C. Tissues were washed three times with PBS-T (5 min each) and incubated for 2 h with appropriate secondary antibodies (Table 2) diluted in PBS-T at room temperature. For triple-labeling, this procedure was repeated twice with primaries raised in different species (Table 1). In some cases, FG was detected by auto-fluorescence. Some sections were counterstained with a nuclear marker [NeuroTrace® 640/660 Deep-Red Fluorescent Nissl Stain, 1:100, Invitrogen®, Thermo Fisher Scientific Cat#N21483, Lot1851967, RRID: AB_2572212], for 20 min, at room temperature. Finally, sections were washed with PBS-T, mounted on gelatin-coated slides and cover-slipped with 60/40 glycerol: PBS-T.

Gas chromatography

Serum ethanol concentrations were analyzed by gas chromatography. Trace 1310 gas chromatograph (ThermoScientific, USA) with a capillary column Rtx-BAC PLUS 1 (Restek, USA) (30 m × 0.53 mm i.d., 3.0 µm film thickness), a split-splitless injector (temperature 140°C) and a flame ionization detector (temperature 250°C) was used. After dilution (1/20) in water added with internal standard Propanol-1, 0.8 µl of sample was injected with automatic sampler on CPG injector. Constant oven temperature (60°C) was required. The carrier gas was helium (99.9999%) at a constant pressure of 3 bars (44 psi). The hydrogen flow was 20 mL/min and air flow was 200 mL/min. Ethanol was identified by comparison with retention time of ethanol standard solutions analyzed at the same conditions. Quantitative determination of ethanol was performed relatively to propanol-1 and calibration range.

Image acquisition and processing

Sections were analyzed on an ApoTome.2 microscope (Axio Imager Zeiss), and images were obtained through a numeric camera (Digital Camera Hamamatsu C11440) using the Imager.Z2 software (Zen 2).

Electrophysiological recordings and firing rate analysis

Animals: Fifty male Hooded Lister rats (265-450 g) were anaesthetized with an i.p. injection of urethane (ethyl carbonate; 1.25 g/kg as a 25% aqueous solution) and mounted in a stereotaxic frame with the skull level. Body temperature was maintained at 37°C with a thermostatically controlled heating blanket. Two stainless steel electrodes (E363-1, Plastics One, Roanoke, VA) were inserted into the left hindpaw, one under the skin of the plantar surface of the foot and the other under the skin of the medial aspect of the lower leg/ankle. Craniotomies were then performed to allow access to the STN and the PSTN.

STN recordings: Extracellular single unit recordings were made from STN or PSTN neurons located contralaterally to the stimulated hindpaw, using glass microelectrodes pulled via a vertical electrode puller (Narashige Laboratory Instruments Ltd. Tokyo, Japan) and broken back to a tip diameter of approximately 1 µm (impedances 5-20 MΩ, measured at 135 Hz in 0.9% NaCl). Electrodes were filled with

0.5 M saline and 2% Pontamine Sky Blue (BDH Chemicals Ltd., Poole, UK). The electrode was lowered into the STN/PSTN with a hydraulic microdrive (Trent Wells Inc.).

Stimulation procedure: As previously described *(26, 27)*, the noxious footshocks was induced by single pulses (0.5 Hz, 2 ms duration) at an intensity of 5.0 mA. The activity of the cells was recorded during a control period (120 trials of sham stimulation) and during the application of noxious footshocks (120 trials).

Histology and analysis: The final recording site for the STN recording electrode was marked by passing a constant cathodal current of 27.5 µA (constant current source) through the electrode for a period of 30 min to eject Pontamine Sky Blue. Animals were then killed by an overdose of pentobarbital and perfused with 0.9 % saline followed by 4 % paraformaldehyde. Brains were removed and postfixed overnight in 4% paraformaldehyde at 4 °C, before being transferred into sucrose for 36 h. Serial coronal (30 µm) sections were cut, mounted on slides and processed with a Nissl stain (Cresyl Violet). Once sections had been processed, recording sites were reconstructed onto sections taken from the atlas of Paxinos and Watson (2005).

Peri-stimulus time interval histograms (PSTNs) were constructed based on SC/PBN multi-unit (bin width 1 ms) and STN single-unit data (bin width 10 ms). PSTNs were imported into an Excel program (Peter Furness, University of Sheffield, *(26-29)*) which determined the following response characteristics: i). Baseline activity: was the mean number of single- multi-unit events during the 500 ms bins prior to the footshock. ii). Response latency: The latency of a visually-evoked response was marked as the point when the value of post-stimulation events exceeded 1.96 S.D. of the baseline mean. (iii) Response duration: Response offset was recorded when post-stimulation activity returned to a value 1.96 S.D. of the baseline mean. iii). Amplitude of the response is the maximum amplitude during the response. iv). Magnitude of the response: is the mean number of single- multi-unit events between response onset and offset minus the baseline mean.

Behavioral sessions

Experiments in the rat

Neophobic test

Ten male rats weighing 250 g were randomly distributed into two groups. All rats were handled daily during a week before the experiment and kept 2 or 3 animals per cage. Then, animals of the control 'habituated' group were individually handled and given during 30 min a bottle containing a 20% sucrose solution each day during an additional 5 days. During the same period, neophobic rats were handled and given a bottle of water. The day before the experiment, drinking water was removed. The day of the experiment, each rat were handled as before and were presented to a bottle containing a 20% sucrose solution during 30 min. Immediately after, rats were anesthetized (Dolethal 1ml/Kg, i.p.) and perfused with the fixative (PFA4%). Often, neophobia is done by using a saccharin solution. However, previous unpublished experiment with this product showed that the c-Fos response in the PSTN is very weak with this molecule compared to sucrose. In a past experiment *(11)*, we also showed that i.p. injection of glucose do not induce a c-Fos response in the PSTN and that therefore the c-Fos expression is not modulated by glycemia.

LPS and cisplatin

Three group of male rats (LPS, n = 9; cisplatin, n = 9 and NaCl, n = 9), weighing 200 g, were i.p. injected with a solution of LPS (5 mg/kg), or cisplatin (6 mg/kg), or NaCl (0.9%) and killed 3 h later by perfusion of the fixative solution after being anesthetized (Dolethal 1ml/Kg, i.p.).

Alcohol exposure

The experiment was designed in the rats as to obtain a voluntary alcohol consumption and is described in the figure 1. A total of 44 male rats weighing 200 g were used. Rats were first habituated to their living

condition during a week. They were housed by 2 or 3 per cages and handled by the experimenter once a day. Eight groups of rats were then constituted. Drinking water was replaced by a solution of 15% alcohol or quinine (0,3 mM) at day-1 in their home cage. At the evening of day -1, all animals were deprived of any drinking solution during the night. Those of one group quinine and of one group alcohol (groups Day 0) had then individually free access to a bottle containing respectively the quinine or the alcohol solution during 30 min before to be perfused 30 min later. The same procedure was used to other groups of rats at Day 2, Day 5 and Day 20. In addition, two other groups of 4 rats were forced to drink either the alcohol or the quinine solution and were used to perform a double choice experiment against water at day 0 and day 20.

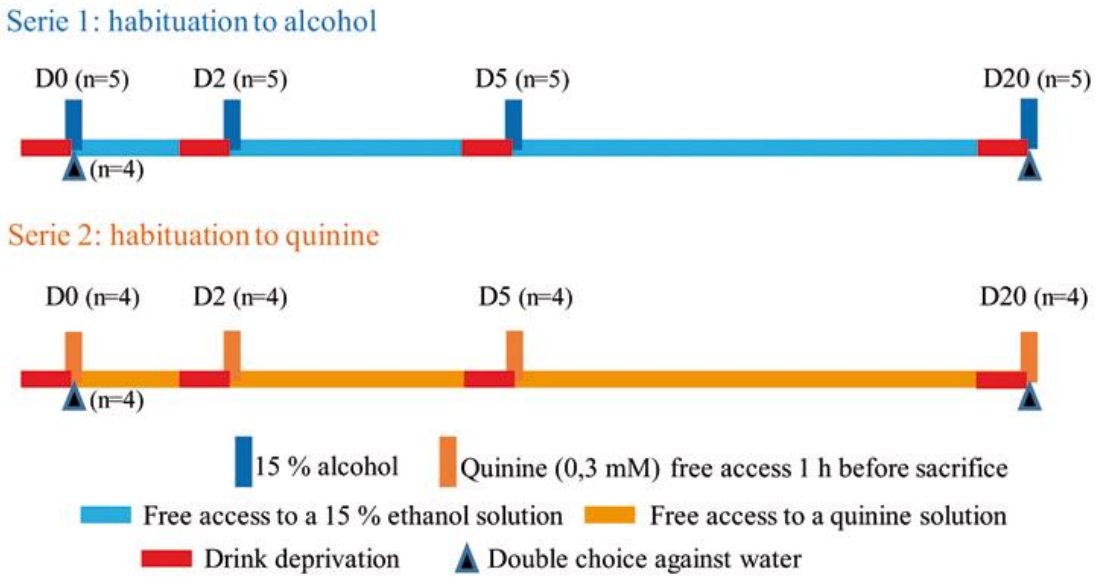

Figure 1. Diagram summarizing the experiment.

Experiments in mice

Food intake

TAC1-Cre mice (Controls, n = 18; DREADD, n = 12 and M.P., n = 5) were placed in operant chambers (MedAssociates) to monitor pellets consumption during 1 h. Before the test, mice were habituated to eat pellets in the operant chamber three times per week for two consecutive weeks. The day of the test, each mouse received an i.p. injection of CNO (1 mg/kg) 1 h before the start of the session. At the end of the session, all pellets were weighed.

Open field tests

To assess locomotor activity in response to our treatments, TAC1-Cre mice (Controls, n = 6; DREADD, n = 9 and M.P. n = 3; the M.P. animals were determined after the histological validation of the injection site) were placed on a novel Plexiglas arena (40 × 40 x 40 cm). The total area was divided into a virtual central (34 × 34 cm), and a surrounding peripherical subareas. The central subarea was lit with a 100-lux lamp to induce natural aversion to this particular location, as usually performed. Animals were tested once in this arena. The 5 min sessions were digitally recorded with a CCD camera. Data were analyzed by replaying the sessions in slow-motion to verify the results obtained with the VideoTrack View Point software (Lyon, France). Outcomes were the number of sequential crossings over different subareas (representing total locomotor activity), and relative time spent within the illuminated central part of the arena.

Forced swim test

TAC1-Cre mice (Controls, n = 6; DREADD, n = 9 and M.P., n = 3) were placed into a glass cylinder (height 26 cm, diameter 18 cm) containing water at a temperature of 32 ± 2 °C and a depth of 15 cm. Many

parameters (time before 1st immobilization, number and duration of stops and movements) were programmed with the VideoTrack View Point software (Lyon, France). Each test lasted 6 min and was video recorded for subsequent scoring of the total time spent immobile by a blind observer. Mice were considered immobile when they ceased struggling and remained floating motionless in the water.

Neophobic test
One group of TAC1-Cre mice (neophobic; n = 5) was exposed only once to a 10% sucrose solution (primo exposure to a novel taste). A second group (habituated, n = 5) was exposed to this same solution every 2 days for 2 weeks. The day of the test, after 12 h of water withdrawal, each animal received an i.p. injection of CNO (1 mg/kg) and was placed 1h later in operant chambers equipped with lickometers (MedAssociates) to monitor sucrose (10% v/v) solution consumption during 15 min.

LPS and cisplatin
Group of TAC1-Cre mice (LPS, n = 10; NaCl, n = 13 and M.P., n = 7) were i.p. injected with a solution of LPS (50 µg/kg), or NaCl (0.9%) and killed at the end of the experiment. With injection of LPS or NaCl, each mouse receives another i.p. injection of CNO (1 mg/kg) and a last 1 h apart. Mice were placed 1 h later in operant chambers equipped with lickometers (MedAssociates) to monitor sucrose (10% v/v) solution consumption during 15 min.

Statistical analyses

Data analyses were performed using GraphPad Prism 5 (GraphPad). Data distribution was assumed to be normal, but this was not formally tested due to normality tests being inconclusive when small sample sizes are employed (normal probability plots instead). Consistently with the overall experimental design and group assignments, statistical analyses only made use of standard linear model (Pearson correlation) analyses as well as one-way ANOVAs and post-hoc t-tests whenever relevant. All P values associated with the t-tests performed correspond to two-tailed tests, and all post-hoc tests were corrected for multiple comparisons by employing Bonferroni correction. All data are reported as mean ± s.e.m. Every experimental group entered in statistical analyses was associated with the corresponding computation of its mean ± s.e.m.

Supplemental data 2: Characterization of the PSTN/CbN region.

The caudo-lateral lateral hypothalamic area (LHA) is made of several differentiated nuclei (fig. 1). In that it differs from more rostral LHA regions (tuberal) that are not nuclearly organized and share many cytoarchitectural features with the reticular formation. Chometton *et al.* provided a careful analysis of the cytoarchitecture of the PSTN region and the present description is based on this work *(11)*.

The parasubthalamic nucleus (PSTN) lies adjacent to the STN and is a nucleus initially characterized by the expression of TAC1 *(30)*. This nucleus is illustrated in the atlas of Paxinos and Watson and in the Brain Maps of L.W. Swanson *(31, 32)*. Besides TAC1, this nucleus does not contain GAD (while the tuberal LHA is rich in GABAergic neurons), but its neurons express VGluT2 and are probably glutamatergic *(33)*. It is selectively innervated by CGRP axons from the parabrachial nucleus (PBN) along the closely related CbN *(11)*.

The calbindin nucleus (CbN) is a small round shaped nucleus that was described by Chometton *et al*. in the rat *(11)*. It contains, as indicated by the name, a condensation of small round shaped cells that are labeled for calbindin. It receives, like the PSTN, an intense input from the CGRP neurons in the PBN, and both nuclei form the PSTN/CbN complex.

The paravafox nucleus was essentially described by the groups of Celio and Alvarez-Bolado *(34)*. The rostral aspect of this nucleus corresponds to the *parateretе* nucleus of Paxinos *(32)*, but it extends in the caudal LHA where it was first identified by Celio as the PV1 nucleus because it contains a dense parvalbumin labeling. It was renamed Parvafox because some neurons also contain the Foxb1 protein *(4)*. This nucleus is the bed of a small tract of axons originating in the deep layer of the olfactory tubercle and named the ventrolateral hypothalamic tract (vlt). This tract was described by Price *(35)* and figures in the Brain Maps *(31)*. At premammillary level, the vlt arches dorsally and terminates in a small nucleus named the nucleus gemini (NG) *(11)*. This nucleus was described first during the 1960's but has been largely ignored since.

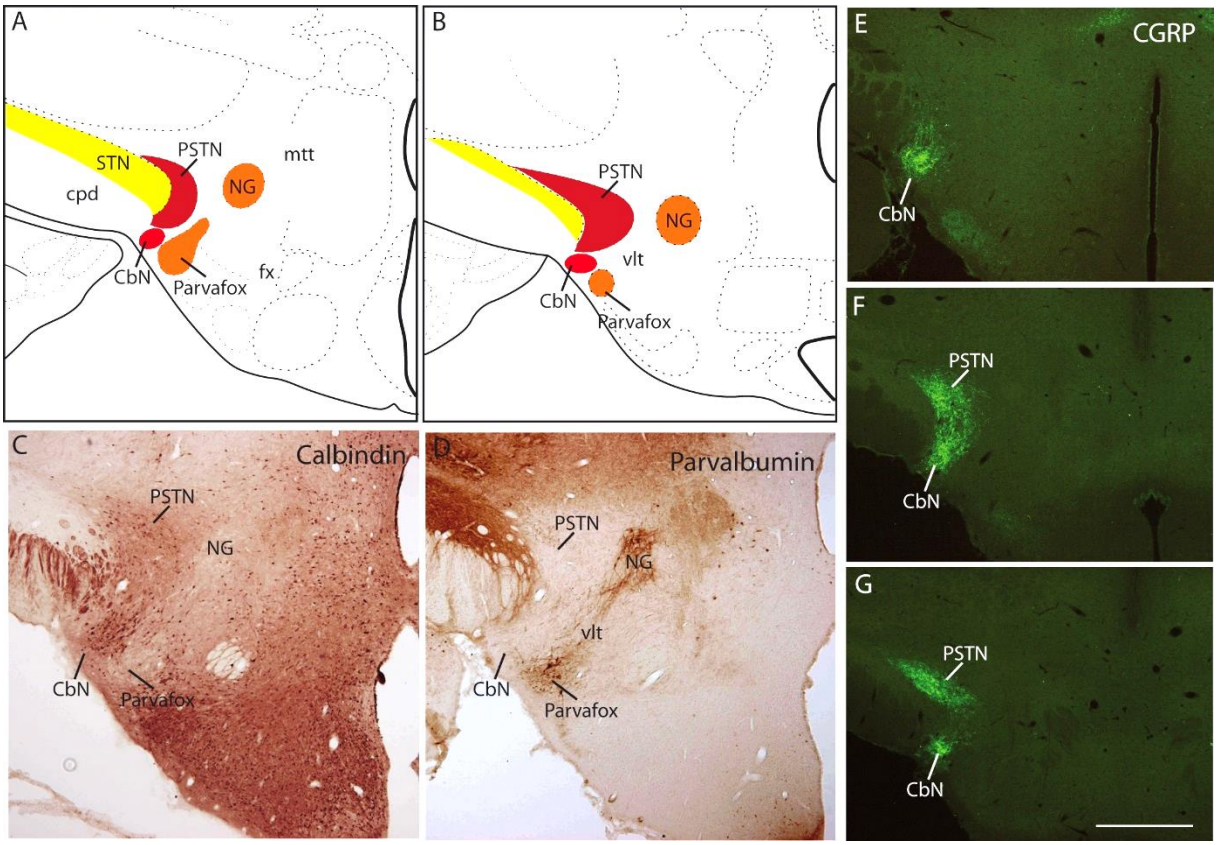

Figure 1. A, B: Line drawings adapted from Chometton *et al.* and the Brain Maps *(11, 31)*, illustrating the nuclear organization of the caudo-lateral LHA. C, D: Photomicrographs illustrating the distribution of calbindin (C) and parvalbumin (D) using immunohistochemistry (with permission from Chometton *et al.*). E-G: Photomicrographs illustrating the CGRP projections in the PSTN/CbN using immunofluorescence on three sections through the premammillary region and arranged from rostral (E) to caudal (G). Scale bar in g = 500 µm.

Supplemental data 3: Nomenclature for the insular cortex and injection sites.

The insular cortex is usually divided into granular, dysgranular and agranular areas, mostly depending on the presence or absence of a 4th granular layer found in the granular areas (see the figure below). The granular area is ventrally adjacent to the somatosensory cortex and most of it corresponds to the visceral area (VISC) according to Swanson 2004 *(31)*. The dysgranular area, that may also contain few granular cells, is ventral to the insular granular area but extends more rostrally, ventral to the rostral motor isocortex. It corresponds mostly to the gustatory cortex (GU). However, following the Swanson's nomenclature, the gustatory area extends over rostral granular fields. Agranular areas (AI) occupy ventral parts of insular cortical mantle, around the rhinal fissure, just dorsal to the piriform cortex. Its frontal pole is also ventrally adjacent to the motor cortex, lateral to the lateral orbital area. It is divided into dorsal (AId), ventral (AIv) areas in its rostral half, and forms the posterior area (AIp) caudally.
PHAL injections were obtained in each of these divisions, including one in the visceral, two in the gustatory (one rostral in the dysgranular cortex and one in the granular insular area rostral to visceral areas), three in the AId, one in the AIv and one in the AIp. The respective localization of the injection sites was determined by the cytoarchitecture. However, the projections into the thalamus were also a clear evidence of the location of the injection site: The GU and VISC project heavily respectively in the parvicellular part of the ventral posteromedial thalamic nucleus (VPMpc) or the parvicellular part of the ventral posterolateral thalamic nucleus (VPLpc); the AId and dysgranular GU (anterior) innervate intensely the mediodorsal thalamic nucleus (MD) in addition to the VPMpc ; agranular areas (AIp, AIv) did not innervate the VPM or VPL but send dense inputs to the medial part of the MD. In addition, control injections were obtained in motor (two), somatosensory (two), lateral orbital (one) and piriform (one) areas.

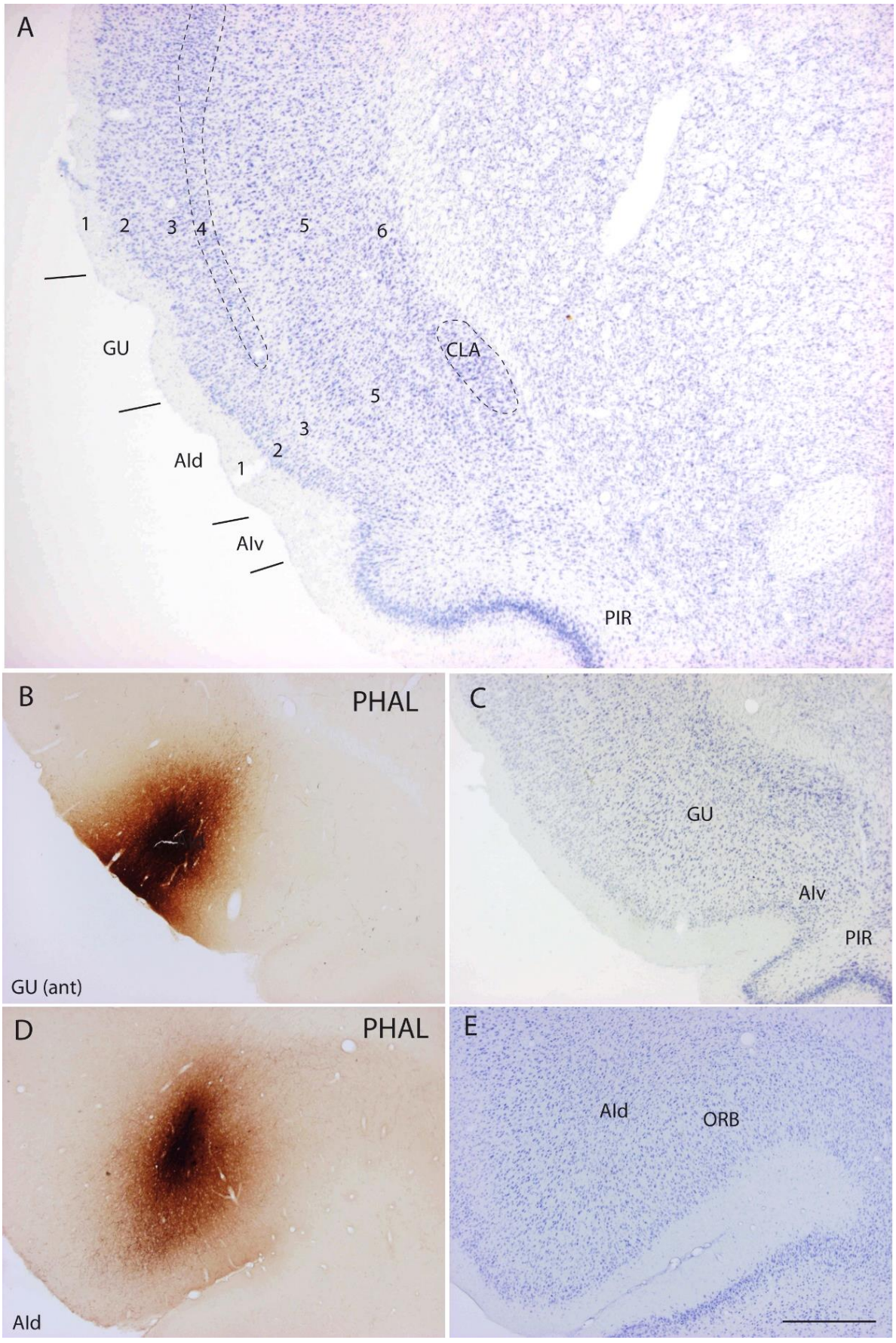

Figure 1. A, C, E: Photomicrographs of toluidine blue labeled sections through the insular cortex. B, D: Sections adjacent to B and D respectively and illustration the injection site in the GUant (dysgranular GU) (B), and in the AId (D). Scale bar = 500 µm in B to E and 200 µm in A.

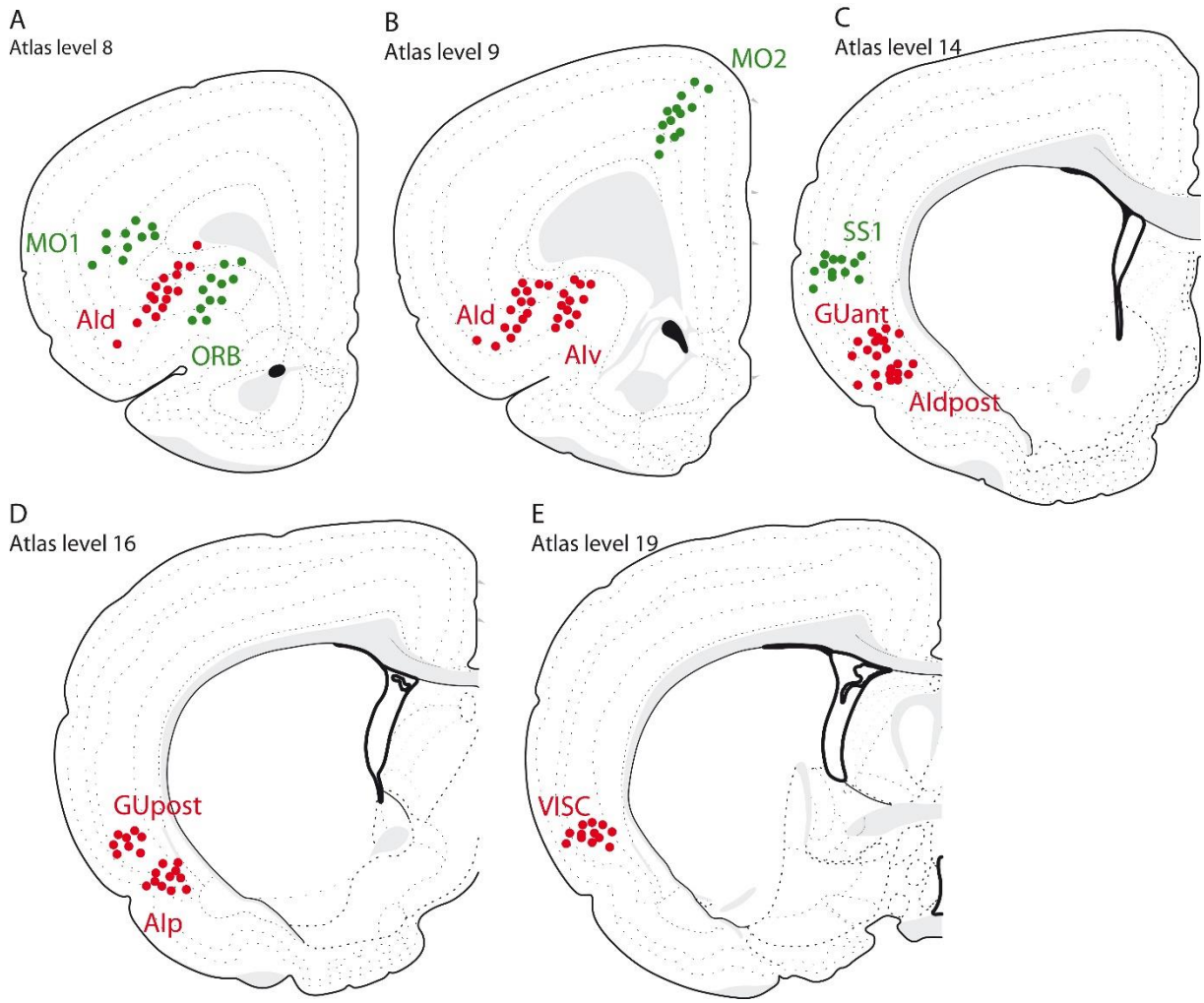

Figure 2. Line drawings to illustrate the locations of PHAL injection sites in the INS (in red) and of some control experiments (in green). PHAL injection sites were obtained in each of the division of the INS. Line drawings are arranged from rostral (A) to caudal (E). Atlas levels refer to the Swanson's Brain Maps *(31)*.

Supplemental data 4: Additional data on the innervation of the PSTN/CbN from the insula.

The distributions of PHAL axons from injection sites in the INS were compared with that of CGRP axons and calbindin neurons labeled by immunohistochemistry. After injection in the AIv, parvalbumin labeling was used to identify the Parvafox nucleus.

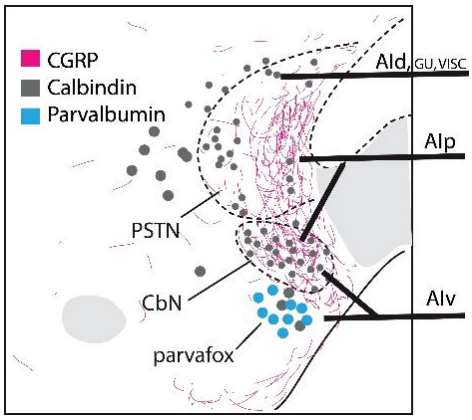

Figure 1. Line drawing summarizing the distribution of INS axons in the PSTN/CbN with regard to the neurochemical heterogeneity of the PSTN. Injection site in the INS provided distinct patterns of innervation of the PSTN/CbN, confirming that the PSTN is not homogeneous in the rat. AId provided a denser innervation of dorsal aspects of the nucleus characterized as containing calbindin-containing cells. GU and VISC innervated the same region but projections were weaker. The innervation provided by the AIp was intense and with a pattern identical to that provided by the CGRP projections within the nucleus. Finally, the AIv mostly innervated the CbN and the adjacent Parvafox labeled for parvalbumin.

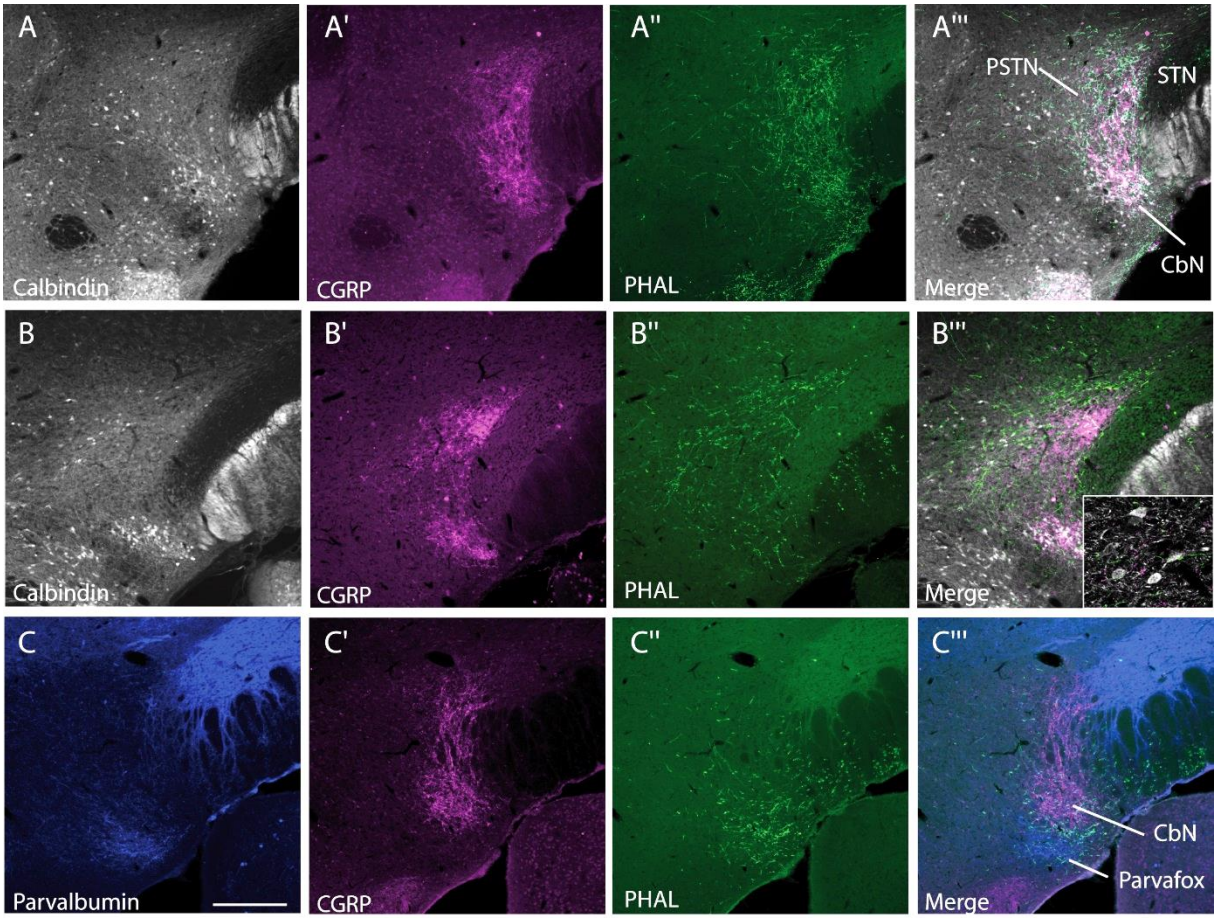

Figure 2. Photomicrographs illustrating the co-distribution of PHAL axons with that of CGRP, calbindin or parvalbumin signals. Triple immunofluorescence labeling procedures were used.

Scale bar = 500 µm.

A-A''': Projections from AIp were intense and overlapped with the distribution of CGRP terminal field in the PSTN and CbN.

B-B’’’: Projections from the AId were significant but tended to avoid the CGRP rich region of the PSTN and innervated dorsal regions containing more calbindin cells. Some of these cells were contacted by PHAL containing axons and boutons. The framed picture in B’’’ illustrates axons establishing close relationships with calbindin labeled cells and evocating synaptic contacts.

C-C’’’: Projections from the AIv extended over the CbN and Parvafox nucleus but spared the PSTN.

Figure 3. Photomicrographs illustrating the co-distribution of PHAL axons with that of CGRP, calbindin or parvalbumin labeling. Triple immunofluorescence labeling procedures were used. Scale bar = 500 µm in A, C; = 250 µm in D; = 100 µm in B.

A-A’’, B: Projections from the GU were weak but distributed similarly to that from the AId. At higher magnifications and using the Apotome device of the microscope (B), axons obviously displayed *en passant* boutons, seemingly in contact with cell bodies or dendrites labeled with the calbindin antibody (arrows).

C-C’’’ and D-D’’’: Projections from the VISC were also weak and also distributed dorsal in the PSTN. At higher magnification it was clear that many of these axons changed appearance as they crossed the border to enter the PSTN and displayed more boutons and collaterals.

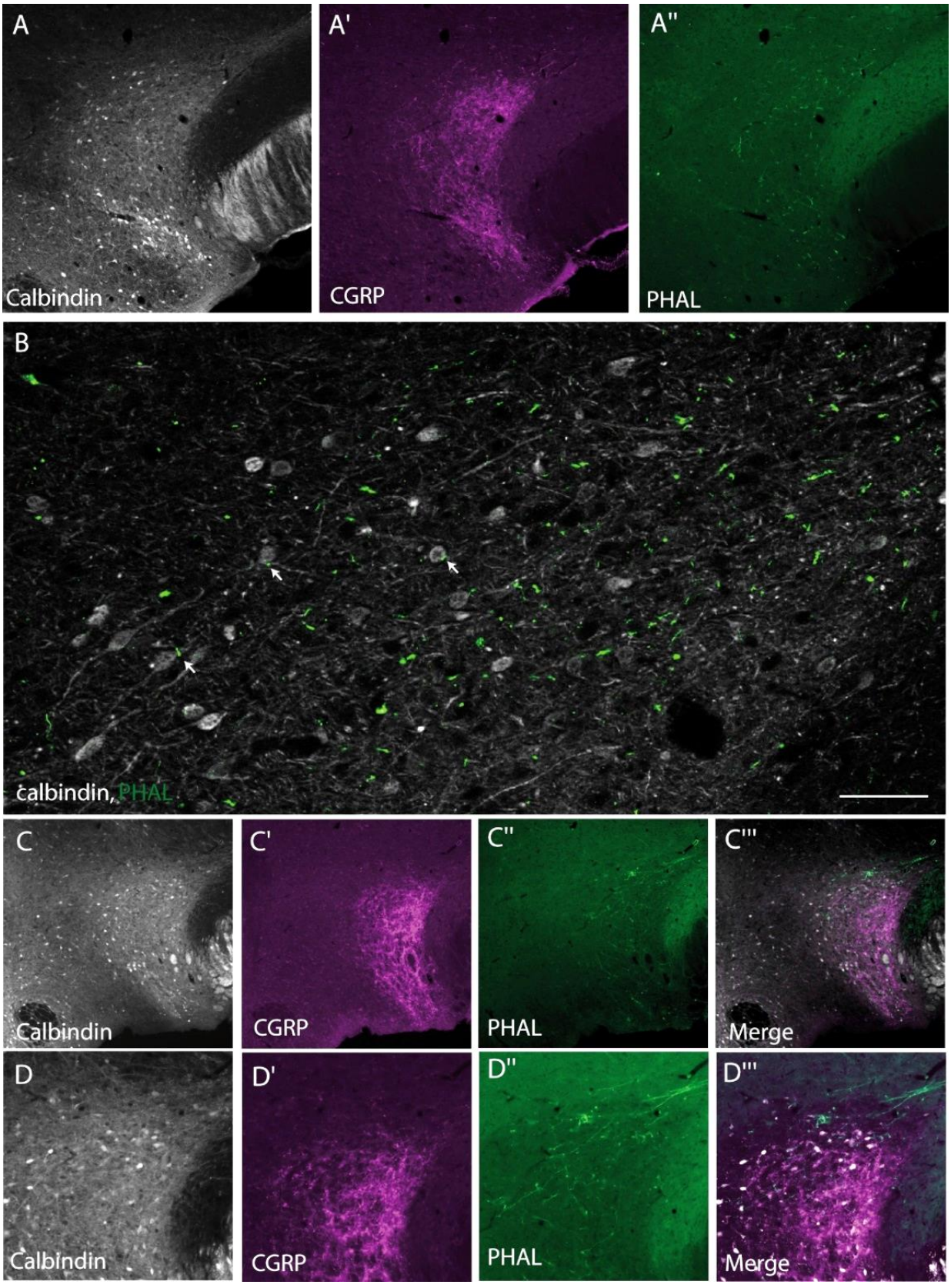
A
A'
A''
Calbindin
CGRP
PHAL
B
calbindin, PHAL
C
C'
C''
C'''
Calbindin
CGRP
PHAL
Merge
D
D'
D''
D'''
Calbindin
CGRP
PHAL
Merge

Supplemental data 5: Distribution of PHAL axons in the striatal compartment.

The striatal compartment is made of the dorsal striatum (caudoputamen nucleus, CP) and a complex ventral striatum comprising the nucleus accumbens (divided into core and shell; ACBc, ACBs), the olfactory tubercle (OT), the fundus striatum (FS, named by some the IPAC). Besides, the CP region just dorsal to the CEA is also named the amygdalostriatal transitory part (ASt) (Paxinos *(32)*).

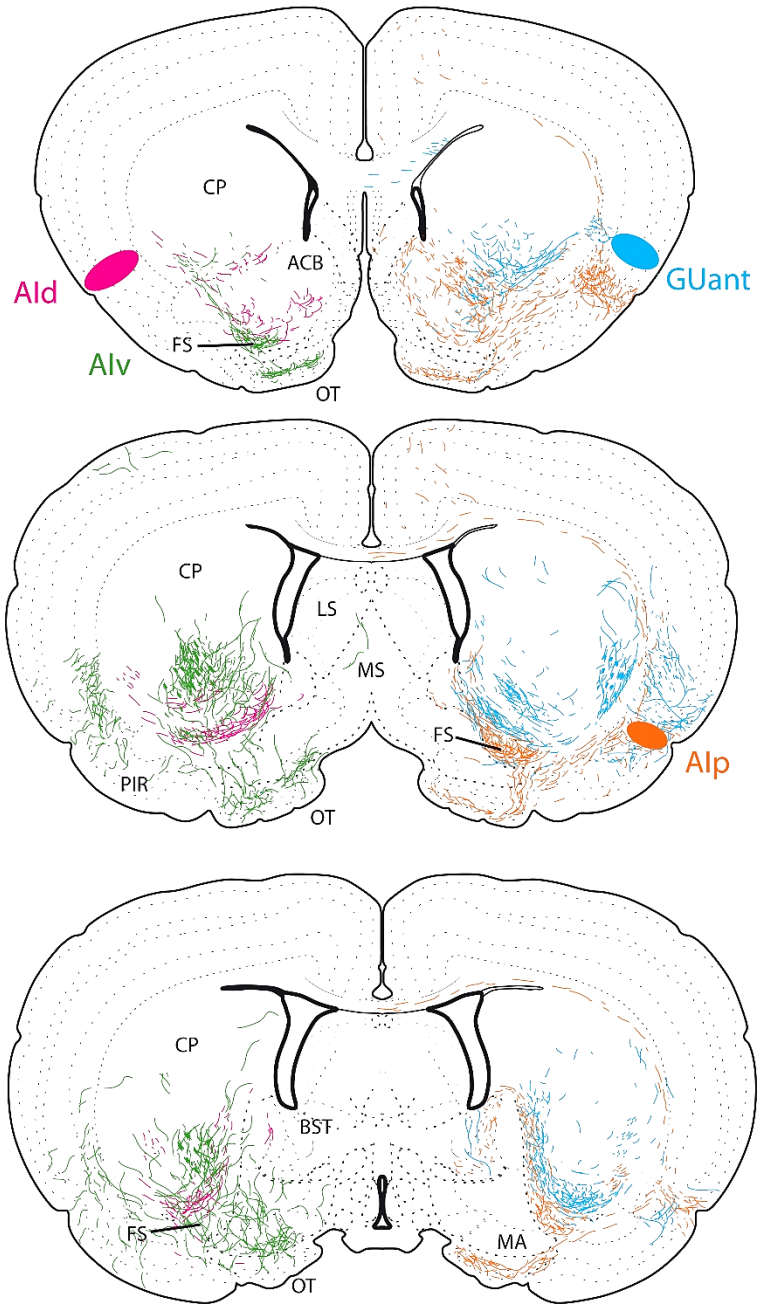

Figure 1. Line drawings to illustrate the distribution of PHAL axons after injections in the AId, AIv, GU and AIp on brain sections from rostral (top) to caudal (bottom).

The organization of projections from the IC into the striatum is topographically organized:

-The AIv and AIp innervated predominantly the ACB, the FS and the OT.

-The AId projections innervate the ventral CP and the ACB, but the main projections are for a specific caudal part of the FS.

-The GU and VISC innervate mostly ventral and central regions of the CP including ASt (see fig. 2), but also the ACBc and the FS.

ACB: accumbens nucleus; AId/v: aire agranulaire insulaire dorsale / ventrale; BST: bed nucleus of the stria terminalis; CP: caudoputamen nucleus; FS: fundus striatum; GUant: anterior part of the gustatory area; LS: lateral septal nucleus; MA: magnocellular preoptic nucleus; MS: medial septal nucleus; OT: olfactory tubercle; PIR: piriform cortex. *(31)*

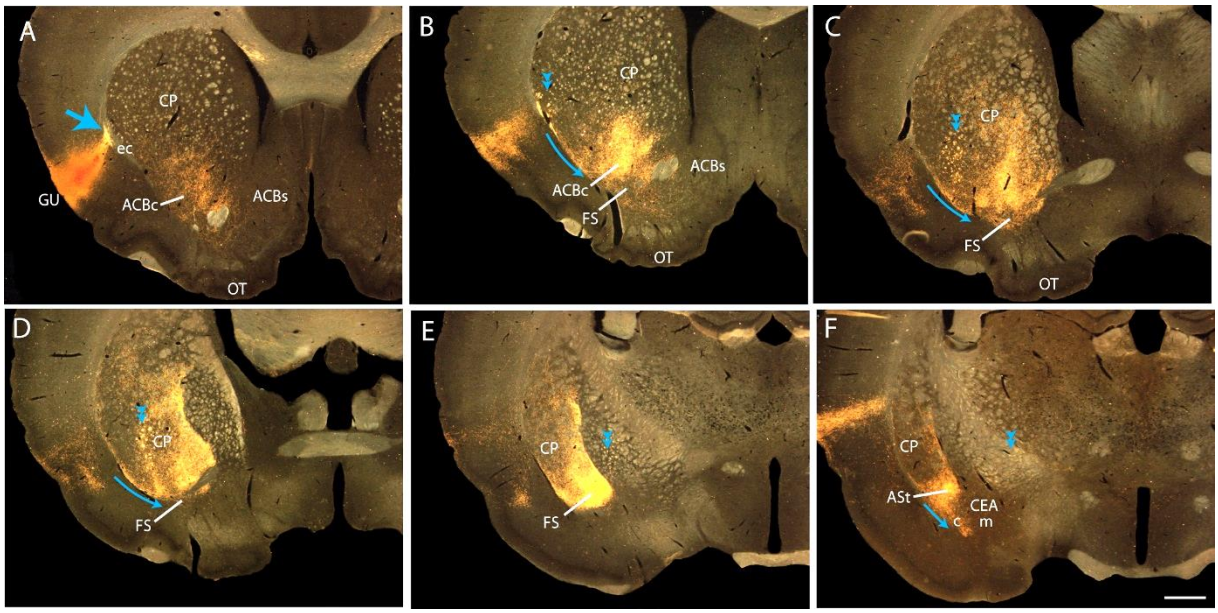

Figure 2. Photomicrographs illustrating the course of PHAL axons in the striatal compartment after PHAL injection in the GU. PHAL axons enter the external capsule (large blue arrow in A) and some join the internal capsule (double arrowheads) and travel through the striatum and the pallidum to reach the diencephalon, while others (blue arrows) take a ventral route to enter the striatal compartment. It is clear, and shall be emphasized in sup data 6, that the innervation of the CEAc arises from axons extending from the FS or from the ASt and, therefore, is an extension of the ventral striatal pathway.

Scale bar in F = 1mm

Supplemental data 6: Innervation of the lateral parts of the CEA are from axons extending from the striatum.

The INS projects topographically into the lateral parts (lateral and capsular) of the CEA.

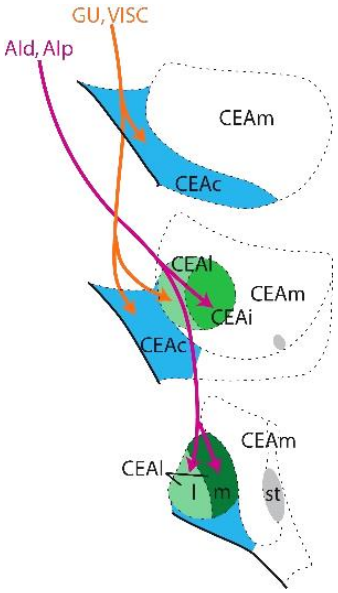

Figure 1. Line drawing summarizing the projections from the INS into the lateral CEA. These projections extend from the ASt or from the FS to innervate the CEAc (VISC, GU), lateral regions of the CEAl (GU) or the whole CEAl including a specific intermediate part of the CEA (AId, AIp). This last division of the CEA (CEAi) is most often considered as a component of the CEAl *(36)*. The remaining CEAl can also be divided into two domains: a lateral and a medial domain.

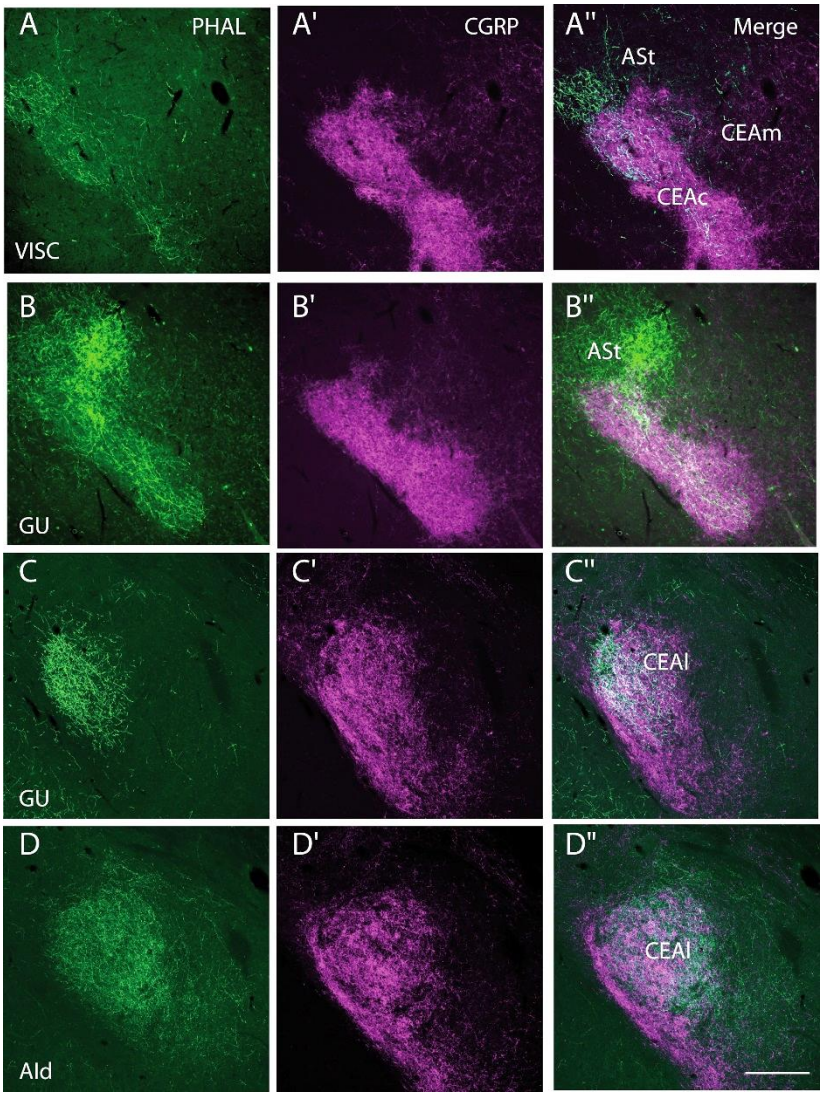

Figure 2. Photomicrographs to illustrate the distribution of PHAL axons from the INS in the CEA, compared with that of CGRP axons that intensely innervate the CEAc and CEAl.

A-A": The VISC innervated moderately and exclusively the CEAc.

B-B" and C-C": The GU innervated the CEAc as the VISC (B-B"), but this projection extended into the lateral CEAl (C-C"), avoiding the CEAi.

D-D": Projections from the AId intensely innervated the whole CEAl and CEAi (not shown for the CEAi, see *(36)*).

Scale bar = 100 µm.

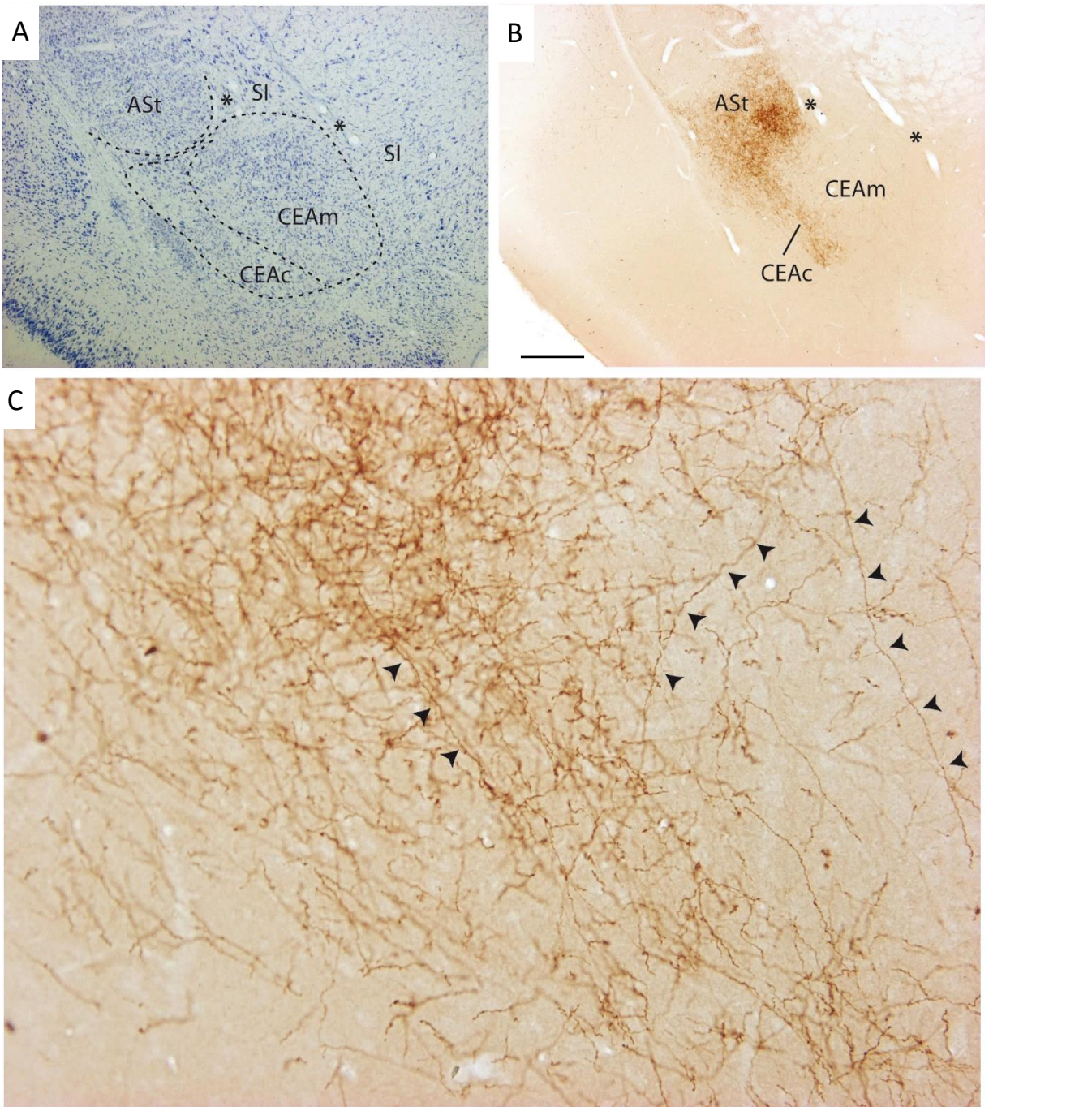

Figure 3. Innervation of the CEA by axons extending from adjacent striatal compartments.

A, B: Photomicrographs that illustrate the innervation of the ASt and CEAc after PHAL injection in the GU. Both structures are adjacent, as shown on the toluidine blue (Nissl) stained section (A).

C: At high magnification, it is very clear that axons innervating the CEAc come from the ASt. It is possible to individually follow several of them (arrowheads).

Scale bar = 250 µm in A, B and 25 µm in C.

Supplemental Data 7: The indirect pathway from the lateral CEA to the PSTN.

A: Line drawings schematizing the distribution of PHAL axons in the ventral telencephalon after PHAL injections in the lateral amygdala (CEAc in red, CEAl/CEAi in green).

B, C: Rats were injected with PHAL in the CEA, and FG in the PSTN. The photomicrograph in B illustrates the injection site in the CEAi/CEAl. The same animal was injected with FG in the PSTN (C).

D, E: Photomicrographs to illustrate the dual labeling in the SI for PHAL and FG. The fields corresponding to the pictures are illustrated in A. PHAL axons innervated parts of the posterior SI adjacent to the GP that contained many FG cells after FG injection in the PSTN. Many axons (frame pictures in E) made contacts on FG cells suggesting an innervation of these neurons projecting in the PSTN.

Scale bar = 500 µm in B and C, = 150 µm in D and E.

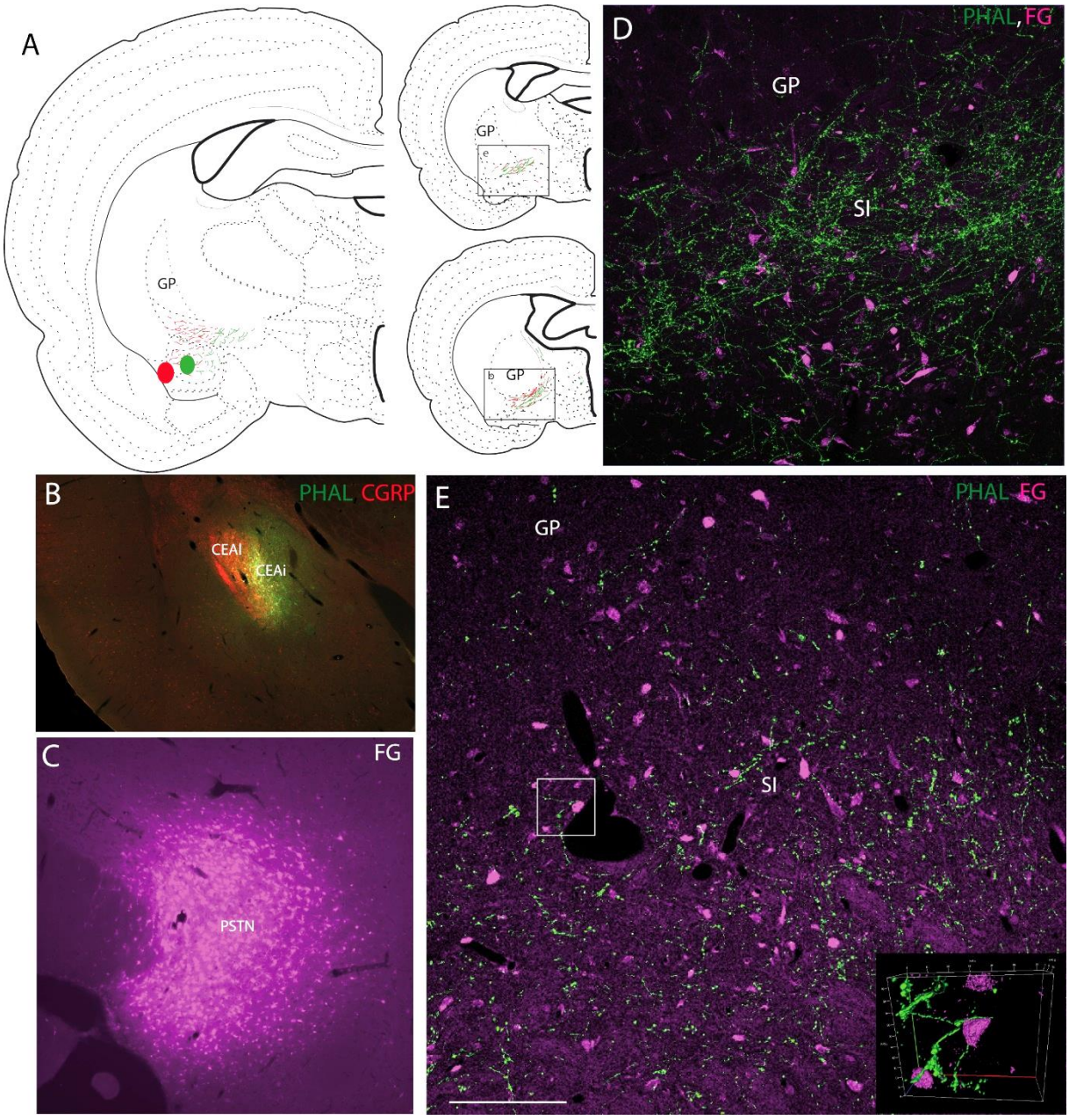

Supplemental data 8: Electrophysiological profile of PSTN neurons.

A recent experiment found that STN neurons presented various nociceptive responses to noxious footshock delivered in the rat hind paw *(37)*. This experiment analyzed cells located in both the STN and PSTN. We thus compared the electrophysiological characteristic of those noxious responses between the PSTN (n = 19) and the STN (n = 80).

PSTN and STN neurons: The PSTN neurons sampled in the present study were characterized by a triphasic action potential (n = 19, mean duration: 2.45 ± 0.16 ms). The STN neurons were also characterized by a triphasic action potential in majority of cases (n = 70, mean duration: 2.04 ± 0.07 ms), but an additional group of cells had a biphasic action potential (n = 10, 1.58 ± 0.13 ms). Neurons in the PSTN had a significant lower spontaneous firing rate than those in the STN (Mann-Whitney test: U = 431; $p < 0.01$; mean ± SEM: PSTN: 4.27 ± 0.57 Hz; STN: 8.08 ± 0.61 Hz) however both structures exhibited the same pattern of activity such as irregular, regular or bursting.

Phasic nociceptive response: Following noxious stimulation performed on the contralateral hindpaw (120, 0.5 Hz), 16 cells responded to the footshock (84%) in the PSTN and 64 cells (80%) in the STN. Contingency analysis on the number of responding and non-responding cells did not show a significant difference between both structures ($\chi2 = 0.1755$, *df* = 1, $p = 0.3376$). As illustrated in table 1, the same patterns of response can be found within the PSTN and the STN.

RESPONSE TYPE		*STN*	*PSTN*
Monophasic excitation	Single initial excitation	31	9
Biphasic +/+	Initial excitation followed by longer latency excitation	21	3
Biphasic +/-	Initial excitation followed by longer latency inhibition	8	3
Triphasic +/-/+	Initial excitation, then an inhibition followed by a third late latency excitation	3	2

Table 1: Response type in the STN and the PSTN.

Baseline firing rate: We performed an individual analysis on each of the total 99 cells to test if the introduction of the noxious stimulation induced a significant change of STN or PSTN baseline firing rate, and if so, in which direction the change took place. In the PSTN, we identified 5 (26%) and 3 (16%) cells showing a significant increase ("up" group) or decrease ("down" group) of their baseline firing rate with the stimulation, respectively and no significant change for the remaining 11 cells (58%, "no change" group). In the STN, the "up" and "down" groups included 28 (35%) and 19 (24%) cells, respectively and 33 cells (41%) in the "no change" group. Contingency analysis on the number of cells within each category did not show a significant difference between the PSTN and the STN ($\chi2 = 1.742$, *df* = 2, $p = 0.4185$).

Supplemental data 9: Response of the PSTN to neophobia.

C-Fos expression induced by a primo exposure to a 20% sucrose solution was researched. A first group of rats (neophobic; n = 5) was exposed only once to the 20% sucrose solution. A second group (habituated, n = 5) was exposed to this same solution every 2 days during 12 days. The day of sacrifice, after 12 h of water withdrawal, each animal was exposed 30 min to the sucrose solution and killed 30 min later. Ingested volumes were measured, and the licking profile was recorded.

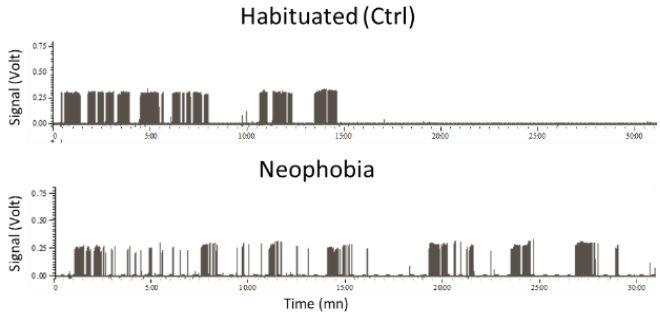

Figure 1. Example of licking profiles for habituated (control) and neophobic rats. Habituated rats drunk rapidly a large amount of the solution, while the neophobic rats spread their consumption of the same solution over the entire 30 min period.

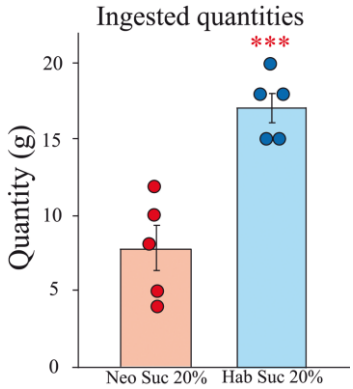

Figure 2. Graphs illustrating that habituated (controls) rats drunk significantly more of the 20% sucrose solution than the neophobic rats. N = 5 in each group, unpaired *t*-test, p = 0.0008, ***p < 0.001.

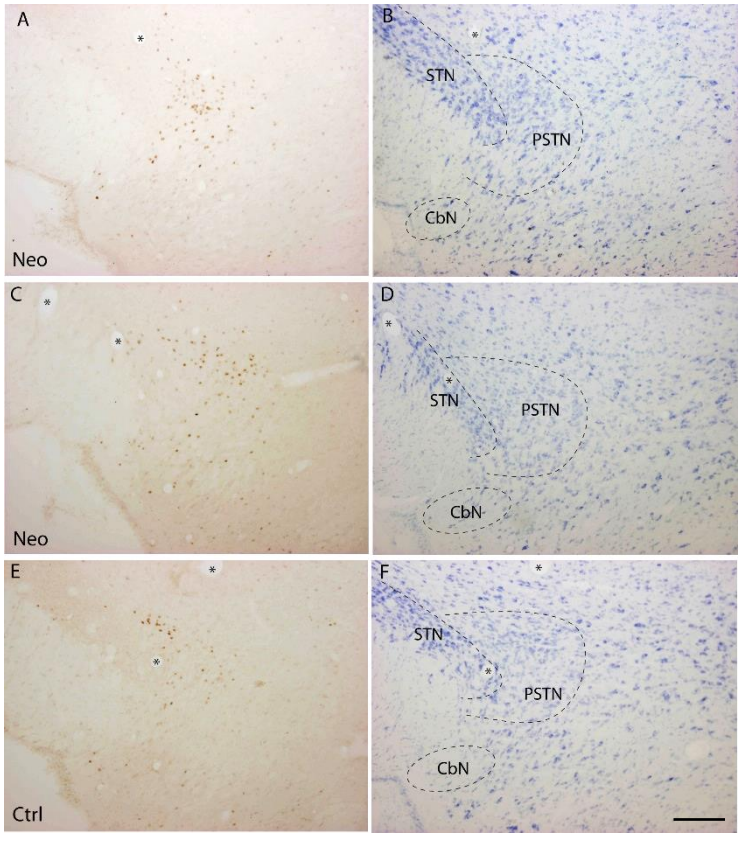

Figure 3. Photomicrographs that illustrate the c-Fos expression in the PSTN of neophobic rats (A, C) and a control animal (E). Pictures B, D, F are from adjacent Nissl stained sections for cytoarchitectonic purpose.

Scale bar = 200 µm.

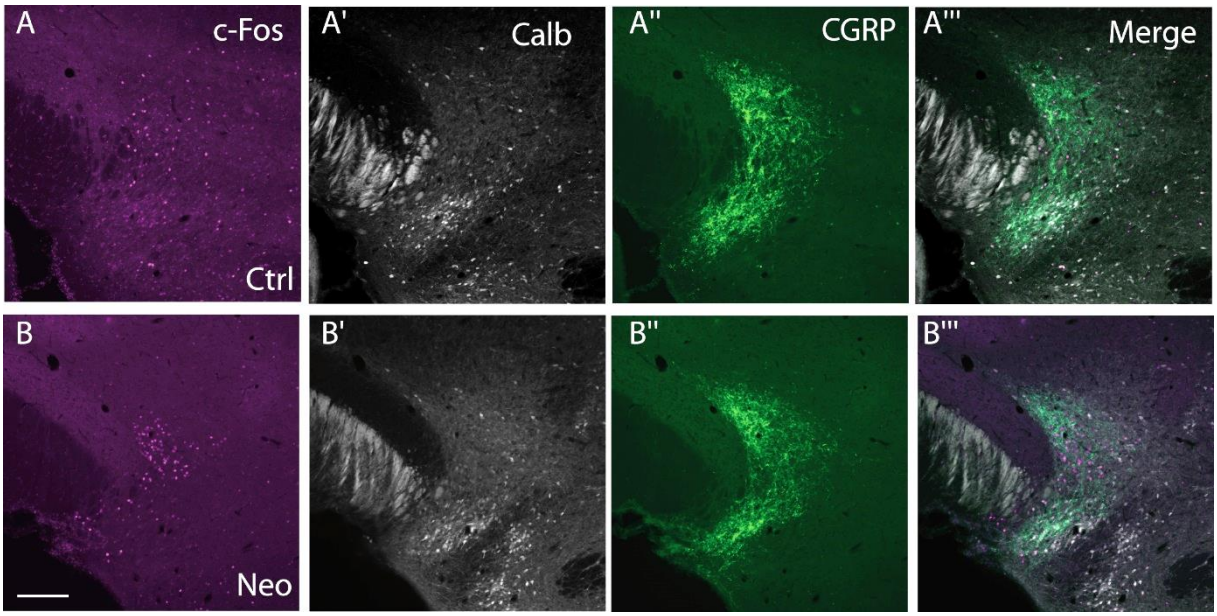

Figure 4. Photomicrographs that illustrate the co-distributions of c-Fos labeled nuclei, calbindin-containing cells and CGRP axons. Note that in both controls and neophobic rats, c-Fos labeled nuclei have a distribution mostly in the PSTN that spare the CGRP rich region of the nucleus. Close to 50% of the c-Fos nuclei belonged to calbindin expressing neurons, and the proportion was identical in neophobic rats and controls (fig. 5). Scale bar = 200 µm.

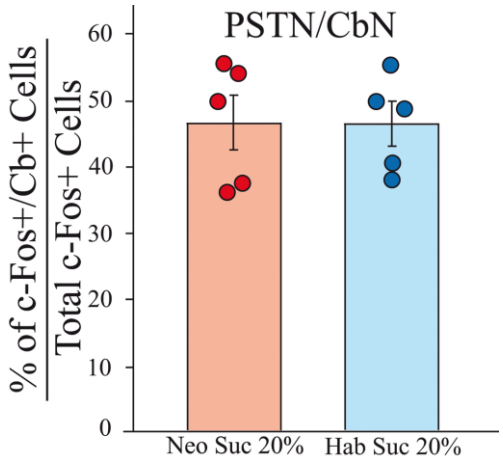

Figure 5. The ratio of double labeled cells for c-Fos and calbindin was identical in the neophobic and the control groups. N = 5 in each group, unpaired *t*-test, p = 0.9428, ns.

Supplemental data 10: Response of the PSTN to induced sickness.

C-Fos expression in the PSTN/CbN was analyzed 3 h after a single injection of LPS (5 mg/kg) or cisplatin (6 mg/kg) and compared to controls (injection of NaCl).

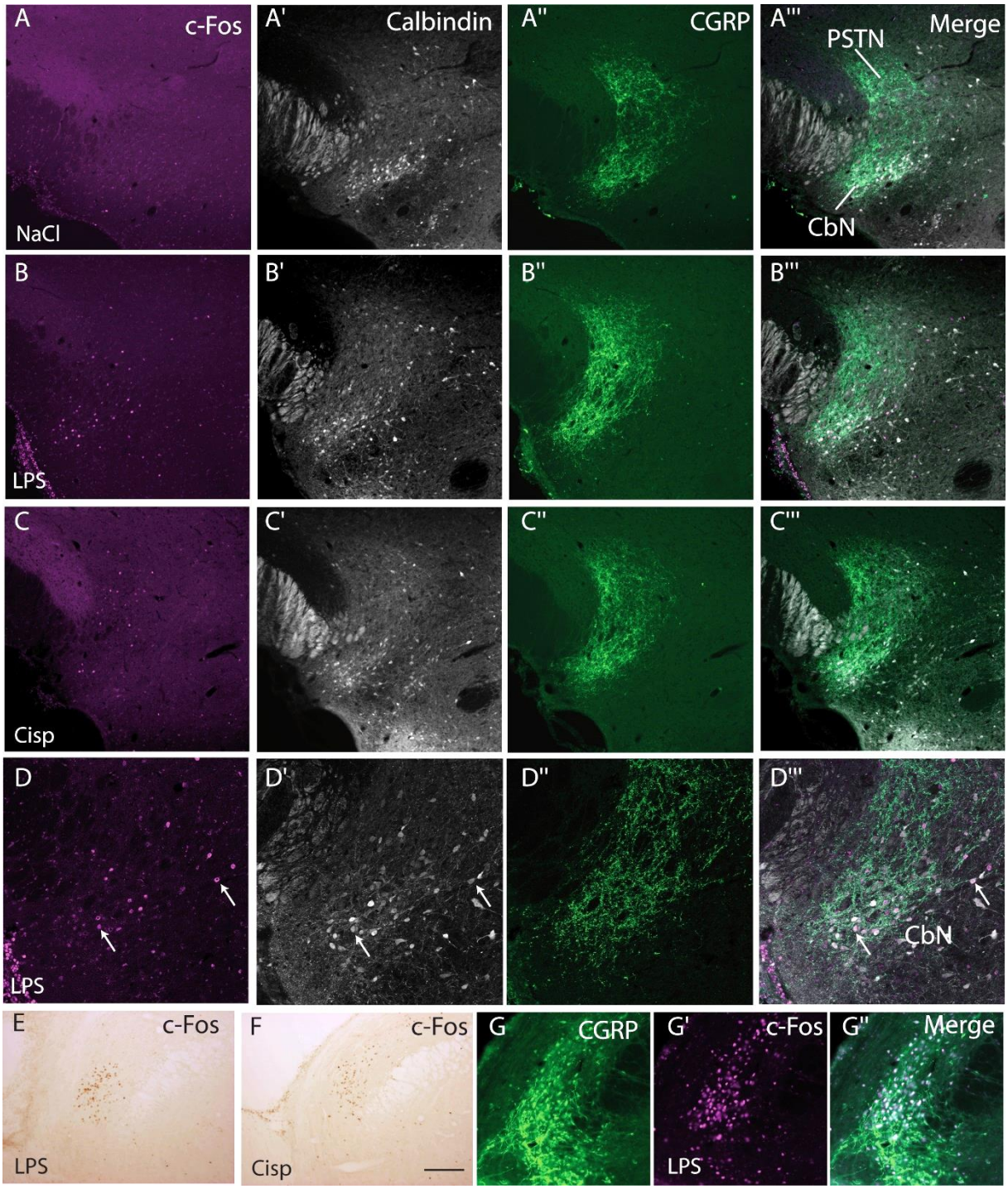

Figure 1. Photomicrographs to illustrate the patterns of the c-Fos labeling compared with that of CGRP and calbindin. Scale bar in A to C''', E to G'' = 200 µm and 50 µm in D to D'''.

A-A''': Low c-Fos expression in control animals.

B-B''': LPS induced an intense c-Fos expression that affected the CbN and to a lesser extend the PSTN.

C-C''': Cisplatin also induced a c-Fos expression, but that is less intense than LPS.

D-D’’’: At higher magnification, many c-Fos labeled nuclei were observed in calbindin positive cells (arrows), here after LPS injection.

E-G’’: LPS (E) and cisplatin (F) induced a very intense c-Fos expression in the dorsolateral parabrachial region, as expected. Dual labeling for c-Fos and CGRP confirmed literature data that c-Fos labels almost all CGRP neurons after LPS injection.

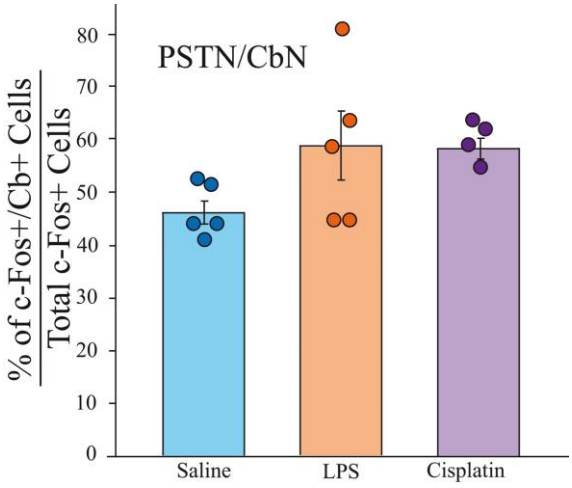

Figure 2. The number of dual labeled cells for c-Fos and calbindin was verified. Although, the treatment appeared to induce a slight increase of c-Fos expression in calbindin positive cells, the difference was not statistically significant. Saline n = 5, LPS n = 5, Cisplatin n = 4, One-way ANOVA, p = 0.1326; F = 2.441.

Supplemental data 11: Effect of alcohol or quinine ingestion on c-Fos expression in the PSTN/CbN.

The objective of this experiment was to verify the effect of an alcoholic intoxication on the c-Fos expression in the PSTN/CbN. The experiment was designed as to obtain a voluntary alcohol consumption from the rats. Administration of an alcohol solution by gavage or i.p. injection could have been envisaged but was not chosen as these procedures would have induced discomfort and/or pain, and we have seen that the PSTN/CbN responds to sickness conditions. Furthermore, we also had to take into account that the expression of c-Fos in PSTN/CbN is dependent of the hedonic nature of the aliment. We assumed that the oral sensation from a first-time ingestion of a 15% alcohol solution could be aversive. We therefore choose to run a parallel control experiment with a 0,3 mM quinine solution instead of 15% alcohol. Quinine is known to be disliked by rats because of its bitterness that is unpleasant. The detail of the experiment is described in the Sup. data 1.

1- Ingested quantities

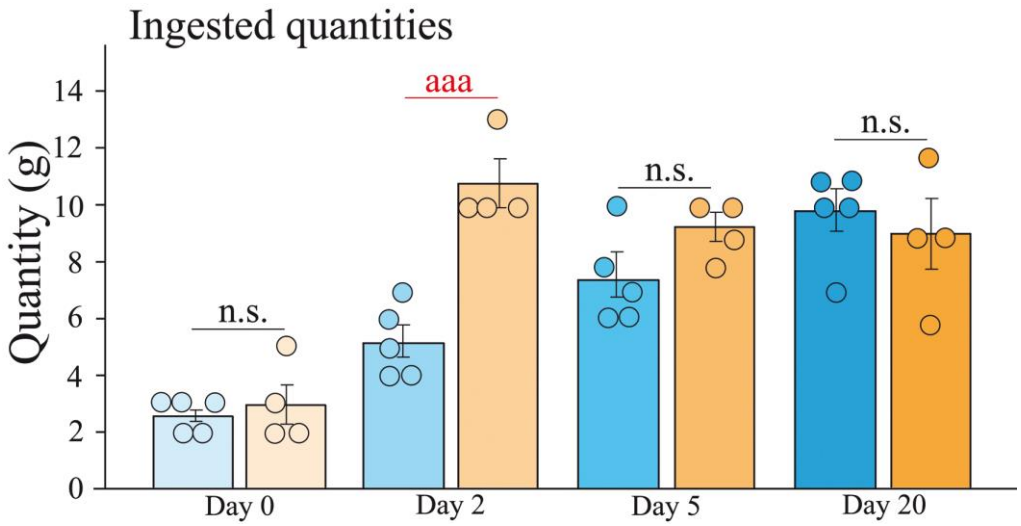

Figure 1. This graphic illustrates ingested quantities by the 8 groups of rats. Rats of the groups Day 0 drunk very little of the alcohol or quinine solutions, showing a clear neophobic response. However, already at Day 2, rats drunk quite normal amount of the quinine solution. This is easily understandable, as rats were strongly dehydrated and probably very thirsty. On the other hand, rats slowly habituated to the alcohol solution and only at Day 5 the amount of consummated alcohol solution was not statistically significant, even if it was slightly lower than that of quinine. Quinine n = 4, alcohol n = 5; two-way ANOVA, group x session interaction: p = 0.0008, F = 7.44; group x session treatment (alcohol or quinine): p = 0.0017, F = 12.

2- Double choice preference test Day 0 – Day 20

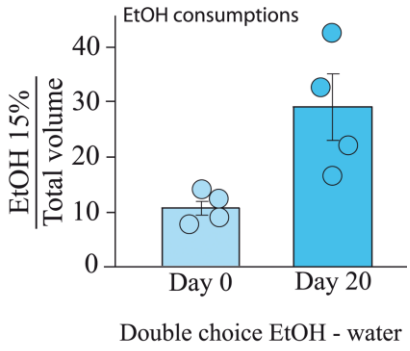

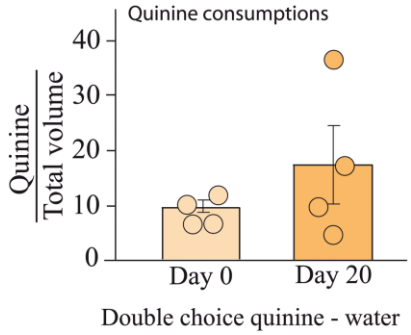

Figure 2. The double choice preference test indicates that both the alcohol and quinine solutions were equally aversive to the rats at

Day 0 (rats ingested 90% water for 10% EtOH or quinine). At Day 20, the animals were more familiar to the taste of the solutions, suggesting an absence of wariness toward alcohol or quinine, but still rats preferred water over alcohol or quinine solutions. Therefore, this result indicates that the habituation to the alcoholic solution cannot be associated with the development of an addiction, as the rat still drunk twice as much water (+/-70%) than the alcohol solution (+/- 30%).

3 - C-Fos expression in the PSTN/CbN

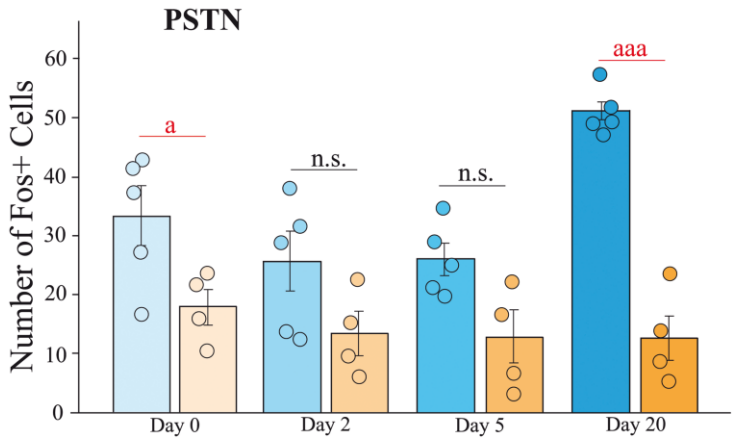

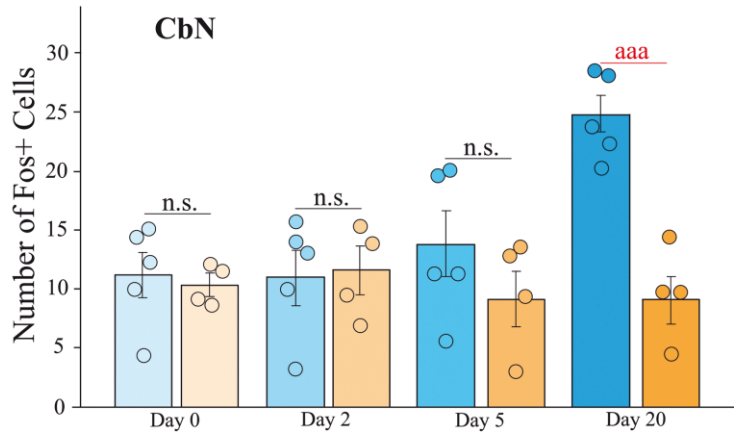

The figure 3 shows the results of the c-Fos expression associated with the alcohol or quinine consummation. Quinine n = 4, alcohol n = 5; for the PSTN, two-way ANOVA, group x session interaction: $p = 0.0057$, $F = 5.165$; group x session treatment (alcohol or quinine): $p < 0.0001$, $F = 51.07$. For the CbN, two-way ANOVA, group x session interaction: $p = 0.0026$, $F = 6.060$; group x session treatment (alcohol or quinine): $p = 0.0019$, $F = 11.68$.

-Quinine ingestion is never associated with an increase of c-Fos expression in the PSTN/CbN. This confirm our previous observation that, in normal (non-sick animals) the c-Fos response in the PSTN/CbN is associated to the hedonistic quality of the aliment and independent of the ingested volume. As quinine is not palatable, the c-Fos response is low.

-C-Fos expression level in the PSTN is always slightly higher in the alcohol group than in the quinine group maybe suggesting that the bitter taste of the quinine is more aversive than alcohol.

The slight increased preference for alcohol in the double choice preference test at Day 20 might reflect this. The c-Fos expression shows statistical significance only at Day 0 and might be associated to a neophobic response associated to a first exposure to the tastant, visible in the PSTN but not in the CbN.

-Finally, the increase in the c-Fos expression is very significant at Day 20 of the alcohol group in both the PSTN and CbN. This data is to be compared to the alcohol levels of animals of this group (close to 3 g/l see Fig. 3 in the main text). We have here a situation resembling to a binge drinking behavior as the animals have ingested voluntarily a large quantity of the alcoholic solution in a short period of time, resulting in a strong alcoholic intoxication. Considering that c-Fos expression does not increase in these nuclei in relation to the ingested volume and that animals do not show a strong preference for this beverage, as they would for sucrose for example, we may assume that the c-Fos expression results of the sickness consecutive to the alcohol intoxication. The pattern, with a strong expression in the CbN, as intense as in the LPS experiment, suggests this interpretation. However, the analysis of c-Fos expression in the parabrachial nucleus failed to show a strong expression in the dorsolateral/CGRP rich region of the nucleus. Therefore, in contrary than that in with LPS and cisplatin, the response is associated to a centrally induced sickness by alcohol (drunkenness) and do not strongly rely on peripheric information.

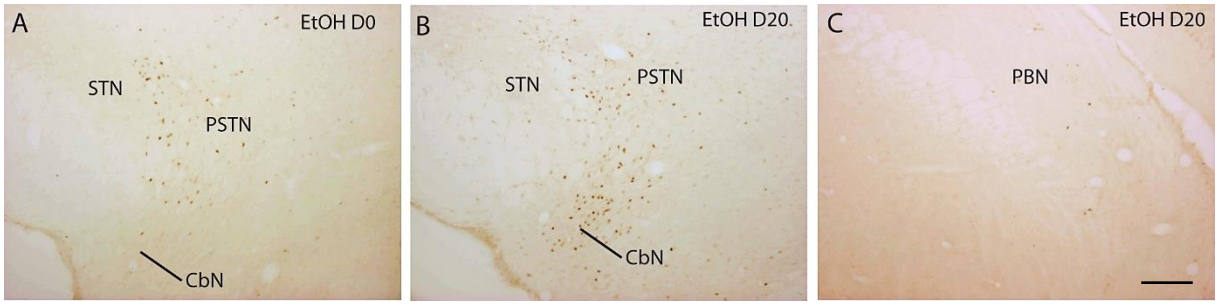

Figure 4. Photomicrographs illustrating the c-Fos labeling in the PSTN/CbN of a rat representative at D20 (A) and D0 (B) of rats from the ethanol groups. The picture in C illustrates the labeling in the parabrachial nucleus of a rat D20 ethanol group. Scale bar = 200 µm.

Supplemental data 12: The mouse PSTN.

The PSTN is signaled in the latest mouse brain atlases of Paxinos and of the Allen Institute *(25, 32)*. However, virtually nothing is found in the general literature about its anatomy and function. Therefore, it was necessary to identify here some of the major features of the nucleus in this species as mice are now a very common model for genetic and functional studies. Differences with the rat PSTN/CbN complex are observed, but by in large, the connections of the complex are similar in both species.

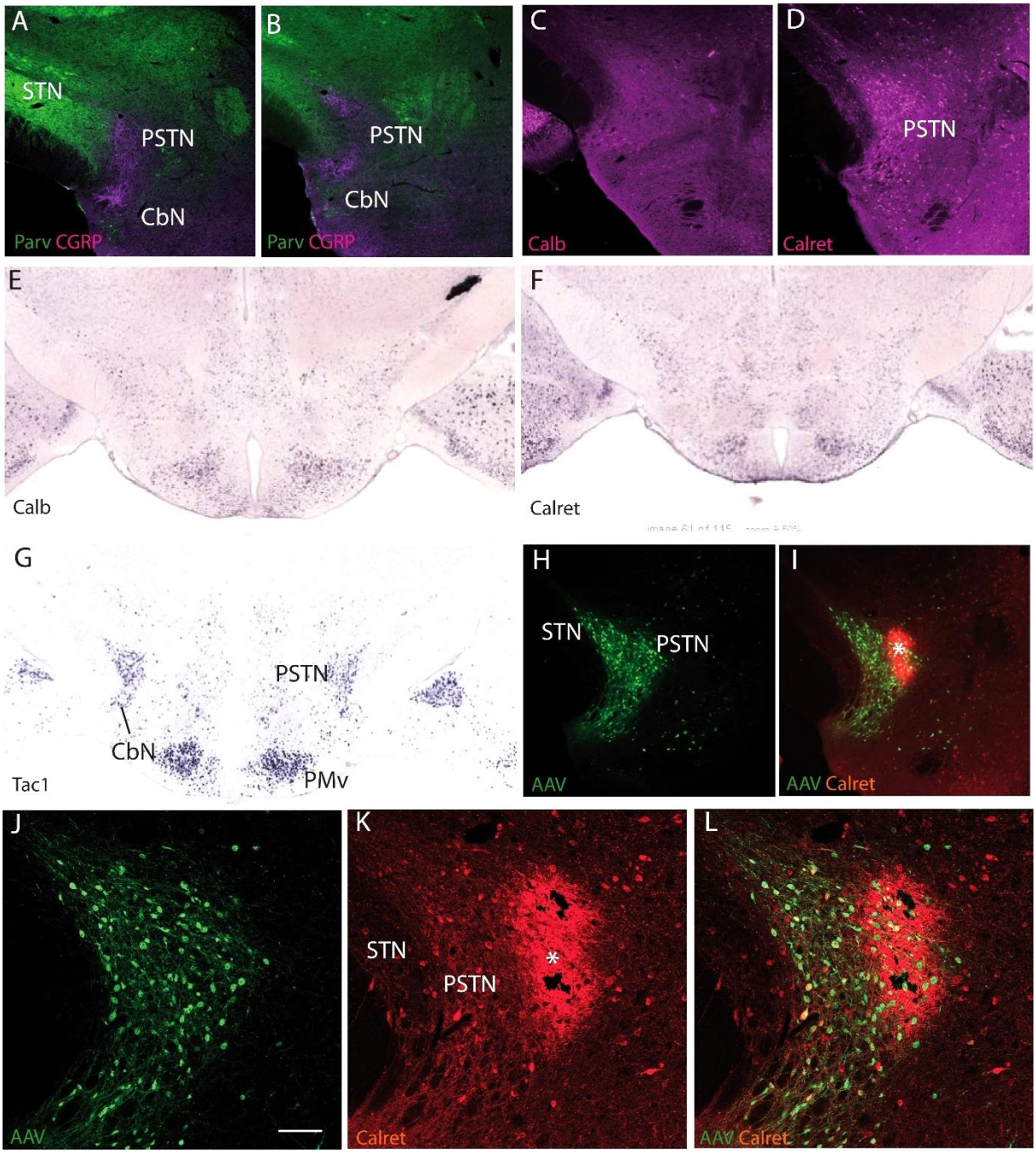

Figure 1. Photomicrographs to illustrate the neuro-chemical characteristics of the PSTN/CbN in the mouse. Scale bar = 200 µm in A to D and H, I; = 500 µm in E to G and = 100 µm in J to L.

A, B: dual immuno-fluorescence for CGRP and parvalbumin. Like in the rat, the PSTN/CbN receive a CGRP input, while STN receive intense parvalbumin projections as well as the medially adjacent Parvafox and NG that also contains parvalbumin cells.

C, D: Immunofluorescence for calbindin and calretinin. In contrary to that in the rat, a dense calbindin cell cluster is not found in the mouse. The calretinin expression seem similar and extends into the adjacent STN.

E, F: In situ hybridization images from the Allen Brain Atlas (with permission) for calbindin and calretinin. *In situ* data is coherent with our immunohistochemical observation.

G: Allen Brain Atlas in situ hybridization for *Tac1*. The expression of the *tac1* gene is very abundant in the mouse and extend in the CbN which is not labeled in the rat.

H-L: After injection of the AAV pCAG-FLEX-EGFP-WPRE. in the PSTN of TAC1-Cre mice, the PSTN and CbN are intensely labeled. Few cells are also stained outside the nucleus. Dual labeling for calretinin allow to see the lesion of the injection site (*). Some cells are double labeled for the AAV and calretinin. However, calretinin cells in the STN are do not contain the *tac1* gene expression and are not labeled for the AAV (J-L). Therefore, TAC1-Cre mice appear to be a good starting model to study the function of the nucleus through the DREAD technology.

Figure 2. AAV pCAG-FLEX-EGFP-WPRE injection in the PSTN allowed to identify the projections of the nucleus in the mouse. Like in the rat with the PHAL *(38)*, projections were observed in the BST and posterior SI (A, B) in the CEAm (B), the parabrachial nucleus (C) and in the nucleus of the solitary tract (D). Overall the projections of the PSTN^{tac1} cells are very similar to those described for the PSTN in the rat (E). Scale bar = 200 µm.

A, B, D, E: Photomicrographs illustrating the distribution of axons labeled axons after AAV injection in the PSTN (fig. 1 H-L). Sections are counterstained with a nuclear marker ([NeuroTrace® 640/660 Deep-Red Fluorescent Nissl Stain, 1:100, Invitrogen®, Thermo Fisher Scientific Cat#N21483, Lot1851967, RRID: AB_2572212).

C: Dual fluorescence to illustrate the innervation of the CEAm and caudal SI by axons while the CEAc that contains an intense CGRP innervation is not targeted by PSTN^{tac1} axons.

F: Line drawing to schematize the distribution of axons after the AAV injection in the PSTN.

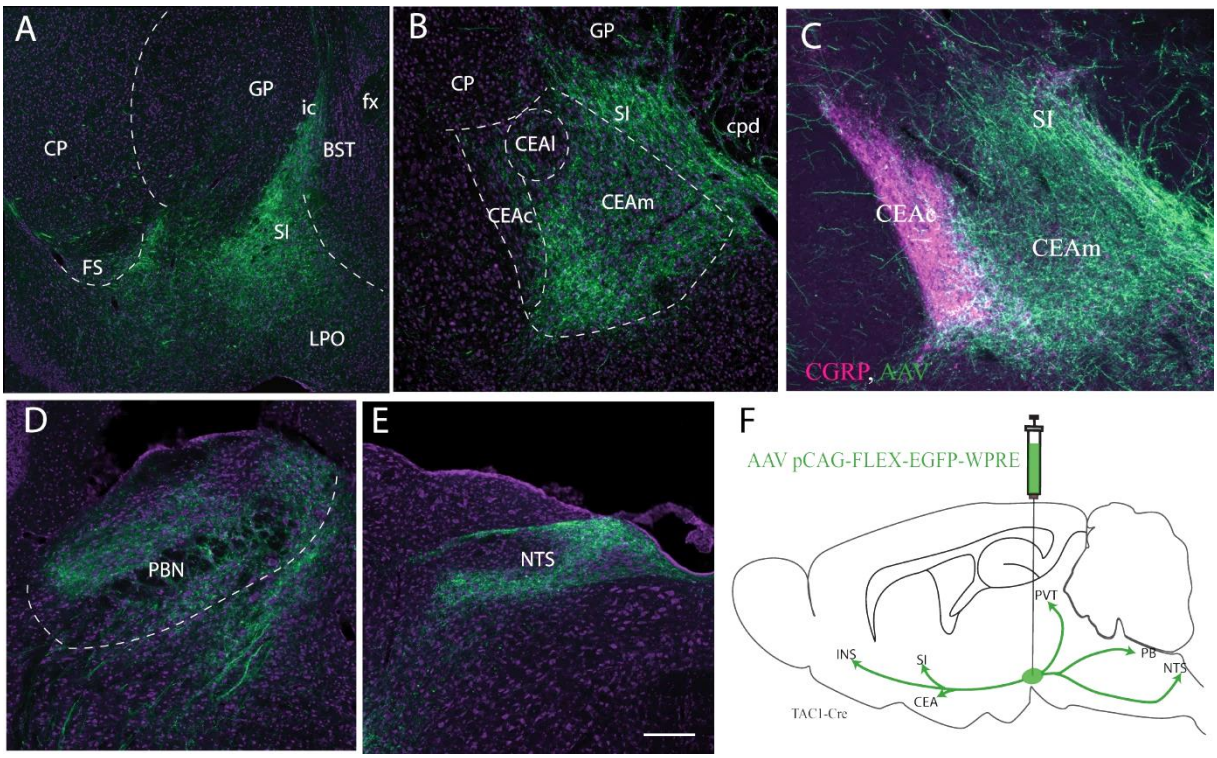

Figure 3. Connections of the mouse PSTN next.

A: PRV152 and 2001 were injected in the CEA to analyze the specificity of the projections from the PSTN to the CEA in TAC1-cre mice. Survival times were short (1 or 2 days) and only resulted in a dense accumulation of the virus within the border of the PSTN/CbN but not adjacent structures, suggesting that the PSTN is part of a network specifically involving the PSTN in the premammillary region of the hypothalamus.

B, C: After injection of the PRV152 (microbeads deposit) in the CEA, a dense cluster of cells is specifically observed in the PSTN.

D, E: Injection of the PRV2001 in the CEA of a TAC1-Cre mice (B). Many cells are labeled in the PSTN and CbN.

C-E: After injection of the retrograde tracer cholera toxin in the PSTN of a mouse, many cells are observed in the INS as well as in the CEAm and caudal SI, while the CEAc and CEAl are not labeled. This confirm the bidirectional nature of the connections between the CEAm/SI and the PSTN/CbN also observed in the rat. Scale bar = 500 µm in B, C, E and = 100 µm in D, F to H.

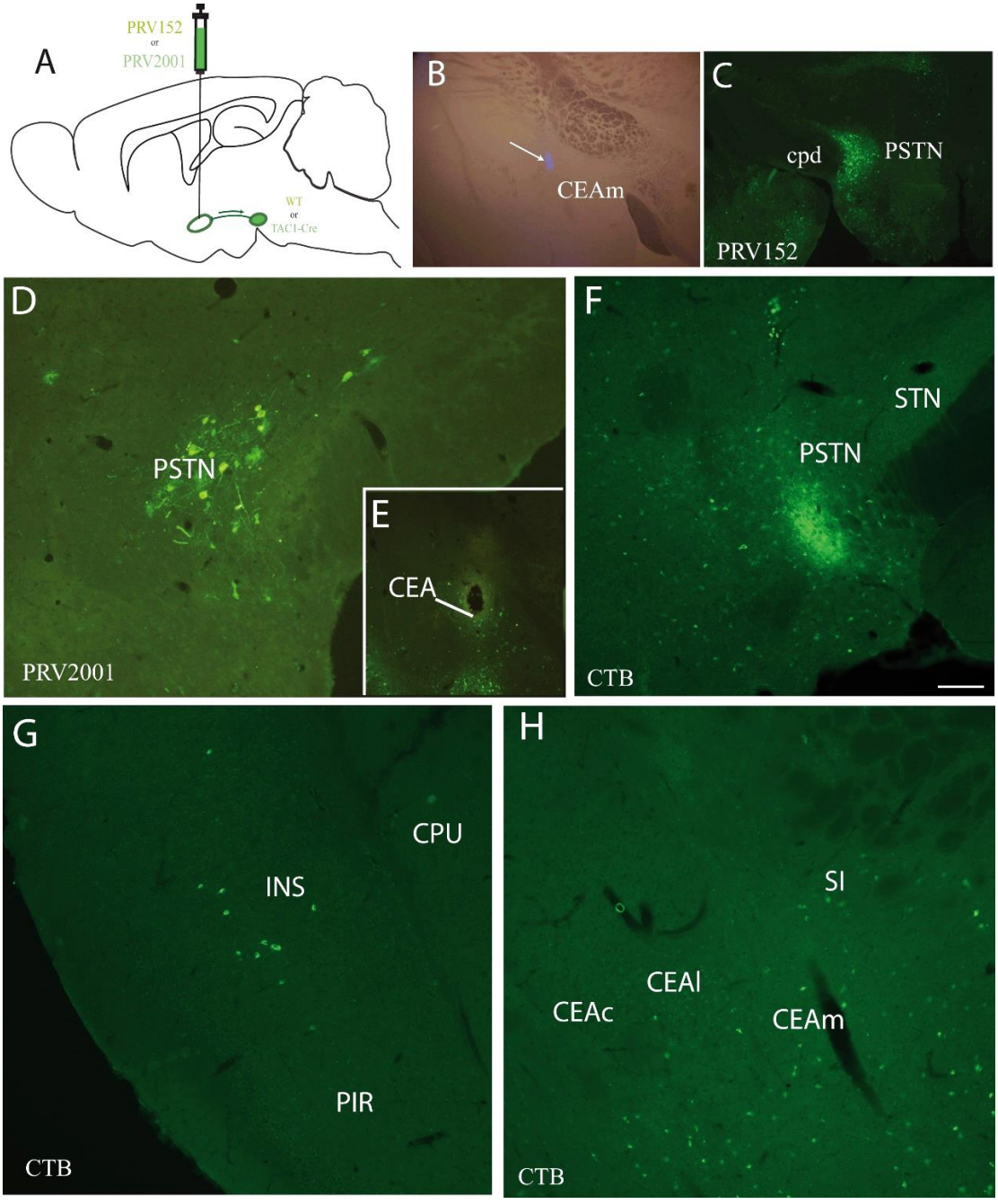

Images from the Allen Brain Institute *(25)* also confirmed the anatomical observation made in the rat. Overall the INS, caudal SI and CEAm send intense projections that specifically target the PSTN/CbN complex, but not surrounding structures such as the STN. Therefore, the PSTN is part of a network involving these telencephalic structures.

Figure 4. Images from the Allen Brain Atlas mouse connectivity.

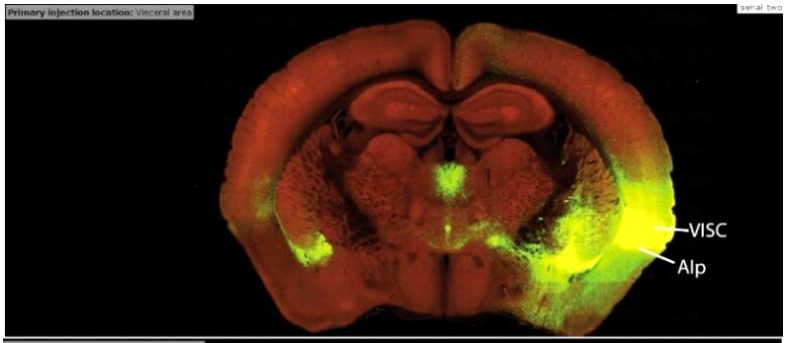

Injection site in the VISC but that obviously involves the AIp as well, as indicated by the anterograde distribution ion the OT and in the PVT of the thalamus.

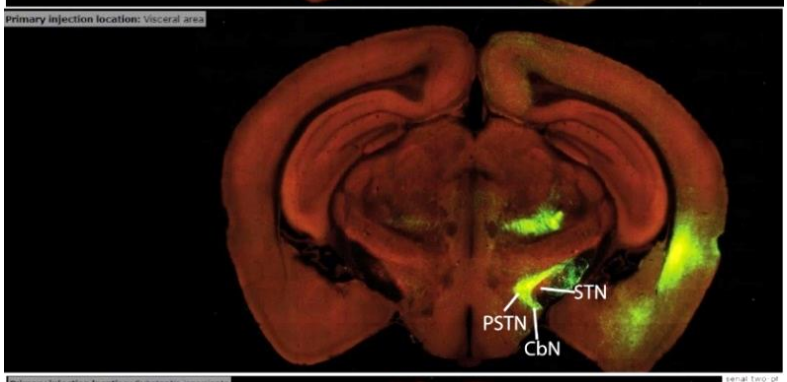

An intense innervation of the PSTN/CbN is observed. In the rat, the AIp is the main input to the PSTN. Nevertheless, the image illustrates that the STN is not innervated.

Injection site in the SI.

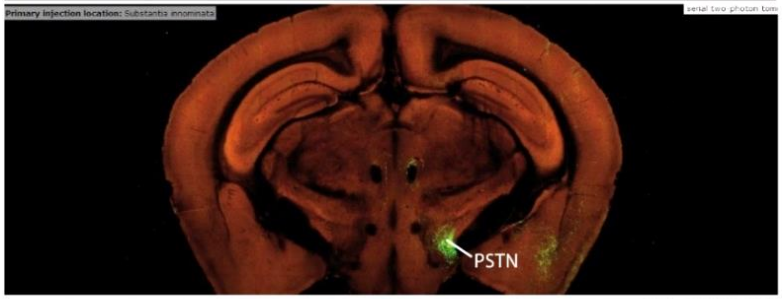

SI innervate the PSTN. This is also a confirmation of the rat data.

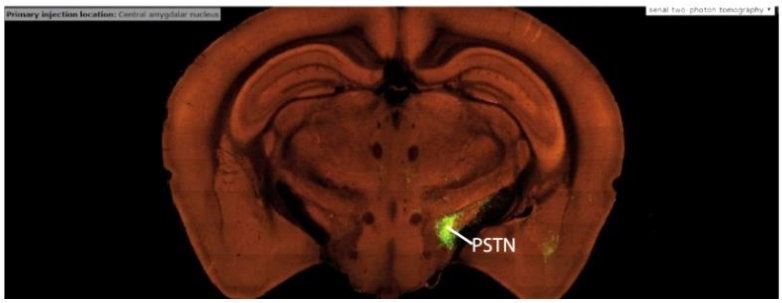

Finally, after an injection in the CEA (injection site not shown), the PSTN is also the main target in the hypothalamus for the efferent axons from this nucleus.

Supplemental Data 13: Additional DREADD results.

Figure 1. A-D: Photomicrographs of additional AAV injection sites in the PSTN. C-F: Photomicrographs of two misplaced injection sites dorsal to the PSTN in the zona incerta (ZI). G: Inhibition of TAC1-Cre neurons in the PSTN did not significantly affect the quantity of food ingestion. Controls n = 12; DREADD n = 18; DREADD M.P. n = 5; One-way ANOVA and Bonferroni's multiple comparison test, p = 0.6135, F = 0.4947. H: No difference on the forced swim test was obtained. Several parameters were analyzed: latency before first immobilization, duration of immobilization and total time of swimming. Controls n = 6; DREADD n = 9; DREADD M.P. n = 3; Two-way ANOVA and Bonferroni's multiple comparison test, p = 0.9146, F = 0.09. I: Open field test performances were also not affected by the DREADD inhibition of TAC1 neurons. Controls n = 6; DREADD n = 9; DREADD M.P. n = 3; two-way ANOVA and Bonferroni's multiple comparison test, For the "Time": p = 1, F = 0. For the "Distance": p = 0.1350, F = 2.09. Scale bar = 200 µm.

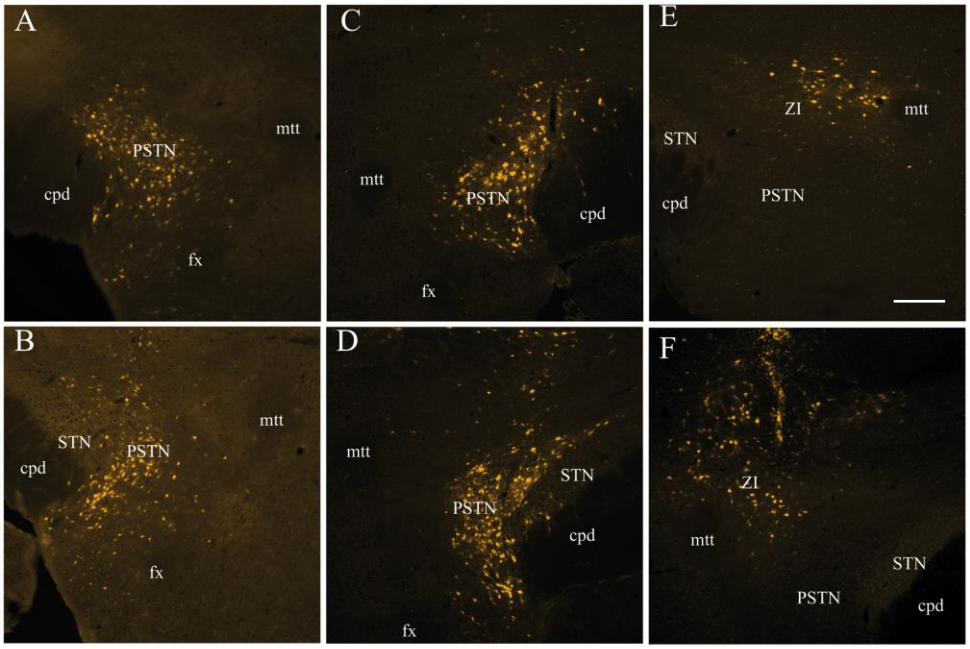
A
PSTN
mtt
cpd
fx
C
mtt
PSTN
cpd
fx
E
ZI
mtt
STN
cpd
PSTN
B
STN
PSTN
mtt
cpd
fx
D
mtt
STN
PSTN
cpd
fx
F
ZI
mtt
STN
PSTN
cpd

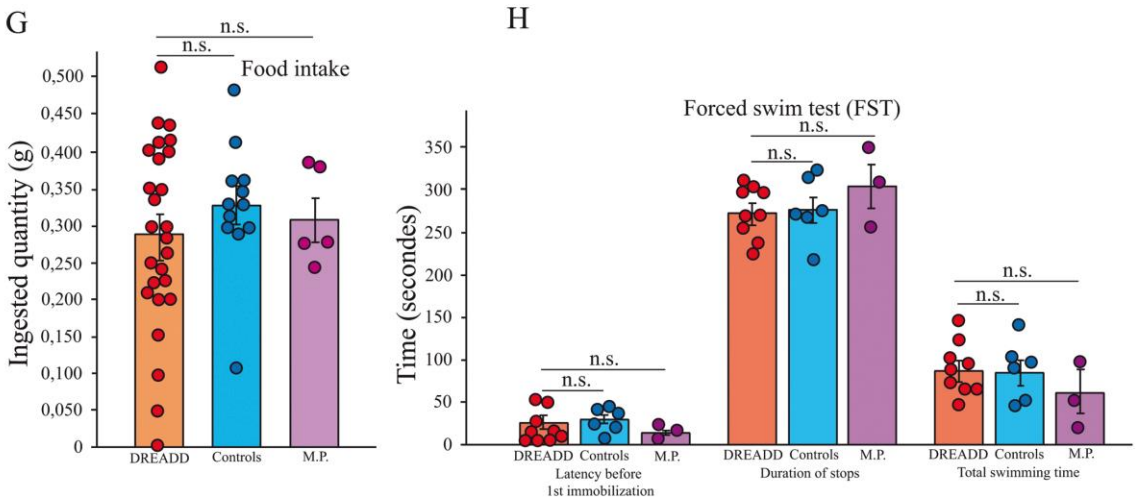
G
Food intake
Ingested quantity (g)
0,500
0,450
0,400
0,350
0,300
0,250
0,200
0,150
0,100
0,050
0
n.s.
n.s.
DREADD
Controls
M.P.
H
Forced swim test (FST)
Time (secondes)
350
300
250
200
150
100
50
0
n.s.
DREADD Controls M.P.
Latency before 1st immobilization
Duration of stops
Total swimming time

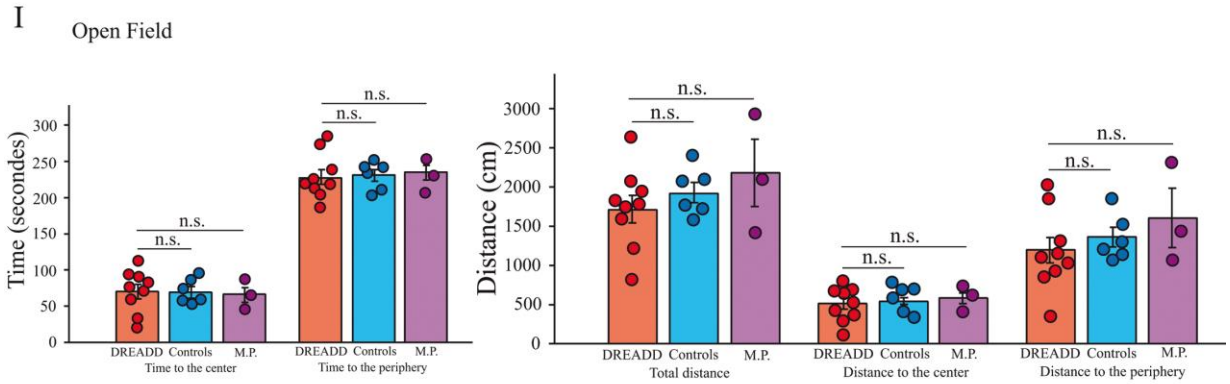
I
Open Field
Time (secondes)
300
250
200
150
100
50
0
n.s.
DREADD Controls M.P.
Time to the center
Time to the periphery
Distance (cm)
3000
2500
2000
1500
1000
500
0
Total distance
Distance to the center
Distance to the periphery

Données complémentaires

En plus des données décrites dans l'article n°4, quelques observations supplémentaires ont été obtenues et sont brièvement exposées ci-après. Ces résultats complémentaires sont présentés car ils nourriront certains aspects spécifiques de la discussion.

1. Patrons d'expression de la protéine c-Fos dans le CEA

L'expression de la protéine c-Fos a été quantifiée chez le rat dans les trois principales divisions du CEA (capsulaire, latérale et médiane) identifiées dans les atlas (Swanson, 2004; Paxinos & Watson, 2013) dans toutes les conditions expérimentales décrites précédemment (néophobie, malaise et intoxication à l'alcool). Il ne s'agit pas ici d'entamer une analyse fine de ces résultats, qui nécessiteront d'autres investigations, mais simplement de constater les différences dans les profils d'expression de la protéine c-Fos dans chacune des parties du CEA. Les amplitudes des réponses sont particulièrement élevées dans le CEAl en lien avec les états de malaise. Le CEAc réagit beaucoup plus dans le cas d'une intoxication alcoolique (Figure 29). En fait, le profil d'expression de la protéine c-Fos est similaire dans le CEAc et le CEAl (Figure 30) à celui décrit dans l'article pour le complexe PSTN/CbN. Au contraire, le profil d'expression de la protéine c-Fos dans le CEAm (Figure 31) présente des amplitudes de réponses assez faibles, même si l'analyse statistique (ANOVA) montre qu'elles sont significatives. L'expression de la protéine c-Fos a tendance à augmenter dans toutes les conditions expérimentales par rapport à la condition "NaCl" (Contrôle).

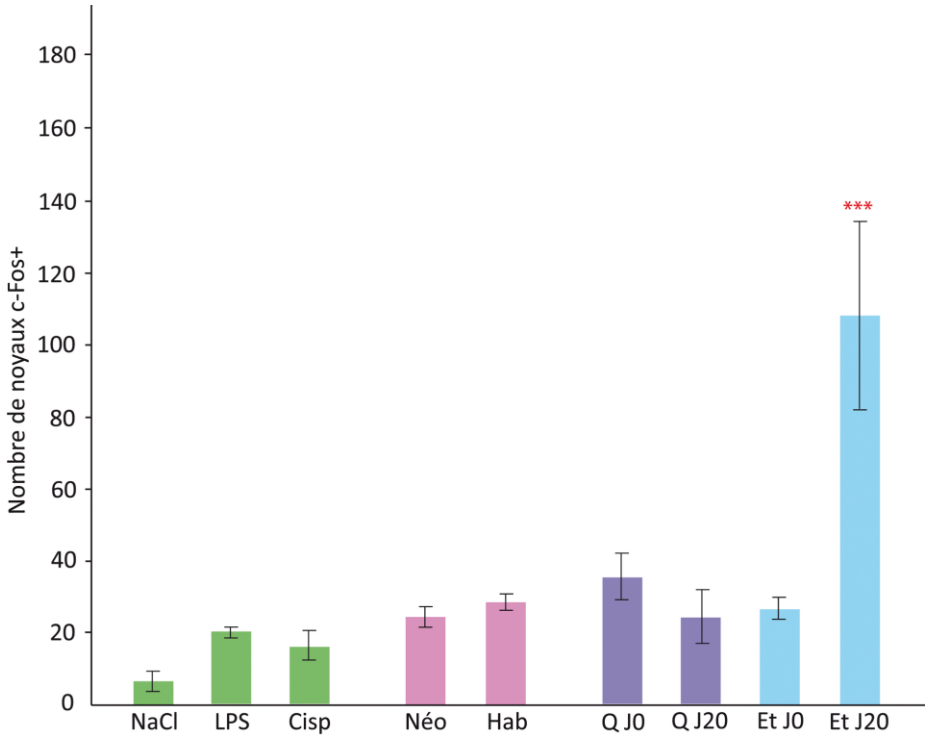

Figure 29. Diagramme de l'expression de la protéine c-Fos dans la division capsulaire du CEA dans différentes conditions expérimentales.

A : alcool ; Cisp : cisplatine ; Hab : habitué ; J : jour ; LPS : lipopolysaccharide ; Néo : néophobique ; Q : quinine.

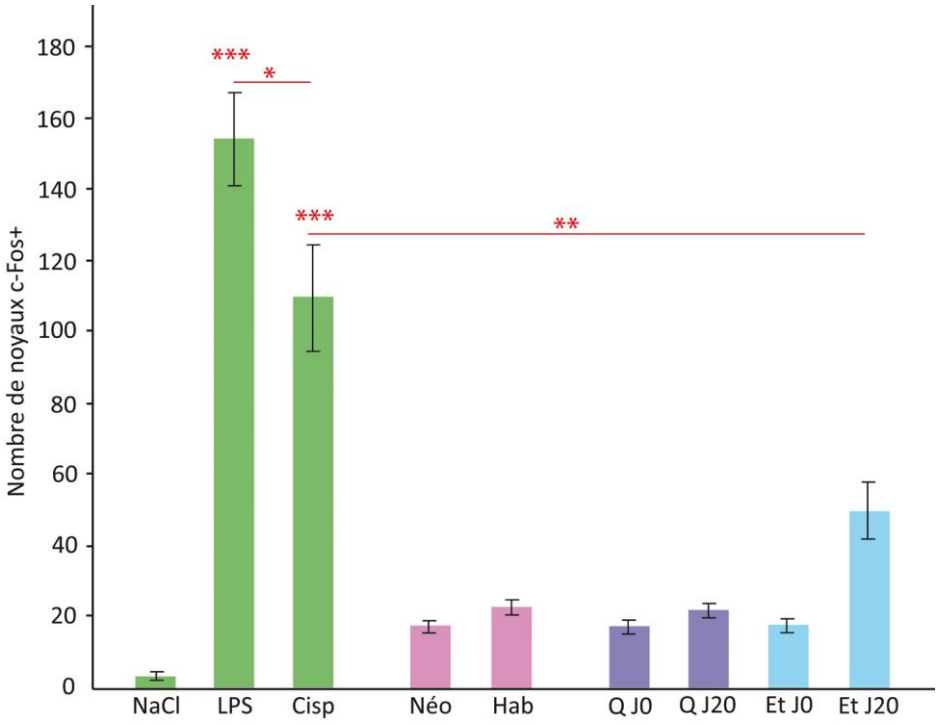

Figure 30. Diagramme de l'expression de la protéine c-Fos dans la division latérale du CEA dans différentes conditions expérimentales.

A : alcool ; Cisp : cisplatine ; Hab : habitué ; J : jour ; LPS : lipopolysaccharide ; Néo : néophobique ; Q : quinine.

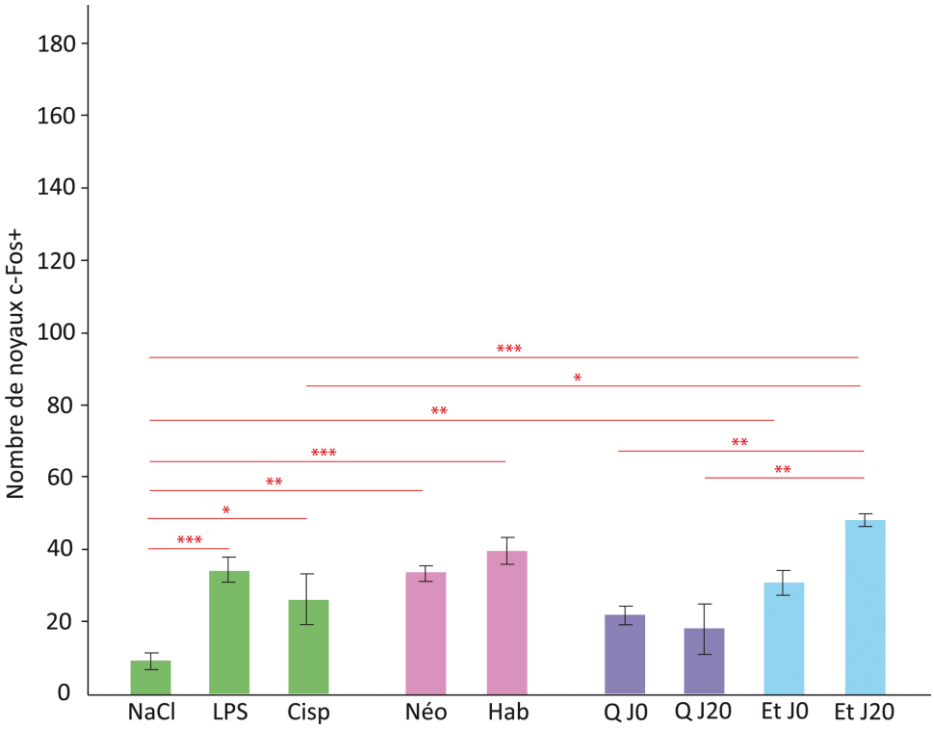

Figure 31. Diagramme de l'expression de la protéine c-Fos dans la division médiane du CEA dans différentes conditions expérimentales.

A : alcool ; Cisp : cisplatine ; Hab : habitué ; J : jour ; LPS : lipopolysaccharide ; Néo : néophobique ; Q : quinine.

Les diagrammes des figures 29 à 31 sont utiles pour comparer l'intensité de l'expression de la protéine c-Fos globalement dans chaque partie. Cependant, l'analyse histologique (Figure 32) révèle que cette expression est souvent restreinte à des groupes cellulaires spécifiques au moins dans le CEAl, i et le CEAc. Le groupe de rats exposé 20 jours à la solution d'éthanol à 15% ("alcool J20") (A-A", D) présente une condensation de noyaux dans la partie ventrale de la région antérieure du CEAc, spécifique à cette condition expérimentale. L'ingestion d'une solution sucrée à 20% (B-B", E) et l'injection de LPS (C-C", F) induisent une expression intense de la protéine c-Fos dans la partie latérale du CEA. Mais cette expression correspond au CEAi dans le cas "solution sucrée" et dans lequel aucun neurone c-Fos positif n'a été observé dans le groupe "LPS". D'autre part, l'injection de LPS induit une expression de la protéine c-Fos intense dans la région postérieure du CEAl. Cette région du CEAl est faiblement marquée dans le groupe "solution sucrée", mais contient quelques cellules c-Fos dans le groupe "alcool J20".

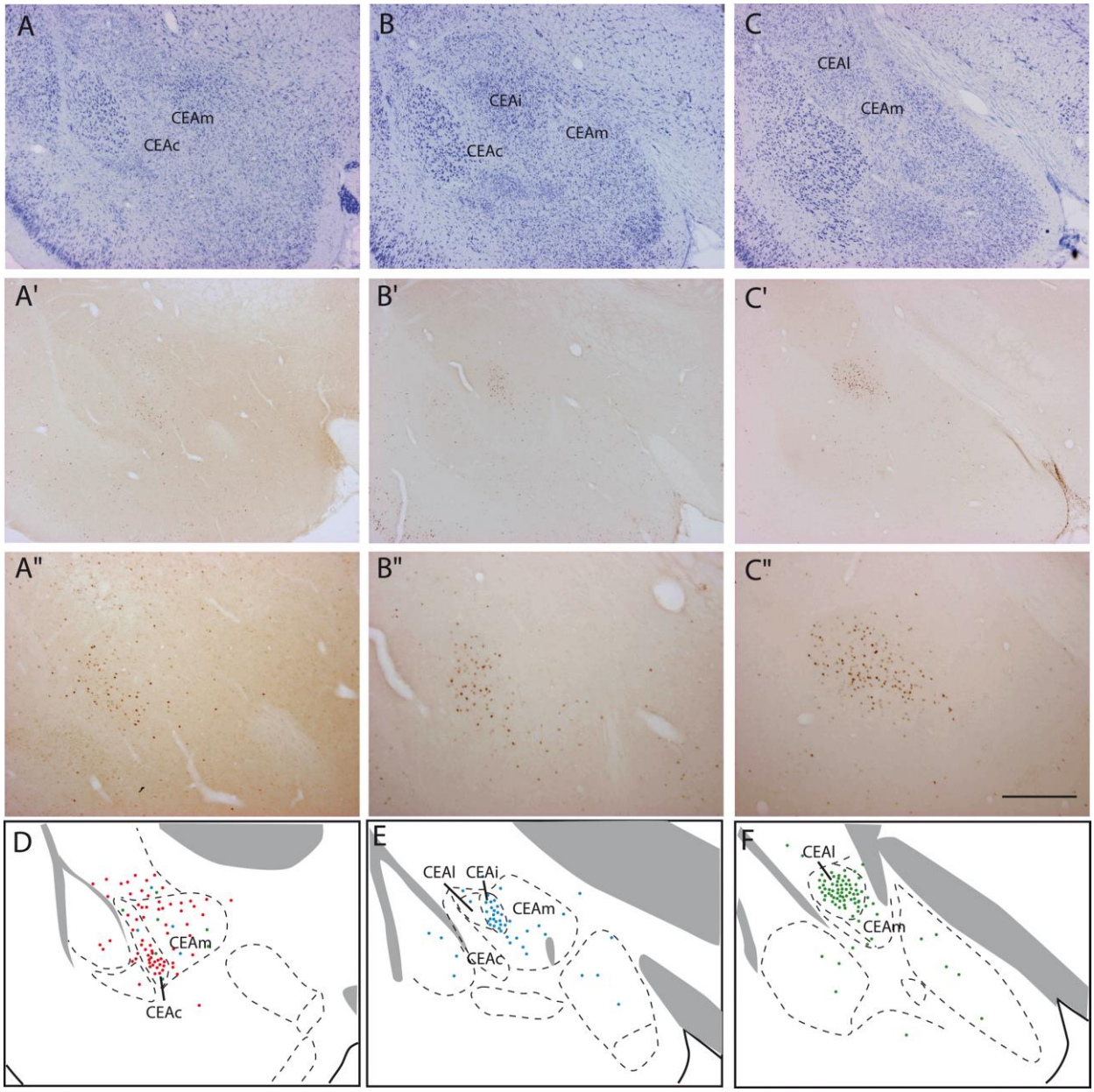

Figure 32. Photographies et schémas illustrant la distribution des noyaux c-Fos positifs dans le CEA dans différentes conditions expérimentales (néophobie, malaise et intoxication à l'alcool).

Les photographies (A, A" – C, C") et les cartographies (D, E, F) illustrent l'expression de la protéine c-Fos dans le CEA après intoxication alcoolique (A, A' et A"), ingestion de solution sucrée (B, B' et B") et malaise induit par injection i.p. de LPS (C, C' et C"). Barre d'échelle = 500 µm in A to C'; = 250 µm in A" to C".

CEAc/i/l/m : noyau central de l'amygdale, partie capsulaire/intermédiaire/latérale/médiane.

Ces données préliminaires devront par la suite être complétées par l'identification des types cellulaires exprimant la protéine c-Fos. Néanmoins, elles confirmeront déjà la très grande hétérogénéité du CEA.

2. Projections des neurones à NT du PB dans le CEA et le complexe PSTN/CbN

Le LHA reçoit des informations convergentes de l'INS et du CEA (Yasui *et al*, 1991; Bourgeais *et al*, 2001; González *et al*, 2016) et serait donc un centre intégrateur des informations télencéphaliques. Dans les publications n°1 et n°3, plusieurs régions du LHA ont été identifiées comme cibles préférentielles du CEA, en particulier le complexe PSTN/CbN (Barbier *et al*, 2017, 2018b). Ce complexe, tout comme le CEA, reçoit des projections directes de l'INS (Chometton *et al*, 2016; Schiff *et al*, 2018) ainsi que des projections des neurones à CGRP du PB impliquées dans des processus viscéraux et nociceptifs (Yamamoto *et al*, 1990; Carter *et al*, 2013, 2015; Campos *et al*, 2016, 2018; Chen *et al*, 2018; Palmiter, 2018). Les projections des neurones à CGRP du PB se distribuent principalement dans les parties latérale et capsulaire du CEA. Dans le LHA, des collatérales de ces axones délimitent clairement le complexe PSTN/CbN (Chometton *et al*, 2016). Dans la publication n°2 concernant la chémoarchitecture du CEA chez le rat, il avait été repéré un marquage NT intense dans la région ventrale du CEAc (Barbier *et al*, 2018a). Des marquages multiples ont d'ailleurs montré que le CEAc ventral est innervé par des axones contenant à la fois CGRP et NT, tandis que la partie dorsale du CEAc et le CEAl sont innervés par des projections CGRP mais ne contenant pas NT. Le PB contient des neurones CGRP dont certains coexpriment NT ; il a donc été réalisé chez des souris NT-Cre des injections de traceur viral antérograde dans le PB. La distribution des projections à NT dans le CEA et le LHA a été identifiée (Figure 33). Il a été observé que le signal antérograde occupe tout le CEAc et ne se limite pas à sa partie ventrale, contrairement au signal NT détecté par immunohistochimie chez le rat. Cette observation illustre donc une différence entre rat et souris dans l'étendue des projections CGRP/NT dans le CEAc.

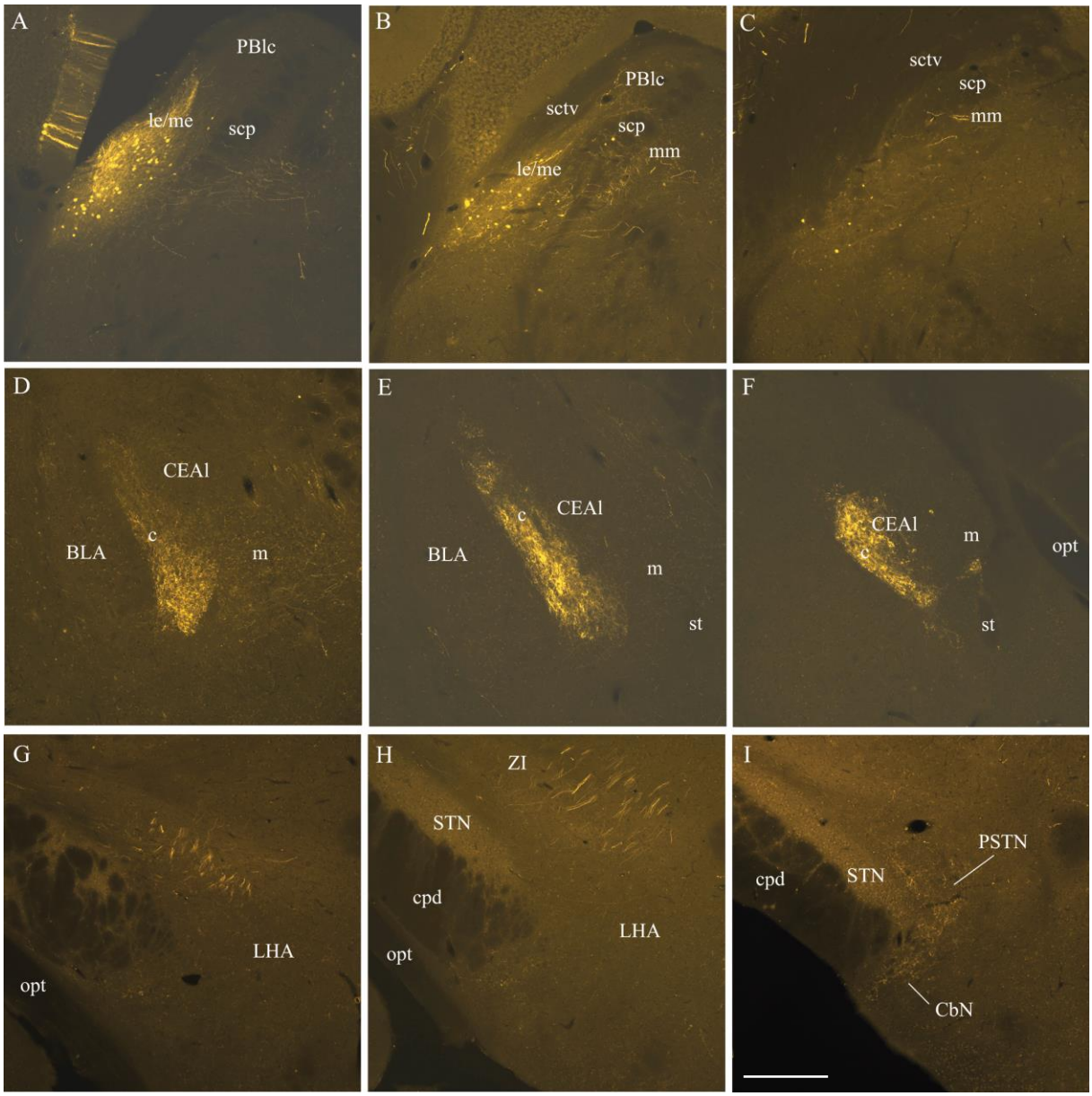

Figure 33. Photographies du site d'injection dans le PB et des projections des neurones à NT dans le CEA et l'hypothalamus.

Ces photographies illustrent la distribution des projections des neurones à NT après injection de virus AAV (AAV.CAG.LSL.tdTomato) dans la partie latéro-médiane du PB chez une souris NT-Cre. Les niveaux de coupes ci-dessus passent par le site d'injection (A-C), le CEA (D-F) et l'hypothalamus (G-I). Le CEAc est intensément innervé par les axones NT (E). Des axones de passage sont visibles dans la partie dorsale du LHA et dans la zona incerta (G et H). Une innervation modeste du PSTN est observée sur la photographie I. Barre d'échelle = 500 µm.

BLA : noyau basolatéral de l'amygdale ; CbN : noyau calbindine ; CEAc/l/m : noyau central de l'amygdale, partie capsulaire/latérale/médiane ; cpd : pédoncule cérébral ; opt : tractus optique ; LHA : aire hypothalamique latérale ; PBlc/le, me/mm : noyau parabrachial, partie centrale/externe de la division latérale, partie externe/médiane de la division médiane ; PSTN : noyau parasousthalamique ; scp : pédoncule cérébelleux supérieur ; sctv : tractus spinocérébelleux ventral ; st : strie terminale ; STN : noyau sousthalamique ; ZI : zona incerta.

DISCUSSION

Les résultats obtenus lors de ce travail de thèse mettent en évidence l'existence d'un réseau impliquant des structures télencéphaliques et de l'hypothalamus postérieur qui est comparable dans son organisation à certains de ceux décrits pour les "noyaux de la base". Dans une première étape, le PSTN a été reconnu comme la cible majeure des projections issues du CEA. Par la suite, un réseau a été identifié, mettant en jeu différentes aires de l'INS, les sous-divisions du CEA dans le télencéphale basal et le complexe PSTN/CbN dans l'hypothalamus prémamillaire. Le rôle du complexe PSTN/CbN a ensuite été exploré, notamment en lien avec le contrôle de la prise alimentaire et l'état de maladie.

I. Organisation anatomique du réseau impliquant le complexe PSTN/CbN

L'étude plus approfondie du réseau impliquant le complexe PSTN/CbN a été menée en deux étapes : tout d'abord, il a été tenté de comprendre l'organisation des liens entre le CEA et le complexe PSTN/CbN. D'autres noyaux de l'amygdale ont alors aussi attiré notre attention tel que le BMAa. Cette première partie a été étendue à l'analyse des connexions du CEA dans le LHA et a permis l'obtention de données originales concernant l'anatomie du CEA chez le rat et la souris. Dans un second temps, il s'agissait d'élargir le champ de nos investigations afin d'y inclure l'INS. Les aspects fonctionnels en lien avec cette seconde partie seront discutés dans le chapitre suivant (II).

1. Organisation des connexions entre le CEA et le complexe PSTN/CbN

a. Le PSTN est la cible majeure de la partie médiane du CEA

a.1. Organisation des projections du CEA dans le LHA

Des connexions entre le CEA et le LHA avaient déjà été observées par de nombreux auteurs (Krettek & Price, 1978; Ottersen, 1980; Veening *et al*, 1982, 1984; Ono *et al*, 1985; Gray *et al*, 1989; Gonzales & Chesselet, 1990; Petrovich & Swanson, 1997; Bourgeais *et al*, 2001; Tsumori *et al*, 2006; Oka *et al*, 2008; Shirasu *et al*, 2011; Niu *et al*, 2012; Chometton *et al*, 2016). Cependant, la cible majeure de ces efférences dans le LHA postérieur n'avait encore jamais été clairement décrite. Il a été montré dans l'introduction que le LHA n'est pas une structure homogène. Les travaux anatomiques antérieurs à la découverte du PSTN faisaient parfois référence aux aires postéro-latérales du LHA, terme vague mais il n'y avait pas d'alternative. Le travail de Chometton *et al* (2015, 2016) puis le nôtre (Barbier *et al*, 2017) place définitivement le PSTN comme un acteur incontournable dans le réseau des projections descendantes depuis le CEA. Ce noyau est effectivement la structure la plus innervée de l'hypothalamus par le CEA dans son ensemble et l'intensité de cette innervation est similaire à celle relevée dans d'autres territoires cibles mais extra-hypothalamiques tels que le NTS

(voir la discussion de Barbier *et al*, 2017). Cependant d'autres secteurs du LHA, comme le LHAs, le LHAd et plus encore le LHAppstn sont aussi la cible d'afférences du CEAm. L'intensité de ces projections est moindre, voire parfois modeste, ce qui ne préjuge pas de leur importance fonctionnelle. Néanmoins, ces projections respectent certaines des divisions chémoarchitectoniques du LHA tubéral (Barbier *et al*, 2018b) (voir page 50 de l'introduction). Ainsi, chez le rat, les divisions définies par J.D. Hahn et L.W. Swanson correspondent aussi à des patrons de distribution d'afférences issues de structures spécifiques, renforçant l'hypothèse de ces auteurs qu'elles correspondent à des entités distinctes possiblement impliquées dans des fonctions spécifiques. Dans l'introduction, l'intérêt que présentait l'identification de divisions basée sur des observations chémoarchitectoniques a été modulé. Il est vrai que la distribution de ces marqueurs "spécifiques" varie suivant les espèces. Ceci a encore été confirmé pour le complexe PSTN/CbN qui présente des différences significatives entre rat et souris et dont certaines sont décrites dans les données supplémentaires de l'article 4 *("Supplemental data 12"* page 181). Néanmoins, l'analyse de ces marqueurs, combinée à la distribution d'afférences depuis des structures bien identifiées, peut permettre de mieux comprendre l'organisation de régions par ailleurs peu différenciées d'un point de vue cytoarchitectural. Un exemple classique dans la littérature concerne l'identification des compartiments associés au "patch" ou à la matrice dans le striatum. Ces derniers ne sont identifiables que par des marqueurs neurochimiques dont la distribution varie entre les espèces mais dont les afférences d'origines corticales sont conservées (Graybiel & Ragsdale, 1978; Gerfen *et al*, 1985; Gerfen & Wilson, 1996). Appliquée au LHA et notamment au LHA tubéral, une telle approche s'avérera très utile pour identifier et comparer entre les espèces certaines divisions du LHA qu'il sera souvent très difficile d'identifier par ailleurs.

La région prémamillaire du LHA est beaucoup mieux différenciée d'un point de vue cytoarchitectural que le LHA tubéral. Notre étude a confirmé que chacune de ces divisions est irriguée par un tractus spécifique. Cette organisation se distingue clairement encore une fois de celle du LHA tubéral et renforce l'hypothèse de régions anatomiques différentes.

a.2. Trajet des projections sur le complexe PSTN/CbN et organisation du LHApm

Les résultats publiés en 2016 par notre équipe (Chometton *et al*, 2016) ont donc été confirmés et approfondis dès la première publication par des injections de traceurs PHAL et FG réalisées dans l'amygdale et le PSTN respectivement (Barbier *et al*, 2017). Dans le LHA postérieur, le complexe PSTN/CbN a été montré comme étant la principale cible hypothalamique des projections descendantes depuis le CEAm et le BMAa via deux voies bien différenciées à travers le mfb : une voie ventrale depuis le CEAm et le BMAa qui a été nommée vlah, en référence au vlt adjacent et une voie dorsale depuis le CEAm.

La voie ventrale est connue puisque J.G. Veening et ses collègues avaient déjà observé que des projections télencéphaliques, en particulier de l'amygdale, empruntent le mfb en passant latéralement et ventralement dans le LHA (Veening *et al*, 1982, 1984), mais sans en illustrer de trajet spécifique. Le PSTN et le CbN n'étaient pas identifiés, mais des études de traçage antérograde rapportaient des projections denses dans la partie caudale du LHA (Krettek & Price, 1978; Gonzales & Chesselet, 1990; Bourgeais *et al*, 2001). L'intérêt de la caractérisation du vlah en tant que tractus différencié réside dans la compréhension qu'il permet, lorsqu'il est comparé à d'autres tractus voisins, de l'organisation des projections du télencéphale dans la région prémamillaire. En effet, comme indiqué dans la discussion de M. Barbier *et al* (2017), les projections massives du BMAa, mais aussi reportées pour la partie antérieure du noyau cortical amygdalien (COAa) par ce tractus, dénotent la nature olfactive de certaines des informations qui y transitent. Le COAa reçoit des projections du bulbe olfactif par le tractus olfactif latéral et le BMAa reçoit des projections du COAa ainsi que du cortex piriforme. Le vlah est voisin du vlt. Le vlt, bien repéré par marquage parvalbumine (Chometton *et al*, 2016), est originaire du tubercule olfactif. Dans la région prémamillaire, ce trajet innerve le NG relié au Parvafox. Ainsi, deux tractus indépendants relaient des informations olfactives issues des tubercules olfactifs (vlt) ou du cortex amygdalien (vlah) et irriguent pour l'un, le Parvafox et le NG et pour l'autre, le CbN et le PSTN. Il est a noté que ces noyaux occupent le LHApm alors que dans la région médiane se localise le PMv. Ce dernier noyau reçoit des informations phéromonales transitant par la strie terminale depuis le noyau médian de l'amygdale. Ainsi, ces premières observations pointaient déjà un début d'organisation anatomique liant un noyau de l'hypothalamus médian et d'autres de l'hypothalamus latéral. Ces observations sont illustrées dans la figure 20 de notre premier article (Barbier *et al*, 2017).

Le tractus dorsal était uniquement emprunté par les projections du CEA dans notre étude et quasi uniquement depuis le CEAm. A la différence du CEAm, le CEAc et le CEAl projettent peu dans le LHA postérieur (Gray *et al*, 1989; Petrovich & Swanson, 1997). En revanche, des projections comparables à celles du CEAm ont été décrites des régions dorsales postérieures de la SI, adjacentes au CEAm, qui contiennent des neurones également à l'origine d'une innervation intense du complexe PSTN/CbN (Grove, 1988; Spooren *et al*, 1991; Groenewegen *et al*, 1993; Allen Institute, 2004; Barbier *et al*, 2017).

En comparant les données de la littérature, il a été remarqué que certains auteurs ne décrivent parfois que l'un ou l'autre des deux trajets après injections de traceur antérograde dans le CEAm (Gonzales & Chesselet, 1990; Bourgeais *et al*, 2001; Shirasu *et al*, 2011). En fait, ces différences d'observations s'expliquent par la localisation respective des sites d'injections dans le CEAm selon qu'ils soient plus ou moins rostraux ou caudaux. Ils illustrent surtout que le CEA est un noyau encore incomplètement caractérisé bien que faisant l'objet d'un nombre important de travaux.

Ces dernières observations ont attiré notre attention et ont mené à l'étude plus approfondie du CEA. En effet, afin de comprendre l'organisation du réseau impliquant le PSTN, il était indispensable de s'intéresser avant à celle de ce noyau.

b. Organisation cytoarchitectonique, chémoarchitectonique et hodologique du CEA

Le CEA présente une organisation complexe, mal représentée par les atlas actuels qui le divisent simplement en trois parties (capsulaire, latérale et médiane) et qui ne lui délimitent pas tous les mêmes frontières (Swanson, 2004; Paxinos & Watson, 2013). Cette complexité est encore accentuée par les études neurochimiques. Contrairement au CEAm, le CEAl est très riche en neurones et en axones qui expriment de nombreux neuropeptides et enzymes. La partie latérale, particulièrement bien repérée par marquage PKC-δ, peut par exemple elle-même être divisée en trois zones (Cassell *et al*, 1999; Marchant *et al*, 2007; Kim *et al*, 2017). Notre étude du CEA était donc destinée à répondre à une question spécifique : comment expliquer les différences reportées dans la littérature dans l'intensité et la distribution des projections de ce noyau vers le LHA ? La stratégie utilisée a consisté en l'analyse de la distribution des neurones rétrogradement marqués après injection de FG dans le complexe PSTN/CbN ou dans les régions antérieures du LHA (périfornical). Notre première observation a été de constater que les patrons de distribution des neurones différaient. Notamment, après injection dans les régions antérieures, un groupe compact de cellules a été marqué, qui correspondait à la partie "intermédiaire" décrite par A.J. McDonald il y a plusieurs décennies, mais très largement ignorée depuis. Singulièrement, ce marquage avait déjà été observé mais le lien avec le CEAi n'avait pas été fait. Les injections dans le PSTN marquaient des neurones très majoritairement localisés dans le CEAm mais peu dans le CEAi. Ce trait ainsi que l'observation de l'intense innervation par l'INS et l'absence d'afférence depuis le FS, nous ont convaincu de laisser le CEAi dans un complexe "latéral" du CEA et donc distinct du CEAm. Par ailleurs, chez la souris, un CEAi différencié ne semble pas exister et les cellules qui projettent dans le LHApfx sont dispersées dans la partie antérieure du CEAl, confirmant encore un rapprochement CEAi-CEAl. Par la suite, l'analyse de l'expression de la protéine c-Fos dans diverses conditions expérimentales chez le rat a permis de constater que le CEAi est activé spécifiquement suite à l'ingestion d'une solution d'eau sucrée, alors que le CEAl réagit plus intensément à des signaux nociceptifs périphériques (suite à une injection intrapéritonéale de LPS ou de cisplatine). Ce dernier point concernant le CEAl est parfaitement connu (Hunt & Mantyh, 2001; Han *et al*, 2015) et cohérant avec l'innervation CGRP qu'il reçoit du PB (Schwaber *et al*, 1988; D'Hanis *et al*, 2007; Carter *et al*, 2013; Han *et al*, 2015), qui par ailleurs innerve aussi le complexe PSTN/CbN (Chometton *et al*, 2016). En revanche, la réponse du CEAi était inédite. Après injection de PHAL dans cette partie (Barbier *et al*, 2018a), les projections du CEAi ont été identifiées dans le LHAs, impliqué par J.D. Hahn et L.W. Swanson dans la prise alimentaire, mais aussi dans le noyau

paraventriculaire de l'hypothalamus, ce qui est cohérent avec un contrôle de l'activité du système nerveux autonome. Il s'agit donc d'un circuit prometteur à étudier dans le futur proche, mais qui sera plus difficile à analyser chez la souris du fait de l'absence d'un CEAi bien différencié.

Le CEA est également constitué d'une partie capsulaire (CEAc). Nos observations ont confirmé celles de la littérature concernant la complexité de cette partie avec au moins deux divisions chez le rat : l'une dorsale (CGRP) et l'autre ventrale (CGRP et NT). La partie ventrale est innervée depuis le PB par des neurones coexprimant CGRP et NT. L'intérêt de cette observation a émergé lorsque, après intoxication alcoolique, il a été observé que l'expression de la protéine c-Fos marquait un groupe compact de neurones dans cette division chez le rat, suggérant qu'elle peut jouer un rôle plus spécifiquement dans les phénomènes d'addiction ou d'intoxication à l'alcool. Ce point particulier n'a pas pu être approfondi, cependant, des premiers tests de traçage génétique chez des souris NT-Cre depuis le PB montrent que chez cette espèce, les projections CGRP/NT innervent le CEAc dans son ensemble. Encore une fois, des différences importantes entre rat et souris pointent sur les limites du modèle souris pour de nombreux "problèmes" anatomiques.

En tout état de cause, cette étude limitée du CEA a permis d'en apprendre assez sur ce noyau pour poursuivre notre projet. Nous avions notamment compris la différence majeure qui existe entre le CEAm d'une part et les parties plus latérales (CEAi, l, c) d'autre part. La première semble plus homogène d'un point de vue neurochimique, alors que les secondes sont très riches en neuropeptides. Ces derniers définissent des divisions qu'il est ensuite possible de comparer à la distribution des projections de l'INS. Tout n'est toujours pas compris concernant ce noyau et des points obscures sont soulevés aussi dans la discussion de notre article (Barbier *et al*, 2018a) et qui ne seront pas repris ici.

2. Organisation des connexions entre l'INS et le complexe PSTN/CbN

Après avoir analysé l'organisation et constaté l'abondance des connexions entre le CEA et le complexe PSTN/CbN, le projet initial a été poursuivi avec l'étude des projections depuis l'INS. Les résultats sont décrits et brièvement discutés dans l'article 4. Deux types de connexions ont été observées :

- Des projections directes depuis la plupart des aires insulaires, mais pas toutes avec la même intensité.

- Des liens indirects par l'intermédiaire des divisons latérales du CEA (c, l, i) qui elles-mêmes innervent le CEAm et la SI qui sont bi-directionnellement connectés au complexe PSTN/CbN.

Interprétées dans le cadre de la compréhension de l'organisation du télencéphale, ces connexions ont été comparées à celles décrites pour ce qui est généralement appelé les "ganglions de la base". Ainsi, les projections de l'INS sur le complexe PSTN/CbN ont été assimilées au trajet

"hyperdirect" décrit depuis l'isocortex sur le STN. Nos arguments en faveur de cette interprétation sont purement structuraux et basés sur la constatation d'une organisation topographique des projections depuis l'isocortex et l'INS dans la région incluant STN et PSTN/CbN. Ces régions sont également *GAD* négatives et donc pauvres en neurones GABAergiques. En revanche, le complexe PSTN/CbN est VGluT2 (transporteur 2 vésiculaire de glutamate) positif et donc probablement glutamatergique (Chometton *et al*, 2016) tout comme le STN (Gerfen & Wilson, 1996; Pautrat *et al*, 2018). Nos arguments sont aussi supportés par les ressemblances observées dans le profil électrophysiologique des neurones du PSTN et du STN et révélées par le Dr V. Coizet (adresse : veronique.coizet@univ-grenoble-alpes.fr) qui a partagé avec nous ses données exposées dans l'article 4. Dans la littérature, H.J. Groenewegen et H.W. Berendse ont signalé la grande ressemblance des neurones du STN avec ceux du LHA voisin et qui correspond donc au PSTN (Groenewegen & Berendse, 1990). Enfin, chez le primate, les aires du LHA adjacentes au STN ont aussi été assimilées à une division médiane du STN sur la base d'afférences depuis certaines aires préfrontales médianes (Haynes & Haber, 2013) (Figure 34).

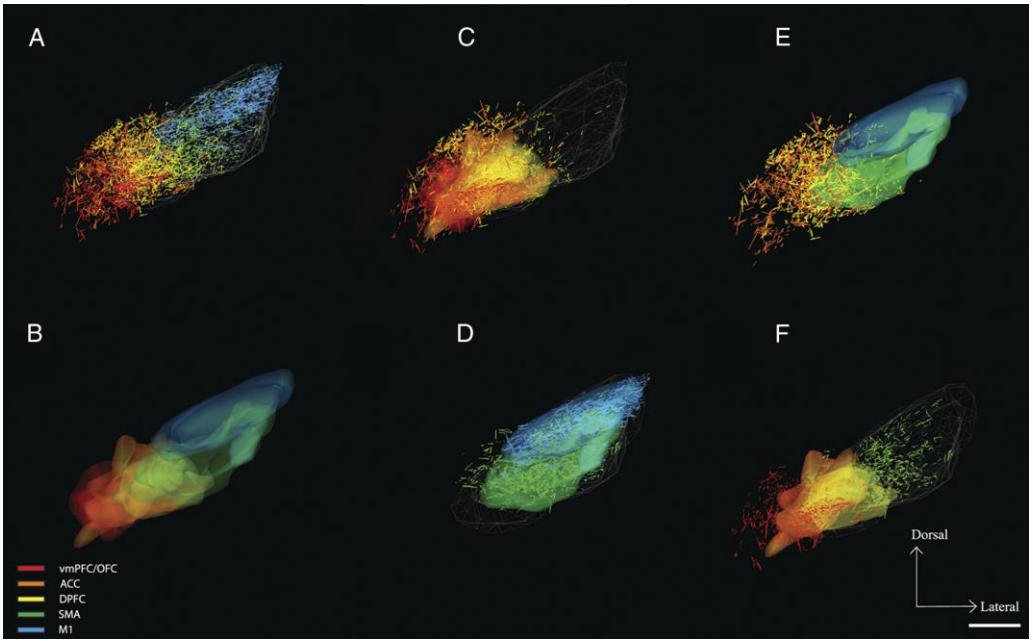

Figure 34. Représentations en vues 3D de projections corticales dans le STN et le LHA adjacent (Haynes & Haber, 2013).

Les projections préfrontales, orbitofrontales et cingulaires sont signalées en rouge-jaune et les projections motrices en vert-bleu. Barre d'échelle = 1 mm.

Le complexe PSTN/CbN n'a pas été caractérisé chez ces espèces, mais ces aires du LHA ne contiennent pas de neurones à MCH. Chez l'homme, il a été montré que la région du LHA adjacente au STN est riche en marquage pour calbindine et calrétinine, ce qui est une des caractéristiques neurochimiques de ces noyaux chez le rat. D'ailleurs, sur les illustrations du papier de S.J. Augood *et al*, il est possible d'apercevoir une condensation de marquage calbindine positive (Figure 35 C) en

position basale qui évoque fortement le CbN (Augood *et al*, 1999). Sur des coupes d'encéphale humain marqué par technique d'injection intravasculaire à l'encre de Chine (matériel prêté par le Pr. H. Duvernoy), il est possible de deviner le complexe PSTN/CbN par étude angioarchitecturale (Figure 35 D). Ainsi, sur des modèles rongeurs, le PSTN reçoit des projections corticales qui ressemblent à celles décrites chez le primate pour des régions du LHA déjà assimilées par les auteurs à du STN. Les données chémoarchitecturales chez l'homme suggèrent aussi que les régions voisines du STN dans le LHA correspondent au complexe PSTN/CbN du rongeur.

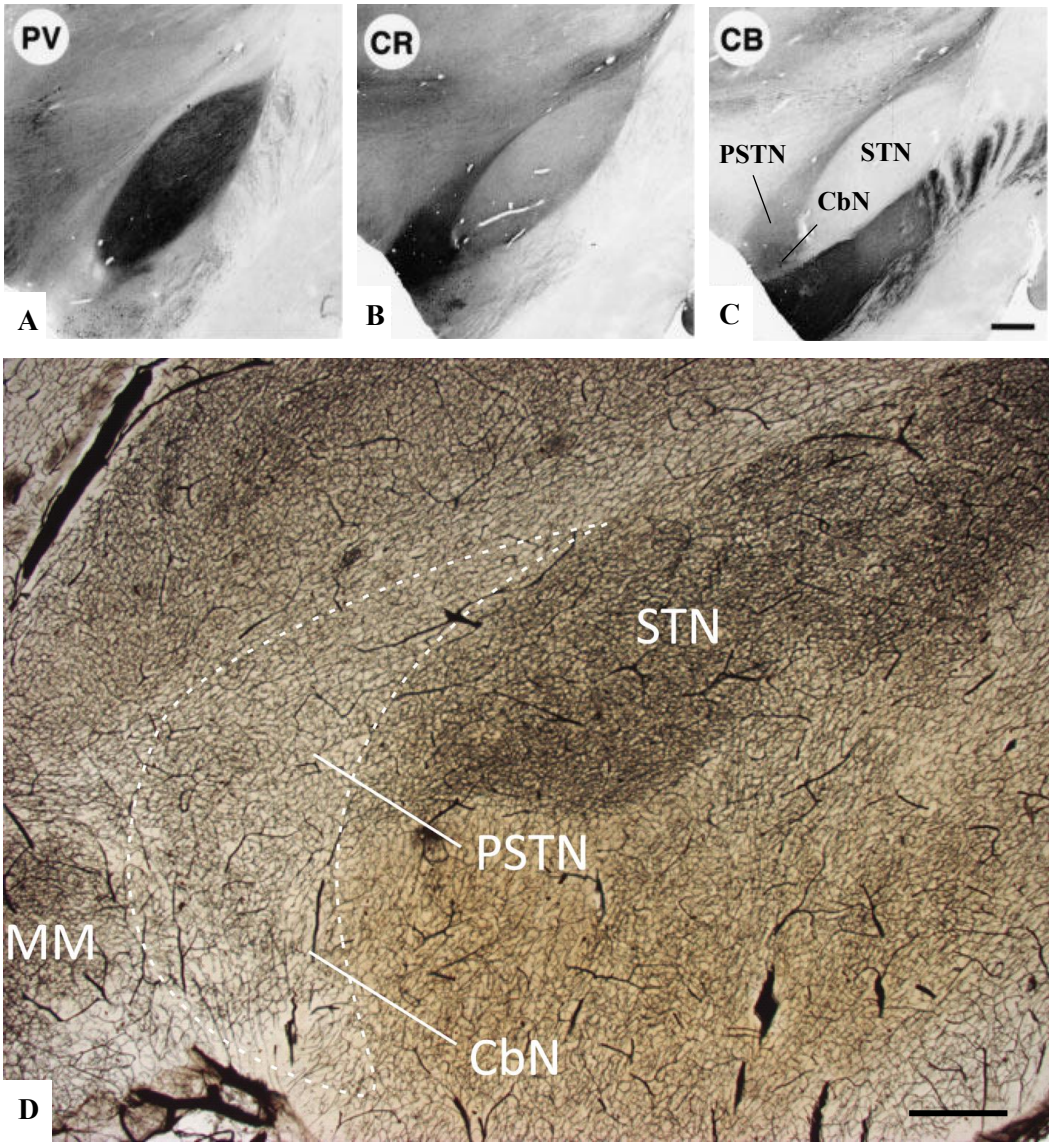

Figure 35. Photographies du STN en coupes coronales chez l'humain.

Coupes immunomarquées pour la parvalbumine (PV en A), la calrétinine (CR en B) et la calbindine (CB en C) (Augood *et al*, 1999) et injecté à l'encre de Chine révélant l'architecture vasculaire de plusieurs noyaux.

CB : calbindine ; CbN : noyau calbindine ; CR : calrétinine ; MM : noyau mamillaire médian ; PSTN : noyau parasousthalamique ; STN : noyau sousthalamique. Barre d'échelle (A, B et C) = 1 cm ; (D) = 1 mm.

L'assimilation du trajet INS-CEA/SI-PSTN/CbN à une voie indirecte est plus originale, mais là encore, certaines données actuelles de la littérature viennent en support de notre hypothèse. Notre argumentation est purement basée sur des considérations architecturales des trajets. Afin d'affermir cette hypothèse il sera indispensable de vérifier l'expression d'un certain nombre de marqueurs neurochimiques spécifiques : par exemple les neurones du striatum à l'origine de la voie indirecte expriment le récepteur D2 à la dopamine. Des marquages avec des anticorps anti-D2 commerciaux ont été tentés, malheureusement la qualité de ces marquages (ou plus exactement l'absence de qualité) nous a empêché de les utiliser dans notre démonstration. Néanmoins, dans un travail récent, J. Kim *et al* décrivent les projections depuis le noyau basolatéral de l'amygdale dans le CEA comme présentant les caractéristiques neurochimiques de connexions cortico-striatales (Kim *et al*, 2017) (Figure 36). Le CEA exprime des marqueurs de la voie indirecte, mais la cible potentielle dans l'hypothalamus des neurones du CEA n'était pas recherchée dans ce travail.

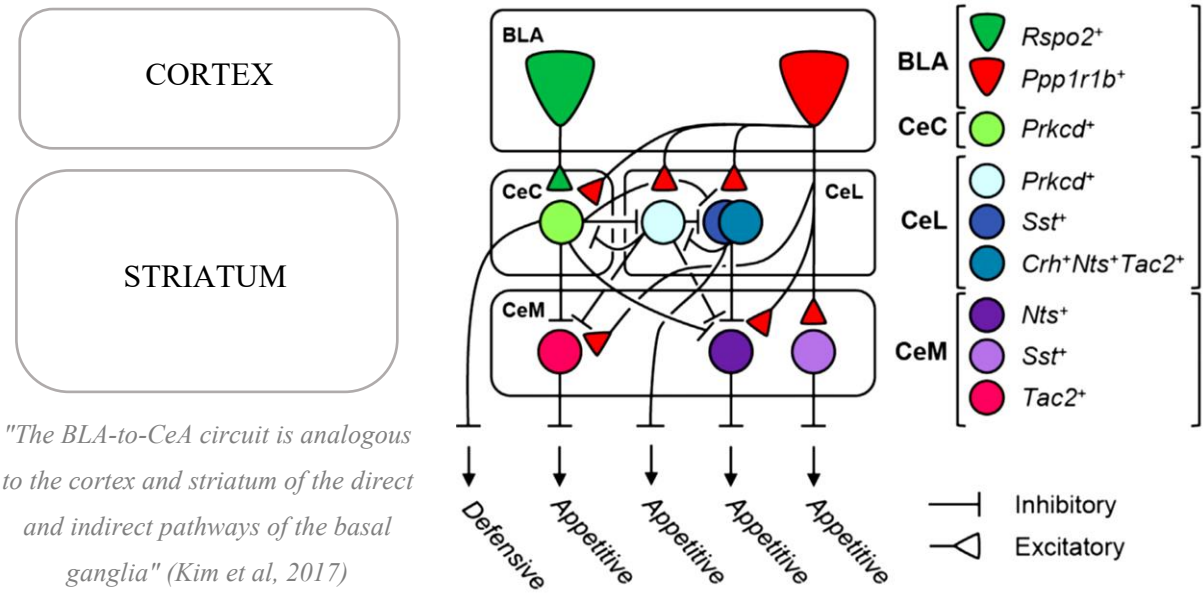

"The BLA-to-CeA circuit is analogous to the cortex and striatum of the direct and indirect pathways of the basal ganglia" (Kim et al, 2017)

Figure 36. Modèle structural et fonctionnel des connexions entre les noyaux basolatéral et central de l'amygdale spécifiques de types cellulaires, d'après Kim *et al* (2017).

Les connexions ont été déterminées par des expériences de traçage viral monosynaptique.

BLA : noyau basolatéral de l'amygdale ; CeC : division capsulaire du noyau amygdalien central (Ce) ; CeL : division latérale du Ce ; CeM : division médiane du Ce ; Crh : corticolibérine ; Nts : neurotensine ; Ppp1r1b : protéine phosphatase 1 régulatrice de la sous-unité 1B ; Prkcd : protéine kinase C delta ; Rspo2 : R-spondine 2 ; Sst : somatostatine ; Tac2 : tachykinine 2.

Il n'en reste pas moins que l'origine striatale des parties capsulaire et latérale du CEA, ainsi que le fait que leurs neurones principaux sont des neurones épineux qui sont identiques dans leur morphologie à ceux du CP voisin (voir l'introduction), sont des arguments qui plaident en faveur de notre hypothèse.

Un dernier point dans ce chapitre reste à discuter qui n'a été que très succinctement évoqué dans l'article 4 mais qui semble essentiel. Il concerne la complexité du réseau descendant depuis l'INS. L'INS est à l'origine de projections sur divers secteurs du striatum : avec une innervation des régions ventrales du CP et du striatum ventral, il est susceptible d'influencer différents processus en liens avec les circuits issus de ces régions. Mais les différentes aires de l'INS innervent de manière topographiquement organisée le CEAc, l, i. Ainsi, il est possible de tracer depuis chaque site d'injection de traceur antérograde dans l'INS, un réseau ramifié en plusieurs branches et susceptible de contrôler de nombreuses réponses motrices ou comportementales, cognitives, motivationnelles ou associées à la récompense, ou encore émotionnelles. La figure 37 schématise l'organisation de ces réseaux. Elle permet notamment d'illustrer que le complexe PSTN/CbN en est la cible de plusieurs des branches : par les divisions capsulaire et latérale du CEA, mais aussi par le FS. Illustré dans l'article 1 et 2, le FS est une des sources afférentes abondantes du CEAm. Le FS a la même origine développementale que les régions voisines du striatum telles que le CP et le tubercule olfactif. Le FS est innervé par plusieurs aires insulaires dont les parties dorsale (AId) et postérieure (AIp) de l'aire agranulaire. Le schéma de la figure 37 illustre notamment que si les projections corticales affectent de nombreux secteurs du striatum, les trajets à partir de plusieurs de ces secteurs par l'intermédiaire de branches distinctes convergent dans le complexe PSTN/CbN.

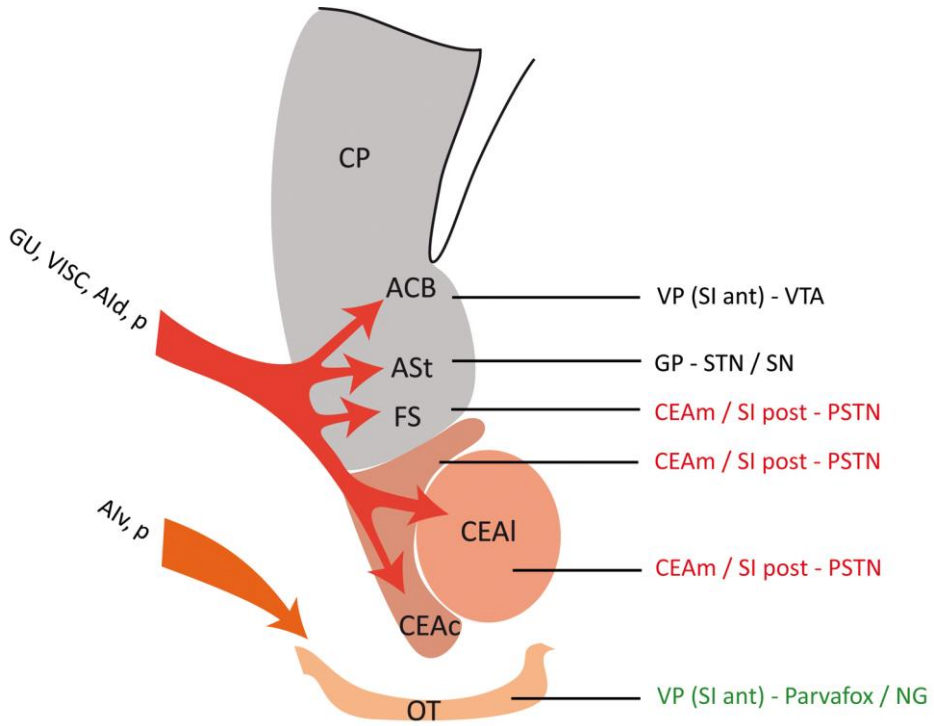

Figure 37. Schéma des projections depuis plusieurs aires insulaires dans diverses régions striatales et convergeant dans l'hypothalamus prémamillaire ou la SN et la VTA.

ACB : noyau accumbens ; AId : partie dorsale de l'aire insulaire agranulaire ; AIv, p : parties ventrale, postérieure de l'aire insulaire agranulaire ; ASt : aire transitionnelle amygdalo-striatale ; CEAc : division capsulaire du noyau amygdalien central ; CEAl : division latérale du noyau amygdalien central ; CP : caudoputamen ; FS : fundus striatum ; GU : aire insulaire gustative ; OT : tubercule olfactif ; VISC : aire insulaire viscérale.

La signification de cette confluence nous échappe encore, mais pointe clairement vers un rôle crucial du complexe PSTN/CbN. Les connexions illustrées dans la figure 37 expliquent donc le très large éventail des fonctions dans lesquelles l'INS est impliqué, et justifient notamment le regain d'intérêt pour ces aires corticales dans l'étude des processus associés à la prise de décision. Notre analyse ne fait pour autant que pointer vers cette complexité sans encore en disséquer chaque aspect, ce qui nécessitera un grand nombre de travaux d'anatomie afin de caractériser en détail chaque réseau issu de chaque aire insulaire et d'en disséquer chacune des branches. Néanmoins, comprendre que chacune des branches en question est organisée suivant un plan similaire semble déjà une étape préliminaire indispensable.

II. Fonctions attribuées au réseau impliquant le complexe PSTN/CbN

1. Le LHA et le comportement alimentaire

Le comportement de prise alimentaire est complexe, il implique des signaux d'ordre métabolique qui peuvent être modulés par des signaux gustatifs, odorants et hédoniques. L'hypothalamus et plus particulièrement le noyau arqué jouent un rôle clé dans le contrôle métabolique de ce comportement, permettant le maintien de la balance énergétique (Aponte *et al*, 2011). Les données de la littérature ciblent classiquement les neurones du LHA en tant que centre hypothalamique de contrôle du comportement d'ingestion, recevant des efférences de plusieurs structures impliquées dans le traitement d'informations sensorielles et motrices. Il serait donc plus largement engagé dans les aspects motivationnels de la prise alimentaire. Cependant, les circuits de la gustation sont décrits de manière assez diffuse dans l'hypothalamus, originaires notamment de la région rostrale du NTS, du PB, et des régions insulaires. Les auteurs tentent depuis de nombreuses années de comprendre l'organisation de ces réseaux mais peinent à identifier le schéma complet. Ce comportement est en partie élaboré dans des structures télencéphaliques qui médient les stratégies d'adaptabilité et d'apprentissage influencées par les aspects hédoniques et de récompense de la nourriture. Les propositions de schémas d'organisation des réseaux impliqués dans le contrôle du comportement de prise alimentaire mettent en évidence des circuits hiérarchiquement ordonnés responsables d'un aspect particulier de ce comportement (Watts *et al*, 2007) (Figure 38). Même si de nombreuses données expérimentales impliquent fortement certaines parties du LHA en tant que contributeurs importants au réseau de contrôle, aucune structure n'a été précisément identifiée, c'est-à-dire avec des frontières précises.

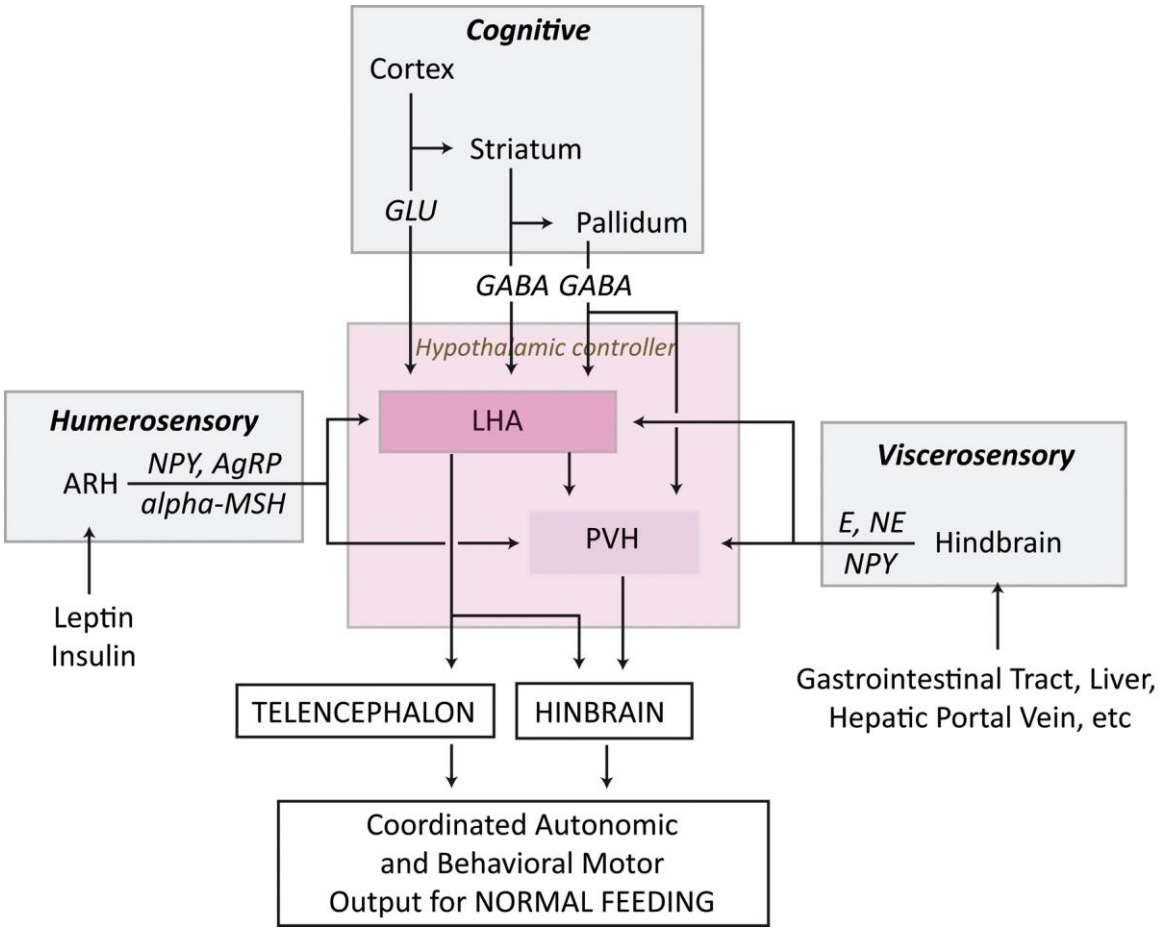

Figure 38. Schéma du réseau de contrôle du comportement alimentaire impliquant l'hypothalamus, d'après Watts *et al* (2007).

AgRP : *"agouti related peptide"* ; ARH : noyau arqué ; E : épinéphrine ; GABA : acide gamma-aminobutyrique ; GLU : glutamate ; LHA : aire hypothalamique latérale ; αMSH : hormone mélanotrope ; NE : norépinephrine ; NPY : neuropeptide Y ; PVH : noyau paraventriculaire.

Les travaux récents pointent vers des populations ou sous-populations de neurones (Hcrt, NT, glutamate, GABA) dont la distribution n'a jamais sérieusement été établie en rapport avec le contrôle du comportement alimentaire. Il est souvent fait référence au LHApfx qui peut-être correspond au LHAs de L.W. Swanson. Cependant, rien n'a été réellement formalisé dans ce domaine et les territoires, décrits anatomiquement chez le rat, sont le plus souvent étudiés au niveau fonctionnel chez la souris. Des différences importantes entre les deux espèces ont déjà été soulevées plusieurs fois dans ce travail. En revanche, dans le cadre de la prise alimentaire, les régions postéro-latérales du LHA n'ont que très peu été prises en compte. Or, par ses connexions (Goto & Swanson, 2004) ainsi que par les premières données fonctionnelles obtenues par notre équipe mais aussi par d'autres (Chometton *et al*, 2016; Zséli *et al*, 2016, 2018), le PSTN ressort comme un acteur important de la prise alimentaire. Dans ce travail, les données obtenues apportent un éclairage particulier quant à la manière dont le complexe PSTN/CbN est susceptible d'influencer les comportements d'ingestion.

2. Le complexe PSTN/CbN et la prise alimentaire

a. Le complexe PSTN/CbN et le contrôle volumique et métabolique de la prise alimentaire

Les conditions dans lesquelles le complexe PSTN/CbN réagit à la prise alimentaire sont diverses. Elles incluent par exemple les aspects hédoniques de la nourriture, mais le volume ingéré par l'animal n'influence pas l'amplitude de cette réponse mesurée par l'expression de la protéine c-Fos (Chometton *et al*, 2016). Contrairement au LHA tubéral, aucune variation d'expression de la protéine c-Fos n'a été observée à la suite de l'ingestion d'un volume plus ou moins important de nourriture ou de boisson. Ces données ont été confirmées dans notre dernière étude, chez des souris, par inhibition du complexe PSTN/CbN en condition de prise alimentaire. En effet, aucune différence de quantité de nourriture ingérée entre les animaux "contrôles" et les animaux "DREADD", chez lesquels le complexe PSTN/CbN a été inhibé, n'a été observée. Récemment, une équipe a signalé l'activation du complexe PSTN/CbN après ingestion de nourriture suite à un jeûne et lui attribue un rôle dans la satiété (Zséli *et al*, 2016, 2018). Cependant, ils ne tiennent pas compte de l'aspect plaisant de la réalimentation et réalisent leurs observations après quelques heures. Or, dans nos expériences, la réponse du complexe PSTN/CbN est induite en seulement 30 minutes, ce qui permet d'éviter les signaux résultants des processus de digestion ou de satiété. Elle n'est pas non plus liée à des modifications rapides de glycémie puisque des injections de glucose n'induisent pas de variation d'expression de la protéine c-Fos dans cette région (Chometton *et al*, 2016). Le complexe PSTN/CbN n'innerve pas le noyau arqué et que très peu le noyau paraventriculaire. Ce complexe ne semble donc pas intervenir dans le contrôle métabolique de la prise alimentaire.

b. Le complexe PSTN/CbN et le contrôle cognitif de la prise alimentaire

Le complexe PSTN/CbN est activé chez des rats assoiffés soumis à des goûts agréables, mais pas chez ceux soumis à l'ingestion d'aliments ayant un goût aversif, et l'amplitude de la réponse varie avec l'intensité de ce goût. Pour un volume ingéré similaire, l'expression de la protéine c-Fos est très significativement plus abondante dans le complexe nucléaire lorsque l'aliment ou la boisson est gustativement palatable que lorsqu'elle est légèrement aversive (Chometton *et al*, 2016). De plus, le complexe PSTN/CbN répond plus intensément à l'ingestion d'une solution nouvelle, inconnue de l'animal mais hédonique (Chometton, 2015). Il a été montré que le complexe PSTN/CbN reçoit une innervation intense de plusieurs aires insulaires (GU, VISC, AId, p) dont certaines (GU et AId en particulier) ont un rôle dans la reconnaissance d'un goût nouveau ou familier (Stehberg *et al*, 2011; Lin & Reilly, 2012; Moraga-Amaro *et al*, 2014; Lin *et al*, 2015). Le CEA avec lequel il est aussi

connecté est mis en jeu dans les états anxiogènes (Kalin *et al*, 2004; Tye *et al*, 2011; Gilpin *et al*, 2015; Skórzewska *et al*, 2015) incluant le comportement néophobique (Lin *et al*, 2012; Raab *et al*, 2018). D'ailleurs, les souris à qui l'on inhibe le complexe PSTN/CbN boivent davantage de solution au cours des premières minutes d'exposition que les animaux "contrôles", à la manière d'animaux dits "habitués". Ainsi, ce complexe semble intervenir dans le contrôle de l'ingestion d'aliments palatables en fonction de facteurs cognitifs qui vont en atténuer la consommation.

Le rôle du complexe PSTN/CbN n'est donc à priori pas lié au rôle de récompense généralement associé à la consommation d'aliments palatables. Ce phénomène de récompense, qui associe le striatum ventral (ACB) et la VTA, conduit à consommer davantage un aliment agréable au goût. A l'inverse, le complexe PSTN/CbN pourrait freiner la consommation de cet aliment si par exemple, n'étant pas connu, l'animal est méfiant quant aux conséquences potentielles de son ingestion.

c. Le complexe PSTN/CbN et les afférences viscéro-sensorielles nociceptives

Plusieurs résultats obtenus impliquent le complexe PSTN/CbN dans le contrôle de l'ingestion de nutriments en fonction de l'état pathologique de l'individu. En effet, le complexe PSTN/CbN est intensément et spécifiquement innervé dans le LHA par des projections CGRP issues du PB. Ces projections qui innervent aussi les parties capsulaire et latérale du CEA (Carter *et al*, 2013, 2015; Chometton *et al*, 2016) jouent un rôle dans les réponses anorexigènes et de conditionnement gustatif aversif. Les neurones à CGRP du PB intègrent des informations viscérales et nociceptives et communiquent avec le CEA pour induire un état de satiété ou de malaise (Carter *et al*, 2013, 2015; Campos *et al*, 2016; Barna *et al*, 2018; Chen *et al*, 2018).

Trois expériences ont été réalisées qui effectivement impliquent le complexe PSTN/CbN dans la réponse à l'état de malaise. Tout d'abord, l'injection de LPS, un composé provoquant une réaction inflammatoire intense, ou celle de cisplatine, un produit utilisé en oncologie et provoquant nausées et malaises, induisent une augmentation de l'expression de la protéine c-Fos dans le complexe PSTN/CbN en absence de tout stimulus gustatif.

Dans une autre série expérimentale, il a été constaté que l'intoxication alcoolique volontaire, mimant un *"binge drinking"*, induit une augmentation très importante de la protéine c-Fos dans le complexe PSTN/CbN. Cette augmentation était significativement corrélée au taux d'alcool sanguin pour le CbN. Il est à noter, dans la même expérience, que des animaux ayant consommés un volume équivalent d'une solution de quinine ne présentaient pas d'augmentation de l'expression de la protéine c-Fos, confirmant l'absence de corrélation entre le volume ingéré et l'expression de la protéine c-Fos dans le complexe PSTN/CbN.

Enfin, dans une troisième expérience effectuée chez des souris TAC1-Cre, il a été montré que l'inhibition par la technique DREADD du complexe contrecarre l'anorexie induite par l'état de malaise provoqué par une injection de LPS à l'individu.

Les résultats de ces trois expériences pointent donc dans la même direction, corrélant une réponse du complexe à des stimuli nociceptifs susceptibles d'entrainer une réaction anorexique. Il est intéressant de noter que nos observations chez le rat pointent pour des réponses légèrement différentes entre le PSTN et le CbN : le premier réagit plus intensément lorsque l'animal ingère un aliment ou une boisson palatable. La réaction à la néophobie est aussi plus intense dans ce noyau. En revanche, la réponse du CbN était plus intense, même en l'absence d'ingestion, en fonction de l'état de malaise.

d. Mécanismes impliqués dans la mise en jeu du complexe PSTN/CbN et conclusions

L'ensemble du réseau impliquant le complexe PSTN/CbN suggère que les fonctions de ce complexe hypothalamique postérieur sont liées à des informations d'ordre gustatives et sous le contrôle d'afférences viscéro-sensorielles, émotionnelles et cognitives. Les réponses de ce complexe semblent dépendre de l'état physiologique et pathologique (malaise, besoin de s'alimenter) de l'animal mais également de son état "émotionnel" et cognitif (apprentissage, néophobie). Cependant, nous n'avons travaillé par la technique pharmacogénétique (DREADD) que sur une des populations du complexe PSTN/CbN que sont les neurones TAC1. Nos données sont donc préliminaires. Afin de comprendre les mécanismes qui peuvent expliquer les réponses initiées par le complexe PSTN/CbN, de nombreuses autres expériences par d'autres approches seront nécessaires. En particulier, des expériences d'optogénétique afin d'étudier le rôle des innervations réciproques entre le CEAm et le PSTN peuvent être envisagées.

Le CEA joue un rôle important dans le contrôle de la motivation et de la valeur hédonique ainsi que dans l'établissement de la peur conditionnée (Touzani *et al*, 1997; Bourgeais *et al*, 2001). Il participe grâce à ses différentes divisions à l'expression de comportements dits "positifs" ou "négatifs" (Kim *et al*, 2017). Il est ainsi capable de favoriser ou de diminuer l'appétit par la mise en jeu de projections glutamatergiques et GABAergiques.

Les afférences glutamatergiques portées par les axones corticaux et parabrachiaux CGRP peuvent activer les neurones GABA du CEAc et du CEAl qui en retour inhibent les neurones GABA du CEAm (voie indirecte) (Figure 39). On peut donc faire l'hypothèse que l'inhibition du CEAm lève l'inhibition des neurones du complexe PSTN/CbN qui sont aussi activés directement par les neurones CGRP du PB et de l'INS (voie hyperdirecte). Le PSTN et CbN, probablement glutamatergiques (Chometton *et al*, 2016), peuvent également avoir une influence excitatrice sur le CEAm. Ce dernier peut à son tour entrainer l'inhibition du complexe PSTN/CbN. Ces connections entre le complexe

PSTN/CbN et le CEAm ressemblent à une boucle de rétrocontrôle qui pourrait moduler l'activité du CEAl. Cette voie dite indirecte est le pendant de celle du STN. En effet, les projections isocorticales glutamatergiques activent les neurones GABA du CP qui en retour inhibent les neurones GABA du GPe. Cette dernière inhibition lève alors l'inhibition des neurones du STN qui sont aussi activés par l'isocortex (voie hyperdirecte). Les neurones du CEAl et du CEAc peuvent, par la voie directe, inhiber les neurones de la VTA et de la SN comme les neurones du CP avec la SNr pour les "noyaux de la base".

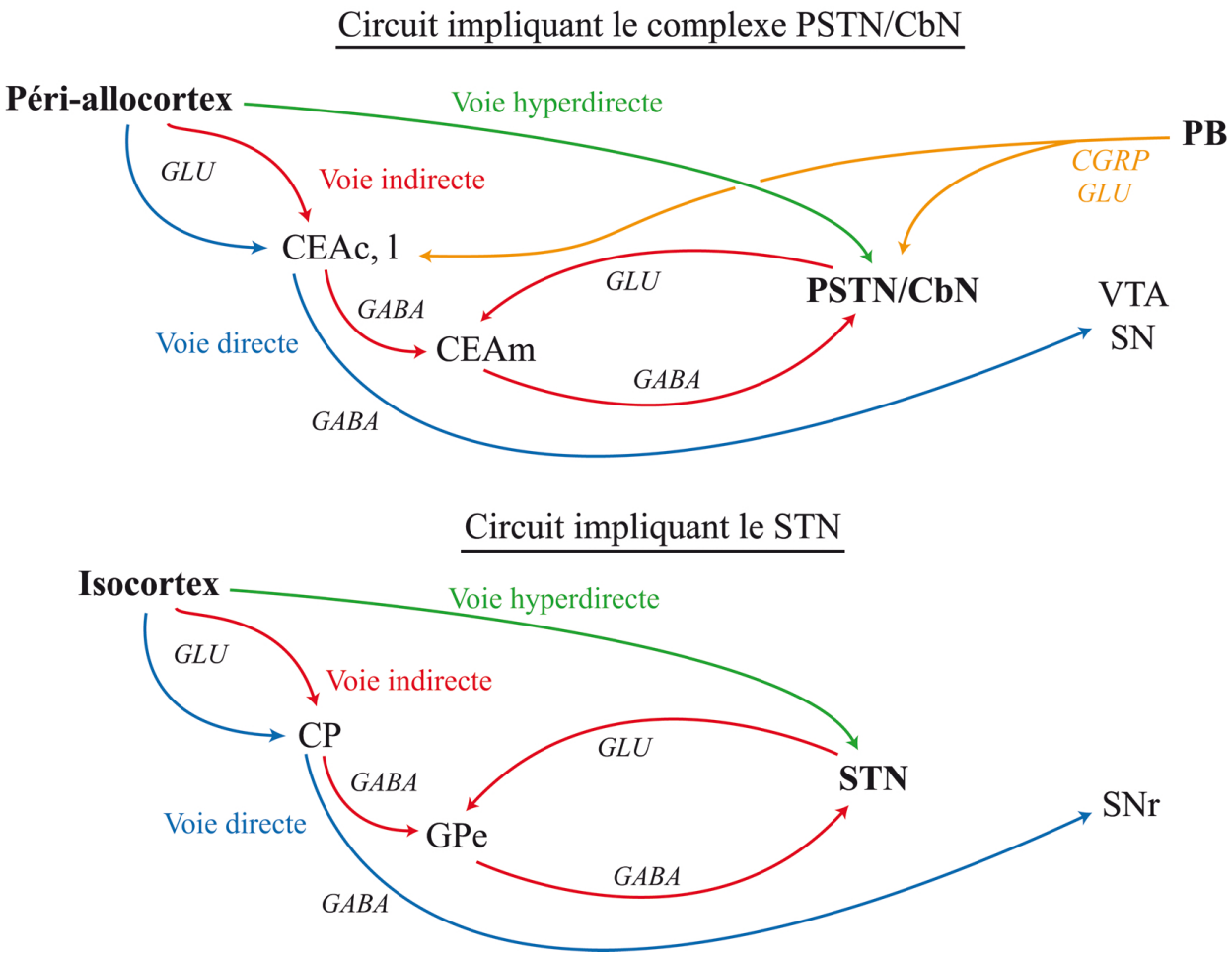

Figure 39. Comparaison des réseaux incluant le complexe PSTN/CbN et le STN.

CbN : noyau calbindine ; CEAc/l/m : noyau central de l'amygdale, partie capsulaire/latérale/médiane ; CGRP : *calcitonin gene-related peptide* ; CP : caudoputamen ; GABA : acide gamma-aminobutyrique ; GLU : glutamate ; GPe : segment externe du globus pallidus ; PB : noyau parabrachial ; PSTN : noyau parasousthalamique ; SN : substance noire ; STN : noyau sousthalamique ; VTA : aire tegmentale ventrale.

Le CEAm reçoit aussi des projections GABAergiques du FS qui lui-même reçoit des afférences de plusieurs aires insulaires. Des mécanismes similaires à ceux précédemment décrits peuvent donc être impliqués mais dont l'exacte "chaine synaptique" n'a pas pu être étudiée ici. Le PSTN est aussi la cible de la partie latérale du BST (Dong & Swanson, 2004) dont les connexions dans le LHA modulent la prise alimentaire (Petrovich *et al*, 2002; Jennings *et al*, 2013). Comme il a été mentionné dans

l'introduction (page 37), le BST, comme le CEA, a une origine à la fois striatale et pallidale. Un travail similaire à celui qui a été entrepris pour le CEA pourrait également être mené. Le BST est aussi connecté avec le FS, la SI et le complexe PSTN/CbN (Grove, 1988; Chometton *et al*, 2016). Ces structures peuvent aussi probablement sous-tendre des mécanismes permettant la modulation du comportement émotionnel et cognitif de l'animal dans la prise alimentaire.

III. Organisation de l'hypothalamus postérieur

Les résultats obtenus nous permettent d'améliorer notre compréhension de l'organisation de l'hypothalamus postérieur. Combinées aux connaissances acquises et exposées dans l'introduction, nos observations montrent que l'organisation des régions *GAD* négatives, qui forment la vaste majorité de l'hypothalamus postérieur, est totalement corrélée à celle du télencéphale. Cette région *GAD* négative s'étend du STN au corps mamillaire, incluant le complexe PSTN/CbN, le Parvafox/NG et les noyaux prémamillaires. Nous avons vu dans l'introduction les arguments développementaux qui ont menés les anatomistes à rattacher le STN à l'hypothalamus, alors que ce noyau est en général associé aux "ganglions de la base". Un point qui semble curieux, c'est que l'assimilation de ce noyau à l'hypothalamus ne s'est accompagnée d'aucune réflexion sur la signification qu'un tel changement de sa position anatomique pouvait révéler. Le STN est une structure essentielle du circuit des "noyaux de la base" et ses fonctions dans le contrôle de l'activité motrice ne correspondent en rien à des fonctions hypothalamiques "classiques". En ce sens, il se rapproche un peu des noyaux mamillaires médian et latéral qui forment le corps mamillaire. Cette structure, en position médiane, répond au rythme thêta de l'hippocampe et est impliquée dans la mémorisation mais pas dans des réponses endocrines ou végétatives (Vertes, 1986; Vann & Aggleton, 2004; Vann, 2013). Elle a été identifiée à peu près en même temps que le STN et associée initialement aux aires "sub-thalamiques". Elle est, depuis His (1893), considérée comme une structure emblématique de l'hypothalamus.

Ces deux structures, STN et corps mamillaire, forment donc deux pôles, l'un latéral, l'autre médian de l'hypothalamus postérieur. Mais ils ont été étudiés séparément sans qu'aucun lien n'ai été identifié jusqu'à présent, qui puisse les rapprocher, mis à part, récemment, une origine développementale proche. Latéral au corps mamillaire, les noyaux prémamillaires ont été identifiés au début du XX^{ème} siècle et leur appartenance à l'hypothalamus n'a jamais été questionnée. Le PMd est anatomiquement proche du corps mamillaire et les deux reçoivent des projections par le système du fornix (tractus cortico-hypothalamique médian pour le premier et pilier du fornix pour le second). Le PMv est en revanche une cible de la strie terminale, et ainsi, noyaux prémamillaires et mamillaires partagent des connexions avec l'ancien système dit "limbique".

Les noyaux de l'hypothalamus latéral postérieur, appelé LHApm (Chometton *et al*, 2016), ont été identifiés tardivement : le NG, reconnu dans les années 1960, n'a quasi pas été étudié, tout comme le Parvafox, dont l'historique a été rappelé dans l'introduction (page 51). Le PSTN, reconnu en 1999, fait partie du complexe PSTN/CbN caractérisé par notre équipe il y a quelques années. En s'intéressant à cette région, nous avons étudié la dernière structure positionnée entre le corps mamillaire et le STN. Chometton *et al* (2016) avaient signalé les ressemblances neurochimiques chez le rat entre PSTN et PMv/PMd, puisque ces trois noyaux expriment le gène *Tac1* et sont glutamatergiques. Dans notre étude, nous avons montré une organisation topographique dans l'organisation des projections olfactives et phéromonales sur le CbN, le Parvafox et le PMv, associant ainsi ces noyaux ventraux dans le LHApm, aux noyaux plus médians de l'hypothalamus postérieur. Par la suite, nous avons montré que le complexe PSTN/CbN est connecté avec l'INS et le CEA/SI par des trajets qui sont organisés de manière structurellement similaire avec ceux impliquant le STN. D'ailleurs, chez le primate, pour lequel l'hypothalamus est moins attentivement étudié, les aires les plus postérieures du LHA sont déjà assimilées à du STN.

En conséquence, commence à se dessiner un modèle d'organisation de l'hypothalamus postérieur s'étendant du STN au corps mamillaire. D'un point de vue neurochimique, toutes ces structures sont pauvres en neurones GABAergiques et sont très largement glutamatergiques. Notre hypothèse est que chacun de ces noyaux est aussi connecté à des aires spécifiques du télencéphale suivant un modèle d'organisation qui a été le mieux décrit pour les "noyaux de la base", mais qui présente de nombreuses ressemblances et sont parallèles les uns aux autres.

1. Organisation des connexions depuis le pallium, la voie hyperdirecte

Le cortex cérébral est divisé en isocortex, allocortex et périallocortex. La région postérieure de l'hypothalamus est organisée autour de deux grands pôles : un pôle latéral, le STN, qui concentre des afférences depuis de nombreuses aires isocorticales ; et un pôle médian, le corps mamillaire, qui est la cible du fornix constituant le tractus le plus différencié de l'allocortex et issu du subiculum dorsal. Entre ces deux pôles, les noyaux prémamillaires sont aussi dominés par des afférences allocorticales qui irriguent certaines structures du LHApm (Figure 40). Ces dernières projections forment les tractus vlah, vlt et strie terminale et trouvent leurs origines dans le cortex amygdalien. Cependant, le LHApm semble dominé par des afférences périallocorticales : celles issues de l'INS, décrites dans ce travail, ou celles qui viennent du cortex préfrontal médian et décrites chez le primate. Le Parvafox/NG reçoit quant à lui des projections du cortex orbital (observations personnelles non publiées) (Babalian *et al*, 2019) qui suivent la voie des projections olfactives par le noyau magnocellulaire préoptique et le vlt.

Ainsi, le pallium, dans son ensemble, innerve par une voie analogue à la voie hyperdirecte, l'ensemble des structures glutamatergiques de l'hypothalamus postérieur.

2. Organisation des connexions depuis les "noyaux de la base", la voie indirecte

A côté des projections issues du pallium, la région postérieure de l'hypothalamus est aussi la cible d'afférences issues des "noyaux de la base". Ces projections sont originaires du pallidum en ce qui concerne le STN, et celles issues du CEAm et des régions postérieures de la SI dans le PSTN peuvent être considérées de même nature. Le Parvafox/NG est innervé par le pallidum ventral sus-jacent au tubercule olfactif et constituant donc encore une voie de même ordre (Figure 40). Les afférences du télencéphale basal dans le corps mamillaire sont toutes originaires du complexe du septum médian et sont GABAergiques (Gonzalo-Ruiz *et al*, 1992). D'après P.Y. Risold et L.W. Swanson (voir l'introduction page 39), le complexe du septum médian est assimilable au pallidum médian ; par conséquent, la ressemblance avec la voie indirecte est troublante. Reste le PMd et le PMv, dont il a été montré dans l'introduction qu'ils sont inclus dans deux réseaux intra-hypothalamiques : l'un avec le noyau hypothalamique antérieur et l'autre avec le noyau préoptique médian. Pour de nombreux auteurs, la région préoptique naît proche des régions donnant naissance au pallidum et en partage de nombreuses caractéristiques, tant dans l'expression de facteurs de transcription que comme source d'interneurones pour le cortex et le striatum. En ce sens, les connexions bidirectionnelles entre le noyau préoptique médian (GABAergique) et le PMv (glutamatergique) présentent encore une fois des ressemblances avec la voie indirecte. Il existe peu de données concernant le noyau hypothalamique antérieur, mis à part que ses parties postérieures (parties centrale, postérieure et dorsale), qui innervent le PMd, sont GABAergiques (Okamura *et al*, 1990). Sans spéculer plus avant, nous pronostiquons que des liens avec certaines divisions du pallidum seront observés et que les connexions bidirectionnelles de ce noyau avec le PMd suivent le même modèle que celles des autres structures de l'hypothalamus postérieur.

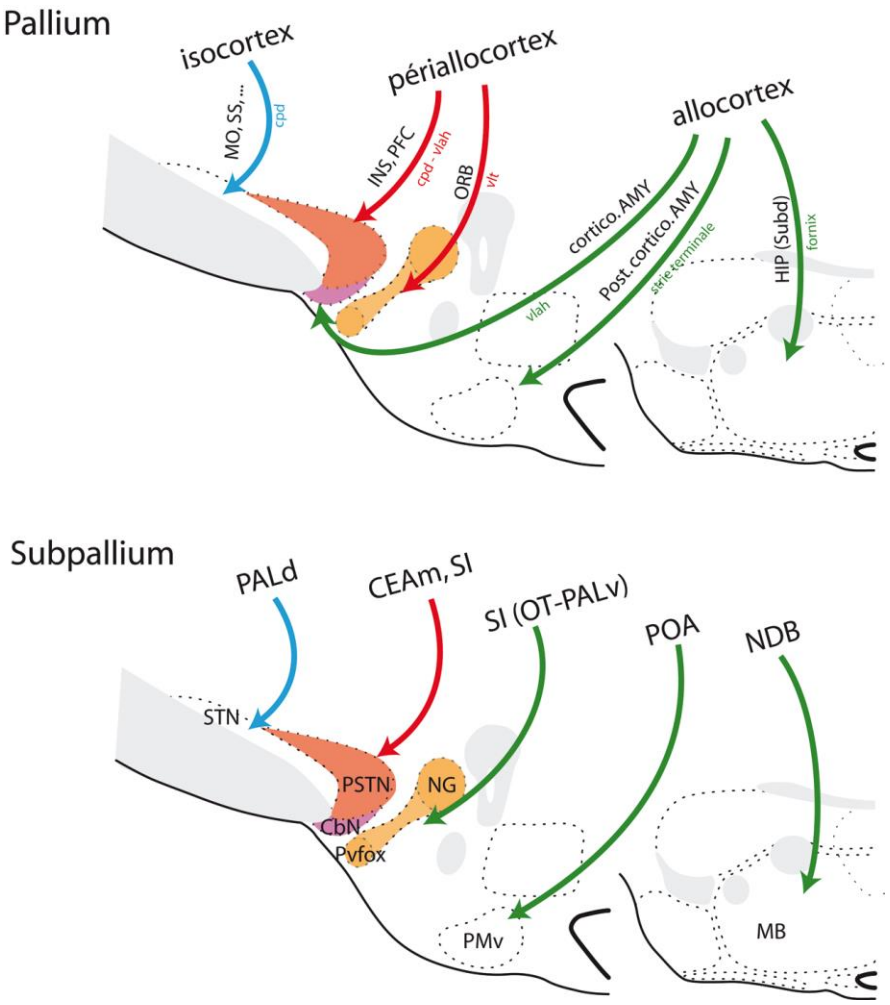

Figure 40. Schéma de l'organisation des projections issues du pallium et du subpallium dans la région postérieure de l'hypothalamus.

Chaque noyau reçoit des projections du pallium transitant par des voies différenciées et similaires. Les principales afférences subpalliales à ces structures trouvent leurs origines dans des formations associées à du pallidum.

CEAm : partie médiane du noyau central de l'amygdale ; (Post.) cortico. AMY : tractus cortico-hypothalamique médian (postérieur) ; cpd : pédoncule cérébral ; HIP : hippocampe ; INS : aires insulaires ; MB : corps mamillaire ; MO : aires somatomotrices ; NDB : noyau de la bandelette diagonale ; NG : noyau gémini ; ORB : aire orbitale ; OT : tubercule olfactif ; PALd : pallidum dorsal ; PALv : pallidum ventral ; PFC : cortex préfrontal ; POA : aire préoptique ; PMv : noyau prémamillaire ventral ; PSTN : noyau parasousthalamique ; Pvfox : noyau Parvafox ; SI : substance innominée ; SS : aires somatosensorielles ; STN : noyau sousthalamique ; Subd : subiculum dorsal ; vlah : tractus amygdalo-hypothalamique ventro-latéral ; vlt : tractus hypothalamique ventro-latéral.

3. Perspectives

L'interprétation des données anatomiques que nous avons obtenues dépasse le simple cadre du complexe PSTN/CbN et de ses fonctions. En effet, elles permettent la compréhension de l'organisation des régions postérieures de l'hypothalamus. Cependant, de nombreux travaux sont encore nécessaires afin de compléter notre hypothèse. Ces travaux intéresseront tous les domaines des Neurosciences :

- Le développement afin d'acquérir des données complémentaires concernant la différenciation des régions hypothalamiques postérieures.

- L'anatomie et l'anatomie comparée pour affiner notre modèle et tenter de comprendre comment ces régions évoluent d'un point de vue phylogénétique. La notion d'un hypothalamus conservé est quelque peu remise en question si l'on considère que l'organisation de certaines de ses divisions importantes suit celle du télencéphale et en particulier du pallium.

- Enfin, même si nous avons beaucoup orienté ce discours sur les aspects anatomiques, le complexe PSTN/CbN semble une structure dont l'étude apparait comme particulièrement prometteuse afin de comprendre des processus associés à la prise alimentaire et à l'état de maladie. C'est sur ces aspects plus fonctionnels, peut-être susceptibles de déboucher sur des applications pratiques voire cliniques intéressantes, que je souhaite poursuivre mes investigations futures. En effet, ce complexe semble très bien se prêter aux travaux par les approches modernes de manipulations génétiques de son activité. Vérifier les effets de son activation ou inactivation par optogénétique chez des animaux sains ou malades peut apporter des informations importantes pour le traitement d'anorexie ou les phénomènes de cachexie associés à des pathologies graves.

Bibliographie

Affaticati P, Yamamoto K, Rizzi B, Bureau C, Peyriéras N, Pasqualini C, Demarque M & Vernier P (2015) Identification of the optic recess region as a morphogenetic entity in the zebrafish forebrain. *Sci Rep* **5:** 8738

Albin RL, Young AB & Penney JB (1989) The functional anatomy of basal ganglia disorders. *Trends Neurosci.* **12:** 366–375

Alexander GE, DeLong MR & Strick PL (1986) Parallel organization of functionally segregated circuits linking basal ganglia and cortex. *Annu. Rev. Neurosci.* **9:** 357–381

Alheid GF (2003) Extended amygdala and basal forebrain. *Ann. N. Y. Acad. Sci.* **985:** 185–205

Allen GV & Cechetto DF (1992) Functional and anatomical organization of cardiovascular pressor and depressor sites in the lateral hypothalamic area: I. Descending projections. *J. Comp. Neurol.* **315:** 313–332

Allen GV & Cechetto DF (1993) Functional and anatomical organization of cardiovascular pressor and depressor sites in the lateral hypothalamic area. II. Ascending projections. *J. Comp. Neurol.* **330:** 421–438

Allen Institute (2004) Allen Mouse Brain Atlas. Available at: http://mouse.brain-map.org/

Altman J & Bayer SA (1986) The development of the rat hypothalamus. *Adv Anat Embryol Cell Biol* **100:** 1–178

Alvarez-Bolado G, Paul FA & Blaess S (2012) Sonic hedgehog lineage in the mouse hypothalamus: from progenitor domains to hypothalamic regions. *Neural Dev* **7:** 4

Alvarez-Bolado G, Rosenfeld MG & Swanson LW (1995) Model of forebrain regionalization based on spatiotemporal patterns of POU-III homeobox gene expression, birthdates, and morphological features. *J. Comp. Neurol.* **355:** 237–295

Alvarez-Bolado G & Swanson LW (1996) Developmental brain maps: structure of the embryonic rat brain. Amsterdam: Elsevier

Anand BK & Brobeck JR (1951) Localization of a 'feeding center' in the hypothalamus of the rat. *Proc. Soc. Exp. Biol. Med.* **77:** 323–324

Aponte Y, Atasoy D & Sternson SM (2011) AGRP neurons are sufficient to orchestrate feeding behavior rapidly and without training. *Nat Neurosci* **14:** 351–355

Arendt D, Tosches MA & Marlow H (2016) From nerve net to nerve ring, nerve cord and brain--evolution of the nervous system. *Nat. Rev. Neurosci.* **17:** 61–72

Augood SJ, Waldvogel HJ, Münkle MC, Faull RL & Emson PC (1999) Localization of calcium-binding proteins and GABA transporter (GAT-1) messenger RNA in the human subthalamic nucleus. *Neuroscience* **88:** 521–534

Aujla PK, Naratadam GT, Xu L & Raetzman LT (2013) Notch/Rbpjκ signaling regulates progenitor maintenance and differentiation of hypothalamic arcuate neurons. *Development* **140:** 3511–3521

Babalian A, Eichenberger S, Bilella A, Girard F, Szabolcsi V, Roccaro D, Alvarez-Bolado G, Xu C & Celio MR (2019) The orbitofrontal cortex projects to the parvafox nucleus of the ventrolateral hypothalamus and to its targets in the ventromedial periaqueductal grey matter. *Brain Struct Funct* **224:** 293–314

Barbier M, Chometton S, Peterschmitt Y, Fellmann D & Risold P-Y (2017) Parasubthalamic and calbindin nuclei in the posterior lateral hypothalamus are the major hypothalamic targets for projections from the central and anterior basomedial nuclei of the amygdala. *Brain Struct Funct* **222:** 2961–2991

Barbier M, Fellmann D & Risold P-Y (2018a) Characterization of McDonald's intermediate part of the Central nucleus of the amygdala in the rat. *J. Comp. Neurol.* **526:** 2165–2186

Barbier M, Fellmann D & Risold P-Y (2018b) Morphofunctional Organization of the Connections From the Medial and Intermediate Parts of the Central Nucleus of the Amygdala Into Distinct Divisions of the Lateral Hypothalamic Area in the Rat. *Front Neurol* **9:** 688

Bargmann W (1949) Über die Neurosekretorische Verknüpfung von Hypothalamus und Neurohypophyse. *Z. Zellforsch.* **34:** 610–634

Barna J, Renner E, Arszovszki A, Cservenák M, Kovács Z, Palkovits M & Dobolyi A (2018) Suckling induced activation pattern in the brain of rat pups. *Nutr Neurosci* **21:** 317–327

Bayer SA (1979a) The development of the septal region in the rat. I. Neurogenesis examined with 3H-thymidine autoradiography. *J. Comp. Neurol.* **183:** 89–106

Bayer SA (1979b) The development of the septal region in the rat. II. Morphogenesis in normal and x-irradiated embryos. *J. Comp. Neurol.* **183:** 107–120

Bayer SA & Altman J (2004) CHAPTER 2 - Development of the Telencephalon: Neural Stem Cells, Neurogenesis, and Neuronal Migration. In *The Rat Nervous System (Third Edition)*, Paxinos G (ed) pp 27–73. Burlington: Academic Press

Bergquist H & Kallen B (1953) Studies on the topography of the migration areas in the vertebrate brain. *Acta Anat (Basel)* **17:** 353–369

Bergquist H & Kallen B (1954) Notes on the early histogenesis and morphogenesis of the central nervous system in vertebrates. *J. Comp. Neurol.* **100:** 627–659

Berthoud H-R & Münzberg H (2011) The lateral hypothalamus as integrator of metabolic and environmental needs: from electrical self-stimulation to opto-genetics. *Physiol. Behav.* **104:** 29–39

Bilella A, Alvarez-Bolado G & Celio MR (2014) Coaxiality of Foxb1- and parvalbumin-expressing neurons in the lateral hypothalamic PV1-nucleus. *Neurosci. Lett.* **566:** 111–114

Bilella A, Alvarez-Bolado G & Celio MR (2016) The Foxb1-expressing neurons of the ventrolateral hypothalamic parvafox nucleus project to defensive circuits. *J. Comp. Neurol.* **524:** 2955–2981

Bittencourt JC, Presse F, Arias C, Peto C, Vaughan J, Nahon JL, Vale W & Sawchenko PE (1992) The melanin-concentrating hormone system of the rat brain: an immuno- and hybridization histochemical characterization. *J. Comp. Neurol.* **319:** 218–245

Bolam JP, Ingham CA, Izzo PN, Levey AI, Rye DB, Smith AD & Wainer BH (1986) Substance P-containing terminals in synaptic contact with cholinergic neurons in the neostriatum and basal forebrain: a double immunocytochemical study in the rat. *Brain Res.* **397:** 279–289

Bolam JP, Wainer BH & Smith AD (1984) Characterization of cholinergic neurons in the rat neostriatum. A combination of choline acetyltransferase immunocytochemistry, Golgi-impregnation and electron microscopy. *Neuroscience* **12:** 711–718

Boulant JA & Bignall KE (1973) Hypothalamic neuronal responses to peripheral and deep-body temperatures. *Am. J. Physiol.* **225:** 1371–1374

Bourgeais L, Gauriau C & Bernard JF (2001) Projections from the nociceptive area of the central nucleus of the amygdala to the forebrain: a PHA-L study in the rat. *Eur. J. Neurosci.* **14:** 229–255

Braak H (1980) Architectonics of the human telencephalic cortex. Springer, Berlin; New York

Bresson JL, Clavequin MC, Fellmann D & Bugnon C (1989) Human hypothalamic neuronal system revealed with a salmon melanin-concentrating hormone (MCH) antiserum. *Neurosci. Lett.* **102:** 39–43

Brischoux F, Cvetkovic V, Griffond B, Fellmann D & Risold PY (2002) Time of genesis determines projection and neurokinin-3 expression patterns of diencephalic neurons containing melanin-concentrating hormone. *Eur. J. Neurosci.* **16:** 1672–1680

Brischoux F, Fellmann D & Risold PY (2001) Ontogenetic development of the diencephalic MCH neurons: a hypothalamic 'MCH area' hypothesis. *Eur. J. Neurosci.* **13:** 1733–1744

Bulchand S, Grove EA, Porter FD & Tole S (2001) LIM-homeodomain gene Lhx2 regulates the formation of the cortical hem. *Mech. Dev.* **100:** 165–175

Bupesh M, Abellán A & Medina L (2011a) Genetic and experimental evidence supports the continuum of the central extended amygdala and a mutiple embryonic origin of its principal neurons. *J. Comp. Neurol.* **519:** 3507–3531

Bupesh M, Legaz I, Abellán A & Medina L (2011b) Multiple telencephalic and extratelencephalic embryonic domains contribute neurons to the medial extended amygdala. *J. Comp. Neurol.* **519:** 1505–1525

Bupesh M, Vicario A, Abellán A, Desfilis E & Medina L (2014) Dynamic expression of tyrosine hydroxylase mRNA and protein in neurons of the striatum and amygdala of mice, and experimental evidence of their multiple embryonic origin. *Brain Struct Funct* **219:** 751–776

Cajal SR (1909) Histologie du système nerveux de l'homme & des vertébrés. Paris : Maloine

Campos CA, Bowen AJ, Roman CW & Palmiter RD (2018) Encoding of danger by parabrachial CGRP neurons. *Nature* **555:** 617–622

Campos CA, Bowen AJ, Schwartz MW & Palmiter RD (2016) Parabrachial CGRP Neurons Control Meal Termination. *Cell Metab.* **23:** 811–820

de Carlos JA, López-Mascaraque L & Valverde F (1996) Dynamics of cell migration from the lateral ganglionic eminence in the rat. *J. Neurosci.* **16:** 6146–6156

Carter ME, Han S & Palmiter RD (2015) Parabrachial calcitonin gene-related peptide neurons mediate conditioned taste aversion. *J. Neurosci.* **35:** 4582–4586

Carter ME, Soden ME, Zweifel LS & Palmiter RD (2013) Genetic identification of a neural circuit that suppresses appetite. *Nature* **503:** 111–114

Cassell MD, Freedman LJ & Shi C (1999) The intrinsic organization of the central extended amygdala. *Ann. N. Y. Acad. Sci.* **877:** 217–241

Celio MR (1990) Calbindin D-28k and parvalbumin in the rat nervous system. *Neuroscience* **35:** 375–475

Chen JY, Campos CA, Jarvie BC & Palmiter RD (2018) Parabrachial CGRP Neurons Establish and Sustain Aversive Taste Memories. *Neuron* **100:** 891-899.e5

Chevalier G, Vacher S, Deniau JM & Desban M (1985) Disinhibition as a basic process in the expression of striatal functions. I. The striato-nigral influence on tecto-spinal/tecto-diencephalic neurons. *Brain Res.* **334:** 215–226

Chometton S (2015) Thèse : Organisation morphofonctionnelle de l'hypothalamus latéral postérieur chez le rongeur.

Chometton S, Franchi G, Houdayer C, Mariot A, Poncet F, Fellmann D, Tillet Y & Risold PY (2014) Different distributions of preproMCH and hypocretin/orexin in the forebrain of the pig (Sus scrofa domesticus). *J. Chem. Neuroanat.* **61–62:** 72–82

Chometton S, Pedron S, Peterschmitt Y, Van Waes V, Fellmann D & Risold P-Y (2016) A premammillary lateral hypothalamic nuclear complex responds to hedonic but not aversive tastes in the male rat. *Brain Struct Funct* **221:** 2183–2208

Chu H-Y, McIver EL, Kovaleski RF, Atherton JF & Bevan MD (2017) Loss of Hyperdirect Pathway Cortico-Subthalamic Inputs Following Degeneration of Midbrain Dopamine Neurons. *Neuron* **95:** 1306-1318.e5

Cobos I, Puelles L & Martínez S (2001) The avian telencephalic subpallium originates inhibitory neurons that invade tangentially the pallium (dorsal ventricular ridge and cortical areas). *Dev. Biol.* **239:** 30–45

Cocas LA, Miyoshi G, Carney RSE, Sousa VH, Hirata T, Jones KR, Fishell G, Huntsman MM & Corbin JG (2009) Emx1-lineage progenitors differentially contribute to neural diversity in the striatum and amygdala. *J. Neurosci.* **29:** 15933–15946

Comoli E, Ribeiro-Barbosa ER, Negrão N, Goto M & Canteras NS (2005) Functional mapping of the prosencephalic systems involved in organizing predatory behavior in rats. *Neuroscience* **130:** 1055–1067

Croizier S, Amiot C, Chen X, Presse F, Nahon J-L, Wu JY, Fellmann D & Risold P-Y (2011) Development of Posterior Hypothalamic Neurons Enlightens a Switch in the Prosencephalic Basic Plan. *PLoS ONE* **6:** e28574

Croizier S, Cardot J, Brischoux F, Fellmann D, Griffond B & Risold PY (2013) The vertebrate diencephalic MCH system: a versatile neuronal population in an evolving brain. *Front Neuroendocrinol* **34:** 65–87

Croizier S, Chometton S, Fellmann D & Risold P-Y (2015) Characterization of a mammalian prosencephalic functional plan. *Front Neuroanat* **8:** 161

Croizier S, Franchi-Bernard G, Colard C, Poncet F, La Roche A & Risold P-Y (2010) A Comparative Analysis Shows Morphofunctional Differences between the Rat and Mouse Melanin-Concentrating Hormone Systems. *PLoS ONE* **5:** e15471

Crosby EC & Woodburne RT (1940) The comparative anatomy of the preoptic area and the hypothalamus. *Assoc Res Nerv Ment Dis* **20:** 52–169

Cvetkovic V, Poncet F, Fellmann D, Griffond B & Risold PY (2003) Diencephalic neurons producing melanin-concentrating hormone are influenced by local and multiple extra-hypothalamic tachykininergic projections through the neurokinin 3 receptor. *Neuroscience* **119:** 1113–1145

Daitz HM & Powell TP (1954) Studies of the connexions of the fornix system. *J. Neurol. Neurosurg. Psychiatry* **17:** 75–82

Deniau JM & Chevalier G (1985) Disinhibition as a basic process in the expression of striatal functions. II. The striato-nigral influence on thalamocortical cells of the ventromedial thalamic nucleus. *Brain Res.* **334:** 227–233

D'Hanis W, Linke R & Yilmazer-Hanke DM (2007) Topography of thalamic and parabrachial calcitonin gene-related peptide (CGRP) immunoreactive neurons projecting to subnuclei of the amygdala and extended amygdala. *J. Comp. Neurol.* **505:** 268–291

Diez-Roux G, Banfi S, Sultan M, Geffers L, Anand S, Rozado D, Magen A, Canidio E, Pagani M, Peluso I, Lin-Marq N, Koch M, Bilio M, Cantiello I, Verde R, De Masi C, Bianchi SA, Cicchini J, Perroud E, Mehmeti S, et al (2011) A high-resolution anatomical atlas of the transcriptome in the mouse embryo. *PLoS Biol.* **9:** e1000582

Dobolyi A, Irwin S, Makara G, Usdin TB & Palkovits M (2005) Calcitonin gene-related peptide-containing pathways in the rat forebrain. *J. Comp. Neurol.* **489:** 92–119

Dong H-W & Swanson LW (2004) Organization of axonal projections from the anterolateral area of the bed nuclei of the stria terminalis. *J. Comp. Neurol.* **468:** 277–298

Duncan RN, Xie Y, McPherson AD, Taibi AV, Bonkowsky JL, Douglass AD & Dorsky RI (2016) Hypothalamic radial glia function as self-renewing neural progenitors in the absence of Wnt/β-catenin signaling. *Development* **143:** 45–53

Eisenstat DD, Liu JK, Mione M, Zhong W, Yu G, Anderson SA, Ghattas I, Puelles L & Rubenstein JL (1999) DLX-1, DLX-2, and DLX-5 expression define distinct stages of basal forebrain differentiation. *J. Comp. Neurol.* **414:** 217–237

Elias CF, Lee CE, Kelly JF, Ahima RS, Kuhar M, Saper CB & Elmquist JK (2001) Characterization of CART neurons in the rat and human hypothalamus. *J. Comp. Neurol.* **432:** 1–19

Elias CF, Sita LV, Zambon BK, Oliveira ER, Vasconcelos L a. P & Bittencourt JC (2008a) Melanin-concentrating hormone projections to areas involved in somatomotor responses. *J. Chem. Neuroanat.* **35:** 188–201

Elias WJ, Ray DK & Jane JA (2008b) Lennart Heimer: concepts of the ventral striatum and extended amygdala. *Neurosurgical Focus* **25:** E8

Elshatory Y & Gan L (2008) The LIM-homeobox gene Islet-1 is required for the development of restricted forebrain cholinergic neurons. *J. Neurosci.* **28:** 3291–3297

Engelhardt E (2013) Meynert and the basal nucleus. *Dement Neuropsychol* **7:** 435–438

Epstein A (1971) The lateral hypothalamic syndrome: Its implications for the physiological psychology of hunger and thirst. *Progress in Physiological Psychology* **4:** 263–317

Feldblum S, Erlander MG & Tobin AJ (1993) Different distributions of GAD65 and GAD67 mRNAs suggest that the two glutamate decarboxylases play distinctive functional roles. *J. Neurosci. Res.* **34:** 689–706

Fernandez De Molina A & Hunsperger RW (1962) Organization of the subcortical system governing defence and flight reactions in the cat. *J. Physiol. (Lond.)* **160:** 200–213

Ferrier D (1876) The Functions of the brain. London: Smith, Elder & Co.

Filimonoff IN (1947) A rational subdivision of the cerebral cortex. *Arch Neurol Psychiatry* **58:** 296–311

Fitzsimons JT (1979) The physiology of thirst and sodium appetite. *Monogr Physiol Soc* **35:** 1–572

Flames N, Pla R, Gelman DM, Rubenstein JLR, Puelles L & Marín O (2007) Delineation of multiple subpallial progenitor domains by the combinatorial expression of transcriptional codes. *J. Neurosci.* **27:** 9682–9695

Flandin P, Kimura S & Rubenstein JLR (2010) The progenitor zone of the ventral medial ganglionic eminence requires Nkx2-1 to generate most of the globus pallidus but few neocortical interneurons. *J. Neurosci.* **30:** 2812–2823

Fujiyama F, Takahashi S & Karube F (2015) Morphological elucidation of basal ganglia circuits contributing reward prediction. *Front Neurosci* **9:** 6

Fulton JF, Ranson SW & Frantz AM (1940) The hypothalamus and central levels of autonomic function. Baltimore: The Williams & Wilkins Co.

Ganser SJM (1882) Vergleichend-anatomische studien über das gehirn des maulwurfs. *Morphol. Jb.* **7:** 591–725

García-Cabezas MÁ, Zikopoulos B & Barbas H (2019) The Structural Model: a theory linking connections, plasticity, pathology, development and evolution of the cerebral cortex. *Brain Struct Funct* **224:** 985–1008

García-López M, Abellán A, Legaz I, Rubenstein JLR, Puelles L & Medina L (2008) Histogenetic compartments of the mouse centromedial and extended amygdala based on gene expression patterns during development. *J. Comp. Neurol.* **506:** 46–74

Geeraedts LM, Nieuwenhuys R & Veening JG (1990) Medial forebrain bundle of the rat: IV. Cytoarchitecture of the caudal (lateral hypothalamic) part of the medial forebrain bundle bed nucleus. *J. Comp. Neurol.* **294:** 537–568

Gerfen CR, Baimbridge KG & Miller JJ (1985) The neostriatal mosaic: compartmental distribution of calcium-binding protein and parvalbumin in the basal ganglia of the rat and monkey. *Proc. Natl. Acad. Sci. U.S.A.* **82:** 8780–8784

Gerfen CR & Bolam JP (2016) Chapter 1 - The Neuroanatomical Organization of the Basal Ganglia. In *Handbook of Behavioral Neuroscience*, Steiner H & Tseng KY (eds) pp 3–32. Elsevier

Gerfen CR & Wilson CJ (1996) Chapter II. The basal ganglia. In *Integrated Systems of the CNS, Part III* pp 371–468. Amsterdam: Elsevier

Gilpin NW, Herman MA & Roberto M (2015) The central amygdala as an integrative hub for anxiety and alcohol use disorders. *Biol. Psychiatry* **77:** 859–869

Gonzales C & Chesselet MF (1990) Amygdalonigral pathway: an anterograde study in the rat with Phaseolus vulgaris leucoagglutinin (PHA-L). *J. Comp. Neurol.* **297:** 182–200

González A, López JM & Marín O (2002) Expression pattern of the homeobox protein NKX2-1 in the developing Xenopus forebrain. *Brain Res. Gene Expr. Patterns* **1:** 181–185

González JA, Iordanidou P, Strom M, Adamantidis A & Burdakov D (2016) Awake dynamics and brain-wide direct inputs of hypothalamic MCH and orexin networks. *Nat Commun* **7:** 11395

Gonzalo-Ruiz A, Alonso A, Sanz JM & Llinás RR (1992) Afferent projections to the mammillary complex of the rat, with special reference to those from surrounding hypothalamic regions. *J. Comp. Neurol.* **321:** 277–299

Goto M & Swanson LW (2004) Axonal projections from the parasubthalamic nucleus. *J. Comp. Neurol.* **469:** 581–607

Gray TS, Carney ME & Magnuson DJ (1989) Direct projections from the central amygdaloid nucleus to the hypothalamic paraventricular nucleus: possible role in stress-induced adrenocorticotropin release. *Neuroendocrinology* **50:** 433–446

Graybiel AM & Ragsdale CW (1978) Histochemically distinct compartments in the striatum of human, monkeys, and cat demonstrated by acetylthiocholinesterase staining. *Proc. Natl. Acad. Sci. U.S.A.* **75:** 5723–5726

Griffond B & Risold PY (2009) MCH and feeding behavior-interaction with peptidic network. *Peptides* **30:** 2045–2051

Grillner S & Robertson B (2016) The Basal Ganglia Over 500 Million Years. *Curr. Biol.* **26:** R1088–R1100

Groenewegen HJ & Berendse HW (1990) Connections of the subthalamic nucleus with ventral striatopallidal parts of the basal ganglia in the rat. *J. Comp. Neurol.* **294:** 607–622

Groenewegen HJ, Berendse HW & Haber SN (1993) Organization of the output of the ventral striatopallidal system in the rat: ventral pallidal efferents. *Neuroscience* **57:** 113–142

Grove EA (1988) Neural associations of the substantia innominata in the rat: afferent connections. *J. Comp. Neurol.* **277:** 315–346

Grupp L, Wolburg H & Mack AF (2010) Astroglial structures in the zebrafish brain. *J. Comp. Neurol.* **518:** 4277–4287

Gurdjian ES (1927) The diencephalon of the albino rat. Studies on the brain of the rat. No. 2. *J. Comp. Neurol.* **43:** 1–114

Hahn JD (2010) Comparison of melanin-concentrating hormone and hypocretin/orexin peptide expression patterns in a current parceling scheme of the lateral hypothalamic zone. *Neurosci. Lett.* **468:** 12–17

Hahn JD & Swanson LW (2010) Distinct patterns of neuronal inputs and outputs of the juxtaparaventricular and suprafornical regions of the lateral hypothalamic area in the male rat. *Brain Res Rev* **64:** 14–103

Han S, Soleiman MT, Soden ME, Zweifel LS & Palmiter RD (2015) Elucidating an Affective Pain Circuit that Creates a Threat Memory. *Cell* **162:** 363–374

Han W, Tellez LA, Rangel MJ, Motta SC, Zhang X, Perez IO, Canteras NS, Shammah-Lagnado SJ, van den Pol AN & de Araujo IE (2017) Integrated Control of Predatory Hunting by the Central Nucleus of the Amygdala. *Cell* **168:** 311-324.e18

Haynes WIA & Haber SN (2013) The organization of prefrontal-subthalamic inputs in primates provides an anatomical substrate for both functional specificity and integration: implications for Basal Ganglia models and deep brain stimulation. *J. Neurosci.* **33:** 4804–4814

Heimer L & Wilson RD (1975) The subcortical projections of the allocortex: similarities in the neural associations of the hippocampus, the piriform cortex and the neocortex. In *Golgi centennial symposium proceedings* pp 177–193. New York: Santini M

Hendrickson AE, Wagoner N & Cowan WM (1972) An autoradiographic and electron microscopic study of retino-hypothalamic connections. *Z Zellforsch Mikrosk Anat* **135:** 1–26

Herrick CJ (1910) The morphology of the forebrain in amphibia and reptilia. *Journal of Comparative Neurology and Psychology* **20:** 413–547

Hetherington AE & Ranson S (1939) Experimental hypothalamico-hypophyseal obesity in the rat. *Proc. Soc. Exp. Biol. Med.* **41:** 465–466

Hirata T, Li P, Lanuza GM, Cocas LA, Huntsman MM & Corbin JG (2009) Identification of distinct telencephalic progenitor pools for neuronal diversity in the amygdala. *Nat. Neurosci.* **12:** 141–149

His W (1893) Vorschläge zur Einteilung des Gehirns. *Arch. Anat. Entwicklungsgesch (Leipzig)* **17:** 172–179

Hof PR, Young WG, Bloom FE, Belichenko PV & Celio MR eds. (2000) Comparative Cytoarchitectonic Atlas of the C57BL/6 and 129/Sv Mouse Brains. Amsterdam: Elsevier

Holmgren N (1925) Points of View Concerning Fore-Brain Morphology in Higher Vertebrates. *Acta Zoologica* **6:** 413–459

Hunt SP & Mantyh PW (2001) The molecular dynamics of pain control. *Nat. Rev. Neurosci.* **2:** 83–91

Huxley TH (1871) The anatomy of vertebrated animals.

Jennings JH, Rizzi G, Stamatakis AM, Ung RL & Stuber GD (2013) The Inhibitory Circuit Architecture of the Lateral Hypothalamus Orchestrates Feeding. *Science* **341:** 1517–1521

Kalin NH, Shelton SE & Davidson RJ (2004) The role of the central nucleus of the amygdala in mediating fear and anxiety in the primate. *J. Neurosci.* **24:** 5506–5515

Kappers CUA, Huber GC & Crosby EC (1936) The comparative anatomy of the nervous system of vertebrates including man. The Macmillan Company. New York

Kemp JM & Powell TP (1971) The structure of the caudate nucleus of the cat: light and electron microscopy. *Philos. Trans. R. Soc. Lond., B, Biol. Sci.* **262:** 383–401

Keyser A (1972) The development of the diencephalon of the Chinese hamster. An investigation of the validity of the criteria of subdivision of the brain. *Acta Anat Suppl (Basel)* **59:** 1–178

Keyser A (1979) Development of the hypothalamus in mammals, An investigation into its morphological position during ontogenesis. In *Handbook of the hypothalamus. Anatomy of the hypothalamus.* pp 65–136. New York: Morgane PJ and Pankseep J.

Kim J, Zhang X, Muralidhar S, LeBlanc SA & Tonegawa S (2017) Basolateral to Central Amygdala Neural Circuits for Appetitive Behaviors. *Neuron* **93:** 1464-1479.e5

Köhler C & Chan-Palay V (1983) Distribution of gamma aminobutyric acid containing neurons and terminals in the septal area. An immunohistochemical study using antibodies to glutamic acid decarboxylase in the rat brain. *Anat. Embryol.* **167:** 53–65

Köhler C, Haglund L & Swanson LW (1984) A diffuse alpha MSH-immunoreactive projection to the hippocampus and spinal cord from individual neurons in the lateral hypothalamic area and zona incerta. *J. Comp. Neurol.* **223:** 501–514

Krettek JE & Price JL (1978) Amygdaloid projections to subcortical structures within the basal forebrain and brainstem in the rat and cat. *J. Comp. Neurol.* **178:** 225–253

Krolewski DM, Medina A, Kerman IA, Bernard R, Burke S, Thompson RC, Bunney WE, Schatzberg AF, Myers RM, Akil H, Jones EG & Watson SJ (2010) Expression patterns of corticotropin-releasing factor, arginine vasopressin, histidine decarboxylase, melanin-concentrating hormone, and orexin genes in the human hypothalamus. *J. Comp. Neurol.* **518:** 4591–4611

Künzle H (1975) Bilateral projections from precentral motor cortex to the putamen and other parts of the basal ganglia. An autoradiographic study in Macaca fascicularis. *Brain Res.* **88:** 195–209

Le Gros Clark WE, Beattie J, Riddoch G & Dott NM (1939) The Hypothalamus: Morphological, Functional, Clinical and Surgical Aspects. *Can Med Assoc J* **40:** 422

Lee HJ, Gallagher M & Holland PC (2010) The central amygdala projection to the substantia nigra reflects prediction error information in appetitive conditioning. *Learn. Mem.* **17:** 531–538

Lee HJ, Groshek F, Petrovich GD, Cantalini JP, Gallagher M & Holland PC (2005) Role of Amygdalo-Nigral Circuitry in Conditioning of a Visual Stimulus Paired with Food. *J. Neurosci.* **25:** 3881–3888

Lin J-Y, Arthurs J & Reilly S (2015) Gustatory insular cortex, aversive taste memory and taste neophobia. *Neurobiol Learn Mem* **119:** 77–84

Lin J-Y & Reilly S (2012) Amygdala-gustatory insular cortex connections and taste neophobia. *Behav. Brain Res.* **235:** 182–188

Lin J-Y, Roman C, Arthurs J & Reilly S (2012) Taste neophobia and c-Fos expression in the rat brain. *Brain Res.* **1448:** 82–88

Marchant NJ, Densmore VS & Osborne PB (2007) Coexpression of prodynorphin and corticotrophin-releasing hormone in the rat central amygdala: evidence of two distinct endogenous opioid systems in the lateral division. *J. Comp. Neurol.* **504:** 702–715

Marin O, Anderson SA & Rubenstein JL (2000) Origin and molecular specification of striatal interneurons. *J. Neurosci.* **20:** 6063–6076

Marin O & Rubenstein JL (2001) A long, remarkable journey: tangential migration in the telencephalon. *Nat. Rev. Neurosci.* **2:** 780–790

Martin DM, Skidmore JM, Philips ST, Vieira C, Gage PJ, Condie BG, Raphael Y, Martinez S & Camper SA (2004) PITX2 is required for normal development of neurons in the mouse subthalamic nucleus and midbrain. *Dev. Biol.* **267:** 93–108

McDonald AJ (1982) Cytoarchitecture of the central amygdaloid nucleus of the rat. *J. Comp. Neurol.* **208:** 401–418

McDonald AJ (1997) Calbindin-D28k immunoreactivity in the rat amygdala. *J. Comp. Neurol.* **383:** 231–244

McGeorge AJ & Faull RL (1989) The organization of the projection from the cerebral cortex to the striatum in the rat. *Neuroscience* **29:** 503–537

Medina L & Abellán A (2009) Development and evolution of the pallium. *Semin. Cell Dev. Biol.* **20:** 698–711

Medina L, Abellán A, Vicario A & Desfilis E (2014) Evolutionary and developmental contributions for understanding the organization of the basal ganglia. *Brain Behav. Evol.* **83:** 112–125

Medina L, Bupesh M & Abellán A (2011) Contribution of genoarchitecture to understanding forebrain evolution and development, with particular emphasis on the amygdala. *Brain Behav. Evol.* **78:** 216–236

Medina L & Reiner A (1995) Neurotransmitter organization and connectivity of the basal ganglia in vertebrates: implications for the evolution of basal ganglia. *Brain Behav. Evol.* **46:** 235–258

Mészár Z, Girard F, Saper CB & Celio MR (2012) The lateral hypothalamic parvalbumin-immunoreactive (PV1) nucleus in rodents. *J. Comp. Neurol.* **520:** 798–815

Millhouse OE (1969) A Golgi study of the desending medial forebrain bundle. *Brain Res.* **15:** 341–363

Millhouse OE (1979) A golgi anatomy of the rodent hypothalamus. In *Handbook of the hypothalamus, Anatomy of the hypothalamus* pp 221–265. New York and Basel: Morgane P, Panksepp J

Millhouse OE (1987) Granule cells of the olfactory tubercle and the question of the islands of Calleja. *J. Comp. Neurol.* **265:** 1–24

Moga MM, Herbert H, Hurley KM, Yasui Y, Gray TS & Saper CB (1990) Organization of cortical, basal forebrain, and hypothalamic afferents to the parabrachial nucleus in the rat. *J. Comp. Neurol.* **295:** 624–661

Mogenson GJ, Swanson LW & Wu M (1983) Neural projections from nucleus accumbens to globus pallidus, substantia innominata, and lateral preoptic-lateral hypothalamic area: an anatomical and electrophysiological investigation in the rat. *J. Neurosci.* **3:** 189–202

Mogenson GJ, Swanson LW & Wu M (1985) Evidence that projections from substantia innominata to zona incerta and mesencephalic locomotor region contribute to locomotor activity. *Brain Res.* **334:** 65–76

Montiel JF & Aboitiz F (2015) Pallial patterning and the origin of the isocortex. *Front Neurosci* **9:** 377

Moore RY & Lenn NJ (1972) A retinohypothalamic projection in the rat. *J. Comp. Neurol.* **146:** 1–14

Moraga-Amaro R, Cortés-Rojas A, Simon F & Stehberg J (2014) Role of the insular cortex in taste familiarity. *Neurobiol Learn Mem* **109:** 37–45

Moreno N & González A (2011) The non-evaginated secondary prosencephalon of vertebrates. *Front Neuroanat* **5:** 12

Moreno N, González A & Rétaux S (2009) Development and evolution of the subpallium. *Semin. Cell Dev. Biol.* **20:** 735–743

Morgane PJ & Panksepp J eds. (1979) Handbook of the hypothalamus : Anatomy of the hypothalamus. New York: Marcel Dekker

Nambu A, Tokuno H & Takada M (2002) Functional significance of the cortico-subthalamo-pallidal 'hyperdirect' pathway. *Neurosci. Res.* **43:** 111–117

Nieuwenhuys R, Donkelaar HJ ten & Nicholson C (1998) The central nervous system of vertebrates. Berlin: Springer-Verlag

Nieuwenhuys R, Geeraedts LMG & Veening JG (1982) The medial forebrain bundle of the rat. I. General introduction. *J. Comp. Neurol.* **206:** 49–81

Nieuwenhuys R & Puelles L (2016) Towards a new neuromorphology. London: Springer International Publishing

Niu J-G, Yokota S, Tsumori T, Oka T & Yasui Y (2012) Projections from the anterior basomedial and anterior cortical amygdaloid nuclei to melanin-concentrating hormone-containing neurons in the lateral hypothalamus of the rat. *Brain Res.* **1479:** 31–43

Nóbrega-Pereira S, Gelman D, Bartolini G, Pla R, Pierani A & Marín O (2010) Origin and molecular specification of globus pallidus neurons. *J. Neurosci.* **30:** 2824–2834

Ocaña FM, Suryanarayana SM, Saitoh K, Kardamakis AA, Capantini L, Robertson B & Grillner S (2015) The lamprey pallium provides a blueprint of the mammalian motor projections from cortex. *Curr. Biol.* **25:** 413–423

Oka T, Tsumori T, Yokota S & Yasui Y (2008) Neuroanatomical and neurochemical organization of projections from the central amygdaloid nucleus to the nucleus retroambiguus via the periaqueductal gray in the rat. *Neurosci. Res.* **62:** 286–298

Okamura H, Abitbol M, Julien JF, Dumas S, Bérod A, Geffard M, Kitahama K, Bobillier P, Mallet J & Wiklund L (1990) Neurons containing messenger RNA encoding glutamate decarboxylase in rat hypothalamus demonstrated by in situ hybridization, with special emphasis on cell groups in medial preoptic area, anterior hypothalamic area and dorsomedial hypothalamic nucleus. *Neuroscience* **39:** 675–699

Olds J (1962) Hypothalamic substrates of reward. *Physiol. Rev.* **42:** 554–604

de Olmos JS, Beltramino CA & Alheid G (2004) CHAPTER 19 - Amygdala and Extended Amygdala of the Rat: A Cytoarchitectonical, Fibroarchitectonical, and Chemoarchitectonical Survey. In *The Rat Nervous System (THIRD EDITION)*, Paxinos G (ed) pp 509–603. Burlington: Academic Press

de Olmos JS & Heimer L (1999) The concepts of the ventral striatopallidal system and extended amygdala. *Ann. N. Y. Acad. Sci.* **877:** 1–32

Ono T, Luiten PG, Nishijo H, Fukuda M & Nishino H (1985) Topographic organization of projections from the amygdala to the hypothalamus of the rat. *Neurosci. Res.* **2:** 221–238

Onteniente B, Tago H, Kimura H & Maeda T (1986) Distribution of gamma-aminobutyric acid-immunoreactive neurons in the septal region of the rat brain. *J. Comp. Neurol.* **248:** 422–430

Orr H (1887) Contribution to the embryology of the lizard; With especial reference to the central nervous system and some organs of the head; together with observations on the origin of the vertebrates. *J. Morphol.* **1:** 311–372

Ottersen OP (1980) Afferent connections to the amygdaloid complex of the rat and cat: II. Afferents from the hypothalamus and the basal telencephalon. *J. Comp. Neurol.* **194:** 267–289

Palmiter RD (2018) The Parabrachial Nucleus: CGRP Neurons Function as a General Alarm. *Trends Neurosci.* **41:** 280–293

Panula P, Revuelta AV, Cheney DL, Wu JY & Costa E (1984) An immunohistochemical study on the location of GABAergic neurons in rat septum. *J. Comp. Neurol.* **222:** 69–80

Papez JW (1995) A proposed mechanism of emotion. 1937. *J Neuropsychiatry Clin Neurosci* **7:** 103–112

Pautrat A, Rolland M, Barthelemy M, Baunez C, Sinniger V, Piallat B, Savasta M, Overton PG, David O & Coizet V (2018) Revealing a novel nociceptive network that links the subthalamic nucleus to pain processing. *Elife* **7:** e36607

Paxinos G & Franklin KBJ (2007) The Mouse Brain in Stereotaxic Coordinates. Third Edition. Amsterdam: Academic Press

Paxinos G & Watson C (2005) The rat brain in stereotaxic coordinates. Fifth Edition. San Diego: Elsevier Academic Press

Paxinos G & Watson C (2013) The rat brain in stereotaxic coordinates. Seventh Edition. New York: Academic Press

Petrovich GD, Setlow B, Holland PC & Gallagher M (2002) Amygdalo-hypothalamic circuit allows learned cues to override satiety and promote eating. *J. Neurosci.* **22:** 8748–8753

Petrovich GD & Swanson LW (1997) Projections from the lateral part of the central amygdalar nucleus to the postulated fear conditioning circuit. *Brain Res.* **763:** 247–254

Peyron C, Tighe DK, van den Pol AN, de Lecea L, Heller HC, Sutcliffe JG & Kilduff TS (1998) Neurons containing hypocretin (orexin) project to multiple neuronal systems. *J. Neurosci.* **18:** 9996–10015

Pombero A, Bueno C, Saglietti L, Rodenas M, Guimera J, Bulfone A & Martinez S (2011) Pallial origin of basal forebrain cholinergic neurons in the nucleus basalis of Meynert and horizontal limb of the diagonal band nucleus. *Development* **138:** 4315–4326

Potter GB, Petryniak MA, Shevchenko E, McKinsey GL, Ekker M & Rubenstein JLR (2009) Generation of Cre-transgenic mice using Dlx1/Dlx2 enhancers and their characterization in GABAergic interneurons. *Mol. Cell. Neurosci.* **40:** 167–186

Poulain P (1983) Hypothalamic projection to the lateral septum in the guinea pig an HRP study. *Brain Res. Bull.* **10:** 309–313

Poulain P, Martin-Bouyer L, Beauvillain JC & Tramu G (1984) Study of the efferent connections of the enkephalinergic magnocellular dorsal nucleus in the guinea-pig hypothalamus using lesions, retrograde tracing and immunohistochemistry: evidence for a projection to the lateral septum. *Neuroscience* **11:** 331–343

Puelles L (1995) A segmental morphological paradigm for understanding vertebrate forebrains. *Brain Behav. Evol.* **46:** 319–337

Puelles L (2017) Comments on the Updated Tetrapartite Pallium Model in the Mouse and Chick, Featuring a Homologous Claustro-Insular Complex. *Brain Behav. Evol.* **90:** 171–189

Puelles L, Harrison M, Paxinos G & Watson C (2013) A developmental ontology for the mammalian brain based on the prosomeric model. *Trends Neurosci.* **36:** 570–578

Puelles L, Martinez-de-la-Torre M, Bardet S & Rubenstein JLR (2012) Hypothalamus. In *The mouse nervous system* pp 221–312. San Diego: Elsevier

Puelles L & Rubenstein JL (1993) Expression patterns of homeobox and other putative regulatory genes in the embryonic mouse forebrain suggest a neuromeric organization. *Trends Neurosci.* **16:** 472–479

Puelles L & Rubenstein JLR (2003) Forebrain gene expression domains and the evolving prosomeric model. *Trends Neurosci.* **26:** 469–476

Puelles L & Rubenstein JLR (2015) A new scenario of hypothalamic organization: rationale of new hypotheses introduced in the updated prosomeric model. *Front Neuroanat* **9:** 27

Puelles L, Tvrdik P & Martínez-de-la-Torre M (2019) The Postmigratory Alar Topography of Visceral Cranial Nerve Efferents Challenges the Classical Model of Hindbrain Columns. *Anat Rec (Hoboken)* **302:** 485–504

Raab A, Popp S, Lesch K-P, Lohse MJ, Fischer M, Deckert J & Hommers L (2018) Increased fear learning, spatial learning as well as neophobia in Rgs2-/- mice. *Genes Brain Behav.* **17:** e12420

Rakic P (2009) Evolution of the neocortex: a perspective from developmental biology. *Nat. Rev. Neurosci.* **10:** 724–735

Risold (2004) CHAPTER 20 - The Septal Region. In *The Rat Nervous System (Third Edition)*, Paxinos G (ed) pp 605–632. Burlington: Academic Press

Risold PY, Canteras NS & Swanson LW (1994) Organization of projections from the anterior hypothalamic nucleus: a Phaseolus vulgaris-leucoagglutinin study in the rat. *J. Comp. Neurol.* **348:** 1–40

Risold PY, Croizier S, Legagneux K, Brischoux F, Fellmann D & Griffond B (2009) The development of the MCH system. *Peptides* **30:** 1969–1972

Risold PY & Swanson LW (1995) Evidence for a hypothalamothalamocortical circuit mediating pheromonal influences on eye and head movements. *Proc Natl Acad Sci U S A* **92:** 3898–3902

Risold PY & Swanson LW (1996) Structural evidence for functional domains in the rat hippocampus. *Science* **272:** 1484–1486

Risold PY & Swanson LW (1997a) Chemoarchitecture of the rat lateral septal nucleus. *Brain Res. Brain Res. Rev.* **24:** 91–113

Risold PY & Swanson LW (1997b) Connections of the rat lateral septal complex. *Brain Res. Rev.* **24:** 115–195

Risold PY, Thompson RH & Swanson LW (1997) The structural organization of connections between hypothalamus and cerebral cortex. *Brain Res. Brain Res. Rev.* **24:** 197–254

Roberts A, Dale N, Ottersen OP & Storm-Mathisen J (1987) The early development of neurons with GABA immunoreactivity in the CNS of Xenopus laevis embryos. *J. Comp. Neurol.* **261:** 435–449

Robins SC, Stewart I, McNay DE, Taylor V, Giachino C, Goetz M, Ninkovic J, Briancon N, Maratos-Flier E, Flier JS, Kokoeva MV & Placzek M (2013) α-Tanycytes of the adult hypothalamic third ventricle include distinct populations of FGF-responsive neural progenitors. *Nat Commun* **4:** 2049

Rolls BJ & Rolls ET (1982) Thirst. New York: Cambridge University Press

Rubenstein JL, Martinez S, Shimamura K & Puelles L (1994) The embryonic vertebrate forebrain: the prosomeric model. *Science* **266:** 578–580

Rubenstein JL & Puelles L (1994) Homeobox gene expression during development of the vertebrate brain. *Curr. Top. Dev. Biol.* **29:** 1–63

Sanides F (1970) Functional architecture of motor and sensory cortices in primates in the light of a new concept of neocortex evolution. In *The primate brain: advances in primatology.* pp 137–208. New York: Appleton-Century-Crofts Educational Division/ Meredith Corporation

Saper CB (1985) Organization of cerebral cortical afferent systems in the rat. II. Hypothalamocortical projections. *J. Comp. Neurol.* **237:** 21–46

Saper CB (2004) CHAPTER 24 - Central Autonomic System. In *The Rat Nervous System (Third Edition)*, Paxinos G (ed) pp 761–796. Burlington: Academic Press

Saper CB, Akil H & Watson SJ (1986) Lateral hypothalamic innervation of the cerebral cortex: immunoreactive staining for a peptide resembling but immunochemically distinct from pituitary/arcuate alpha-melanocyte stimulating hormone. *Brain Res. Bull.* **16:** 107–120

Saper CB, Lu J, Chou TC & Gooley J (2005) The hypothalamic integrator for circadian rhythms. *Trends Neurosci.* **28:** 152–157

Scharrer E & Scharrer B (1940) Secretory cells within the hypothalamus. *Proc. Assoc. Res. Nervous Mental Dis.***:** 170–194

Schiff HC, Bouhuis AL, Yu K, Penzo MA, Li H, He M & Li B (2018) An Insula-Central Amygdala Circuit for Guiding Tastant-Reinforced Choice Behavior. *J. Neurosci.* **38:** 1418–1429

Schulze G, Tetzner M & Topolinski H (1981) Operant thermoregulation of rats with anterior hypothalamic lesions. *Naunyn-Schmiedeberg's Arch. Pharmacol.* **318:** 43–48

Schwaber JS, Sternini C, Brecha NC, Rogers WT & Card JP (1988) Neurons containing calcitonin gene-related peptide in the parabrachial nucleus project to the central nucleus of the amygdala. *J. Comp. Neurol.* **270:** 416–426, 398–399

Shimogori T, Lee DA, Miranda-Angulo A, Yang Y, Wang H, Jiang L, Yoshida AC, Kataoka A, Mashiko H, Avetisyan M, Qi L, Qian J & Blackshaw S (2010) A genomic atlas of mouse hypothalamic development. *Nat. Neurosci.* **13:** 767–775

Shin J-W, Geerling JC, Stein MK, Miller RL & Loewy AD (2011) FoxP2 brainstem neurons project to sodium appetite regulatory sites. *J. Chem. Neuroanat.* **42:** 1–23

Shirasu M, Takahashi T, Yamamoto T, Itoh K, Sato S & Nakamura H (2011) Direct projections from the central amygdaloid nucleus to the mesencephalic trigeminal nucleus in rats. *Brain Res.* **1400:** 19–30

Simerly RB (2004) CHAPTER 14 - Anatomical Substrates of Hypothalamic Integration. In *The Rat Nervous System (Third Edition)*, Paxinos G (ed) pp 335–368. Burlington: Academic Press

Skidmore JM, Cramer JD, Martin JF & Martin DM (2008) Cre fate mapping reveals lineage specific defects in neuronal migration with loss of Pitx2 function in the developing mouse hypothalamus and subthalamic nucleus. *Mol. Cell. Neurosci.* **37:** 696–707

Skórzewska A, Lehner M, Wisłowska-Stanek A, Turzyńska D, Sobolewska A, Krząścik P & Płaźnik A (2015) GABAergic control of the activity of the central nucleus of the amygdala in low- and high-anxiety rats. *Neuropharmacology* **99:** 566–576

Smidt MP, Cox JJ, van Schaick HS, Coolen M, Schepers J, van der Kleij AM & Burbach JP (2000) Analysis of three Ptx2 splice variants on transcriptional activity and differential expression pattern in the brain. *J. Neurochem.* **75:** 1818–1825

Spooren WP, Veening JG, Groenewegen HJ & Cools AR (1991) Efferent connections of the striatopallidal and amygdaloid components of the substantia innominata in the cat: projections to the nucleus accumbens and caudate nucleus. *Neuroscience* **44:** 431–447

Stehberg J, Moraga-Amaro R & Felipe Simon (2011) The role of the insular cortex in taste function. *Neurobiol Learn Mem* **96:** 130–135

Stenman J, Toresson H & Campbell K (2003) Identification of two distinct progenitor populations in the lateral ganglionic eminence: implications for striatal and olfactory bulb neurogenesis. *J. Neurosci.* **23:** 167–174

Stühmer T, Anderson SA, Ekker M & Rubenstein JLR (2002) Ectopic expression of the Dlx genes induces glutamic acid decarboxylase and Dlx expression. *Development* **129:** 245–252

Subramanian L, Remedios R, Shetty A & Tole S (2009) Signals from the edges: the cortical hem and antihem in telencephalic development. *Semin. Cell Dev. Biol.* **20:** 712–718

Sussel L, Marin O, Kimura S & Rubenstein JL (1999) Loss of Nkx2.1 homeobox gene function results in a ventral to dorsal molecular respecification within the basal telencephalon: evidence for a transformation of the pallidum into the striatum. *Development* **126:** 3359–3370

Swanson LW (1987) The hypothalamus. In: A. Björklund TH, L.W. Swanson editor. Handbook of chemical neuroanatomy, Integrated systems of the CNS, Part I. Amsterdam: Elsevier

Swanson LW (1998) Brain maps: structure of the rat brain. A laboratory guide with printed and electronic templates for data, models, and schematics. Second Edition. Amsterdam, The Netherlands: Elsevier

Swanson LW (1999) The neuroanatomy revolution of the 1970s and the hypothalamus. *Brain Res. Bull.* **50:** 397

Swanson LW (2000) Cerebral hemisphere regulation of motivated behavior. *Brain Res.* **886:** 113–164

Swanson LW (2004) Brain Maps: Structure of the Rat Brain. Third Edition. San Diego: Elsevier

Swanson LW (2012) Brain Architecture: understanding the basic plan. New York: Oxford University Press

Swanson LW & Cowan WM (1979) The connections of the septal region in the rat. *J. Comp. Neurol.* **186:** 621–655

Swanson LW & Mogenson GJ (1981) Neural mechanisms for the functional coupling of autonomic, endocrine and somatomotor responses in adaptive behavior. *Brain Res.* **228:** 1–34

Swanson LW & Petrovich GD (1998) What is the amygdala? *Trends Neurosci.* **21:** 323–331

Swanson LW & Risold P-Y (2000) On the Basic Architecture of the Septal Region. In *The Behavioral Neuroscience of the Septal Region*, Numan R (ed) pp 1–14. New York, NY: Springer New York

Swanson LW, Sanchez-Watts G & Watts AG (2005) Comparison of melanin-concentrating hormone and hypocretin/orexin mRNA expression patterns in a new parceling scheme of the lateral hypothalamic zone. *Neurosci. Lett.* **387:** 80–84

Swanson LW & Sawchenko PE (1983) Hypothalamic integration: organization of the paraventricular and supraoptic nuclei. *Annu. Rev. Neurosci.* **6:** 269–324

Szechtman H, Caggiula AR & Wulkan D (1978) Preoptic knife cuts and sexual behavior in male rats. *Brain Res.* **150:** 569–595

Tecuapetla F, Jin X, Lima SQ & Costa RM (2016) Complementary Contributions of Striatal Projection Pathways to Action Initiation and Execution. *Cell* **166:** 703–715

Thompson RH & Swanson LW (2003) Structural characterization of a hypothalamic visceromotor pattern generator network. *Brain Res. Brain Res. Rev.* **41:** 153–202

Tillet Y, Batailler M & Fellmann D (1996) Distribution of melanin-concentrating hormone (MCH)-like immunoreactivity in neurons of the diencephalon of sheep. *J. Chem. Neuroanat.* **12:** 135–145

Timsit S, Martinez S, Allinquant B, Peyron F, Puelles L & Zalc B (1995) Oligodendrocytes originate in a restricted zone of the embryonic ventral neural tube defined by DM-20 mRNA expression. *J. Neurosci.* **15:** 1012–1024

Torterolo P, Sampogna S, Morales FR & Chase MH (2006) MCH-containing neurons in the hypothalamus of the cat: searching for a role in the control of sleep and wakefulness. *Brain Res.* **1119:** 101–114

Touzani K, Taghzouti K & Velley L (1997) Increase of the aversive value of taste stimuli following ibotenic acid lesion of the central amygdaloid nucleus in the rat. *Behav. Brain Res.* **88:** 133–142

Tsumori T, Yokota S, Qin Y, Oka T & Yasui Y (2006) A light and electron microscopic analysis of the convergent insular cortical and amygdaloid projections to the posterior lateral hypothalamus in the rat, with special reference to cardiovascular function. *Neurosci. Res.* **56:** 261–269

Tye KM, Prakash R, Kim S-Y, Fenno LE, Grosenick L, Zarabi H, Thompson KR, Gradinaru V, Ramakrishnan C & Deisseroth K (2011) Amygdala circuitry mediating reversible and bidirectional control of anxiety. *Nature* **471:** 358–362

Vann SD (2013) Dismantling the Papez circuit for memory in rats. *Elife* **2:** e00736

Vann SD & Aggleton JP (2004) The mammillary bodies: two memory systems in one? *Nat. Rev. Neurosci.* **5:** 35–44

Vaughan JM, Fischer WH, Hoeger C, Rivier J & Vale W (1989) Characterization of melanin-concentrating hormone from rat hypothalamus. *Endocrinology* **125:** 1660–1665

Veening JG, Swanson LW, Cowan WM, Nieuwenhuys R & Geeraedts LM (1982) The medial forebrain bundle of the rat. II. An autoradiographic study of the topography of the major descending and ascending components. *J. Comp. Neurol.* **206:** 82–108

Veening JG, Swanson LW & Sawchenko PE (1984) The organization of projections from the central nucleus of the amygdala to brainstem sites involved in central autonomic regulation: a combined retrograde transport-immunohistochemical study. *Brain Res.* **303:** 337–357

Vertes RP (1984) Brainstem control of the events of REM sleep. *Prog. Neurobiol.* **22:** 241–288

Vertes RP (1986) Brainstem Modulation of the Hippocampus. In *The Hippocampus* pp 41–75. Springer, Boston, MA

Vogt C & Vogt O (1919) Allgemeinere Ergebnisse unserer Hirnforschung. *J Psychol Neurol* **25:** 279–462

Waite MR, Skidmore JM, Micucci JA, Shiratori H, Hamada H, Martin JF & Martin DM (2013) Pleiotropic and isoform-specific functions for Pitx2 in superior colliculus and hypothalamic neuronal development. *Mol. Cell. Neurosci.* **52:** 128–139

Walaas SI & Ouimet CC (1989) The ventral striatopallidal complex: an immunocytochemical analysis of medium-sized striatal neurons and striatopallidal fibers in the basal forebrain of the rat. *Neuroscience* **28:** 663–672

Wallace DM, Magnuson DJ & Gray TS (1992) Organization of amygdaloid projections to brainstem dopaminergic, noradrenergic, and adrenergic cell groups in the rat. *Brain Res. Bull.* **28:** 447–454

Wang PY & Zhang FC (1995) Outline and atlas of learning rat brain slices.

Watts AG (2011) Structure and function in the conceptual development of mammalian neuroendocrinology between 1920 and 1965. *Brain Res Rev* **66:** 174–204

Watts AG, Salter DS & Neuner CM (2007) Neural network interactions and ingestive behavior control during anorexia. *Physiol. Behav.* **91:** 389–396

Webster KE (1961) Cortico-striate interrelations in the albino rat. *J. Anat.* **95:** 532–544

Welagen J & Anderson S (2011) Origins of neocortical interneurons in mice. *Dev Neurobiol* **71:** 10–17

Xie Y & Dorsky RI (2017) Development of the hypothalamus: conservation, modification and innovation. *Development* **144:** 1588–1599

Yakovlev PI (1959) Pathoarchitectonic studies of cerebral malformations. III. Arrhinencephalies (holotelencephalies). *J. Neuropathol. Exp. Neurol.* **18:** 22–55

Yamamoto K, Bloch S & Vernier P (2017) New perspective on the regionalization of the anterior forebrain in Osteichthyes. *Dev. Growth Differ.* **59:** 175–187

Yamamoto K & Vernier P (2011) The evolution of dopamine systems in chordates. *Front Neuroanat* **5:** 21

Yamamoto T, Matsuo R, Ichikawa H, Wakisaka S, Akai M, Imai Y, Yonehara N & Inoki R (1990) Aversive taste stimuli increase CGRP levels in the gustatory insular cortex of the rat. *Neurosci. Lett.* **112:** 167–172

Yasui Y, Breder CD, Saper CB & Cechetto DF (1991) Autonomic responses and efferent pathways from the insular cortex in the rat. *J. Comp. Neurol.* **303:** 355–374

Yetnikoff L, Lavezzi HN, Reichard RA & Zahm DS (2014) An update on the connections of the ventral mesencephalic dopaminergic complex. *Neuroscience* **282:** 23–48

Zahm DS & Heimer L (1990) Two transpallidal pathways originating in the rat nucleus accumbens. *J. Comp. Neurol.* **302:** 437–446

Zhao Y, Marín O, Hermesz E, Powell A, Flames N, Palkovits M, Rubenstein JLR & Westphal H (2003) The LIM-homeobox gene Lhx8 is required for the development of many cholinergic neurons in the mouse forebrain. *Proc. Natl. Acad. Sci. U.S.A.* **100:** 9005–9010

Ziehen GT (1901) Das Centralnervensystem der Monotremen und Marsupalier, II. Mikroskopische Anatomie, 1. Der Faserverlauf im Hirnstamm von Pseudochirus peregrinus. *Denkschr. med.- nat. Ges. Jena.* **6:** 677–728

Zséli G, Vida B, Martinez A, Lechan RM, Khan AM & Fekete C (2016) Elucidation of the anatomy of a satiety network: Focus on connectivity of the parabrachial nucleus in the adult rat. *J. Comp. Neurol.* **524:** 2803–2827

Zséli G, Vida B, Szilvásy-Szabó A, Tóth M, Lechan RM & Fekete C (2018) Neuronal connections of the central amygdalar nucleus with refeeding-activated brain areas in rats. *Brain Struct Funct* **223:** 391–414

ANNEXES

I. Do s compl entaires concernant l'hypothalamus pos rieur

1. Innervation MCH du claustrum (Publication n°5)

Des travaux menés au laboratoire concernaient l'étude des projections des neurones à MCH sur le télencéphale. Ces travaux avaient montré que les neurones producteurs de MCH sont distribués dans le LHA postérieur, mais projettent abondamment à travers le prosencéphale basal avec une organisation topographique de ces projections sur des structures cholinergiques (GP, complexe septal médian et SI). Les neurones à MCH innervent également plusieurs structures sous-corticales connectées au cortex. Dans ce travail, il a été identifié et analysé la distribution de certaines projections spécifiques de l'hypothalamus latéral (MCH et Hcrt) et du mésencéphale (TH, précurseur de la dopamine) dans la région du claustrum. Le claustrum est une petite structure allongée, située entre la capsule externe et l'INS, caractérisée chez le rongeur par une condensation de cellules exprimant la parvalbumine. Il possède des connections bidirectionnelles avec des structures corticales et projette dans le LHA. Il reçoit une innervation sérotoninergique du noyau du Raphé et certaines de ses afférences proviennent également du LHA et de groupes cellulaires catécholaminergiques. Dans cette étude, il a été observé que le claustrum est innervé par les axones MCH, alors qu'il est dépourvu de projections TH et les axones Hcrt sont dispersés dans toute la région. Cette observation a été discutée principalement en ce qui concerne le rôle du claustrum dans les fonctions cognitives et celui de MCH dans le sommeil paradoxal.

RESEARCH ARTICLE

Melanin-Concentrating Hormone Axons, but Not Orexin or Tyrosine Hydroxylase Axons, Innervate the Claustrum in the Rat: An Immunohistochemical Study

Marie Barbier, Christophe Houdayer, Gabrielle Franchi, Fabrice Poncet, and Pierre-Yves Risold*

EA3922, UFR Sciences Médicales et Pharmaceutiques, IFR IBCT, Université de Bourgogne-Franche-Comté, 25030 Besançon, France

ABSTRACT

The claustrum is a small, elongated nucleus close to the external capsule and deep in the insular cortex. In rodents, this nucleus is characterized by a dense cluster of parvalbumin labeling. The claustrum is connected with the cerebral cortex. It does not project to the brainstem, but brainstem structures can influence this nucleus. To identify some specific projections from the lateral hypothalamus and midbrain, we analyzed the distribution of projections labeled with antibodies against tyrosine hydroxylase (TH), melanin-concentrating hormone (MCH), and hypocretin (Hcrt) in the region of the claustrum. The claustrum contains a significant projection by MCH axons, whereas it is devoid of TH projections. Unlike TH and MCH axons, Hcrt axons are scattered throughout the region. This observation is discussed mainly with regard to the role of the claustrum in cognitive functions and that of MCH in REM sleep. J. Comp. Neurol. 525:1489–1498, 2017.

INDEXING TERMS: cerebral cortex; anatomy; external capsule; RRID:AB_10000343; RRID:AB_2536180; RRID:AB 2616562; RRID:AB_653610; RRID:AB_2313745; RRID:AB_10562715; RRID:AB_2340400; RRID:AB_2313606; RRID:SCR_013672

The claustrum is a poorly understood cell group located adjacent to the external capsule, deep in the insular cortex. This structure has strong bilateral connections with many cortical fields (Kim et al., 2016) and was thought until recently to project into several brainstem structures such as the lateral hypothalamic area (LHA; Mathur, 2014). In the rat, the borders of the claustrum were recently reevaluated based on its neurochemical content and pattern of projections. The claustrum is now better viewed as a cell mass that can be labeled immunohistochemically by parvalbumin (PV), without a rostral extension to the level of the caudoputamen (Mathur et al., 2009). Given this definition, neurons projecting into the medial forebrain bundle belong to the deep layer of the insular cortex and not to the claustrum proper. This "revised" rat claustrum shares many more characteristics with the primate claustrum and may serve as a model for studying the functions of this nucleus (Mathur et al., 2009; Pirone et al., 2014). Interconnections with the cerebral cortex have received increasing attention from investigators (White et al., 2016). Specific afferences from the brainstem may also provide important pieces of information, but the small size of the nucleus makes it difficult to use classical retrograde tract-tracing techniques. Serotonin inputs from the dorsal raphe nucleus have previously been described as uniformly innervating the claustrum (Baizer, 2001; Rahman and Baizer, 2007; Mathur, 2014). Other source of afferences may originate in the lateral hypothalamus and catecholaminergic cell groups of the midbrain and pons (Mathur, 2014). Among those inputs, peptidergic neurons in the LHA, such as MCH and hypocretinergic neurons, may project to the claustrum (Bittencourt et al., 1992; Peyron et al., 1998). However, the distribution of these inputs with regard to the new borders of the claustrum is unknown. Such information may be important for a nucleus that could be involved in higher cognitive functions because both

Grant sponsor: Region Franche-Comté, France.

*CORRESPONDENCE TO: Pierre-Yves Risold, EA3922, UFR Sciences Médicales et Pharmaceutiques, 19 rue Ambroise Paré, IFR IBCT, Université de Bourgogne-Franche-Comté, 25030 Besançon cedex, France. E-mail: pierre-yves.risold@univ-fcomte.fr

Received April 22, 2016; Revised July 12, 2016;
Accepted August 24, 2016.
DOI 10.1002/cne.24110
Published online October 21, 2016 in Wiley Online Library (wileyonlinelibrary.com)

hypothalamic cell populations are differentially involved in control of the behavioral state and the sleep–wake cycle. This report describes projections labeled by immunohistochemistry for melanin-concentrating hormone (MCH), hypocretin (Hcrt), and tyrosine hydroxylase (TH) in the region of the claustrum as identified based on PV expression.

MATERIALS AND METHODS

Animals

All animal use and care protocols were in accordance with institutional guidelines, and the investigators were authorized. Eight male Sprague-Dawley rats weighing 300–350 g were obtained from Janvier (Le Genest-Saint-Isle, France). Rats were housed with a standard 12-hour light/dark cycle at a constant room temperature and had free access to standard laboratory diet and water.

Characterization of primary antisera

Table 1 lists the antigen, immunogen, manufacturer, catalog/lot number, species in which the antibody was raised, and the working dilution for each of the primary antibodies employed.

Anti-MCH

The sMCH antibody has been tested on hypothalamic sections from many species (Croizier et al., 2013). Its specificity has been verified by liquid-phase inhibition, dot blot, and affinity column analyses (Fellmann et al., 1987; Risold et al., 1992). For mice, it was also shown that the labeling was observed exclusively in MCH-GFP cells in the lateral hypothalamus (Croizier et al., 2011).

Anti-Orexin A

The orexin antibody used in the present study was a goat polyclonal antibody (catalog No. sc-8070, C-19, lot No. GO 813; Santa Cruz Biotechnology, Santa Cruz, CA; Lee et al., 2013) raised against a peptide mapping to the carboxy-terminus of human orexin A (residues 48–66 of the orexin precursor, identical to corresponding mouse sequence; manufacturer's technical information). The orexin antiserum recognizes the fully processed orexin A/hypocretin 1 peptide (manufacturer's data sheet) from various mammalian species, including rat (Harris et al., 2005; Henny and Jones, 2006), mouse (Lutter et al., 2008), buffalo (Tafuri et al., 2009), and pig (Chometton et al., 2014b). The specificity of this antibody has previously been verified by preabsorption with orexin, which abolished all staining (Florenzano et al., 2006), and by Western blotting, which shows specificity for rat, mouse, and human orexin A (manufacturer's technical information). The antibody was also shown to label hypothalamic cell bodies in the LHA (Harris et al., 2005; Lutter et al., 2008), perifornical region, and dorsomedial nucleus (Florenzano et al., 2006), consistent with the known pattern of orexin neurons (de Lecea et al., 1998; Sakurai et al., 1998) and orexin/hypocretin-immunoreactive fibers in the locus coeruleus of rats (Henny et al., 2010) and mice (Puskás et al., 2010).

Abbreviations

CL	claustrum
CPu	caudoputamen
ec	external capsule
EPd	dorsal endopiriform nucleus
IC	insular cortex
LHA	lateral hypothalamic area
lot	lateral olfactory tract
OT	olfactory tubercle
PIR	piriform area
vl	lateral ventricle
VTA	ventral tegmental area

Anti-PV

Anti-PV mouse monoclonal antibody (SWant, Belinzona, Switzerland; code No. 235, lot No. 10-11[F]; Clarke et al., 2009) was raised against purified carp muscle PV (Celio et al., 1988). The antibody reacts specifically with PV in tissue originating from human, monkey, rabbit, rat, mouse, chicken, and fish. The antibody specifically identifies 12-kDa, IEF-4.9 PV by 2D immunoblot and shows an absence of staining in the brain of a PV knockout mouse (manufacturer's technical information).

Anti-TH

To detect TH, we used the polyclonal anti-TH antibody (No. C.P. 208020234 from the "Institute de Biotechnologies Jacques Boy," Reims, France; Goncharuk et al., 2011) raised in rabbit after immunization with TH purified from rat pheochromocytoma (Table 1). According to the manufacturer's description, the specificity of this antibody was examined by using Ouchterlony double diffusion (1958), also known as an agar gel immunodiffusion test, and by Western blot. This antibody provides a strong labeling of all regions known to contain dopaminergic neuronal elements, such as the ventral midbrain and the striatum.

Double immunofluorescent staining

Rats were deeply anesthetized with an intraperitoneal injection of pentobarbital (CEVA, 50 mg/kg). They were then perfused transcardially with 0.9% NaCl, followed by ice-cold 4% paraformaldehyde (PFA; Roth) fixative in 0.1 M phosphate-buffered saline (PBS) at pH 7.4. Brains were extracted, postfixed for 20 hours in the same fixative at 4 °C, and cryoprotected by saturation in a 15% sucrose solution (Sigma, St. Louis, MO) in 0.1 M PB for

TABLE 1.
Primary Antibodies Used in This Study

Antibody	Immunogen	Source	Dilution
Anti-MCH (melanin-concentrating hormone)	Synthetic salmon MCH; full 17-amino-acid sequence: DTMRKMVGRVYRPCWEV	Our laboratory (Risold et al., 1992), rabbit, polyclonal, PMID:1641182, ISSN 0304-3940, RRID:AB_2616562	1:1,000
Anti-OrxA (hypocretin)	Human orexin A, 19 aa of the c-terminal fragment	Santa Cruz Biotechnology, goat, polyclonal, sc-8070, No. GO 813, RRID:AB_653610	1:500
Anti-PV	Hybridization of mouse myeloma cells with spleen cells from mice immunized with PV purified from carp muscles	SWant, mouse, monoclonal IgG1, McAB 235, lot No. 10-11 (F), RRID:AB_10000343	1:2,000
Anti-TH	Pure TH rat pheochromocytoma	Biotechnologies Institute Jacques Boy (Reims), rabbit, polyclonal IgG, lot No. 900101A, REF 208020234, RRID:AB_2313745	1:1,000

TABLE 2.
Secondary Antibodies Used in This Study

Antibody	Type	Source	Dilution
Alexa Fluor 488	Anti-rabbit IgG	Invitrogen, goat, A11034, lot No. 1141875, RRID:AB_10562715	1:1,000
Alexa Fluor 555	Anti-mouse IgG	Invitrogen, donkey, A31570, lot No. 1117032, RRID:AB_2536180	1:1,000
Biotinylated	Anti-rabbit IgG	Vector Laboratories, goat, BA-1000, lot No. ZA0520, RRID:AB_2313606	1:1,000
Fluorescein (FITC)	Anti-goat IgG	Jackson Immunoresearch, donkey, code 705-095-003, lot No. 33899, RRID:AB_ 2340400	1:500

24 hours at 4 °C. Tissues were cut into four series of 30-µm-thick coronal sections, collected in a cryoprotective solution (1:1:2 glycerol/ethylene glycol/PBS), and stored at −40 °C.

After being rinsed in PBS with 0.3% Triton X-100 (PBS-T), free-floating sections were incubated with primary anti-PV antibody (Table 1; SWant, catalog No. 235, RRID:AB_10000343) dissolved in PBS-T for 48 hours at 4 °C. Tissues were washed three times with PBS-T (5 minutes each) and incubated with Alexa Fluor 555 donkey anti-mouse IgG antibody (Table 2, Thermo Fisher Scientific, Fair Lawn, NJ; catalog No. A-31570, RRID:AB_2536180) diluted in PBS-T for 2 hours at room temperature.

Then, after the first staining, free-floating sections were washed with PBS-T and incubated with the anti-MCH (RRID:AB 2616562), anti-Hcrt (Santa Cruz Biotechnology; catalog No. sc-8070, RRID:AB_653610), or anti-TH antibodies (Institut de Biotechnologies Jacques Boy; catalog No. 208020234, RRID:AB_2313745; Table 1) dissolved in milk solution (PBS-T, 1% bovine serum albumin, 10% lactoproteins, and 0.01% sodium azide) for 48 hours at 4 °C. Tissues were then incubated with Alexa Fluor 488 goat anti-rabbit IgG (Thermo Fisher Scientific; catalog No. A11034, RRID:AB_10562715) or fluorescein isothiocyanate (FITC)-conjugated AffiniPure donkey anti-goat IgG antibodies (Table 2; Jackson Immunoresearch, West Grove, PA; catalog No. 705-095-003, RRID:AB_2340400) diluted in PBS-T for 2 hours at room temperature.

Finally, sections were washed with PBS-T, mounted on gelatin-coated slides, and coverslipped with 60/40 glycerol/PBS-T. An adjacent series was always stained in a solution of 1% toluidine blue (Roth) in water to serve as a reference series for cytoarchitectonic purposes.

Immunohistochemistry MCH

After being rinsed in PBS-T, free-floating sections were incubated with the anti-MCH antibody (Table 1; Fellmann et al., 1987; Risold et al., 1992) in milk solution for 48 hours at 4 °C. Sections were incubated for 4 hours at room temperature in a solution of biotinylated goat anti-rabbit IgG (Vector Laboratories, Burlingame, CA; catalog No. BA-1000, RRID:AB_2313606) at a dilution of 1:1000 in PBS-T. Then, sections were placed in a mixed avidin-biotin horseradish peroxidase (HRP) complex solution (ABC Elite Kit; Vector Laboratories) for 1 hour at room temperature. The peroxidase complex was visualized by using a 6-minute exposure to a chromogen solution containing 0.04% 3,3′-diaminobenzidine tetrahydrochloride (DAB; Sigma) with 0.006% hydrogen peroxide (Sigma) in PBS. The reaction was stopped by extensive washing in PBS. Sections were mounted on

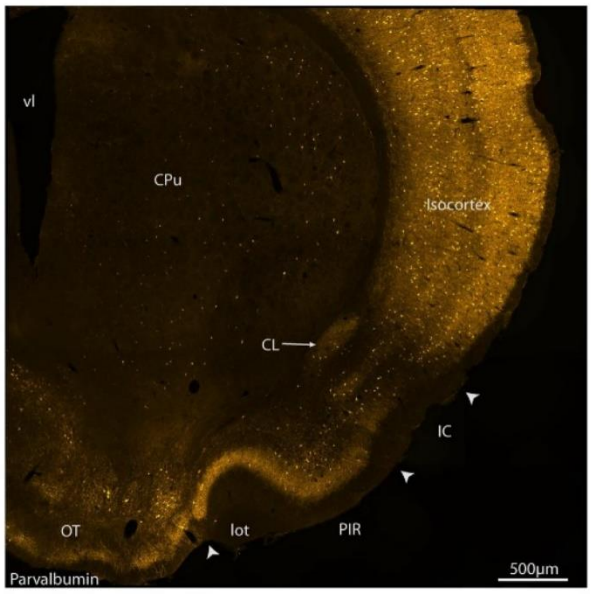

Figure 1. Photomicrograph of a section passing through the claustrum and labeled via immunohistochemistry for PV. Note the condensation corresponding to the claustrum (CL) deep in the insular cortex (IC). Note also the very intense labeling through the isocortex. Scale bar = 500 µm.

gelatin-coated slides and then stained in a solution of 1% toluidine blue (Roth) or by the Kluver-Barrera method in water to serve as a reference for cytoarchitectonic purposes. Finally, sections were dehydrated and coverslipped with Canada balsam (Roth).

Image acquisition and processing

Sections were analyzed with an ApoTome.2 microscope (Axio Imager Zeiss), and images were obtained through a numeric camera (Digital Camera Hamamatsu C11440) using the Imager.Z2 software (Zen2; ZEN Digital Imaging for Light Microscopy; RRID:SCR_013672). The labeling was observed with appropriate filters: 38 HE green fluorescent protein (BP excitation 450–490, emission 500–550) and 43 HE DsRed (BP excitation 538–562, emission 570–540). Pictures were taken with the advanced features "Z-Stack" and "Deconvolution" of the Zen software. No additional processing was performed, except for the fluorescence intensity.

RESULTS

The pattern of labeling obtained with the anti-PV AS was identical to that previously reported by Mathur et al. (2009). At low magnification, a dense network of fine axons labeled by the PV-AS could be observed

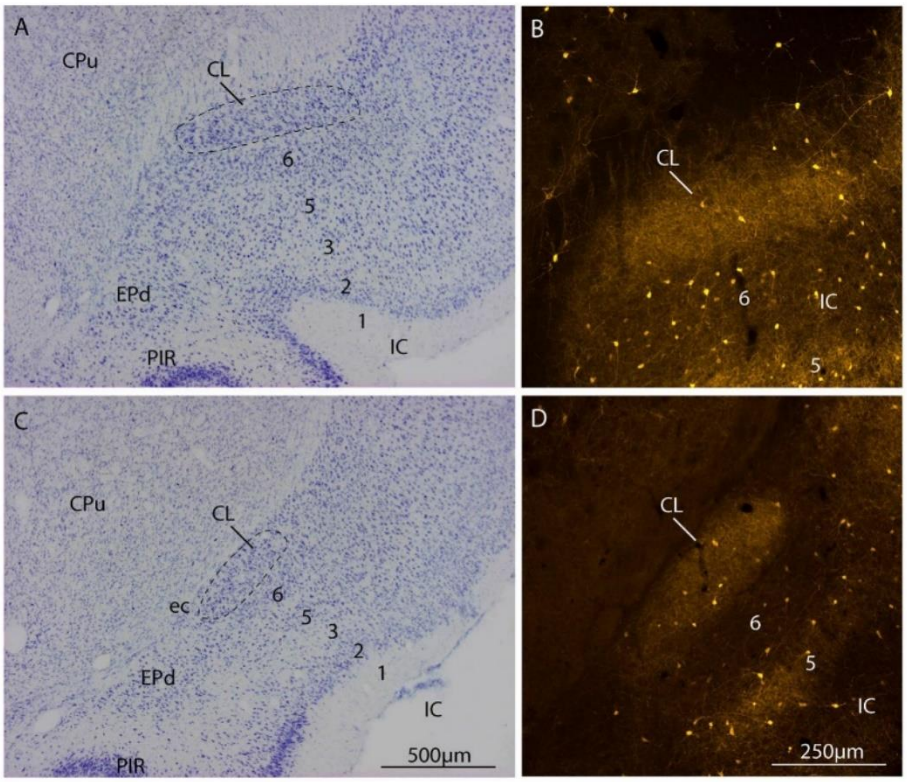

Figure 2. Photomicrographs of the claustrum at rostral (**A,B**) and caudal (**C,D**) levels. The condensation of PV labeling (B,D) corresponds to a cluster of cells embedded in layer 6 of the insular cortex, representing the claustrum. Scale bars = 500 µm in C (applies to A,C); 250 µm in D (applies to B,D).

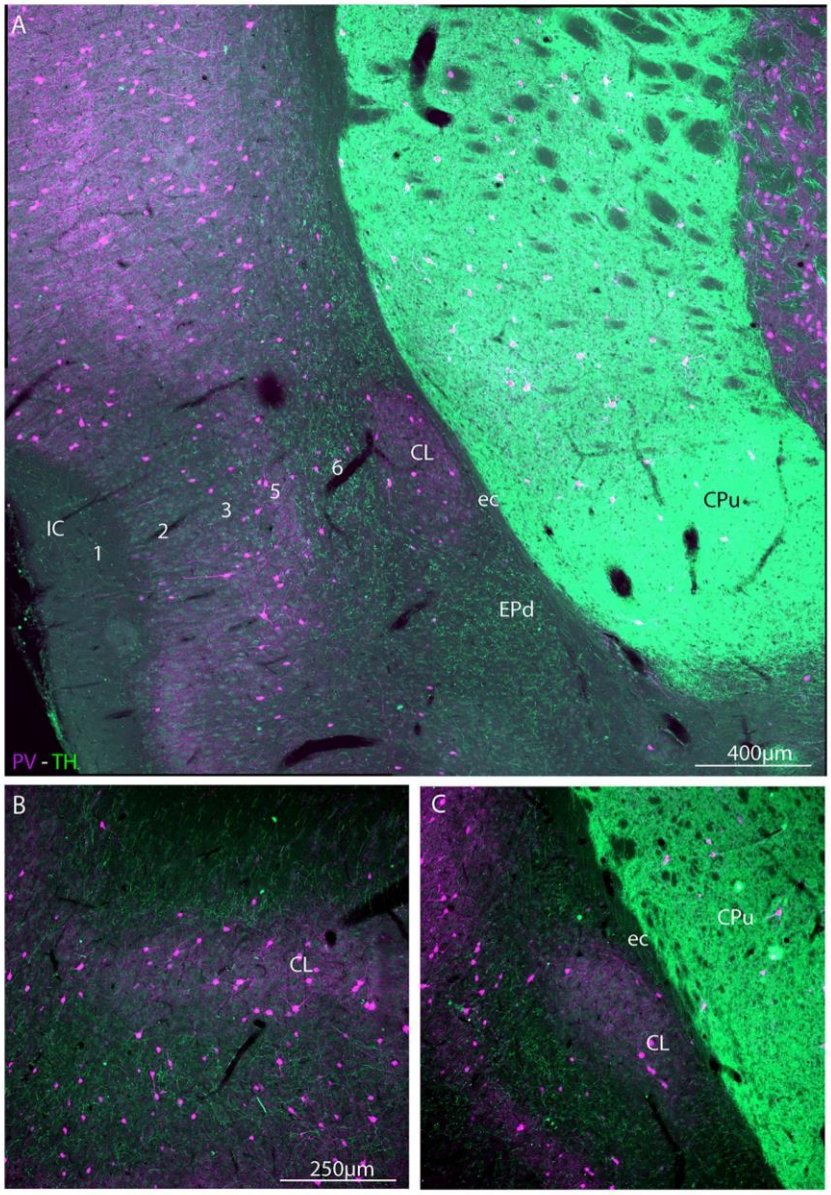

Figure 3. Photomicrographs illustrating the distribution of TH in the region of the claustrum. Note the very intense innervation of the caudoputamen nucleus as well as the innervation of layer 6 of the insular cortex. The claustrum is not innervated. This pattern is clear at rostral (**B**) and more caudal (**A,C**) levels. Scale bars = 400 µm in A; 250 µm in B (applies to B,C).

deep into the insular cortex, close to the external capsule. Few cell bodies displayed the fluorescent staining (Figs. 1, 2). At higher magnifications, PV-containing axons formed pericellular nets around cell bodies, but the PV-expressing cells were not targeted by these axons. From adjacent sections labeled with toluidine blue for cytoarchitectonic purposes, we could observe that the PV innervation corresponded to the discrete cell condensation of the claustrum (Fig. 2). In the following analysis, we therefore used PV expression to define the borders of this nucleus and to compare them for the distributions of TH, MCH, and Hcrt.

The innervation of the striatum by TH axons was extremely intense, as expected, but showed the high quality of labeling provided by the antibody (Fig. 3A). By comparison, insular fields in the cerebral cortex were moderately innervated. This innervation involved mainly layer 6 and extended dorsally in layer 6 of the isocortex. Layers 1, 2, and 3 contained fewer projections, and TH axons tended to avoid layer 5. Ventrally from the insular cortex, the endopiriform nucleus was also well innervated. However, the TH labeling avoided the claustrum as defined by PV expression (Fig. 3A–C). Observation of sections labeled with a dual immunostaining procedure showed that the distribution of TH axons scrupulously respected the PV-rich region corresponding to the claustrum. Only very few, thin, and smooth-looking axons could be observed within the

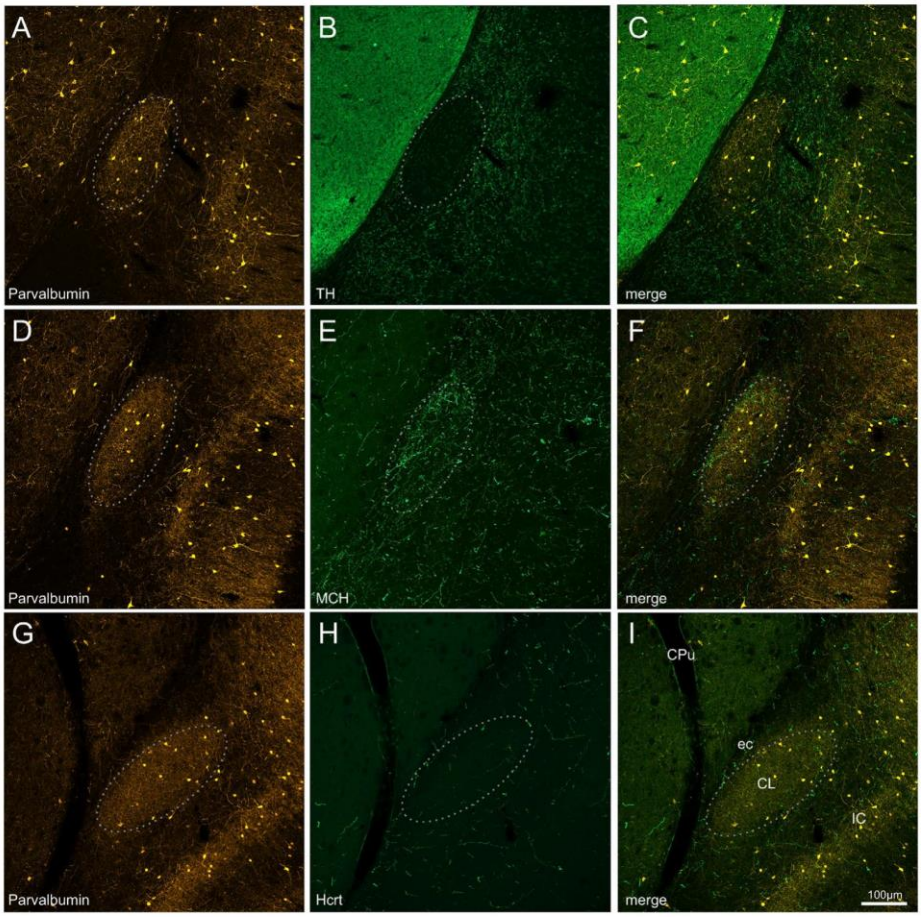

Figure 4. Photomicrographs illustrating the distributions of TH, MCH, and Hcrt axons in the claustrum. **A–C**: TH-labeled axons innervate the deep insular layers of the IC but avoid the claustrum (CL) labeled for PV. **D–F**: MCH axons provide a significant innervation of the claustrum. Axons penetrated the nucleus from its ventral side or by following the external capsule (ec). The medial aspect of the nucleus contains a denser input than more lateral aspects. **G–I**: Hcrt axons provide a modest input to the IC region. Even fewer axons penetrated the borders of the claustrum. Scale bar = 100 µm.

limits of the claustrum, suggesting that this nucleus is not targeted by TH axons (Fig. 4A–C). The same observation was made at both rostral and caudal levels of the nucleus.

Among the two other markers analyzed in this study, only MCH was observed in a significant number of labeled axons in the claustrum (Fig. 4D–F). MCH axons reached the nucleus via two pathways: many entered the nucleus through its ventral border, but we also observed that a large proportion of the axons entered the claustrum from the external capsule. This innervation by MCH axons was moderate to intense; they formed a plexus denser than that observed in the surrounding cortical tissue. MCH axons are not distributed homogeneously in the nucleus. Medial regions closest to the external capsule were more densely innervated (Fig. 4E). This impression was also reinforced because medial axons appeared thicker than in more lateral regions of the nucleus. The neuronal target of this innervation was not identified, but, based on double immunofluorescence, PV-containing neurons are not contacted, given that very few boutons were observed in their immediate proximity (Fig. 4F). This impression was confirmed by the 3D analysis with a ×60 objective and the Z-Stack function of the Zen2 software. Using an immunoperoxidase approach, we observed that many boutons were in close apposition to cell bodies, suggesting axosomatic synapses (Fig. 5A–F). However, electron microscopy is required to confirm this particular point. Caudally, as the PV labeling decreased, the MCH innervation also decreased in intensity. However, rostrally, deep layers of the prefrontal cortex were also intensely innervated.

Hcrt-labeled axons were sparse throughout this region (Fig. 4G–I). They obviously followed the same pathways as MCH axons, including in the external capsule. However, very few entered the claustrum (Fig. 6). The surrounding insular cortical fields and endopiriform nucleus were also moderately innervated. Axons could be seen running alongside the borders of the claustrum. Some axons from the external capsule crossed its borders, but they often had the appearance only of axons of passage, displaying few boutons and leaving the impression that the surrounding tissue was more

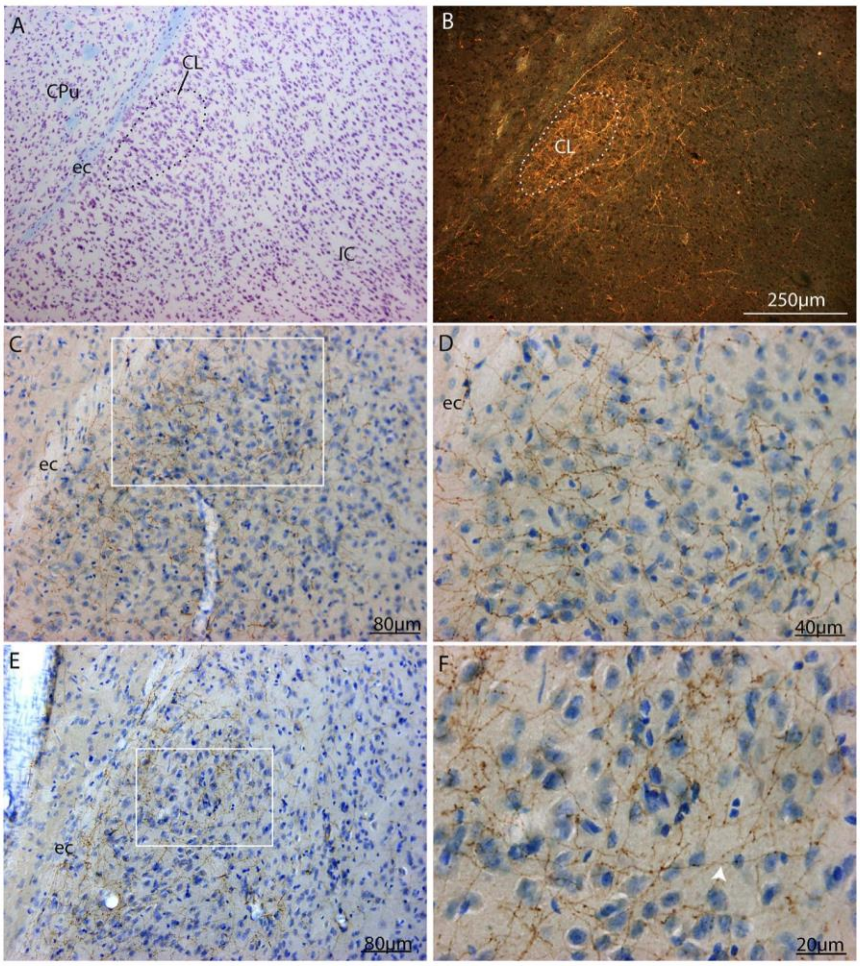

Figure 5. Photomicrographs illustrating the distribution of MCH in the region of the claustrum vi immunohistochemistry. **A,B**: Note the innervation of the claustrum at low magnification and under darkfield illumination (B). A is the adjacent section to B and was stained with the Kluver-Barrera technique for cytoarchitectonic purposes. **C–F**: At higher magnifications and after counterstaining with toluidine blue, we can observe that MCH axons appear to innervate cell bodies: boutons labeled by the DAB product in brown are in close proximity to cell bodies. Closer to the external capsule, fibers are more abundant and appear more darkly labeled. However, axons displaying at least boutons en passant are observed throughout the claustrum; for example, see the axon indicated by the arrowhead in F, which appears to form boutons en passant on each cell body that it passes. The boxed area in C corresponds to D, and that in E corresponds to F. Scale bars = 500 µm in C (applies to A,C); 250 µm in D (applies to B,D). Scale bars = 250 µm in B (applies to A,B); 80 µm in C,E; 40 µm in D; 20 µm in F.

abundantly targeted, even if only moderately so, than the claustrum itself.

DISCUSSION

The main finding of this work is that ascending projections labeled with TH, Hcrt, or MCH show distinct and differentiated distribution patterns in the region of the claustrum. The results can be discussed with regard to the recent parcellation of the nucleus based on PV expression. However, they also provide relevant information regarding actual hypotheses about the cognitive functions of this nucleus.

The borders of the claustrum have always been problematic in rodents, especially at rostral levels (Mathur, 2014). Our report did not seek to resolve that issue, but it seems to us that the identification of specific markers of this cell group is a major step toward establishing its borders in these species. In particular, PV immunohistochemistry appears to be a reliable and easy way to identify the nucleus (Mathur et al., 2009; Mathur, 2014; Kim et al., 2016), and our observations agree quite well with those reports.

The distributions of TH- and MCH-labeled axons show complementary patterns in the region of the claustrum. TH-labeled axons scrupulously respected the borders of

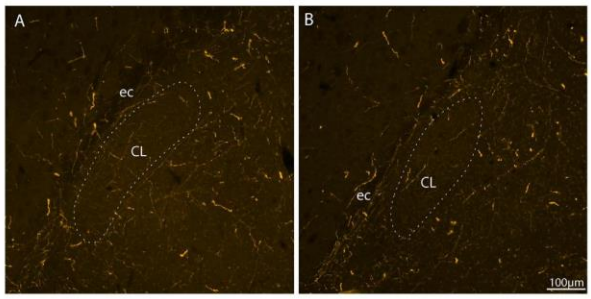

Figure 6. Photomicrographs illustrating the distribution of Hcrt in the region of the claustrum. More axons are seen around and close to the borders of the claustrum than within the nucleus itself, giving the impression that these axons tend to avoid the claustrum. Scale bar = 100 µm.

the nucleus while innervating all areas adjacent to it. The literature contains very few data regarding TH innervation of the claustrum, but at least one previous study also signaled a poor innervation of this nucleus (Fallon and Moore, 1978). By comparison, MCH innervation is dense within the PV-rich nucleus, thereby indicating that some neurons of the LHA innervate the claustrum even if this structure does not project into the LHA. However, Hcrt neurons that are colocalized in the LHA with MCH neurons send projections that tend to avoid the claustrum.

Current hypotheses regarding the functions of the claustrum suggest that this nucleus is involved in cognitive processes and perception of stimuli by facilitating intercortical synchrony, possibly related to salience detection (Chau et al., 2015; Goll et al., 2015). However, as stated by Mathur, (2014) and based on a report by Remedios et al. (2014), the quiescent nature of claustral neurons does not support the claustrum being involved in conscious states, and the observation that it responds to sudden stimuli suggests that the claustrum serves as a salience filter for corticocortical communication. Furthermore, based on our observations, the functions of this nucleus would be independent from direct ascending brainstem inputs related to waking, motivation and arousal. Indeed, TH-labeled axons correspond to both the dopaminergic inputs of the mesotelencephalic path and the noradrenergic axons from the locus coeruleus (Oades and Halliday, 1987; Chandler, 2015). Functionally, the locus coeruleus is involved in behavioral arousal and waking state (Aston-Jones and Waterhouse, 2016; Mather and Harley, 2016). The ventral tegmental area (VTA), where dopaminergic axons originate, is involved in reward and motivation (Berridge and Robinson, 2003). Hcrt neurons in the LHA are active during wake but are also involved in arousal and project to the locus coeruleus and VTA (Horvath et al., 1999; Estabrooke et al., 2001; Winsky-Sommerer et al., 2003; España et al., 2005; Aston-Jones et al., 2009; Nunez et al., 2009; Richardson and Aston-Jones, 2012; Jones and Hassani, 2013). In contrast, MCH neurons are signaled to be active during REM sleep and less active during the waking period (Estabrooke et al., 2001; Verret et al., 2003; Jones and Hassani, 2013). We observed a significant input by MCH-containing axons in the claustrum. MCH neurons in the LHA are GABAergic and, because we did not observe that these axons target PV interneurons of the claustrum, we may assume that they inhibit non-GABAergic neurons. MCH neurons are active during REM sleep, and activation of the claustrum was otherwise induced during REM sleep (Renouard et al., 2015). Therefore, MCH projections may influence the claustral processing during this phase of sleep, perhaps controlling the claustrum activation and modifying the level of salience detection in that nucleus. Studies in humans indicate that the claustrum could be involved in regaining consciousness rather than in maintaining consciousness (Chau et al., 2015). Given that MCH neurons are GABAergic, a GABAergic/MCH projection into this nucleus could therefore be involved in controlling a rise in consciousness during REM sleep.

MCH axons are observed at multiple telencephalic sites related to the control of cortical activity, including the entire cerebral cortex but also the cholinergic-rich regions of the ventral telencephalon (globus pallidus, medial septal complex), the subthalamic nucleus, and even the medial mammillary nucleus, which fires rhythmically with the hippocampal theta rhythm in the rat (Casatti et al., 2002; Chometton et al., 2014a,b). The claustrum is an additional site through which MCH could influence cortical activity during REM sleep.

In conclusion, the claustrum, when defined as a PV-rich structure, is scarcely innervated by TH- or Hcrt-containing axons. It is, however, innervated by MCH axons. These projections may be related to the role of MCH neurons in REM sleep and to that of the claustrum in salience detection of sensory stimuli.

ACKNOWLEDGMENTS

The authors thank Louis Foucault for technical help.

COMPETING INTEREST

The authors declare that they have no competing interests.

ROLE OF AUTHORS

Conceived and designed the experiments: Pierre-Yves Risold. Performed the experiments and illustration production: Marie Barbier. Technical help and animal handling: Christophe Houdayer, Gabrielle Franchi and Fabrice Poncet. Analyzed the data and wrote the text: Marie Barbier and Pierre-Yves Risold.

LITERATURE CITED

Aston-Jones G, Waterhouse B. 2016. Locus coeruleus: from global projection system to adaptive regulation of behavior. Brain Res. Available from: http://linkinghub.elsevier.com/retrieve/pii/S0006899316301172

Aston-Jones G, Smith RJ, Moorman DE, Richardson KA. 2009. Role of lateral hypothalamic orexin neurons in reward processing and addiction. Neuropharmacology 56:112–121.

Baizer J. 2001. Serotonergic innervation of the primate claustrum. Brain Res Bull 55:431–434.

Berridge KC, Robinson TE. 2003. Parsing reward. Trends Neurosci 26:507–513.

Bittencourt JC, Presse F, Arias C, Peto C, Vaughan J, Nahon JL, Vale W, Sawchenko PE. 1992. The melanin-concentrating hormone system of the rat brain: an immuno- and hybridization histochemical characterization. J Comp Neurol 319:218–245.

Casatti CA, Elias CF, Sita LV, Frigo L, Furlani VCG, Bauer JA, Bittencourt JC. 2002. Distribution of melanin-concentrating hormone neurons projecting to the medial mammillary nucleus. Neuroscience 115:899–915.

Celio MR, Baier W, Schärer L, de Viragh PA, Gerday C. 1988. Monoclonal antibodies directed against the calcium binding protein parvalbumin. Cell Calcium 9:81–86.

Chandler DJ. 2015. Evidence for a specialized role of the locus coeruleus noradrenergic system in cortical circuitries and behavioral operations. Brain Res. Available from: http://linkinghub.elsevier.com/retrieve/pii/S0006899315008665

Chau A, Salazar AM, Krueger F, Cristofori I, Grafman J. 2015. The effect of claustrum lesions on human consciousness and recovery of function. Conscious Cogn 36:256–264.

Chometton S, Cvetkovic-Lopes V, Houdayer C, Franchi G, Mariot A, Poncet F, Fellmann D, Risold P-Y. 2014a. Anatomical organization of MCH connections with the pallidum and dorsal striatum in the rat. Front Syst Neurosci 8:185.

Chometton S, Franchi G, Houdayer C, Mariot A, Poncet F, Fellmann D, Tillet Y, Risold PY. 2014b. Different distributions of preproMCH and hypocretin/orexin in the forebrain of the pig (*Sus scrofa domesticus*). J Chem Neuroanat 61/62:72–82.

Clarke JH, Emson PC, Irvine RF. 2009. Distribution and neuronal expression of phosphatidylinositol phosphate kinase IIγ in the mouse brain. J Comp Neurol 517:296–312.

Croizier S, Amiot C, Chen X, Presse F, Nahon J-L, Wu JY, Fellmann D, Risold P-Y. 2011. Development of posterior hypothalamic neurons enlightens a switch in the prosencephalic basic plan. PLoS One 6:e28574.

Croizier S, Cardot J, Brischoux F, Fellmann D, Griffond B, Risold PY. 2013. The vertebrate diencephalic MCH system: a versatile neuronal population in an evolving brain. Front Neuroendocrinol 34:65–87.

de Lecea L, Kilduff TS, Peyron C, Gao X, Foye PE, Danielson PE, Fukuhara C, Battenberg EL, Gautvik VT, Bartlett FS, Frankel WN, van den Pol AN, Bloom FE, Gautvik KM, Sutcliffe JG. 1998. The hypocretins: hypothalamus-specific peptides with neuroexcitatory activity. Proc Natl Acad Sci U S A 95:322–327.

España RA, Reis KM, Valentino RJ, Berridge CW. 2005. Organization of hypocretin/orexin efferents to locus coeruleus and basal forebrain arousal-related structures. J Comp Neurol 481:160–178.

Estabrooke IV, McCarthy MT, Ko E, Chou TC, Chemelli RM, Yanagisawa M, Saper CB, Scammell TE. 2001. Fos expression in orexin neurons varies with behavioral state. J Neurosci 21:1656–1662.

Fallon JH, Moore RY. 1978. Catecholamine innervation of the basal forebrain IV. Topography of the dopamine projection to the basal forebrain and neostriatum. J Comp Neurol 180:545–579.

Fellmann D, Bugnon C, Risold PY. 1987. Unrelated peptide immunoreactivities coexist in neurons of the rat lateral dorsal hypothalamus: human growth hormone-releasing factor1–37-, salmon melanin-concentrating hormone- and alpha-melanotropin-like substances. Neurosci Lett 74: 275–280.

Florenzano F, Viscomi MT, Mercaldo V, Longone P, Bernardi G, Bagni C, Molinari M, Carrive P. 2006. P2X2R purinergic receptor subunit mRNA and protein are expressed by all hypothalamic hypocretin/orexin neurons. J Comp Neurol 498:58–67.

Goll Y, Atlan G, Citri A. 2015. Attention: the claustrum. Trends Neurosci 38:486–495.

Goncharuk VD, Buijs RM, Jhamandas JH, Swaab DF. 2011. Vasopressin (VP) and neuropeptide FF (NPFF) systems in the normal and hypertensive human brainstem. J Comp Neurol 519:93–124.

Harris GC, Wimmer M, Aston-Jones G. 2005. A role for lateral hypothalamic orexin neurons in reward seeking. Nature 437:556–559.

Henny P, Jones BE. 2006. Innervation of orexin/hypocretin neurons by GABAergic, glutamatergic or cholinergic basal forebrain terminals evidenced by immunostaining for presynaptic vesicular transporter and postsynaptic scaffolding proteins. J Comp Neurol 499:645–661.

Henny P, Brischoux F, Mainville L, Stroh T, Jones BE. 2010. Immunohistochemical evidence for synaptic release of glutamate from orexin terminals in the locus coeruleus. Neuroscience 169:1150–1157.

Horvath TL, Peyron C, Diano S, Ivanov A, Aston-Jones G, Kilduff TS, van Den Pol AN. 1999. Hypocretin (orexin) activation and synaptic innervation of the locus coeruleus noradrenergic system. J Comp Neurol 415:145–159.

Jones BE, Hassani OK. 2013. The role of Hcrt/Orx and MCH neurons in sleep-wake state regulation. Sleep 36:1769–1772.

Kim J, Matney CJ, Roth RH, Brown SP. 2016. Synaptic organization of the neuronal circuits of the claustrum. J Neurosci 36:773–784.

Lee SJ, Kirigiti M, Lindsley SR, Loche A, Madden CJ, Morrison SF, Smith MS, Grove KL. 2013. Efferent projections of neuropeptide Y-expressing neurons of the dorsomedial hypothalamus in chronic hyperphagic models: projections of DMH NPY neurons. J Comp Neurol 521:1891–1914.

Lutter M, Krishnan V, Russo SJ, Jung S, McClung CA, Nestler EJ. 2008. Orexin signaling mediates the antidepressant-like effect of calorie restriction. J Neurosci 28:3071–3075.

Mather M, Harley CW. 2016. The locus coeruleus: essential for maintaining cognitive function and the aging brain. Trends Cogn Sci 20:214–226.

Mathur BN. 2014. The claustrum in review. Front Syst Neurosci 8:48.

Mathur BN, Caprioli RM, Deutch AY. 2009. Proteomic analysis illuminates a novel structural definition of the claustrum and insula. Cereb Cortex 19:2372–2379.

Nunez A, Rodrigo-Angulo M, De Andres I, Garzon M. 2009. Hypocretin/orexin neuropeptides: participation in the control of sleep–wakefulness cycle and energy homeostasis. Curr Neuropharmacol 7:50–59.

Oades RD, Halliday GM. 1987. Ventral tegmental (A10) system: neurobiology. 1. Anatomy and connectivity. Brain Res 434:117–165.

Peyron C, Tighe DK, van den Pol AN, de Lecea L, Heller HC, Sutcliffe JG, Kilduff TS. 1998. Neurons containing hypocretin (orexin) project to multiple neuronal systems. J Neurosci 18:9996–10015.

Pirone A, Castagna M, Granato A, Peruffo A, Quilici F, Cavicchioli L, Piano I, Lenzi C, Cozzi B. 2014. Expression of calcium-binding proteins and selected neuropeptides in the human, chimpanzee, and crab-eating macaque claustrum. Front Syst Neurosci 8:99.

Puskás N, Papp RS, Gallatz K, Palkovits M. 2010. Interactions between orexin–immunoreactive fibers and adrenaline or noradrenaline-expressing neurons of the lower brainstem in rats and mice. Peptides 31:1589–1597.

Rahman FE, Baizer JS. 2007. Neurochemically defined cell types in the claustrum of the cat. Brain Res 1159:94–111.

Remedios R, Logothetis NK, Kayser C. 2014. A role of the claustrum in auditory scene analysis by reflecting sensory change. Front Syst Neurosci 8:44.

Renouard L, Billwiller F, Ogawa K, Clement O, Camargo N, Abdelkarim M, Gay N, Scote-Blachon C, Toure R, Libourel P-A, Ravassard P, Salvert D, Peyron C, Claustrat B, Leger L, Salin P, Malleret G, Fort P, Luppi P-H. 2015. The supramammillary nucleus and the claustrum activate the cortex during REM sleep. Sci Adv 1:e1400177–e1400177.

Richardson KA, Aston-Jones G. 2012. Lateral hypothalamic orexin/hypocretin neurons that project to ventral tegmental area are differentially activated with morphine preference. J Neurosci 32:3809–3817.

Risold PY, Fellmann D, Rivier J, Vale W, Bugnon C. 1992. Immunoreactivities for antisera to three putative neuropeptides of the rat melanin-concentrating hormone precursor are coexpressed in neurons of the rat lateral dorsal hypothalamus. Neurosci Lett 136:145–149.

Sakurai T, Amemiya A, Ishii M, Matsuzaki I, Chemelli RM, Tanaka H, Williams SC, Richarson JA, Kozlowski GP, Wilson S, Arch JR, Buckingham RE, Haynes AC, Carr SA, Annan RS, McNulty DE, Liu WS, Terrett JA, Elshourbagy NA, Bergsma DJ, Yanagisawa M. 1998. Orexins and orexin receptors: a family of hypothalamic neuropeptides and G protein-coupled receptors that regulate feeding behavior. Cell 92:696.

Tafuri S, Pavone LM, Mastellone V, Spina A, Avallone L, Vittoria A, Staiano N, Scala G. 2009. Expression of orexin A and its receptor 1 in the choroid plexuses from buffalo brain. Neuropeptides 43:73–80.

Verret L, Goutagny R, Fort P, Cagnon L, Salvert D, Léger L, Boissard R, Salin P, Peyron C, Luppi P-H. 2003. A role of melanin-concentrating hormone producing neurons in the central regulation of paradoxical sleep. BMC Neurosci 4: 19.

White MG, Cody PA, Bubser M, Wang H-D, Deutch AY, Mathur BN. 2016. Cortical hierarchy governs rat claustrocortical circuit organization: cortical hierarchy and claustrocortical circuitry. J Comp Neurol (in press).

Winsky-Sommerer R, Boutrel B, De Lecea L. 2003. The role of the hypocretinergic system in the integration of networks that dictate the states of arousal. Drug News Perspect 16:504–512.

2. Connexions entre le noyau supramamillaire et le claustrum (Publication n°6)

En réalisant des injections de traceur antérograde PHAL chez le rat dans la région du complexe PSTN/CbN afin de poursuivre la caractérisation de l'hypothalamus prémamillaire, des sites ont été obtenus dans les régions plus postérieures. Deux de ces injections ont été retrouvées dans le noyau supramamillaire, une dans sa partie antérieure et l'autre dans sa partie postérieure. Comme décrit dans la littérature, il a été retrouvé des projections dans le gyrus denté de l'hippocampe et dans la région septale. Mais ce qui nous a le plus intrigué fut les projections intenses dans le claustrum. Des précédents travaux avaient déjà étudié le circuit impliquant le noyau supramamillaire mais négligeaient les connexions de ce dernier avec le claustrum. Afin de vérifier si les cellules à l'origine de cette innervation sont bien distribuées dans le noyau supramamillaire, des injections de traceur rétrograde FG ont donc été réalisées dans l'hippocampe et le claustrum. Cette étude a permis de mettre en évidence l'importance des liens anatomiques entre le noyau supramamillaire et le claustrum pouvant avoir des conséquences non négligeables en termes d'apprentissage/mémoire et de navigation spatiale.

NEUROSCIENCE
RESEARCH ARTICLE

Marie Barbier, P.-Y. Risold / Neuroscience 409 (2019) 261–275

The claustrum is a target for projections from the supramammillary nucleus in the rat

Marie Barbier* **and Pierre-Yves Risold**

EA481, Neurosciences Intégratives et Cliniques, UFR Santé, 19 rue Ambroise Paré, Université de Bourgogne Franche-Comté, 25030 Besançon cedex, France

Abstract—Injection of the anterograde tracer *Phaseolus vulgaris* leucoagglutinin (PHAL) into the rat rostral and caudal supramammillary nucleus (SUM) provided expected patterns of projections into the hippocampus and the septal region. In addition, unexpectedly intense projections were observed into the claustrum defined by parvalbumin expression. Injections of the retrograde tracer fluorogold (FG) into the hippocampus and the region of the claustrum showed that the cells of origin of these projections distributed similarly within the borders of the SUM. The SUM is usually involved in control of hippocampal theta activity, but the observation of intense projections into the claustrum indicates that it may also influence isocortical processes. Therefore, the SUM may coordinate sensory processing in the isocortex with memory formation in the hippocampus.

Key words: parvalbumin, septum, dentate gyrus, salience, tract tracing.

INTRODUCTION

The rat supramammillary nucleus (SUM) is a heterogenic cell group dorsal to the body of the medial mammillary nucleus (MM). It is anatomically divided into medial (SUMm) and lateral (SUMl) parts. Functionally, it relates to the septum and the hippocampus (Swanson and Cowan, 1977, 1979; Gonzalo-Ruiz et al., 1992; Risold, 2004). The SUMl is thought to be involved in the control of behavioral states and of hippocampal theta activity related to spatial information processing (Vertes, 1986; Kocsis and Vertes, 1994; Hernández-Pérez et al., 2015). Indeed, SUM projections to the dentate gyrus (DG) enhance the functional connectivity of the network during exploratory behaviors, by theta discharge of granule cells, which tetanizes CA3 pyramidal neurons (Kocsis and Vertes, 1994). In rats, its neurons discharge rhythmically with the hippocampal theta rhythm (Kocsis and Vertes, 1994; Pan and McNaughton, 2002; Kirk and Mackay, 2003; Pan and McNaughton, 2004; Kocsis, 2006; Ruan et al., 2011; Renouard et al., 2015).

During a study aimed at characterizing premammillary structures of the hypothalamus, we injected the anterograde tracer *Phaseolus vulgaris* Leucoagglutinin (PHAL) into SUMl. Besides the very large outputs into the lateral and medial septal nuclei, as well as in the hippocampus, we were surprised by unexpectedly dense projections into the claustrum (CLA), which is located deep in the insular cortex (IC), adjacent to the external capsule. The CLA is mainly characterized by interconnections with vast regions of the isocortex (Rae, 1954). Currently, in addition to its cortical connections (Sherk, 1986), this poorly understood cell group is defined by a dense cluster of parvalbumin (PV) labeling (Mathur et al., 2009). Moreover, a proteomic

*Corresponding author. Tel.: +33 3 63 08 22 20.
E-mail address: marie.barbier03@edu.univ-fcomte.fr (Marie Barbier).

Abbreviations: AI, Agranular insular area; ARH, Arcuate hypothalamic nucleus; CA1–3, Field CA1–3, Ammon's horn; CA1slm, Field CA1, stratum lacunosum-moleculare; CA1so, Field CA1, stratum oriens; CA1sp, Field CA1, pyramidal layer; CA1sr, Field CA1, stratum radiatum; CbN, Calbindin nucleus; cc, Corpus callosum; CLA, Claustrum; Cpd, Cerebral peduncle; CP, Caudoputamen; DG, Dentate gyrus; DGlb-mo, Dentate gyrus, lateral blade-molecular layer; DGlb-po, Dentate gyrus, lateral blade-polymorph layer; DGlb-sg, Dentate gyrus, lateral blade-granule cell layer; DGmb, Dentate gyrus, medial blade; DMH, Dorsomedial hypothalamic nucleus; ec, External capsule; ENT, Entorhinal area; EPd, Dorsal endopiriform nucleus; fr, Fasciculus retroflexus; fx, Columns of the fornix; FG, Fluorogold; Hcrt, Hypocretin; IC, Insular cortex; IG, Induseum griseum; ILA, Infralimbic area; LHA, Lateral hypothalamic area; LM, Lateral mammillary nucleus; LS, Lateral septal nucleus; LSr, Lateral septal nucleus, rostral part; MCH, Melanin-concentrating hormone; ml, Medial lemniscus; MM, Body of the medial mammillary nucleus; mp, Mammillary peduncle; MS, Medial septal nuclei; mtt, Mammillothalamic tract; NG, Nucleus Gemini; OT, Olfactory tubercle; PH, Posterior hypothalamic nucleus; PHAL, *Phaseolus vulgaris* Leucoagglutinin; PL, Prelimbic area; pm, Principal mammillary tract; PMd, Dorsal premammillary nucleus; PMv, Ventral premammillary nucleus; PSTN, Parasubthalamic nucleus; PV, Parvalbumin; PVp, Periventricular hypothalamic nucleus, posterior part; RE, Nucleus reuniens; SNc, Substantia nigra, compact part; SNr, Substantia nigra, reticular part; SO, Supraoptic nucleus; STN, Subthalamic nucleus; SUM, Supramammillary nucleus; SUMl, Supramammillary nucleus, lateral part; SUMl, Supramammillary nucleus, medial part; TH, Tyrosine-hydroxylase; TTd2, Tenia tecta, dorsal part, layers 2; TU, Tuberal nucleus; VMH, Ventromedial hypothalamic nucleus; ZI, Zona incerta; ZIrm, Zona incerta, rostromedial part; VTA, Ventral tegmental area.

https://doi.org/10.1016/j.neuroscience.2019.03.045
0306-4522/

analysis identified a G-protein gamma2 subunit (Gng2) as a new claustral marker (Mathur et al., 2009). At a functional level, electrophysiology experiments have shown that the CLA responds to sudden stimuli, suggesting that it serves as a saliency filter for cortico-cortical communications. Furthermore, recent findings support CLA roles in a variety of cognitive processes, such as in signaling novel stimuli, directing attention, and setting vigilance states (Mathur, 2014; Remedios et al., 2014; Goll et al., 2015; White et al., 2017; Brown et al., 2017; Wang et al., 2017). In addition to these strong bilateral connections with many cortical fields (Kim et al., 2016), the CLA receives inputs from several brainstem structures (Baizer, 2001; Rahman and Baizer, 2007; Mathur, 2014). Recent data also indicate that the CLA contains a significant ascending projection from the lateral hypothalamus, by melanin-concentrating hormone (MCH) axons (activated in REM sleep), whereas it is devoid of tyrosine-hydroxylase (TH) axons, and hypocretin (Hcrt) projections are scattered throughout the region (Bittencourt et al., 1992; Peyron et al., 1998; Barbier et al., 2017b).

Previous attempts to explore the SUM circuitry largely overlooked the connections of this nucleus into the CLA. Therefore, the aim of this study was to highlight the abundance of this anatomical pathway, as the connections between both nuclei might have important consequences in terms of learning/memory, and spatial navigation.

EXPERIMENTAL PROCEDURES

Animals

Seven Sprague–Dawley male rats, weighing 300–350 g, were utilized in this study. They were obtained from Janvier (Le Genest-Saint-Isle, France). Rats were housed with a standard 12-h light/dark cycle, at a constant room temperature, and had free access to the standard laboratory diet and water. All animal use and care protocols were in accordance with institutional guidelines, and with the Directive 2010/63/EU of the European Parliament, and of the Council of 22 September 2010, on the protection of animals used for scientific purposes. The protocols were approved by the Franche-Comté University's Animal Care Committee (protocol number: 2015-002), and the investigators received authorization to conduct the study.

Characterization of primary antisera

We used antibodies described in previous studies. The readers may refer to these articles to find necessary information about their specificity, and their respective antigens: anti-Fluorogold (FG) (Schmued and Fallon, 1986; García Del Caño et al., 2000; White et al., 2017), anti-MCH (Fellmann et al., 1987; Risold et al., 1992; Croizier et al., 2011, 2013), anti-Orexin A (Hcrt) (de Lecea et al., 1998; Sakurai et al., 1998; Harris et al., 2005; Florenzano et al., 2006; Henny and Jones, 2006; Lutter et al., 2008; Tafuri et al., 2009; Henny et al., 2010; Puskás et al., 2010; Lee et al., 2013; Chometton et al., 2014), anti-PV (Celio et al., 1988; Clarke et al., 2009), and anti-PHAL (Balcita-Pedicino et al., 2011). Table 1 lists the antigen, immunogen, manufacturer, catalog/lot number, species in which the antibodies were raised, and the working dilution for each of them.

Tracer injections

All injections were performed under anesthesia, with an intraperitoneal (i.p.) injection of a mixture of xylazine and ketamine (1 mg/100 g and 10 mg/100 g of body weight, respectively; Vetoquinol®, France), and once the rats were fully anesthetized, they were placed into a stereotaxic device.

Anterograde tracer into the SUMl, the ventral tegmental area (VTA) and the parasubthalamic nucleus (PSTN)

Four rats received a unilateral iontophoretic injection of a 2.5% PHAL diluted in sodium phosphatebuffer saline (NaPBS) pH 7.2. Coordinates were taken from Bregma using the Paxinos and Watson (2005) atlas. For the anterior SUMl, the coordinates are AP: −4.0 mm, ML: 1.25 mm, and DV:−8.8 mm, and for the posterior SUMl, the coordinates are AP:−4.4 mm, ML: 0.8 mm, and DV: −8.6 mm. For the VTA, the coordinates are AP: −5.25 mm, ML: 1.0 mm, and DV:−8.0 mm, and for the PSTN, the coordinates are AP: −4.2 mm, ML: 1.5 mm, and DV: −8.4 mm. The procedures for the iontophoresis injections were previously described (Barbier et al., 2017a, 2018a,b).

Table 1. Primary antibodies used in this study.

Antibody	Immunogen	Source	Dilution
Anti-FG	Fluorogold	Rabbit, polyclonal, Millipore® Cat# 153, Lot LV1644476	1:3000
Anti-MCH	Synthetic salmon MCH; full 17-amino-acid sequence: DTMRKMVGRVYRPCWEV	Our laboratory (Risold et al., 1992), rabbit, polyclonal, PMID:1641182, ISSN 0304–3940	1:1000
Anti-Orexin A (Hcrt)	Mouse anti human Orexin A, immunogen AA 34–66, clone MM0500-8G22	Mouse, monoclonal IgG1, Angio-Proteomie, Cat# ABIN1983384	1:2000
Anti-PHAL	PHA-E et PHA-L	Goat, polyclonal, Vector Laboratories® Cat# AS-2224, lot No. ZD0504	1:1000
Anti-PHAL	PHA-E et PHA-L	Rabbit, polyclonal, Vector Laboratories® Cat# AS-2300, lot No. ZC0303	1:1000
Anti-PV	Hybridization of mouse myeloma cells with spleen cells from mice immunized with PV purified from carp muscles	Mouse, monoclonal IgG1, Swant®, McAB Cat#235, Lot 10–11 (F)	1:2000

Retrograde tracer into the CLA and the hippocampus

Three rats received a unilateral iontophoretic injection of a 10% solution of FG diluted in 0.9% sodium chloride (NaCl) into the CLA and into the hippocampus. For the CLA, the coordinates are AP: 1.0 mm, ML: 2.4 mm, and DV: −6.6 mm, angle: 20° and for the hippocampus, the coordinates are AP: −2.5 mm, ML: 1.2 mm, DV: −4.0 mm. The procedure was similar to that for the PHAL (Barbier et al., 2017a, 2018a,b).

Tissue preparation

Rats were deeply anesthetized with an i.p. injection of Pentobarbital (CEVA®, 50 mg/kg). Animals were perfused transcardially with 0.9% NaCl, followed by ice-cold 4% paraformaldehyde (PFA, Roth®), fixative in 0.1 M phosphate buffer (PB) at pH 7.4. Brains were extracted, post-fixed for 20 h in the same fixative at 4 °C, and cryoprotected by saturation in a 15% sucrose solution (Sigma®) in 0.1 M PB, for 24 h at 4 °C. Tissues were cut in four series of 30-µm-thick coronal sections, collected in a cryoprotective solution [1:1:2 glycerol/ethylene glycol/ phosphate buffer saline (PBS)], and stored at −40 °C.

Enzymatic immunohistochemistry

The procedure for immunohistochemistry was amply described (Barbier et al., 2017a,b, 2018a,b). The biotinylated goat anti-rabbit IgG was diluted to 1:1000 in PBS-T, and the labeling revealed using the ABC Elite Kit (Vector Laboratories®), and 3,3′diaminobenzidine tetrahydrochloride (DAB, Sigma®). A series of sections was mounted on gelatin-coated slides, and then stained in a solution of 1% toluidine blue (Roth®) in water, to serve as a reference for cytoarchitectonic purposes.

Immunofluorescent staining

Secondary antibodies are listed in Table 2 and the procedure described elsewhere (Barbier et al., 2017a,b, 2018a, b). Some sections were counterstained with a nuclear marker [NeuroTrace® 640/660 Deep-Red Fluorescent Nissl Stain, 1:100, Invitrogen®, Thermo Fisher Scientific Cat#N21483, Lot1851967, RRID:AB_2572212 (De la Huerta et al., 2012)], for 20 min, at room temperature. Finally, an adjacent series was always stained in a solution of 1% toluidine blue (Roth) in water, to serve as a reference series for cytoarchitectonic purposes.

Image acquisition and processing

Sections were analyzed on an ApoTome.2 microscope (Axio Imager Zeiss), and images were obtained through a numeric camera (Digital Camera Hamamatsu C11440) using the Imager.Z2 software (Zen 2) (ZEN Digital Imaging for Light Microscopy, RRID:SCR_013672). The labeling was observed with appropriate filters: 38 HE Green Fluorescent Protein (BP excitation 450–490, emission 500–550), 43 HE DsRed (BP excitation 538–562, emission 570–540), 50 Cy5 (BP excitation 625–655, emission 665–715) and DAPI (BP excitation 372–401, emission 421–456).

Some pictures were taken using the advanced features “Z-Stack”, and “Deconvolution”, of the Zen software. Neither additional treatment was made, except the fluorescence intensity. Nomenclature and nuclear parcellation are from Swanson (2004) except for the PSTN-calbindin nucleus (CbN)-nucleus Gemini (NG) region, whose nomenclature and parceling are from Chometton et al. (2016).

RESULTS

PHAL injection sites into the SUM, the VTA, and the PSTN

Four PHAL experiments are described in this study. One PHAL injection (experiment SUM-1) was in the rostral pole of the SUM, at levels 32–33 of Swanson's Brain Maps, adjacent dorsally to the columns of the fornix (fx), and ventral to the mammillothalamic tract (mtt) (Fig. 1A). The second PHAL injection (experiment SUM-2) was centered at the mid rostro-caudal level within the cytoarchitectonic borders of the SUMl, at level 34 of Swanson's Brain Maps, lateral to the principal mammillary tract (pm), as it exits the MM (Fig. 1B). Very few PHAL neurons were observed in the MM, and did not result in any transport as no axons were found in the anterior thalamic nuclei. Co-immunolabelings were obtained with PV to highlight the parvafox and gemini nuclei, whichare lateral to the SUM, but difficult to identify solely based on Nissl stains. Two control PHAL injections were obtained. The first involved the PSTN, at level 33 of Swanson's Brain Maps, and the second was centered in the ventral VTA, at level 37 of Swanson's Brain Maps.

Innervation of the hippocampus and septum

Innervation of the hippocampus and the septal region is a hallmark of the SUM (Haglund et al., 1984; Björklund et al., 1987; Kocsis and Vertes, 1994; Pan and McNaughton, 2004). Because experiment SUM-1 was very rostral, a short account and a comparison of the projections in the two

Table 2. Secondary antibodies used in this study.

Antibody	Type	Source	Dilution
Alexa Fluor 488	Anti-rabbit IgG	Invitrogen®, goat, Thermo Fisher Scientific Cat#A11034, Lot 1141875	1:1000
Alexa Fluor 488	Anti-rabbit IgG	Invitrogen®, donkey, Thermo Fisher Scientific Cat#A21206, Lot 1874771	1:1000
Alexa Fluor 555	Anti-mouse IgG	Invitrogen®, donkey, Thermo Fisher Scientific Cat#A31570, Lot 1117032	1:1000
Cyanine 3	Anti-goat IgG	Interchim®, donkey, Jackson ImmunoResearch, Code number 705-165-003, Lot 127,717	1:1000
Cyanine 5	Anti-mouse IgG	Interchim®, donkey, Jackson ImmunoResearch, Code number 715-175-150, Lot 126,435	1:1000
Biotinylated	Anti-rabbit IgG	Vector Laboratories®, goat, Cat#BA-1000, Lot ZA0520	1:1000

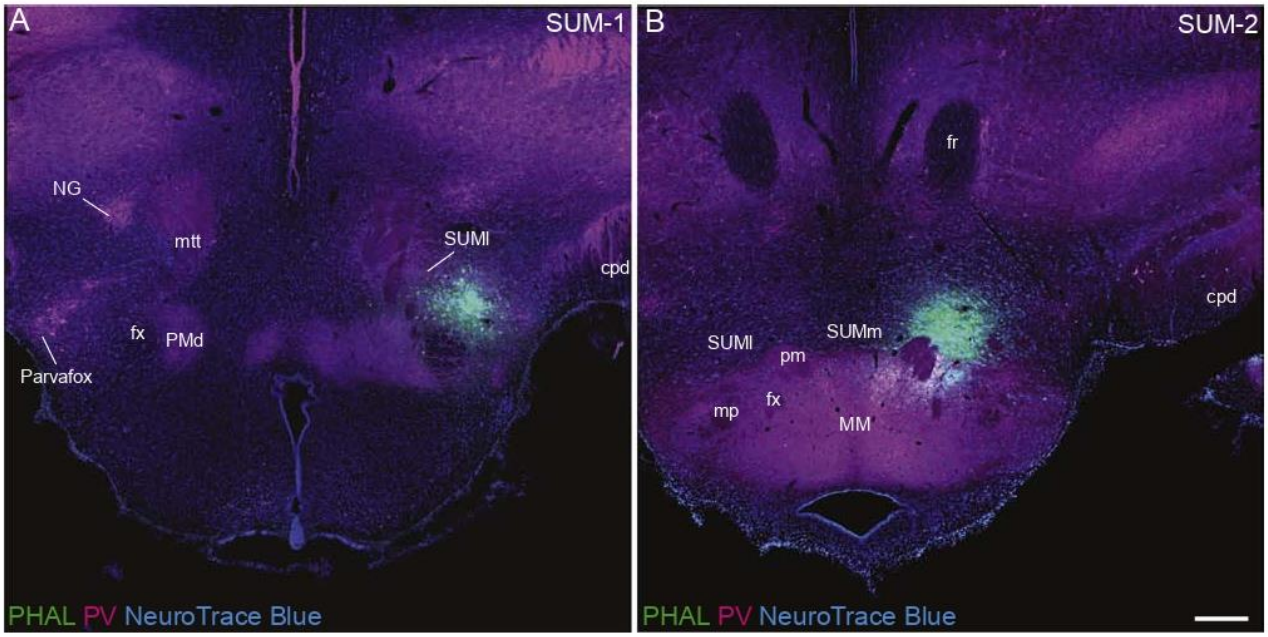

Fig. 1. Photomicrographs to illustrate the PHAL injection sites in the lateral part of the SUM. PHAL was revealed using immunofluorescence (green), but sections were also labeled for PV, as this marker is expressed in many structures surrounding the SUM. Sections were also counterstained with NeuroTraceBlue for cytoarchitectonic purpose. The experiment SUM-1 was centered in the rostral pole of the nucleus (level 33 (A) of the Swanson's Brain Maps), and the experiment SUM-2 was more caudal (level 34 (B)) just dorsal to the MM. Note that the parvafox nucleus and the nucleus Gemini, which are characterized by PV expression, are respectively rostro-lateral and dorso-lateral to the SUM.Scale bar = 250 µm.

experiments, SUM-1 and SUM-2, are provided and illustrated. The distribution of PHAL axons in the two experiments was very similar to that described by Vertes (1992) and Haglund et al. (1984). Indeed, both experiments provided a similar pattern of PHAL labeling in the hippocampus with a very intense innervation of the DG (Fig. 2A, A′), and less abundant in CA2. Innervation of the septal pole of CA3 was also noted. Labeled axons showed complex morphologies in the granule cell layer of the lateral blade of the DG. However, SUM-2 provided a more intense innervation of the DG than SUM-1. Hippocampal rudiments, especially the induseum griseum (IG) labeled with PV (Fig. 2E), were also labeled (Fig. 2B, C, E). Heavy projections in the septal region innervated both the lateral (LS) and medial (MS) septal nuclei, as well as the septofimbrial nucleus which can be regarded as a division of the LS (Risold and Swanson, 1997) (Fig. 2C, D). In the MS, the innervation involved mainly lateral parts, while medial (PV rich) regions were less innervated (Fig. 2D). The dorsal part of the tenia tecta (TTd), IG, and the LSr of experiment SUM-1 received less abundant innervation than that in experiment SUM-2. By contrast, descending projections of experiment SUM-1 innervated the periaqueductal gray and the superior colliculus more intensely, while SUM-2 provided a more intense innervation of the VTA, substantia nigra (SN), and the interpeduncular nucleus.

Pathway in the LHA

Axons reached the telencephalon through the medial forebrain bundle (mfb) in the lateral hypothalamic area (LHA) (Fig. 3). The LHA contains MCH and Hcrt neurons that also project into the hippocampus and the CLA (for MCH neurons). A triple labeling was then performed, on sections through the LHA of SUM-1 and SUM-2 experiments, to verify if PHAL axons innervated MCH or Hcrt neurons on their way to the telencephalon. SUM axons traveled mostly ventromedially through the mfb, but distributed axons in more dorsal regions of the LHA (Fig. 3). However, these axons appeared to provide a light innervation of the tuberal LHA. Most of them were axons of passage with few *en passant* boutons.

SUM axons mostly avoided the dorsal perifornical region where Hcrt neurons are abundant. More putative contact could be observed with MCH perikarya, in the rostromedial zona incerta (ZIrm). The SUM innervates the nucleus reuniens (RE), in the thalamus, by axons that reach this nucleus through the ZIrm (Fig. 3B). This region of the ZI is rich in MCH cell bodies. However, using the Apotome device of the microscope, only a few *en passant* putative contacts may be effectively observed on MCH neurons.

FG injection in the hippocampus

A direct projection into the DG is a clear characteristic of the SUMl. The distribution of retrogradely labeled cells in the region of the SUM, after retrograde tracer injection in the DG, shall help to better characterize its border, especially with regard to inconspicuous cell groups, such as the nucleus gemini (NG), or the parvafox nucleus, that, to date, are little investigated, but are located close to the SUM borders, at least for the NG (Alvarez-Bolado and Celio, 2016; Bilella et al., 2016). Two FG injections were centered in the DG (Fig. 4A). The halo of diffusion extended into the CA3.

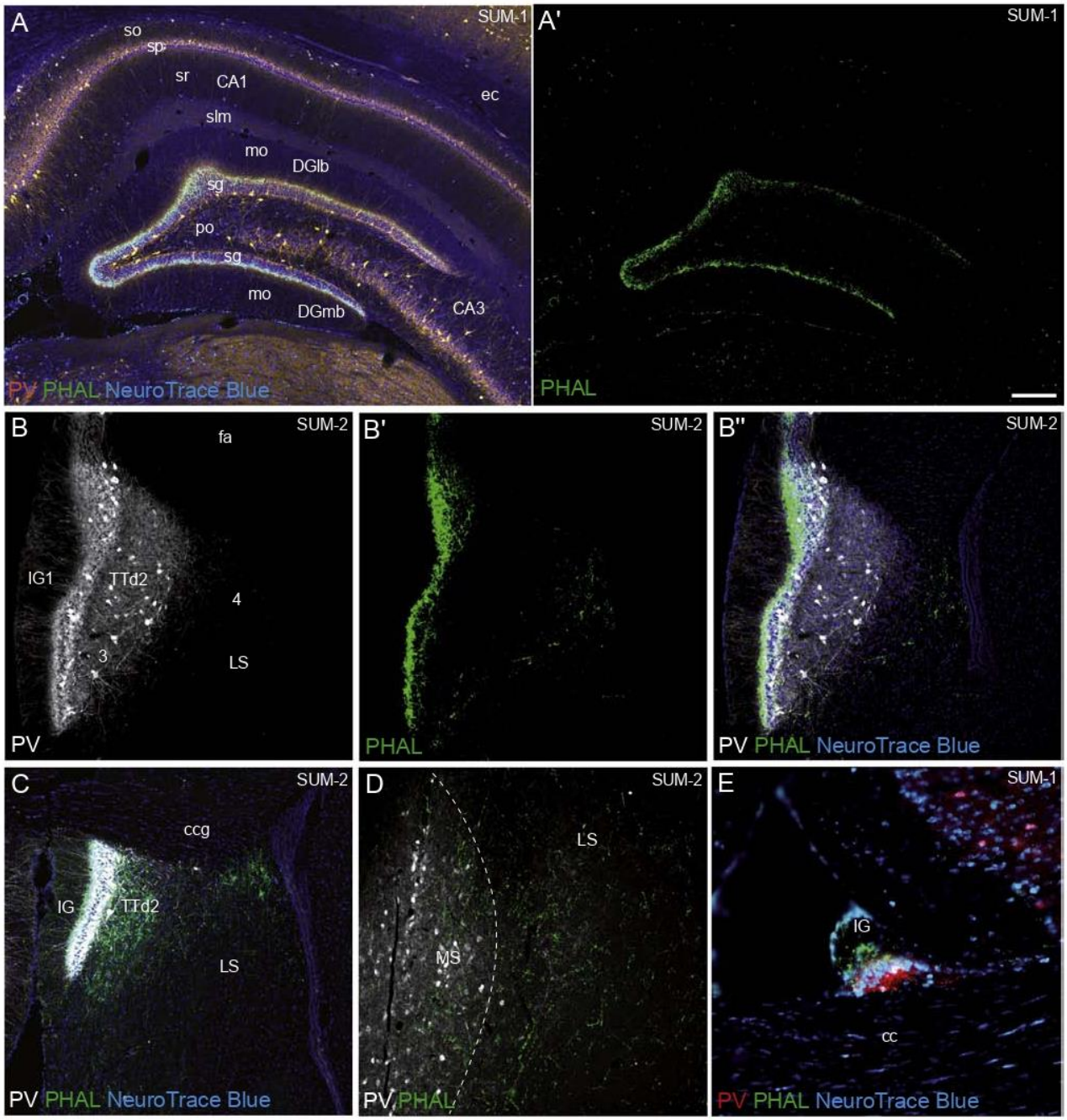

Fig. 2. Photomicrographs of coronal sections illustrating the distribution of PHAL in several of the most representative regions, after PHAL injection in the SUM.A–A′: Immunofluorescence in the hippocampus with PHAL revealed in green, and PV revealed in orange. The section is counterstained using NeuroTrace Blue. Note the intense PHAL innervation in the DG (A′).B–B″: Immunofluorescence in the region of the induseum griseum (IG), and tenia tecta (TT), with PHAL revealed in green, and PV revealed in white. The sections are counterstained using NeuroTrace Blue. Note the intense labeling of the external side of layer 2 of the IG, remembering by its aspect and intensity the innervation of the DG.C–E: Photomicrographs to illustrate PHAL axons in the caudal TT (C), the LS (D), and in the IG, just dorsal to the corpus callosum. Section are also co-labeled for PV and counterstained with NeuroTrace Blue.Scale bar: A–A′ = 250 μm; B–B″ = 100 μm; C–D = 150 μm; E = 50 μm.

Distribution of FG labeled cells in the SUM

Fig. 4 (A–J) depicts patterns of distribution of labeled neurons on 10 rostrocaudal sections, through the ipsilateral SUMl, after a typical FG injection in the DG (Fig. 4A). As expected, very abundant retrogradely labeled neurons were observed in the SUM, mostly in the lateral part of the nucleus. Retrogradely labeled perikarya are also distributed rostrally to the admitted cytoarchitectonic borders of the SUM, around the mtt. Indeed, neurons were observed at the most rostral level in the posterior hypothalamic nucleus

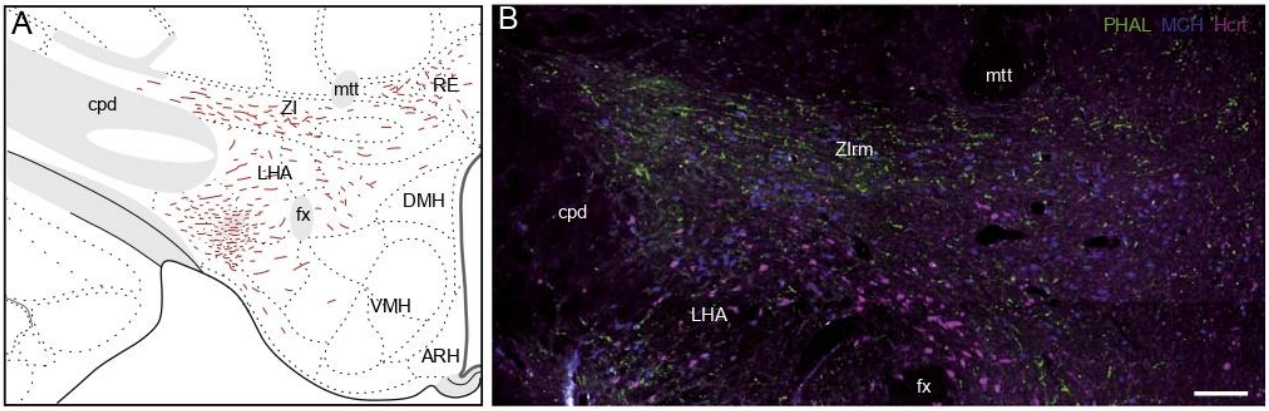

Fig. 3. Line drawing (A) and photomicrograph (B) to illustrate PHAL axons in the LHA (experiment SUM-2). Most ascending axons traveled through the ventrolateral LHA to reach the telencephalon. However, neurons in the LHA itself appear little innervated. Triple labeling experiments (B) for MCH, Hcrt, and PHAL showed few *en passant* boutons could close to MCH and Hcrt neurons. The rostromedial ZI (ZIrm) seemed more intensely targeted by axons *en route* to innervate the reuniens nucleus (RE). The ZIrm contains numerous MCH cell bodies. Some PHAL boutons could be observed close to these neurons.Scale bar = 50 µm.

(PH) (corresponding to level 31 of Swanson's Brain Maps), medial to the mtt, and a few in the LHA area, ventrolateral to the mtt and dorsal to the fx (Fig. 4A, B). These medial cells were similar, in shape and staining intensity, to those observed in the SUMl.

At levels 32 and 33 of Swanson's Brain Maps (Fig. 4C–E), an abundant FG cell group was observed dorsal to the fx, in the SUMl. Indeed, they were distributed lateral to the pm and dorsal to the fx, between the NG and the parvafox nucleus labeled for PV (Fig. 5).

At levels 34 and 35 of Swanson's Brain Maps, almost all the FG neurons were distributed in the SUMl, dorsal to the pm, except for a few observed more dorsally to the SUMl, and ventral to the fr (Fig. 4F–H). More caudally, in addition to the SUMl, FG neurons were found in the SUMm (Fig. 4I), and extended ventrolaterally to the fr, in the PH (Fig. 4J).

Because MCH and Hcrt cells in the posterior LHA innervate the hippocampal formation (Peyron et al., 1998; Croizier et al., 2015), double labeling experiments, MCH-FG and Hcrt-FG, were realized to confirm that FG neurons, in the SUM/PHA region, were distinct of the MCH and Hcrt neurons in the LHA. Indeed, these FG neurons, in the region of the SUM, are different to the MCH and Hcrt neurons projecting on the hippocampus (data not shown), which are rostral in the LHA, compared to those observed in the rostral borders of the SUM.

Innervation of the CLA after PHAL injection in the SUMl

In this study, the CLA was defined as a cell mass that contains a dense immunohistochemical labeling for PV (Mathur et al., 2009; Barbier et al., 2017b). Both SUM PHAL injections provided dense projections, which were restricted to the PV-rich claustrum and could not be observed more rostrally or caudally (Figs. 6, 7).

In experiment SUM-1, axons innervated a restricted, mostly rostral part of the CLA (Figs. 6 and 7 A1–A2), whereas in experiment SUM-2, axons were observed through the whole nucleus (Figs. 6 and 7B1–B2).

High magnification analysis showed that PHAL axons within the borders of the CLA have a complex morphology with very clear grapes of boutons and potential synaptic contacts with CLA's perikarya, suggesting a significant innervation of the CLA (Fig. 8). Some PV containing cells seemed contacted by PHAL axons, as varicosities were observed in their immediate proximity. Specific regions rostral to the PV-rich claustrum and abutting the corpus callosum (cc) and rostral to the onset of the caudoputamen (CP) nucleus were not innervated (Fig. 9). To verify the origin of these projections from the SUM, injections of FG were performed into the CLA (Fig. 10).

FG injection site in the CLA

Because of the small size of the nucleus, it was very difficult to perform an FG injection into the CLA without contaminating adjacent structures. As a consequence, none of our injections was restricted to this nucleus, but the halo of diffusion extended into adjacent structures including the IC and the CP. However, one FG injection was centered in the rostral CLA (Fig. 10A1, A1″). The illustration of the distribution of retrogradely labeled cells in Fig. 10 (B–G) is based on this CLA experiment.

Distribution of FG labeled cells in the region of the SUM

FG-containing neurons were observed in the lateral and medial parts of the SUMl (Fig. 10E). These cells formed a group of middle-sized neurons, with long branched dendrites, distributed in the lateral region of the SUMl. This experiment then confirmed that neurons in the SUMl innervate the CLA, as adjacent IC and CP are not innervated by PHAL axons from the SUM. However, as our FG injection sites extended into the IC and CP, the distribution pattern of FG neurons extended beyond the SUMl. Control PHAL in the PSTN and VTA were useful to verify if these additional sites, which contained FG cell bodies, effectively project into the CLA.

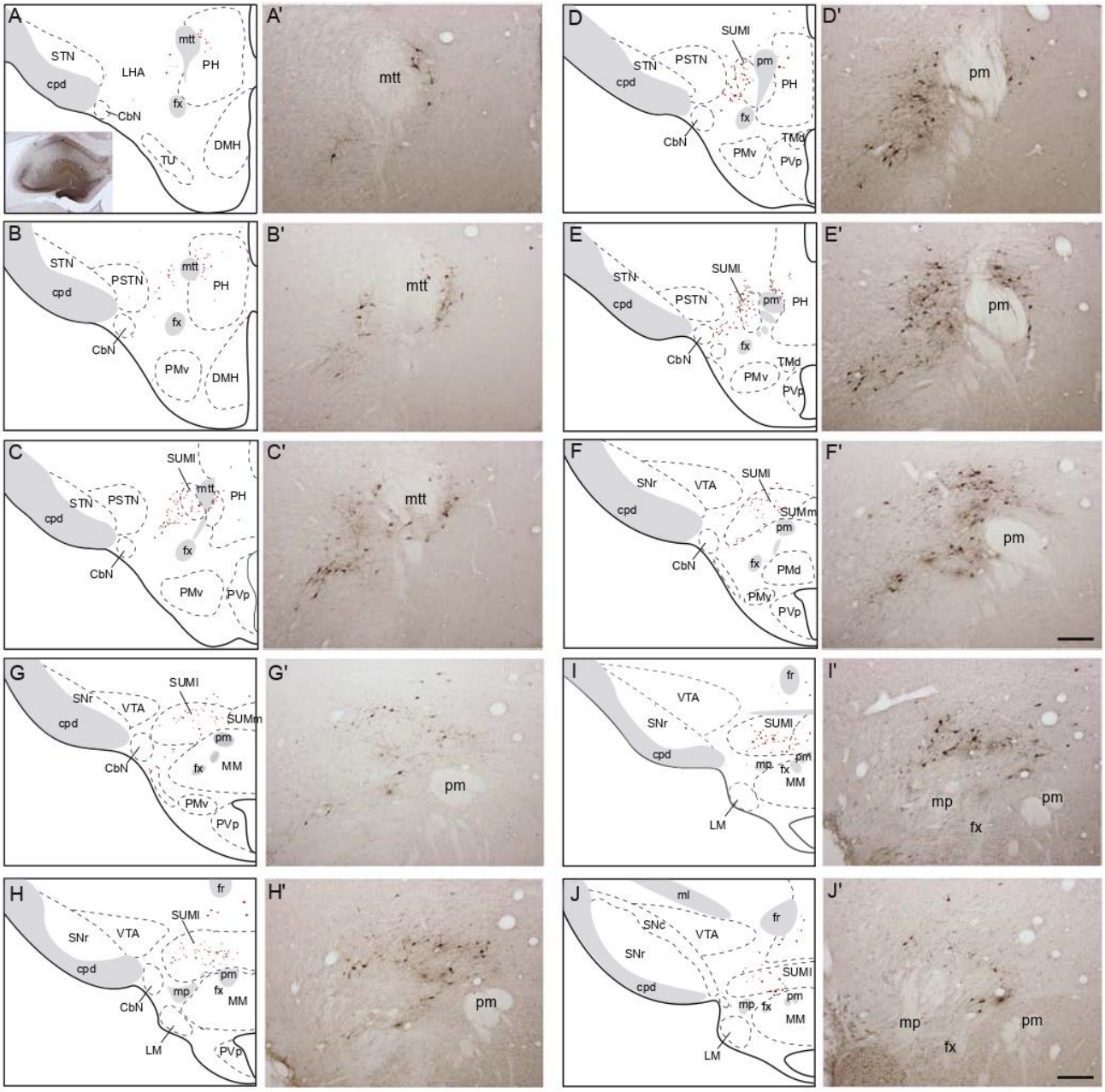

Fig. 4. Line drawings (A–J) and photomicrographs (A′–J′) to illustrate the distribution of FG cells after injection of this retrograde tracer in the DG (frame in A). Note that the distribution of these cells closely follows the mtt along its course in the caudal hypothalamus.Scale bar = 100 µm.

At rostral levels, many FG neurons were observed in the PSTN adjacent to the NG. Indeed, our PHAL injection site into the PSTN yielded evidence of innervation in the IC but not in the CLA. Additional, but less abundant FG cells, were observed in the LHA immediately medial to the PSTN and dorsal to the calbindin (CbN) and parvafox nuclei. One or two neurons were found in the subthalamic nucleus (STN). These patterns are illustrated in Fig. 10 (B, C). This cell group extends far caudally on sections corresponding to the lateral part of the PSTN/CbN complex. One FG neuron was observed in the ZI (Fig. 10D). At level 34 of Swanson's Brain Maps, FG neurons were observed into the SNr and dorsal into the VTA. Indeed, our control PHAL site into the ventral VTA was important to verify that no innervation into the CLA arises from these two structures; therefore, retrograde neurons within them were the results of the CP or insular contaminations by the fluorogold injection.

DISCUSSION

The most important point of our study is that the SUMl sends dense projections into the CLA, defined by PV expression. In the following discussion, we will re-examine the previous literature concerning the SUM network, and

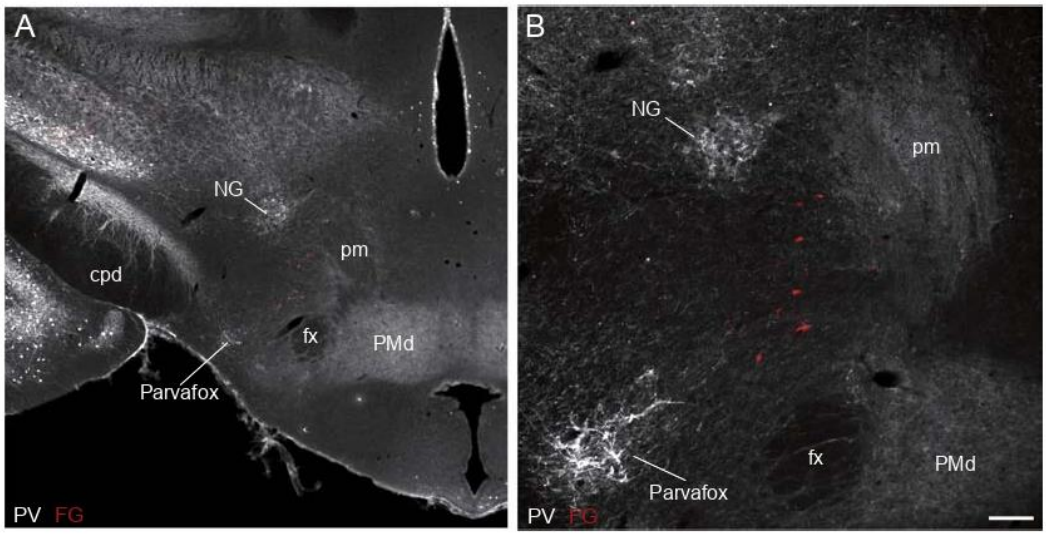

Fig. 5. Photomicrographs of FG-retrogradely labeled neurons after a FG injection in the DG. Note that FG cell bodies are observed in the SUMl lateral to the principal mammillary tract (pm), and dorsal to the fx. The nucleus gemini (NG), labeled with PV antibodies, is just dorsal to the SUM, and does not contain FG cells.Scale bar: A = 250 µm; B = 100 µm.

the functional implication of these projections. Some aspects of the SUM cytoarchitectonic organization, especially with regard to its rostral borders that extend in the dorsal premammillary region, will also be addressed.

Characterization of the rostral borders of the SUMl

The caudal and ventral borders of the SUM are easy to distinguish with the VTA and the MM, respectively (Swanson, 1982; Paxinos and Watson, 2005). However, rostral borders of the nucleus are drawn differently, depending on authors. Distribution of the retrograde labeling from the hippocampus appears to be a good marker of the SUMl rostral borders. FG-containing cells were observed associated with the mtt, laterally adjacent to the posterior hypothalamic nucleus (PH). This distribution was identical to that reported by previous authors, such as Riley and Moore (1981) and Haglund et al. (1984). Therefore, a rostral border of the nucleus extending beyond the rostral limit of the MM is proposed, as illustrated by Swanson (Dahlström and Fuxe, 1964; Swanson, 2004). Therefore, the SUM may as well laterally covert the dorsal premammillary nucleus, as illustrated by Haglund et al. (1984). The dorsal premammillary nucleus (PMd) is regarded as closely related to the MM, in terms of its afferent projections from the ventral tegmental nucleus, and efferent projections into the anterior thalamic nucleus (Canteras and Swanson, 1992). Therefore, a SUM extending dorsolateral to this nucleus is not anomalous. The SUM-1 injection in this region provided a similar pattern of projections than the more caudal SUM-2 injection site, especially regarding axons into the septal region, and a dense innervation to the DG which is a hallmark of the SUM (Segal and Landis, 1974a,b; Wyss et al., 1979; Riley and Moore, 1981; Haglund et al., 1984; Vertes, 1992). The SUMl, however, appears clearly distinct from the NG, this small enigmatic cell group, whichis connected to the olfactory tubercle (Price et al., 1991), being intensely labeled for PV (Chometton et al., 2016), while the SUM is not.

CLA innervation by SUM projections

Projections from the SUM to the CLA were already mentioned by Vertes (1992). A recent work in the mouse also described connections from the SUM to the CLA, but authors indicated that borders of the CLA might extend beyond the PV-rich zone, in particular, in connection with somatomotor networks (Zingg et al., 2018). At neurochemical levels, the borders of the CLA have been revised during the last decade. Neurochemical data indicate that the CLA is smaller than what the cytoarchitecture suggested. In particular, Mathur based a definition of the CLA on the pattern of projections, but also on an intense PV labeling (Mathur et al., 2009; Mathur, 2014). The CLA is also devoid of TH projections, while the surrounding tissue is intensely innervated by TH-containing axons (Barbier et al., 2017b). At the molecular level, Mathur also identified a claustrum-specific protein, the G-protein gamma2 subunit (Gng2), which enriched the nucleus, but not adjacent structures of the rat forebrain (Mathur et al., 2009). In light of these anatomical considerations, it was necessary to re-examine the connections from the SUM as they may have important functional implications.

Both our PHAL experiments in the SUM resulted in an intense labeling into the borders of the CLA, as defined by PV expression. The rostral injection sites provided a more restricted input to the rostral half of the nucleus, maybe revealing a weak degree of topographical organization. PHAL axons in both experiments were evocative of a very significant innervation of the nucleus. Axons showed a complex morphology, displaying many buttons, suggesting numerous synaptic contacts. Compared to the input into the DG, obviously the CLA projections are less abundant. However, PHAL injection sites

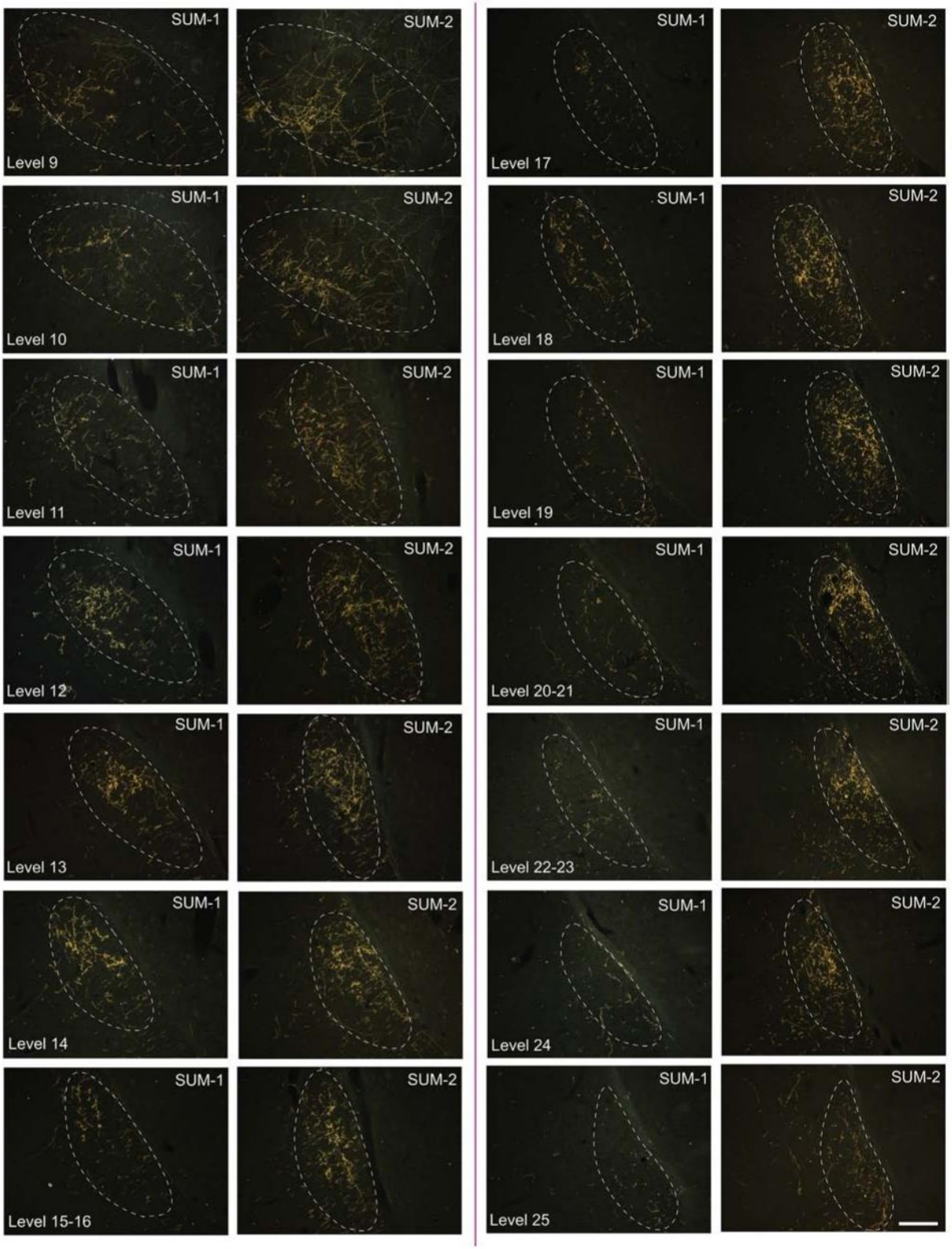

Fig. 6. Photomicrographs illustrating the distribution of PHAL axons in the CLA in experiments SUM-1 (A–J), and SUM 2 (A′–J′). Pictures are arranged from rostral (A–A′) to caudal (J–J′).Scale bar = 50 μm.

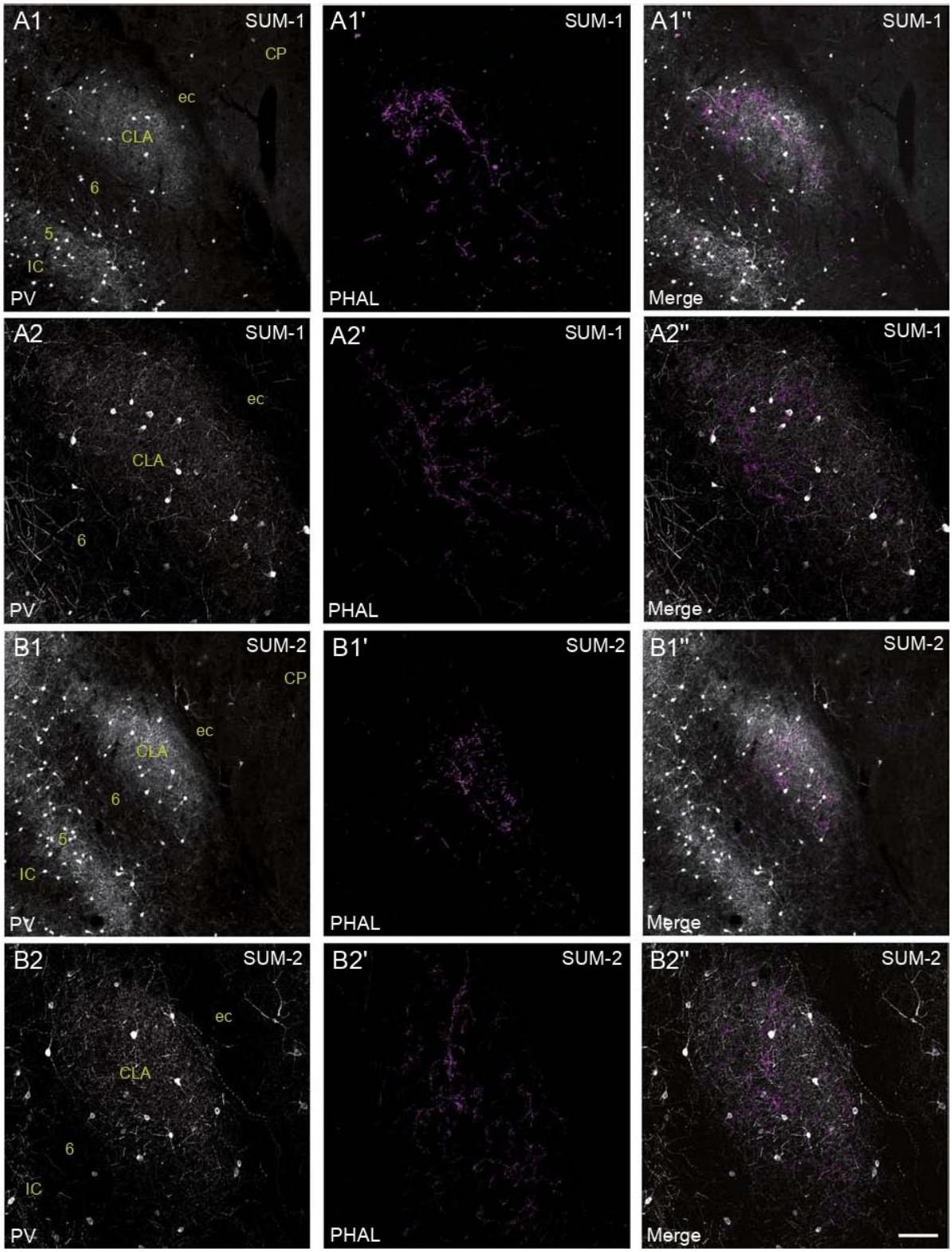

Fig. 7. Photomicrographs at × 10 (A1–A1″ and B1–B1″) and at × 20 (A2–A2″ and B2–B2″) illustrating the distribution of PHAL axons from the SUMl in the region of the CLA at level 13–14 of Swanson Brain maps. The condensation of PV-labeling corresponds to a cluster of cells embedded in layer 6 of the IC, representing the CLA. From the SUM-1 (A1–A2″), PHAL axons innervate the nucleus from its dorsal side whereas from the SUM-2 (B1–B2″), PHAL axons innervate the CLA from its ventral side.Scale bar = 50 μm.

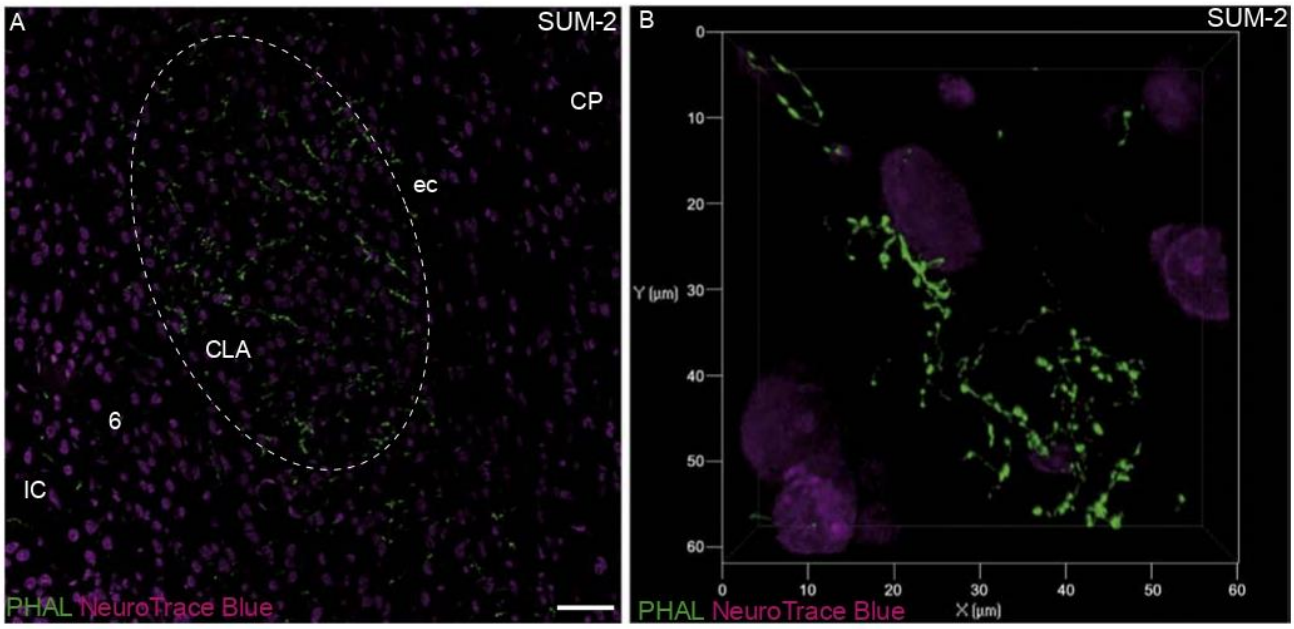

Fig. 8. Photomicrographs to illustrate aspects of PHAL axons in the CLA. (A) Optic slice using the ApoTome device of the microscope to illustrate the innervation of the CL by PHAL axons (green) (B). At higher magnification, labeled PHAL axons show complex morphologies with many varicosities and clear boutons. These pictures were taken in the CLA of experiment SUM-2. The section was counterstained using NeuroTrace Blue (in purple).Scale bar = 30 µm.

in the SUM involved a very small fraction of the SUM neurons, and the true abundance of the CLA innervation by the SUM should certainly not be underestimated.

To confirm the origin of the SUM projections into the CLA, FG was injected into this nucleus. The distribution of FG neurons in the SUMl was reminiscent of that after FG injection in the DG. Because of the small size of the CLA, our FG injection contaminated adjacent IC and CP, resulting in abundant retrograde signals into the PSTN and the SNr/VTA, However, our control injections confirmed that these last structures do not project into the CLA, but innervate the IC and/or the striatum (Björklund et al., 1987; Gerfen and Wilson, 1996; Goto and Swanson, 2004). Again, they were also confirmed by a recent genetic tract tracing study in the mouse (Zingg et al., 2018).

Functional considerations

The SUM is a key player in the pathways that modulate the expression of the theta rhythm by the hippocampus (Fig. 11). This electrical activity is related to behavioral expression, spatial learning, and memory formation. It involves the SUM projections to the DG, but those into the MS are central in these processes, as the medial septum is seen as a pacemaker of the theta rhythm in the hippocampus (Vertes, 1986; Wang, 2002; Varga et al., 2008).

The CLA is very well connected with a major sensory cortical network (Torgerson and Van Horn, 2014) and is thought to have cognitive functions related to the salience of sensory stimuli. Neurons in this nucleus discharge with the appearance of a particular external stimulus. The CLA does not project to the brainstem, but brainstem structures can influence this nucleus. In this context, the innervation by the SUMl of the CLA is quite significant. The isocortex feeds forward information to the hippocampal formation through the entorhinal cortex (Fig. 11). The entorhinal cortex is in turn at the origin of the perforant path that innervates the DG. Therefore, the projections from the SUMl into the CLA and the DG could very well modify the excitability of this nucleus, as well as the DG, facilitating the spatial encoding of prominent sensory inputs by the hippocampus.

Finally, both the SUM and CLA are also involved in REM sleep (Luppi et al., 2017). Indeed, Renouard et al. (2015) reported that CLA neurons are activated during paradoxical sleep (PS) and are responsible for neocortical activation, while the SUMl neurons are responsible for activating the DG granule cells during PS. It is tempting to hypothesize that the SUMl might also be involved in activating CLA neurons during PS. In this context, it was also appealing to search for specific connections from SUM axons onto MCH cell bodies, as SUM axons run through the medial forebrain bundle and LHA MCH neurons are important for REM sleep. We did not find that MCH cell bodies were specifically targeted by SUM axons and few *en passant* putative contacts were observed. However, many SUM axons traveled through the ZIrm, and provided a light input to this structure believed to be involved in attention (Chometton et al., 2017) and might be compared to the executive role of the CLA functional network (White et al., 2018).

To conclude, the hippocampal formation and isocortex are connected through several channels. The projections

Fig. 9. Photomicrographs to illustrate aspects of PHAL axons rostral to the CLA. Regions rostral to the PV-rich claustrum, immediately ventral to the corpus callosum but at a level of section rostral to the level at which the CP is emerging, contain only few axons. The picture illustrates the innervation in experiment SUM-1 but the same observation was made in experiment SUM-2.Scale bar: A–B = 500 μm; C = 50 μm.

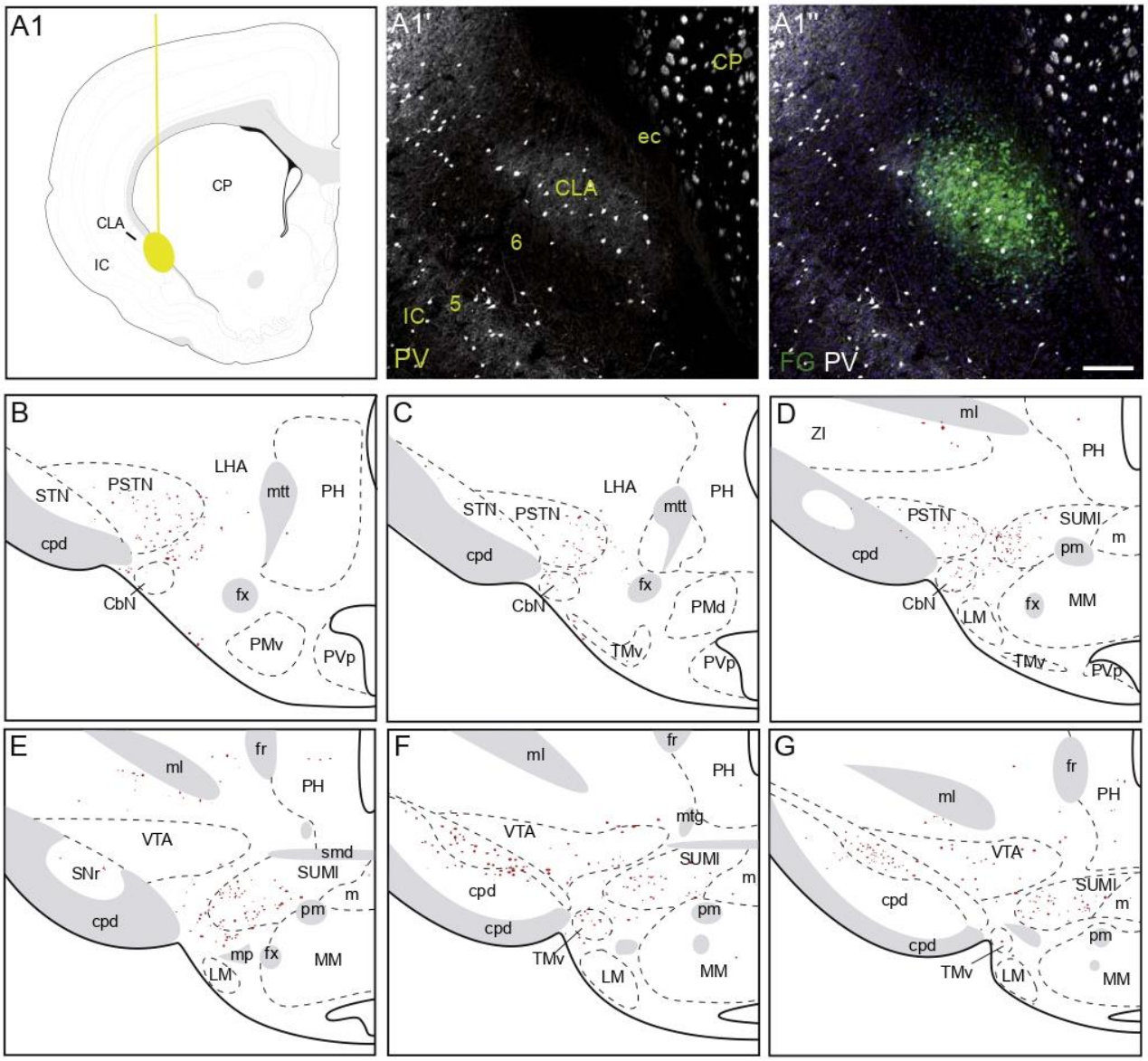

Fig. 10. Line drawing to illustrate the FG injection site in the region of the claustrum (A), and photomicrographs (A′, A″) illustrating the same FG injection site in the region of the rostral CLA labeled using immunohistochemistry for PV (B1–A1″). The injection site contaminated the IC and the CP adjacent to the CLA, but the CP contamination was more obvious caudally. Line drawings of coronal sections passing through the premammillary and the mammillary areas, arranged from rostral (B) to caudal (G), and illustrating the distribution of retrogradely labeled cells (containing the FG) in the SUM after FG injection in the CLA. Abundant labeling was also seen in the PSTN and VTA, but resulted of the contamination in the IC and CP (see text for details).Scale bar = 50 μm.

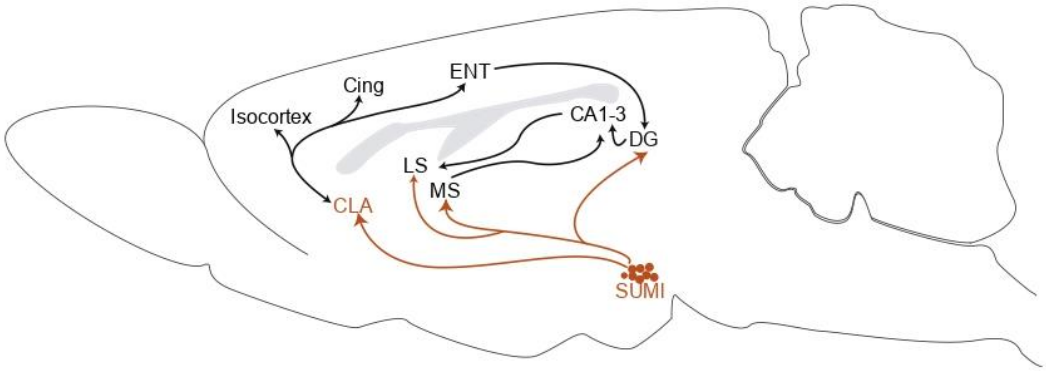

Fig. 11. Summary diagram illustrating the hypothesis of the functional organization of the circuitry linking the lateral part of the SUMl, the DG, and the CLA (see text for details).

from the SUM to the CLA are a pathway that has not been investigated so far, but that might be promising to understand the coding of information and memory formation.

ACKNOWLEDGMENT

This work was supported by the Region Franche-Comté, France.

ROLE OF AUTHORS

Conceived and designed the experiments: Pierre-Yves Risold. Performed the experiments and illustration production: Marie Barbier and Pierre-Yves Risold. Animal handling: Marie Barbier. Analyzed the data and wrote the text: Marie Barbier and Pierre-Yves Risold.

REFERENCES

Alvarez-Bolado G, Celio MR. (2016) The ventrolateral hypothalamic area and the parvafox nucleus: role in the expression of (positive) emotions? J Comp Neurol 524:1616-1623.

Baizer J. (2001) Serotonergic innervation of the primate claustrum. Brain Res Bull 55:431-434.

Balcita-Pedicino JJ, Omelchenko N, Bell R, Sesack SR. (2011) The inhibitory influence of the lateral habenula on midbrain dopamine cells: ultrastructural evidence for indirect mediation via the rostromedial mesopontine tegmental nucleus. J Comp Neurol 519:1143-1164.

Barbier M, Chometton S, Peterschmitt Y, Fellmann D, Risold P-Y. (2017) Parasubthalamic and calbindin nuclei in the posterior lateral hypothalamus are the major hypothalamic targets for projections from the central and anterior basomedial nuclei of the amygdala. Brain Struct Funct 222:2961-2991.

Barbier M, Houdayer C, Franchi G, Poncet F, Risold P-Y. (2017) Melanin-concentrating hormone axons, but not orexin or tyrosine hydroxylase axons, innervate the claustrum in the rat: an immunohistochemical study. J Comp Neurol 525:1489-1498.

Barbier M, Fellmann D, Risold P-Y. (2018) Characterization of McDonald's intermediate part of the central nucleus of the amygdala in the rat. J Comp Neurol 526(14):2165-2186, https://doi.org/10.1002/cne.24470.

Barbier M, Fellmann D, Risold P-Y. (2018) Morphofunctional organization of the connections from the medial and intermediate parts of the central nucleus of the amygdala into distinct divisions of the lateral hypothalamic area in the rat. Front Neurol 9:688.

Bilella A, Alvarez-Bolado G, Celio MR. (2016) The Foxb1-expressing neurons of the ventrolateral hypothalamic parvafox nucleus project to defensive circuits: *Foxb1*-expressing neurons of the VL hypothalamic Parvafox nucleus. J Comp Neurol 524:2955-2981.

Bittencourt JC, Presse F, Arias C, Peto C, Vaughan J, Nahon JL, Vale W, Sawchenko PE. (1992) The melanin-concentrating hormone system of the rat brain: an immuno- and hybridization histochemical characterization. J Comp Neurol 319:218-245.

Björklund A, Hökfelt T, Swanson LW. (1987) Handbook of chemical neuroanatomy. Elsevier, 1987.

Brown SP, Mathur BN, Olsen SR, Luppi P-H, Bickford ME, Citri A. (2017) New breakthroughs in understanding the role of functional interactions between the neocortex and the claustrum. J Neurosci Off J Soc Neurosci 37:10877-10881.

Canteras NS, Swanson LW. (1992) The dorsal premammillary nucleus: an unusual component of the mammillary body. Proc Natl Acad Sci U S A 89:10089-10093.

Celio MR, Baier W, Schärer L, de Viragh PA, Gerday C. (1988) Monoclonal antibodies directed against the calcium binding protein parvalbumin. Cell Calcium 9:81-86.

Chometton S, Franchi G, Houdayer C, Mariot A, Poncet F, Fellmann D, Tillet Y, Risold PY. (2014) Different distributions of preproMCH and hypocretin/orexin in the forebrain of the pig (Sus scrofa domesticus). J Chem Neuroanat 61–62:72-82.

Chometton S, Pedron S, Peterschmitt Y, Van Waes V, Fellmann D, Risold P-Y. (2016) A premammillary lateral hypothalamic nuclear complex responds to hedonic but not aversive tastes in the male rat. Brain Struct Funct 221:2183-2208.

Chometton S, Charrière K, Bayer L, Houdayer C, Franchi G, Poncet F, Fellmann D, Risold PY. (2017) The rostromedial zona incerta is involved in attentional processes while adjacent LHA responds to arousal: c-Fos and anatomical evidence. Brain Struct Funct 222:2507-2525.

Clarke JH, Emson PC, Irvine RF. (2009) Distribution and neuronal expression of phosphatidylinositol phosphate kinase II$\hat{1}^3$ in the mouse brain. J Comp Neurol 517:296-312.

Croizier S, Amiot C, Chen X, Presse F, Nahon J-L, Wu JY, Fellmann D, Risold P-Y. (2011) Development of posterior hypothalamic neurons enlightens a switch in the prosencephalic basic plan Henrique D. PLoS ONE 6e28574.

Croizier S, Cardot J, Brischoux F, Fellmann D, Griffond B, Risold PY. (2013) The vertebrate diencephalic MCH system: a versatile neuronal population in an evolving brain. Front Neuroendocrinol 34:65-87.

Croizier S, Chometton S, Fellmann D, Risold P-Y. (2015) Characterization of a mammalian prosencephalic functional plan. Front Neuroanat 8 Available at http://journal.frontiersin.org/article/10.3389/fnana.2014.00161/abstract.

Dahlström A, Fuxe K. (1964) Localization of monoamines in the lower brain stem. Experientia 20:398-399.

De la Huerta I, Kim I-J, Voinescu PE, Sanes JR. (2012) Direction-selective retinal ganglion cells arise from molecularly specified multipotential progenitors. Proc Natl Acad Sci U S A 109:17663-17668.

de Lecea L, Kilduff TS, Peyron C, Gao X, Foye PE, Danielson PE, Fukuhara C, Battenberg EL, Gautvik VT, Bartlett FS, Frankel WN, van den Pol AN, Bloom FE, Gautvik KM, Sutcliffe JG. (1998) The

hypocretins: hypothalamus-specific peptides with neuroexcitatory activity. Proc Natl Acad Sci U S A 95:322-327.
Fellmann D, Bugnon C, Risold PY. (1987) Unrelated peptide immunoreactivities coexist in neurons of the rat lateral dorsal hypothalamus: human growth hormone-releasing factor1-37-, salmon melanin-concentrating hormone- and alpha-melanotropin-like substances. Neurosci Lett 74:275-280.
Florenzano F, Viscomi MT, Mercaldo V, Longone P, Bernardi G, Bagni C, Molinari M, Carrive P. (2006) P2X2R purinergic receptor subunit mRNA and protein are expressed by all hypothalamic hypocretin/orexin neurons. J Comp Neurol 498:58-67.
García Del Caño G, Gerrikagoitia I, Martínez-Millán L. (2000) Morphology and topographical organization of the retrospleniocollicular connection: a pathway to relay contextual information from the environment to the superior colliculus. J Comp Neurol 425:393-408.
Gerfen CR, Wilson CJ. (1996) Chapter II. The basal ganglia. Integrated systems of the CNS, part III. Amsterdam: Elsevier. p. 371-468.
Goll Y, Atlan G, Citri A. (2015) Attention: the claustrum. Trends Neurosci 38:486-495.
Gonzalo-Ruiz A, Alonso A, Sanz JM, Llinás RR. (1992) Afferent projections to the mammillary complex of the rat, with special reference to those from surrounding hypothalamic regions. J Comp Neurol 321:277-299.
Goto M, Swanson LW. (2004) Axonal projections from the parasubthalamic nucleus. J Comp Neurol 469:581-607.
Haglund L, Swanson LW, Köhler C. (1984) The projection of the supramammillary nucleus to the hippocampal formation: an immunohistochemical and anterograde transport study with the lectin PHA-L in the rat. J Comp Neurol 229:171-185.
Harris GC, Wimmer M, Aston-Jones G. (2005) A role for lateral hypothalamic orexin neurons in reward seeking. Nature 437:556-559.
Henny P, Jones BE. (2006) Innervation of orexin/hypocretin neurons by GABAergic, glutamatergic or cholinergic basal forebrain terminals evidenced by immunostaining for presynaptic vesicular transporter and postsynaptic scaffolding proteins. J Comp Neurol 499:645-661.
Henny P, Brischoux F, Mainville L, Stroh T, Jones BE. (2010) Immunohistochemical evidence for synaptic release of glutamate from orexin terminals in the locus coeruleus. Neuroscience 169:1150-1157.
Hernández-Pérez JJ, Gutiérrez-Guzmán BE, López-Vázquez MÁ, Olvera-Cortés ME. (2015) Supramammillary serotonin reduction alters place learning and concomitant hippocampal, septal, and supramammillar theta activity in a Morris water maze. Front Pharmacol 6 Available at https://www.frontiersin.org/articles/10.3389/fphar.2015.00250/full.
Kim J, Matney CJ, Roth RH, Brown SP. (2016) Synaptic organization of the neuronal circuits of the claustrum. J Neurosci 36:773-784.
Kirk IJ, Mackay JC. (2003) The role of theta-range oscillations in synchronising and integrating activity in distributed mnemonic networks. Cortex J Devoted Study Nerv Syst Behav 39:993-1008.
Kocsis B. (2006) The effect of descending theta rhythmic input from the septohippocampal system on firing in the supramammillary nucleus. Brain Res 1086:92-97.
Kocsis B, Vertes RP. (1994) Characterization of neurons of the supramammillary nucleus and mammillary body that discharge rhythmically with the hippocampal theta rhythm in the rat. J Neurosci 14:7040-7052.
Lee SJ, Kirigiti M, Lindsley SR, Loche A, Madden CJ, Morrison SF, Smith MS, Grove KL. (2013) Efferent projections of neuropeptide Y-expressing neurons of the dorsomedial hypothalamus in chronic hyperphagic models: projections of DMH NPY neurons. J Comp Neurol 521:1891-1914.
Luppi P-H, Billwiller F, Fort P. (2017) Selective activation of a few limbic structures during paradoxical (REM) sleep by the claustrum and the supramammillary nucleus: evidence and function. Curr Opin Neurobiol 44:59-64.
Lutter M, Krishnan V, Russo SJ, Jung S, McClung CA, Nestler EJ. (2008) Orexin signaling mediates the antidepressant-like effect of calorie restriction. J Neurosci 28:3071-3075.
Mathur BN. (2014) The claustrum in review. Front Syst Neurosci 8:48.
Mathur BN, Caprioli RM, Deutch AY. (2009) Proteomic analysis illuminates a novel structural definition of the claustrum and insula. Cereb Cortex 19:2372-2379.
Pan W-X, McNaughton N. (2002) The role of the medial supramammillary nucleus in the control of hippocampal theta activity and behaviour in rats. Eur J Neurosci 16:1797-1809.
Pan W-X, McNaughton N. (2004) The supramammillary area: its organization, functions and relationship to the hippocampus. Prog Neurobiol 74:127-166.
Paxinos G, Watson C. (2005) The rat brain in stereotaxic coordinates. 5th ed. Amsterdam ; Boston: Elsevier Academic Press, 2005.
Peyron C, Tighe DK, van den Pol AN, de Lecea L, Heller HC, Sutcliffe JG, Kilduff TS. (1998) Neurons containing hypocretin (orexin) project to multiple neuronal systems. J Neurosci 18:9996-10015.
Price JL, Slotnick BM, Revial M-F. (1991) Olfactory projections to the hypothalamus. J Comp Neurol 306:447-461.
Puskás N, Papp RS, Gallatz K, Palkovits M. (2010) Interactions between orexin-immunoreactive fibers and adrenaline or noradrenaline-expressing neurons of the lower brainstem in rats and mice. Peptides 31:1589-1597.
Rae AS. (1954) The form and structure of the human claustrum. J Comp Neurol 100:15-39.
Rahman FE, Baizer JS. (2007) Neurochemically defined cell types in the claustrum of the cat. Brain Res 1159:94-111.
Remedios R, Logothetis NK, Kayser C. (2014) A role of the claustrum in auditory scene analysis by reflecting sensory change. Front Syst Neurosci 8:44.
Renouard L, Billwiller F, Ogawa K, Clement O, Camargo N, Abdelkarim M, Gay N, Scote-Blachon C, Toure R, Libourel P-A, Ravassard P, Salvert D, Peyron C, Claustrat B, Leger L, Salin P, Malleret G, Fort P, Luppi P-H. (2015) The supramammillary nucleus and the claustrum activate the cortex during REM sleep. Sci Adv 1 e1400177–e1400177.
Riley JN, Moore RY. (1981) Diencephalic and brainstem afferents to the hippocampal formation of the rat. Brain Res Bull 6:437-444.
Risold PY. (2004) The septal region. The rat nervous system. Elsevier. p. 605-632. Available at: http://linkinghub.elsevier.com/retrieve/pii/B9780125476386500213.
Risold PY, Swanson LW. (1997) Connections of the rat lateral septal complex. Brain Res Brain Res Rev 24:115-195.
Risold PY, Fellmann D, Rivier J, Vale W, Bugnon C. (1992) Immunoreactivities for antisera to three putative neuropeptides of the rat melanin-concentrating hormone precursor are coexpressed in neurons of the rat lateral dorsal hypothalamus. Neurosci Lett 136:145-149.
Ruan M, Young CK, McNaughton N. (2011) Minimal driving of hippocampal theta by the supramammillary nucleus during water maze learning. Hippocampus 21:1074-1081.
Sakurai T, et al. (1998) Orexins and orexin receptors: a family of hypothalamic neuropeptides and G protein-coupled receptors that regulate feeding behavior. Cell 92 1 page following 696.
Schmued LC, Fallon JH. (1986) Fluoro-gold: a new fluorescent retrograde axonal tracer with numerous unique properties. Brain Res 377:147-154.
Segal M, Landis S. (1974) Afferents to the hippocampus of the rat studied with the method of retrograde transport of horseradish peroxidase. Brain Res 78:1-15.
Segal M, Landis SC. (1974) Afferents to the septal area of the rat studied with the method of retrograde axonal transport of horseradish peroxidase. Brain Res 82:263-268.
Sherk H. (1986) The claustrum and the cerebral cortex. Sensory-motor areas and aspects of cortical connectivity. Cerebral CortexBoston, MA: Springer. p. 467-499. Available at: https://link.springer.com/chapter/10.1007/978-1-4613-2149-1_13.
Swanson LW. (1982) The projections of the ventral tegmental area and adjacent regions: a combined fluorescent retrograde tracer and immunofluorescence study in the rat. Brain Res Bull 9:321-353.
Swanson LW. (2004) Brain maps: structure of the rat brain. third edition. San Diego: Elsevier, 2004.

Swanson LW, Cowan WM. (1977) An autoradiographic study of the organization of the efferent connections of the hippocampal formation in the rat. J Comp Neurol 172:49-84.
Swanson LW, Cowan WM. (1979) The connections of the septal region in the rat. J Comp Neurol 186:621-655.
Tafuri S, Pavone LM, Mastellone V, Spina A, Avallone L, Vittoria A, Staiano N, Scala G. (2009) Expression of orexin A and its receptor 1 in the choroid plexuses from buffalo brain. Neuropeptides 43:73-80.
Torgerson CM, Van Horn JD. (2014) A case study in connectomics: the history, mapping, and connectivity of the claustrum. Front Neuroinform 8:83.
Varga V, Hangya B, Kránitz K, Ludányi A, Zemankovics R, Katona I, Shigemoto R, Freund TF, Borhegyi Z. (2008) The presence of pacemaker HCN channels identifies theta rhythmic GABAergic neurons in the medial septum. J Physiol 586:3893-3915.
Vertes RP. (1986) Brainstem modulation of the hippocampus. The hippocampus. Boston, MA: Springer. p. 41-75. Available at: https://link.springer.com/chapter/10.1007/978-1-4615-8024-9_2.
Vertes RP. (1992) PHA-L analysis of projections from the supramammillary nucleus in the rat. J Comp Neurol 326:595-622.
Wang X-J. (2002) Pacemaker neurons for the theta rhythm and their synchronization in the septohippocampal reciprocal loop. J Neurophysiol 87:889-900.
Wang Q, Ng L, Harris JA, Feng D, Li Y, Royall JJ, Oh SW, Bernard A, Sunkin SM, Koch C, Zeng H. (2017) Organization of the connections between claustrum and cortex in the mouse. J Comp Neurol 525:1317-1346.
White MG, Cody PA, Bubser M, Wang H-D, Deutch AY, Mathur BN. (2017) Cortical hierarchy governs rat claustrocortical circuit organization. J Comp Neurol 525:1347-1362.
White MG, Panicker M, Mu C, Carter AM, Roberts BM, Dharmasri PA, Mathur BN. (2018) Anterior cingulate cortex input to the claustrum is required for top-down action control. Cell Rep 22:84-95.
Wyss JM, Swanson LW, Cowan WM. (1979) Evidence for an input to the molecular layer and the stratum granulosum of the dentate gyrus from the supramammillary region of the hypothalamus. Anat Embryol (Berl) 156:165-176.
Zingg B, Dong H-W, Tao HW, Zhang LI. (2018) Input-output organization of the mouse claustrum. J Comp Neurol 526:2428-2443.

(Received 7 December 2018, Accepted 20 March 2019)
(Available online 28 March 2019)

II. Liste des communications

1. Article scientifique en co-auteur

Peterschmitt Y, Abdoul-Azize S, Murtaza B, **Barbier M**, Khan AS, Millot J-L & Khan NA (2018) Fatty Acid Lingual Application Activates Gustatory and Reward Brain Circuits in the Mouse. *Nutrients* **10:** 1246

2. Communication orale

Barbier M., Risold P.Y., Fellmann D. (2016) Structures de l'hypothalamus postérieur impliquées dans la réaction aux états de malaise. *Société de Biologie de Besançon (SBB)*; 8 décembre 2016

3. Communications affichées

1. Barbier M., Risold P-Y (2018) Direct and indirect connections from the insular cortex into the parasubthalamic nucleus in the rat. C*ongrès de la Society For Neuroscience (SFN)*, San Diego (USA); 3-7 novembre 2018

2. Barbier M., Fellmann D., Risold P-Y. (2018) Immunohistochemical characterization of McDonald's intermediate part of the central amygdalar nucleus in the rat. *Congrès de la Federation of European Neuroscience Societies (FENS)*, Berlin (Allemagne); 7-11 juillet 2018

3. Risold P-Y., Fellmann D., **Barbier M.** (2018) Organization of Projections from the CEA into the lateral hypothalamic area. *Congrès de la Federation of European Neuroscience Societies (FENS)*, Berlin (Allemagne); 7-11 juillet 2018

4. Barbier M., Houdayer C., Peterschmitt Y., Fellmann D., Risold P.Y. (2017) Organization of connections between insular cortex, central amygdala and caudal hypothalamus. *Colloque de la Société de Neuroendocrinologie*, Dijon (France); 18-21 septembre 2017

5. Barbier M., Chometton S., Houdayer C., Franchi G., Peterschmitt Y., Fellmann D., Risold P.Y. (2017) Characterization of a premammillary region of the hypothalamus. *Congrès de la Société des Neurosciences (NeuroFrance 2017)*, Bordeaux (France); 17-19 mai 2017

6. Risold P.Y., **Barbier M.**, Houdayer C., Franchi G., Fellmann D. (2017) Claustrum is a target for projections from the supramammillary nucleus. *Congrès de la Société des Neurosciences (NeuroFrance 2017)*, Bordeaux (France); 17-19 mai 2017

7. Barbier M., Chometton S., Houdayer C., Franchi G., Mariot A., Poncet F., Miguet-Alfonsi C., Peterschmitt Y., Fellmann D., Risold PY. (2016) Functional exploration of the parasubthalamic and calbindin nuclei. *Congrès de la Federation of European Neuroscience Societies (FENS)*, Copenhague (Danemark); 2-6 juillet 2016

8. Risold PY., **Barbier M.**, Chometton S., Franchi G., Houdayer C., Poncet F., Mariot A., Peterschmitt Y., Fellmann D. (2016) Organization of projections from the insular cortex to the parasubthalamic region in the rat. *Congrès de la Federation of European Neuroscience Societies (FENS)*, Copenhague (Danemark); 2-6 juillet 2016

9. Peterschmitt Y., Abdoul-Azize S., **Barbier M.**, Millot JL., Khan NA. (2016) Linoleic acid activates gustatory and reward brain circuits. *Congrès de la Federation of European Neuroscience Societies (FENS)*, Copenhague (Danemark); 2-6 juillet 2016

10. Barbier M., Chometton S., Houdayer C., Franchi G., Mariot A., Poncet F., Peterschmitt Y., Fellmann D., Risold PY. (2016) Le complexe PSTN/CbN répond à l'exposition à une solution d'éthanol. *Forum des Jeunes Chercheurs (FJC)*, Besançon (25); 16 juin 2016

Abstract

The hypothalamus is involved in a wide range of functions involving neuroendocrine, visceral, metabolic or behavioral responses. However, recent work challenges the classical boundaries of this brain region. The borders of the hypothalamus with the telencephalon are difficult to define and some networks, including the nuclei of the medial hypothalamus, recall in their organization those best described and connecting the basal telencephalon with the diencephalon. For large areas of the hypothalamus, especially the lateral hypothalamic areas (LHA), there is little data in the literature that can illustrate their integration into the same prosencephalic networks.

Therefore, the objectives of our work were to analyze some of the networks between of a small nuclear complex of the posterior LHA, formed by the parasubthalamic (PSTN) and the calbindin (CbN) nuclei, and the insular cortex (INS) as well as the central amygdala nucleus (CEA), with which it shares abundant connections. Axonal tract tracing techniques have been combined with the detailed neurochemical study of some of these regions. We confirmed the bidirectional nature of the anatomical links that it maintains with the CEA, identifying a division of this nucleus (the intermediate part) which was not recognized in classical atlases. Then, we showed that this complex maintains direct, with the INS, but also indirect pathways after relay in the CEA and the neighboring regions of the substantia innominata. These networks are structurally similar to those conventionally described for the adjacent subthalamic nucleus (STN) and connected to the isocortex and the "basal nuclei" by the hyperdirect and indirect pathways respectively. This work was then supplemented by functional studies in rats, but also in mice using genetic tracing and pharmacogenetic approaches. We were able to show the role of this complex in the cognitive and interoceptive control of food intake.

The interpretation of these data sheds new light on the organization of the most posterior areas of the hypothalamus including the PSTN/CbN complex but also the STN.

Résumé

L'hypothalamus est impliqué dans un large éventail de fonctions engageant des réponses neuroendocrines, viscérales, métaboliques ou encore comportementales. Cependant, les travaux récents remettent en question les frontières classiques de cette région cérébrale. Les frontières de l'hypothalamus avec le télencéphale sont difficiles à définir et certains réseaux, impliquant notamment les noyaux de l'hypothalamus médian, rappellent dans leur organisation ceux mieux décrits et connectant le télencéphale basal avec le diencéphale. Pour de vastes régions de l'hypothalamus, surtout des aires hypothalamiques latérales (LHA), peu de données de la littérature sont susceptibles d'illustrer leur intégration dans les mêmes réseaux prosencéphaliques.

Les objectifs de notre travail étaient donc d'analyser les réseaux entre un petit complexe nucléaire du LHA postérieur, formé par les noyaux parasousthalamique (PSTN) et calbindine (CbN), et le cortex insulaire (INS) ainsi que le noyau central de l'amygdale (CEA) avec lesquels il partage des connexions abondantes. Des techniques de traçage des voies nerveuses ont été combinées à l'étude neurochimique détaillée de certaines de ces régions. Nous avons confirmé la nature bidirectionnelle des liens anatomiques qu'il entretient avec le CEA, identifiant au passage une division de ce noyau (la partie intermédiaire) qui n'était pas reconnue dans les atlas classiques. Puis, nous avons montré que ce complexe entretient avec l'INS des réseaux directs, mais aussi indirects après relais dans le CEA et les régions voisines de la substance innominée. Ces réseaux sont proches dans leur structure de ceux classiquement décrits pour le noyau sousthalamique, adjacent au PSTN et connecté à l'isocortex et aux "noyaux de la base" par les voies hyperdirectes et indirectes respectivement. Ces travaux ont ensuite été complétés par des études fonctionnelles chez le rat, mais aussi chez la souris, faisant appel dans ce dernier modèle aux approches de traçage génétique et de pharmacogénétique. Nous avons pu ainsi montrer le rôle de ce complexe dans le contrôle cognitif et intéroceptif de la prise alimentaire.

L'interprétation de ces données apporte un éclairage nouveau concernant l'organisation des aires les plus postérieures de l'hypothalamus incluant ce complexe PSTN/CbN mais aussi le noyau sousthalamique.